DOCKET: EPA-HQ-OAR-2019-0534

TECHNICAL SUPPORT DOCUMENT FOR SECTION 194.24

EVALUATION OF THE COMPLIANCE RECERTIFICATION APPLICATION (CRA-2019) ACTINIDE SOURCE TERM, GAS GENERATION, BACKFILL EFFICACY, WATER BALANCE, AND CULEBRA DOLOMITE DISTRIBUTION COEFFICIENT VALUES

U. S. Environmental Protection Agency
Office of Radiation and Indoor Air
Center for Waste Management and Regulations
1200 Pennsylvania Ave. N.W.
Washington, DC 20460

April 2022

EXECUTIVE SUMMARY AND REPORT OUTLINE

The Waste Isolation Pilot Plant (WIPP) in southeastern New Mexico is an underground facility designed for the permanent disposal of defense-related transuranic (TRU) waste. The U.S. Department of Energy (DOE) operates the WIPP repository under the regulatory oversight of the U.S. Environmental Protection Agency (EPA or the Agency). DOE submitted the Compliance Certification Application (CCA) to the EPA in 1996. After extensive review of the CCA and supplemental information provided by DOE, including additional performance assessment (PA) calculations referred to as Performance Assessment Verification Testing (PAVT), EPA certified that DOE had met the regulatory requirements and WIPP began accepting waste in March 1999.

DOE is required to submit a Compliance Recertification Application (CRA) every 5 years after the initial receipt of waste at WIPP, and DOE submitted the first CRA (CRA-2004, DOE 2004) to EPA in March 2004. As required, DOE also submitted the CRA-2009 in March 2009 (DOE 2009) and the CRA-2014 in March 2014 (DOE 2014) to EPA. The Agency reviewed these CRAs and supplemental information provided by DOE and certified that DOE continued to meet WIPP regulatory requirements (EPA 2006a, EPA 2010b, EPA 2017a).

DOE submitted the fourth CRA (CRA-2019) in March 2019 (DOE 2019), with a deferred PA (CRA-2019 DPA) submitted in December 2019 (Sosson 2019). This Technical Support Document (TSD) summarizes EPA's review of chemistry-related parameters, assumptions, and documentation important to PA, including actinide source term modeling, gas generation, backfill efficacy, water balance calculations, and actinide transport in the Culebra Dolomite above the repository for the WIPP CRA-2019.

Section 1.0 summarizes WIPP certification and recertification activities since the CCA. It also summarizes the regulatory requirements and important waste chemical characteristics and repository chemical processes considered during certification and recertification. WIPP waste characteristics and components that have been identified as potentially affecting the chemistry of the system and repository releases include actinide solubilities and oxidation state distributions; formation of colloidal suspensions containing radionuclides; production of gas from steel corrosion and waste degradation; ferrous metals inventory; cellulosic, plastic, and rubber material (CPR) inventory; chelating agents (organic ligands), oxyanions, and cements; and the activity of each isotope of the radionuclides present in the waste [40 CFR 194.24(b), EPA 1997a]. For the first time, DOE (2019) also included the processes of brine consumption and gas generation caused by radiolysis in the CRA-2019 DPA based on an increased radionuclide inventory, specifically of plutonium isotopes and ^{241}Am in surplus plutonium waste.

A summary of the geologic setting, mineralogy of the Salado Formation surrounding the repository, and WIPP brine chemistry is provided in Section 2.0. The WIPP repository is excavated within the Salado Formation, a relatively thick bedded salt that is composed mainly of layers of impure halite [NaCl], with interbedded layers of anhydrite [$CaSO_4$(s)], polyhalite [$K_2MgCa_2(SO_4)_4 \cdot 2H_2O$(s)], and mudstone. The Salado Formation is underlain by the Castile Formation. The Castile Formation is mainly composed of thick beds of high-purity halite, alternating with thick beds of interlaminated carbonate and anhydrite. Pressurized brines are associated with the deformed areas of this formation. The Salado Formation is overlain by the Rustler Formation, and the Culebra Dolomite Member of the Rustler Formation is the most

significant to WIPP PA. The Culebra Dolomite, which is mostly composed of dolomite [$CaMg(CO_3)_2(s)$] with small amounts of anhydrite or gypsum [$CaSO_4 \bullet 2H_2O(s)$], is the most transmissive continuously saturated unit above the WIPP facility. It therefore provides the most direct pathway from the repository to the accessible environment, apart from human-induced releases directly to the surface.

WIPP PA calculations have used representations of both Salado and Castile brines. Small quantities of intergranular and intragranular Salado brines are associated with the salt at the repository horizon. These brines are highly concentrated (ionic strengths up to 8 M), with a composition of mostly sodium, magnesium, potassium, chloride, and sulfate, and with smaller concentrations of calcium, carbonate, and borate. The brine formulation used to represent Salado brine in WIPP laboratory experiments and PA calculations is denoted as Generic Weep Brine (GWB). This brine formulation was used to represent Salado brine in the CRA-2004 PA and all subsequent PA calculations (Snider 2003b). Castile brine may enter the repository if a borehole penetrates a waste panel and also penetrates an area of pressurized brine in the underlying Castile Formation. DOE uses the brine composition from the ERDA-6 borehole to represent Castile brines in WIPP-related laboratory experiments and WIPP PA calculations. Brine obtained from the ERDA-6 borehole has lower magnesium and chloride concentrations and a lower ionic strength than the GWB Salado brine formulation.

Section 3.0 provides a review and discussion of the Gas Generation conceptual model and its implementation for WIPP PA. Gas generation is important to PA calculations as gases generated (e.g., CO_2 and H_2) will impact repository chemical conditions such as pH and redox. Generated gases will also increase repository pressure, which can affect repository saturation, brine releases to the surface, and spallings. The Gas Generation conceptual model includes the assumption that significant gas generation will occur in the repository through corrosion of ferrous metals and microbial degradation of CPR. Because of an increased radionuclide inventory for the CRA-2019 DPA, DOE (2019) also included gas generation from brine radiolysis by dissolved, colloidal, and wetted radionuclide solids in the CRA-2019 DPA. The conceptual model also assumes that essentially all carbon dioxide [CO_2] will be removed from the gas phase by reaction with the magnesium oxide (MgO) backfill.

WIPP PA uses either humid or inundated anoxic steel corrosion rates depending on brine saturation. These rates are proportional to the estimated surface area of iron-based waste and steel waste containers. Anoxic corrosion of iron-based metals in the waste and waste containers produces hydrogen gas and two solids, $Fe(OH)_2 \bullet xH_2O(s)$ and FeS(s). DOE used project-specific data in the CRA-2019 DPA to modify the inundated and humid corrosion rates from those used in prior PAs. EPA has determined that the inundated and humid corrosion rates used by DOE for the CRA-2019 DPA are consistent with current theoretical and experimental data. EPA's evaluation of the steel surface area calculations demonstrated that the steel surface area per unit volume used in the CRA-2019 DPA was a reasonable value for WIPP waste based on the CRA-2019 DPA inventory. For future WIPP PAs, EPA recommends that DOE evaluate the steel surface area per unit volume using future inventories and waste emplacement data to demonstrate that the value used in PA continues to be representative.

DOE assumed for the CRA-2014 PA that all $H_2S(g)$ generated by CPR degradation would instantaneously react with Fe(s) and $Fe(OH)_2(s)$. This assumption resulted in lower repository

gas pressures and higher brine volumes. EPA's assessment of the available experimental data concluded that this assumption is inconsistent with data indicating H_2S passivation of iron surfaces. For the CRA-2019 DPA, DOE therefore assumed $H_2S(g)$ would not react with Fe(s) and $Fe(OH)_2(s)$ in the CRA-2019 DPA.

The CRA-2019 DPA lead inventory is significantly higher than in previous WIPP PAs because of the increased number of shielded RH containers. DOE demonstrated that lead corrosion will have insignificant effects on overall gas generation rates because of the relatively low lead surface area and lower lead corrosion rate compared to the steel surface area and corrosion rates.

For the CRA-2004 Performance Assessment Baseline Calculations (PABC04) and all later PA calculations, DOE assumed significant microbial degradation of cellulosics for 100% of the PA realizations, and assumed significant microbial degradation of plastics and rubber for 25% of the PA realizations. For the PABC04 and all later PA calculations, DOE used an initial gas pressure to account for rapid initial microbial gas generation rates, and used lower rates to account for slower long-term microbial gas generation through CPR degradation. Based on the available data that include WIPP-specific long-term degradation experiments, the current approach for modeling microbial gas generation rates is appropriate.

DOE included gas generation from brine radiolysis in the CRA-2019 DPA, and assumed radiolytic gas generation would occur in brine from dissolved and colloidal radionuclides and from radiolysis of brine by wetted radionuclide solids. DOE demonstrated that including gas generation from radiolysis of CPR and other wastes would not significantly affect repository releases for the CRA-2019 DPA. However, additional investigation is necessary to determine the relative importance of gas generation by radiolysis of adsorbed water on waste under unsaturated conditions and of gas generation by CPR radiolysis, including the potential effects of increased gas generation rates during the first 1,000 years post-closure. EPA expects DOE to provide a more extensive evaluation of gas generation by radiolysis of adsorbed water and CPR and the effects on repository releases for future WIPP PAs. Because surplus plutonium waste stream SR-KAC-PuOx contains a large fraction of the plutonium isotopes and ^{241}Am that will cause radiolytic gas generation, EPA also expects DOE to assess the effects on radiolytic gas generation and repository releases of placing this waste stream in a limited number of waste panels.

Section 4.0 describes the MgO backfill emplaced in the WIPP repository to control repository chemical conditions and minimize actinide solubilities in the post-closure repository. EPA determined that the MgO backfill met the requirements for an engineered barrier to control CO_2 fugacity and buffer brine pH during review of the CCA. MgO reacts with water in the repository to create brucite [$Mg(OH)_2(s)$] and Phase 5 [$Mg_3(OH)_5Cl{\bullet}4H_2O$], and dissolution of brucite or Phase 5 prevents low brine pH values that could increase actinide solubilities. Brucite and Phase 5 also react with CO_2 produced by microbial degradation of CPR to form hydromagnesite [$Mg_5(CO_3)_4(OH)_2{\bullet}4H_2O(s)$], controlling CO_2 fugacity at low levels that minimize actinide solubilities in repository brines. Hydromagnesite may convert over long time periods to magnesite [$MgCO_3(s)$], which is the more stable phase that will control CO_2 fugacity at even lower levels.

Evaluation of the available data indicates that the MgO backfill will control CO_2 fugacity under inundated conditions and maintain chemical conditions in WIPP brines that limit actinide solubilities. The current emplacement plan ensures adequate amounts of MgO will be present in the repository because the quantities of CPR and MgO are monitored in each room of the repository during emplacement and additional MgO is emplaced if necessary. Because of uncertainties in the rate at which hydromagnesite will convert to magnesite in the repository environment, DOE assumes for PA that the brucite-hydromagnesite reaction will buffer CO_2 fugacity at levels consistent with relatively low actinide solubilities under inundated conditions. DOE has not completed an experimental determination of MgO hydration rates using Martin Marietta-supplied MgO, which constitutes the majority of the MgO in the repository and hydrates more rapidly than MgO in the repository that was supplied by other vendors. EPA recommends that DOE provide updated hydration rates for future WIPP PAs that are consistent with the characteristics of MgO in the repository.

Section 5.0 summarizes the actinide elements and isotopes included in WIPP PA calculations. Not all radionuclides in the WIPP inventory are included in PA calculations because of computational and time constraints. Consequently, the radionuclides included in PA have been reduced according to an algorithm initially developed for the CCA. The results of the CRA-2019 DPA calculations indicate that radionuclide releases are dominated by isotopes of plutonium and americium.

Section 6.0 provides a review of the expected oxidation states of actinides that are dissolved in WIPP repository brines or present as solid phases. The actinide oxidation states assumed for the CRA-2019 DPA have remained unchanged since the CCA. DOE assumes that Am(III), Cm(III), and Th(IV) are the only stable oxidation states for these radionuclides in all realizations. DOE assumed for the CRA-2019 DPA that uranium may exist in either the U(IV) or U(VI) oxidation state and neptunium may exist in either the Np(IV) or Np(V) oxidation state. U(IV) and Np(IV) are likely to be the most stable oxidation states under the reducing conditions in the WIPP repository. Using the Np(V) and U(VI) oxidation states for 50% of PA realizations has relatively little effect on PA results because neptunium and uranium are not significant contributors to total actinide releases.

DOE has assumed that plutonium concentrations in the 50% of PA realizations with the most reducing conditions are controlled by equilibrium between Pu(III) solid and Pu(III) aqueous species. For the 50% of PA realizations with more oxidizing conditions, DOE has assumed plutonium solubilities are controlled by equilibrium between Pu(IV) solid and Pu(IV) aqueous species. The Agency believes DOE's use of the Pu(IV) oxidation state for 50% of PA realizations resulted in an underestimation of total mobilized plutonium in WIPP brines, and an underestimation of plutonium releases through Direct Brine Releases (DBRs) or by transport through the Culebra or Salado. Based on EPA's evaluation of the available experimental data and highly reducing conditions expected in the long-term repository, the Agency expects that chemical conditions will overwhelmingly favor the Pu(III) oxidation state over Pu(IV). DOE can address this issue in WIPP PA by assuming plutonium will be present only in the Pu(III) oxidation state, which would provide a reasonable upper bound on plutonium mobilization in brine. If DOE does not take this approach, then DOE needs to identify data that support its alternative approach. The Agency does not believe that the current assumption of an equal

probability of the Pu(III) and Pu(IV) oxidation states should be used in future WIPP PA calculations.

Section 7.0 addresses the calculation of actinide solubilities used in PA. Representative Salado or Castile brines are equilibrated with Salado minerals, MgO hydration and carbonation products, and actinide solid phases. The CRA-2019 DPA solubilities of Am(III), Th(IV), and Np(V) were calculated for WIPP repository conditions using the EQ3/6 code and database. The Dissolved Actinide Source Term conceptual model includes the assumption that actinides in the same oxidation state will exhibit the same solubilities and aqueous speciation. Accordingly, DOE assumes that the solubilities of Cm(III) and Pu(III) are equal to the solubility calculated for Am(III) and the solubilities of U(IV), Np(IV), and Pu(IV) are equal to the calculated Th(IV) concentration. DOE uses calculated Np(V) solubilities only for neptunium because it is the only actinide predicted to be present in WIPP brines in the +V oxidation state. Because DOE has not developed an aqueous speciation and solubility model for U(VI), DOE assumes an upper limit dissolved concentration of 10^{-3} M for PA.

The organic ligands acetate, citrate, ethylenediaminetetraacetic acid (EDTA), and oxalate could affect actinide solubilities in the repository because these ligands are water soluble and present in significant quantities in the WIPP inventory. The effects of organic ligands on actinide solubilities were not included in the CCA PAVT actinide solubility calculations because DOE assumed that other constituents, including transition metals in the waste and magnesium from the MgO backfill, would compete with the actinides for binding sites on the organic ligands. The effects of organic ligands on actinide solubilities have been included in subsequent PAs, showing that EDTA may significantly affect dissolved +III actinide concentrations.

DOE used the DATA0.FM4 EQ3/6 database for the CRA-2019 DPA actinide solubility calculations. The DATA0.FM4 database included revisions to the solubility of hydromagnesite and organic ligands data, and data were added for iron and lead reactions. EPA's review identified issues with the DATA0.FM4 thermodynamic database, including incomplete revisions to the EDTA aqueous speciation data, which resulted in significant underestimation of the dissolved +III actinide concentrations in WIPP brines. EPA found that the lead data added to the database are inadequate because DOE did not include Pitzer interaction parameters to account for the effects of ionic strength. DOE has not updated the solubility and aqueous speciation data for Am(III) and Th(IV) since the PABC04, and the Am(III) solubility data are not consistent with currently available data. Potential inconsistencies have also been identified in the WIPP Am(III) model, which could affect stability constants and Pitzer parameters in the WIPP thermodynamic database. EPA has provided a detailed list of database issues that the Agency expects to be addressed prior to future WIPP PAs (Attachment B). EPA expects DOE to continue updating the EQ3/6 database for future WIPP PAs so that it remains consistent with recent information. If data are to be excluded from any updates, EPA expects DOE to provide documentation containing defensible justification for that exclusion.

For the CRA-2019 DPA baseline actinide solubility calculations, DOE assumed that calcite [$CaCO_3$(s)] would precipitate to equilibrium. This assumption resulted in large amounts of Phase 5 (a product of MgO hydration) precipitation and water consumption. Actinide solubilities were not greatly affected by these processes, but the precipitation of large quantities of solids and consumption of a large amount of water are inconsistent with the Chemical Conditions

conceptual model. EPA expects DOE to assume in actinide solubility calculations for future WIPP PAs that calcite remains slightly oversaturated because of the presence of known calcite precipitation inhibitors, such as magnesium and sulfate, in WIPP repository brines. EPA also recommends that DOE evaluate the Phase 5 solubility constant for future WIPP PAs to determine if an excessively low solubility contributed to the precipitation of large amounts of Phase 5 and water consumption in the CRA-2019 DPA actinide solubility calculations.

The calculated solubilities for the +III, +IV, and +V actinides are constant values, with associated uncertainties. The actinide solubility uncertainty distributions are developed by comparing the measured solubilities of actinides in published studies to DOE's modeling of the solubilities under the experimental conditions. The studies used for the uncertainty distributions are chosen using a set of selection criteria. For the CRA-2019 DPA actinide solubility uncertainty distributions, DOE used selection criteria that included an October 31, 2011 cutoff date for published experimental solubility data. In response to EPA's request that DOE evaluate and include data published between the CRA-2014 and CRA-2019, DOE identified additional Nd(III) solubility data for use in the uncertainty evaluation for Am(III). These data increased the mean, median, and maximum difference values relative to the Am(III) solubility uncertainty distribution sampled for the CRA-2019 DPA. EPA expects that for future WIPP PAs, the cutoff date for publications used to develop the +III and +IV actinide solubility uncertainty distributions will be the latest practical date to ensure that the uncertainty distributions remain consistent with current data.

The revised +III actinide solubility uncertainty distribution provided by DOE in response to EPA's request includes additional solubility data published since the CRA-2014 and contains more +III actinide solubility data for more-soluble amorphous and microcrystalline solids than for crystalline solids solubility data. As a result, the revised +III actinide solubility uncertainty distribution may overemphasize the persistence of more-soluble +III actinide solids in the long-term WIPP repository. DOE should consider whether the availability of more actinide solubility data for some conditions may bias the resulting actinide uncertainty distributions, and whether a defensible approach is available to address this potential effect. Although the current approach used for WIPP PA appears to provide uncertainty distributions that adequately represent the potential ranges of dissolved actinide solubilities, EPA suggests that a review of other possible approaches and the relative advantages and disadvantages of these alternatives would provide additional support for the current approach for addressing +III and +IV actinide solubility uncertainties.

The WIPP colloidal actinide source term is summarized in Section 8.0. Four types of colloids can form in WIPP repository brines, including microbial, humic, intrinsic, and mineral fragment colloids. Actinide concentrations associated with microbial and humic colloids are based on proportionality constants with maximum values. The concentrations of actinide intrinsic colloids and mineral fragment colloids used in PA are constant values based on the results of experimental investigations.

Parameter values reflecting mineral fragment colloids have remained unchanged since the CCA PAVT, and these values are consistent with the available data. DOE investigated for the CRA-2019 whether mineral fragment colloids that transport actinides might form during reaction of MgO in WIPP brines. EPA suggests that DOE could resolve remaining uncertainties regarding

formation of pseudocolloids from MgO hydration and carbonation products by performing additional investigations of adsorption of +III and +IV actinide analogues. Formation of actinide(IV)-silica colloids that could increase actinide mobilization has been reported in the literature (Section 8.1.6). EPA recommends that DOE evaluate the potential effects of structural silica colloid formation with actinide(IV) species, including evaluating the effects of high ionic strength and high pcH on silica solubilities in repository brines.

Absent evidence of the formation of actinide intrinsic colloids for radionuclides other than plutonium, the concentrations of thorium, uranium, neptunium, and americium intrinsic colloids were set to zero for PAs prior to the CRA-2014. More recent publications, however, identified the existence of intrinsic Th(IV) colloids in dilute solution and in brines (Section 8.1.5). DOE performed experiments to evaluate the formation of intrinsic Nd(III), Th(IV), and U(VI) colloids in WIPP brines and used data from these experiments to establish the intrinsic colloid parameters used in the CRA-2019 DPA. EPA's evaluation of the data for Pu(III) indicates that the intrinsic colloid concentration used for plutonium in the CRA-2019 DPA is consistent with measured Pu(III) intrinsic colloid concentrations. Examination of the Nd(III) data, however, indicates that the Am(III) intrinsic colloid concentration used in the CRA-2019 DPA should be increased to provide an appropriate upper bound for the data. Similarly, the Th(IV) intrinsic colloid concentration used in the CRA-2019 DPA should be increased to a concentration that is consistent with WIPP-specific data and available literature data. EPA expects DOE to increase the Am(III) and Th(IV) intrinsic colloid parameters to be consistent with the experimental data. The neptunium and uranium intrinsic colloid concentrations used in the CRA-2019 DPA are reasonable and are not expected to affect repository releases.

The humic colloid parameters were revised for the CRA-2019 DPA and provide reasonable values for the actinide concentrations associated with humic colloids. EPA expects that for future WIPP PAs, DOE will make appropriate corrections to the EDTA stability constants and Pitzer parameters in the EQ3/6 database (Section 7.4.5). Because the experiments used to determine the humic colloid parameters contained EDTA, DOE should recalculate the humic colloid proportionality constants after these corrections to the EDTA data are completed.

DOE revised the microbial colloid proportionality constants and maximum actinide concentrations associated with microbial colloids for the CRA-2019 DPA. As a result of these modifications, CRA-2019 DPA actinide concentrations associated with microbial colloids were less than CRA-2014 PA concentrations. EPA evaluated the data provided by DOE and surveyed the available scientific literature to determine the potential ranges of the microbial colloid proportionality constants and maximum actinide concentrations. EPA concluded that the CRA-2019 DPA parameters do not reflect the large variability in the literature, because the CRA-2019 DPA values were determined using a single organism. EPA determined that americium, thorium, neptunium, and uranium proportionality constant values from the CCA and a plutonium proportionality constant value of 2.18 from an independent EPA study conducted after CRA-2014 (Section 8.3.4), should be used for future WIPP PAs. In addition, DOE should use the maximum microbial colloid-associated concentrations of actinides recalculated from data provided by Papenguth (1996c) for future WIPP PAs because these concentrations appear to bound most literature values. EPA expects DOE to use these proportionality constants and recalculated maximum concentration values until more data applicable to the WIPP environment are collected.

Distribution coefficient (K_d) values used to calculate radionuclide transport through the Culebra Dolomite are described in Section 9.0. DOE based these distribution coefficients on the results of WIPP-specific sorption studies carried out on Culebra Dolomite rock samples and pure dolomite. DOE used the K_d distributions from the CRA-2009 Performance Assessment Baseline Calculations (PABC09) for the CRA-2019 DPA. These distributions continue to be appropriate.

Section 10.0 examines the assumption of homogeneous waste emplacement for WIPP PA. This assumption is potentially significant because of heterogeneous waste loading that has occurred in the WIPP repository. Empirical data and theoretical evaluations of excavated openings in salt indicate each waste panel will be isolated for the majority of the regulatory period due to the creep-closure process. Therefore, it is unlikely that brine in contact with waste in one panel of the repository will contact brine in another panel.

Because DOE assumes chemical equilibrium between brine and actinide solubility-controlling solids, heterogeneous distribution of the radionuclide inventory between the panels will not affect the calculated actinide solubilities. DOE has adequately accounted for the effects of possible heterogeneous distribution of organic ligands between panels in the actinide solubility calculations.

Most shielded containers that will be used at WIPP will be placed in currently unfilled panels. Consequently, these panels will contain large inventories of steel and lead packaging materials relative to the other filled panels. Because the steel surface area to weight ratio for shielded containers is relatively low, the increased mass of steel is unlikely to significantly increase gas generation rates in panels with large numbers of shielded containers. Relatively low lead corrosion rates and a low surface area to mass ratio for lead in the shielded containers will limit the effects of lead corrosion on gas generation rates in panels with large numbers of shielded containers.

A surplus plutonium waste stream, SR-KAC-PuOx, was added to the CRA-2019 DPA waste inventory. Addition of this waste stream is a significant change to the WIPP inventory because SR-KAC-PuOx significantly increased the radionuclide inventory for the CRA-2019 DPA. Waste stream SR-KAC-PuOx represents about 3.5% of the total waste volume, but contains approximately 30% of the radionuclides that are predicted to cause radiolytic gas generation and brine consumption in WIPP PA. If this waste stream is emplaced in a limited number of panels, these panels may exhibit higher gas generation rates and greater brine consumption than other panels, possibly leading to fewer DBRs and more spallings releases. EPA expects DOE to evaluate for future WIPP PAs whether the current PA calculations adequately address the radiolytic effects of this waste form on brine consumption, gas generation, and repository releases if this waste is placed in a limited number of panels.

Section 11.0 addresses the effects of chemical processes on the repository water balance. Anoxic corrosion was the only chemical process included in calculations of the quantity of brine in the repository for the CCA PAVT, PABC04, and PABC09. The CRA-2014 PA water balance and the CRA-2019 DPA water balance included the effects of iron sulfidation, microbial degradation of CPR, MgO hydration, MgO and brucite carbonation, and the hydromagnesite conversion reaction. For the CRA-2019 DPA, DOE also included radiolytic brine consumption by dissolved, colloidal, and wetted radionuclide solids.

MgO hydration rates included in the water balance were based on data from Premier-supplied MgO, which is present in the repository in smaller quantities and hydrates more slowly than Martin Marietta MgO. Because this parameter is not consistent with the limited experimental data for Martin Marietta MgO hydration, EPA recommends that DOE develop hydration rates using Martin Marietta MgO and use these rates in combination with Premier MgO hydration rates in future WIPP PAs. A 'composite' hydration rate will likely decrease brine volumes in the repository under some conditions. EPA also expects DOE to evaluate the potential for brine consumption by radiolysis of water adsorbed on waste materials for future WIPP PAs. MgO hydration to produce Phase 5 consumes more water than MgO hydration to brucite, but the formation of Phase 5 is not included in the CRA-2019 DPA water balance. DOE should assess whether formation of significant quantities of Phase 5 in the backfill may occur and whether it should be included in water balance calculations for future WIPP PAs.

Section 12.0 compares the mean total mobilized actinides calculated for the CRA-2014 PA, CRA-2019 DPA, and sensitivity calculations performed by EPA during the CRA-2019 DPA review. Evaluation of the mean total mobilized actinide concentrations calculated for these PAs demonstrates that the baseline +III and +IV actinide solubilities combined with the uncertainty distributions significantly affect total mobilized actinide concentrations. Mineral fragment colloids make only minor contributions to mean total mobilized concentrations for all actinides. Intrinsic colloids contribute significantly to mobilization of the +IV actinides. Humic colloids have small effects on +III actinide mobilization and little effect on +IV actinide mobilization using the updated CRA-2019 DPA parameters. Total mobilized actinide concentrations are sensitive to the proportionality constants and maximum concentration limits for actinides associated with microbial colloids, demonstrating the importance of establishing defensible values for these parameters. Issues associated with the baseline +III actinide solubilities, Th(IV) intrinsic colloid concentrations, microbial colloid proportionality constants and maximum concentration limits, and actinide oxidation state assumption caused the CRA-2019 DPA calculations to underestimate the total mobilized concentrations of americium, plutonium, and thorium.

Section 13.0 summarizes the results of sensitivity calculations performed to assess the effects of the chemistry parameter changes identified by EPA in Section 12.0 on repository releases. EPA performed a series of sensitivity calculations during the CRA-2019 review to evaluate the effects of individual and combined parameter changes on predicted actinide releases from the repository. The evaluated chemistry parameter changes included: 1) revised baseline actinide solubilities; 2) revised baseline actinide solubilities and +III actinide solubility uncertainty distribution; 3) revised baseline actinide solubilities and microbial and intrinsic colloid parameters; and 4) revised baseline actinide solubilities, revised intrinsic and microbial colloid parameters, and reduced actinide oxidation states.

The increased baseline actinide solubilities used in the first sensitivity calculation significantly increased total mobilized Am(III) and Pu(III) concentrations, which significantly increased DBRs relative to the CRA-2019 DPA. The increased DBRs caused increased total repository releases only at low probabilities because total repository releases are dominated by cuttings and cavings at higher probabilities. These results show that because DOE underpredicted the baseline +III actinide solubility, CRA-2019 DPA mean DBRs and mean total repository releases were

underpredicted. However, mean total releases remained below repository release limits for the sensitivity calculation with the revised baseline actinide solubilities.

The second sensitivity calculation included increased baseline actinide solubilities and a revised +III actinide solubility uncertainty distribution with additional data from recent publications. Mean DBRs were significantly increased by the revised +III actinide solubility uncertainty distribution. These increased mean DBRs increased mean total repository releases at low probabilities. Mean total releases remained below repository release limits in this sensitivity calculation. The sensitivity of total releases to the +III actinide solubility uncertainty distribution is consistent with the sensitivity evaluation of repository releases to sampled parameters for the CRA-2019 DPA (Zeitler 2019b). However, EPA did not include the updated +III actinide solubility uncertainty distribution in the other sensitivity calculations, because the revised uncertainty distribution likely provides an overly conservative estimate of the uncertainty associated with the +III actinide solubilities.

The third sensitivity calculation tested the effects of increased baseline actinide solubilities, increased Am(III) and Th(IV) intrinsic colloid concentrations, and revised microbial colloid parameters. Modification of the intrinsic and microbial colloid parameters increased mean DBRs, and also increased mean total repository releases at low probabilities. Mean total releases remained below repository release limits in this sensitivity calculation.

The fourth sensitivity calculation combined EPA-identified chemistry parameter changes, including revised baseline actinide solubilities, revised microbial and intrinsic colloid parameters, and the assumption that plutonium, uranium, and neptunium would be present only in their most reduced oxidation states [Pu(III)), U(IV), and Np(IV)]. The assumption of reduced oxidation states in the fourth sensitivity calculation significantly increased mean DBRs because of the higher concentration of total mobilized Pu(III) compared to total mobilized Pu(IV) concentrations. The increased mean DBRs contributed to increased mean total repository releases at low probabilities. Despite the increased mean total releases in this sensitivity calculation, mean total repository releases remained below the regulatory limits for all of the calculations.

The most important chemistry parameters affecting americium and plutonium mobilized in brine and repository releases include:

- Baseline actinide solubilities for the +III and +IV actinides;
- +III and +IV actinide solubility uncertainty distributions;
- Actinide oxidation state parameter;
- Microbial colloid proportionality constants and maximum concentrations;
- Humic colloid proportionality constants; and
- Intrinsic colloid parameters.

EPA's review of the CRA-2019 DPA has identified significant issues with the baseline +III actinide solubility parameters, microbial colloid parameters, Am(III) and Th(IV) intrinsic colloid concentrations, and the actinide oxidation state assumption used in the CRA-2019 DPA.

Parameters that affect repository brine saturation and pressures may significantly affect DBRs and spallings releases. The most significant of these parameters, based on review of the CRA-2019 DPA include:

- Inundated and humid steel corrosion parameters;
- Microbial gas generation parameters;
- Brine radiolysis parameters; and
- Stoichiometric parameters for steel sulfidation reactions.

The microbial gas generation, steel corrosion, and steel sulfidation stoichiometric parameters are well-supported by currently available data and do not require additional investigation at this time. Processes that were not included in the CRA-2019 DPA may affect brine saturation and repository pressure, including radiolysis of water adsorbed on waste and CPR radiolysis. EPA expects DOE to continue to evaluate the effects of these processes along with brine radiolysis by dissolved, colloidal, and wetted radionuclide solids for future WIPP PAs.

Section 14.0 summarizes EPA's conclusions regarding CRA-2019 chemistry issues. EPA expects DOE to prioritize resolution of the following issues for future WIPP PAs, which are listed in their approximate order of importance:

- Revise the EQ3/6 database, especially addressing issues related to the EDTA data, possible inconsistencies in Am(III) stability constants and Pitzer parameters, Th(IV)-carbonate aqueous speciation, Phase 5 solubility, addition of missing iron-sulfate data, and removal of lead data, as well as all other issues identified in Attachment B;
- Assume Pu(III), Np(IV), and U(IV) are the dominant oxidation states for actinide solubility and mobilization calculations;
- Evaluate the potential effects of the radiolytic brine consumption and gas generation that will occur when the surplus plutonium waste stream SR-KAC-PuOx is placed in a limited number of panels;
- Continue investigating radiolytic gas generation and brine consumption, including the relative importance and timing of radiolysis of brine by dissolved, colloidal and wetted radionuclide solids, radiolysis of water adsorbed on waste, and CPR radiolysis;
- Update the cutoff date for publications used to develop the +III and +IV actinide solubility uncertainty distributions to the most recent date that can be implemented for future WIPP PAs;
- Determine whether the availability of more actinide solubility data for some conditions (e.g., less-crystalline, more-soluble solid phases) may bias the resulting actinide uncertainty distributions, and whether a defensible approach is available to address this potential effect;
- Revise parameters used to calculate actinide concentrations associated with microbial colloids (PROPMIC and CAPMIC) to be consistent with the available literature data and project-specific data;
- Increase the Th(IV) and Am(III) intrinsic colloid parameters (TH:CONCINT and AM:CONCINT) to be consistent with available data;
- Assume a reasonable degree of calcite oversaturation in actinide solubility calculations to prevent unrealistic amounts of Phase 5 precipitation and water consumption;

- Determine whether Phase 5 formation could affect the water balance calculations after re-evaluating its solubility and investigating its formation in Martin Marietta MgO hydration experiments; and
- Remove lead data from DATA0.FM4, because the data are incomplete and should not be used in WIPP actinide solubility calculations.

The following issues are listed in the order that they are considered in this TSD. These issues should be addressed to minimize uncertainty for future WIPP PAs:

- Calculate D_s using projected total container counts at closure from DOE's inventory calculations and bounding estimates for iron-based waste;
- Evaluate MgO hydration rates using Martin Marietta MgO to improve the water balance;
- Use the appropriate brine volumes to calculate the initial solid phases in the 2-, 3-, 4-, and 5-times minimum brine volume actinide solubility calculations;
- Evaluate the potential effects of sulfides and phosphates on lead and iron solubilities, if lead or iron interactions with organic ligands are added to the actinide solubility calculations;
- Continue evaluating the potential effects of borate on actinide aqueous speciation and solid phase solubilities;
- Re-evaluate the available mineralogy data to provide a more realistic estimate of polyhalite concentrations in the Salado Formation;
- Review other possible approaches for evaluating actinide solubility uncertainties and their relative advantages and disadvantages to provide additional support for the current approach for addressing +III and +IV actinide solubility uncertainties;
- Resolve remaining uncertainties regarding formation of pseudocolloids from MgO hydration and carbonation products by performing sequential filtration experiments with brine samples from the MgO hydration and carbonation experiments after spiking the solution aliquots with Th(IV) and a +III actinide or analogue such as Nd(III);
- Investigate the effects of revised EDTA data in the EQ3/6 database on humic colloid parameters;
- Investigate the effects of silica aqueous species, solid phases, and formation of silica colloids with +IV actinides; and
- Calculate the possible ranges of microbial cell counts of representative organisms in addition to *Bacillus* spores (such as bacteria and fungi), similar to the calculation performed in Swanson et al. (2021). These calculations should include various organisms that could be introduced into WIPP through waste and archaea that could be introduced in brine to provide a clearer picture of which organisms will likely dominate the biomass in the post-closure environment.

EPA's review included sensitivity calculations performed using various combinations of chemistry parameters that were revised to address the identified issues. The results of the Agency's review and these sensitivity calculations show that there is a reasonable expectation that repository releases will remain within regulatory numerical release limits (40 CFR 191.13) if the chemistry parameters in question are revised.

TABLE OF CONTENTS

Acronym and Abbreviation List xxii
Executive Summary and Report Outline ii
1.0 Introduction 1
2.0 Geologic Setting, Salado Formation Mineralogy, and Brine Chemistry 3
2.1 Geologic Setting 3
2.2 Salado Mineralogy 3
2.3 Salado Formation and Castile Formation Brine Chemistry 4
2.4 Conclusions 6
3.0 Gas Generation 7
3.1 Iron Corrosion 7
3.1.1 Corrosion Reaction Products and Stoichiometry 8
3.1.2 Corrosion Rates 9
3.1.3 Passivation of Iron Surfaces by H_2S 12
3.1.4 Steel Surface Area 13
3.1.5 PA Implementation of Gas Generation by Anoxic Steel Corrosion 14
3.1.6 Effects of Anoxic Corrosion Gas Generation Rates on Repository Releases 15
3.2 Corrosion of Lead, Aluminum, and Other Metals 15
3.2.1 Lead Corrosion 16
3.2.2 Corrosion of Aluminum and Other Metals 19
3.3 Galvanic Coupling 19
3.4 Microbial Gas Generation 20
3.4.1 CCA PA, PAVT, and CRA-2004 PA Microbial Gas Generation 20
3.4.2 Microbial Gas Generation Evaluation during AMWTF Review 22
3.4.3 PABC04 Microbial Gas Generation 22
3.4.4 Microbial Gas Generation Review for MgO Planned Change Request 26
3.4.5 Microbial Gas Generation for the CRA-2009 PA and PABC09 27
3.4.6 Microbial Gas Generation for the CRA-2014 PA and CRA-2019 DPA 28
3.4.7 PA Implementation of Microbial Gas Generation 28
3.5 Effects of Chemically Incompatible Materials on Gas Generation 29
3.6 Radiolytic Gas Generation 30
3.6.1 Brine Radiolysis 31
3.6.2 Adsorbed Water Radiolysis 36
3.6.3 CPR Radiolysis 38
3.6.4 Radiolysis of Other Wastes 42

3.6.5 Gamma Radiolysis 42
3.6.6 PA Implementation of Radiolytic Gas Generation 43
3.7 Total Gas Production Rate 44
3.8 WIPP Gas Generation Summary and Conclusions 45
4.0 Backfill Efficacy 48
4.1 MgO Reactions in the Repository 48
4.2 MgO Characterization 50
4.2.1 Characterization of Premier MgO 50
4.2.2 Characterization of Martin Marietta MgO 51
4.3 Potential Formation of Impermeable MgO Reaction Products 51
4.4 Hydromagnesite Conversion to Magnesite 51
4.5 Effects of Calcium Carbonate Precipitation on CO_2 Consumption 52
4.6 Placement of MgO Backfill and Excess Factor Calculations 52
4.6.1 CCA MgO Placement and Excess Factor Calculations 52
4.6.2 MgO Placement and Excess Factor Changes Through the CRA-2004 53
4.6.3 Planned Change Request to Reduce MgO Excess Factor 54
4.6.4 CRA-2009 MgO Placement and Excess Factor 56
4.6.5 Planned Change Request for MgO Placement and Supersack Weight 56
4.6.6 CRA-2014 and CRA-2019 MgO Placement and Excess Factors 56
4.7 Backfill Efficacy Conclusions 57
5.0 Radionuclides Included in Brine Mobilization Calculations 59
6.0 Actinide Oxidation States 60
6.1 Actinide Oxidation State Information Developed for the CCA PAVT, PABC04, and PABC09 61
6.2 Actinide Oxidation State Information Developed for the CRA-2014 PA 62
6.2.1 Uranium and Neptunium Oxidation States 62
6.2.2 Plutonium Oxidation States 62
6.3 Actinide Oxidation State Information Developed for the CRA-2019 DPA 64
6.3.1 Uranium and Neptunium Oxidation States 64
6.3.2 Plutonium Oxidation States 64
6.4 Actinide Oxidation States Summary and Conclusions 68
7.0 Dissolved Actinide Source Term 70
7.1 Dissolved Actinide Source Term For the CCA PA Through PABC09 70
7.1.1 FMT Code and Database 71
7.1.2 Salado Brine Formulation 72
7.1.3 Carbon Dioxide Buffering Reactions 73
7.1.4 Oxidation-State Analogy 73
7.1.5 Uranium(VI) Solubility 73

7.1.6 Minimum Brine Volume 74
7.1.7 Waste Inventory 74
7.1.8 Effects of Organic Ligands on Actinide Solubilities 75
7.1.9 Results of the Actinide Solubility Calculations for the CCA PAVT, PABC04, and PABC09 78
7.1.10 Actinide Solubility Uncertainties 81
7.2 CRA-2014 PA Dissolved Actinide Source Term 85
7.2.1 Waste Inventory 85
7.2.2 Brine Chemistry 86
7.2.3 Brine Volumes and Organic Ligand Concentrations 86
7.2.4 EQ3/6 Code and Database 86
7.2.5 Actinide Solubility Calculations 87
7.2.6 Actinide Solubility Uncertainties 88
7.3 CRA14_SEN4 PA Dissolved Actinide Source Term 91
7.4 CRA-2019 DPA Dissolved Actinide Source Term 92
7.4.1 Waste Inventory 92
7.4.2 Brine Chemistry 93
7.4.3 EQ3/6 Code and Database 93
7.4.4 CRA-2019 DPA Actinide Solubility Calculations 94
7.4.5 DATA0.FM4 Database 95
7.4.6 Calcite Saturation 98
7.4.7 Iron and Lead Phases 100
7.4.8 Polyhalite Effects 102
7.4.9 Cement Effects 102
7.4.10 Sensitivity Calculations of Actinide Solubilities 103
7.4.11 Actinide Solubility Uncertainties 105
7.5 Dissolved Actinide Source Term Summary and Conclusions 111
8.0 Colloidal Actinide Source Term 114
8.1 Mineral Fragment and Intrinsic Colloids 114
8.1.1 CCA Mineral Fragment Colloid Concentrations Used in WIPP PA 115
8.1.2 Mineral Fragment Colloid Formation by MgO Hydration and Carbonation Products 115
8.1.3 Plutonium Mineral Fragment and Intrinsic Colloids 116
8.1.4 Neodymium(III) Mineral Fragment and Intrinsic Colloids 119
8.1.5 Thorium(IV) Mineral Fragment and Intrinsic Colloids 120
8.1.6 Actinide(IV) – Silica Colloids 123
8.1.7 Uranium(VI) Mineral Fragment and Intrinsic Colloids 124
8.1.8 Neptunium(V) Mineral Fragment and Intrinsic Colloids 124

8.1.9 EPA Evaluation of Mineral Fragment and Intrinsic Colloid Parameters 125
8.2 Humic Colloids 125
8.2.1 Humic Colloid Concentrations for the CCA PAVT through CRA-2014 PA 125
8.2.2 Humic Colloid Concentrations for the CRA-2019 DPA 127
8.3 Microbial Colloids 129
8.3.1 Microbial Colloids from the CCA PAVT to PABC09 129
8.3.2 Microbial Colloids for CRA-2014 PA 130
8.3.3 Microbial Colloids for the CRA-2019 DPA 131
8.3.4 EPA Study of the PROPMIC and CAPMIC Parameter 133
8.3.5 EPA Evaluation of PROPMIC and CAPMIC 143
8.4 Colloids Summary and Conclusions 144
9.0 Culebra Dolomite Distribution Coefficients 147
9.1 Distribution Coefficients Used in the CCA PA and PAVT 147
9.2 Distribution Coefficients Used in the CRA-2004 PA, PABC04, and CRA-2009 PA 147
9.3 Distribution Coefficients used in the PABC09 and CRA-2014 PA 148
9.4 Distribution Coefficients used in the CRA-2019 DPA 149
9.5 Culebra Dolomite Distribution Coefficients Conclusions 149
10.0 Heterogeneous Waste Loading 150
11.0 Effects of Chemical Processes on Repository Water Balance 153
11.1 Anoxic Corrosion and Sulfidation of Iron-Based Metals 154
11.2 Lead Corrosion 154
11.3 Microbial Degradation of CPR 155
11.4 Backfill Reactions 155
11.4.1 MgO Hydration Rate 155
11.4.2 MgO and Brucite Carbonation Rates 156
11.4.3 Hydromagnesite Conversion Rate 157
11.5 Brine Radiolysis 157
11.6 Total Brine Consumption Rate 158
11.7 Water Balance Summary and Conclusions 158
12.0 Total Mobilized Actinide Calculations for PA 159
12.1 CRA-2014 PA and CRA-2019 DPA Total Mobilized Actinides 159
12.2 EPA Recalculations of Total Mobilized Actinides 161
12.3 EPA Evaluation of the Sensitivity of Total Mobilized Actinide Concentrations to PA Parameters 165
13.0 Sensitivity of Repository Releases to Chemistry Parameters 167

13.1 DOE Evaluation of the Sensitivity of CRA-2019 DPA Repository Releases to Chemistry Parameters 167
13.2 EPA Evaluation of the Sensitivy of Repository Releases to Chemistry Parameters 168
13.2.1 Sensitivity to Baseline Actinide Solubilities (GCHM_S0) 168
13.2.2 Sensitivity to Baseline Actinide Solubilities and the Revised +III Actinide Solubility Uncertainty Distribution (GCHM_S1) 170
13.2.3 Sensitivity to Baseline Actinide Solubilities and Revised Colloid Parameters (GCHM_S2) 171
13.2.4 Effects of Combined Parameter Changes (GCHM_S3) 171
13.3 Chemistry Parameters Likely to Affect Calculated Repository Releases 173
14.0 Summary and Conclusions 175
14.1 Gas Generation 175
14.2 Backfill Efficacy 177
14.3 Actinide Oxidation States 177
14.4 Dissolved Actinide Source Term 177
14.5 Colloidal Actinide Source Term 180
14.6 Culebra Dolomite Distribution Coefficients 181
14.7 Heterogeneous Waste Loading 181
14.8 Repository Water Balance 181
14.9 Actinide Mobilization in WIPP Brines 182
14.10 Prioritization of Chemistry-Related Issues 182
15.0 References 1

LIST OF TABLES

Table 2-1. Brine A, GWB, and ERDA-6 Compositions 5
Table 3-1. CRA-2014 PA and CRA-2019 DPA Inventories of Iron-Based Metals and Alloys 7
Table 3-2. WIPP PA Inundated Steel and Humid Steel Corrosion Rates 9
Table 3-3. CRA-2014 PA and CRA-2019 DPA Inventories of Aluminum, Lead and Other Metals and Alloys 16
Table 3-4. Inundated Iron and Lead Corrosion Rate Measurements Statistics, 0 and 350 ppm CO_2 from Roselle (2013a) 17
Table 3-5. Inundated Microbial Gas Generation Rates (WAS_AREA:GRATMICI) 21
Table 3-6. Humid Microbial Gas Generation Rates (WAS_AREA:GRATMICH) 21
Table 3-7. CPR Inventories and Initial Gas Pressures 25
Table 3-8. G Values for $H_2(g)$ in Alpha-Irradiated Chloride Brines 33
Table 3-9. Fraction of Alpha Particle Energy Escaping from PuO_2 Particles as a Function of Particle Diameter and Initial Energy 34
Table 3-10. Radionuclides Included in WIPP Brine Radiolysis Calculations 43

Table 5-1. Radionuclides Included in DBRs and Transport Calculations through the Salado and Culebra 59
Table 7-1. Mass Balance Calculations Comparing Moles of Portlandite in Cement to Moles of Magnesium Available from Brine and Polyhalite, Minimum Brine Volume of 17,400 m^3 75
Table 7-2. Organic Ligand Concentrations Calculated for the CCA PAVT, PABC04, PABC09, CRA-2014 PA, and CRA-2019 DPA 76
Table 7-3. Organic Ligand Inventories for the PABC04, PABC09, CRA-2014 PA, and CRA-2019 DPA 76
Table 7-4. Actinide Solubility Calculations for the CCA PAVT, PABC04, PABC09, CRA-2014 PA, CRA-2019 DPA, and CRA-2019 Sensitivity Calculations (Minimum Brine Volume) 79
Table 7-5. Am(III) Solubility Uncertainty Distribution Statistics for the PABC04, PABC09, CRA-2014 PA, CRA-2019 DPA, and CRA-2019 Sensitivity Calculations 81
Table 7-6. Th(IV) Solubility Uncertainty Distribution Statistics for the PABC04, PABC09, CRA-2014 PA, CRA-2019 DPA, and CRA-2019 Sensitivity Calculations 82
Table 7-7. CRA-2019 DPA Actinide Solubility Calculation Results, Results Obtained Using PHREEQC with Converted DATA0.FM4 Database, and Results Obtained with EPA-Modified Database 96
Table 7-8. Calcite Saturation Index Values, Am(III) Concentrations, and CO_2 Fugacity Calculated for ERDA-6 Brine (Minimum Brine Volume) in Recent PAs 98
Table 7-9. Am(III) Solubilities Calculated for the CRA-2019 DPA, EPA PHREEQC Calculations with Revised Database, and Revised DOE EQ3/6 Calculations 104
Table 8-1. Actinide Concentrations Associated with Intrinsic Colloids (Parameter CONCINT) 116
Table 8-2. Proportionality Constants and Maximum Concentrations for Humic Colloids 126
Table 8-3. Proportionality Constants and Maximum Concentrations for Microbial Colloids 130
Table 9-1. Comparison of Matrix K_d Values 148
Table 11-1. Hydromagnesite Conversion Rates (parameter WAS_AREA:HYMAGCON) 157
Table 12-1. CRA-2019 DPA Mean Dissolved, Colloidal, and Total Mobilized Actinides 162
Table 12-2. CRA-2014 PA Mean Dissolved, Colloidal, and Total Mobilized Actinides 163
Table 12-3. EPA CRA-2019 Sensitivity Calculation Mean Dissolved. Colloidal, and Total Mobilized Actinides 164
Table 12-4. Mean Total Mobilized Concentrations in ERDA-6 Brine for the PABC09, CRA-2014 PA, CRA-2019 DPA, and CRA-2019 EPA Calculations 165

LIST OF FIGURES

Figure 3-1. Humid Steel Corrosion Rate Data 12
Figure 3-2. Lead Corrosion Rate Data Obtained with Fully Submerged and Partially Submerged Coupons 18
Figure 3-3. Equations Fit to Radiolytic Gas Generation Data Collected by Zerwekh (1979) Over the 5-year Data Collection Period 38
Figure 3-4. Equations Fit to Radiolytic Gas Generation Data Collected by Zerwekh (1979) Adjusted for the Higher Activity in the Experiments 40
Figure 6-1. Reactions that Control Plutonium Solubility as a Function of pH and Redox Conditions (pe), Showing the Expanded Stability Field for Pu(III) Aqueous Species and Solids at Elevated H_2(g) Pressure (3 m NaCl and 1×10^{-8} m Total Plutonium) 66
Figure 7-1. CRA-2019 DPA +III Actinide Solubility Difference Values 106
Figure 7-2. CRA-2019 DPA +III Actinide Solubility Difference Values from Runde and Kim (1994), Rao et al. (1999), and Neck et al. (2009) 107
Figure 7-3. +III Actinide Solubility Difference Values for Microcrystalline $Nd(OH)_3$(s) from Herm et al. (2015), Hinz et al. (2015), and Xiong et al. (2017) 109
Figure 7-4. CRA-2019 DPA Difference Values Compared to All +III Actinide Solubility Difference Values 110
Figure 8-1. Pu(III) Mineral Fragment Colloid Concentrations Calculated from Reed (2020) Data with CRA-2019 DPA Parameter PU:CONCMIN 118
Figure 8-2. Pu(III) Intrinsic Colloid Concentrations Calculated from Reed (2020) Data with CRA-2019 DPA Parameter PU:CONCINT 119
Figure 8-3. Nd(III) Intrinsic Colloid Concentrations Calculated from Reed et al. (2013) Data with CRA-2019 DPA Parameter AM:CONCINT 120
Figure 8-4. Th(IV) Mineral Fragment Colloid Concentrations Calculated from Borkowski (2012b) Data with CRA-2019 DPA Parameter TH:CONCMIN 121
Figure 8-5. Th(IV) Intrinsic Colloid Concentrations Calculated from Borkowski (2012b) Data with CRA-2019 DPA Parameter TH:CONCINT and Data from Altmaier et al. (2004) in 5 M NaCl 122
Figure 8-6. Calculated PROPMIC Values from the Literature by Oxidation State 136
Figure 8-7. Calculated PROPMIC Values from the Literature by Actinide, Including Swanson (2019) 137
Figure 8-8. Calculated PROPMIC Values from the Literature by Cell Life Cycle 138
Figure 8-9. Calculated PROPMIC Values from the Literature by Domain 139
Figure 8-10. Literature PROPMIC Values vs. Experimental Time 140
Figure 8-11. Viable and Total Cell Counts in WIPP-related Environments vs. TDS as a Proxy for Salinity 141
Figure 8-12. Calculated CAPMIC Values from the Literature by Actinide, Including Data from Papenguth (1996c) and recalculated CCA CAPMIC 142

Figure 8-13. Calculated Literature CAPMIC Values by Oxidation State Compared to CRA-2019 DPA CAPMIC Values and Recalculated CCA CAPMIC 142
Figure 13-1. Mean DBRs Calculated for the CRA-2019 DPA (CRA19), the Baseline Actinide Solubility Sensitivity Calculation (GCHM_S0), and the Baseline Actinide Solubility plus +III Actinide Solubility Uncertainty Sensitivity Calculation (GCHM_S1) 169
Figure 13-2. Mean Total Releases Calculated for the CRA-2019 DPA (CRA19), the Baseline Actinide Solubility Sensitivity Calculation (GCHM_S0), and the Baseline Actinide Solubility plus +III Actinide Solubility Uncertainty Sensitivity Calculation (GCHM_S1) 170
Figure 13-3. Mean DBRs Calculated for the CRA-2019 DPA (CRA19); the Baseline Actinide Solubility Sensitivity Calculation (GCHM_S0); the Baseline Actinide Solubility plus Intrinsic and Microbial Colloid Sensitivity Calculation (GCHM_S2); and the Sensitivity Calculation Combining Revised Baseline Actinide Solubility, Revised Intrinsic and Microbial Colloid, and Revised Actinide Oxidation State Parameters (GCHM_S3) 172
Figure 13-4. Mean Total Repository Releases Calculated for the CRA-2019 DPA (CRA19); the Baseline Actinide Solubility Sensitivity Calculation (GCHM_S0); the Baseline Actinide Solubility plus Intrinsic and Microbial Colloid Sensitivity Calculation (GCHM_S2); and the Sensitivity Calculation Combining Revised Baseline Actinide Solubility, Revised Intrinsic and Microbial Colloid, and Revised Actinide Oxidation State Parameters (GCHM_S3).....172

LIST OF ATTACHMENTS

ATTACHMENT A. EPA Completeness Questions

ATTACHMENT B. DATA0.FM4 Database Review

ATTACHMENT C. CRA-2019 Sensitivity Calculation Parameters

ATTACHMENT D. PHREEQC QA Summary Report

LIST OF ACRONYMS AND ABBREVIATIONS

A_d	Surface area of steel associated with a waste disposal drum, PA parameter REFCON:ASDRUM
AMWTF	Advanced Mixed Waste Treatment Facility
B_{fc}	Uncertainty related to long-term microbial degradation of CPR, PA parameter WAS_AREA:BIOGENFC
Brine A	Simulated Salado brine formulation
CCA	Compliance Certification Application
CCDF	Complementary cumulative distribution function
CDF	Cumulative distribution function
CFR	*Code of Federal Regulations*
CH	Contact handled
Ci	Curie
CPR	Cellulosics, plastics, and rubber
CRA	Compliance Recertification Application
CRA-2004	First Compliance Recertification Application, March 2004
CRA-2009	Second Compliance Recertification Application, March 2009
CRA-2014	Third Compliance Recertification Application, March 2014
CRA-2019	Fourth Compliance Recertification Application, March 2019
CRA-2019 DPA	Deferred PA for the CRA-2019, December 2019
CRA14_SEN4 PA	Sensitivity study of CRA-2014 PA
D	Difference value, $\log_{10}$(measured solubility) – $\log_{10}$(predicted solubility), PA parameter SOLVAR
DATA0.FM1	EQ3/6 thermodynamic database used for the CRA-2014 PA
DATA0.FM2	Revised EQ3/6 thermodynamic database
DATA0.FM4	Revised EQ3/6 thermodynamic database used for the CRA-2019 DPA
DBR	Direct brine release
D_c	Mass concentration of cellulosics in the repository (kg biodegradable material/m^3 disposal volume)
DPA	Deferred performance assessment
DOE	U.S. Department of Energy
DRSPALL	Spallings released to accessible environment from a future drilling event
DRZ	Disturbed rock zone
D_S	Steel surface area per unit disposal volume (m^2/m^3)
$E_{dis,i}$	Total emitted disintegration energy of radionuclide i, PA parameter DECAYNRG
EDTA	Ethylenediaminetetraacetic acid

EEF	Effective excess factor
EF	Excess factor
Eh	Oxidation/reduction potential
EPA	U.S. Environmental Protection Agency
EPS	Extracellular polymeric substances
EQ3/6	Geochemical modeling code used for CRA-2014 PA
ERDA-6	Simulated Castile brine formulation
FMT	Fracture Matrix Transport geochemical modeling code
FEP	Feature, event, and process
FMT_021120.CHEMDAT	FMT thermodynamic database used for the CRA-2004 PA
FMT_050405.CHEMDAT	FMT thermodynamic database used for the PABC04 and PABC09
FMT_970407.CHEMDAT	FMT thermodynamic database used for the PAVT
g	Uncertainty in the moles of CO_2 produced per mole of microbially consumed organic carbon
G	Amounts of chemical species consumed or produced by radiolysis per unit energy (molecules/100 eV)
$G(H_2)_{avg}$	Average hydrogen yield, parameter GLOBAL:GH2AVG (molecules/100 eV)
GWB	Generic Weep Brine, simulated Salado brine formulation
K_d	Distribution coefficient
kPa	Kilopascal
λ_i	Radioactive decay constant for radionuclide i
LANL	Los Alamos National Laboratory
LWB	Land Withdrawal Boundary
m	Moles of MgO available for CO_2 consumption
m	Molal, moles/kg H_2O
M	Molar, moles/liter
MB	Marker bed
M_c	Total moles of organic carbon in emplaced CPR
M_{CO2}	Maximum moles of CO_2 that could be generated by microbial consumption of all carbon in the CPR inventory
meq	Milliequivalent
M_{H2}	Molecular weight of H_2, PA parameter REFCON:MW_H2
M_{MgO}	Total moles of emplaced MgO
MPa	Megapascal
μ^0/RT	Standard chemical potential (dimensionless)
$M(t)_{sol,i}$	Amount of dissolved plus colloidal radionuclide i
$M(t)_{sol,i}$	Amount of wetted solid radionuclide i

n_d	Number of waste drums that can be closely packed into a single room in the repository, PA parameter REFCON:DRROOM
NEA-TDB	Nuclear Energy Agency Thermochemical Database
Pa	Pascal
PA	Performance assessment
PABC04	CRA-2004 Performance Assessment Baseline Calculations
PABC09	CRA-2009 Performance Assessment Baseline Calculations
PAVT	Performance Assessment Verification Testing
PCR	Planned change request
P_{dep}	Energy deposition probability for wetted radionuclide solids, PA parameter GLOBAL:GDEPFAC
ρ_{Fe}	Molar density of steel
pH	Negative log of the hydrogen ion activity
pcH	Negative log of the hydrogen ion concentration, molar units
pmH	Negative log of the hydrogen ion concentration, molal units
PVC	Polyvinylchloride
q_{rb}	Total rate of brine consumption or production per unit volume of waste in the model grid ($kg/m^3/sec$)
q_{rbc}	Rate of brine consumption per unit volume of waste due to anoxic corrosion of iron-based metals in the model grid ($kg/m^3/sec$)
q_{rbh}	Rate of brine consumption per unit volume of waste due to MgO hydration to brucite in the model grid ($kg/m^3/sec$)
q_{rbhc}	Rate of brine production per unit volume of waste due to hydromagnesite conversion to magnesite in the model grid ($kg/m^3/sec$)
q_{rbm}	Rate of brine production per unit volume of waste due to microbial degradation of CPR in the model grid ($kg/m^3/sec$)
q_{rbr}	Rate of brine consumption per unit volume of waste due to radiolysis in the model grid ($kg/m^3/sec$)
q_{rbs}	Rate of brine production per unit volume of waste due to iron sulfidation reactions in the model grid ($kg/m^3/sec$)
q_{rg}	Total rate of gas production per unit volume of waste in the model grid ($kg/m^3/sec$)
q_{rgc}	Rate of gas production per unit volume of waste due to anoxic corrosion of iron-based metals in the model grid ($kg/m^3/sec$)
q_{rgm}	Rate of microbial gas production per unit volume of waste in the model grid ($kg/m^3/sec$)
q_{rgr}	Rate of gas production per unit volume of waste due to brine radiolysis in the model grid ($kg/m^3/sec$)

q_{rgs}	Rate of gas production per unit volume of waste due to steel sulfidation in the model grid ($kg/m^3/sec$)
r	Uncertainty in the moles of CO_2 consumed per mole of emplaced MgO
R_{ci}	Corrosion rate under inundated conditions, PA parameter STEEL:CORRMCO2 (m/s)
R_{ch}	Corrosion rate under humid conditions, PA parameter STEEL:HUMCORR (m/s)
$R_{H2,i}$	$H_2(g)$ generation rate by dissolved and colloidal radionuclides and by the wetted solid form of the radionuclide for each radionuclide i
R_{mh}	Rate of CO_2 production from cellulose biodegradation under humid conditions, PA parameter WAS_AREA:GRATMICH (moles C consumed/kg $C_6H_{10}O_5$/sec)
R_{mi}	Rate of CO_2 production from cellulose biodegradation under inundated conditions, PA parameter WAS_AREA:GRATMICI (moles C consumed/kg $C_6H_{10}O_5$/sec)
RH	Remote handled
RSI	Institute for Regulatory Science
$S_{b,eff}$	Effective brine saturation due to capillary action in the waste materials
S_m	Measured solubility
SNL	Sandia National Laboratories
S_p	Solubility predicted by FMT or EQ3/6 calculations
SIT	Specific Ion Interaction Theory
TIC	Total inorganic carbon
TRU	Transuranic
TSD	Technical support document
V_R	Initial volume of a single room in the repository, PA parameter REFCON:VROOM
WDS	WIPP Waste Data System
WIPP	Waste Isolation Pilot Plant
XANES	X-ray absorption near-edge spectroscopy
$X_C(H_2 \mid Fe)$	Stoichiometric coefficient for gas generation due to the corrosion of steel, PA parameter STEEL:STOIFX
$X_m(H_2 \mid C)$	Average stoichiometric factor for microbial gas generation of cellulose, i.e., moles of H_2 generated per mole of carbon consumed by microbial action (moles H_2/mole C)
XRD	X-ray diffraction

Support for this TSD was provided by SC&A, Arlington, Virginia, under Contract 68HERD20A0005, Task Order 68HERH20F0404, Task 1132-0003-001-001-02b. Although issues of both technical practice and regulatory intent are addressed in this report, final interpretation of the EPA rule and ultimate acceptance or rejection of the EPA expectations expressed in this report is only within the purview of the Agency.

1.0 INTRODUCTION

The Waste Isolation Pilot Plant (WIPP) in southeastern New Mexico is an underground facility designed for the permanent disposal of transuranic (TRU) defense-related waste. The U.S. Department of Energy (DOE) operates the WIPP repository under the regulatory oversight of the U.S. Environmental Protection Agency (EPA or the Agency). DOE submitted the Compliance Certification Application (CCA) to the EPA in 1996. After extensive review of the CCA and supplemental information provided by DOE, including an additional performance assessment (PA) calculation referred to as the Performance Assessment Verification Testing (PAVT), EPA certified that DOE had met the regulatory requirements and WIPP began accepting waste in March 1999.

Waste characteristics and waste components must be analyzed, and the results must be included in any certification application [40 CFR 194.24(b)]. Those waste characteristics and components that could affect releases must be incorporated into PA [40 CFR 194.32(a)]. All additional data collected since the most recent CCA or Compliance Recertification Application (CRA) must be included in the CRA [40 CFR 194.15(a)], including any geochemical information, analyses, or results of laboratory experiments that are relevant to the performance of the repository. WIPP waste characteristics and components that have been identified as potentially affecting the chemistry of the system and releases include actinide solubilities and oxidation state distributions; formation of colloidal suspensions containing radionuclides; production of gas from the waste; ferrous metals inventory; cellulosic, plastic, and rubber material (CPR) inventory; chelating agents (organic ligands), oxyanions and cements; and the activity of each isotope of the radionuclides present in the waste [40 CFR 194.24(b), EPA 1997a].

DOE is required to submit a CRA every 5 years after the initial acceptance of waste at WIPP and the first CRA (CRA-2004) was submitted to EPA in March 2004 (DOE 2004). EPA reviewed the CRA-2004 and supplemental information provided by DOE, including PA calculations referred to as the CRA-2004 Performance Assessment Baseline Calculations (PABC04), and certified that DOE continued to meet WIPP regulatory requirements (EPA 2006a).

DOE submitted the second CRA (CRA-2009) to EPA in March 2009 (DOE 2009). EPA performed a completeness review of the CRA-2009 and instructed DOE to perform a new PA to capture changes since the 2004 recertification (Cotsworth 2009a). DOE performed this revised PA, the CRA-2009 Performance Assessment Baseline Calculations (PABC09). Based on its review of the CRA-2009 and PABC09, EPA certified that DOE continued to meet WIPP regulatory requirements (EPA 2010a). At the time of the recertification decision, EPA (2010b) noted some uncertainties related to WIPP chemistry and also identified issues related to WIPP repository chemical processes for additional investigation by DOE prior to the CRA-2014.

DOE submitted the third CRA (CRA-2014) in March 2014 (DOE 2014) that included the CRA-2014 PA. Because of uncertainties associated with some of the parameters used in the PA, EPA requested a sensitivity study of the CRA-2014 PA (CRA14_SEN4 PA. EPA (2017a) certified that DOE continued to meet WIPP regulatory requirements based on EPA's review of the CRA-2014 and the CRA14_SEN4 PA.

DOE submitted the fourth CRA (CRA-2019) in March 2019 (DOE 2019), with a deferred PA (CRA-2019 DPA) submitted in December 2019 (Sosson 2019). This Technical Support Document (TSD) summarizes EPA's review of chemistry-related issues important to the CRA-2019 DPA, including actinide source term modeling, gas generation, backfill efficacy, and actinide transport in the Culebra Dolomite above the repository for the WIPP CRA-2019. The principal portions of CRA-2019 (DOE 2019) addressed in this review are Appendix SOTERM and its supporting references, Appendix GEOCHEM and its supporting references, portions of §194.44 and Appendix MgO and their supporting references, portions of Appendix PA and its supporting references, portions of Appendix MASS and its supporting references, and portions of §194.24 and its supporting references. Information has also been obtained from DOE's responses to EPA's requests for additional information and from the results of reviews of chemistry-related issues carried out by EPA since the CCA.

Chemistry-related topics addressed in this report include Salado Formation mineralogy surrounding the repository and the chemistry of Salado and Castile brines (Section 2.0); gas generation caused by microbial degradation of CPR, anoxic corrosion of metals in the repository, and radiolysis (Section 3.0); the ability of the magnesium oxide (MgO) backfill to control chemical conditions (Section 4.0); an assessment of the actinides included in PA (Section 5.0); actinide oxidation states assumed in source term modeling (Section 6.0); dissolved actinide source term modeling (Section 7.0); colloidal actinide source term modeling (Section 8.0); distribution coefficients (K_ds) used in PA to model the release of actinides by transport through the Culebra Dolomite Member of the Rustler Formation (Section 9.0); the effects of heterogeneous waste loading (Section 10.0); the effects of chemical processes on repository water balance (Section 11.0); the sensitivity of total mobilized actinides in WIPP brines to chemistry parameters (Section 12.0); and the sensitivity of repository releases to chemistry parameter changes (Section 13.0). The resolution of a number of editorial comments, requests for computer code input and output files, and requests for cited documents are summarized in Attachment A. Attachment B provides detailed information regarding EPA's review of the DATA0.FM4 EQ3/6 database used to model CRA-2019 DPA baseline actinide solubilities. Attachment C summarizes the revised parameters used by EPA in CRA-2019 sensitivity calculations.

The results of this review indicate that DOE has modified its assessment of repository chemical processes as additional information has become available since the CCA PAVT, PABC04, PABC09, and CRA-2014 PA. EPA has identified additional modifications to incorporate in DOE's assessment of repository chemical processes for future WIPP PAs.

2.0 GEOLOGIC SETTING, SALADO FORMATION MINERALOGY, AND BRINE CHEMISTRY

WIPP repository chemical processes are influenced by the chemistry of the waste, by interaction of the waste with brines that may contact the waste, and by interaction of brine with the minerals in the Salado Formation that surrounds the repository. As a result, the geologic setting, Salado Formation mineralogy, and the chemistry of brines that could contact the waste can affect actinide releases from the repository and subsequent transport. The Salado mineralogy and the chemistry of brines that may contact WIPP waste are described in the CRA-2019 (DOE 2019, Appendix SOTERM).

2.1 GEOLOGIC SETTING

The WIPP repository is excavated within the Salado Formation. The low permeability of the Salado Formation surrounding the WIPP repository provides a significant hydrologic barrier between the repository and other, more transmissive water-bearing strata. A more permeable, transitory region forms within the Salado around the repository in response to the stress field caused by repository excavation; this region is called the Disturbed Rock Zone (DRZ). The DRZ is relatively thin compared to the thickness of the Salado Formation surrounding the repository (DOE 2019, Appendix SOTERM, Table SOTERM-1).

The Salado Formation is underlain by the Castile Formation. The Castile Formation is mainly composed of thick beds of high-purity halite, alternating with thick beds of interlaminated carbonate and anhydrite [$CaSO_4$(s)] (DOE 2019, Appendix SOTERM). The Castile Formation has been significantly deformed in some areas near the WIPP repository and pressurized brines are associated with the deformed areas.

The Salado Formation is overlain by the Rustler Formation (DOE 2019, Appendix SOTERM). This formation is composed of evaporite layers called, from bottom to top, the Los Medaños Member, the Culebra Dolomite Member, the Tamarisk Member, the Magenta Dolomite Member, and the Forty-Niner Member. The Culebra Dolomite is mostly composed of dolomite [$CaMg(CO_3)_2$(s)], with small amounts of anhydrite or gypsum [$CaSO_4 \cdot 2H_2O$(s)] (Lambert 1992). The Culebra Dolomite is the most transmissive continuously saturated unit above the WIPP facility. It therefore provides the most direct pathway from the repository to the accessible environment, apart from releases directly to the surface (DOE 2004). As a consequence, this aquifer has been studied more extensively than other portions of the Rustler Formation (Lambert 1992; DOE 2004).

2.2 SALADO MINERALOGY

In the area around WIPP, the Salado Formation is a thick bedded salt, composed mainly of layers of impure halite [NaCl], with interbedded layers of anhydrite, polyhalite [$K_2MgCa_2(SO_4)_4 \cdot 2H_2O$(s)], and mudstone (Lambert 1992). These sulfate-bearing interbeds are called Marker Beds (MB). Within the Salado Formation, these beds are labeled using numbers that range from MB 100 near the top of the formation to MB 144 near the bottom (DOE 2004).

Stein (1985) provided mineralogical analyses of drill core from the Salado Formation above and below the repository horizon. Based on x-ray diffraction (XRD) data, Stein (1985) identified quartz [SiO_2(s)], magnesite [$MgCO_3$(s)], anhydrite, gypsum, halite, polyhalite, bassanite [$CaSO_4 \cdot 0.5H_2O$(s)], alkali feldspar [(Na,K)$AlSi_3O_8$(s)], and clay minerals in the Salado Formation. Brush (1990) used these data to calculate the average mineralogical composition of the Salado for use in geochemical modeling. Because the XRD evaluation of the mineralogical composition was only semiquantitative, Brush (1990) assumed that halite constituted 93.2 wt% of the Salado Formation, with the remaining fraction composed of equal parts magnesite, anhydrite, gypsum, and polyhalite (1.7 wt% each). Brush (1990) did not include clay minerals, feldspar, and quartz in the assumed mineralogy because Pitzer data for aqueous silica species were unavailable at that time for use in geochemical modeling. Bassanite was not included in the assumed mineralogy, because it was identified in only one sample.

The assumption by Brush (1990) of equal percentages of the non-halite minerals in the Salado Formation likely overestimates the amount of polyhalite. Stein (1985) identified polyhalite in only four of the 44 tested samples, and polyhalite appeared to be less abundant than the other non-halite minerals in three of these four samples. SC&A (2008b) reviewed the Stein (1985) data from within the estimated extent of the DRZ above and below the waste rooms, and found that polyhalite was identified by XRD only in sample FH-224. These results indicate that much less polyhalite is likely accessible to repository brines than has been assumed for calculating the effects of cements on brine pcH (DOE 1996, Appendix SOTERM; EPA 2017d). The available amount of polyhalite may also affect the modeled precipitation of hydrated magnesium minerals and predicted brine consumption in actinide solubility calculations.

2.3 SALADO FORMATION AND CASTILE FORMATION BRINE CHEMISTRY

Small quantities of intergranular and intragranular Salado brines are associated with the salt at the repository horizon. These brines are highly concentrated (ionic strengths up to 8), with a composition of mostly sodium, magnesium, potassium, chloride, and sulfate, and with smaller amounts of calcium, carbonate, and borate. Two formulations of these Salado brines, Brine A and Generic Weep Brine (GWB), have been used in WIPP laboratory experiments and PA calculations (Snider 2003b). In the CCA PAVT, the Brine A formulation was used to simulate intergranular Salado brines. However, the GWB Salado brine formulation has been used in the CRA-2004 PA and all subsequent WIPP PA calculations. A detailed discussion of GWB brine and a comparison to Brine A were provided by Snider (2003b).

GWB was developed based on chemical analyses of intergranular fluids that seep into the WIPP excavations from the DRZ (Snider 2003b). DOE developed the GWB formulation because of the potential effects of magnesium concentrations in the brine on the modeled and experimental chemical behavior of the MgO backfill. Snider (2003b) verified the calculations supporting the formulation of GWB and compared the concentrations of major cations and anions in several WIPP brines. The comparison between GWB and Brine A indicated that GWB has higher boron, sodium, bromide, chloride, and sulfate concentrations, and lower calcium, potassium, and magnesium than Brine A. Brine A has a relatively low reported inorganic carbon concentration,

whereas none was reported for GWB (Table 2-1). The ionic strength[1] of GWB is approximately 6.5 compared to approximately 5.9 for Brine A.

Table 2-1. Brine A, GWB, and ERDA-6 Compositions

Component	Brine A	GWB	ERDA-6
Boron	0.020	0.155	0.063
Calcium	0.020	0.014	0.012
Potassium	0.770	0.458	0.097
Magnesium	1.44	1.00	0.019
Sodium	1.83	3.48	4.87
Bromide	0.010	0.026	0.011
Chloride	5.35	5.51	4.8
Sulfate	0.040	0.175	0.170
Total Inorganic Carbon	0.010	Not reported	0.016
pH	6.5	Not reported	6.17
Specific Gravity (kg/L)	1.2	1.2	1.216
Total Dissolved Solids (mg/L)	306,000	Not reported	330,000

All units are moles/L solution, unless otherwise specified
Source: Brush and Xiong (2003a)

EPA (2006c) reviewed DOE's proposed use of the GWB brine formulation to model actinide solubilities for the CRA-2004 PA and concluded that the GWB formulation was adequately documented. EPA concurred with DOE that the GWB brine formulation more closely matches the composition of Salado intergranular brines than Brine A, and that use of the GWB formulation in place of Brine A for the CRA-2004 PA and future actinide solubility calculations is appropriate. Only minor differences were observed between actinide solubility calculations carried out with GWB and Brine A.

Castile brine may enter the repository if a borehole that penetrates the repository also penetrates an area of pressurized brine in the underlying Castile Formation. Borehole ERDA-6 encountered pressurized brine in the Castile Formation. The composition of this ERDA-6 brine has been used to represent the likely composition of Castile brine in laboratory experiments and all WIPP PA calculations (Table 2-1).

Silica has not been included in the synthetic Salado or Castile brines used in WIPP experiments or modeling calculations. Dissolved silica likely was omitted from the brine formulations because silica was not analyzed in some studies of WIPP brines (Stein and Krumhansl 1986, Krumhansl et al. 1991). However, silica has been observed in both Salado (Abitz et al. 1990) and Castile brines (Popielak et al. 1983). The presence of silica in WIPP brines, sourced from clay

[1] Ionic strength (I) is defined by the equation $I = \frac{1}{2} \Sigma_I c_i Z_i^2$. This summation is carried out for all cations and anions in the solution, and c_i and Z_i are the concentrations and charges, respectively, of all ions in solution.

minerals in the Salado or from WIPP waste, may require future consideration, especially in the context of silica colloids discussed in Section 8.1.6.

2.4 CONCLUSIONS

EPA has reviewed the available information regarding the WIPP repository geologic setting, as well as the Salado Formation mineralogy and the compositions of Salado Formation and Castile Formation brines used in WIPP PA. Based on this review, EPA has found:

- The assumption that the Salado contains 1.7 wt% polyhalite appears to overestimate the amount of polyhalite based on the reported analytical data. Because of the potential effects of polyhalite on mineral precipitation and water consumption in the baseline actinide solubility calculations (Section 7.4.8), EPA recommends that DOE re-evaluate the available mineralogical data to establish a more realistic estimate of the polyhalite concentration in the Salado Formation.
- The GWB (Salado) and ERDA-6 (Castile) brine formulations used in WIPP PA do not include silica, likely because silica was not included in some reported WIPP brine analyses. Dissolved silica has been detected in both Salado and Castile brines, and silicate minerals are present in WIPP waste and the Salado Formation. Because the potential formation of silica colloids containing structural +IV actinides has been reported in the literature (Section 8.1.6), EPA recommends that DOE evaluate for future WIPP PAs the likely concentrations of silica that may be achieved in WIPP brines under the moderately alkaline conditions created by the MgO backfill, as well as potentially increased actinide mobilization because of the formation of +IV actinide-silica colloids under WIPP repository conditions.

3.0 GAS GENERATION

The Gas Generation conceptual model developed for the CCA and used through CRA-2014 included the assumption that significant gas generation will occur in the repository from corrosion of ferrous metals and from microbial degradation of CPR. The Gas Generation conceptual model also includes the assumption that essentially all carbon dioxide [CO_2] will be removed from the gas phase by reaction with the MgO backfill (Wilson et al. 1996a and 1996b). Another assumption is that corrosion of other metals in the WIPP inventory, such as aluminum and lead, will not contribute significantly to gas generation rates because of low inventories. The Gas Generation conceptual model used in WIPP PA through the CRA-2014 is described in detail by SC&A (2008b, Appendix A).

Before the CRA-2019, DOE assumed that radiolysis of brine and CPR in the waste would not significantly affect gas generation rates (Wilson et al. 1996a and 1996b). EPA (2017d) noted during its review of the CRA-2014 that it was no longer certain that gas generation caused by radiolysis of brine and CPR will be insignificant because of the lower microbial degradation rates and lower anoxic steel corrosion rates used in the CRA-2014 PA. DOE subsequently reevaluated the potential importance of radiolytic gas generation (Day 2019b; DOE 2019, Appendix SCR). Because of increases in alpha-emitting radionuclides in the inventory that could contribute to increased gas generation through brine radiolysis, gas generation from radiolysis of brine was included in the CRA-2019 DPA (DOE 2019, Appendix PA). Gas generation from CPR radiolysis continued to be screened out of the CRA-2019 DPA (DOE 2019, Appendix SCR).

3.1 IRON CORROSION

Large quantities of reduced iron will be present in the repository in the form of steel waste containers and as iron-based alloys in the waste. Van Soest (2012, 2018) provides inventory estimates of the masses of iron-based waste material and packaging materials in contact-handled (CH) and remote-handled (RH) waste for the CRA-2014 PA and CRA-2019 DPA. These estimates are based on the annual inventory reports as of December 31, 2011 (DOE 2012a) for the CRA-2014 PA and as of December 31, 2017 for the CRA-2019 DPA (DOE 2018). The inventory estimates include emplaced, stored, and projected WIPP waste, which are scaled to a full repository. The estimated WIPP inventory at closure of iron-based metals and alloys for the CRA-2019 has increased from 49,000 metric tons to 63,000 metric tons (Table 3-1). CH and RH waste constitutes approximately 25% of the iron-based metals and alloys inventory, and packaging materials make up 75% of both inventories. The increased repository total for iron-based metals and alloys is chiefly due to increased RH packaging materials from shielded containers (DOE 2018).

Table 3-1. CRA-2014 PA and CRA-2019 DPA Inventories of Iron-Based Metals and Alloys

Parameter	CRA-2014 PA		CRA-2019 DPA	
	(kg)	(%)	(kg)	(%)
CH Waste Iron-Based Metal and Alloys	10,900,000	22	14,100,000	22
CH Steel Packaging Materials	30,000,000	61	31,200,000	49
RH Waste Iron-Based Metal and Alloys	1,350,000	3	1,330,000	2

RH Steel Packaging Materials	6,860,000	14	16,500,000	26
Repository Total	49,110,000	100	63,130,000	100

Sources: Van Soest (2012, Table 5-5), Van Soest (2018, Table 5-5)

The Gas Generation conceptual model includes assumptions related to iron corrosion (Wilson et al. 1996a and 1996b, SC&A 2008b):

- The small amounts of oxygen trapped in the repository immediately after closure will be consumed by oxic corrosion or aerobic microbial degradation, and these processes will not generate a significant amount of gas;
- Anoxic corrosion can occur in the repository as soon as the shafts are sealed;
- The anoxic corrosion rate of steel is a function of both brine saturation and steel surface area;
- CO_2 generated by microbial degradation of CPR will not passivate steel, because CO_2 will be consumed by reaction with the MgO backfill;
- Hydrogen sulfide (H_2S) might passivate steel by forming FeS(s) on the steel surfaces if H_2S is produced in sufficient quantities; however, reducing chemical conditions would continue to be maintained by the FeS(s); and
- Fe is represented by Fe(s) and/or $Fe(OH)_2(s)$.[2]

3.1.1 Corrosion Reaction Products and Stoichiometry

Anoxic corrosion of steel in the waste and waste containers produces hydrogen gas [$H_2(g)$]. The chemical reactions that represent the stoichiometry of anoxic corrosion of steel in the WIPP repository for CRA-2014 are:

$$Fe(s) + (x+2)\ H_2O(l) \leftrightharpoons Fe(OH)_2 \bullet xH_2O(s) + H_2(g) \quad \textbf{(1)}$$

$$Fe(s) + H_2S(g) \leftrightharpoons FeS(s) + H_2(g) \quad \textbf{(2)}$$

In the CRA-2004 (DOE 2004, Appendix PA, Attachment SOTERM-2.2.3) and CRA-2009 (DOE 2009, Appendix SOTERM-2.3.4), DOE listed additional iron corrosion reactions based on WIPP-specific experiments (Telander and Westerman 1993 and 1997):

$$3\ Fe(s) + 4\ H_2O(l) \leftrightharpoons Fe_3O_4(s) + 4\ H_2(g) \quad \textbf{(3)}$$

$$Fe(s) + H_2O(l) + CO_2(g) \leftrightharpoons FeCO_3(s) + H_2(g) \quad \textbf{(4)}$$

Reactions (3) and (4) indicate that iron corrosion could produce magnetite [$Fe_3O_4(s)$] or siderite [$FeCO_3(s)$]. Magnetite production through reaction (3) is potentially important, because reaction (3) produces 1.33 moles of gas per mole of iron, whereas reactions (1) and (2) produce only one

[2] The product of iron metal corrosion is most accurately represented as $Fe(OH)_2 \bullet xH_2O(s)$. However, because the waters of hydration in this reaction product are indeterminate, $Fe(OH)_2(s)$ is used for stoichiometric calculations

mole of gas per mole of iron. DOE (2019, Appendix GEOCHEM) discussed the uncertainty regarding whether magnetite will form from anoxic corrosion at WIPP temperatures. Experimental data from Telander and Westerman (1997) indicate that magnetite formation may not occur at the low temperatures expected in the WIPP repository, and additional low-temperature iron corrosion experiments carried out by Roselle (2009, 2010, 2011a, 2011b, 2013a) did not produce magnetite as a corrosion product. Siderite formation is not expected to be a significant process in the repository, because of the presence of the MgO backfill, which will control CO_2 fugacity at low levels.

DOE (2014, Appendix SOTERM) stated that based on new iron corrosion experiments, Roselle (2013a) had identified green rust [idealized formula $Fe(III)_2Fe(II)_4(OH)_{12}CO_3 \cdot 2H_2O$] as the "most likely corrosion product in experiments with low atmospheric CO_2 concentrations (<350 ppm)." The corrosion reaction to form green rust was given as:

$$6\ Fe(s) + CO_2(g) + 15\ H_2O(l) \leftrightharpoons Fe(III)_2Fe(II)_4(OH)_{12}CO_3 \bullet 2H_2O(s) + 7\ H_2(g) \qquad \textbf{(5)}$$

DOE (2019, Appendix GEOCHEM) also stated that the possible formation of green rust had been demonstrated in WIPP steel corrosion experiments (Roselle 2009, 2010, 2011a, 2011b, 2013a). DOE evaluated the available data regarding likely iron corrosion products in response to a comment from EPA during the CRA-2014 review (Shrader 2016), including WIPP-specific data from Telander and Westerman (1993, 1997), Roselle (2009, 2010, 2011a, 2011b, 2013a) and Nemer et al. (2011) as well as data related to corrosion of iron archaeological artifacts in chloride-rich environments (Neff et al. 2005, Réguer et al. 2007, Bellot-Gurlet et al. 2009, Rémazeilles et al. 2009, Saheb et al. 2009). The available data indicated that the most likely corrosion product is $Fe(OH)_2 \bullet xH_2O(s)$, as observed by Telander and Westerman (1993), or possibly hibbingite [$Fe_2(OH)_3Cl(s)$]:

$$Fe(s) + 0.5\ Cl^- + 2\ H_2O(l) \leftrightharpoons 0.5\ Fe_2(OH)_3Cl(s) + 0.5\ OH^- + H_2(g) \qquad \textbf{(6)}$$

Reaction (6) produces one mole of gas per mole of iron. Consequently, EPA believes the molar ratio of hydrogen gas [$H_2(g)$] produced per mole of iron should remain equal to 1 for anoxic corrosion of iron in the WIPP environment.

3.1.2 Corrosion Rates

DOE uses two parameters in PA to represent iron corrosion rates, STEEL:CORRMCO2, representing the inundated steel corrosion rate (m/s) and STEEL:HUMCORR, representing the humid steel corrosion rate (m/s). DOE used the same values and distributions for these parameters for the CCA PAVT, PABC04, and PABC09 (Table 3-2). In these PAs, DOE assumed the humid steel corrosion rate was 0.0 m/s (Wang and Brush 1996).

Table 3-2. WIPP PA Inundated Steel and Humid Steel Corrosion Rates

	Distribution	Maximum	Mean	Minimum
Inundated Steel Corrosion Rates (STEEL:CORRMCO2, m/s)				
CCA PA	Uniform	1.59×10^{-14}	7.95×10^{-15}	0.0
CCA PAVT, PABC04, PABC09	Uniform	3.17×10^{-14}	1.585×10^{-14}	0.0

CRA-2014 PA	Student	1.84×10^{-14}	6.06×10^{-15}	3.29×10^{-16}
Zeitler and Hansen (2015a)	CDF	3.96×10^{-14}	6.76×10^{-15}	0.0
CRA-2019 DPA (Kim and Feng 2019)	CDF	7.92×10^{-14}	1.33×10^{-14}	0.0
Humid Steel Corrosion Rates (STEEL:HUMCORR, m/s)				
CCA PA, CCA PAVT, PABC04, PABC09, CRA 2014 PA	--	0.0	0.0	0.0
Zeitler and Hansen (2015c) 0.58 ppm CO_2	CDF	1.02×10^{-15}	2.68×10^{-16}	0.0
Zeitler and Hansen (2015b) 3.14 ppm CO_2	CDF	1.03×10^{-15}	2.71×10^{-16}	0.0
Zeitler (2018) 5 ppm CO_2	CDF	1.03×10^{-15}	2.73×10^{-16}	0.0
CRA-2019 DPA (Kim and Feng 2019)	CDF	1.03×10^{-15}	2.43×10^{-16}	0.0

For the CCA PA, DOE estimated the inundated corrosion rate would range from 0.0 to 1.59×10^{-14} m/s, with a uniform distribution over this range (Wang and Brush 1996). However, EPA requested that DOE double the upper bound of the inundated corrosion rate because of the rate increase observed at pressures from 70 to 127 atm by Telander and Westerman (1997), which are comparable to WIPP repository gas pressures (Camphouse 2013a). MFG (2000) confirmed these corrosion rates and established that iron corrosion would maintain repository reducing conditions. Consequently, the sampled range for the inundated steel corrosion rate was from 0 to 3.17×10^{-14} m/s, with a uniform distribution for the CCA PAVT, PABC04, and PABC09 (Fox 2008).

DOE (2014, Appendix PA) established a revised range and distribution for the inundated steel corrosion rate for the CRA-2014 PA (Table 3-2) based on WIPP-specific experiments (Roselle 2009, 2010, 2011a, 2011b, 2013). The humid corrosion rate remained unchanged for the CRA-2014 PA at zero, based on a recommendation by Roselle (2013a). EPA noted that the revised inundated steel corrosion rate was calculated using only data obtained at a CO_2 atmospheric concentration of 0 ppm (Edwards 2015a). EPA observed that CO_2 atmospheric concentrations in equilibrium with repository brines, while low, are nonzero and corrosion experiments conducted at higher CO_2 appeared to have higher maximum corrosion rates. DOE responded with a revised assessment of the corrosion rate data that included experiments conducted with nonzero CO_2 concentrations (Shrader 2016, Zeitler and Hansen 2015a). Zeitler and Hansen (2015a) recalculated the inundated steel corrosion rate by including data collected at CO_2 concentrations of 0 and 350 ppm and 1 atm total pressure (Table 3-2). Zeitler and Hansen (2015a) also included a corrosion rate of 0 m/s to account for possible passivation of the steel surface. Zeitler and Hansen (2015a) accumulated these rates into a cumulative distribution function (CDF) to represent in PA the range of variability in the inundated corrosion rate data. EPA (2017d) found this data analysis and distribution to be reasonable but observed that it did not account for the previously noted effects of higher repository pressure on the inundated corrosion rate. For the CRA-2019 DPA, DOE increased the inundated corrosion rates measured by Roselle (2013a) by a factor of two and accumulated the increased rates into a CDF, which accounts for higher rates measured at higher pressure (Table 3-2). The CRA-2019 DPA inundated steel corrosion rate

distribution is supported by the corrosion rate measurements of Roselle (2009, 2010, 2011a, 2011b, 2013a) and are consistent with the earlier corrosion rate data (Telander and Westerman 1997).

Humid steel corrosion rates previously used in PA have been zero based on assessments of data available from Telander and Westerman (1993, 1997). EPA observed that the Roselle (2013a) data appeared to be non-zero and requested that DOE assess the humid steel corrosion rate using data obtained with gas-phase CO_2 concentrations of 0 and 350 ppm, which bracket anticipated repository conditions (Edwards 2015a). DOE responded with a revised assessment of the humid corrosion rate data (Shrader 2016, Zeitler and Hansen 2015b).

DOE (Zeitler and Hansen 2015b) considered 16 data points from Roselle (2013a), eight each for samples tested at 0 ppm and 350 ppm CO_2. Four of the 350 ppm CO_2 rates were negative and were therefore excluded from the evaluation. After constructing separate CDFs for the 0 ppm and 350 ppm CO_2 data, Zeitler and Hansen (2015b) developed a common set of percentiles by linearly interpolating between the CDFs using a CO_2 concentration of 3.14 ppm (Table 3-2), consistent with predicted WIPP repository conditions from Brush and Domski (2013b). Zeitler and Hansen (2015c) used the same approach to develop a CDF for the humid steel corrosion rate for a CO_2 concentration of 0.58 ppm (Table 3-2), consistent with predicted repository conditions from Domski and Xiong (2015b). Because of the minimal differences between the rates calculated using CO_2 concentrations of 0.58 and 3.14 ppm and to avoid recalculating the humid corrosion rate each time the expected repository CO_2 concentration is recalculated, Zeitler (2018) calculated the humid steel corrosion rate for a bounding CO_2 concentration of 5 ppm (Table 3-2).

The maximum value for the humid corrosion rate distribution calculated by Zeitler (2018) is reasonable, because only a single data point obtained at 350 ppm CO_2 exceeds this rate (Figure 3-1). A lower bound of zero is appropriate considering the possible surface passivation by H_2S and low to slightly negative rates observed in some of the experiments. A nonzero humid corrosion rate represents a change from previous WIPP PAs, but this change is adequately supported by the new experimental data.

The mean value for the humid corrosion rate distribution provided in the parameter data report (Kim and Feng 2019) is slightly lower than the value presented by Zeitler (2018) (Table 3-2), and the standard deviation reported by Kim and Feng (2019) is also slightly lower (2.47×10^{-16} compared to 3.32×10^{-16} m/s). In response to a comment from EPA (Peake 2020f, Comment CC6-GEOCHEM-33), DOE confirmed the cumulative distribution of humid steel corrosion rate data was correctly sampled for the CRA-2019 DPA (Knerr 2021b). The mean and standard deviation values in Kim and Feng (2019) are the correct values.

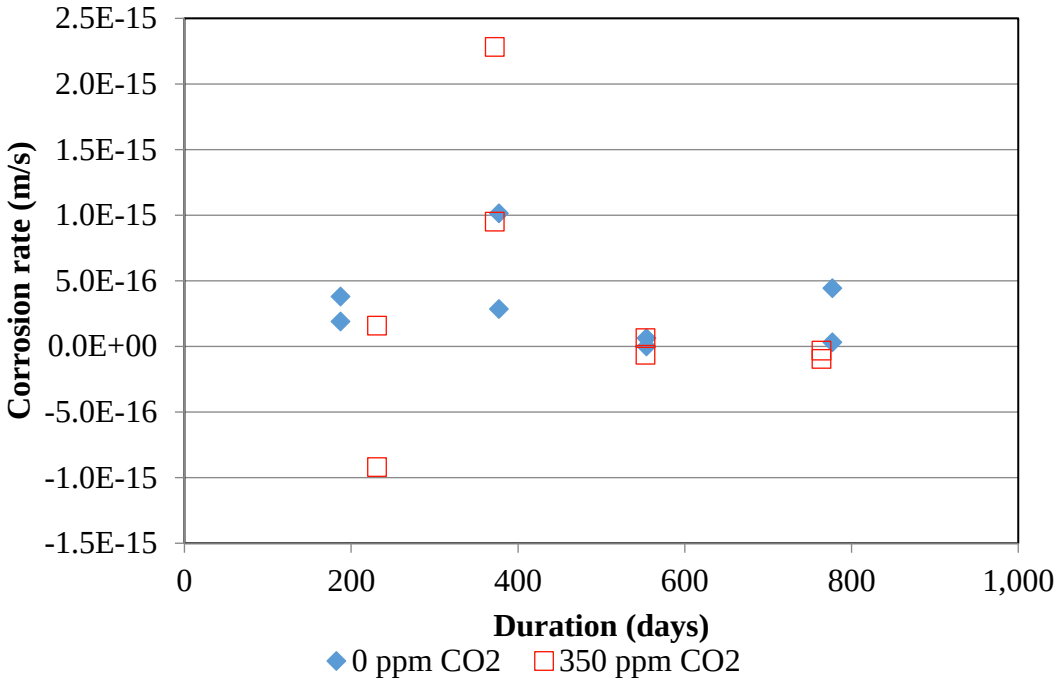

Figure 3-1. Humid Steel Corrosion Rate Data (Roselle 2013a)

Both the inundated steel corrosion rate (STEEL:CORRMCO2) and the humid steel corrosion rate (STEEL:HUMCORR) parameters were sampled for the CRA-2019 DPA using the LHS code (Zeitler 2019a). For the inundated and humid steel corrosion rates, DOE specified a conditional relationship so that the sampled humid rate was equal to or less than the sampled inundated rate (Zeitler 2019a).

3.1.3 Passivation of Iron Surfaces by H_2S

For the CRA-2014 PA, DOE assumed that all H_2S produced by microbial degradation of cellulose will instantaneously react to produce iron sulfide. EPA (2017d) questioned this assumption, noting that WIPP-specific corrosion experiments had indicated H_2S passivated steel (Telander and Westerman 1997). The iron metal sulfidation and ferrous hydroxide sulfidation reactions are reaction (2) and:

$$Fe(OH)_2(s) + H_2S(g) \leftrightharpoons FeS(s) + 2\ H_2O(l) \qquad \textbf{(7)}$$

Reaction (2) has no net effect on the amount of gas or brine in the repository. However, reaction (7) reduces the amount of gas and increases the brine volume. Because H_2S was presumed to preferentially react with iron hydroxide versus metallic iron for the CRA-2014 PA (DOE 2014, CRA-2014 Appendix MASS), overestimation of the iron sulfidation rate results in an underestimation of the gas pressure and overestimation of the brine volume in the repository [reaction (7)].

The effects of removing iron sulfidation reactions from the PA were tested by setting the stoichiometric coefficients for reactions (2) and (7) equal to zero for the CRA14_SEN4 PA

(Zeitler and Day 2016). The effects of this change combined with an increased probability of encountering pressurized brine during a drilling intrusion resulted in increased DBRs (EPA 2017c). For the CRA-2019 DPA, DOE removed the iron sulfidation reactions (2) and (7) by setting the stoichiometric parameters REFCON:STCO_31 and REFCON:STCO_32 to zero (DOE 2019 Appendix PA Section PA-1.1.9, Kim and Feng 2019).

3.1.4 Steel Surface Area

The gas generation rate caused by anoxic corrosion of iron-based metal in the repository is proportional to the steel surface area per unit disposal volume, D_S (DOE 2019 Appendix GEOCHEM Equation GEOCHEM.4). DOE calculates the value of D_S from (Appendix GEOCHEM equation GEOCHEM.14):

$$D_S = \frac{A_d n_d}{V_R} \quad \textbf{(8)}$$

Where:

A_d is the surface area of steel associated with a waste disposal drum (parameter REFCON:ASDRUM, m^2/drum),

V_R is the initial volume of a single room in the repository (parameter REFCON:VROOM, m^3), and

n_d is the ideal number of waste drums that can be closely packed into a single room (parameter REFCON:DRROOM).

Based on information developed prior to the CCA PA, DOE estimated that the steel surface area of a 55-gallon waste disposal drum (A_d) is approximately 6 m^2/drum (Brush 1990). This estimated surface area included both the surface area of the steel drum and the iron-based waste contents. DOE assumed a generic room size of 33 ft by 300 ft by 13 ft (V_R, 3,640 m^3) allowing for 6,800 (n_d) 55-gallon drums. These parameters result in D_S = 11.2 m^2/m^3, which has been used in all WIPP PA calculations. EPA (2017d) considered the potential effects of waste inventory and emplacement data collected since the CCA PAVT on the likely repository-wide steel surface area per unit volume. The information considered by EPA included calculations performed by Day (2015) based on the number of different containers emplaced in WIPP as of December 31, 2014. EPA (2017d) calculated that average D_S values would range from 10.0 m^2/m^3 to 11.6 m^2/m^3, from slightly below to slightly above the 11.2 m^2/m^3 value used in the CRA-2014 PA. EPA (2017d) found that the D_s value used in the CRA-2014 was acceptable based on these calculations. EPA (2017d) also recommended that DOE confirm for the CRA-2019 that the steel surface area per unit disposal volume remained representative of WIPP waste using updated inventory and waste emplacement data.

The CRA-2019 DPA iron-based metals and alloys inventory increased by 14,000 metric tons since the CRA-2014 PA (Table 3-1), primarily because of increased RH packaging materials from shielded containers (DOE 2018). However, DOE (2019) did not address whether the increased number of shielded containers significantly affects D_s. Because of the substantial increase in the number of RH shielded containers, EPA requested that DOE provide information

to support retaining the existing REFCON:ASDRUM, REFCON:DRROOM, and REFCON:VROOM parameters in the CRA-2019 DPA (Peake 2020f, Comment CC6-GEOCHEM-32). DOE provided a response (Knerr 2021b) that: 1) referenced its CRA-2014 PA calculations, 2) stated that DOE and EPA had agreed that no change to the steel surface area calculation was needed for CRA-2019 but that this calculation would be addressed in future WIPP PAs, and 3) asserted that because the steel surface area per drum equivalent for shielded containers is low, increased numbers of shielded containers would continue to overestimate steel surface area in the repository and PA calculations would continue to overestimate gas generation from steel corrosion. DOE's last assertion implies that overestimation of gas generation rates will result in overestimations of releases. However, in response to a question regarding radiolytic gas generation (Peake 2020c, Comment CC3-GEOCHEM-17c), Knerr (2020c) found that increased radiolytic gas generation rates decreased average total releases from the repository (Section 3.6.1). Consequently, overestimating steel surface area and gas generation might not result in conservative estimates of releases.

Calculations of D_s depend on the proportions of different wastes and waste containers in the repository. The calculations performed by Day (2015) for the CRA-2014 PA used the number of emplaced containers and did not account for the types and numbers of containers that are stored and projected for the WIPP repository at closure. The CRA-2019 DPA projected total container count at closure is included in DOE's WIPP inventory calculations (Table 1, LANL-CO 2018). EPA calculated D_s using these projected container counts for the CRA-2019 DPA and the surface area to tare weights for each container (Day 2015). The surface area of steel waste was approximated by assuming a surface area to weight ratio for 1 cm spheres (spherical surrogate) or assuming a surface area to weight ratio equivalent to a 55-gallon drum (revised sheet metal surrogate). The total surface area for the containers and waste were divided by the total repository volume of 438,000 m^3. The results indicated that the estimated D_s for the CRA-2019 DPA would range from approximately 10.5 m^2/m^3 (spherical surrogate) to 13.2 m^2/m^3 (revised sheet metal surrogate). This range is similar to the range calculated above for the CRA-2014 PA and adequately brackets the value of 11.2 m^2/m^3 used in the CRA-2019 DPA.

In future calculations of steel surface area, DOE should use emplaced, stored, and scaled anticipated container counts that are consistent with the container counts used to estimate CPR emplacement and operation materials in the WIPP inventory. Accurately representing the steel surface area in future WIPP PAs will be important because steel corrosion is the most important gas generation mechanism and the relationship between gas generation rates and repository releases is complex. EPA recommends that DOE use the available total container counts at closure and recalculate D_s for each future WIPP PA to demonstrate that the parameters used to calculate steel surface area remain defensible.

3.1.5 PA Implementation of Gas Generation by Anoxic Steel Corrosion

The equation used to calculate the anoxic steel corrosion gas generation rate is (DOE 2019, Appendix GEOCHEM-2.2):

$$q_{rgc} = (R_{ci}\, S_{b,eff} + R_{ch}\, S_g^*)\, D_s\, \rho_{Fe}\, X_C\, (H_2 \mid Fe)\, M_{H2} \qquad \textbf{(9)}$$

Where:

q_{rgc} is the rate of gas production per unit volume of waste due to anoxic corrosion of iron-based metals ($kg/m^3/sec$);

R_{ci} is the corrosion rate under inundated conditions (parameter STEEL:CORRMCO2, m/s);

$S_{b,eff}$ is the effective brine saturation due to capillary action in the waste materials;

R_{ch} is the corrosion rate under humid conditions (parameter STEEL:HUMCORR, m/s);

S_g* equals 1- $S_{b,eff}$ if $S_{b,eff} > 0$, or equals 0 if $S_{b,eff} = 0$;

D_s is the steel surface area per unit disposal volume in the repository (11.2 m^2/m^3), calculated from the parameters REFCON:ASDRUM (6 m^2/drum), REFCON:DRROOM (6,800 drums/room), and REFCON:VROOM (3,640 m^3/room);

ρ_{Fe} is the molar density of steel calculated from the density of iron (parameter REFCON:DN_FE) and the molecular weight of iron (parameter REFCON:MW_FE);

X_C ($H_2 \mid Fe$) is the stoichiometric coefficient for gas generation due to the corrosion of steel (1 mole H_2 per mole Fe, parameter STEEL:STOIFX, Kim and Feng 2019)]; and

M_{H2} is the molecular weight of H_2 (parameter REFCON:MW_H2, kg H_2 per mole H_2).

For each realization, DOE uses the sampled inundated and humid anoxic corrosion rates to calculate anoxic corrosion gas generation per unit volume of waste as a function of the effective brine saturation.

3.1.6 Effects of Anoxic Corrosion Gas Generation Rates on Repository Releases

The CRA-2019 DPA humid corrosion rate is higher than the previously used humid corrosion rate of 0 m/s. Zeitler (2019b) found that repository releases were not sensitive to the humid steel corrosion rate. The CRA-2019 DPA mean inundated corrosion rate is higher than the CRA-2014 rate and has a similar mean to the CCA-PAVT, PABC04, and PABC09 inundated corrosion rate (Table 3-2). Sensitivity analysis of repository releases to sampled input parameters (Zeitler 2019b) indicated that the importance of the inundated steel corrosion rate to the variability of DBR increased in the CRA-2019 DPA compared to the CRA-2014 PA, but the increased inundated corrosion rate was correlated with decreased DBRs because higher repository brine pressure led to decreased waste area saturation. Zeitler et al. (2019) observed that cumulative gas generation was generally higher in the CRA-2019 DPA, in part because of increased inundated iron corrosion rates. These higher pressures resulted in increased spallings releases compared to the CRA-2014 PA.

3.2 CORROSION OF LEAD, ALUMINUM, AND OTHER METALS

In addition to iron-based metals, corrosion of other metals such as aluminum and lead could contribute to repository gas generation. Inventory data from the CCA PAVT through the CRA-2014 PA showed that the masses of aluminum, lead, and other metals were low compared to iron-based metals, so corrosion of these metals was not expected to significantly contribute to repository gas generation (EPA 2017d). The masses of metals that are tracked in the WIPP

inventory are compared in Table 3-3 for the CRA-2014 PA and CRA-2019 DPA. The significant increase in RH lead packaging materials is caused by the large number (31,942) of shielded container assemblies in the CRA-2019 DPA inventory (LANL-CO 2018).

Table 3-3. CRA-2014 PA and CRA-2019 DPA Inventories of Aluminum, Lead and Other Metals and Alloys

Waste or Packaging Material	CRA-2014 PA (kg)	CRA-2019 DPA (kg)
CH and RH Waste Aluminum-Based Metal and Alloys	457,100	556,600
CH and RH Waste Other Metals and Alloys	1,233,000	984,000
RH Lead Packaging Materials	8,280	13,800,000
Total Waste Other Metals and Alloys and Lead Packaging Materials	1,241,280	14,784,000
Total Iron-Based Waste and Packaging Materials	49,110,000	63,130,000

Source: Van Soest (2012, 2018)

3.2.1 Lead Corrosion

Anoxic corrosion of lead to form oxidized minerals such as litharge [PbO(s)] consumes brine and generates $H_2(g)$:

$$Pb(s) + H_2O(l) \leftrightharpoons PbO(s) + H_2(g) \quad \textbf{(10)}$$

If significant quantities of lead are present in the WIPP inventory, lead corrosion could affect repository gas generation rates and brine volumes. EPA (2017d) evaluated the likely effects of shielded RH containers on the lead inventory for the CRA-2014 PA and found that the lead inventory was likely underestimated. EPA (2017d) recommended that DOE develop reasonable upper bound estimates for the lead inventory and lead surface area per unit disposal volume for the CRA-2019 DPA. EPA (2017d) also stated that if DOE determined that the lead inventory was significant relative to the iron-based metals inventory, DOE should use project-specific lead corrosion rate data to assess the effects of lead corrosion on gas generation and brine consumption in the WIPP repository.

The WIPP lead inventory includes lead shielding used in the RH shielded containers, and also includes lead waste. The lead shielding used as packaging material is reported for PA as packaging material lead. However, lead inventory associated with CH and RH waste is included with "other metals and alloys" (Van Soest 2018). Consequently, the sum of the waste "other metals and alloys" and the lead packaging materials inventory (Table 3-3) provides an upper bound for the total lead in the repository. In WIPP inventories prior to the CRA-2019, packaging material lead was a relatively unimportant contributor to the lead inventory. The packaging material lead for the CRA-2019 DPA increased due to changes in the estimated final form container types from RH canisters to shielded containers for some RH waste streams (DOE 2017, 2018). In the CRA-2019 DPA inventory, RH packaging lead represents about 93% of the upper-bound total lead inventory.

The mass of packaging lead and total "other metals and alloys" in the CRA-2019 DPA inventory equals 23% of the total iron-based metals inventory. The potential contribution of lead corrosion to repository gas generation rates has not been included in previous WIPP PAs based on the low expected lead inventory. Because of the large increase in the lead inventory, however, the

contribution of lead corrosion to gas generation rates can no longer be excluded solely on this basis. DOE (2019, Appendix SCR, FEPs W5 Container Material Inventory and W49 Gases from Metal Corrosion) stated that gas generation from lead corrosion is not included in the CRA-2019 DPA calculations based on an assessment by Kirkes (2019). Kirkes (2019) evaluated WIPP lead corrosion rate data (Roselle 2009, 2010, 2011a, 2011b, 2013a) and concluded that the data were inadequate for determining lead corrosion rates in the WIPP repository. Kirkes also stated that the lead corrosion rate data from Roselle (2013a) indicated likely lead surface passivation.

EPA (Peake 2020e, Comment CC5-SCR-9) observed that if the approach used to develop the inundated steel corrosion rate (Zeitler and Hansen 2015a) for the CRA-2014 is used to develop an inundated lead corrosion rate from the Roselle (2013a) data, 120 samples are available (119 positive rate measurements plus an additional value of 0 m/sec added to the data set). Statistics for these corrosion rates are provided in Table 3-4, which show that the measured rates for the 6- to 24-month experiments are comparable for iron and lead. The lead corrosion rate data for 0 and 350 ppm CO_2 are illustrated in Figure 3-2, which show that although rates decrease with time, positive lead corrosion rates continued to be measured after 24 months.

Table 3-4. Inundated Iron and Lead Corrosion Rate Measurements Statistics, 0 and 350 ppm CO_2 from Roselle (2013a)

Statistic	Steel Corrosion Rate 6- to 24-month data (m/s)[a]	Lead Corrosion Rate 6- to 24-month data (m/s)
Count[b]	125	120
Mean	6.76×10^{-15}	6.79×10^{-15}
Median	5.58×10^{-15}	5.59×10^{-15}
Standard Dev.	5.84×10^{-15}	5.24×10^{-15}
Maximum	3.96×10^{-14}	2.57×10^{-14}
Minimum[b]	0.00	0.00

a – Measured rate statistics from Zeitler and Hansen (2015a); these data were multiplied by a factor of two for the CRA-2019 DPA to account for the effects of high pressure (Section 3.1.2)

b – A value of 0.00 m/s was added to the lead and steel corrosion rate data sets to account for possible surface passivation

EPA requested that DOE perform additional calculations supporting the assertion that lead corrosion would be an insignificant contributor to gas generation in the WIPP repository (Peake 2020e, Comment CC5-SCR-9). EPA requested that DOE assess gas generation by lead corrosion under inundated conditions for time periods up to 10,000 years using the mean lead corrosion rate of 6.79×10^{-15} m/s (Table 3-4), the mass of RH packaging material lead in the CRA-2019 DPA inventory (Table 3-3), and the expected lead surface area per kg in the WIPP inventory and packaging materials. EPA requested a comparison of the results of these lead corrosion gas-generation calculations to equivalent calculations for inundated iron corrosion using the mean inundated steel corrosion rate, iron inventory, and iron surface area per kg used in the CRA-2019 DPA.

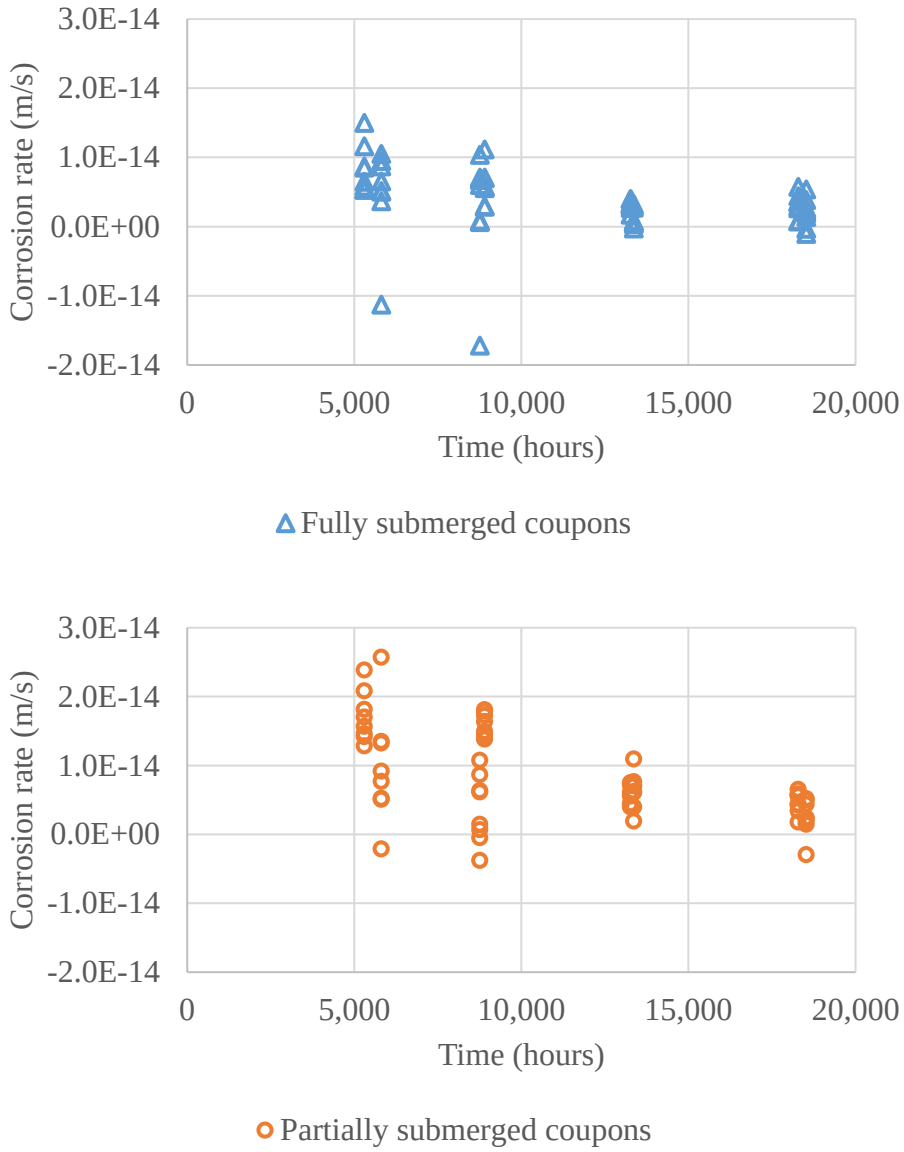

Figure 3-2. Lead Corrosion Rate Data Obtained with Fully Submerged and Partially Submerged Coupons (Roselle 2013a)

Knerr (2021c) calculated the lead gas generation rate using the mean lead corrosion rate. In these calculations, Knerr (2021c) included the conservative assumption that the double-walled steel shell that encases the lead liner in a shielded container assembly would not inhibit lead corrosion. Knerr (2021c) compared the gas generation rates from lead and steel corrosion and demonstrated that gas generation from lead corrosion will be a negligible fraction of overall gas generation rates. This result is caused by the higher mean corrosion rate of steel used in the CRA-2019 DPA (1.33×10^{-14} m/sec) compared to lead (6.79×10^{-15} m/sec), and the significantly higher steel surface area in the repository (4.91×10^{6} m^2) compared to the lead surface area (9.87×10^{4} m^2).

3.2.2 Corrosion of Aluminum and Other Metals

Anoxic corrosion of aluminum and other metals in WIPP waste could affect gas generation rates if the inventory of these metals is sufficiently large. The CRA-2019 DPA inventory of aluminum-based metals and alloys is higher than the CRA-2014 PA aluminum inventory (Table 3-3). However, because the iron inventory also increased, the CRA-2019 DPA aluminum inventory remains less than 1% of the iron-based metals inventory (Table 3-3) and aluminum corrosion remains unlikely to significantly affect repository gas generation rates. The CRA-2019 DPA inventory of "other metals and alloys" is less than the CRA-2014 PA inventory. Anoxic corrosion of these other metals, such as copper, are not expected to significantly affect repository gas generation rates because of their relatively small amounts in the inventory compared to iron-based metals and alloys (Table 3-3).

3.3 GALVANIC COUPLING

Galvanic coupling may affect metal corrosion rates under some circumstances. Galvanic coupling can occur if two metals come into contact in an aqueous electrolyte (such as WIPP brine) because different metals have different electrode potentials, and if in electrical contact, one of these metals may act as an anode, while the other metal acts as a cathode. Galvanic coupling can result in accelerated corrosion of the anodic metal, while the cathodic metal is relatively protected from corrosion. Galvanic coupling within the repository has been screened out from WIPP PAs based on the preponderance of iron over other metals in the repository (DOE 2019, Appendix SCR, FEP W50). However, the increased lead inventory for the CRA-2019 DPA may affect the validity of this screening argument. Publications since the CRA-2014 have indicated that iron oxides and hydroxides, such as those formed by anoxic corrosion in the WIPP repository, may cause galvanic corrosion of lead (Trueman and Gagnon 2016, Trueman et al. 2017).

EPA requested that DOE determine whether galvanic coupling between iron and lead in WIPP waste and packaging materials can continue to be screened out of WIPP PA despite the increased lead inventory in the CRA-2019 DPA (Peake 2020e, Comment CC5-SCR-8). EPA also asked that DOE provide additional information regarding the possible effects on the screening argument for FEP W50 Galvanic Coupling (within the repository) of reported galvanic corrosion of lead by iron oxides and hydroxides (Trueman and Gagnon 2016, Trueman et al. 2017).

In response, Knerr (2021c) observed that lead corrosion coupled with reduction of ferrous hydroxide would have little influence on gas generation rates because this reaction would not result in net gas production. Knerr (2021c) also observed that galvanic corrosion of lead caused by ferrous hydroxide has only been demonstrated under conditions likely in municipal water systems, which are quite different from WIPP repository conditions.

There is currently no evidence that galvanic corrosion will be a significant process in the WIPP repository. However, the current screening argument for FEP W50 Galvanic Coupling (within the repository) relies on the preponderance of iron in the inventory, and does not address the much larger lead inventory introduced in CRA-2019 by increased use of shielded containers. It is also unclear from site-specific lead corrosion experiments that lead surfaces will be passivated in

the repository. EPA expects that the screening argument for this FEP will be updated for future WIPP PAs.

3.4 MICROBIAL GAS GENERATION

Cellulosics, plastics, and rubber are present in WIPP waste and in waste emplacement and packaging materials. Microbial gas generation in the WIPP repository can occur because microbes are likely to be naturally present at the repository horizon or introduced with the waste. As these microbes utilize CPR materials as a carbon source, production of CO_2 could acidify repository brines or increase the solubility of actinides by carbonate complexation. To control chemical conditions and limit the possible effects of acidic conditions and carbonate complexation on actinide solubilities, MgO backfill is included in the repository to react with CO_2 and maintain mildly alkaline conditions with low CO_2 fugacity consistent with relatively low actinide solubilities (Section 4.0).

3.4.1 CCA PA, PAVT, and CRA-2004 PA Microbial Gas Generation

The CCA-PA, PAVT, and CRA-2004 PA conceptual model for gas generation included the assumption that microbial degradation of CPR may occur in the repository and produce methane [CH_4(g)] and CO_2(g). The major pathways for microbial degradation of CPR are predicted to include the following reactions:

$$C_6H_{10}O_5 + 4.8\ H^+ + 4.8\ NO_3^- \rightarrow 7.4\ H_2O(l) + 6\ CO_2(g) + 2.4\ N_2(g) \quad \textbf{(11)}$$

$$C_6H_{10}O_5 + 6\ H^+ + 3\ SO_4^{2-} \rightarrow 5\ H_2O(l) + 6\ CO_2(g) + 3\ H_2S(g) \quad \textbf{(12)}$$

$$C_6H_{10}O_5 + H_2O(l) \rightarrow 3\ CH_4(g) + 3\ CO_2(g) \quad \textbf{(13)}$$

where $C_6H_{10}O_5$ is the chemical formula for cellulose monomer. In reactions (11) and (12), one mole of CO_2 is produced for each mole of organic carbon consumed. However, reaction (13) produces only 0.5 moles of CO_2 per mole of organic carbon consumed. Reactions (11) to (13) are predicted to proceed sequentially according to the energy yield of the reactions (Wang and Brush 1996). As the denitrification and sulfate-reduction reactions [reactions (11) and (12), respectively] proceed, DOE predicted that they would consume the limited amounts of nitrate [NO_3^-] and sulfate [SO_4^{2-}] in the WIPP waste inventory and produce limited quantities of nitrogen [N_2(g)] and hydrogen sulfide [H_2S(g)]. In both the CCA and the CRA-2004, DOE predicted that the methanogenesis reaction (13) would be the dominant reaction pathway and, consequently, that approximately half of the CPR carbon consumed would be converted to CO_2 and the other half converting to CH_4(g) (DOE 1996, Appendix SOTERM; DOE 2004, Appendix PA, Attachment SOTERM).

DOE assumed that microbial consumption of CPR could be limited by the long-term viability of microbes in the repository, and uncertainty associated with whether microbes would consume plastics and rubbers was also considered important in development of the conceptual model. DOE's conceptual model also assumed that the rate of microbial gas generation was dependent on brine saturation (DOE 2004, Appendix PA, Attachment MASS). DOE assumed that MgO backfill will remove CO_2 from the repository brines and gas phase, so CO_2 generated from CPR

degradation will not significantly affect repository gas pressures. The effects of CPR degradation on the amount of brine in the repository were considered uncertain, so these effects were not accounted for in PA. DOE also assumed that gas generation would take place homogeneously throughout the repository, because of the assumed homogeneous distribution of waste.

DOE assumed that microbial gas production would occur at a rate dependent on the availability of brine. DOE assumed significant microbial gas production would not occur in 50% of the realizations for the CCA PA, CCA PAVT, and CRA-2004 PA because of uncertainties associated with microbial processes. In the other half of the PA realizations, DOE assumed that significant microbial consumption of CPR occurred, with an equal likelihood of the microbial consumption of only cellulosics (25% of all realizations) or of all CPR materials (25% of all realizations), including plastics and rubber (DOE 2004).

The ranges of microbial gas generation rates used for the CCA PA, the CCA PAVT, and the CRA-2004 PA (Tables 3-5 and 3-6) were determined using initial results from inundated and humid condition microbial degradation experiments with cellulose (Francis and Gillow 1994; Wang and Brush 1996; DOE 2004, Appendix PA, Attachment PAR). A gas generation rate was calculated in BRAGFLO from the humid and inundated rates based on the effective liquid saturation (DOE 2004). DOE assumes that gas generation rates for plastics and rubber are equal to the rate for cellulose; the larger average carbon content by weight for plastics is accounted for by multiplying the mass of plastics by a factor of 1.7 for calculation of the gas generation rate (Wang and Brush 1996).

Table 3-5. Inundated Microbial Gas Generation Rates (WAS_AREA:GRATMICI)

Performance Assessment	Maximum	Mean	Minimum	Reference
CCA/PAVT and CRA-2004 PA	9.51×10^{-9}	4.60×10^{-9}	3.17×10^{-10}	DOE (1996), DOE (2004)
PABC04, CRA-2009 PA, PABC09, CRA-2014 PA, and CRA-2019 DPA	5.57×10^{-10}	2.94×10^{-10}	3.08×10^{-11}	Nemer et al. (2005), Fox (2008), Kicker and Herrick (2013), Kim and Feng (2019)

Units of moles CO_2/kg cellulose/sec

Table 3-6. Humid Microbial Gas Generation Rates (WAS_AREA:GRATMICH)

Performance Assessment	Maximum	Mean	Minimum	Reference
CCA/PAVT and CRA-2004 PA	1.27×10^{-9}	6.35×10^{-10}	0.00	DOE (1996), DOE (2004)
PABC04, CRA-2009 PA, PABC09, CRA-2014 PA, and CRA-2019 DPA	1.03×10^{-9}	5.14×10^{-10}	0.00	Nemer et al. (2005), Fox (2008), Kicker and Herrick (2013), Kim and Feng (2019)

Units of moles CO_2/kg cellulose/sec

EPA (1998c) reviewed microbial gas generation during its evaluation of the CCA. In its review, EPA noted the uncertainties associated with whether microbial communities capable of degrading CPR would be present in the hypersaline WIPP environment, and numerous factors that may limit microbial gas generation, including the concentrations of nutrient and toxic

compounds and limitations imposed by temperature, salinity, Eh, pH, and the availability of electron acceptors. EPA observed that it is generally difficult to estimate the rate and extent of slow processes, such as CPR degradation, over long periods by extrapolating the results of short-term studies. Based on the available evidence, EPA concluded that DOE's approach to addressing the probability of significant microbial gas generation was an adequately conservative overestimate, and that addition of MgO backfill to the WIPP repository made CO_2 production unlikely to be of significant concern (EPA 1998c).

3.4.2 Microbial Gas Generation Evaluation during AMWTF Review

At the time of the CCA PA, DOE assumed that all carbon in CPR could potentially be converted to CO_2 and used this assumption to calculate the amount of MgO required in the backfill. By the time of the AMWTF review, Gillow and Francis (2003) observed methanogenesis in some of the microbial degradation experiments. DOE stated that methane generation in the experiments demonstrated that methanogenesis will occur in the WIPP repository environment if microbial degradation of CPR occurs. DOE also assumed that only limited amounts of CPR degradation will take place through denitrification and sulfate reduction [reactions (11) and (12)] because of the relatively small amounts of nitrate and sulfate in the waste (Hansen et al. 2003a and 2003b). DOE stated that after sulfate and nitrate inventories in the waste are consumed, CPR degradation will either cease or will proceed through methanogenesis [reaction (13)]. Because methanogenesis produces only 0.5 moles of CO_2 for each mole of CPR carbon, CPR degradation through methanogenesis would significantly reduce the amount of CO_2 that could be produced and the amount of MgO needed to maintain the required chemical conditions in the repository.

TEA (2004) reviewed the information DOE provided (Hansen et al. 2003a and 2003b; Kanney et al. 2004), and concluded that DOE's consideration of the sulfate available for CPR degradation by sulfate reduction did not adequately account for sulfate in the brine and sulfate-bearing minerals in the Salado Formation. EPA considered the available information and the uncertainty associated with possible microbial processes in the repository, and directed DOE to continue calculating required quantities of MgO backfill by assuming all CPR carbon could be converted to CO_2 unless new and convincing evidence became available demonstrating that methanogenesis would occur in the WIPP repository (Cotsworth 2004a, Marcinowski 2004).

3.4.3 PABC04 Microbial Gas Generation

For the CRA-2004 PA, DOE did not change the CCA PA and PAVT microbial Gas Generation conceptual model assumptions or the sampled humid or inundated microbial gas generation rates (DOE 2004, Appendix PA, Attachment SOTERM). EPA's review of the CRA-2004 PA included an evaluation of additional experimental data related to microbial gas generation rates and reaction products (EPA 2006c). These data included results from WIPP-specific experiments that continued after approval of the CCA (Francis et al. 1997; Francis and Gillow 2000; Gillow and Francis 2001a, 2001b, 2002a, 2002b, and 2003), as well as additional experiments carried out under WIPP-relevant conditions (Felicione et al. 2001). The data review assessed both microbial degradation probabilities and gas generation rates.

3.4.3.1 Microbial Degradation Probabilities

EPA requested additional information from DOE regarding microbial degradation probabilities (Cotsworth 2004b). EPA (2006c) evaluated the DOE response to this request and determined that information developed since the CCA indicated an increased probability that microorganisms will be present in the repository when it is filled and sealed, that there is insufficient evidence that MgO will prevent microbial activity in the WIPP environment, that some new evidence was available making long-term viability of microbes appear more probable than at the time of the CCA, and that the amount of nutrients, specifically phosphate, in the inventory had increased, making the microbial degradation of cellulosics in the repository appear more likely.

DOE evaluated the potential effects of a higher probability of significant microbial CPR degradation on microbial gas generation rates by comparing releases through the Culebra, DBRs, spallings releases, and total releases for CRA-2004 PA realizations with and without microbial activity (Detwiler 2004b). Higher releases were observed in microbial realizations for DBRs and for spallings releases. However, total releases were only slightly higher for microbial realizations than non-microbial realizations, because of the importance of cuttings and cavings[3] to total releases, and cuttings and cavings should not be significantly affected by microbial activity (Detwiler 2004b).

EPA (2006c) concluded that information developed since the CCA indicated that microbial degradation of cellulosic materials may be more likely than previously assumed and that this higher probability would be likely to increase calculated releases from the repository. Results from DOE's experiments indicated that rubber materials may be microbially degraded in the WIPP repository environment. On the other hand, no evidence was found in the DOE experiments of microbial degradation of polyethylene or PVC performed for up to 8.4 years (Gillow and Francis 2003). EPA (2006c) concluded that the probability of significant microbial degradation of cellulosic materials should be higher than assumed for the CCA PA, PAVT, and the CRA-2004 PA, and directed DOE to assume that microbial degradation of cellulosics would occur in all realizations (Cotsworth 2005). Because only limited degradation of rubber materials was observed and no degradation of plastics was observed, there was no evidence that the probabilities of plastics or rubber degradation assumed for the CCA PA and PAVT should be revised.

The parameter WAS_AREA:PROBDEG is sampled within BRAGFLO to indicate whether microbial gas generation occurs from plastic and rubber degradation (Nemer 2005). DOE updated this parameter for the PABC04 to reflect the increased probability (0.75) of microbial degradation of only cellulosics materials, and the unchanged probability (0.25) of microbial degradation of all CPR materials. EPA (2006b) found that these changes to WAS_AREA:PROBDEG are consistent with the available data and were an adequate response to EPA's request that significant microbial degradation should be assumed to occur in all PABC04 realizations.

[3] Cuttings are solids that are cut from the borehole by the drill and brought to the surface; cavings are solids that fall from the wall of the borehole

3.4.3.2 Microbial Gas Generation Rates

Wang et al. (2003) recalculated inundated and humid microbial gas generation rates using lower, longer-term CO_2 generation rates from the WIPP-specific experiments that continued after the CCA PA and PAVT. Although Wang et al. (2003) stated that these lower rates were more representative of rates likely to occur in the WIPP repository, DOE used the higher CCA PA and PAVT microbial gas generation rates in the CRA-2004 PA.

Because of the higher probability assumed for microbial degradation in the PABC04, DOE revised the microbial gas generation rates to account for rate data that had become available since the CCA PA and PAVT (Nemer et al. 2005). DOE used a two-step process to simulate microbial gas production rates in the WIPP repository for the PABC04 (Nemer et al. 2005). The initially rapid rates of microbial gas production were simulated by increasing the initial pressure in the BRAGFLO input file. This increased initial repository gas pressure was combined with the use of lower gas generation rates determined from long-term experimental data.

Nemer et al. (2005) described the derivation of the microbial gas generation rates used in the PABC04. The microbial gas generation data were obtained from experiments summarized by Francis et al. (1997) and Gillow and Francis (2002a, 2003). The microbial production of CO_2 as a function of time in these experiments took place at relatively high rates at the beginning of the experiments, but CO_2 production typically slowed after about 1.5 years. The causes of these slowing rates are uncertain, but this type of bacterial growth curve is commonly encountered because of limitations on resources, such as nutrients or readily degradable substrate, or because of increasing concentrations of metabolites. The microbial gas generation rates were modeled by obtaining a least-squares fit of two linear functions to the reported mean values for the CO_2 gas generation data. In this manner, both a short-term and a long-term rate were determined for each experimental dataset. A minimum of three data points was included in each short-term or long-term fit to the data. The best fit was determined by choosing the result with the smallest residual between the observed and fitted values of CO_2 produced as a function of time (Nemer et al. 2005). Nemer et al. (2005) used the 95% upper confidence limit and 95% lower confidence limit about the mean slope values to determine the maximum and minimum possible rates for inundated and humid conditions (Tables 3-5 and 3-6). EPA (2006b) reviewed the derivation of the humid and inundated microbial gas generation rates and found that they were reasonable and adequately supported by the available experimental data.

3.4.3.3 PABC04 Implementation of Microbial Gas Generation Rates

Nemer and Stein (2005) described the implementation of the revised microbial gas generation rates in BRAGFLO for the PABC04. The two zero-order microbial gas generation rates for humid (WAS_AREA:GRATMICH) and inundated (WAS_AREA:GRATMICI) conditions were determined as described by Nemer et al. (2005), with units converted to those used by BRAGFLO (moles C/kg cellulose/sec) and accounting for the dissolution of CO_2 in water for the inundated rates. The rates used in the different PAs are compared in Tables 3-5 and 3-6. The revised inundated long-term microbial gas generation rate used in the PABC04 and subsequent PA calculations is more than an order of magnitude lower than the previous rate. The revised humid long-term microbial gas generation rate is only slightly lower than the previous humid rate.

Because DOE believed the humid rate should be lower than the inundated rate, the sampled humid and inundated rates were compared within BRAGFLO for the PABC04. If the sampled humid rate exceeded the sampled inundated rate, the humid rate was set equal to the inundated rate. Stein and Nemer (2005) did not provide information on the likely effects of assuming that the humid rate would always be lower than the inundated rate. However, because the maximum inundated and humid rates differ by only about a factor of two (Tables 3-5 and 3-6), it is likely that the humid rates used in BRAGFLO were not significantly reduced by this assumption.

The revised microbial gas generation rates were based on long-term experimental data. Therefore, gas generation during the early stages of the repository was accounted for in BRAGFLO for the PABC04 by assuming a fixed amount of gas was present in the repository at the beginning of the calculations (Nemer et al. 2005). Nemer et al. (2005, Appendix B) provides a detailed description of the calculation of the initial pressure in the repository from short-term microbial gas generation. The initial repository gas pressure is a function of the CPR inventory, the short-term gas generation rate, and the volume of the repository, which is calculated from the excavated storage volume of the repository (4.38×10^5 m^3, parameter REFCON:VREPOS) and the effective porosity of the waste-filled repository (0.848, parameter WAS_AREA:POROSITY). The initial gas pressure calculated by Nemer et al. (2005) was 128.039 kPa (Table 3-7).

Table 3-7. CPR Inventories and Initial Gas Pressures

Inventory	Total Cellulose Equivalent (kg)[a]	Initial Gas (moles)	Initial Pressure (kPa)
CRA-2004 PA (Nemer et al. 2005)	28,875,700	1.069×10^9	128.0
PABC04 (Leigh et al 2005)	32,454,720	1.201×10^9	131.9
PABC09 (Crawford et al. 2009)	28,873,157	1.063×10^9	128.5
CRA-2014 (Van Soest 2012)	22,076,080	8.169×10^8	122.1
CRA-2019 (Van Soest 2018)	25,173,170	9.315×10^8	125.0

a –total cellulose equivalent (kg) = cellulose (kg) + (1.7 × plastics (kg)) + rubber (kg) (Wang and Brush 1996)

At EPA's direction, DOE changed the probability of microbial degradation to account for new evidence regarding the presence and viability of microbes capable of degrading CPR in the WIPP repository. The revised probability parameters resulted in microbial gas generation in all realizations for the PABC04 (Section 3.4.3.1). However, DOE asserted that uncertainties remained regarding the viability of microbes in the repository, because of different conditions in the repository compared to the conditions in the experiments (Nemer et al. 2005). DOE therefore introduced an additional sampled parameter, WAS_AREA:BIOGENFC. This parameter, which has a uniform distribution from 0 to 1, was multiplied by the sampled humid and inundated microbial gas generation rates to reduce the rates from the experimentally determined long-term rates. EPA (2006b) concluded that because of the inherent uncertainties associated with extrapolating experimentally measured microbial gas generation rates to repository conditions, it was reasonable to add an uncertainty factor to these rates.

DOE reported that implementation of lower long-term microbial gas generation rates reduced both the rate of pressurization and the pressure in the undisturbed repository (Nemer et al. 2005,

Leigh et al. 2005). This implementation also resulted in slightly higher brine saturation for the undisturbed repository. For the disturbed repository, pressures are relatively unchanged by the different microbial gas generation rates, but the brine saturation is higher using the lower long-term rates. Higher brine saturation may lead to increased flow up the borehole and DBR of radionuclides. Therefore, lower microbial gas generation rates may have had some previously unanticipated effects, in that the likelihood of DBR of radionuclides was increased. However, the frequency and volume of spallings releases were decreased in the PABC04 compared to the CRA-2004 PA because of lower gas pressures (Leigh et al. 2005).

DOE's implementation of an initially rapid microbial gas generation rate, followed by slower long-term rates, is more likely to be representative of future repository conditions. Assuming a rapid initial rate followed by slower long-term rates is more consistent with the experimental data and with general patterns of microbial processes. A consequence of this change is likely to be longer persistence of microbial gas-generating processes and higher brine saturations in both the disturbed and undisturbed repository scenarios.

3.4.4 Microbial Gas Generation Review for MgO Planned Change Request

At DOE's request, an expert panel was convened by the Institute for Regulatory Science (RSI) to consider issues associated with the MgO backfill and microbial degradation of CPR in the WIPP repository (RSI 2006). The expert panel recommended that an expert elicitation panel be formed to determine the likely extent of degradation of CPR materials and to determine if the amounts of MgO currently placed in the repository could be safely reduced. To address the potential need for an expert elicitation panel related to gas generation from CPR, EPA carried out a review to identify technical questions and uncertainties related to gas generation from CPR degradation (SC&A 2006). This review included the potential CO_2-generating microbial degradation reactions that could occur within the repository and the extent to which these reactions could occur.

SC&A (2006) performed a review of WIPP-specific data and a survey of the scientific literature regarding gas generation from CPR degradation under WIPP repository conditions. SC&A (2006) concluded that uncertainties in CPR inventories in the WIPP should be addressed before changes in the MgO backfill engineered barrier were made. SC&A (2006) evaluated the potential effects of radiolysis, and found that additional information should be obtained related to the radiolytic degradation of CPR, along with the potential interactions of radiolytic and microbial processes. SC&A (2006) concluded that cellulosics could potentially be completely degraded in the repository environment over the 10,000-year regulatory period, but that more investigation of radiolytic and microbial degradation of plastics and rubber would be required to assess likely extents of degradation of these materials.

EPA regulations require that expert judgment should not be substituted for available experimental data or data that could be obtained from a reasonable set of experiments (40 CFR 194.26). The results of the review by EPA (SC&A 2006) indicated that literature data were available that might reduce the uncertainties associated with the extent of CPR degradation in the WIPP repository and improve understanding of WIPP's future performance. SC&A (2006) concluded that the use of expert judgment to assess the likely extent of CPR degradation in the

WIPP repository would require further justification from DOE that included an in-depth analysis of the available data.

3.4.5 Microbial Gas Generation for the CRA-2009 PA and PABC09

No changes were made to the implementation of microbial gas generation or to microbial gas generation rate parameters for the PABC09 from the PABC04. DOE assumed that the initial gas pressure in the repository resulting from the short-term, rapid microbial degradation of CPR was equal to the pressure of 128.039 kPa calculated for the PABC04 (Nemer and Clayton 2008). This initial pressure is very close to the value calculated from the PABC09 inventory (Table 3-7), and is not expected to significantly affect repository pressures. The long-term rates used in the CRA-2009 PA were the same as the rates used in the PABC04 (Tables 3-5 and 3-6).

The sampled humid and inundated rates were compared within BRAGFLO for the PABC04. If the sampled humid rate exceeded the sampled inundated rate, the humid rate was set equal to the inundated rate. For the CRA-2009 PA, DOE determined that changing the higher sampled humid rate to equal the inundated rate introduced a small error into the sensitivity analysis, because the regression analysis was based on the sampled values rather than the lower conditional values for the humid rate. Consequently, DOE applied a conditional relationship for the CRA-2009 and later PAs, so that the sampled inundated rate is used as the maximum value for humid rate sampling (DOE 2009, Kirchner 2008). The effects of this change on predicted repository performance are small.

DOE (2009) attributed slower changes in repository pressure after 2,000 years to cessation of room closure, slowing of brine inflow and consumption of CPR. To understand whether complete consumption of CPR contributes to slower changes in repository pressure after 2,000 years, EPA requested that DOE provide information regarding whether the slower rates of microbial degradation assumed for the CRA-2009 resulted in the persistence of CPR in the PA realizations (Cotsworth 2009a). The response from DOE (Moody 2009a) showed that for most CRA-2009 PA realizations, 70% or more of the initial CPR remained in the undisturbed repository at the end of the 10,000-year period of performance. Nemer and Clayton (2008, Figures 6-65 and 6-66) illustrated the fraction of cellulosics remaining versus time for all realizations in Replicate R1, Scenarios S2 and S4, which are disturbed repository scenarios. These figures show that, in the vast majority of disturbed realizations, undegraded CPR also remained at the end of the 10,000-year period of performance. The persistence of CPR in the repository under most conditions is a reasonable result, because of the likely resistance to rapid microbial degradation of plastics and rubber and potential limitations on the amounts of brine in the repository.

During review of the CRA-2009 PA, EPA requested additional information from DOE regarding whether it was reasonable to assume that plastic and rubber degradation, in the 25% of realizations where it occurred, will take place at the same rate as cellulose degradation when normalized to the assumed carbon content of the CPR (Cotsworth 2009a). EPA noted that this assumption may no longer be appropriate, based on WIPP-specific experimental results showing essentially no plastic degradation and limited degradation of rubber over periods of up to 8.4 years (Gillow and Francis 2003), evaluations of literature data regarding plastics and rubber degradation process that have become available since the PABC04 (SC&A 2006), and evidence

from the PABC04 that lower microbial gas generation rates resulted in a slight increase in releases. EPA accordingly requested that DOE consider the possible effects on PA of lower microbial gas generation rates from plastics and rubber degradation.

DOE noted in its response that there is a high level of uncertainty regarding the rates of degradation of plastics and rubber over the 10,000-year repository period of performance (Moody 2009a). DOE explained that this uncertainty is addressed in PA by only modeling significant degradation of plastics and rubber in 25% of the realizations, and by using a lower bound of zero for the sampled microbial degradation rate range. DOE stated that the effects on releases for lower microbial degradation rates implemented for the PABC04 were not calculated, and that Nemer and Stein (2005) showed very little difference between the CRA-2004 PA and PABC04 intermediate results. DOE stated that it did not believe that reduction in gas generation rates increases releases. DOE also noted that reducing the rates of plastic and rubber degradation would likely have only minor effects on the gas volumes generated, because on average, gas generation rates from iron corrosion are three times greater than from CPR degradation, and plastics and rubber degradation is modeled to occur in only 25% of the realizations.

DOE's conclusions regarding the lack of effect of lower microbial gas generation rates differ from the conclusions drawn by EPA (2006b) during review of the PABC04. Higher releases were calculated at low probability for the PABC04 than for the CCA PAVT, which EPA (2006b) found were caused by increased DBRs. EPA (2006b) believed these higher DBRs were primarily due to higher brine saturations resulting from lower microbial gas generation rates, and to changes in the PABC04 that increased actinide solubilities. Although DOE and EPA appear to have reached different conclusions regarding potential effects on releases of lower gas generation rates from microbial degradation of plastic and rubber in the WIPP inventory, comparison of the results of the CCA PAVT and PABC04 shows that large decreases in microbial gas generation rates had relatively small effects on repository releases and only at low probabilities. Consequently, although the relatively high microbial gas generation rates used for plastic and rubber in the CRA-2009 PA may not be consistent with the available data, it is likely that reducing these rates would have insignificant effects on repository releases. Consequently, the assumption that microbial gas generation from plastic and rubber degradation will occur at the same rate as from cellulosics degradation remains adequate for the purposes of the PA.

3.4.6 Microbial Gas Generation for the CRA-2014 PA and CRA-2019 DPA

Implementation of microbial gas generation and microbial gas generation rate parameters remained unchanged for the CRA-2014 PA and CRA-2019 DPA. The initial gas pressure was 128.039 kPa, which is only slightly higher than the pressures calculated using the CRA-2014 PA and CRA-2019 DPA inventories (Table 3-7). DOE has not analyzed the sensitivity of the PA results to the initial gas pressure in the repository, but because the pressure difference is small, it is reasonable to assume that its effects on releases will also be small.

3.4.7 PA Implementation of Microbial Gas Generation

The microbial gas generation rate is calculated using the following equation (DOE 2019, Appendix GEOCHEM-2.2):

$$q_{rgm} = (R_{mi}\, S_{b,eff} + R_{mh} S^{*}_{g})\, D_c\, X_m\, (H_2 \mid C)\, M_{H2}\, B_{fc} \quad \textbf{(14)}$$

Where:

q_{rgm} is the rate of microbial gas production per unit volume of waste ($kg/m^3/sec$);

R_{mi} is the rate of CO_2 production from cellulose biodegradation under inundated conditions (parameter WAS_AREA:GRATMICI, moles C consumed/kg $C_6H_{10}O_5$/sec);

R_{mh} is the rate of CO_2 production from biodegradation under humid conditions (parameter WAS_AREA:GRATMICH, moles C consumed/kg $C_6H_{10}O_5$/sec);

$S_{b,eff}$ is the effective brine saturation due to capillary action in the waste materials;

S^{*}_{g} equals 1 - $S_{b,eff}$ if $S_{b,eff} > 0$, or equals 0 if $S_{b,eff} = 0$;

D_c is the mass concentration of cellulosics in the repository (kg biodegradable material/m^3 disposal volume);

$X_m(H_2 \mid C)$ is the average stoichiometric factor for microbial gas generation of cellulose, i.e., moles of H_2 generated per mole of carbon consumed by microbial action (moles H_2/mole C);

M_{H2} is the molecular weight of H_2 (parameter REFCON:MW_H2, kg H_2 per mole H_2); and

B_{fc} is the variable representing uncertainty related to long-term microbial degradation of CPR (parameter WAS_AREA:BIOGENFC).

The variable D_c is calculated from the initial CPR inventory, with the inventory mass of plastics increased by a factor of 1.7 to account for the higher average carbon concentration per kg of plastic (Wang and Brush 1996). The modeled microbial gas generation rate is zero-order with respect to the mass of CPR, meaning that the rate does not change as CPR is degraded.

DOE (2019, Appendix GEOCHEM) stated that the parameter WAS_AREA:BIOGENFC would be set equal to 1 for the CRA-2019 DPA. EPA noted in a comment to DOE (Peake 2020a, Comment CC1-GEOCHEM-2) that DOE (2019, Appendix PA-2019) stated that WAS_AREA:BIOGENFC is uniformly sampled from 0 to 1. In addition, Kim and Feng (2019, Tables 1 and 4) listed WAS_AREA:BIOGENFC as an LHS sampled parameter for the CRA-2019. DOE acknowledged this editorial error and confirmed that this parameter was appropriately sampled for the CRA-2019 DPA (Sosson 2020a).

3.5 EFFECTS OF CHEMICALLY INCOMPATIBLE MATERIALS ON GAS GENERATION

On February 14, 2014, an incident occurred in the WIPP underground that released radioactive material (Wilson et al. 2015). This release was caused by incompatibility of chemicals within a waste drum (Drum 68660) that led to a thermal runaway reaction, buildup of gases within the drum, displacement of the drum lid, and venting of radioactive materials. During review of the CRA-2014, EPA requested additional information about the chemically incompatible materials in WIPP waste streams, including the potential effects of these materials on gas generation

(Edwards 2014). DOE performed bounding calculations that demonstrated that gas generation by chemical incompatibilities in the affected waste streams are unlikely to significantly affect PA results.

DOE (2020b) has established new waste characterization activities and process enhancements in response to the 2014 radiological release event. This response included increased consideration of possible chemical combinations in each waste stream and evaluation of potential adverse chemical reactions. DOE now includes formal documentation of a chemical compatibility evaluation for each waste stream or waste stream sub-population. Evaluations that identify potential chemical incompatibility are the basis for placing an administrative hold on the waste stream. EPA agrees that these efforts by DOE are likely to decrease the inadvertent acceptance of waste with chemically incompatible materials that result in an uncontrolled release of gas in the repository.

3.6 RADIOLYTIC GAS GENERATION

Radionuclides in WIPP waste will emit alpha, beta, and gamma radiation. Irradiation of water adsorbed on waste in unsaturated regions of the repository, brine, CPR, and other waste may consume water from brine and produce gases and dissolved species that affect repository conditions. DOE's evaluation of these radiolytic gas generation processes is addressed in this section. Alpha radiolysis is potentially important because of the concentrations of alpha-emitting radionuclides in the TRU waste, such as plutonium. Gamma radiolysis is less likely to be important because CH waste, which constitutes a large volume fraction of the waste inventory, is limited to a 200 mrem per hour payload surface dose rate.

The Gas Generation conceptual model developed for the CCA included the assumption that radiolysis of water in the waste and brine and of CPR in the waste will not have significant effects on gas generation rates or quantities (SC&A 2008b). In its initial evaluation of the Gas Generation conceptual model, the CCA Peer Review Panel found that possible radiolytic $H_2(g)$ and $O_2(g)$ generation from wetted and dissolved actinides and gas generation from radiolysis of CPR had not been adequately evaluated (Wilson et al. 1996a). DOE supplied additional information about radiolytic gas generation in the CCA (DOE 1996, Appendix SCR). In DOE's CCA analysis, brine radiolysis occurred only from dissolved and colloidal radionuclides, and this radiolytic gas generation rate was determined to be small relative to gas generation rates from microbial degradation and anoxic corrosion of steel. DOE's calculations also demonstrated that gas generation through brine radiolysis would not significantly affect repository releases. DOE evaluated gas generation rates from CPR radiolysis in WIPP-specific experiments (Molecke 1979) and found that these rates were much less than gas generation rates from microbial degradation and anoxic corrosion of steel. The Peer Review Panel accepted DOE's conclusion that radiolysis would not be an important source of gas generation in WIPP (Wilson et al. 1996b).

EPA (SC&A 2006) reviewed WIPP-specific data and literature data regarding radiolytic gas generation from CPR. SC&A (2006) concluded that radiolytic gas production would occur in the WIPP repository, but also concluded that whether it would significantly affect repository performance was uncertain. During review of the CRA-2014, EPA (2017d) noted that microbial and anoxic corrosion gas generation rates had decreased since the CCA, so it was no longer

certain that radiolytic gas generation will be insignificant. EPA (2017d) recommended that DOE reexamine the potential importance of brine and waste radiolysis to WIPP gas generation rates.

Kicker (2019b) identified ^{241}Am, ^{238}Pu, ^{239}Pu, ^{240}Pu, and ^{242}Pu as the radionuclides in the CRA-2019 DPA inventory that represent greater than 96% of the radionuclide inventory that would contribute to radiolysis. The inventories of these five radionuclides increased significantly between the CRA-2014 and CRA-2019, mostly because surplus plutonium waste stream SR-KAC-PuOx was added to the inventory (Van Soest 2018). The increased radionuclide inventory combined with decreased microbial degradation and anoxic corrosion rates since the CCA prompted DOE to re-evaluate the importance of radiolytic gas generation and brine consumption for the CRA-2019.

DOE re-assessed the potential effects of radiolysis of brine and of CPR for the CRA-2019 DPA (Day 2019b). Day (2019b) considered the effects of alpha radiolysis of brine by dissolved, colloidal, and wetted radionuclide solids. Based on the results of this evaluation, DOE found that gas generation by alpha radiolysis of brine was potentially important to repository performance and added alpha radiolysis of brine to the CRA-2019 DPA gas generation calculations (DOE 2019, Appendix SCR-6.5.1.6, FEP W52). DOE (2019) did not include gas generation caused by CPR radiolysis in the CRA-2019 DPA calculations on the basis of low consequence (DOE 2019, Appendix SCR-6.5.1.7, FEP W53). DOE (2019) did not address radiolytic gas generation from other wastes, such as cements, hydrated minerals in waste soils, or solidified organic wastes, and did not address gas generation by radiolysis of water adsorbed on wastes under unsaturated conditions.

EPA reviewed DOE's CRA-2019 DPA implementation of gas generation and brine consumption by alpha radiolysis of brine by wetted radionuclide solids and dissolved and colloidal radionuclides. As summarized below, EPA also reviewed other radiolytic gas generation and brine consumption processes that were not included in the CRA-2019 DPA to determine whether DOE (2019) adequately justified omission of these processes.

3.6.1 Brine Radiolysis

Alpha radiolysis of chloride brines produces gases [H_2(g), O_2(g), and Cl_2(g)] and oxidizing ionic species such as chlorate [ClO_3^-], hypochlorite [ClO^-], and chlorite [ClO_2^-] (Jenks 1972, Kelm et al. 1999). The oxidizing ionic species and O_2(g) are expected to rapidly react with metallic iron or other reductants in the repository (Day 2019b). Consequently, it is expected that only radiolytic H_2(g) production has the potential to significantly affect repository conditions.

The rates at which brine radiolysis will produce gas or consume brine depend on:

- The quantities of various radionuclides in the waste inventory,
- The disintegration energies of the radionuclides,
- The amounts of chemical species consumed or produced per unit energy, and
- For alpha radiation, the fraction of radiation that is not self-attenuated.

Day (2019b) obtained the disintegration energies from Eckerman and Endo (2008) for the radionuclides identified in Kicker (2019b) (^{241}Am, ^{238}Pu, ^{239}Pu, ^{240}Pu, and ^{242}Pu). These ranged

from 4.99 MeV for ^{242}Pu to 5.64 MeV for ^{241}Am. The radionuclide disintegration energies were included in the CRA-2019 DPA as new parameters for each of the five radionuclides (e.g., AM241:DECAYNRG).

The amounts of chemical species consumed or produced by radiolysis per unit energy are represented by G values, which are the number of molecules of reactant consumed or product formed per 100 eV of energy absorbed. G values are influenced by the type of radiation (alpha, beta, or gamma) and the linear energy transfer (LET), which is the energy loss per unit length of an ionizing particle traveling through a material (Anderson et al. 2000). G values are also affected by factors such as the material composition, environmental factors such as temperature and pH, the absorbed dose, and the dose rate. EPA reviewed the available data regarding the rate of H_2(g) production by alpha radiolysis of chloride brines to assess the defensibility of the G value used in the CRA-2019 DPA.

Reported G values for H_2(g) production by alpha radiolysis of chloride brines are listed in Table 3-8. Reed et al. (1993) carried out radiolysis experiments with WIPP brines and reported the results of individual experiments and a summary table with "best values." Reed et al. (1993) did not explain the basis for selection of these values, although the values are near the higher end of the measured ranges. Day (2019b) used a G value of 1.4 molecules/100 eV to model radiolytic H_2(g) production by alpha radiolysis of WIPP brines (parameter GLOBAL:GH2AVG). This parameter value is at the high end of the range reported for Salado brines by Reed et al. (1993) and is above the range of values measured for the Castile brine (Table 3-8). Day (2019b) did not explain the selection of this G value compared to using sampled values from the reported range in WIPP brines and did not address the likely effects of a higher radiolytic H_2(g) production rate on releases from the repository. Selection of a relatively high G value may not be conservative. Although a high G value can increase gas production and may yield higher pressures, which could increase spallings releases, a larger G value also increases brine consumption, which could decrease DBRs. Consequently, EPA requested that DOE compare the effects on repository releases of using a single, higher G value compared to releases obtained using a sampled range of G values for the production of H_2(g) by alpha radiolysis (Peake 2020b, Comment CC2-GEOCHEM-15).

DOE's response (Knerr 2020c) cited uncertainties in the Reed et al (1993) experimental results because of difficulties sampling the small volumes of generated gas and precipitation of solids that occurred over longer time periods and resulted in decreased dose to the brine. Reed et al. (1993) accounted for these uncertainties by recommending G values at the higher end of the measured ranges. Knerr (2020c) noted that Kelm (1999) determined a higher G value for 5 M NaCl solutions (Table 3-8), which provided additional support for higher G values within the measured ranges in WIPP brines. Knerr (2020c) also pointed out that uncertainty in the radiolytic gas generation rate calculations is accounted for in the sampled energy deposition probability (parameter GLOBAL:GDEPFAC) range for wetted radionuclide solids. Because the uncertainty in energy deposition probability is greater than the variability in the measured G values, Knerr (2020c) stated that adding an additional uncertainty variable for the G value would be redundant. Knerr (2020c) also noted that the sampled energy deposition probability parameter does not significantly influence the variability of any release mechanism or total releases in CRA-2019 DPA results (Zeitler 2019b), so DOE does not expect that PA results are sensitive to uncertainty

in the G value. DOE's response provided adequate justification for the G value of 1.4 molecules/100 eV used in the CRA-2019 DPA.

Table 3-8. G Values for H_2(g) in Alpha-Irradiated Chloride Brines

Brine	Isotope	Measured G (molecules/100 eV)	"Best Value" G (molecules/100 eV)	Reference
Brine A (Salado)	Pu-239	>0.8 1.1 ± 0.1 1.3 ± 0.1 1.4 ± 0.1	1.4 ± 0.1	Reed et al. (1993)
DH-36 (Salado)	Pu-239	1.3 1.5 0.8 – 1.5	1.3 ± 0.1	Reed et al. (1993)
G8-B (Salado)	Pu-239	1.3 1.5 0.7 – 1.5	1.3 ± 0.1	Reed et al. (1993)
ERDA-6 (Castile)	Pu-239	0.9 0.6 0.2 – 0.7	0.9 ± 0.2	Reed et al. (1993)
5 M NaCl	Pu-238	1.52	--	Kelm et al. (1999)

The G values in Table 3-8 are directly applicable to brine radiolysis if radionuclides are dissolved or present as colloids in brine because all of the decay energy can be assumed to contribute to radiolytic gas generation. However, most of the radionuclides in the WIPP repository will be present in solid form. Only a fraction of alpha disintegration energy is released from solid particles because of self-attenuation, and the fraction of the disintegration energy released decreases with increasing particle size. Day (2019b) refers to the fraction of alpha-decay energy that is not self-absorbed and causes brine radiolysis as the energy deposition probability. Day (2019b, Figure 2) provided a graph illustrating the fraction of energy escaping from a spherical PuO_2 particle as a function of particle radius for an initial decay energy of 5.15 eV from DOE (2012b).

DOE (2012b) calculated the fraction of alpha decay energy escaping from a spherical particle of PuO_2 as a function of the particle diameter from 0 μm to 200 μm for initial energies of 5.15 eV (^{239}Pu) and 5.49 eV (^{238}Pu). These results show that the fraction of energy escaping a PuO_2 particle is only slightly affected by the different decay energies (Table 3-9). For particles with diameters less than about 4 μm, more than 90% of the alpha decay energy will escape from the particle. As the particle diameter increases above about 20 μm, less than 50% of the alpha decay will escape. Day (2019b, Figure 2) shows that above a particle diameter of about 80 μm, less than 10% of the alpha decay energy will escape a PuO_2 particle.

Day (2019b) used data provided by Narlesky et al. (2012) to estimate the particle size distribution of plutonium waste in the WIPP inventory. The reported particle sizes ranged from 3.6 to 79.6 μm, with an average of 20.5 μm (Day 2019b). For this particle diameter range, the fractional energy released would vary from about 0.10 to 0.90 (Table 3-9). Day (2019b) noted

that if a radionuclide particle is adhered to or embedded in a non-hydrogenous surface, only 50% of the disintegration energy could contribute to brine radiolysis based on geometry.

Table 3-9. Fraction of Alpha Particle Energy Escaping from PuO_2 Particles as a Function of Particle Diameter and Initial Energy

Particle Diameter (μm)	Fraction of Energy Escaping from Particle	
	E_0 = 5.15 MeV	E_0 = 5.49 MeV
19	0.476	0.515
14	0.607	0.647
9	0.766	0.790
7	0.823	0.840
5	0.877	0.888
3	0.927	0.934
1.5	0.964	0.967
0.56	0.987	0.988

Source: DOE (2012b), Table B2-1

Day (2019b) established a uniform distribution of 0.0 to 0.50 for the energy deposition probability for gas generation from brine radiolysis by wetted radionuclide solids (parameter GLOBAL:GDEPFAC). The upper limit corresponds to the fraction of energy released from a particle with the mean particle size of the plutonium materials characterized by Narlesky et al. (2012). The lower limit accounts for the possibility that brine radiolysis from wetted radionuclide solids does not significantly contribute to gas generation for reasons such as the formation of coatings by non-hydrogenous materials (Day 2019b). Day (2019b) provided reasonable justification for the range and distribution of the GLOBAL:GDEPFAC parameter, provided the PuO_2 materials characterized by Narlesky et al. (2012) adequately represent plutonium-bearing wastes in the WIPP inventory.

The materials characterized by Narlesky et al. (2012) are representative of plutonium stored in DOE-STD-3013 containers. Because surplus plutonium waste stream SR-KAC-PuOx contains a large fraction of the current WIPP plutonium and ^{241}Am inventories, EPA requested additional information from DOE to establish whether the materials characterized by Narlesky et al. (2012) adequately represent the characteristics of waste stream SR-KAC-PuOx and other plutonium wastes in the WIPP inventory (Peake 2020c).

The materials characterized by Narlesky et al. (2012) are products and byproducts produced by aqueous processing, metal oxidation, mixed actinide operations, and molten salt operations at Hanford, Rocky Flats, and Los Alamos National Laboratory (LANL) and were originally destined for conversion to mixed oxide fuel. EPA asked DOE to clarify whether the SR-KAC-PuOx material originated at the same sites as the materials in the Narlesky et al. (2012) investigation (Peake 2020c, Comment CC3-GEOCHEM-17a). EPA also requested that DOE identify the process or processes that produced the SR-KAC-PuOx material (Peake 2020c, Comment CC3-GEOCHEM-17b).

Knerr (2020c) responded that a large fraction of the SR-KAC-PuOx material originated at the Hanford, Rocky Flats, and LANL sites, but some of the material also originated from Savannah River Site (SRS) and Lawrence Livermore National Laboratory (LLNL). Each of the materials from SRS and LLNL are represented by specific materials evaluated by Narlesky et al. (2012) based on processing history or impurities present in the materials following stabilization. The aqueous processing, metal oxidation, mixed actinide operations, and molten salt processes identified by Narlesky (2012) represent the processes supplying materials for surplus plutonium disposition as part of waste stream SR-KAC-PuOx. DOE's responses to Comments CC3-GEOCHEM-17a and 17b demonstrated that the materials characterized by Narlesky et al. (2012) are reasonably representative of the sites and processes that produced the SR-KAC-PuOx material.

Narlesky et al. (2012) characterized plutonium solids after they were passed through 40 mesh (0.42 mm) sieves, but these materials were not reported to be crushed or ground. On the other hand, repackaging at Savannah River for waste stream SR-KAC-PuOx appears to include grinding and sieving (McAlhany 2018). Crushing or grinding of other waste prior to repackaging for WIPP has also been reported (e.g., Hopkins et al. 2003). EPA requested that DOE evaluate the effects on predicted radiolytic gas generation of particle size reduction during the repackaging process for the SR-KAC-PuOx waste stream and other plutonium wastes in the WIPP inventory. EPA additionally requested that DOE assess the modeling uncertainty introduced as a result of a higher proportion of smaller particle sizes than the distribution reported by Narlesky et al. (2012) (Peake 2020c, Comment CC3-GEOCHEM-17c).

DOE (Knerr 2020c) responded that particle size distributions for WIPP wastes are uncertain and are not tracked in typical waste stream data. The Narlesky et al. (2012) data are believed to be the best available particle size distribution for PuO_2 waste, and the PuO_2 characterized represents a variety of processes used throughout the DOE complex. DOE noted that in the Narlesky et al. (2012) study, the PuO_2 was ultrasonically suspended in an electrolyte solution, which would tend to break down agglomerated materials. Although Narlesky et al (2012) used short sonication times to minimize break down of agglomerated materials, it is reasonable to believe that ultrasonic suspension led to some break down of agglomerated materials. DOE stated that the size reduction step for the dilute and dispose operation utilizes the minimum mechanical processing necessary to break down PuO_2 materials to pass a 2 mm sieve, which is much larger than the measured particle sizes of mostly less than 0.1 mm (Narlesky et al. 2012, Appendix 4). DOE adequately demonstrated in its response to comment CC3-GEOCHEM-17c that the size reduction step used in the dilute and dispose process is more likely to disaggregate agglomerated materials than to significantly reduce the sizes of the PuO_2 particles.

A decreased PuO_2 particle size would be expected to increase the energy deposition probability. To evaluate the potential effects of smaller particle sizes on gas generation by brine radiolysis, DOE performed gas generation calculations to demonstrate that a higher energy deposition probability increased gas generation rates and waste panel brine pressures, decreased waste panel brine saturation, and slightly decreased average total releases from the repository at low probabilities because of decreased DBRs (Knerr 2020c). DOE has therefore adequately demonstrated that decreased PuO_2 particle size would not increase repository releases under the conditions modeled for the CRA-2019.

Plutonium-bearing wastes from sites other than Hanford, Rocky Flats, and LANL are present in the WIPP inventory, and the inventory also includes forms of plutonium-bearing waste such as contaminated soils and incinerator ash (Behrens et al. 1995) that were not included in the materials characterized by Narlesky et al. (2012). EPA requested that DOE assess the uncertainty introduced into the particle size ranges and distributions and the radiolytic gas generation calculations by the presence in the WIPP inventory of plutonium wastes that were not included in the Narlesky et al. (2012) investigation, and the presence of plutonium contamination on waste materials surfaces (Peake 2020c, CC3-GEOCHEM-17d). DOE acknowledged uncertainties associated with particle sizes in WIPP waste and noted that calculations performed with higher gas generation rates caused by smaller particle sizes resulted in lower mean repository releases (Knerr 2020c).

The Agency has reviewed the information provided by DOE regarding the calculation of $H_2(g)$ production and brine consumption by alpha radiolysis of brine for the CRA-2019 DPA. DOE identified the radionuclides in the WIPP inventory that would contribute significantly to brine radiolysis and provided the required disintegration energies for these radionuclides. The information provided by Day (2019b) for the CRA-2019 and by Knerr (2020c) in response to EPA's requests for additional information established that the G value used to calculate the rate of $H_2(g)$ generation is a reasonable value for WIPP brine radiolysis. Information provided by Day (2019b) and Knerr (2020c) also showed that the particle size distribution and resulting energy deposition probability range used to model $H_2(g)$ production by brine radiolysis is reasonably representative of plutonium wastes in WIPP, which are expected to be the dominant cause of gas generation through brine radiolysis (Section 3.6.6). Knerr (2020c) also presented the results of gas generation calculations with a higher maximum energy deposition probability that resulted in lower mean repository releases. Day (2019a) found that gas generation rates from alpha radiolysis of brine by dissolved and colloidal radionuclides and wetted radionuclide solids were approximately equal to microbial gas generation rates for the CRA-2019 DPA. Consequently, DOE concluded that gas generation by brine radiolysis is potentially important to WIPP performance and that it is appropriate to include this radiolytic gas generation process in WIPP PA.

3.6.2 Adsorbed Water Radiolysis

Day (2019b) considered radiolytic $H_2(g)$ generation from brine by dissolved and colloidal radionuclides, and $H_2(g)$ generation by brine radiolysis from wetted solid radionuclides. As currently modeled in PA, significant radiolytic $H_2(g)$ generation requires saturated conditions. Production of $H_2(g)$ by radiolysis of adsorbed water on various surfaces has been reported (e.g., LaVerne and Tandon 2003, Le Caër 2011, Veirs et al. 2012). These studies indicate that $H_2(g)$ yields (G values) from adsorbed water can be significantly higher than from bulk water, due to the efficient energy transfer that can occur at the interface. EPA requested that DOE evaluate the likely rates of $H_2(g)$ production due to radiolysis of adsorbed water on waste material surfaces under unsaturated conditions to justify omitting this process from the gas generation calculations (Peake 2020c, Comment CC3-GEOCHEM-20).

DOE evaluated the average dissolved, wetted, and non-wetted masses of plutonium in the WIPP inventory and determined that the average amount of non-wetted radionuclide solids will exceed the combined amounts of dissolved, colloidal, and wetted radionuclide solids (Knerr 2020c).

DOE stated that there is evidence that G values for gas production from non-wetted radionuclide solids may exceed the G values for dissolved, colloidal, and wetted solid radionuclides. DOE concluded there is evidence that radiolysis of water adsorbed on waste could contribute to $H_2(g)$ generation at a rate on the order of the rates already considered from brine radiolysis by dissolved, colloidal, and wetted radionuclide solids. DOE noted that increased gas generation rates by radiolysis of brine by wetted solids had already been determined to decrease repository releases using CRA-2019 DPA assumptions (Section 3.6.1), and concluded that additional gas generation by of adsorbed water radiolysis would be expected to decrease repository releases. DOE stated that a complete evaluation of gas generation by radiolysis of adsorbed water would require additional investigation, including an assessment of the fraction of non-wetted radionuclide solids that would be exposed to humid air and the amount of energy transferred to the relatively thin water layer on waste surfaces (Knerr 2020c).

DOE has provided reasonable justification for omitting gas generation from radiolysis of adsorbed water from the CRA-2019 DPA because DOE's calculations show that increased radiolytic gas generation rates would likely decrease repository releases under the conditions modeled for the CRA-2019 DPA. However, some uncertainty remains in these calculations because the relationships between gas generation rates, repository pressure, brine saturation, and releases are complex. The sensitivity calculations performed by DOE did not fully account for uncertainty regarding the G value for $H_2(g)$ generation from adsorbed water radiolysis, and average brine saturations were assumed in DOE's screening calculations. Another uncertainty is related to the timing of gas generation by radiolysis of adsorbed water because this process would occur in unsaturated conditions whereas other significant gas generation processes, including anoxic corrosion and microbial degradation, occur at higher rates under saturated conditions. It is also possible that significant gas generation by radiolysis of adsorbed water could increase repository pressures during early periods and interfere with creep closure. In addition, waste stream SR-KAC-PuOx contains a significant fraction of the radionuclide inventory important to radiolysis and could be placed in a limited number of panels. In this case, gas generation from radiolysis of adsorbed water may have different effects on releases from these panels than calculated using the CRA-2019 DPA assumption of homogenous waste loading (Section 10.0).

EPA expects DOE to evaluate radiolytic $H_2(g)$ generation from adsorbed water in greater detail for the next PA. The gas generation rate from radiolysis of adsorbed water may be similar to or even larger than the gas generation rate from brine radiolysis by wetted solid, dissolved, and colloidal radionuclides, which has been screened in for PA. In addition, because gas generation from adsorbed water radiolysis will be an inverse function of brine saturation, the timing of gas generation by adsorbed water radiolysis may affect repository performance. This evaluation should include an assessment of the likely G values, the amounts of non-wetted radionuclide solids exposed to humid air in the repository, the thickness of the adsorbed water layer under WIPP repository conditions, the effects of placement of surplus plutonium waste streams in a limited number of panels, and the expected effects of gas generation by radiolysis of adsorbed water on repository releases.

3.6.3 CPR Radiolysis

Ionizing radiation may affect the chemical properties of CPR in WIPP waste and emplacement materials. The changes that may occur in the CPR polymers include (O'Donnell 1991):

- Scission (breakage) of polymer molecules leading to a decrease in molecular weight,
- Crosslinking of polymer molecules leading to an increase in molecular weight,
- Changes in the molecular composition and structure of the polymer molecules, including unsaturation (C=C bonds) in PVC, and
- Evolution of gas molecules, such as H_2, carbon monoxide (CO), CO_2, and methane.

Radiolytic gas production from organic materials such as CPR can decrease over time because of a process called matrix depletion. When an alpha-emitting material is present in waste in dispersed, particulate form, only a small, spherical volume of the surrounding material is affected because of the relatively short distance that alpha particles can travel in solid materials. Over time, the nearby hydrogen-bearing material is depleted and the effective G value decreases to a limit that is characteristic of the affected matrix (INEEL 1999).

Day (2019b) used the time-dependent G values for CPR measured by Zerwekh (1979, Figure 3-3) and assumed that the equations developed by Zerwekh (1979) could be used to predict G values over time periods considerably longer than the experiments. Day (2019b) found that because of matrix depletion, the average predicted G value for all waste matrices at 100 years would be less than 1% of the initial average G value. Consequently, Day (2019b) concluded that CPR radiolysis would result in insignificant amounts of gas production compared to other processes in the WIPP repository.

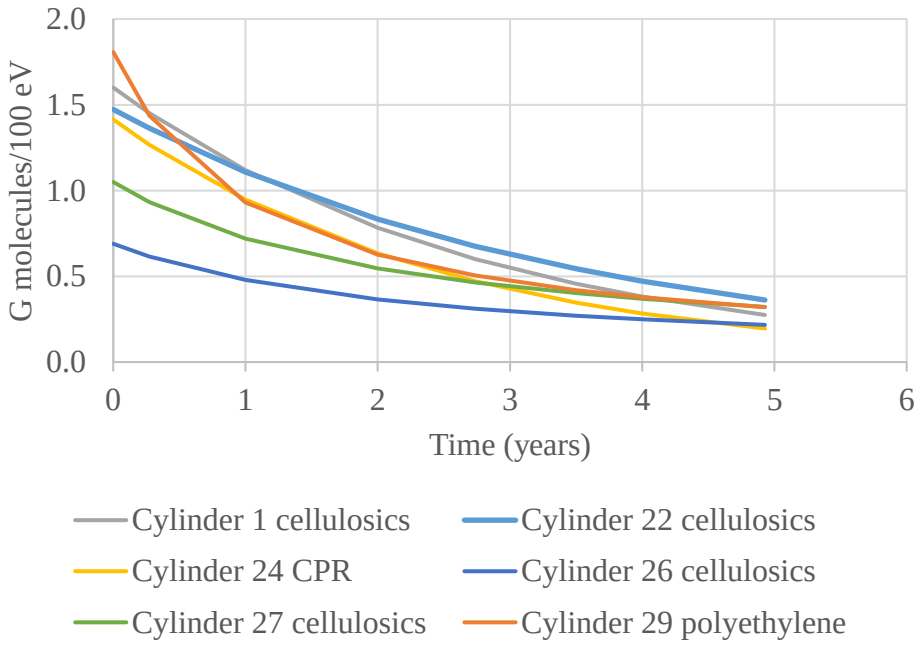

Figure 3-3. Equations Fit to Radiolytic Gas Generation Data Collected by Zerwekh (1979) Over the 5-year Data Collection Period

Zerwekh (1979) used high Pu-238 concentrations per kg of waste (~20 Ci/kg) to investigate radiolytic gas generation from organic materials. The WIPP waste material radionuclide concentrations are much lower and are predicted to range from about 0.1 Ci/kg in 2033 to about 0.01 Ci/kg in 12033 based on the current inventory (DOE 2018, Van Soest 2018). The high Pu-238 concentrations used by Zerwekh (1979) would increase the rate at which matrix depletion would occur, causing a more rapid decrease in the experimental G values than would occur in the WIPP repository. EPA requested that DOE analyze the effects of matrix depletion on G values for CPR in the WIPP repository after adjusting the Zerwekh (1979) data to be consistent with the much lower radionuclide activities in the WIPP inventory (Peake 2020c, Comment CC3-GEOCHEM-19a).

DOE agreed that the high radionuclide activity used in the Zerwekh (1979) experiments accelerated the effects of matrix depletion on G values (Knerr 2020c). Knerr (2020c) considered the effects of a 40-fold difference in radionuclide activity based on the maximum allowable radionuclide activity cited by Zerwekh (1979), and assumed that the effects of the higher radionuclide activity would be linear. Using these assumptions, Knerr (2020c) determined that the average G value would decrease to less than 5% of its initial value within 1,000 years. Knerr (2020c) also noted that the CPR inventory is subject to biodegradation, which would compete with radiolysis for the available CPR inventory. Knerr (2020c) stated that a larger G value would shift gas production to an earlier time during the repository regulatory period but would not increase total gas generation.

The average radionuclide density in WIPP waste materials is predicted to be 0.1 Ci/kg in 2033, which differs from the radionuclide density in the Zerwekh (1979) experiments by a factor of 200 (20 Ci/kg ÷ 0.1 Ci/kg) and is also much less than the radionuclide density assumed by Knerr (2020c). EPA generated the G values in Figure 3-4 using the equations developed by Zerwekh (1979), with the time associated with each G value increased by a factor of 200 to account for the lower radionuclide activities in WIPP waste. The initial G value calculated from the average of the six experiments in Figure 3-4 is 1.34 molecules/100 eV. After 1,000 years, the average G value is predicted to decrease to 0.28 molecules/100 eV (21% of the initial average G value).

Day (2019b) used the equations developed by Zerwekh (1979) to project extremely low G values and radiolytic gas generation rates after approximately 100 years (Day 2019b, Figure 3). However, EPA noted that the equations would be expected to have increasing uncertainties at longer times, and the G values as a function of time may have been asymptotically approaching a G value of approximately 0.3 molecules/100 eV at the end of the 4.9-year experiments (Figure 3-3). EPA requested a bounding analysis of the amount of radiolytic gas generation from CPR in the WIPP repository by assuming a constant G value of 0.3 moles/100 eV throughout the repository regulatory period (Peake 2020c, Comment CC3-GEOCHEM-19b).

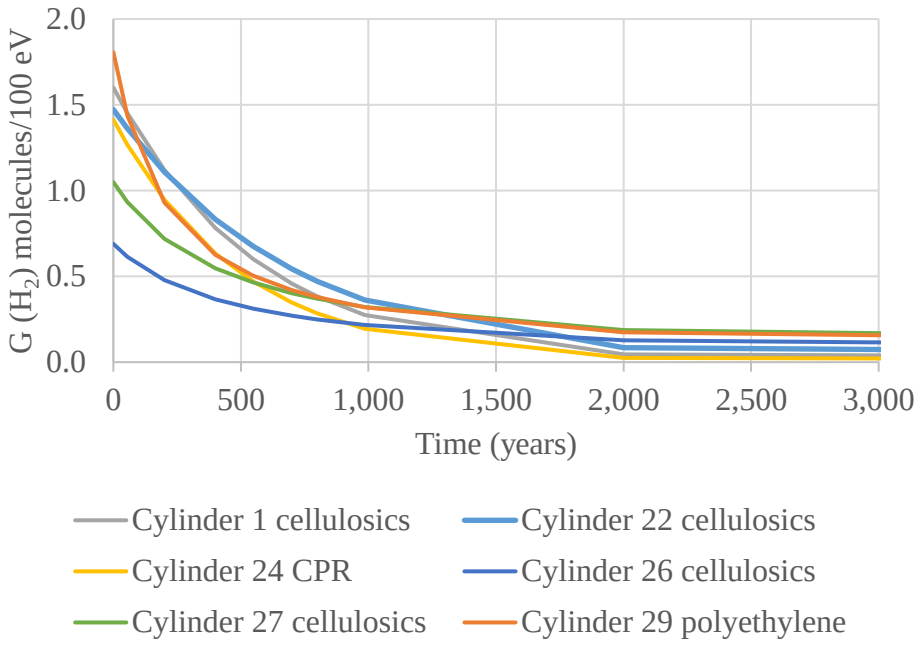

Figure 3-4. Equations Fit to Radiolytic Gas Generation Data Collected by Zerwekh (1979) Adjusted for the Higher Activity in the Experiments

DOE provided the requested analysis using a two-step modeling process (Knerr 2020c). In the first step, DOE modeled the amount of gas generated as a function of time. Because the radionuclide inventory can contribute to either radiolysis of brine or CPR, DOE apportioned the radiolytic effects of the radionuclide inventory between these processes by assuming that only the non-wetted radionuclide solid inventory that does not already contribute to brine radiolysis may contribute to CPR radiolysis. The results of the calculation of CPR radiolytic gas generation show that gas generation from CPR radiolysis slightly exceeded the CRA-2019 DPA gas generation by microbial degradation of CPR and gas generation from brine radiolysis in scenarios without a Castile brine encounter (scenarios S1-BF and scenario S4-BF, Knerr 2020c). For scenarios that included a Castile brine encounter (scenarios S2-BF and S6-BF), brine saturations are significantly higher than in the scenarios without Castile brine. Under these higher brine saturation conditions, more brine radiolysis occurs at the expense of CPR radiolysis, and microbial gas generation from CPR degradation and steel corrosion gas generation also increase, so gas generation from CPR radiolysis is much lower than all other gas generation processes. The results of these calculations indicate that CPR radiolysis might affect gas generation under conditions of lower brine saturation but may be less important under high brine saturation conditions.

In the second calculation step, DOE approximated the rate of gas generation from CPR radiolysis by assuming that it is equal to the rate of gas generation from microbial degradation of CPR and that the effects of CPR radiolytic gas generation could be simulated by doubling the microbial gas generation rate. DOE then recalculated all 100 vectors of replicate 1 from the CRA-2019 DPA. Compared to the CRA-2019 DPA results, the increased gas generation rates increased brine pressures, inhibited brine flow into the repository, and reduced brine saturation. DOE

found that these changes had only very small effects on modeled repository releases compared to the results of the CRA-2019 DPA.

Knerr (2020c) stated that the requested calculation overestimates the radiolytic gas generation from CPR because it does not account for the finite amount of CPR in the repository, which would decrease over time and may be entirely consumed by microbial degradation and CPR radiolysis. However, in 75% of the PA realizations, microbial degradation of plastics and rubber does not occur (Section 3.4.3.1), and gas generation by radiolysis of these materials would not compete with microbial degradation and could result in increased total gas generation. Further, Moody (2009a) found CPR was not completely degraded in the majority of CRA-2009 PA realizations, which used the same microbial gas generation rates as the CRA-2019 DPA (Section 3.4.5). The persistence of plastic and rubber in 75% of PA realizations is significant because plastics and rubber comprise 66% of the CPR mass in the CRA-2019 DPA inventory. Another limitation of the Knerr (2020c) calculations is that higher G values for CPR radiolysis during the first 1,000 years after closure are not included in the assessment (Figure 3-4). These higher gas generation rates early in the repository regulatory period could affect creep closure and other processes, as previously noted for adsorbed water radiolysis in Section 3.6.2. The assumption that gas generation from CPR radiolysis will only occur in non-wetted waste is another limitation. As waste becomes saturated with brine, some of the alpha radiation from the wetted waste will cause brine radiolysis instead of CPR radiolysis. However, some gas generation due to CPR radiolysis within the wetted waste will still occur.

There is some evidence that CPR radiolysis could increase microbial degradation rates because polymer cleavage of recalcitrant materials could create materials that are more susceptible to microbial degradation (SC&A 2006). Increased CPR degradation rates associated with radiolysis is consistent with WIPP experiments that found irradiation of rubber increased CO_2 production in microbial gas generation experiments (Gillow and Francis 2003). DOE did not address these potential interactions between radiolytic processes and microbial degradation of CPR, which is another possible source of uncertainty.

The calculations performed by DOE (Knerr, 2020c) indicate that long-term gas generation from CPR radiolysis may be similar in magnitude to gas generation from brine radiolysis and microbial degradation of CPR under some repository conditions. Uncertainties associated with this assessment of the effects of gas generation by CPR radiolysis include:

- Effects on repository releases of higher rates of CPR radiolysis in the first 1,000 years post closure before matrix depletion reduces the G value to approximately 0.3 molecules/100 eV or less,
- Potential for radiolytic effects on CPR polymer properties that could result in higher gas generation rates from microbial degradation,
- The fractions of alpha radiation emitted by the WIPP inventory radionuclides that will cause gas generation from brine, adsorbed water, or CPR or that will interact with non-hydrogenous materials and not cause radiolytic gas generation, and
- The effects of placing waste stream SR-KAC-PuOx, which contains a large fraction of the radionuclides that cause radiolytic gas generation and that also includes significant cellulose and plastic packaging materials, in a limited number of panels.

Addressing these uncertainties would likely increase gas generation rates from CPR radiolysis earlier in the repository history. DOE (Knerr 2020c) has adequately demonstrated that CPR radiolysis is unlikely to have major effects on WIPP repository performance for the CRA-2019 DPA using the assumption of homogeneous waste loading because gas generation is dominated by anoxic corrosion of iron and the results of the bounding gas generation calculations have indicated that CPR radiolytic gas generation will have only small effects on repository releases. EPA expects DOE to continue evaluating the potential importance of gas generation from CPR radiolysis for the future WIPP PAs, including an analysis of the effects on repository releases of potentially higher gas generation rates during the first 1,000 years post closure and the effects on repository releases if waste stream SR-KAC-PuOx is placed in a limited number of panels.

3.6.4 Radiolysis of Other Wastes

Radiolytic gas generation has been reported for other waste materials in the WIPP inventory, including the hydrated mineral montmorillonite (e.g., Fourdrin et al. 2013), solidified inorganic wastes, solidified organic wastes (e.g., Barber et al. 2001), and cements (e.g., Bouniol and Bjergbakke 2008). EPA requested that DOE provide screening analyses for other waste forms to indicate whether they could contribute significant H_2(g) to the repository, including: 1) hydrated minerals, such as clays in waste soils; 2) solidified inorganic wastes; 3) solidified organic wastes; and 4) cements (Peake 2020c, Comment CC3-GEOCHEM-21).

DOE (Knerr 2020c) provided an analysis for these other wastes that relied upon the CPR radiolysis analysis (Section 3.6.3). In the analysis, DOE assumed that only the non-wetted radionuclide solid inventory that does not already contribute to brine radiolysis may contribute to radiolysis of CPR and other wastes. Knerr (2020c) examined the range of reported G values for soils, solidified inorganic wastes, solidified organic wastes, and cements from the literature, and selected an upper-bound initial G value for each material. DOE used these G values with the inventory masses of the CPR and other waste materials to calculate inventory-weighted initial G values for each material. The total of these inventory-weighted initial G values was less than the initial G value for CPR. Because the inventory-weighted G values for the other waste materials are less than the G value for CPR and the other wastes are a smaller fraction of the inventory, DOE demonstrated that radiolysis of the other waste materials should have little effect on overall gas generation rates in the repository.

3.6.5 Gamma Radiolysis

Based on the WIPP inventory, alpha radiation is likely to have the largest effects on repository conditions. Day (2019b) cited low gamma dose rates from CH waste as part of the justification for omitting gamma radiolysis from radiolytic gas generation calculations. EPA requested that DOE address the omission of RH waste gamma radiation from the gas generation calculations (Peake 2020b, Comment CC2-GEOCHEM-16). In response, Knerr (2020c) explained that the screening process for inclusion of radionuclides in radiolytic gas generation calculations (Kicker 2019b) considered both the CH and RH inventories and the disintegration energy used was the sum of the alpha, beta, and gamma disintegration energies for each radionuclide. An analysis of decay heat by decay type (alpha, beta, or gamma) showed that alpha decay would comprise 97.1% of the decay heat at the WIPP closure date of 2033 (Knerr 2020c). This percentage increases over time, to 99.8% in 12033. Knerr (2020c) acknowledged that gamma radiation

would have less self-attenuation than alpha radiation, leading to a higher energy deposition probability. However, this increased energy deposition probability would likely be balanced out by a lower G value for gamma radiolysis of brine compared to alpha radiolysis (Gray and Simonson 1984). The additional information provided by Knerr (2020c) demonstrated that gamma radiation from RH waste is unlikely to be a significant source of radiolytic gas generation in the WIPP repository.

3.6.6 PA Implementation of Radiolytic Gas Generation

Kicker (2019b) performed a screening assessment to identify radionuclides in the WIPP inventory that are the principal contributors to decay heat and should therefore be included in radiolytic gas generation and brine consumption calculations. The decay heat calculated for each radionuclide is a function of the sum of its CH and RH inventory, decay heat specific power, and its specific activity. Kicker (2019b) calculated that the five radionuclides in Table 3-10 represent greater than 99% of the total inventory decay heat from 100 to 10,000 years after WIPP repository closure. These radionuclides are included in the radiolytic gas generation calculations, with the decay energy parameters listed in Table 3-10.

Table 3-10. Radionuclides Included in WIPP Brine Radiolysis Calculations

Radionuclide	Wattage Fraction in 2133 (%)	Wattage Fraction in 12033 (%)	Parameter	Decay Energy (MeV)
^{241}Am	39.85	0.00	AM241:DECAYNRG	5.64
^{238}Pu	16.84	0.00	PU238:DECAYNRG	5.59
^{239}Pu	31.44	85.17	PU239:DECAYNRG	5.24
^{240}Pu	11.43	14.47	PU240:DECAYNRG	5.26
^{242}Pu	0.01	0.02	PU242:DECAYNRG	4.99
Total	99.57	99.65	--	--

Sources: Kicker (2019b), Kim and Feng (2019)

Calculation of the gas generation rate due to brine radiolysis in the WIPP repository is described by Day (2019b). Day (2019b) defined the H_2(g) generation rate for each radionuclide i ($R_{H2,i}$) from brine radiolysis by dissolved and colloidal radionuclides and by the wetted solid form of the radionuclide:

$$R_{H2,i} = (M(t)_{sol,i} + (M(t)_{wet,i} \times P_{dep})) \times (\lambda_i \times E_{dis,i} \times G(H_2)_{avg}) \quad \textbf{(15)}$$

Where:

$M(t)_{sol,i}$ is the amount of dissolved plus colloidal radionuclide i;

$M(t)_{wet,i}$ is the quantity of wetted solid radionuclide i, calculated from the difference between the total inventory and the dissolved or colloidal inventory, multiplied by the brine saturation;

P_{dep} is the energy deposition probability for wetted solids (parameter GLOBAL:GDEPFAC, uniform distribution from 0.0 to 0.5);

λ_i is the radionuclide radioactive decay constant, which is a function of the radionuclide half-life ($t_{1/2}$, parameter HALFLIFE): $\lambda_i = \ln(2)/t_{1/2}$;

$E_{dis,i}$ is the total emitted disintegration energy of radionuclide i (parameter DECAYNRG, Table 3-10); and

$G(H_2)_{avg}$ is the average hydrogen yield (parameter GLOBAL:GH2AVG, 1.4 molecules/100 eV).

The total gas generation rate through brine radiolysis (q_{rgr}) is the sum of the radiolytic gas generation rates for the isotopes in Table 3-10:

$$q_{rgr} = R_{H2,Am-241} + R_{H2,Pu-238} + R_{H2,Pu-239} + R_{H2,Pu-240} + R_{H2,Pu-242} \quad \textbf{(16)}$$

Radiolysis of water in brine to create $H_2(g)$ also produces oxidized species that may ultimately react to form $O_2(g)$, with the potential formation of 0.5 moles of $O_2(g)$ per mole of $H_2(g)$. Day (2019b) accounted for the potential formation of $O_2(g)$ by establishing the parameter GLOBAL:SRADO2, which is a stoichiometric coefficient that is 0.5 if $O_2(g)$ does not react and remains in the repository gas phase, and is 0.0 if all $O_2(g)$ reacts with other repository materials and does not contribute to repository pressure. For the CRA-2019 DPA, the GLOBAL:SRADO2 parameter was 0.0 (Kim and Feng 2019), consistent with the assumption that all oxidized species created by radiolysis quickly react with reducing materials in the repository.

DOE has modeled gas production from brine radiolysis by dissolved, colloidal, and wetted radionuclide solids using reasonable parameter values for the energy deposition probability and hydrogen yield. DOE provided additional information in response to EPA comments that demonstrated that gas generation from CPR radiolysis and radiolysis of other wastes including hydrated minerals, solidified inorganics, solidified organics, and cements will not significantly increase repository releases modeled for the CRA-2019 DPA. The rate of gas generation by radiolysis of water adsorbed on waste material surfaces under unsaturated conditions was not included in the CRA-2019 DPA. A complete evaluation of gas generation by radiolysis of adsorbed water will require additional investigation. EPA expects DOE to evaluate this process in greater detail for future WIPP PAs, including an assessment of the likely G values, the amounts of non-wetted radionuclide solids exposed to air in the repository, and the expected effects of this process on repository releases, to determine whether gas generation by radiolysis of adsorbed water should be included in calculations of gas generation rates for WIPP PA. EPA also expects DOE to continue evaluating the potential importance of gas generation from CPR radiolysis for future WIPP PAs, particularly the effects on repository releases of higher gas generation rates during the first 1,000 years post closure. Because the surplus plutonium waste stream SR-KAC-PuOx contains a large fraction of the radiolysis-causing radionuclides in the WIPP inventory, EPA also expects DOE to assess the effects on radiolytic gas generation and repository releases if this waste stream is placed in a limited number of waste panels.

3.7 TOTAL GAS PRODUCTION RATE

DOE (2019, Appendix GEOCHEM) described the total repository gas production rate as the sum of gas production by corrosion of iron-based metals, by microbial degradation of CPR, and by sulfidation of iron-based metals (Equation GEOCHEM.2). DOE (2019, Appendix GEOCHEM)

acknowledged gas production by brine radiolysis by stating that Day (2019b) addressed this process. However, EPA noted that DOE should have included the contributions of brine radiolysis to the gas generation rate in Equation GEOCHEM.2 (Peake 2020f, Comment CC6-GEOCHEM-35). In addition, sulfidation of iron-based metals does not contribute to gas generation in the CRA-2019 DPA (Section 3.1.3). Although brine radiolysis was omitted from Equation GEOCHEM.2, DOE stated in its response to Comment CC6-GEOCHEM-35 that this process was included in the CRA-2019 DPA model (Knerr 2021b).

Including all processes that contributed to modeled gas generation in the CRA-2019 DPA results in the following equation for the total gas generation rate (q_{rg}):

$$q_{rg} = q_{rgc} + q_{rgm} + q_{rgs} + q_{rgr} \quad \textbf{(17)}$$

The gas generation rate from corrosion of iron-based metals and alloys (q_{rgc}) is calculated using equation (9), the microbial gas generation rate (q_{rgm}) is calculated using equation (14), and the brine radiolysis gas production rate (q_{rgr}) is calculated using equation (16). The gas generation rate from steel sulfidation (q_{rgs}) was set equal to zero for the CRA-2019 DPA (Section 3.1.3).

Zeitler et al. (2019) provided an overview of the gas generation processes and results of the CRA-2019 DPA calculations. Gas generation was generally increased over all scenarios in the CRA-2019 DPA compared to the CRA-2014 PA because of the inclusion of gas generation caused by brine radiolysis, increased CPR inventory, increased inundated iron corrosion rates, and increased iron inventory. Iron corrosion was the most important contributor to gas generation, and microbial and radiolytic gas generation were less important to overall moles of gas generation.

3.8 WIPP GAS GENERATION SUMMARY AND CONCLUSIONS

WIPP PAs through the CRA-2014 PA have included anoxic corrosion of iron-based metals and alloys and microbial degradation of CPR as significant gas generation processes. Because of the increased inventories of plutonium isotopes and ^{241}Am, DOE included gas generation by brine radiolysis by dissolved and colloidal radionuclides and wetted waste in the modeled CRA-2019 DPA gas generation processes.

EPA has reviewed gas generation from anoxic corrosion of iron and other metals in the WIPP repository, and concludes:

- The conceptual model assumptions and DOE's implementation of gas generation by anoxic corrosion of iron-based metals and alloys have remained unchanged since the CCA PAVT. The available data continue to support the conceptual model and overall approach for gas generation by anoxic corrosion of iron-based metals and alloys.
- Review of the available data regarding reaction products of anoxic corrosion of iron-based metals and alloys indicates that the reaction stoichiometry used in the CRA-2019 DPA remains appropriate.
- DOE increased the sampled inundated corrosion rate from the CRA-2014 PA by a factor of two for the CRA-2019 DPA to account for the effects of elevated repository pressure

on the corrosion rate. The CRA-2019 DPA inundated and humid anoxic corrosion rates for iron-based metals and alloys are based on project-specific data, are well-documented, and are appropriate for use in WIPP PA.

- DOE adequately accounted for potential surface passivation of iron metals and alloys by setting the iron sulfidation REFCON:STCO_31 and REFCON:STCO_32 stoichiometric parameters to zero.
- DOE did not recalculate the potential range for the steel surface area per unit disposal volume (D_S) for the CRA-2019 DPA. EPA calculations indicate that the D_s value used for the CRA-2019 DPA continues to be consistent with the range calculated based on the iron inventory in the waste and anticipated waste containers. DOE should calculate the range of D_S values for future WIPP PAs using emplaced, stored, and scaled anticipated container counts and surface areas and reasonable assumptions about the iron-based waste surface areas in the WIPP inventory.
- The CRA-2019 DPA lead inventory is significantly higher than in previous WIPP PAs because of the increased number of anticipated shielded RH containers. DOE demonstrated for the CRA-2019 DPA lead inventory that lead corrosion will have insignificant effects on overall gas generation because of the relatively low lead surface area and corrosion rate compared to the steel surface area and corrosion rates.
- Corrosion of aluminum and other metals is not expected to contribute significantly to gas generation because of the low inventory of these metals.
- Galvanic coupling is unlikely to significantly affect gas generation in the WIPP repository. The current screening argument for FEP W50 Galvanic Coupling (within the repository) should be reworded to account for the increased mass of lead owing to a higher lead inventory and increased use of shielded containers.

The microbial gas generation rates used for the CRA-2019 DPA were the same rates used for the PABC04, CRA-2009 PA, PABC09, and CRA-2014 PA. EPA has concluded based on review of the CRA-2019:

- The microbial gas generation rates are based on WIPP-specific microbial gas generation experiments carried out with cellulose. Consequently, these rates are appropriate for modeling gas generation rates from degradation of cellulosic materials but may overestimate gas generation rates from the degradation of plastics and rubber. DOE accounts for uncertainties regarding the rates of plastic and rubber degradation in the WIPP repository environment by assuming it occurs in only 25% of PA realizations.
- The approach and parameters used to model microbial gas generation rates for the CRA-2019 DPA are appropriate.

Gas generation from brine radiolysis was included in the CRA-2019 DPA. EPA reviewed the information regarding radiolytic gas generation in the WIPP repository and found:

- DOE assumed radiolytic gas generation will occur only in brine from dissolved and colloidal radionuclides and from radiolysis of brine by wetted solids.
- DOE demonstrated that gas generation from radiolysis of CPR and other wastes is not expected to significantly affect repository releases for the CRA-2019 DPA, but EPA expects DOE to continue to investigate the potential for significant gas generation from

CPR radiolysis for future WIPP PAs, particularly the effects of increased gas generation rates during the first 1,000 years post closure on repository releases and the effects on repository releases if surplus plutonium waste stream SR-KAC-PuOx is placed in a limited number of panels.

- Additional investigation will be necessary to determine the importance of adsorbed water radiolysis under unsaturated conditions because gas generation rates from adsorbed water radiolysis may equal or exceed the rates from brine radiolysis or microbial degradation. In addition, the timing of gas generation from radiolysis of adsorbed water may differ significantly from anoxic corrosion and microbial degradation, because the latter processes have higher rates under saturated conditions. EPA expects a more detailed evaluation of the rates and timing of gas generation by radiolysis of adsorbed water for future WIPP PAs.

4.0 BACKFILL EFFICACY

MgO backfill is included in the WIPP repository design to control chemical conditions and thereby minimize actinide solubilities in the post-closure repository (DOE 1996, Appendix BACK). DOE selected MgO as an engineered barrier based on an analysis described in the CCA (DOE 1996, Appendix EBS). The CCA described the expected performance of the MgO backfill (DOE 1996, Appendices BACK and SOTERM) and DOE provided additional information during EPA's review of the CCA (EPA 1997b). EPA determined that MgO met the engineered barrier requirements (40 CFR Part 194.44).

4.1 MGO REACTIONS IN THE REPOSITORY

The MgO chemical reactions and their ability to control chemical conditions in WIPP brines were addressed in the Chemical Conditions conceptual model, which was peer reviewed and accepted for the CCA (Wilson et al. 1996a, 1996b, 1997a, 1997b). The MgO backfill consumes CO_2 produced by microbial degradation or radiolysis of CPR and buffers brine pH to moderately alkaline values (approximately 8 to 10). Both actions control actinide solubilities in brine within the post-closure repository.

MgO will initially react with brine to form brucite [$Mg(OH)_2(s)$]:

$$MgO(s) + H_2O(l) \leftrightharpoons Mg(OH)_2(s) \quad \textbf{(18)}$$

In GWB brine, MgO hydration may also produce Phase 5[4] [$Mg_3(OH)_5Cl{\bullet}4H_2O$]:

$$3\ MgO(s) + 6\ H_2O(l) + H^+ + Cl^- \leftrightharpoons Mg_3(OH)_5Cl{\bullet}4H_2O(s) \quad \textbf{(19)}$$

Brucite and Phase 5 dissolution is expected to buffer brine pH in the repository by consuming acidity:

$$Mg(OH)_2(s) + 2\ H^+ \leftrightharpoons Mg^{2+} + 2\ H_2O(l) \quad \textbf{(20)}$$

$$Mg_3(OH)_5Cl{\bullet}4H_2O(s) + 5\ H^+ \leftrightharpoons 3\ Mg^{2+} + Cl^- + 9\ H_2O(l) \quad \textbf{(21)}$$

Microbial degradation and radiolysis of CPR will produce CO_2, which can react with brucite to form magnesium-carbonate phases such as magnesite ($MgCO_3$):

$$Mg(OH)_2(s) + CO_2(g) \leftrightharpoons MgCO_3(s) + H_2O(l) \quad \textbf{(22)}$$

[4] This magnesium hydroxychloride is referred to as "Phase 5" in the cement industry, and this term is adopted for consistency with other WIPP documents (e.g., Xiong et al. 2010a).

Brucite also consumes CO_2 to form hydromagnesite[5] [reaction (23)] and nesquehonite [reaction (24)]:

$$5\ Mg(OH)_2(s) + 4\ CO_2(g) \leftrightharpoons Mg_5(CO_3)_4(OH)_2 \bullet 4H_2O(s) \quad \textbf{(23)}$$

$$Mg(OH)_2(s) + CO_2(g) + 2\ H_2O(l) \leftrightharpoons MgCO_3 \bullet 3H_2O(s) \quad \textbf{(24)}$$

Phase 5 would react with CO_2 in a manner similar to the brucite reactions. Because of the magnesium ion's high energy of hydrolysis, magnesite does not precipitate directly from low-temperature solutions. Instead, metastable formation of hydrated magnesium-carbonate phases, such as hydromagnesite and nesquehonite, are more likely to occur. Because these phases are not thermodynamically stable under repository conditions, they are expected to eventually dehydrate to form magnesite, for example:

$$Mg_5(CO_3)_4(OH)_2 \bullet 4H_2O(s) + CO_2(g) \leftrightharpoons 5\ MgCO_3(s) + 5\ H_2O(l) \quad \textbf{(25)}$$

At equilibrium in the repository, magnesite is expected to be the most stable magnesium-carbonate phase (EPA 1998c). However, the rate at which metastable hydrated magnesium-carbonate phases will convert to stable magnesite is uncertain.

The reaction of brucite or Phase 5 to form magnesium-carbonate solids in the repository will control the CO_2 fugacity. In the CCA PA, DOE assumed that the brucite-magnesite reaction (22) would control CO_2 fugacity (DOE 1996, Appendix SOTERM). EPA (1998c) reviewed experimental data on magnesium-carbonate solids formation in WIPP brines (SNL 1997) and found that nesquehonite formed initially in the experiments, but nesquehonite converted within a few days to a solid phase with a composition similar to proto-hydromagnesite [$(MgCO_3)_4 \bullet Mg(OH)_2 \bullet 4H_2O(s)$]. Hydromagnesite formation was observed in other scoping experiments (SNL 1997). There was no evidence of hydromagnesite conversion to magnesite in the SNL (1997) experiments.

Based on a review of the literature, EPA (1998c) conceptualized the sequence and time scales of reactions between infiltrating brine and MgO backfill in the WIPP repository:

1. Rapid reaction of MgO with brine to produce brucite (or Phase 5) (hours to days)
2. Rapid carbonation of brucite (or Phase 5) to produce nesquehonite and possibly hydromagnesite (hours to days)
3. Rapid conversion of nesquehonite to hydromagnesite (days to weeks)
4. Slow conversion of hydromagnesite to magnesite (hundreds to thousands of years)

---

[5] DOE has reported two compositions for hydromagnesite: hydromagnesite$_{5424}$ [$Mg_5(CO_3)_4(OH)_2 \bullet 4H_2O(s)$] and hydromagnesite$_{4323}$ [$Mg_4(CO_3)_3(OH)_2 \bullet 3H_2O(s)$] (DOE 2009, Appendix MgO). Only the hydromagnesite$_{5424}$ composition has been observed to form in WIPP-specific experiments and hydromagnesite$_{5424}$ is the composition recognized by the International Mineralogical Association (www.ima-mineralogy.org/Minlist.htm). Consequently, all references to hydromagnesite in this document refer to the hydromagnesite$_{5424}$ composition.

EPA (1998c) found that brucite in combination with the different magnesium carbonates buffered CO_2 fugacity at different values, with the highest value observed for nesquehonite, intermediate values for hydromagnesite, and the lowest fugacity for magnesite. Higher CO_2 fugacity generally increases actinide solid solubilities, because of the formation of aqueous actinide-carbonate aqueous complexes.

4.2 MGO CHARACTERIZATION

MgO has been supplied to WIPP by three companies since the repository began accepting waste in March 1999. National Magnesia Chemicals provided MgO from March 1999 to mid-April 2000, and MgO from this supplier was placed only in Panel 1, Room 7 (DOE 2019, Appendix MgO). Consequently, MgO from National Magnesia Chemicals represents a very small fraction of the MgO in the repository. Premier Chemicals provided MgO from mid-April 2000 through January 2005, and Martin Marietta Magnesia Specialties LLC has been supplying MgO to WIPP since January 2005 (DOE 2019, Appendix MgO). Most of the MgO currently emplaced in the repository was provided by Premier Chemicals and Martin Marietta MgO.

4.2.1 Characterization of Premier MgO

At the time of the CRA-2004, WIPP MgO backfill was obtained from Premier Chemicals. Premier MgO was manufactured from mined sedimentary magnesite that was calcined to expel all CO_2 (DOE 2004, Appendix BARRIERS-2.3.1). Premier MgO was characterized by XRD and found to contain primarily periclase [MgO], along with minor phases, such as forsterite [Mg_2SiO_4(s)], lime [CaO(s)], monticellite [$CaMgSiO_4$(s)], spinel [$MgAl_2O_4$(s)] and ulvospinel [$FeTi_2O_4$(s)]. Periclase and lime, which are expected to be reactive, made up approximately 90 wt% of the Premier MgO, with the unreactive constituents forming the remaining 10 wt% (Snider 2003a). Particle-size analysis data are available for two batches of Premier MgO (Bryan and Snider 2001a; DOE 2004, Appendix BARRIERS). These samples yielded distinctly different results, with 37 wt% of one sample having a particle size greater than 2 mm, and only 1.5 wt% of the other sample having a particle size greater than 2 mm.

DOE (2004, Appendix BARRIERS) reported the results of Premier MgO hydration and carbonation experiments (Bryan and Snider 2001a; Zhang et al. 2001; Snider 2001; Bryan and Snider 2001b; Snider 2002; Snider 2003a; Snider and Xiong 2002; Xiong and Snider 2003). These experiments included hydration experiments under humid conditions, using a range of relative humidities and temperatures up to 90°C. Inundated hydration experiments were carried out using deionized water, sodium chloride [NaCl] solutions, GWB brine, and ERDA-6 brine at temperatures up to 90°C. The hydration products in deionized water, NaCl solutions, and ERDA-6 brine were identified as brucite using XRD. In experiments with GWB brine, Phase 5 formed initially (Snider 2002). In longer-term experiments, there was XRD evidence that Phase 5 was slowly being replaced by brucite (Snider 2003a).

MgO carbonation experiments were carried out under inundated conditions at CO_2 concentrations that ranged from atmospheric conditions up to 5%, using deionized water, 4 M NaCl, GWB brine, and ERDA-6 brine. Nesquehonite formation [reaction (24)] was only observed at the highest CO_2 partial pressure, and nesquehonite appeared to be replaced by hydromagnesite as these experiments progressed (DOE 2004, Appendix BARRIERS-2.3.2.2). In

all GWB and ERDA-6 inundated experiments with Premier MgO at atmospheric CO_2 partial pressures, hydromagnesite was the only magnesium-carbonate phase detected.

4.2.2 Characterization of Martin Marietta MgO

Particle size data have been reported from a single lot of Martin Marietta MgO. Particle-size analysis carried out by sieving the Martin Marietta MgO indicated that 75 wt% of the MgO particles were between 0.075 and 2 mm (Deng et al. 2007). The mole percent of periclase and lime in this lot of MgO was determined to be 95 ± 2 mole % and the average lime content was determined to be 0.87 ± 0.03 mole %. Additional reactivity testing of Martin Marietta MgO has been carried out for each shipment received at WIPP (see Section 4.6.4).

Deng et al. (2007) reported results of hydration tests in deionized water at 70ºC. These tests were designed to evaluate the potential influence of MgO particle size, stirring rate, and solid-to-liquid ratio. Deng et al. (2007) observed that the Martin Marietta MgO hydrated more quickly in deionized water at 70°C than Premier MgO. Deng et al. (2009) described preliminary results from long-term MgO inundated hydration experiments using Martin Marietta MgO. These experiments included two MgO to brine ratios (3 g/11 ml and 3.1 g/77 ml), three brines (GWB, ERDA-6, and simplified GWB), and three particle-size ranges (as received, 1.0 to 2.0 mm, and less than 0.075 mm). All experiments were conducted at the predicted repository temperature of 28°C. Based on XRD examination, the MgO hydration reaction products were brucite in ERDA-6 brine and brucite plus Phase 5 in GWB and simplified GWB brines. The results showed that MgO particle size affected the hydration rates, with more rapid hydration of smaller particles. The MgO hydration rate was faster in simplified GWB than in GWB or ERDA-6.

4.3 POTENTIAL FORMATION OF IMPERMEABLE MGO REACTION PRODUCTS

Formation of impermeable rims of reaction products on individual periclase grains and impermeable reaction rinds on the masses of MgO in the repository might limit the availability of MgO for complete reaction. The CCA Conceptual Models Peer Review Panel (Wilson et al. 1996a, 1996b, 1997a, 1997b) considered the possible formation of such reaction rims on individual periclase grains or impermeable rinds on masses of MgO. The Panel concluded that formation of magnesium-carbonate reaction products would not inhibit the access of brine to the surfaces of the MgO, and would not render any of the MgO unavailable for reaction with brine and CO_2. SC&A (2008a) determined that no new data had been developed since the time of the peer review to contradict this assumption, and concluded that it was reasonable to assume that essentially all MgO in the backfill will be available for reaction with brine and CO_2. Kanney and Vugrin (2006) evaluated aqueous diffusion of CO_2 in the repository; their results indicated that the gases and liquids in the repository will be sufficiently well mixed to permit contact and reaction of the MgO with brine and CO_2.

4.4 HYDROMAGNESITE CONVERSION TO MAGNESITE

After MgO has reacted to form hydromagnesite, the rate at which it will convert to magnesite affects the moles of CO_2 consumed per mole of MgO reacted during the 10,000-year repository regulatory period. SC&A (2008a) examined the available experimental and natural analogue data

that indicated the hydromagnesite to magnesite reaction rate could be relatively slow, and concluded that this reaction may not be complete during the WIPP repository regulatory period.

4.5 EFFECTS OF CALCIUM CARBONATE PRECIPITATION ON CO_2 CONSUMPTION

Significant amounts of CPR degradation by sulfate reduction would require dissolution of sulfate minerals in the Salado Formation, including anhydrite, gypsum, and polyhalite. Dissolution of these solid phases would release calcium ion into the brine. Elevated calcium concentrations would be expected to cause calcium-carbonate precipitation and increased net consumption of CO_2 per mole of MgO in the backfill. For calculations of the required amounts of MgO in the repository, DOE assumes that no calcium carbonate precipitation will occur. This is a bounding assumption that will lead to an underestimation of the amount of CO_2 consumed per mole of MgO in the backfill.

4.6 PLACEMENT OF MGO BACKFILL AND EXCESS FACTOR CALCULATIONS

MgO emplaced in the repository is obtained from the supplier in a dry granular form (WTS 2009b). This form was selected to minimize dusting in case of a premature bag rupture, ensure sufficient permeability for access of brine for reaction, reduce possible entrainment of MgO in brine flow, and provide sufficient density so adequate amounts can be placed in the repository (DOE 1996, Appendix BACK; DOE 2004, Appendix BARRIERS). Adequate reactivity of supplied MgO has been tested using laboratory procedures (Krumhansl et al. 1997; WTS 2003, WTS 2009b).

MgO is obtained from the supplier packaged in large polypropylene supersacks (WTS 2009b). The MgO supersacks are constructed of woven polypropylene material and are designed to provide a barrier to atmospheric moisture and CO_2 (WTS 2003). The supersacks are provided with a plastic support sheet that remains under the supersacks after placement on the waste containers (WTS 2009b).

4.6.1 CCA MgO Placement and Excess Factor Calculations

At the time of the CCA, DOE calculated the required amount of MgO by assuming that all CPR carbon in the repository could be converted to CO_2. DOE determined that the amount of MgO required to react with this amount of CO_2 would be 43,700 tons (EPA 1997b). The MgO Excess Factor (EF) is defined as:

$$EF = \frac{M_{MgO}}{M_{CO2}} \quad \textbf{(26)}$$

Where:

M_{MgO} is the total moles of emplaced MgO, and

M_{CO2} is the maximum possible number of moles of CO_2 that could be generated by microbial consumption of all carbon in the CPR.

An appropriate EF was included in the engineered barrier design by setting the amount of MgO at 85,000 tons. This quantity was based on the density of the MgO, the volume of the backfill packages, and the amount of space available in the repository for the backfill. The amount of MgO backfill in the CCA provided an EF of 1.95 (EPA 1997b).

Initially, MgO was placed in the repository in 4,200-pound supersacks and 25-pound minisacks. The supersacks were placed on top of various combinations of waste containers, whereas the minisacks were placed among the waste containers and between the waste containers and the sides of the disposal rooms.

4.6.2 MgO Placement and Excess Factor Changes Through the CRA-2004

DOE requested EPA's approval to eliminate the MgO minisacks to enhance worker safety and EPA approved this change in January 2001 (DOE 2004, Appendix BARRIERS; EPA 2001a and 2001b). Elimination of the MgO minisacks decreased the EF to 1.67 (EPA 2001a).

EPA addressed the MgO EF during its review of DOE's request for AMWTF waste disposal at WIPP (Section 3.4.2). This review was required because of the higher CPR densities in AMWTF waste and the potential effects on the amounts of MgO required to maintain an adequate EF (TEA 2004). EPA approved DOE's request to dispose of AMWTF compressed waste at WIPP, subject to the conditions that DOE maintain the MgO EF of 1.67 by adding extra MgO backfill with the compressed waste and that the MgO EF would be calculated on a room-by-room basis assuming that all CPR carbon in the waste could be converted to CO_2 (Marcinowski 2004).

The MgO EF calculations for the CRA-2004 were performed concurrently with the AMWTF review of issues associated with the CPR microbial degradation reactions and effects on the MgO EF (Section 3.4.2). Consequently, EPA's requirement that DOE should assume all CPR carbon could be completely converted to CO_2 was not included in DOE's CRA-2004 calculations. In addition, when calculating the amount of CPR in the repository for the CRA-2004 PA, DOE did not include the CPR materials external to the waste containers, such as shrink wrap placed around the 55-gallon drum 7-packs or the support sheets and packaging materials used for the MgO supersacks (Cotsworth 2004b). EPA pointed out that the MgO EF had not been appropriately computed for the 2004 CRA (Cotsworth 2004b). EPA reiterated the condition that DOE maintain a 1.67 MgO EF on a room-by-room basis, and requested that DOE provide a plan for implementing this condition (Cotsworth 2004b).

DOE provided an emplacement plan designed to ensure the MgO EF was maintained on a room-by-room basis (Detwiler 2004a, Detwiler 2004d). Under this plan, DOE monitors the amounts of MgO backfill and CPR during their emplacement in each room to ensure that the required MgO EF is maintained on a room-by-room basis (Detwiler 2004a). EPA (2006c) concurred with this plan.

Because the AMWTF compressed waste contains higher than average concentrations of CPR, DOE was required to emplace additional MgO. Consequently, in addition to the one supersack per stack of waste that had previously been used in WIPP, DOE began emplacing additional MgO supersacks on racks placed in the repository to achieve the required EF in each room. Each rack contained five supersacks identical to those placed on top of the waste containers and

spanned the same vertical distance normally occupied by the waste containers. Thus, emplacement of additional MgO in the repository used space normally occupied by CH waste (DOE 2009).

4.6.3 Planned Change Request to Reduce MgO Excess Factor

DOE submitted a planned change request (PCR) to EPA to reduce the MgO EF from 1.67 to 1.20 (Moody 2006). EPA requested additional information about the uncertainties related to MgO effectiveness, the size of these uncertainties and their potential impacts on WIPP's long-term performance (Gitlin 2006). DOE responded with an analysis of the uncertainties associated with the effectiveness of MgO and provided an assessment of the effects of these uncertainties on the calculation of required MgO quantities (Vugrin et al. 2006, Vugrin et al. 2007). The uncertainties were divided into four categories:

- Uncertainties in the quantity of CPR that will be consumed
- Uncertainties associated with the quantities of CO_2 produced by microbial degradation of CPR
- Uncertainties related to the amount of MgO available to react with CO_2
- Uncertainties in the moles of CO_2 consumed per mole of available MgO, and in the moles of CO_2 that could be consumed by reaction with other materials

To evaluate the uncertainties associated with the performance of the MgO backfill, Vugrin et al. (2006, 2007) defined the Effective Excess Factor (EEF) as:

$$EEF = \frac{\left(m \times M_{MgO}\right)}{\left(g \times M_c\right)} \times r \qquad \textbf{(27)}$$

Where:

g is the uncertainty in the moles of CO_2 produced per mole of consumed organic carbon,

m is the uncertainty in the moles of MgO available for CO_2 consumption,

M_c is the total moles of organic carbon in the emplaced CPR reported by DOE,

r is the uncertainty in the moles of CO_2 consumed per mole of emplaced MgO, and

M_{MgO} is the total moles of emplaced MgO.

If the EEF equals one or greater, then sufficient MgO is expected to be available to react with all CO_2 produced by CPR degradation and maintain low CO_2 concentrations in the repository.

Vugrin et al. (2006, 2007) addressed the uncertainties associated with the parameters in equation (27). Vugrin et al. (2006, 2007) accounted for the uncertainty associated with the estimated CPR quantities in each container, and made the bounding assumption that all CPR could degrade during the 10,000-year WIPP regulatory period. Vugrin et al. (2006, 2007) also assumed that sufficient sulfate was present in the waste, brines, and Salado minerals for complete degradation

of all CPR carbon in the repository through sulfate reduction and denitrification. Consequently, each mole of organic carbon consumed would produce a mole of CO_2.

SC&A (2008a) observed that the reported masses of CPR in the inventory must be converted to moles of carbon to determine the amount of CO_2 that could be produced by CPR degradation. These calculations require assumptions regarding the chemical composition of the CPR. Assumptions summarized by Wang and Brush (1996) have been used in the past to perform these calculations. EPA (SC&A 2008a) used assumptions regarding the compositions of the CPR to develop reasonable upper-range and lower-range estimates of the moles of carbon in the CPR inventory, which added uncertainty to the estimated moles of CPR carbon in the inventory.

SC&A (2008a) found that preliminary hydration data provided by Wall (2005) indicated the Martin Marietta MgO will likely hydrate and carbonate more rapidly than MgO from the previous suppliers. Deng et al. (2006) calculated that the Martin Marietta MgO contained 96 ± 2 (1σ) mole % reactive periclase plus lime, with periclase making up 95 mole % and lime making up approximately 1 mole %.

In the presence of CO_2 under WIPP repository conditions, hydromagnesite is expected to form initially from brucite or Phase 5, with eventual reaction to form the more stable magnesite phase. SC&A (2008a) examined the available experimental and natural analogue data that indicated the hydromagnesite to magnesite reaction rate could be relatively slow, so this reaction may not be complete during the WIPP repository regulatory period. Vugrin et al. (2007) accordingly used an uncertain variable with a uniform distribution to represent the moles of CO_2 consumed per mole of reacted MgO. This variable ranged from 0.8 (hydromagnesite only) to 1.0 (magnesite only). Vugrin et al. (2007) assumed for the EEF calculation that CO_2 consumption would occur only through precipitation of magnesium carbonate solids, and that no calcium carbonate precipitation would occur. This is a bounding assumption, and will lead to an underestimation of the EEF.

Vugrin et al. (2007) calculated a mean EEF of 1.03, with a standard deviation of 0.0719. SC&A (2008a) found that incorporating the effects of uncertainty associated with the chemical composition of the CPR reduced the EEF to 1.00, with a standard deviation of 0.078. This EEF indicates that if the EF is reduced to 1.20, the average amount of MgO in a disposal room could equal the quantity required to react with CO_2. The EEF calculation, however, includes a number of bounding assumptions, including the assumptions that all CPR will degrade, all carbon in the CPR will react to form CO_2, and carbonate minerals other than hydromagnesite or magnesite will not precipitate, including calcite or aragonite [$CaCO_3$(s)], iron carbonates, or lead carbonates. SC&A (2008a) determined that given these bounding assumptions, it was probable that if the EF was reduced to 1.20, the EEF in the disposal rooms will be greater than 1.00. Consequently, SC&A (2008a) determined that reduction of the EF to 1.20 would be expected to have no significant effects on repository chemistry.

EPA concluded that the available data supported a 1.20 MgO EF (Reyes 2008). EPA approved the PCR, stipulating that DOE should continue to calculate and track both the CPR carbon disposed and the required MgO needed on a room-by-room basis. EPA also required DOE to annually verify the reactivity (periclase plus lime) of the MgO and ensure that it is maintained at 96 ± 2 mole %, as assumed in DOE's supporting documentation.

4.6.4 CRA-2009 MgO Placement and Excess Factor

During review of the CRA-2009, EPA requested that DOE provide additional characterization data for the Martin Marietta MgO (Cotsworth 2009a). EPA noted that the information provided in the CRA-2009 was based on a single lot of this material, and questioned whether analysis of a single lot would be representative (Section 4.2). EPA also questioned whether the reactivity test developed by Krumhansl et al. (1997) for MgO material acceptance was likely to reliably detect MgO with insufficient reactive periclase plus lime (Cotsworth 2009a). In response, DOE provided its revised procedure for MgO acceptance testing (Nemer 2008), and confirmed that characterization and reactivity testing are performed on all Martin Marietta MgO shipments (Moody 2009b).

Nemer (2009) performed a study using samples with known quantities of inert materials to demonstrate that the MgO acceptance test (Nemer 2008) would reliably detect MgO shipments with a percentage of reactive MgO less than the specified 96 ± 2 mole % reactive periclase plus lime. EPA (2010b) concluded that the Nemer (2008) procedure is adequate for testing the moles of periclase plus lime that would rapidly react with brine in the repository.

4.6.5 Planned Change Request for MgO Placement and Supersack Weight

DOE (Franco 2012) notified EPA of planned changes in the emplacement of MgO and MgO supersack weight. Since EPA's approval of the PCR reducing the MgO EF from 1.67 to 1.2 (Section 4.6.3), 4,200 lb supersacks were placed on top of each waste stack and the EF was calculated at the end of each shift after data was uploaded to the Waste Data System (WDS). Based on this EF calculation, additional MgO was placed during the next waste disposal shift to maintain a minimum EF of 1.2. Franco (2012) noted that using this emplacement process, a large excess of MgO was sometimes emplaced, resulting in a range of EF values from 1.22 to 2.85. DOE requested a change to 3,000 lb supersacks placed on alternating waste stacks, with additional supersacks emplaced if required to maintain a minimum EF of 1.2 based on calculations at the end of a waste emplacement shift.

Franco (2012) supported this change with an analysis based on calculations by Kanney and Vugrin et al. (2006). These calculations showed that diffusion alone will be sufficient for CO_2 to reach MgO placed on an adjacent waste stack. Because advection would be expected to increase mixing, emplacement of MgO supersacks on alternating waste stacks was found to be a reasonable emplacement process. DOE also demonstrated using data from a Comprehensive Inventory Database query as of December 31, 2010, that approximately half of the stored and projected waste inventory would require 0.5 or fewer 3,000 lb MgO supersacks per waste stack to maintain an EF of 1.2 (Franco 2012). EPA reviewed the information provided by DOE related to the PCR for MgO emplacement and supersack weight and had no objection to this modification of site procedures (Peake 2012).

4.6.6 CRA-2014 and CRA-2019 MgO Placement and Excess Factors

DOE (2014, Appendix MgO) and DOE (2019, Appendix MgO) describe the emplacement of MgO backfill. WTS (2009a) specifies both 3,000- and 4,200-lb MgO supersacks because using both sizes is more economical and decreases the number of MgO supersack racks required to

maintain a minimum EF of 1.2. Supersacks are placed on every other row of waste stacks and DOE uses WDS information to calculate the sizes of the emplaced supersacks to maintain a minimum EF of 1.2 in each disposal room and minimize the use of supersack racks. The EF in individual WIPP panels and rooms has changed over time because of the elimination of minisacks with reduction of the minimum EF from 1.95 to 1.67 (Section 4.6.2), the approved PCR for reduction of the minimum EF from 1.67 to 1.2 (Section 4.6.3), and increased efficiency achieved by placing supersacks on alternating waste stack rows (Section 4.6.5).

For the CRA-2014, it was reported that as of the inventory cutoff date of December 31, 2012, the overall EF in the WIPP repository was 1.81 (Kouba 2013, DOE 2014 Appendix MgO). The highest EF (2.186) was calculated for Panel 2, which was filled in October 2005, and the lowest EF (1.557) was calculated for Panel 6, which was filled in March 2013 (Kouba 2013). The information provided by Kouba (2013) demonstrated that EF values in each panel exceeded the minimum 1.2 EF. DOE (2014, Appendix MgO) provided the results of 370 reactivity tests carried out on 37 MgO shipments received from April 2009 to December 2012. These results demonstrated the MgO reactivity exceeded the minimum 96 ± 2 mole % reactivity specified by EPA (Reyes 2008).

During review of the CRA-2014, EPA requested additional information about whether the larger lateral distance between MgO supersacks resulting from the emplacement changes since the PABC09 still allows sufficient reaction between MgO and CO_2 (Edwards 2015b). DOE (Franco 2015b) responded with an update of the calculations performed by Kanney and Vugrin (2006). DOE demonstrated that the minimum calculated lateral diffusion length of 1.43 m will allow sufficient reaction between MgO and CO_2 (Franco 2015b).

For the CRA-2019, DOE reported that as of January 8, 2018, which is close to the inventory cutoff date of December 31, 2017, the overall EF in the WIPP repository was 1.792 (Offner 2018, DOE 2019 Appendix MgO). As of December 31, 2017, the highest EF (4.03) was calculated for Panel 3 Room 7, and the lowest EF values (1.22) were calculated for Panel 4 Room 2 and Panel 6 Room 2 (Klein 2018). The information provided by Klein (2018) documents that EF values in each waste disposal room exceed the minimum 1.2 value.

DOE provided the results of 73 reactivity tests carried out on seven MgO shipments received from January 2013 to December 2014 (DOE 2019, Appendix MgO, Batchelder 2018). These results demonstrate the MgO reactivity during this time period met the requirement for 96 ± 2 mole % reactivity specified by EPA (Reyes 2008). Because of the fire and radiological release event in February 2014, waste emplacement was suspended and 385 MgO supersacks were in surface storage from January through December 2016. The stored MgO was resampled, and 18 reactivity tests indicated an average reactivity of 95.9% (DOE 2019, Appendix MgO, Batchelder 2018). From January through December 2017, 21 reactivity tests returned an average reactivity of 96.1%. These results demonstrate that the Martin Marietta MgO met the 96 ± 2 mole percent reactivity specified by EPA (Reyes 2008).

4.7 BACKFILL EFFICACY CONCLUSIONS

The available data indicate that the MgO backfill will continue to control CO_2 fugacity under inundated conditions and maintain chemical conditions in WIPP brines that limit actinide

solubilities. EPA has reviewed the current characterization, testing, and emplacement of MgO in the repository and concluded:

- The current emplacement plan ensures adequate amounts of MgO. The quantities of CPR and MgO are monitored in each room of the repository during emplacement, and additional MgO is emplaced if necessary to maintain the MgO EF of 1.2.
- Because of uncertainties regarding the rate at which hydromagnesite will convert to magnesite in the repository environment, PA calculations of actinide solubilities assume that the brucite-hydromagnesite reaction will buffer CO_2 fugacity at levels consistent with relatively low actinide solubilities under inundated conditions over the 10,000-year regulatory time period.
- EPA has reviewed documentation from DOE regarding the characterization of the Martin Marietta MgO currently used as WIPP backfill and the acceptance testing that is carried out for this material. The MgO reactivity testing procedure and test results provided by DOE (Moody 2009b) demonstrate that the current Martin Marietta backfill material contains a sufficient percentage of reactive periclase plus lime to control chemical conditions in the repository, and that the testing procedure would detect any MgO shipments with inadequate percentages of reactive periclase plus lime. The testing procedure has been incorporated in the MgO specifications (WTS 2009b).
- DOE has not completed an experimental determination of MgO hydration rates using Martin Marietta MgO. Because the majority of MgO in the repository is Martin Marietta MgO and MgO hydration rates are important to repository water balance calculations (Section 12.4.1), DOE should provide updated hydration rates for future WIPP PAs that are consistent with the characteristics of MgO in the repository.

5.0 RADIONUCLIDES INCLUDED IN BRINE MOBILIZATION CALCULATIONS

Mobilization of radionuclides in brine as dissolved or colloidal species is important for calculating radionuclide releases through DBRs, and for calculating releases by transport through the Culebra or Salado to the WIPP boundary. DOE uses the PANEL code to calculate the radionuclide source term for DBRs and for releases via a borehole to the Culebra Member of the Rustler Formation. DOE uses the NUTS code to calculate radionuclide releases via transport through the Salado Formation or the Culebra Member to the WIPP boundary.

Not all elements and isotopes in the WIPP inventory contribute significantly to DBRs or to releases by transport through the Salado and Culebra. The radionuclides included in solubility calculations and colloid formation were identified for the CCA as americium, neptunium, plutonium, thorium, and uranium (DOE 1996, Appendix WCA). DOE (1996) assumed curium would exhibit the same chemical behavior and oxidation state as americium. DOE (1996) assumed that mobilized concentrations of cesium and strontium in brine would be controlled by their limited waste inventories, and radium was excluded because of its short half-life.

DOE has noted that inclusion of all radionuclides in the WIPP inventory in the PA calculations would be computationally complex and time consuming. Consequently, the number of radionuclides directly included in PA is reduced using an algorithm originally developed for the CCA (DOE 2014, Appendix PA, Figure PA-17; DOE 2019, Appendix PA). Kicker (2019b) describes the selection process for radionuclides included in modeling releases for the CRA-2019 DPA, with additional information provided by Sarathi (2019a). The isotopes included in PA calculations are summarized in Table 5-1. The oxidation states of these radionuclides modeled in the actinide solubility calculations are summarized in Section 6.0. Calculations of the mobilized concentrations of these actinides as dissolved and colloidal materials are described in Sections 7.0 and 8.0, respectively. The radionuclides included for the CRA-2019 DPA calculations remain appropriate.

Table 5-1. Radionuclides Included in DBRs and Transport Calculations through the Salado and Culebra

Direct Brine Release	Culebra and Salado Release
^{238}Pu, ^{239}Pu, ^{240}Pu, ^{241}Pu, ^{242}Pu	^{239}Pu, ^{240}Pu, ^{242}Pu
^{241}Am, ^{243}Am	^{241}Am
^{233}U, ^{234}U, ^{235}U, ^{236}U, ^{238}U	^{233}U, ^{234}U
^{229}Th, ^{230}Th, ^{232}Th	^{229}Th, ^{230}Th
^{237}Np	
^{243}Cm, ^{244}Cm, ^{245}Cm	

Source: DOE (1996, Appendix WCA)

6.0 ACTINIDE OXIDATION STATES

The actinide oxidation states assumed for the CRA-2019 DPA have remained unchanged since the CCA. Assumptions regarding the actinide oxidation states were peer reviewed and approved for the CCA as part of the Dissolved Actinide Source Term and Chemical Conditions conceptual models (Wilson et al. 1996a, 1996b, 1997a, 1997b).

The Chemical Conditions conceptual model does not include the assumption of equilibrium for redox reactions among the actinides. Actinide oxidation states were determined based on the assumption that reducing conditions would be established relatively quickly in the WIPP repository, combined with the results of a literature review and experimental investigations. The actinide oxidation states that were predicted to persist in the WIPP repository environment over the long term were (DOE 1996, Appendix SOTERM):

- Am(III), Cm(III), and Th(IV),
- Pu(III) and Pu(IV),
- Np(IV) and Np(V), and
- U(IV) and U(VI).

DOE used the Fracture-Matrix Transport code (FMT) to calculate actinide solubilities for the CCA PAVT, PABC04, and PABC09 and used the EQ3/6 code to calculate actinide solubilities for the CRA-2014 PA and CRA-2019 DPA. FMT does not include the calculation of oxidation states. Consequently, DOE based the actinide oxidation states for the CCA PAVT, PABC04, and PABC09 on sampling of an oxidation-state parameter. The EQ3/6 code can be used to calculate oxidation states, but DOE retained the same approach for assigning oxidation states for plutonium, neptunium, and uranium for the CRA-2014 PA and CRA-2019 DPA to remain consistent with the Chemical Conditions conceptual model.

Plutonium, neptunium, and uranium may be present in either of two oxidation states in WIPP PA calculations, so the parameter GLOBAL:OXSTAT is sampled from a uniform distribution that ranges from 0.0 to 1.0 (DOE 2019, Appendix PA; Kim and Feng 2019). DOE assumes the Pu(III), Np(IV), and U(IV) oxidation states are present for half of the PA realizations (sampled GLOBAL:OXSTAT values less than or equal to 0.5), and the Pu(IV), Np(V), and U(VI) oxidation states are present for the other half of the PA realizations (sampled GLOBAL:OXSTAT values greater than 0.5).

The actinide oxidation states assumed for the PA calculations are important because of the effects of redox state on actinide solubilities (Section 7.0) and colloidal concentrations (Section 8.0). Reduced actinides [Pu(III), Pu(IV), Np(IV), and U(IV)] form solids that have lower solubilities than actinides in higher oxidation states [Pu(V), Pu(VI), Np(V), and U(VI)]. In contrast, Pu(III) is more soluble than Pu(IV) under the moderately alkaline pH conditions in the WIPP repository, and the mean total mobilized Pu(III) concentration in WIPP brines is higher than the mean total mobilized Pu(IV) concentration (Section 9.0)

6.1 ACTINIDE OXIDATION STATE INFORMATION DEVELOPED FOR THE CCA PAVT, PABC04, AND PABC09

EPA (1998c) reviewed and agreed with the expected oxidation states used in the CCA PA and PAVT. At the time of the CCA, most stakeholder questions about actinide oxidation states concerned the possible persistence of Pu(VI) in the WIPP repository. EPA (1998c) considered several experimental studies indicating that reductants, including soluble iron, metallic iron, humic substances, and other organic ligands would reduce plutonium to the Pu(III) and Pu(IV) oxidation states under equilibrium conditions in the repository (Weiner 1996; Felmy et al. 1989; Rai and Ryan 1985; Choppin 1991).

For the PABC04, EPA (2006c) reviewed additional information regarding likely actinide oxidation states in WIPP brines. The investigations considered by EPA (2006c) included Grambow et al. (1996), Villareal et al. (2001), Haschke et al. (2000), Slater et al. (1997), Xia et al. (2001), Reed et al. (1997), ANL (1997), and André and Choppin (2000). Based on this review, EPA (2006c) concluded the available evidence continued to support the actinide oxidation state assumptions used for the WIPP PABC04 calculations.

For the PABC09, EPA (2010b) concluded that the assumption that uranium may exist in either the U(IV) or U(VI) oxidation state in the WIPP repository remained valid based on a review of data from numerous uranium studies, including Grambow et al. (1996), Gu et al. (1998), Dodge et al. (2002), O'Loughlin et al. (2003), Fiedor et al. (1998), Xia et al. (2001), Hua et al. (2006), Lovley and Phillips (1992), Frederickson et al. (2000), Suzuki et al. (2003), Brooks et al. (2003), Neiss et al. (2007), Francis and Dodge (2008), and Francis et al. (2000). EPA (2010b) concluded that U(IV) is likely to be the most stable oxidation state under the reducing conditions in the WIPP repository, but U(VI) might persist because of the effects of aqueous speciation on uranium reduction.

EPA (2010b) reviewed neptunium oxidation state investigations for the PABC09 that included Rai and Ryan (1985), Xia et al. (2001), Banaszak et al. (1999), Rittmann et al. (2002), and Icopini et al. (2007). EPA (2010b) concluded that neptunium will most likely be present in the Np(IV) oxidation state and the assumption that neptunium may be present in the Np(V) oxidation state in the WIPP repository brines is conservative because of the greater solubility of Np(V) solid phases. Because of the relatively small neptunium inventory, the assumption of higher neptunium solubility in half of the PA realizations is unlikely to significantly affect repository releases.

EPA (2010b) found that the available data continued to support DOE's assumption that plutonium will be present in the less-soluble Pu(III) and Pu(IV) oxidation states, rather than the more-soluble Pu(V) and Pu(VI) oxidation states. Investigations related to plutonium oxidation states reviewed by EPA (2010b) included Rai et al. (2002), Ding et al. (2006), Reed et al. (2006), Neck et al. (2007), Altmaier et al. (2009), Xia et al. (2001), Reed et al. (2010), Reed et al. (2007), Boukhalfa et al. (2007), Ohnuki et al. (2007), and Icopini et al. (2009). EPA (2010b) noted that the relatively more soluble Pu(III) oxidation state may be stable or may metastably persist under anticipated WIPP repository conditions. Radiolytic effects on actinide oxidation states have been assumed to be mitigated by the effects of reducing materials, mainly iron metal,

in the WIPP repository and EPA (2010b) found that the available data continued to support this assumption.

6.2 ACTINIDE OXIDATION STATE INFORMATION DEVELOPED FOR THE CRA-2014 PA

Actinide oxidation state assumptions used in the CRA-2014 PA remained unchanged from previous PA assumptions (DOE 2014).

6.2.1 Uranium and Neptunium Oxidation States

EPA (2017d) reviewed information provided by DOE (2014) and observed that extensive experimental data showed that Fe(II) aqueous species and magnetite can reduce U(VI) to U(IV). These data were provided by Regenspurg et al. (2009), Du et al. (2011), Myllykylä and Ollila (2011), Scott et al. (2005), Duro et al. (2008), Latta et al. (2012), and Huber et al. (2012). Singer et al. (2012a, 2012b) found that formation of Ca-U(VI)-CO_3 aqueous species limited U(VI) reduction by magnetite, but these aqueous species are unlikely to form in significant quantities in WIPP brines because of low carbonate concentrations maintained by the MgO backfill. Gallegos et al. (2013) and Hyun et al. (2012) found that mackinawite [FeS(s)] reduced U(VI) to U(IV). These data indicate that U(IV) is likely to be the predominant oxidation state in WIPP brines under the highly reducing conditions established by iron metal and iron sulfides in the repository. The relatively low calcium and carbonate concentrations anticipated in WIPP brines are likely to be conducive to uranium reduction and low solubilities. Consequently, the assumption that U(VI) will be present in half of the PA realizations is likely to be quite conservative.

No new data were identified regarding neptunium oxidation states. Consequently, EPA (2017d) found that the assumption that neptunium will be present as either Np(IV) or Np(V) continued to be conservative.

6.2.2 Plutonium Oxidation States

DOE (2014, Appendix SOTERM) stated that Pu(IV) was the most likely oxidation state in WIPP brines and equilibrium solid phases. DOE indicated that inclusion of the Pu(III) oxidation state in the actinide solubility calculations used in PA was a conservative assumption because of the generally higher solubilities of Pu(III) solids in WIPP brines. However, EPA (2017d) observed that more recent data (e.g., Altmaier et al. 2009, Reed et al. 2011) show that Pu(III) in WIPP repository brines and equilibrium solid phases may be more important than was previously recognized.

In response to completeness comments from EPA, DOE acknowledged that data developed since the CRA-2009 PA suggest that Pu(III) may be more important for WIPP PA than previously understood (Shrader 2015). In this response, DOE discussed the likely effects of reduced iron, organic ligands such as EDTA, and microbial processes on plutonium oxidation states. DOE concluded that although Pu(III) could be formed under some conditions, Pu(IV) would continue to be important because of its stabilization by EDTA and its production by radiolysis (Shrader 2015). Because DOE's response (Shrader 2015) raised issues related to radiolytic effects on actinide oxidation states and the potential effects of reductive dissolution of Pu(IV) solid to form Pu(III) aqueous species, EPA (2017d) carried out a detailed review of the available data. In this

assessment of likely plutonium oxidation states in the WIPP repository, EPA (2017d) considered the highly reducing conditions likely in the long-term WIPP repository, including $H_2(g)$ pressures much greater than 1 atm. EPA (2017d) reviewed the likely effects of iron solids and aqueous species on plutonium oxidation states, including additional data provided by Reed et al. (2011) from experiments with WIPP brines with added Pu(VI) and magnetite, iron coupons, and iron powder that equilibrated for about 5.8 years. The plutonium solid phase in these experiments was predominantly Pu(III), and over time, transformation of the Pu(IV) solids to Pu(III) solids coincided with increased aqueous plutonium concentrations. Altmaier and Geckeis (2011) performed long-term experiments in 3.5 M $MgCl_2$ and found that plutonium reduction by powdered metallic iron resulted in Pu(III) solids in equilibrium with Pu(III) aqueous species as well as $PuO_2(s)$ reductive dissolution, with Pu(IV) solids in equilibrium with Pu(III) aqueous species:

$$PuO_2(am) + 4\ H^+ + e^- \leftrightharpoons Pu^{3+} + 2\ H_2O(l) \quad \textbf{(28)}$$

Additional evidence of reductive dissolution of $PuO_2(s)$ by iron solids was provided by Felmy et al. (2011, 2012) in experiments with goethite [FeOOH(s)] and magnetite. EPA (2017d) evaluated the available literature on the effects of organic ligands on plutonium oxidation states, including AlMahamid et al. (1996), Reed et al. (1996), Reed et al. (1998), Boukhalfa et al. (2003, 2004), and Rai et al. (2008). EPA (2017d) concluded that organic ligands potentially increase the likelihood of reductive dissolution and the presence of Pu(III) under WIPP repository conditions. Investigations by Choppin (1991), André and Choppin (2000), Marquardt et al. (2004, 2008) and Banik (2006) indicated that humic substances reduced Pu(V) and Pu(VI) to a mixture of Pu(III) and Pu(IV).

EPA (2017d) reviewed literature related to microbial reduction of Pu(VI) and Pu(V) to Pu(IV) and/or Pu(III) (Rusin et al. 1994, Bolton et al. 2006, Boukhalfa et al. 2007, Francis et al. 2007, Icopini et al. 2009, Plymale et al. 2012). EPA (2017d) found that there are extensive data that show biotic plutonium reduction can occur under low-ionic-strength conditions and that EDTA or other ligands can promote dissolution and reduction, but only limited data are available for high-ionic-strength solutions such as WIPP repository brines. There are limited data available showing that biotic reduction of Fe(III) to Fe(II) can occur in high ionic strength solutions (Reed et al. 2011, Emmerich et al. 2012). This Fe(II) could in turn cause plutonium reduction. However, it is uncertain whether microbes present in WIPP halite can cause either direct plutonium reduction or indirect plutonium reduction via production of Fe(II).

EPA (2017d) concluded that under WIPP conditions, aqueous Pu(III) would likely exist in equilibrium with either Pu(III) or Pu(IV) solid phases [$Pu(OH)_3(s)$ or $PuO_2(s)$] but also concluded there was evidence suggesting the stability of Pu(III) over Pu(IV). EPA (2017d) found that the available data indicated that the existing assumption that plutonium would be present in the Pu(IV) oxidation state in both the aqueous and solid phases in half of the PA realizations would underestimate plutonium solubilities in WIPP brines in those realizations, and recommended an independent technical review to resolve this issue.

6.3 ACTINIDE OXIDATION STATE INFORMATION DEVELOPED FOR THE CRA-2019 DPA

DOE's CRA-2019 DPA actinide oxidation state assumptions remained unchanged from previous PA assumptions. Actinide chemistry, including expected oxidation states in the WIPP repository, is addressed for the CRA-2019 by DOE (2019, Appendix SOTERM).

6.3.1 Uranium and Neptunium Oxidation States

DOE (2019) reviewed investigations of uranium oxidation-reduction reactions published since the CRA-2014, including investigations of U(VI) reduction by zero-valent iron (Yan et al. 2014, Sheng et al. 2014, Xu et al. 2014, Crane and Scott 2014, Crane et al. 2015, Hua et al. 2018, Li et al. 2015, Zhang et al. 2015). Tsarev et al. (2016) investigated U(VI) sorption by clay minerals and subsequent reduction to U(IV) by aqueous Fe(II) at pH values greater than 7.6. Cevirim-Papaioannou et al. (2018) investigated uranium redox behavior under anoxic conditions in 0.1 and 5.0 M NaCl solutions at pmH values ranging from 2 to 14.5 in the presence of various reducing agents. The results showed that U(VI) was reduced to U(IV) under all experimental conditions. DOE (2019) concluded that U(IV) is likely to be the predominant oxidation state under WIPP repository conditions. This conclusion is supported by the available data, and use of U(VI) in half of the PA realizations results in an overprediction of uranium concentrations mobilized in WIPP brines.

Investigations of neptunium oxidation-reduction reactions reviewed by DOE (2019) included an experimental investigation of Np(V) interaction with fresh and corroded iron surfaces under anaerobic conditions (Yang et al. 2017). In this investigation, reductive precipitation of disordered Np(IV) solid was observed on the fresh iron surfaces and on pre-corroded iron with a magnetite surface composition. Altmaier et al. (2017) investigated the ability of different reductants to stabilize the Np(IV) oxidation state, including powdered iron metal. Altmaier et al. (2017) reported that powdered iron is a strong reductant that effectively maintains the Np(IV) oxidation state, but noted that powdered iron can slowly lose its reducing capacity over time above pmH ~ 10 because of surface passivation.

Other recent studies have demonstrated that Fe(II) solids and aqueous species can reduce Np(V) to Np(IV). Scheinost et al. (2016) investigated the sorption of Np(V) onto siderite [$FeCO_3$] and its surface reduction to Np(IV). In this study, addition of Np(V) to an aqueous Fe(II)-carbonate solution resulted in the precipitation of an Np(IV)-pentacarbonate solid phase. Bots et al. (2019) found that interaction of aqueous Np(V) with magnetite produces Np(IV) through a surface-mediated reduction mechanism. Roberts et al. (2019) coprecipitated Fe(II)-bearing magnetite and green rust with $Np(V)O_2^+$ and determined that Np(V) was reduced to Np(IV). The evidence that has accumulated since the CCA PAVT clearly indicates that in the WIPP repository, the presence of large amounts of iron metal and Fe(II)-bearing corrosion products will maintain the Np(IV) oxidation state.

6.3.2 Plutonium Oxidation States

Based on a review of the CRA-2014 and the relevant literature, EPA (2017d) concluded that dissolved plutonium concentrations in WIPP repository brines would likely be controlled by

aqueous Pu(III) in equilibrium with the Pu(III) solid $Pu(OH)_3(s)$ or by the equilibrium between aqueous Pu(III) and the Pu(IV) solid $PuO_2(am)$. The latter process of reductive dissolution results in higher total dissolved plutonium concentrations than the dissolution of Pu(IV) solid to Pu(IV) aqueous species. EPA (2017d) concluded that DOE underpredicted dissolved plutonium concentrations by including dissolved Pu(IV) concentrations in equilibrium with Pu(IV) solids in 50% of PA realizations.

EPA continued to evaluate plutonium oxidation states in the WIPP repository after the CRA-2014 review (Schramke et al. 2020). This evaluation considered the potential effects of high $H_2(g)$ pressures in the post-closure repository caused by anoxic corrosion of iron (Section 3.1). Actinide solubility calculations and predicted total mobilized actinides are important for DBRs, which can occur at repository pressures that are equal to or exceed the hydrostatic pressure of 8 MPa (79 atm). Repository pressures can range up to the lithostatic pressure of 15 MPa (148 atm). Because the repository gas phase will consist mainly of $H_2(g)$, the $H_2(g)$ pressures in the repository during a DBR release will range from approximately 79 to 148 atm. Most pe - pH diagrams illustrating the relative stability of plutonium species, including Figure SOTERM-22 (DOE 2019), are generated assuming 1 atm total pressure. However, the higher $H_2(g)$ pressure expected in the WIPP repository increases the stability field of water, and expands the conditions under which Pu(III) solids are in equilibrium with aqueous Pu(III) to lower pe values (Figure 6-1).

The iron corrosion products in the long-term WIPP repository based on project experiments are most likely to be Fe(II) oxyhydroxides including $Fe(OH)_2(s)$ and hibbingite (Section 3.1.1). Other investigations have identified magnetite as a potential reaction product of anoxic iron corrosion (Selwyn 2004, Saheb et al. 2010). The likely redox conditions in the WIPP repository range from the most reducing, at a P_{H2} of 150 atm, to an upper limit on redox conditions where $Fe(OH)_2(s)$ is in equilibrium with magnetite. Schramke et al. (2020) performed a series of calculations to show that the solubility of Pu(III) solids will control aqueous plutonium concentrations under these WIPP repository conditions using the Specific Ion Interaction Theory (SIT) to calculate activities. Although there are uncertainties associated with use of SIT to model at high ionic strengths, and although there are additional uncertainties regarding the Pu(III) solids that will form, calculations indicate that the extremely reducing WIPP repository conditions will be well within the stability field of the Pu(III) solids. As a result, because of the higher solubility of Pu(III) solids, higher dissolved plutonium concentrations will be present in WIPP brines than are predicted using the solubility of Pu(IV) solid phases.

DOE (2019) provided its perspective on plutonium oxidation states, and Figure SOTERM-22 illustrated DOE's conceptualization of WIPP pH and redox conditions. However, DOE's lower limit for redox conditions is inconsistent with expected extremely reducing post-closure repository conditions. Only Fe(II) solids or possibly magnetite, which is a mixed Fe(II)/Fe(III) solid, are expected to form under WIPP repository conditions. The entire pe range illustrated for WIPP conditions on Figure SOTERM-22 is within the stability field of Fe(III) solid phases. Consequently, the pe range illustrated in Figure SOTERM-22 for WIPP conditions is too high to be consistent with the iron corrosion products expected in the WIPP repository. Calculations performed by Schramke et al. (2020) indicated that the maximum pe values established by equilibrium between magnetite and $Fe(OH)_2(s)$ in WIPP brines will be within the stability field of Pu(III) solids and aqueous species.

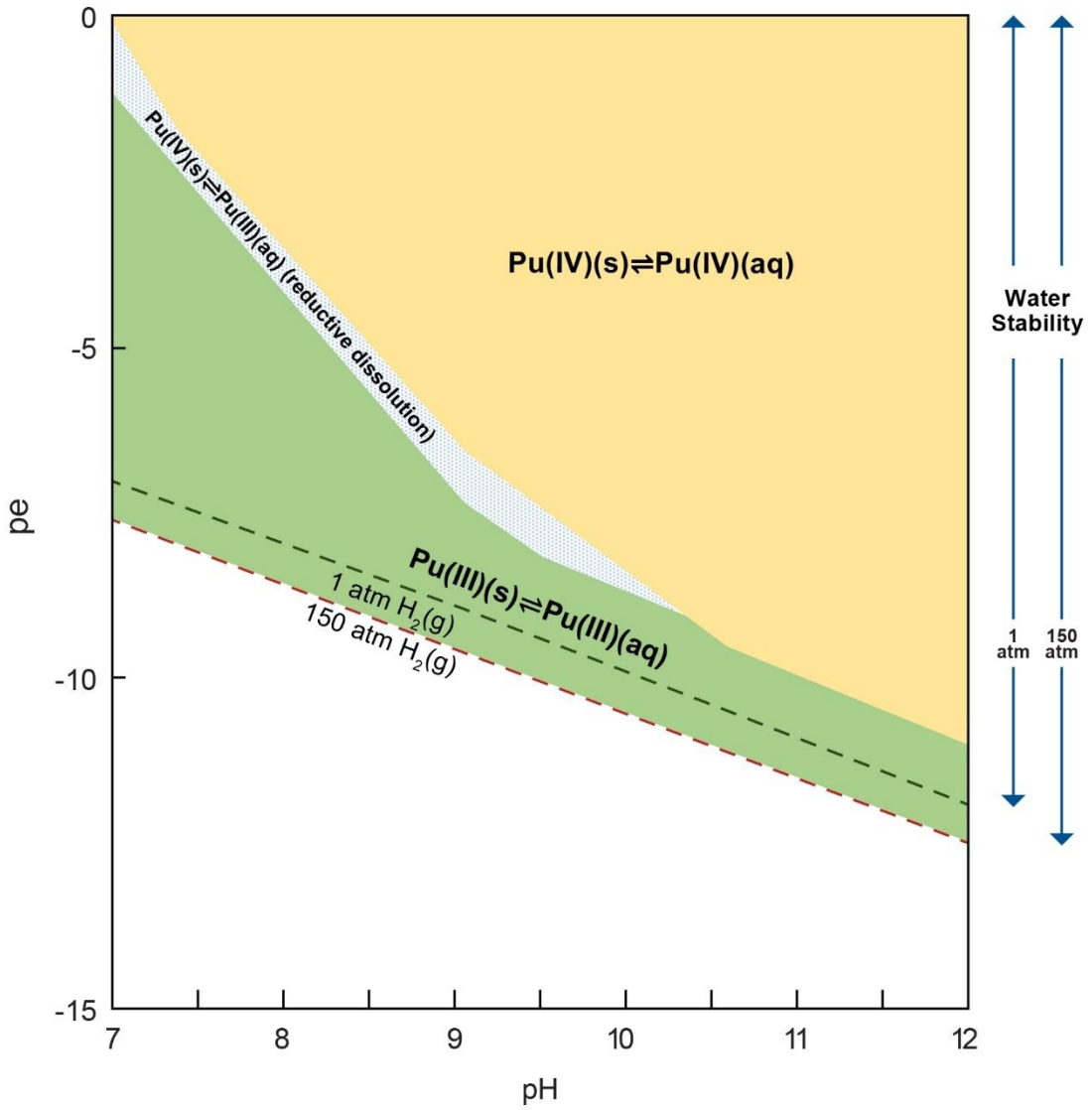

Figure 6-1. Reactions that Control Plutonium Solubility as a Function of pH and Redox Conditions (pe), Showing the Expanded Stability Field for Pu(III) Aqueous Species and Solids at Elevated H_2(g) Pressure (3 m NaCl and 1 × 10^{-8} m Total Plutonium, Schramke et al. 2020)

DOE (2019) cited an investigation by Rai and Ryan (1982) as evidence supporting the radiolytic formation of localized oxidizing zones in the WIPP repository, where higher-valent plutonium oxidation states can exist. Rai and Ryan (1982) conducted experiments with initially crystalline PuO_2(s) and observed that the solid became less crystalline over time. Rai and Ryan (1982) hypothesized that radiolysis produced transient Pu(V) and Pu(VI) aqueous species, which were quickly reprecipitated as amorphous PuO_2(s). However, Rai and Ryan (1982) noted that reducing radiolytic aqueous species, such as a hydrated electron and the hydrogen atom, may also have caused transient dissolution [as Pu(III)] and reprecipitation as amorphous PuO_2(s). These experiments were not carried out under the reducing conditions predicted for the WIPP repository, including the presence of iron metal and high H_2(g) pressure. In addition, the net

effect of radiolysis in these experiments was the formation of less-crystalline PuO_2(s), without any demonstrated change in oxidation state. Consequently, using this study to support the formation of localized oxidizing zones in the WIPP repository is highly speculative.

DOE (2019, Appendix SOTERM) reviewed the literature related to plutonium reduction by EDTA and concluded that there is ample evidence that Pu(V) and Pu(VI) would be reduced by EDTA. DOE (2019) stated that the available data should be interpreted as inconclusive regarding the effects of EDTA on the long-term stability or formation of Pu(III) under WIPP-relevant conditions. However, Plymale et al. (2012) showed that EDTA facilitated abiotic reduction of solid Pu(IV) to aqueous Pu(III) in the presence of H_2, which indicates that in the presence of high H_2(g) pressures in the WIPP repository, EDTA is likely to stabilize Pu(III) over Pu(IV).

Cho et al. (2016) investigated the solubility of $Pu(OH)_3$(am) and the hydrolysis of Pu^{3+} in 0.1 M $NaClO_4$. The total Pu(III) concentrations measured by Cho et al. (2016) are consistent with the concentrations reported by Felmy et al. (1989) at low ionic strength. However, Cho et al. (2016) calculated the $Pu(OH)_3$(am) solubility constant by including an experimentally determined hydrolysis constant for the formation of $PuOH^{2+}$, whereas Felmy et al. (1989) assumed that formation of this hydrolysis species would be negligible in the studied pH range. Cho et al. (2016) demonstrated that their solubility constant differed from the Felmy et al. (1989) value because of the inclusion of this hydrolysis constant in their calculations.

DOE (2019) pointed out that the solubility and hydrolysis constants calculated by Cho et al. (2016) are inconsistent with the NEA-TDB (Nuclear Energy Agency Thermochemical Database) values (Guillaumont et al. 2003). However, a more recent review of the $Pu(OH)_3$(am) solubility and $PuOH^{2+}$ stability data accepted the results of Cho et al. (2016), and revised the solubility and stability constants in the NEA-TDB (Grenthe et al. 2020). The results of the Cho et al. (2016) investigation show that $Pu(OH)_3$(am) is less soluble, and hence more stable, than indicated by the solubility constant calculated by Felmy et al. (1989). The experimental results of the Cho et al. (2016) and Felmy et al. (1989) investigations are in very good agreement if the first hydrolysis constant from Cho et al. (2016) is included in the solubility constant calculation using the Felmy et al. (1989) solubility data (Grenthe et al. 2020). Consequently, the solubility for $Pu(OH)_3$(am) and first hydrolysis constant for Pu^{3+} appear well established.

Tasi et al. (2018) investigated the solubility and redox states of plutonium under a range of redox conditions. The lowest oxidation state experiments included $SnCl_2$ to buffer the pe to values close to the lower stability limit of water at 1 atm. In these experiments, the plutonium solid phase appeared to be a mixture of Pu(III) and Pu(IV) solids. As illustrated by the calculations carried out by Schramke et al. (2020), the Tasi et al. (2018) experimental conditions were more oxidizing than expected WIPP repository conditions and are in a region within the predicted stability of both Pu(III) and Pu(IV).

Dumas et al. (2019) performed plutonium/magnetite coprecipitation experiments under anoxic conditions to determine whether Pu(III) would be structurally incorporated in the magnetite. Initial experiments were performed under anoxic conditions using either Pu(III) or Pu(V) stock solutions. Pu(V) was quickly reduced to Pu(III) during precipitation of magnetite. Freshly precipitated magnetite incorporated Pu(III) in nearly equal proportions by structural incorporation within the magnetite and adsorption. After magnetite recrystallization meant to

simulate long-term aging of the magnetite, Pu(III) continued to be strongly retained but sorption became more important than structural incorporation.

Bone et al. (2019) provided preliminary x-ray absorption near-edge spectroscopy (XANES) data for plutonium solid phases obtained from Reed et al. (2011) experiments, which were previously discussed in Section 6.2.2. The total equilibration period for the experiments at the time of XANES measurement was 11 years. Solids from six experiments were evaluated, five samples from experiments that included powdered metallic iron, and a sixth sample from an experiment with Fe(III) hydroxide solid. Solid samples from experiments with metallic iron were dominantly Pu(III), whereas in the experiment with Fe(III) solid, the plutonium solid was not reduced to Pu(III). These results are consistent with the dominant oxidation state of Pu(III) in the WIPP repository because of the large inventory of metallic iron in the waste and waste containers and the expected absence of Fe(III) solids.

Information developed since the CRA-2014 indicates that Pu(III) solid phases are more stable than previously believed, and EPA expects that the Pu(III) oxidation state will predominate under the highly reducing conditions in the long-term WIPP repository because of the presence of metallic iron, Fe(II) solids, Fe(II) aqueous species, and high H_2(g) pressures. Consequently, EPA expects DOE to assume plutonium will be present in the +III oxidation state in all PA realizations to provide a reasonable upper bound on total mobilized plutonium concentrations in WIPP brines. If DOE does not assume that plutonium mobilization will be controlled by the Pu(III) oxidation state in all future WIPP PA realizations, then DOE must provide data that support its alternative approach.

6.4 ACTINIDE OXIDATION STATES SUMMARY AND CONCLUSIONS

EPA has reviewed the available data related to the assumed actinide oxidation states for WIPP PA:

- DOE appropriately assumes that Am(III), Cm(III), and Th(IV) are the only redox states for these actinides.
- High H_2(g) pressures, ranging from approximately 79 atm to 149 atm, will exist in the WIPP repository under the conditions where a DBR could occur. These high H_2(g) pressures, combined with the presence of iron metal and corrosion products that contain Fe(II) [$Fe(OH)_2$(s), hibbingite, and possibly magnetite], will create strongly reducing conditions.
- For the CRA-2019 DPA and all previous WIPP PAs, half of PA realizations were performed assuming the presence of the more reduced actinide oxidation states [Pu(III), Np(IV), and U(IV)] while half were performed assuming the more oxidized states [Pu(IV), Np(V), and U(VI)].
- Data has become available demonstrating that under long-term WIPP repository conditions, more reduced oxidation states [Pu(III), Np(IV), and U(IV)] will be the dominant oxidation states in WIPP solid phases and aqueous species and EPA expects that all PA realizations in future WIPP PAs will be performed assuming the presence of these reduced oxidation states.

- Using the Np(V) and U(VI) oxidation states for 50% of PA realizations has relatively small effects on PA results because neptunium and uranium do not significantly contribute to total actinide releases.
- Using the Pu(IV) oxidation state for 50% of PA realizations results in an underestimation of total mobilized plutonium and underpredicts plutonium releases through DBRs, or by transport through the Culebra or Salado.

Under the highly reducing conditions in the WIPP repository, the evidence reviewed above demonstrates that the lowest oxidation states for plutonium, neptunium, and uranium are most likely to be the predominant oxidation states. The effects of the assumed plutonium oxidation state on total mobilized plutonium in WIPP PA are further addressed in Section 9.0 and the effects on repository releases are considered in Section 13.4.4.

7.0 DISSOLVED ACTINIDE SOURCE TERM

Actinides in the WIPP waste inventory may dissolve in brine that flows into the repository from the DRZ in the Salado Formation, or in brine that flows up a borehole that intersects both the repository and a pressurized brine region in the underlying Castile Formation. The actinide solubilities calculated for WIPP PA include americium, curium, neptunium, plutonium, thorium, and uranium.

Actinide solubilities are calculated using thermodynamic modeling that depends on a number of assumptions about the chemical conditions in the repository and the chemical behavior of the actinides in solution. Consequently, both the Chemical Conditions and Dissolved Actinide Source Term conceptual models are important for calculating dissolved actinide concentrations used in PA. These conceptual models are described in detail by SC&A (2008b, Appendix A).

The Chemical Conditions conceptual model includes assumptions related to the mineralogy of the Salado Formation in contact with WIPP brines, the compositions of the Salado and Castile brines that may enter the repository, organic ligand concentrations, and the reactions that may control important chemical parameters, such as pH, redox, and CO_2 fugacity. The Chemical Conditions conceptual model also includes assumptions regarding the redox states of actinides and metals in solution. The Dissolved Actinide Source Term conceptual model includes assumptions about the oxidation states of the actinides, equilibrium of the brine with respect to precipitation-dissolution reactions, the existence of reducing conditions in the repository, the important inorganic and organic constituents for determining actinide speciation in brines, and use of the Pitzer activity coefficient model.

The FMT code was used to calculate actinide solubilities for the CCA PAVT, PABC04, and PABC09. FMT was replaced by the EQ3/6 code for the CRA-2014 PA and CRA-2019 DPA. The FMT and EQ3/6 calculations of aqueous concentrations in WIPP brines are based on calculations of aqueous speciation and solubility equilibria performed using the Pitzer activity coefficient model. The actinide solubility calculations do not include redox reactions and the oxidation state of each actinide is instead assumed for the calculations (Section 6.0).

7.1 DISSOLVED ACTINIDE SOURCE TERM FOR THE CCA PA THROUGH PABC09

The Dissolved Actinide Source Term and Chemical Conditions conceptual model assumptions were peer reviewed and approved for the CCA PA (Wilson et al. 1996a, 1996b, 1997a, 1997b). DOE performed FMT modeling calculations for the CCA PAVT to determine the solubilities of Am(III), Th(IV), and Np(V) in end-member Salado (Brine A) and Castile (ERDA-6) brine. DOE assumed that actinide solubilities in brine mixtures would be adequately represented by calculations with the end-member brines. For these solubility calculations, DOE assumed that the brines would be in equilibrium with the Salado minerals anhydrite and halite, as well as brucite and hydromagnesite that would form from hydration and carbonation, respectively, of the MgO backfill. DOE allowed the minerals glauberite [$Na_2Ca(SO_4)_2$] and Phase 3 [$Mg_2Cl(OH)_3 \cdot 4H_2O$(cr)] to precipitate from the brines. Additional details about the CCA and PAVT dissolved actinide source term calculations are provided by Appendix SOTERM of the CCA (DOE 1996) and by EPA (1998c).

DOE (2004) made a few revisions to the actinide solubility calculations for the CRA-2004 PA, but the calculations remained consistent with the Dissolved Actinide Source Term and Chemical Conditions conceptual models. DOE's revisions included a change in the Salado brine composition from Brine A to GWB and updates to the geochemical modeling database (Attachment B) to include the effects of organic ligands on actinide solubilities.

At the direction of EPA (Cotsworth 2005), DOE incorporated a number of changes in the actinide solubility calculations for the PABC04 relative to the CRA-2004 PA. These changes included use of an updated FMT thermodynamic database, revised estimated concentrations of organic ligands, revised actinide solubility uncertainties, and a revised U(VI) concentration. EPA (2006c) provides a detailed review of the CRA-2004 PA and PABC04 actinide solubility calculations.

DOE (2009) used the actinide solubilities calculated for the PABC04 for the CRA-2009 PA dissolved actinide source term. Use of the PABC04 actinide solubilities for the CRA-2009 PA did not consider updated inventory data or new aqueous speciation or solubility data published since the PABC04. DOE revised the actinide solubility calculations for the PABC09, including an updated inventory and a revision to the minimum brine volume necessary for a DBR. Brush et al. (2009) summarized the PABC09 actinide aqueous speciation and solubility calculations for the +III, +IV, and +V actinides. Because DOE has not developed an aqueous speciation and solubility model for actinides in the +VI oxidation state, DOE used a U(VI) concentration of 1×10^{-3} M established by EPA's review of the available literature (Section 7.1.5) for the PABC09. EPA (2010b) provides a detailed review of the CRA-2009 PA and PABC09 actinide solubility calculations.

7.1.1 FMT Code and Database

Actinide solubility calculations for the CCA PA and PAVT were performed with FMT Version 2.0, and subsequent calculations for the CRA 2004 PA through PABC09 were performed with FMT Version 2.4. DOE used the FMT code with an associated database that contains the solid phase solubility, aqueous speciation, and Pitzer parameter data needed for the calculations. Development of the FMT databases used for the CCA PA through PABC09 is summarized in Attachment B of this TSD, and detailed database reviews are provided in EPA (1998c, 2006c, 2010b).

EPA (1998c) identified the FMT database used for the CCA calculations as FMT_HMW_345_960501FANG.CHEMDAT, but noted that it was not clear which database DOE had used. Based on the date indicated in the file name, EPA (1998c) believed the database was representative of the database used for the CCA PA actinide solubility calculations. Novak and Moore (1996), however, stated that DOE used HMW_3456_960318.CHEMDAT and HMW_3456_960325.CHEMDAT for the FMT calculations, and that the data in these two files were identical.

DOE used the FMT_021120.CHEMDAT database for the CRA-2004 PA (Brush and Xiong 2003a; DOE 2004, Appendix PA, Attachment SOTERM-3.3). Changes to the database since the CCA PAVT included revisions to the thermodynamic data for Am(III) aqueous species and solids, and minor revisions to the thermodynamic data for some Th(IV) aqueous species and

Pitzer interaction parameters. A significant database change was incorporation of thermodynamic data for the protonation of organic ligands and complexation of organic ligands with actinides and magnesium, based on data from Choppin et al. (2001). Giambalvo (2002a, 2002b, 2002c, 2002d, 2002e, 2003) documented changes to the FMT database between the CCA PAVT and CRA-2004 PA (Attachment B).

The FMT database used in the CRA-2004 PA actinide solubility calculations (FMT_021120.CHEMDAT) was revised to create the version used in the PABC04 actinide solubility calculations (FMT_050405.CHEMDAT). The database changes since the CRA-2004 PA actinide solubility calculations included a revision of the thermodynamic data for $Th(OH)_4(aq)$, correction of the molecular weight of oxalate, and addition of whewellite [$CaOxalate \bullet H_2O(s)$] solubility data (Attachment B).

The FMT_050405.CHEMDAT was also used for the CRA-2009 PA and PABC09 actinide solubility calculations. EPA (2010b) noted some differences between the chemical models in the FMT database and the published literature, and recommended that DOE perform a review and update of this database prior to the CRA-2014, including consideration of:

- Information summarized by Neck et al. (2009) for the +III actinides;
- Results of WIPP-specific Nd(III) experiments (Borkowski et al. 2009, Borkowski 2010) for the +III actinides;
- Results for Th(IV) hydroxide solubility and carbonate speciation provided by Neck et al. (2002), Rothe et al. (2002), and Altmaier et al. (2004, 2005, 2006);
- Results from continuing WIPP-specific experiments regarding the speciation and solubility of U(VI) (Lucchini et al. 2010); and
- Other literature data published in time for inclusion in the FMT database before the CRA-2014 PA.

On the basis of its CRA-2009 review of the available data for Th(IV), U(VI), Np(V), and Am(III) solubility and aqueous speciation, EPA (2010b) also concluded that:

- Formation of calcium-Th(IV)-hydroxide complexes would likely be unimportant under WIPP pH conditions.
- Borate complexation of U(VI), if it occurs to a significant extent, would not substantially change the current understanding of likely U(VI) solubility in WIPP brines because uranyl carbonate species are expected to dominate aqueous speciation under WIPP repository conditions.

7.1.2 Salado Brine Formulation

The Salado brine formulations used in WIPP PA are described in Section 2.3. For the CCA PAVT actinide solubility calculations, DOE used the brine formulation referred to as Brine A to simulate intergranular Salado brines. However, DOE used the GWB Salado brine formulation in the CRA-2004 PA and all subsequent actinide solubility calculations. Brush and Xiong (2003a) discussed the use of both GWB and Brine A in the CRA-2004 PA to simulate intergranular Salado brines, and provided the compositions of these brines. Snider (2003b) provided a detailed discussion of GWB brine and a comparison of GWB brine to Brine A. EPA (2006c) reviewed

this information and concluded that use of the GWB formulation for Salado brine instead of Brine A for the CRA-2004 PA and future actinide solubility calculations is appropriate.

7.1.3 Carbon Dioxide Buffering Reactions

For the CCA PAVT through PABC09 actinide solubility calculations that included significant CO_2 production by microbial activity, the MgO hydration and carbonation phases assumed to be present in solubility calculations with Salado (Brine A and GWB) brine were brucite, Phase 3, and hydromagnesite. For actinide solubility calculations with Castile (ERDA-6) brine, brucite and hydromagnesite were the assumed MgO hydration and carbonation phases. These MgO hydration and carbonation phases control the calculated pH and CO_2 fugacity. EPA (1998c, 2006c, 2010b) agreed that these phases are the most likely to control pH and CO_2 fugacity in WIPP repository brines during the 10,000-year regulatory period.

7.1.4 Oxidation-State Analogy

DOE uses the oxidation-state analogy to extend the calculated Am(III), Th(IV), and Np(V) solubilities to the other actinides and oxidation states important to WIPP PA. The oxidation-state analogy, part of the Dissolved Actinide Source Term conceptual model, is the assumption that all actinides in the same oxidation state will form the same aqueous species and isostructural compounds. Consequently, DOE assumes that Pu(III) and Cm(III) solubilities in WIPP brines are equal to calculated Am(III) solubilities, and that U(IV), Pu(IV), and Np(IV) solubilities are equal to calculated Th(IV) solubilities. DOE uses calculated Np(V) solubilities only for neptunium because it is the only actinide predicted to be present in WIPP brines in the +V oxidation state.

7.1.5 Uranium(VI) Solubility

Because DOE could not develop an adequate thermodynamic model for U(VI), DOE used fixed concentrations of 8.7×10^{-6} M (Salado brine) and 8.8×10^{-6} M (Castile brine) for the CCA PA and PAVT. EPA (1998c) reviewed DOE's predictions of U(VI) solubilities, including the information in the CCA and supporting documents (Hobart and Moore 1996, Novak and Moore 1996), and additional information that became available after the CCA. EPA (1998c) accepted the use of this single U(VI) concentration in PA because it was consistent with the available data and uncertainties associated with this estimated concentration were believed to be adequately accounted for by the sampled uncertainty distribution. DOE also used this estimated U(VI) concentration for the CRA-2004 PA.

EPA (2006c) noted during review of the CRA-2004 that DOE had not considered new data regarding the solubility of the +VI actinides since the CCA, and reviewed U(VI) solubility data in NaCl brines to determine whether the assumed U(VI) concentrations used in the CRA-2004 PA were still justified. EPA (2006c) determined that a reasonable upper limit for U(VI) solubility in WIPP brines would be approximately 1×10^{-3} M. This concentration is approximately two orders of magnitude higher than the mid-range value used in the CCA PAVT and CRA-2004 PA, and exceeds the upper limit of the solubility uncertainty range used in these PAs. EPA directed DOE to use the revised, higher U(VI) of 1×10^{-3} M for the PABC04 (Cotsworth 2005). DOE has continued to use this upper-limit U(VI) concentration for all subsequent WIPP PAs.

7.1.6 Minimum Brine Volume

DOE uses the minimum brine volume necessary for a brine release with the WIPP inventory data to calculate organic ligand concentrations for the actinide solubility calculations. The minimum brine volume used for the CCA PAVT was 29,841 m^3 (Larson 1996) but was changed to 10,011 m^3 based on an evaluation by Stein (2005) for the PABC04 and the CRA-2009 PA dissolved actinide source term calculations. Clayton (2008) recalculated the minimum brine volume and obtained a value of 17,400 m^3. Increasing the minimum brine volume decreases the organic ligand concentrations used in the actinide solubility calculations. EPA (2010b) found that use of the 17,400 m^3 minimum brine volume to calculate organic ligand concentrations appeared to be conservative and acceptable. DOE used the minimum brine volume of 17,400 m^3 for the PABC09 and all subsequent WIPP PAs.

7.1.7 Waste Inventory

EPA (2010b) calculated the concentrations of curium and neptunium from their PABC09 inventories decayed through repository closure at 2033 (Crawford et al. 2009) and the minimum brine volume of 17,400 m^3 (Clayton 2008). The resulting curium concentration was less than the baseline +III actinide solubilities calculated for the PABC09, but the inventory-based neptunium-237 concentration exceeded the baseline +V actinide solubilities calculated for the PABC09. These results were consistent with previous evaluations of the inventories of curium and neptunium (DOE 2004, EPA 2006c), which concluded that dissolved curium will be present at concentrations below its calculated solubility, and neptunium will be of little significance to repository performance because of its low total curies.

DOE (2009, Appendix SOTERM-2009) did not directly address the influence of the cementitious waste inventory on brine pH in the WIPP repository. The potential effects of cementitious materials in the repository are addressed within the Chemical Conditions conceptual model, where it acknowledges that portlandite [$Ca(OH)_2$] in cementitious materials could react with CO_2 to form calcite. This reaction could buffer pH at relatively high values, compared to the brucite dissolution reaction. Evaluation of the effects of portlandite on brine pH at the time of the CCA showed that the effects of cementitious waste on pH will be minimal because of calcite precipitation and reaction of the portlandite with $MgCl_2$ in the brine to form $CaCl_2$ (SC&A 2008b, Appendix A.2; DOE 1996, Appendix SOTERM):

$$Ca(OH)_2(s) + MgCl_2 \leftrightarrow CaCl_2 + Mg(OH)_2(s) \quad \textbf{(29)}$$

EPA (2010b) evaluated the potential effects of cement in the CRA-2009 waste inventory (Crawford et al. 2009) in the presence of the predicted amount of MgO backfill using mass balance calculations to determine if the amount of portlandite in the cement could exceed the amount of magnesium in the brine and in polyhalite in the Salado Formation. The amount of portlandite in the cement was estimated by assuming the cement contains 5%, 7.5%, or 10% by weight $Ca(OH)_2$ (Storz 1996), resulting in repository-wide estimates of 8.30×10^6 moles, 1.25×10^7 moles, and 1.66×10^7 moles of $Ca(OH)_2$, respectively. EPA (2010b) assumed the repository brine volume was equal to 17,400 m^3, the minimum volume necessary for DBR. EPA (2010b) calculated the amounts of Salado polyhalite in the system assuming a DRZ volume of 1.58×10^6

m^3, a rock density of 1,180 kg/m^3 (Brush et al. 2006), and the assumption that Salado Formation contains 1.7% polyhalite by weight (Brush 1990). EPA (2010b) calculated the moles of portlandite from cement dissolution, polyhalite from the Salado Formation and magnesium in the brine based on 1 kg of H_2O for both GWB and ERDA-6 (Table 7-1).

Table 7-1. Mass Balance Calculations Comparing Moles of Portlandite in Cement to Moles of Magnesium Available from Brine and Polyhalite, Minimum Brine Volume of 17,400 m^3

Brine	Portlandite in Cement (%)	Portlandite (moles/kg H_2O)	Magnesium in Brine (moles/kg H_2O)	Magnesium in Polyhalite (moles/kg H_2O)	Magnesium in Brine and Polyhalite (moles/kg H_2O)
GWB	0	0.000	1.217	6.662	7.879
GWB	5	0.569	1.217	6.662	7.879
GWB	7.5	0.854	1.217	6.662	7.879
GWB	10	1.138	1.217	6.662	7.879
ERDA-6	0	0.000	0.021	6.150	6.171
ERDA-6	5	0.525	0.021	6.150	6.171
ERDA-6	7.5	0.788	0.021	6.150	6.171
ERDA-6	10	1.051	0.021	6.150	6.171

Portlandite dissolution results in brucite precipitation [reaction (29)]. This reaction maintains the moderately alkaline pH predicted for the WIPP brine in the presence of the MgO backfill, provided sufficient magnesium is available in the brine or in polyhalite, which can dissolve and release additional magnesium:

$$K_2MgCa_2(SO_4)_4{\bullet}2H_2O(s) \leftrightharpoons 2K^+ + Mg^{2+} + 2Ca^{2+} + 2SO_4^{2-} + 2H_2O(l) \quad \textbf{(30)}$$

For GWB brine, which has a relatively high magnesium concentration, the moles of magnesium in the brine alone are greater than the moles of portlandite in cement (Table 7-1), so sufficient magnesium would be present to maintain moderately alkaline conditions. ERDA-6 has a much lower magnesium concentration than GWB, and the amount of magnesium initially present in the brine may not be sufficient to maintain the pH. However, magnesium released by polyhalite dissolution would be available to react with hydroxide ion released by portlandite dissolution, precipitating brucite according to reaction (29). The increased potassium, calcium, and sulfate from polyhalite dissolution would be expected to result in precipitation of anhydrite [$CaSO_4(s)$] and syngenite [$K_2Ca(SO_4)_2{\bullet}H_2O(s)$]. Because the moles of magnesium in polyhalite significantly exceed the moles of portlandite in these calculations, the increased cement inventory would be unlikely to cause high brine pH.

7.1.8 Effects of Organic Ligands on Actinide Solubilities

DOE (1996) identified acetate, citrate, EDTA, and oxalate as organic ligands that could potentially affect actinide solubilities, because these ligands are water soluble and present in significant quantities in the WIPP inventory. DOE (1996) estimated the possible concentrations of these ligands using the inventory amounts and a brine volume of 29,841 m^3 (Larson 1996).

These organic ligand concentrations are provided in Table 7-2. DOE (1996) did not include organic ligand complexation of actinides in the CCA PA and PAVT actinide solubility calculations. DOE (1996) reasoned that the presence of organic ligands would not significantly affect actinide solubilities because other constituents, including transition metals in the waste and magnesium from the MgO backfill, would compete with the actinides for binding sites on the organic ligands.

Table 7-2. Organic Ligand Concentrations Calculated for the CCA PAVT, PABC04, PABC09, CRA-2014 PA, and CRA-2019 DPA

Performance Assessment	Brine Volume (m^3)	Acetate[a]	Citrate[b]	EDTA[c]	Oxalate[d]
CCA PA (m) (DOE 1996)	29,841	1.1×10^{-3}	7.4×10^{-3}	4.2×10^{-6}	4.7×10^{-4}
PABC04 (M) (Brush and Xiong 2005)	10,011	1.06×10^{-2}	8.06×10^{-4}	8.14×10^{-6}	4.55×10^{-2}
PABC09 (M) (Brush and Xiong 2009)	17,400	1.94×10^{-2}	2.38×10^{-3}	6.47×10^{-5}	1.73×10^{-3}
CRA-2014 PA (M) (Brush and Domski 2013a)	17,400	2.30×10^{-2}	2.33×10^{-3}	7.40×10^{-5}	1.18×10^{-2}
	34,800	1.15×10^{-2}	1.16×10^{-3}	3.70×10^{-5}	5.90×10^{-3}
	52,200	7.68×10^{-3}	7.76×10^{-4}	2.47×10^{-5}	3.93×10^{-3}
	69,600	5.76×10^{-3}	5.82×10^{-4}	1.85×10^{-5}	2.95×10^{-3}
	87,000	4.61×10^{-3}	4.65×10^{-4}	1.48×10^{-5}	2.36×10^{-3}
CRA-2019 DPA (M) (Domski and Sisk-Scott 2019)	17,400	2.83×10^{-2}	2.30×10^{-3}	7.92×10^{-5}	1.13×10^{-2}
	34,800	1.42×10^{-2}	1.15×10^{-3}	3.96×10^{-5}	5.65×10^{-3}
	52,200	9.45×10^{-3}	7.68×10^{-4}	2.64×10^{-5}	3.77×10^{-3}
	69,600	7.09×10^{-3}	5.76×10^{-4}	1.98×10^{-5}	2.82×10^{-3}
	87,000	5.67×10^{-3}	4.61×10^{-4}	1.58×10^{-5}	2.26×10^{-3}

a – Sum of acetic acid (CH_3COOH) and sodium acetate ($NaCH_3COO$)
b – Sum of citric acid ($C_6H_8O_7$) and sodium citrate ($NaC_6H_7O_7$)
c – Assumed monosodium EDTA
d – Sum of oxalic acid ($H_2C_2O_4$) and sodium oxalate ($NaHC_2O_4$)

DOE (2004, Appendix PA, Attachment SOTERM) included the effects of acetate, citrate, EDTA, and oxalate on the calculated solubilities of the +III, +IV, and +V actinides used in the CRA-2004 PA. Brush and Xiong (2003b) calculated the organic ligand concentrations used in the actinide solubility calculations (Table 7-2) by dividing the total reported ligand inventory by 29,841 m^3 of brine (Larson 1996, DOE 1996). Brush and Xiong (2003c) found that the masses of organic ligands used to calculate concentrations for the CRA-2004 PA were overestimates of the amounts likely to be in the repository. For the PABC04, Brush and Xiong (2005) used the corrected masses of organic ligands (Table 7-3) to calculate organic ligand concentrations. These masses were converted to moles and divided by a revised estimate of the minimum amount of brine that could lead to a release from the repository (10,011 m^3, Stein 2005) to yield the organic ligand concentrations used in the actinide solubility calculations (Table 7-2).

Table 7-3. Organic Ligand Inventories for the PABC04, PABC09, CRA-2014 PA, and CRA-2019 DPA

Compound	PABC04 Inventory [kg] (Leigh 2005)	PABC09 Inventory [kg] (Crawford et al. 2009)	CRA-2014 PA Inventory [kg] (Van Soest 2012)	CRA-2019 DPA Inventory [kg] (Van Soest 2018)
Acetic acid	142	13,200	14,100	15,900
Acetate	8,510	9,700	9,960	13,700
Citric acid	1190.5	5,680	5,230	5,080
Citrate	400	2,550	2,550	2,630
EDTA	25.6	354	376	403
Oxalic acid	13,796	26,600	17,800	17,000
Oxalate	33,940	646	650	700

EPA (2006c) reviewed the CRA-2004 PA and PABC04 actinide solubility calculations and concluded that +III actinide concentrations could be affected by the concentrations of EDTA and the +V actinides could be affected by oxalate and acetate concentrations in repository brines. The available evidence showed that the +IV actinides were relatively insensitive to organic ligands over the evaluated organic ligand concentration range. EPA (2006c) also found that microbially produced lactate is unlikely to significantly affect actinide solubilities. Evaluation of the available data regarding the complexation of U(VI) under anticipated WIPP repository conditions indicated that organic ligands are unlikely to significantly affect U(VI) solubilities in WIPP brines, because of the formation of relatively stable U(VI)-carbonate species EPA (2006c).

DOE (2009) used the actinide solubilities calculated for the PABC04 for the CRA-2009 PA dissolved actinide source term. Comparison of updated inventory information available for the CRA-2009 PA with the quantities used to calculate actinide solubilities for the PABC04 showed that inventory quantities had significantly increased for most organic ligands (Table 7-3). Because of the potential effects of organic ligands on actinide solubilities, EPA instructed DOE to include the revised inventory of organic ligands in the PABC09 actinide solubility calculations (Cotsworth 2009a).

DOE used the most recent inventory data (Table 7-3) and the most recent estimate of the minimum brine volume necessary for DBR (Clayton 2008) to calculate organic ligand concentrations for the PABC09 (Table 7-2). The aqueous speciation and solubility calculations were carried out both with and without the predicted organic ligand concentrations. DOE used the results obtained with organic ligands to determine dissolved actinide source term concentrations for the PABC09.

EPA (2010b) determined that the presence of organic ligands increased the total predicted Am(III) solubilities in both GWB and ERDA-6 brine in the PABC09 calculations. Examination of the reported Am(III) aqueous speciation indicated Am(III)-EDTA complexation caused the higher predicted solubilities. The presence of organic ligands had essentially no effect on predicted Th(IV) solubilities in GWB or ERDA-6 brine. Organic ligands increased predicted Np(V) solubilities by approximately a factor of two because of the complexation of NpO_2^+ by acetate and oxalate.

7.1.9 Results of the Actinide Solubility Calculations for the CCA PAVT, PABC04, and PABC09

The results of the CCA PAVT, PABC04, and PABC09 actinide solubility calculations are summarized in Table 7-4. For the CCA PAVT actinide solubility calculations, $AmOHCO_3(cr)$ was the predicted solubility-controlling solid for the +III actinides. As a result of revisions to the FMT database between the CCA PAVT and the PABC04, $Am(OH)_3(s)$ was the predicted solubility-controlling solid phase for the PABC04 and PABC09 actinide solubility calculations. Predicted dissolved Am(III) concentrations increased between the CCA PAVT and PABC09 because of modifications to the Am(III) data in the FMT thermodynamic database, inclusion of the effects of Am(III)-EDTA complexation in the PABC04 and PABC09 modeling calculations, and increasing EDTA concentrations in WIPP brines (Table 7-2).

The solubilities of $ThO_2(am)$ and $KNpO_2CO_3(s)$ control the predicted Th(IV) and Np(V) concentrations, respectively. Th(IV) concentrations increased from the CCA PAVT to the PABC04 and PABC09 because of modifications to the FMT thermodynamic database. Np(V) concentrations increased from the CCA PAVT to the PABC04 and PABC09 because of modifications to the FMT thermodynamic database, inclusion of acetate and oxalate complexation of Np(V) in the PABC04 and PABC09 modeling calculations, and increasing acetate and oxalate concentrations in WIPP brines (Table 7-2). U(VI) concentrations increased from the CCA PAVT to the PABC04 and PABC09 because of the increased fixed U(VI) concentration assumed for the PABC04 and PABC09 (Section 7.1.5).

The FMT databases used for the CCA PA through PABC09 included Phase 3, a magnesium-hydroxychloride solid phase, and Phase 3 was predicted to precipitate from Salado brine in these calculations. However, as described in Section 4.2.2, experimental investigations with GWB brine and Martin Marietta MgO detected the formation of Phase 5 rather than Phase 3 (Deng et al. 2009). Brush et al. (2009) used an FMT database that included both magnesium-hydroxychloride phases (FMT_090720.CHEMDAT, Xiong 2009) to calculate which phase would be stable under repository conditions and the potential effects of Phase 5 formation on actinide solubilities. The results indicated that Phase 5 is the stable magnesium-hydroxychloride phase, as observed in the MgO hydration experiments in GWB. Predicted formation of this phase in place of Phase 3 had only minor effects on calculated actinide solubilities. DOE did not use the FMT calculations with Phase 5 to predict PABC09 dissolved actinide source term concentrations because the FMT_090720.CHEMDAT database had not yet been reviewed and approved by EPA.

Table 7-4. Actinide Solubility Calculations for the CCA PAVT, PABC04, PABC09, CRA-2014 PA, CRA-2019 DPA, and CRA-2019 Sensitivity Calculations (Minimum Brine Volume)

Property or Actinide Oxidation State	CCA PAVT[a]		PABC04		PABC09	
Brine	Salado (Brine A)	Castile (ERDA-6)	Salado (GWB)	Castile (ERDA-6)	Salado (GWB)	Castile (ERDA-6)
pH	8.69	9.24	8.69	8.94	8.69	8.98
pcH	--	--	9.39	9.64	9.40	9.68
Log CO_2 fugacity	-5.50	-5.50	-5.50	-5.50	-5.50	-5.50
Total Carbon (M)	--	--	2.16×10^{-5}	5.18×10^{-5}	3.50×10^{-4}	4.48×10^{-4}
III (M)	1.2×10^{-7}	1.3×10^{-8}	3.87×10^{-7}	2.88×10^{-7}	1.66×10^{-6}	1.51×10^{-6}
IV (M)	1.3×10^{-8}	4.1×10^{-8}	5.64×10^{-8}	6.79×10^{-8}	5.63×10^{-8}	6.98×10^{-8}
V (M)	2.4×10^{-7}	4.8×10^{-7}	3.55×10^{-7}	8.24×10^{-7}	3.90×10^{-7}	8.75×10^{-7}
VI (M)[b]	8.7×10^{-6}	8.8×10^{-6}	1×10^{-3}	1×10^{-3}	1×10^{-3}	1×10^{-3}
Equilibrium Non-Radionuclide Solid Phases	Anhydrite, halite, brucite, hydromagnesite, Phase 3	Anhydrite, halite, brucite, glauberite, hydromagnesite	Anhydrite, halite, brucite, hydromagnesite, whewellite, Phase 3	Anhydrite, halite, brucite, hydromagnesite, whewellite, glauberite	Anhydrite, halite, brucite, hydromagnesite, whewellite, Phase 3	Anhydrite, halite, brucite, hydromagnesite, whewellite, glauberite
Equilibrium Radionuclide Solid Phases	$AmOHCO_3$(cr), ThO_2(am), $KNpO_2CO_3$(s)		$Am(OH)_3$(s), ThO_2(am), $KNpO_2CO_3$(s)		$Am(OH)_3$(s), ThO_2(am), $KNpO_2CO_3$(s)	
Database	FMT_970407.CHEMDAT		FMT_050405.CHEMDAT		FMT_050405.CHEMDAT	
Output filename	--	--	FMT_CRA1BC_GWB_HMAG_ORGS_007	FMT_CRA1BC_ER6_HMAG_ORGS_007	FMT_PABC09_GWB_HMAG_ORGS_005.OUT	FMT_PABC09_E6_HMAG_ORGS_013

a – organic ligands were not included in the CCA PAVT actinide solubility calculations, but were included in all other actinide solubility calculations in this table

b – DOE did not develop a solubility model for the +VI actinides. Therefore, for all PAs, DOE assumed a fixed concentration for U(VI), which is the only +VI actinide predicted to be present in the WIPP repository in significant concentrations.

Table 7-4 (contd). Actinide Solubility Calculations for the CCA PAVT, PABC04, PABC09, CRA-2014 PA, CRA-2019 DPA, and CRA-2019 Sensitivity Calculations (minimum brine volume)

Property or Actinide Oxidation State	CRA-2014 PA		CRA-2019 DPA		CRA-2019 Sensitivity Calculations	
Brine	Salado (GWB)	Castile (ERDA-6)	Salado (GWB)	Castile (ERDA-6)	Salado (GWB)	Castile (ERDA-6)
pH	8.82	8.99	8.82	8.82	8.58	8.63
pcH	9.54	9.69	9.54	9.52	9.55	9.58
Log CO_2 fugacity	-5.50	-5.50	-5.69	-5.69	-5.71	-5.71
Total Carbon (M)	3.79×10^{-4}	4.55×10^{-4}	2.50×10^{-4}	2.50×10^{-4}	2.80×10^{-4}	2.58×10^{-4}
III (M)	2.59×10^{-6}	1.48×10^{-6}	1.63×10^{-7}	1.78×10^{-7}	2.14×10^{-6}	1.43×10^{-6}
IV (M)	6.05×10^{-8}	7.02×10^{-8}	5.45×10^{-8}	5.44×10^{-8}	5.50×10^{-8}	5.84×10^{-8}
V (M)	2.77×10^{-7}	8.76×10^{-7}	4.02×10^{-7}	1.20×10^{-6}	4.38×10^{-7}	1.82×10^{-6}
VI (M)[a]	1×10^{-3}	1×10^{-3}	1×10^{-3}	1×10^{-3}	1×10^{-3}	1×10^{-3}
Equilibrium Non-Radionuclide Solid Phases	Anhydrite, halite, brucite, hydromagnesite, whewellite, Phase 5	Anhydrite, halite, brucite, hydromagnesite, whewellite, glauberite	Anhydrite, halite, brucite, hydromagnesite, calcite, glauberite, whewellite, Phase 5, cerussite, oxychloride-Fe-3	Anhydrite, halite, brucite, hydromagnesite, calcite, glauberite, whewellite, Phase 5, cerussite, oxychloride-Fe-3, borax	Anhydrite, halite, brucite, hydromagnesite, whewellite, Phase 5	Anhydrite, halite, brucite, hydromagnesite, aragonite, glauberite, whewellite
Equilibrium Radionuclide Solid Phases	$Am(OH)_3(s)$, $ThO_2(am)$, $KNpO_2CO_3(s)$		$Am(OH)_3(s)$, $ThO_2(am)$, $KNpO_2CO_3(s)$		$Am(OH)_3(s)$, $ThO_2(am)$, $KNpO_2CO_3(s)$	
Database	DATA0.FM1		DATA0.FM4		DATA0FM_EPA.dat (PHREEQC)	
Output filename	gwb_1x.6o	erda_1xb.6o	gwb_1x.6o	erda_1xb.6o	gwb_epa.out	erda6_epa.out

a – DOE did not develop a solubility model for the +VI actinides. Therefore, for all PAs, DOE assumed a fixed concentration for U(VI), which is the only +VI actinide predicted to be present in the WIPP repository in significant concentrations.

7.1.10 Actinide Solubility Uncertainties

The baseline actinide solubilities used in WIPP PA are constants. DOE accounts for uncertainties in these solubilities by sampling a cumulative distribution function (CDF) representing uncertainty and multiplying the solubilities by the antilog of the sampled value to determine the actinide concentrations used in PA for each realization. EPA (1998c) reviewed the development of the actinide solubility uncertainty distribution used in the CCA PA and PAVT. To obtain this distribution, DOE compared experimentally measured solubility data used to develop the solubility models in the FMT database to the concentrations predicted by curve-fitting with the code NONLIN (Babb 1996). DOE also compared solubilities reported in the literature with concentrations predicted using FMT for the conditions of the experiments. Difference values (D) between the predicted (S_p) and measured (S_m) solubilities were calculated using the equation:

$$D = \log_{10}S_m - \log_{10}S_p \quad \textbf{(31)}$$

The difference value is negative if the calculated solubility is greater than the measured solubility, positive if the calculated solubility is less than the measured solubility, and zero if the calculated and measured solubilities are equal.

DOE used the population of difference values from these comparisons to generate a cumulative distribution. DOE excluded data for the +IV and +VI actinides from the evaluation, because they believed these datasets to be inconsistent or technically deficient. The remaining data consisted of +III actinide solubility measurements (139 values) and +V actinide solubility measurements (11 values). DOE combined these data to generate a single distribution (Tables 7-5 and 7-6) and used this distribution to represent the uncertainties associated with the solubilities for all four actinide oxidation states.

Table 7-5. Am(III) Solubility Uncertainty Distribution Statistics for the PABC04, PABC09, CRA-2014 PA, CRA-2019 DPA, and CRA-2019 Sensitivity Calculations

Performance Assessment	CCA PAVT	PABC04	PABC09[b]	CRA-2014 PA	CRA14_SEN4 PA	CRA-2019 DPA	CRA-2019 Sensitivity Calculations
Mean	n.r.[a]	0.035	-0.142	-0.678	0.48	0.651	1.16
Median	-0.09	-0.031	0.072	-0.866	0.07	0.516	1.24
Standard Deviation	n.r.[a]	0.900	1.17	1.57	0.93	1.01	1.18
Maximum	1.4	2.85	2.70	2.97	2.97	2.97	3.44
Minimum	-2.0	-3.00	-4.20	-3.55	-1.14	-1.14	-1.14

a – Not reported.

b – The PABC09 Am(III) statistics listed in Xiong et al. (2009) differed slightly from the summary statistics in the spreadsheet (PABC09 Am(III) Uncertainty Analysis 091124.xls) provided to EPA: mean = -0.145, median = 0.090, standard deviation = 1.17, maximum = 2.68 and minimum = -4.16.

Sources: DOE (1996, Appendix SOTERM), Xiong et al. (2009), Brush and Domski (2013c), Xiong and Domski (2016a), Domski (2019d), Knerr (2021f)

Table 7-6. Th(IV) Solubility Uncertainty Distribution Statistics for the PABC04, PABC09, CRA-2014 PA, CRA-2019 DPA, and CRA-2019 Sensitivity Calculations

Performance Assessment	CCA PAVT	PABC04	PABC09[b]	CRA-2014 PA	CRA14_SEN4 PA	CRA-2019 DPA and CRA-2019 Sensitivity Calculations
Mean	n.r.[a]	0.108	-0.346	0.673	-0.011	-0.011
Median	-0.09	0.075	-0.520	1.029	-0.090	-0.090
Standard Deviation	n.r.[a]	0.837	0.995	0.869	0.821	0.821
Maximum	1.4	2.40	3.30	3.19	1.43	1.43
Minimum	-2.0	-1.80	-2.25	-1.52	-2.01	-2.01

a – Not reported.

b – The PABC09 Th(IV) statistics listed in Xiong et al. (2009) differed slightly from the summary statistics in the spreadsheet (PABC09 Th(IV) Uncertainty Analysis 091124.xls) provided to EPA: mean = -0.349, median = -0.517, standard deviation = 0.992, maximum = 3.19 and minimum = -2.21.

Sources: DOE (1996, Appendix SOTERM), Xiong et al. (2009), Brush and Domski (2013c), Domski (2019d)

DOE (2004) used the uncertainty distribution determined for the CCA PA and PAVT to represent the actinide solubility uncertainties for the CRA-2004 PA. Because the available solubility data and the FMT database had changed since the CCA PA and PAVT, EPA requested that DOE re-evaluate the actinide solubility uncertainties using the currently available actinide solubility data (Cotsworth 2004a). DOE provided the requested re-evaluation of the actinide solubility uncertainties for the PABC04 (Triay 2005, Xiong et al. 2004).

Xiong et al. (2004) carried out separate evaluations of the solubility uncertainty distribution for the +III, +IV, and +V actinide oxidation states (Tables 7-5 and 7-6). Xiong et al. (2004) included solubility data used to develop the FMT database as well as additional literature data. For the +III actinides (Table 7-5), the median difference value was slightly less than zero and the median difference value for the +IV actinides was between 0.6 and 0.75 (Xiong et al. 2004). DOE investigated the likely cause of the positive median difference value and determined a revision was necessary to the standard chemical potential (μ^0/RT) value for $Th(OH)_4(aq)$ in the FMT database. Xiong et al. (2005) found that this revised database (FMT_050405.CHEMDAT) resulted in a significant improvement in the ability of the +IV actinide solubility model to predict the available solubility data at high ionic strength, with a median difference value of 0.075 (Table 7-6).

The difference values for the +V actinide solubilities ranged from -1.8 to +1.95, with a median value slightly less than zero (Xiong et al. 2004). Xiong et al. (2005) stated that the uncertainty distribution for the +V actinide solubilities would not be sampled for PA. Neptunium is the only actinide expected to be present in the +V oxidation state in the equilibrium WIPP repository (Section 6.0) and the neptunium inventory is insufficient to affect the long-term performance of the repository, regardless of its solubility (Xiong et al. 2005, EPA 2006c).

EPA (2006b) concluded that the overall approach used in the PABC04 for estimating the uncertainties associated with the actinide solubilities was a substantial improvement over the approach used for the CCA PA and PAVT. The use of a larger dataset and the determination of separate uncertainty distributions for the +III, +IV, and +V actinide solubilities for the PABC04

were more likely to provide reasonable estimates of the uncertainties than the approach taken for the CCA PA, PAVT, and CRA-2004 PA. However, the approach of Xiong et al. (2004, 2005) for selecting the data for the evaluation may not have included all available experimental data. EPA (2006b) also noted inconsistencies in application of the selection criteria because of the inclusion of data used to develop the FMT database in some cases and its exclusion in others. EPA (2006b) recommended implementation of a more thorough and systematic approach for selecting data for development of the actinide solubility uncertainty distributions for future WIPP PAs.

Comparison of the separate PABC04 uncertainty distributions developed for the three modeled actinide oxidation states with the single uncertainty distribution used in the CCA PA, PAVT, and CRA-2004 PA showed that the revised ranges were generally broader, particularly on the upper end of the distributions (Tables 7-5 and 7-6). EPA (2006b) concluded that the revised actinide solubility uncertainty distributions would likely result in the more frequent use of higher actinide solubilities in PA. EPA (2006b) also observed that the larger amount of experimental data used to develop the distributions, the development of uncertainty distributions for each of the modeled actinide oxidation states, and the large ranges developed for the uncertainties indicated that these uncertainty distributions were reasonable and acceptable for use in the PABC04.

For the CRA-2009, the uncertainty distributions for each oxidation state were sampled from the distributions developed for the PABC04 (Xiong et al. 2004, 2005). EPA requested that DOE evaluate the possible effects of recent additional data on the solubility uncertainty distributions developed for the PABC04 (Cotsworth 2009a).

Xiong et al. (2009) described the development of the updated uncertainty distributions for the +III and +IV actinide solubilities that were sampled for the PABC09. Xiong et al. (2009) did not develop an uncertainty distribution for the +V actinides because this distribution is not sampled in PA. The process Xiong et al. (2009) used to develop the uncertainty distributions included use of a set of criteria to select solubility data from the literature. These criteria are reviewed in detail in Section 7.2.6. During an EPA/DOE technical exchange meeting in February 2010, Sandia National Laboratories (SNL) staff stated that an additional requirement for the evaluation was that solubility data used to parameterize the FMT database were not included in the development of the uncertainty distributions. DOE used the FMT code (Version 2.4) and database (FMT_050405.CHEMDAT) to calculate the predicted solubility at the conditions of each experiment. DOE used these calculated solubilities with measured solubilities to generate difference values (Equation 31) for accumulation into a probability distribution.

DOE accumulated the difference values calculated for the +III and +IV oxidation states into separate probability distributions (Tables 7-5 and 7-6). DOE sampled these distributions during the PABC09 calculations and used the sampled uncertainties with the FMT-calculated baseline actinide solubilities in GWB and ERDA-6 under repository conditions (Table 7-4) to calculate the concentrations of the +III and +IV actinides used for each brine in each PA realization.

The mean and median values were lower for the PABC09 +IV actinide solubility uncertainty distribution than for the PABC04 (Table 7-6). EPA (2010b) did not agree with DOE's inclusion of uncentrifuged, unfiltered data and exclusion of ultracentrifuged results from Altmaier et al. (2004). EPA (2010b) also disagreed with DOE's decision to exclude high-ionic-strength solubility data carried out in carbonate-bearing solutions from Altmaier et al. (2005), Altmaier et

al. (2006), and Rai et al. (1995). The mean and median of the uncertainty distributions recalculated by EPA (2010b) were slightly higher than the mean and median values calculated by DOE for the PABC09. Although the higher overall +IV difference values would tend to increase predicted repository releases, EPA (2010b) concluded that these increased releases would be relatively small, would likely occur only at low probabilities where DBR is important and would not significantly affect repository compliance.

The +III actinide solubility uncertainty distribution used for the PABC09 had a lower mean and a slightly higher median value than the uncertainty distribution used in the PABC04 (Table 7-5). EPA (2010b) disagreed with DOE's exclusion of data from Silva (1982) based solely on its date of publication. In addition, because the FMT database did not include Am(III)-borate aqueous speciation data, DOE excluded solubility data obtained at pcH greater than 7.4 in Salado brines and 8.1 in ERDA-6 brine. EPA (2010b) noted that excluding higher-pcH WIPP brine solubility data that contains borate implies that the current WIPP thermodynamic database is inadequate for calculating +III actinide solubilities at the pcH values predicted in the WIPP repository, pcH 9.4 for GWB and pcH 9.7 for ERDA-6. EPA (2010b) also stated that the lack of Am(III)-borate aqueous species in the FMT database might result in the underprediction of total Am(III) concentrations in WIPP brine at higher pcH. Consequently, including these data could result in a larger number of positive difference values in the PABC09 uncertainty distribution. In addition, DOE included data from Borkowski et al. (2009) in the +III actinide solubility uncertainty distribution, even though the solid phases in the experiments were identified only through indirect means. EPA (2010b) determined that these results should not have been included in the PABC09 uncertainty evaluation because of the lack of solid phase characterization.

EPA (2010b) recalculated the +III actinide solubility uncertainty distribution to determine the effects of excluding the Borkowski et al. (2009) data and including data from Silva (1982), Khalili et al. (1994) at pcH 6.4 and 8.4, Meinrath and Kim (1991), Meinrath and Takeishi (1993), Runde and Kim (1994), Rao et al. (1996a, 1996b), and all data from Rao et al. (1999). The recalculated +III actinide solubility distribution had a slightly higher mean, median and maximum than the PABC09 uncertainty distribution and a significantly higher minimum. Because the mean of the recalculated uncertainty distribution was only slightly higher than the mean of the distribution sampled for the PABC09, EPA (2010b) concluded that the effects on mean repository releases would likely have been small.

The process for developing the PABC09 actinide solubility uncertainty distributions was improved in some respects over the PABC04 process. An extensive literature search was carried out to identify actinide solubility data to include in the evaluation and the process included clearly stated data-selection criteria. However, EPA (2010b) identified issues in the application of these criteria, and some of these issues had non-conservative effects or effects that could not be determined using the available information.

The +IV and +III actinide solubility uncertainty distributions were recalculated to address these issues. Although increased mean difference values for the +III and +IV actinide solubility uncertainty distributions would increase mean releases relative to the mean releases calculated for the PABC09, these changes would be relatively small, would likely occur only at low probabilities where DBR is important and would not significantly affect repository compliance.

Consequently, EPA (2010b) determined that the actinide solubility uncertainty distributions sampled for the PABC09 were adequate.

7.2 CRA-2014 PA DISSOLVED ACTINIDE SOURCE TERM

DOE (2014, Appendix SOTERM) summarized the assumptions, data, and calculations of the dissolved actinide source term concentrations used in the CRA-2014 PA. DOE performed solubility calculations for Am(III), Th(IV), and Np(V) using Salado (GWB) and Castile (ERDA-6) brine compositions. DOE did not calculate the U(VI) solubility, but instead assumed the fixed U(VI) upper-limit concentration of 1×10^{-3} M specified by EPA (Section 7.1.5). DOE continued to assume that reaction of brucite to form hydromagnesite would control CO_2 fugacity (Section 7.1.3).

DOE (2014) reviewed information about repository pressure and temperature. The information presented is consistent with the Chemical Conditions conceptual model assumption that pressure will not significantly affect actinide solubilities, and that temperature is not expected to significantly depart from ambient conditions. Consequently, these assumptions continued to be appropriate for the CRA-2014 PA.

New information developed since the PABC09 included revisions to the waste inventory, implementation of a variable brine volume for calculating actinide solubilities for DBR, and calculation of actinide solubilities using the EQ3/6 code instead of FMT. DOE (2014) also reported the results of investigations of the dependence of WIPP brine composition on pH and its long-term stability.

EPA (2017d) identified additional actinide solid solubility and aqueous speciation data that were published since the last revision of the WIPP geochemical modeling database. EPA (2017d) reviewed these data for their potential effects on baseline calculated actinide solubilities and the uncertainty distributions for the Am(III) and Th(IV) actinide solubilities used in PA.

7.2.1 Waste Inventory

As described in Section 7.1.7, cementitious waste in the WIPP inventory could increase brine pH above values established by the brucite dissolution reaction. However, if sufficient magnesium is available in brine and polyhalite in the DRZ, the portlandite in cement is not expected to significantly affect brine pH. EPA (2017d) calculated the moles of portlandite from cement dissolution and moles of magnesium available from polyhalite in the Salado Formation DRZ and in the brine and determined that the moles of magnesium in the brine and polyhalite are significantly greater than the moles of portlandite. Accordingly, the cementitious waste was not expected to have significant effects on repository brine pH.

Previous inventory data had shown curium to be present in quantities below its predicted baseline solubilities when dissolved in the minimum brine volume. Neptunium-237 is also present in relatively low quantities. EPA (2017d) found that dissolution of the CRA-2014 PA inventory quantity of curium in the minimum brine volume of 17,400 m^3 (Clayton 2008) resulted in a curium concentration less than the baseline +III actinide solubilities calculated for the CRA-2014 PA. This result was consistent with previous evaluations of the curium inventory, which

had concluded that curium will be present at concentrations below its calculated solubility (EPA 2006c, EPA 2010b).

Organic ligands inventories reported for the CRA-2014 PA are compared to organic ligands inventories for the PABC04 and PABC09 in Table 7-3. The CRA-2014 PA organic ligands inventories are reasonably similar to the inventories used in the PABC09.

7.2.2 Brine Chemistry

DOE investigated the long-term stability of WIPP brine by analyzing simulated brines that had been stored for up to 6 years. The analytical results showed that the stored WIPP brines remained stable, except for magnesium and borate precipitation from ERDA-6 brine at pcH values greater than 10 (Lucchini et al. 2013b). DOE also evaluated the effects of pcH on brine chemistry by titrating GWB up to approximately pcH 13 and allowing the brine to equilibrate before analysis. The analyzed brine compositions were compared to the compositions predicted by Brush et al. (2011). Lucchini et al. (2013b) observed that the predicted and measured calcium and magnesium concentrations diverged above pcH 10. Comparison of the borate and magnesium concentrations in the experiments (Lucchini et al. 2013b) and calculations (Brush et al. 2011) indicated that additional data are required to improve the modeling of magnesium and borate in WIPP brines at pcH values of 9.5 and greater.

7.2.3 Brine Volumes and Organic Ligand Concentrations

For the PABC04 and PABC09 actinide solubility calculations, DOE determined the concentrations of organic ligands (Table 7-2) by dissolving the ligand inventories (Table 7-3) in the minimum brine volumes required for a DBR. DOE used these concentrations to calculate actinide solubilities for all DBRs, regardless of the volume of brine released. For brine release volumes greater than the minimum brine volume, this approach resulted in larger total dissolved masses of organic ligands than were present in the inventory, and likely caused overestimation of the +III actinide solubilities.

For the CRA-2014 PA, Brush and Domski (2013a) calculated the organic ligand concentrations using the minimum brine volume of 17,400 m^3 established by Clayton (2008), as well as brine volumes that are 2-, 3-, 4- and 5-times greater than this minimum volume. These volumes were determined to span the range of DBRs in the PABC09 (Brush and Domski 2013a). The resulting organic ligand concentrations used in the CRA-2014 PA actinide solubility calculations are summarized in Table 7-2. Using variable brine volumes that more closely match release volumes resulted in lower organic ligand concentrations in brines and slightly decreased dissolved actinide concentrations for the higher release volumes.

7.2.4 EQ3/6 Code and Database

Wolery et al. (2010) qualified the EQ3/6 code for WIPP PA geochemical modeling calculations. EQ3/6 replaced FMT, which DOE used to calculate actinide solubilities for previous WIPP PAs. The EQ3/6 code qualification included reformatting the FMT database used for the PABC09 (FMT_050405.CHEMDAT) into a format compatible with EQ3/6 (Ismail et al. 2009). The reformatted EQ3/6 database file was named data0.fmt.r0. The data0.fmt.r0 database was revised by correcting the parameter A^{ϕ} from 0.39 to 0.392 and correcting the parameter $\beta^{(1)}$ for NaCl

from 0.2644 to 0.2664 to create data0.fmt.r1. The database conversion from the FMT format to the EQ3/6 format (data0.fmt.r0) and the corrections made to the database to create data0.fmt.r1 were reviewed and accepted by EPA (SC&A 2011).

DOE measured the solubility of Phase 5 in $MgCl_2$ - NaCl solutions (Xiong et al. 2010). This solid is produced in addition to brucite by hydration of MgO in GWB brine (Section 4.2.1). Xiong (2011) added the equilibrium constant for Phase 5 to the data0.fmt.r1 database to create data0.fmt.r2. This database is also referred to as DATA0.FM1 (Attachment B).

DOE used the EQ3/6 code version 8.0a and the DATA0.FM1 database for the CRA-2014 PA actinide solubility calculations. In response to EPA concerns about the DATA0.FM1 database, DOE revised DATA0.FM1 to create DATA0.FM2 (Xiong and Domski 2016b) following the procedure summarized in AP-173 Revision 1 (Domski and Xiong 2015a). The revised data included:

- Hydromagnesite solubility,
- Borate chemistry,
- EDTA chemistry,
- Citrate chemistry,
- Magnesium-sulfate dissociation constant, and
- Lead chemistry.

Xiong and Domski (2016b) also provided a review of the available actinide aqueous speciation and solubility data in response to a request for additional information from EPA (Edwards 2015c).

EPA began a review of DATA0.FM2 and the supporting documentation and discussed a number of preliminary comments during technical exchange meetings and a conference call with DOE in February 2016 and August 2016. In its initial review, EPA identified multiple issues and inconsistencies with the updated parameters. Based on the discussions with DOE, EPA determined that a complete review of the supporting information sufficient for accepting DATA0.FM2 or specifying modifications to the database would cause a significant delay in completing the CRA-2014 review. DATA0.FM2 was not accepted by EPA for use in WIPP PA.

In lieu of requesting a revised PABC for the CRA-2014, EPA requested that DOE conduct a sensitivity study to address some of the significant technical concerns arising from EPA's CRA-2014 review. To facilitate completion of the dissolved actinide solubility review for the CRA-2014, EPA and DOE agreed during a technical exchange meeting in September 2016 to use the baseline actinide solubilities calculated for the CRA-2014 PA in the sensitivity study, along with revised +III and +IV actinide solubility uncertainty distributions (Section 7.3).

7.2.5 Actinide Solubility Calculations

Brush and Domski (2013b) used EQ3/6 version 8.0a and the DATA0.FM1 database to calculate actinide solubilities with organic ligand concentrations (Table 7-2) calculated for the range of brine volumes that encompass the expected DBR volumes. Five-fold variation in the brine

volume and organic ligand concentrations affected Am(III) concentrations because of the predicted complexation of Am(III) by EDTA (Brush and Domski 2013b). Np(V) concentrations were affected by variation in the organic ligand concentrations because of complexation by acetate and oxalate (Brush and Domski 2013b). Over the ranges of organic ligand concentrations predicted in the WIPP repository brines for the CRA-2014 PA, organic ligands had minimal effects on Th(IV) concentrations, and Th(IV) speciation was dominated by $Th(OH)_4(aq)$ and $Th(OH)_3CO_3^-$ (Brush and Domski 2013b).

7.2.6 Actinide Solubility Uncertainties

Brush and Domski (2013c) described the development of the uncertainty distributions for the CRA-2014 PA actinide solubilities. Am(III), Nd(III), Cm(III), and Th(IV) solubility studies were evaluated for calculating actinide solubility uncertainty distributions for Am(III) and Th(IV). A solubility uncertainty distribution was not developed for Np(V) solubility because this uncertainty is not sampled for WIPP PA due to neptunium's insignificant effects on long-term WIPP performance. An uncertainty distribution also was not developed for the U(VI) solubility because a WIPP solubility model has not been developed for U(VI) and DOE instead uses a constant, upper-limit U(VI) concentration of 1×10^{-3} M for WIPP PA (Section 7.1.5).

Brush and Domski (2013c) used criteria developed by Xiong et al. (2009) to determine whether data from available solubility studies should be included in the uncertainty analysis. The data cutoff date was modified to include data published through October 31, 2011. Brush and Domski (2013c) also added results from Borkowski et al. (2012) and Borkowski (2012b).

Brush and Domski (2013b) added additional criteria to those of Xiong et al. (2009), including:

> G11. Include only results from experimental studies carried out under conditions at or close to those predicted for WIPP disposal rooms. Specifically, include only results from experiments in which: (1) $I \geq 3$ molal or M, (2) pcH = 8.0 – 11.2, and (3) total inorganic carbon (TIC) = 0 – 0.014 M.
>
> A1: Include only results from GWB brine experiments with $pcH \leq 7.4$ and include only results from ERDA-6 brine experiments with $pcH \leq 8.1$ because Borkowski et al. (2009) determined that significant Nd(III) complexation by borate can occur at higher pcH in WIPP brines.
>
> A2: Include only +III actinide solubility results from concentrated $CaCl_2$ brine experiments with pcH < 10. This pcH limit is included because Neck et al. (2009) found that Cm(III) forms significant $Ca_x[Cm(OH)_y]^{2x+3-y}$ aqueous species at pcH > 10. Significant concentrations of these species are unlikely to form in WIPP repository brines because of the low calcium concentrations maintained by anhydrite precipitation.
>
> A3: Include only Th(IV) actinide solubility results from concentrated $CaCl_2$ brine experiments with pcH < 10. This limit is included because Brendebach et al. (2007) and Altmaier et al. (2008) found that significant concentrations of the $Ca_4[Th(OH)_8]^{4+}$ aqueous species form in concentrated $CaCl_2$ solutions at pcH > 10. Significant concentrations of this species are unlikely to form in WIPP repository brines because of the low calcium concentrations maintained by anhydrite precipitation.

EPA (2017d) reviewed the selection criteria developed by Brush and Domski (2013c) and developed revised selection criteria for the CRA14_SEN4 PA. EPA changed the selection criteria developed by Brush and Domski (2013c) to accommodate the later date of the CRA14_SEN4 PA (Criterion G1), to address the presence of borate in WIPP brines (Criterion G9 and deletion of Criterion A1), and to increase the TIC concentration limit for included solubility data (Criterion G11). Criterion S1 was eliminated as redundant because Criterion G11 addresses both the +III and +IV actinides. Criterion G7 was edited to remove an obsolete reference to the FMT database, because the FMT code and database have been replaced by the EQ3/6 code and database.

Xiong and Domski (2016a) used the revised criteria listed below to evaluate and select solubility data for inclusion in the Am(III) and Th(IV) actinide solubility distribution calculations for the CRA14_SEN4 PA:

> G1: (revised): Include only results from experimental studies published by December 31, 2012.
>
> G2: Include results from papers published in peer-reviewed journals and from unpublished reports (e.g., officially released reports from government laboratories such as Los Alamos National Laboratory, Lawrence Livermore National Laboratory, Pacific Northwest National Laboratory, etc.).
>
> G3: Include only results from solubility studies. Exclude other studies that do not provide solubilities (e.g., studies of corrosion, leaching, sorption, or transport).
>
> G4: Include only results from studies in which water was the solvent. Exclude studies in which other solvents were used (e.g., solids, molten metal or salts, or organic liquids).
>
> G5: Include only results obtained from studies at pressures at or close to atmospheric, at temperatures at or close to those expected in the WIPP (i.e., 20-30°C), and with posttest phase-separation methods similar to those used for the WIPP, because these were the conditions and methods used to parameterize the Th(IV) and Am(III) speciation and solubility models for WIPP compliance-related PA calculations.
>
> G6: Include only results from studies of Th(IV), Nd(III), Am(III), and Cm(III) because these elements were used to parameterize the WIPP Th(IV) and Am(III) solubility models. Exclude studies of U(IV), Np(IV), Pu(IV), and Pu(III) because there could be systematic differences between the solubilities of these elements and those of their oxidation-state analogs used to parameterize the models and because the difficulties inherent in maintaining these elements in these oxidation states could introduce experimental artifacts in the results obtained with these elements.
>
> G7: (revised): Include only results from studies with a characterized solubility-controlling solid for which solubility data are in the WIPP Th(IV) or Am(III) model (currently the DATA0.FM1 database), and in which the quantity of solid initially present was sufficient to prevent complete dissolution of this solid during the experiments.
>
> G8: Include only results from studies with aqueous solutions of known composition. Exclude studies performed with groundwaters, sedimentary pore waters, and soil solutions that may contain unknown quantities of species that can be complexants or

adsorbents (e.g., humic acids or other dissolved organic compounds, microbial colloids, or pseudocolloids).

G9: (revised): Include results from studies with dissolved elements or species that are present in WIPP brines. Exclude studies with dissolved elements or species that are absent in WIPP repository brines and for which our models do not include association/dissociation constants or Pitzer parameters.

G10: Include only results from studies for which the investigators provided a complete description of their experiments and the original solubilities. Exclude literature reviews and summaries, and studies in which the authors only provided average dissolved concentrations or solubility products, thus necessitating back calculation of the solubilities.

G11: (revised). Include only results from experimental studies carried out under conditions at or close to those predicted for WIPP disposal rooms. Specifically, include only results from experiments in which: (1) $I \geq 3$ molal or M, (2) pcH = 8.0 – 11.2, and (3) TIC = 0 – 0.02 M.

A2: Include only +III actinide solubility results from concentrated $CaCl_2$ brine experiments with pcH < 10. This pcH limit is included because Neck et al. (2009) found that Cm(III) forms significant $Ca_x[Cm(OH)_y]^{2x+3-y}$ aqueous species at pcH > 10. Significant concentrations of these species are unlikely to form in WIPP repository brines because of the low calcium concentrations maintained by anhydrite precipitation.

A3: Include only Th(IV) actinide solubility results from concentrated $CaCl_2$ brine experiments with pcH < 10. This limit is included because Brendebach et al. (2007) and Altmaier et al. (2008) found that significant concentrations of the $Ca_4[Th(OH)_8]^{4+}$ aqueous species form in concentrated $CaCl_2$ solutions at pcH > 10. Significant concentrations of this species are unlikely to form in WIPP repository brines because of the low calcium concentrations maintained by anhydrite precipitation.

Brush and Domski (2013c) identified 64 solubility measurements for calculation of the CRA-2014 PA Th(IV) solubility uncertainty distribution:

- 40 values from Borkowski et al. (2012) and Borkowski (2012b),
- 18 values from Felmy et al. (1991), and
- 6 values from Altmaier et al. (2004).

Table 7-6 compares the CRA-2014 PA +IV actinide solubility uncertainty distribution to the CRA-2009 PA distribution. The positive mean and median values suggest a tendency for the CRA-2014 +IV actinide solubility model to predict Th(IV) solubilities less than the measured solubilities.

Brush and Domski (2013c) used 172 solubility measurements to determine the Am(III) solubility uncertainty distribution:

- 109 values from Borkowski et al. (2009), Borkowski et al. (2010), and Borkowski (2012a);
- 56 values from Neck et al. (2009);

- 6 values from Runde and Kim (1994); and
- 1 value from Rao et al. (1999).

The solubility measurements from Neck et al. (2009), Runde and Kim (1994), and Rao et al. (1999) met the selection criteria and were appropriately included in the Am(III) solubility uncertainty distribution calculations. However, the majority of the solubility measurements used to calculate the Am(III) solubility uncertainty distribution for the CRA-2014 PA were from Borkowski et al. (2009). As noted during review of the PABC09, inclusion of the Nd(III) solubility data from Borkowski et al. (2009) in the uncertainty analysis is inconsistent with Criterion G7 because the solid phases were characterized only by indirect means. DOE acknowledged that the Borkowski et al. (2009) data do not meet Criterion G7 and that the large number of solubility measurements from this study may have inordinately affected the uncertainty distribution (Shrader 2016). Table 7-5 compares the results of the CRA-2014 Am(III) uncertainty distribution to the PABC09 uncertainty distribution. The negative mean and median values for the CRA-2014 +III actinide uncertainty distribution suggests a tendency towards predicting Am(III) solubilities that are higher than measured values.

7.3 CRA14_SEN4 PA DISSOLVED ACTINIDE SOURCE TERM

EPA requested that DOE perform a limited sensitivity study of the CRA-2014 PA (Werner 2016). For this PA (CRA14_SEN4 PA), EPA requested that DOE use the baseline actinide solubilities calculated for the CRA-2014 PA with the DATA0.FM1 database (Table 7-4), along with Am(III) and Th(IV) solubility uncertainty distributions developed using data identified by EPA (Peake 2016) using the EPA-modified selection criteria (Section 7.2.6). EPA also requested that DOE use a GLOBAL:PBRINE[6] distribution provided by EPA (EPA 2017b), a modified lower bound for the sampled TAUFAIL[7] distribution for the 50% degraded waste, a corrected version of the DRSPALL code[8], and a corrected representative length of the furthest northern set of panel closures (Werner 2016).

Xiong and Domski (2016a) reported the results of the Th(IV) solubility uncertainty distribution calculations for the CRA14_SEN4 PA. Table 7-6 compares the statistical properties of this distribution to previous WIPP PAs. The mean and median values calculated for the Th(IV) solubility uncertainty distribution for the CRA14_SEN4 PA are close to zero, indicating that there is no general tendency toward under- or over-prediction of the measured Th(IV) solubility measurements.

EPA (2017d) provided a detailed assessment of the effects of data from individual investigations on the Th(IV) solubility uncertainty distribution. The geochemical model consistently predicted Th(IV) concentrations that exceeded measured concentrations in experiments in concentrated NaCl and $MgCl_2$ (Altmaier et al. 2004). This consistent difference may be related to higher ionic strengths in the Altmaier et al. (2004) experiments. This difference could also be caused by more

[6] Parameter representing the probability that a drilling intrusion into the excavated region of the repository encounters a region of pressurized brine below the repository
[7] Effective shear strength for erosion of waste
[8] The DRSPALL code is used to calculate spallings releases

effective removal of nanoscale colloids by the ultracentrifugation method used by Altmaier et al. (2004) than by the 1.8 nm filtration method employed by the Felmy et al. (1991) study that DOE used to parameterize the model. The Th(IV) solubilities measured by Altmaier et al. (2006) in concentrated NaCl solutions with 0.02 M TIC are consistently higher than predicted using the geochemical model. This result indicates the thorium-carbonate speciation in DATA0.FM1 should be re-evaluated (Attachment B, Section B.8.2).

Xiong and Domski (2016a) described the results of the Am(III) solubility uncertainty distribution calculations for the CRA14_SEN4 PA. Table 7-5 compares the statistical properties of this distribution to previous WIPP PAs. The mean and median of the Am(III) difference values are positive, indicating that the model generally underpredicts the experimentally measured Am(III) solubilities.

EPA (2017d) provided a detailed assessment of the effects of data from individual investigations on the Am(III) solubility uncertainty distribution. Neck et al. (2009) measured higher $Nd(OH)_3(s)$ solubilities than previous investigations. This higher solubility and resulting positive difference values are likely related to the amorphous or microcrystalline nature of the solubility-controlling material in the experiments (Attachment B, Section B.7.3). Consequently, including the Neck et al. (2009) data in the +III actinide solubility uncertainty calculations accounts for the possible persistence of amorphous or microcrystalline +III actinide hydroxide solids in the repository.

7.4 CRA-2019 DPA DISSOLVED ACTINIDE SOURCE TERM

Actinide solubilities in WIPP repository brines can be influenced by the repository setting, including Salado mineralogy (Section 2.2), Salado and Castile brine chemistry (Section 2.3), temperature, and pressure. DOE (2019, Appendix SOTERM Section 2.1) reviewed the ambient geochemical conditions created by the repository setting. The assumed repository temperature is 27°C, with a possible transient increase of up to 12°C caused by TRU waste emplacement. The hydrostatic pressure in the repository is 8 MPa. The maximum repository pressure is equal to 15 MPa, which is the lithostatic pressure.

Waste emplacement will alter the ambient chemical conditions in the repository. Components in the waste inventory that can influence dissolved actinide concentrations include CPR, metals, cements, and organic ligands. The effects of the MgO backfill on pH and CO_2 fugacity in repository brines are addressed in Section 4.0, and the effects of iron metal and other reductants on actinide oxidation states are addressed in Section 6.0.

7.4.1 Waste Inventory

The WIPP CPR inventory may affect actinide solubilities because microbial degradation or radiolysis of CPR can produce CO_2. Van Soest (2018) reported the CPR inventory for the CRA-2019 DPA. Because the MgO backfill will react to form hydromagnesite (Section 4.1), CO_2 production by CPR degradation or radiolysis has relatively small effects on actinide solubilities. Actinide solubilities continue to be calculated assuming that hydromagnesite formation by reaction of CO_2 with the MgO backfill will maintain low CO_2 fugacity.

Cementitious waste in the WIPP inventory could increase brine pH above values established by the brucite dissolution reaction. For the CRA-2009 and CRA-2014, EPA used mass-balance calculations to estimate if sufficient amounts of dissolved magnesium would be available to prevent increased brine pH from the dissolution of portlandite in cements (Sections 7.1.7 and 7.2.1). For the CRA-2019, DOE performed geochemical modeling calculations at EPA's request to directly evaluate the effects of portlandite in waste cements on brine pH and actinide solubilities (Section 7.4.9).

Organic ligands inventories reported for the CRA-2019 DPA are compared to organic ligands inventories for previous PAs in Table 7-3. The CRA-2019 DPA organic ligand inventories are reasonably similar to the PABC09 and CRA-2014 PA inventories, although acetic acid and acetate inventories increased from the PABC09 to the CRA-2019 DPA.

The SR-KAC-PuOx waste stream is composed of Pu oxides that have been downblended using a proprietary, classified adulterant. In publicly available documentation, DOE specifies that the adulterant is a multicomponent mixture designed to prevent any criticality issues, provide a stable matrix for the downbleded Pu, and impede recovery of nuclear materials. These adulterant materials are included as part of the SR-KAC-PuOx waste stream and the PA calculations. The waste stream contains ferrous materials (approximately 60-85 wt.%), inorganic materials (10-20 wt.%), non-ferrous metals (5-15 wt.%), and plastics (2-5 wt.%) (Knerr 2022, Wade 2021).

EPA reviewed DOE's preliminary data from a classified scoping study that explored the adulterant's impacts to repository gas generation, pcH, and E_H (i.e., redox conditions) (Knerr 2022). DOE's analysis on the material shows that the geochemical impacts of the adulterant are overwhelmingly mediated by the waste stream's significant iron content. Experimental results indicate no significant impact to repository pcH and impacts to gas generation were previously accounted for in the CRA-2019 DPA. Redox chemistry appears to dominate the adulterant interactions with brine, facilitating the expected, highly reducing chemical conditions of the post-repository system. Consequently, EPA believes that the adulterant associated with the SR-KAC-PuOx waste stream should not impact releases beyond what is already accounted for in the calculations. EPA anticipates reviewing longer-term data on the adulterant as DOE confirms the findings of the classified scoping study.

7.4.2 Brine Chemistry

Domski and Sisk-Scott (2019) performed actinide solubility calculations for the CRA-2019 DPA using GWB and ERDA-6 brines with organic ligand concentrations calculated using the minimum brine volume of 17,400 m^3 (Clayton 2008) and brine volumes that are 2-, 3-, 4-, and 5-times greater than this minimum volume. The organic ligand concentrations used in the CRA-2019 DPA actinide solubility calculations are summarized in Table 7-2. The CRA-2019 DPA organic ligand concentrations are reasonably similar to the CRA-2014 PA concentrations.

7.4.3 EQ3/6 Code and Database

DOE used the EQ3/6 Version 8.0a geochemical modeling code (Wolery et al. 2010) and the DATA0.FM4 database (Domski 2019a) for the CRA-2019 DPA actinide solubility calculations.

DATA0.FM4 was created by revising DATA0.FM1, the WIPP database used for the CRA-2014 PA (Attachment B). Revisions to DATA0.FM1 included:

- Hydromagnesite solubility;
- EDTA aqueous speciation, Pitzer parameters, and $Ca_2EDTA \cdot 7H_2O(s)$ solubility;
- Citrate aqueous speciation;
- Oxalate aqueous speciation and glushinskite [$MgOxalate \cdot 2H_2O(s)$] solubility;
- Iron solids solubilities, aqueous speciation, and Pitzer parameters; and
- Lead solids solubilities and aqueous speciation.

EPA reviewed the DATA0.FM4 database in detail (Attachment B). DOE recalculated the log K_s^0 for hydromagnesite using data from Robie and Hemingway (1973). This recalculated solubility is more internally consistent with other data in the database than the previous DATA0.FM1 value. Issues related to the aqueous stability constants for $CaEDTA^{2-}$, $MgEDTA^{2-}$, and $AmEDTA^{-}$, and to the derivation and testing of some of the $EDTA^{4-}$ Pitzer parameters had significant effects on the dissolved Am(III) concentrations calculated for the CRA-2019 DPA. EPA noted issues associated with citrate, oxalate, and iron data added to the database, and found that the addition of lead to the database was inappropriate because Pitzer parameters associated with lead were not included. The effects of these database issues on dissolved actinide solubilities are evaluated in Section 7.4.10.

7.4.4 CRA-2019 DPA Actinide Solubility Calculations

DOE performed the CRA-2019 DPA actinide solubility calculations in two steps (Domski and Sisk-Scott 2019, Domski 2019c). First, EQ3NR was used to add organic ligands and actinide solid phases [$Am(OH)_3(s)$, $ThO_2(am)$, and $KNpO_2CO_3(s)$] to the WIPP brine and equilibrate the initial solution. A pickup file was created as part of the output that provided input for the next step. In the second step, EQ6 was used to titrate halite, anhydrite, brucite, hydromagnesite, $Fe(OH)_2(s)$, and litharge [PbO(s)] into the equilibrated initial solution from the previous step.

Domski and Sisk-Scott (2019) calculated the moles of solids added in Step 2 based on brine compositions and densities; WIPP inventory data for MgO backfill, iron, and lead; and the volume, mineralogy, and rock density of the DRZ. DOE assumed that the moles of MgO were equal to 1.2 times the moles of carbon in the CPR inventory. Domski and Sisk-Scott (2019) assumed that half of the MgO was initially present as brucite, with the remaining half of the MgO initially present as hydromagnesite. Addition of $Fe(OH)_2(s)$ and litharge represented a change from the CRA-2014 PA calculations, because previous WIPP actinide solubility calculations did not include iron or lead aqueous species and solid phases.

Domski and Sisk-Scott (2019) normalized the moles of solids used in Step 2 of the EQ3/6 calculations to 1 kg of water in the WIPP brine, using the minimum brine volume for a DBR of 17,400 m^3 (Clayton 2008). Domski and Sisk-Scott (2019) calculated the moles of solids using the Excel files Conc_density_calcs_CRA-2019_PA.xlsx and AP-153_Scaling of Solids_2019.xlsx. These files were requested by EPA (Peake 2020b, Comment CC2-GEOCHEM-14) and provided by Knerr (2020a). Domski and Sisk-Scott (2019) calculated the amounts of solids added in all of the EQ3/6 actinide solubility calculations using the minimum brine volume. Using the same amounts of initial solids in all actinide solubility calculations

regardless of brine volume overestimated the solids in the 2-, 3-, 4-, and 5-times minimum brine volume calculations. EPA performed calculations that confirmed that using the smaller quantities of the initial solids for the higher brine volumes did not significantly affect calculated baseline actinide solubilities.

For both the CRA-2014 PA and CRA-2019 DPA actinide solubility calculations, minerals that were not allowed to precipitate if oversaturated (suppressed minerals) included aragonite [$CaCO_3$(s)], magnesite, hydromagnesite with the formula $Mg_4(CO_3)_3(OH)_2 \cdot 3H_2O$(s), dolomite, and nesquehonite. For the CRA-2014 PA calculations, calcite precipitation was suppressed, but Domski and Sisk-Scott (2019) did not suppress calcite precipitation for the CRA-2019 DPA calculations and allowed calcite precipitation to proceed to equilibrium if oversaturation occurred. Domski (2019c) stated that calcite precipitation was allowed to prevent high pcH values and dissolved carbonate concentrations that were predicted if $Fe(OH)_2$(s) was added as an initial solid and calcite precipitation was suppressed. Domski (2019c) justified inclusion of calcite precipitation by noting that Xiong and Lord (2008) observed calcite precipitation in Premier MgO carbonation experiments.

The results of the CRA-2019 DPA actinide solubility calculations for the minimum brine volume are compared to solubilities predicted for previous PAs in Table 7-4. The solubility of the +III actinides decreased by an order of magnitude from the CRA-2014 PA to the CRA-2019 DPA because of changes to the EDTA speciation and Pitzer parameters in DATA0.FM4. The +IV actinide solubility decreased slightly because of a lower $Th(OH)_3CO_3^-$ concentration caused by the decreased solubility of hydromagnesite in DATA0.FM4 and consequent lower CO_2 fugacity. The solubility calculated for Np(V) increased in the CRA-2019 DPA relative to the CRA-2014 PA because of increased formation of NpO_2Acetate(aq), caused at least in part by an increase in the acetate inventory (Table 7-3).

Changes in the EQ3/6 modeling calculations and EQ3/6 thermodynamic database since the CRA-2014 PA affected the nonradioactive solids precipitated during the CRA-2019 DPA calculations and the predicted amounts of water in the modeled system. Domski (2019c) provided detailed information regarding the effects of modeling assumptions on the CRA-2019 DPA actinide solubility calculation results. Knerr (2021a, 2021e) provided additional information requested by EPA (Peake 2020e, Comments CC5-GEOCHEM-24, CC5-GEOCHEM-25, CC5-GEOCHEM-26).

7.4.5 DATA0.FM4 Database

Domski (2019c) compared the modeling results obtained with GWB and ERDA-6 (with the minimum brine volume) using either the DATA0.FM1 or DATA0.FM4 databases, and using the organic ligands inventories from either the CRA-2014 PA or the CRA-2019 DPA. These calculations were performed without calcite precipitation and without iron and lead in the system. The results demonstrated that total carbonate concentrations decreased because of the revised hydromagnesite solubility in DATA0.FM4, and that the dissolved Am(III) concentration was significantly decreased because of the revised EDTA aqueous speciation and Pitzer parameters in DATA0.FM4.

EPA identified issues with some of the revised data in DATA0.FM4 and found that these issues decreased Am(III) concentrations in the CRA-2019 DPA solubility calculations (Attachment B). EPA converted and qualified the DATA0.FM4 EQ3/6 database to the PHREEQC format (DATA0FM.dat). EPA used the PHREEQC geochemical modeling code (Parkhurst and Appelo 2013, version 3.3.8.11723) and the converted database to independently evaluate the CRA-2019 DPA actinide solubility calculations and explore the effects of changes to the thermodynamic database and different modeling assumptions on the calculation results. See the *Quality Assurance Project Plan for: Modeling Analyses and verification of PHREEQC Databases and Input Files Performed to Support EPA's Review of DOE's Compliance Recertification Application 2019 (CRA-2019) at the Waste Isolation Pilot Plant*, (Docket ID No. EPA-HQ-OAR-2019-0534) and Attachment D for details on qualification of the converted database and solubility calculations.

EPA tested the ability to reproduce the CRA-2019 DPA actinide solubility calculation results with PHREEQC and the DATA0FM.dat database using the same assumptions regarding the initial phases added to the brine and allowing calcite to precipitate to equilibrium (Table 7-7). For the calculations with ERDA-6, the calcite saturation index was set equal to 0.02 instead of 0.0 to aid convergence, which should have relatively small effects on the calculated actinide solubilities. Minor differences in CO_2 fugacity and pmH may be caused by slight differences in charge balance calculations by EQ3/6 and PHREEQC and may also be related to different tolerance criteria used by the PHREEQC and EQ3/6 codes. The results of the PHREEQC and EQ3/6 calculations were essentially the same for Th(IV) (Table 7-7), because Th(IV) solubility is relatively insensitive to small variations in CO_2 fugacity and pmH under WIPP repository conditions. The Am(III) and Np(V) concentrations calculated using PHREEQC differed by less than 30% from the CRA-2019 DPA values calculated with EQ3/6. These calculations show that PHREEQC provides reasonably comparable results to EQ3/6 when using the same thermodynamic data and assumptions.

Table 7-7. CRA-2019 DPA Actinide Solubility Calculation Results, Results Obtained Using PHREEQC with Converted DATA0.FM4 Database, and Results Obtained with EPA-Modified Database

		Code and Database	EQ3/6 DATA0.FM4	PHREEQC DATA0FM.dat[a]	PHREEQC DATA0FM_EPA.dat[b]
Constituent	Brine	Multiple of Minimum Brine Volume	Concentration (M)	Concentration (M)	Concentration (M)
Am(III)	GWB	1×	1.63×10^{-7}	1.97×10^{-7}	1.56×10^{-6}
Am(III)	GWB	5×	1.54×10^{-7}	1.84×10^{-7}	4.21×10^{-7}
Am(III)	ERDA-6	1×	1.78×10^{-7}	2.19×10^{-7}	5.13×10^{-6}
Am(III)	ERDA-6	5×	1.52×10^{-7}	1.96×10^{-7}	1.09×10^{-6}
Th(IV)	GWB	1×	5.45×10^{-8}	5.41×10^{-8}	5.56×10^{-8}
Th(IV)	GWB	5×	5.45×10^{-8}	5.41×10^{-8}	5.57×10^{-8}
Th(IV)	ERDA-6	1×	5.44×10^{-8}	5.47×10^{-8}	5.54×10^{-8}
Th(IV)	ERDA-6	5×	5.44×10^{-8}	5.48×10^{-8}	5.55×10^{-8}
Np(V)	GWB	1×	4.02×10^{-7}	4.10×10^{-7}	5.05×10^{-7}
Np(V)	GWB	5×	2.09×10^{-7}	2.08×10^{-7}	3.32×10^{-7}
Np(V)	ERDA-6	1×	1.20×10^{-6}	1.37×10^{-6}	1.45×10^{-6}

Np(V)	ERDA-6	5×	4.05×10^{-7}	5.07×10^{-7}	5.91×10^{-7}
pmH	GWB	1×	9.48	9.50	9.48
pmH	GWB	5×	9.49	9.50	9.48
pmH	ERDA-6	1×	9.45	9.49	9.48
pmH	ERDA-6	5×	9.47	9.50	9.49
log f_{CO2}	GWB	1×	-5.69	-5.71	-5.71
log f_{CO2}	GWB	5×	-5.69	-5.71	-5.71
log f_{CO2}	ERDA-6	1×	-5.69	-5.71	-5.71
log f_{CO2}	ERDA-6	5×	-5.69	-5.71	-5.71

a – calcite saturation set to 0.02 for GWB to aid convergence
b – calcite saturation set to 0.03 for GWB and ERDA-6 to aid convergence

EPA identified issues with DATA0.FM4 (Attachment B). The effects of these issues on the CRA-2019 DPA actinide solubility calculations were assessed by modifying the PHREEQC database:

- Revised stability constants for $AmEDTA^-$, NpO_2EDTA^{3-}, NpO_2HEDTA^{2-}, and $NpO_2H_2EDTA^-$ to values from Hummel et al. (2005);
- Increased stability constant for ThEDTA(aq) to 24.6 to approximate the effects of the $NaEDTA^{3-}$ species;
- Increased $MgEDTA^{2-}$ stability constant to 9.20 to approximate the effects of Pitzer parameter issues;
- Revised $CaEDTA^{2-}$ stability constant to the value from Felmy and Mason (2003);
- $\beta^{(0)}$ for the binary Pitzer parameter for the $Ca^{2+}/EDTA^{4-}$ ion pair was revised (Domski 2019b);
- Corrected α_1 terms for the binary Pitzer parameters for $Ca^{2+}/EDTA^{4-}$, $Mg^{2+}/MgEDTA^{2-}$, and $Mg^{2+}/CaEDTA^{2-}$ ion pairs (Domski 2020);
- Revised AmCitrate(aq) stability constant and added $Am(Citrate)_2^{3-}$ aqueous species based on Hummel et al. (2005);
- Revised $NpO_2Citrate^{2-}$ stability constant to Hummel et al. (2005) value; and
- Added earlandite solubility.

EPA used this database (DATA0FM_EPA.dat) with PHREEQC to perform actinide solubility calculations using the same modeling assumptions as the CRA-2019 DPA. EPA also identified issues with the $Am(OH)_3(s)$ solubility, Am(III) Pitzer parameters, and Th(IV)-carbonate speciation (Attachment B). However, EPA did not make database changes associated with these issues to enable continued use of the +III and +IV actinide solubility uncertainty distributions developed by DOE with the revised baseline solubilities calculated with PHREEQC using DATA0FM_EPA.dat (Section 7.4.10). As discussed below in Section 7.4.10, Domski (2021) repeated these calculations using EQ3/6 and the same modeling assumptions after making the above modifications to DATA0.FM4, and calculated actinide solubilities similar to the solubilities calculated using PHREEQC.

Comparison of the results calculated with PHREEQC using the original and modified databases show that the database changes had significant effects on Am(III) concentrations, essentially no effects on Th(IV) concentrations, and small effects on Np(V) concentrations (Table 7-7). The

issues associated with the EDTA data in DATA0.FM4 are the cause of the Am(III) solubility differences calculated with the two databases.

Oakes et al. (2021) evaluated the +III actinide data available in the literature, and had difficulty reproducing some of the figures from Könnecke et al. (1997). Oakes et al. (2021) concluded that there are potential internal inconsistencies in the WIPP Am(III) model that was derived from Könnecke et al. (1997), which could affect the log β^0 values for $AmCl^{2+}$ and $AmCl_2^+$ and some of the Pitzer parameters. EPA expects DOE to evaluate these possible inconsistencies prior to the next WIPP PA.

7.4.6 Calcite Saturation

Calcite precipitation from WIPP brines under repository conditions was not included in the actinide solubility calculations performed for previous WIPP PAs. In previous actinide solubility calculations, calcite was generally undersaturated to slightly oversaturated in GWB, and moderately oversaturated in ERDA-6 brines (Table 7-8).

For the CRA-2019 DPA actinide solubility calculations, Domski (2019c) evaluated the effects of allowing or suppressing calcite precipitation in the absence or presence of iron and lead solids in the initial solids. For GWB, suppressing calcite precipitation had significant effects if the iron and lead solids were included in the calculation, with pcH increasing to 10.24 and a 24% increase in the mass of water in the system. If calcite precipitation to equilibrium was allowed in GWB calculations that included iron and lead, pcH decreased to 9.54 and the mass of solvent water decreased to 61% of the initial mass.

Table 7-8. Calcite Saturation Index Values, Am(III) Concentrations, and CO_2 Fugacity Calculated for ERDA-6 Brine (Minimum Brine Volume) in Recent PAs

Performance Assessment	Code/Database	Calcite Saturation Index	Am(III) (M)	Log CO_2 Fugacity and TIC (M)	Notes
PABC04	FMT FMT_050405.chemdat	0.55	2.88×10^{-7}	-5.50 5.18×10^{-5}	Phase 5 was not in the database, file FMT_CRA1BC_ER6_HMAG_ORGS_011.out
PABC04	FMT FMT_050405.chemdat	0.64	1.51×10^{-6}	-5.50 4.48×10^{-4}	Phase 5 was not in the database, file FMT_ PABC09_E6_HMAG_ORGS_013.out
CRA-2014 PA	EQ3/6 DATA0.FM1	0.65	1.48×10^{-6}	-5.50 4.55×10^{-4}	Phase 5 was added to the database, file erda_1xb.6o
CRA-2019 DPA	EQ3/6 DATA0.FM4	0.0	2.06×10^{-7}	-5.69 2.50×10^{-4}	Hydromagnesite solubility was revised and Phase 5 was included in the database, file erda_1x.6o

Calcite precipitation had significant effects on the results of CRA-2019 DPA actinide solubility calculations performed with ERDA-6 brines. Calculations with calcite precipitation, both with and without lead and iron solids, resulted in the consumption of a large fraction of the solvent water in the system, with only ~17% of the initial moles of water remaining after reaction (Domski 2019c). Much of the water consumption predicted by the CRA-2019 DPA calculations in ERDA-6 brines was caused by brucite and hydromagnesite dissolution coupled

with precipitation of calcite and Phase 5. In previous PA calculations, Phase 3 or Phase 5 precipitation was predicted from GWB brine, but not from ERDA-6 brine (Table 7-4). The predicted absence of Phase 5 precipitation from ERDA-6 brine in previous WIPP PAs was consistent with the results of WIPP MgO hydration and carbonation experiments (Snider and Xiong 2004, Deng et al. 2009).

Precipitation of large amounts of Phase 5 might significantly affect repository processes, including water balance, MgO reactivity, and room closure. Consumption of large quantities of water by Phase 5 precipitation is not accounted for in the CRA-2019 DPA water balance calculations (DOE 2019, Appendix GEOCHEM). The CRA-2019 DPA water balance calculations include hydration of MgO to form brucite as a brine consumption process, but hydration to Phase 5 consumes twice as many moles of water per mole of MgO (Section 4.1). In addition, Phase 5 is a component of magnesium oxychloride cement, also called Sorel cement. If MgO reacts in the WIPP repository to form a low permeability cementitious mass, efficacy of the backfill for controlling CO_2 fugacity could be limited. The WIPP peer review panel evaluated the possibility of backfill cementation at the time of the CCA (Wilson et al. 1996a, 1996b, 1997a). Based on information provided by DOE (Bynum 1997, SNL 1997), the peer review panel found that the MgO backfill would function as assumed for the CCA, without formation of impermeable masses or reaction rinds (Wilson et al. 1997b). However, the potential formation of large amounts of Phase 5 was not considered during the WIPP conceptual model peer review. Cementation of the MgO backfill might also affect room closure because of physical property changes in the backfill.

Oversaturation with respect to calcite is common in low-temperature aqueous systems and is attributed to slow precipitation kinetics and inhibition of calcite precipitation by constituents that include magnesium, phosphate, sulfate, strontium, barium, lead, and organics (e.g., Katz et al. 1993, LeBron and Suarez 1996, Langmuir 1997, Zavarin and Doner 2005). Although calcite may precipitate from WIPP brines, WIPP brine constituents likely will cause some degree of calcite oversaturation to persist. If calcite precipitation is prevented, more soluble $CaCO_3$(s) polymorphs may precipitate, such as aragonite or vaterite.

EPA requested additional calculations from DOE to compare the effects of varying amounts of calcite oversaturation on the results of the actinide solubility calculations, with saturation indices of 0.5, 0.25 and 0.0 (Peake 2020e, Comment CC5-GEOCHEM-24). DOE initially dismissed this request as irrelevant (Knerr 2021a). After additional discussion with EPA, including a technical exchange meeting in February 2021, DOE agreed to perform these calculations (Peake 2021). The calculation results were provided by Knerr (2021e).

DOE carried out the revised actinide solubility calculations with GWB and ERDA-6, using the organic ligand concentrations for the minimum brine volume. The calculations were performed with calcite precipitation suppressed, and with calcite saturation indices of 0.50, 0.25, and 0.0. These calculations included two different assumptions regarding initial iron and lead solids: $Fe(OH)_2$(s) plus litharge, or hibbingite plus cerussite [$PbCO_3$(s)].

The results of these calculations showed that calcite oversaturation significantly affected the amount of water consumed by the reactions, but had smaller effects on the predicted actinide concentrations. Oversaturation represented by a calcite saturation index of 0.25 or greater, or

allowing aragonite to precipitate instead of calcite prevented Phase 5 precipitation in the ERDA-6 brine calculations and maintained a larger fraction of water in the system. Maintaining a calcite saturation index of 0.25 or allowing aragonite to precipitate instead of calcite in the GWB calculations reduced the amount of predicted Phase 5 precipitation, which resulted in an increased mass of water in the equilibrated solutions.

During review of DATA0.FM4 (Attachment B), EPA was unable to locate calculations demonstrating that the DATA0.FM4 database can be used to accurately model the experimental solubility data for Phase 5. EPA also found that the calculated solubility of Phase 5 may be too low, which would overestimate the stability and precipitation of Phase 5.

CRA-2019 DPA actinide solubility calculations predicting large amounts of Phase 5 precipitation are potentially problematic because of the large amount of water that is consumed, which is inconsistent with the current conceptualization of the water balance. Predictions of large amounts of Phase 5 precipitation also raise questions regarding potential cementation of the MgO backfill, which could alter its ability to control CO_2 fugacity and may also affect room closure because of physical property changes. Phase 5 precipitation in the CRA-2019 DPA may be overpredicted because of the assumption that calcite precipitation will proceed to complete equilibrium despite the presence of multiple brine constituents that are known to inhibit calcite precipitation. EPA expects DOE to evaluate whether some degree of oversaturation with respect to calcite should be maintained in the actinide solubility calculations for future WIPP PAs. DOE also should provide calculations demonstrating that the Phase 5 solubility data in the DATA0.FM4 database is consistent with the measured solubility data prior to the next WIPP PA.

7.4.7 Iron and Lead Phases

For actinide solubility calculations performed for previous WIPP PAs (CCA PAVT, PABC-2004, PABC-2009, and CRA-2014 PA) DOE assumed the initial presence of the minerals halite, anhydrite, brucite, and hydromagnesite and equilibrated these minerals with brine containing Am(III), Th(IV), and Np(V). These calculations differed from the CRA-2019 DPA calculations because the previous calculations included the dissolution and precipitation of fairly small amounts of solid phases and did not include calcite precipitation.

For the CRA-2019 DPA actinide solubility modeling calculations, Domski and Sisk-Scott (2019) included halite, anhydrite, brucite, and hydromagnesite as reactant phases. Domski and Sisk-Scott (2019) also included litharge and $Fe(OH)_2$-hex(s) as initial solid phases. Litharge and $Fe(OH)_2$-hex(s) were unstable under the modeled conditions, were completely dissolved, and much of the lead and iron reprecipitated as cerussite and hibbingite.

In previous WIPP PA calculations, the initial reactant minerals were also present at equilibrium, with relatively small amounts of reaction required to achieve equilibrium solution concentrations. Consequently, changes in the mass of water in the calculations were relatively small. In the CRA-2019 DPA calculations, Domski and Sisk-Scott (2019) included the unstable minerals litharge and $Fe(OH)_2$-hex(s) in the reactants and these solids dissolved completely. These reactions produced large quantities of water during conversion of $Fe(OH)_2$-hex(s) to hibbingite (Domski 2019c, Table 12). The production of this large amount of water is inconsistent with the current WIPP water balance, because most iron in the repository will

initially be present as metallic iron [Fe(s)] that consumes water via anoxic corrosion (Section 3.1.1). Similarly, lead will initially be present in metallic form, and should consume water as it undergoes anoxic corrosion to form litharge or cerussite (Section 3.2.1).

Domski (2019c) evaluated the effects of adding $Fe(OH)_2$(s) and litharge to the CRA-2019 DPA calculations. For these calculations, Domski (2019c) used DATA0.FM4, the CRA-2019 DPA minimum brine volume organic ligand concentrations, and suppressed calcite precipitation. The results of these calculations showed that addition of litharge alone had little effect on the results. Adding $Fe(OH)_2$-hex(s), alone or in combination with litharge, increased the amount of water, increased pH, and decreased Am(III) concentrations because of the effects of dilution and increased pH. Domski (2019c) also showed that if calcite was not suppressed, including $Fe(OH)_2$-hex(s) and litharge had little effect on the results of the actinide solubility calculations for GWB or for ERDA-6.

Knerr (2021e) compared the effects of using either $Fe(OH)_2$-hex(s) plus litharge or the more stable solids hibbingite and cerussite in the actinide solubility calculations. For calculations that included calcite precipitation to equilibrium, the choice of the initial iron and lead solid phases had little effect on the mass of water or actinide concentrations. However, if calcite was not allowed to precipitate, including hibbingite and cerussite resulted in smaller final masses of water and higher Am(III) concentrations.

During review of DATA0.FM4 (Attachment B), EPA found that the lead data are incomplete and should not be used in WIPP PA calculations because DATA0.FM4 lacks Pitzer parameters for lead species, DATA0.FM4 may not include all lead solids that could form in the WIPP repository environment, and DOE has not demonstrated that the DATA0.FM4 can be used to accurately model available experimental solubility data in high ionic strength solutions.

EPA reviewed the iron data in DATA0.FM4 and found that the data are well-documented and adequate for inclusion in the database. However, DOE omitted some Fe^{2+}-sulfate solids solubility and Pitzer parameter data from DATA0.FM4 (Attachment B). These omissions are not expected to have significantly affected the CRA-2019 DPA actinide solubility calculations because sulfate forms weak aqueous complexes with the +III and +IV actinides (Knerr 2021c). DOE should add the missing sulfate data to the database to maintain consistency with the database documentation and minimize uncertainty.

WIPP repository brines are expected to contain sulfide from microbial sulfate reduction and phosphates from the waste inventory. Because reduced iron can form relatively insoluble sulfide and phosphate solid phases, geochemical modeling performed without accounting for the effects of sulfide and phosphate could overpredict Fe^{2+} concentrations. Elevated Fe^{2+} concentrations would increase the competition for organic ligands, leading to the potential underprediction of actinide complexation by organic ligands. Therefore, inclusion of Fe(II) interactions with organic ligands in WIPP actinide solubility calculations will also require consideration of the effects of phosphate and sulfide.

7.4.8 Polyhalite Effects

In response to a request from EPA (Peake 2020e Comment CC5-GEOCHEM-25), Knerr (2021a, 2021e) evaluated the effects of including the Salado Formation mineral polyhalite as an initial solid in the actinide solubility modeling calculations. DOE performed these calculations assuming that the Salado Formation minerals consist of 90 wt% halite, 7.5 wt% anhydrite, and 2.5 wt% polyhalite, and calcite precipitation was allowed to proceed to equilibrium in these calculations. Because polyhalite dissolution released Mg^{2+} to the brines, Phase 5 precipitation consumed water to the extent that the reaction path calculations could not reach completion. Suppression of Phase 5 precipitation allowed the calculations to run to completion. The importance of Phase 5 precipitation to these calculations supports the recommendation that DOE evaluate the Phase 5 solubility data in DATA0.FM4 (Section 7.4.6).

The estimated polyhalite concentration in the Salado Formation of 2.5 wt% is likely to be a significant overestimation. Brush (1990) approximated the mineralogy of the Salado Formation based on data from Stein (1985) and estimated that polyhalite made up 1.7 wt%. SC&A (2008b) evaluated the data reported by Stein (1985) and found that only four out of 44 samples had polyhalite identified by XRD. In three of these samples, polyhalite appeared to be less abundant than other non-halite minerals. SC&A (2008b) concluded that the percentage of polyhalite in the Salado Formation near the repository horizon is probably significantly less than the other non-halite minerals, such as anhydrite, magnesite, and quartz. Because polyhalite dissolution has the potential to consume significant amounts of water through Phase 5 precipitation, a more defensible determination of the amount of polyhalite in the DRZ is recommended.

7.4.9 Cement Effects

The potential effects of cement in the waste inventory have been evaluated for previous WIPP PAs using mass balance calculations to determine if the amount of portlandite in the cement could exceed the amount of magnesium in the brine and in polyhalite in the Salado Formation (Sections 7.1.7 and 7.2.1). A more direct way to evaluate the possible effects of cementitious wastes on brine chemistry is to include portlandite in the actinide solubility calculations.

The amount of portlandite in the cement waste can be calculated by assuming that the cement contains 5 wt%, 7.5 wt%, or 10 wt% $Ca(OH)_2$ (Storz 1996). These percentages of portlandite in the cement can be used with the cement inventory reported for the CRA-2019 DPA (Van Soest 2018) to calculate the total moles of portlandite from cement waste in the repository. In addition to portlandite in cementitious waste, the Martin Marietta MgO is reported to contain 0.63 mole% lime [CaO(s)], which is expected to rapidly hydrate in the repository to form portlandite (Deng et al 2007). When multiplied by the total moles of MgO in the repository, this percentage of portlandite yields an additional 7.0×10^6 moles of portlandite. For the EQ3/6 calculations with GWB and ERDA-6, the moles of portlandite calculated assuming 10% portlandite in cement and normalized to 1 kg solvent water is 1.45 moles for GWB and 1.42 moles for ERDA-6.

Peake (2020e, Comment CC5-GEOCHEM-26) requested that DOE perform EQ3/6 calculations to assess the potential effects of cements on brine chemistry and actinide solubilities. Knerr (2021e) provided calculations that included the assumption that the cement wastes contained 67% portlandite, which is significantly greater than the portlandite content of up to 10%

estimated by Storz (1996). The 67% portlandite value resulted in initial portlandite amounts of 9.2 moles for GWB and 9.0 moles for ERDA-6 when normalized to 1000 g solvent water for the EQ3/6 calculations. DOE performed the calculations using the same assumptions as the CRA-2019 DPA actinide solubility calculations, except for the addition of portlandite to the solid phases. Even at the relatively high portlandite concentrations used by Knerr (2021e), the pmH, CO_2 fugacity, and actinide solubilities were minimally affected by addition of portlandite. In both GWB and ERDA-6, the principal reaction caused by portlandite addition included dissolution of hydromagnesite with precipitation of calcite and brucite:

$$Mg_5(CO_3)_4(OH)_2{\bullet}4H_2O(s) + 4\ Ca(OH)_2(s) \leftrightharpoons 4\ CaCO_3(s) + 5\ Mg(OH)_2(s) + 4H_2O(l) \quad \textbf{(32)}$$

This reaction has no net effect on pmH or CO_2 fugacity. In the GWB calculations, excess hydromagnesite remained at the end of the calculations. However, in the ERDA-6 calculations, hydromagnesite was completely consumed and Phase 5 that was precipitated in the early stages of the calculations began to dissolve. Dissolution of Phase 5 resulted in a larger mass of solvent water than calculated for the CRA-2019 DPA actinide solubility calculations, but the pmH, CO_2 fugacity, and actinide solubilities remained reasonably similar.

EPA used PHREEQC with the converted DATA0.FM4 database to perform additional sensitivity calculations for ERDA-6 brine. In these calculations, EPA did not include iron and lead solid phases, included the higher 9.0 moles of portlandite used by Knerr (2021e), and assumed aragonite precipitation would occur instead of calcite precipitation. Using these assumptions, hydromagnesite was not completely consumed by portlandite addition and reaction (32) appeared to account for most of the effects of portlandite addition. These calculations corroborated the conclusion that portlandite would have minimal effects on actinide solubilities.

EPA also used PHREEQC with the converted DATA0.FM4 database to calculate the amount of CO_2 necessary to maintain moderately alkaline pmH if portlandite is included in the solid phases. EPA performed these calculations by assuming the absence of iron and lead solid phases, the moles of portlandite were equal to the value of 9.0 moles used by Knerr (2021e), and aragonite precipitation occurred instead of calcite. The results of these calculations indicated that less than 15% of the CPR carbon inventory would need to be converted to CO_2 to maintain moderately alkaline pmH values expected in the repository. These results indicate that even at the relatively high portlandite percentages assumed for cementitious wastes by Knerr (2021e), portlandite in the WIPP inventory is unlikely to significantly affect brine chemistry and actinide solubilities.

7.4.10 Sensitivity Calculations of Actinide Solubilities

EPA performed actinide solubility calculations to assess the sensitivity of the results to the issues identified during review of the DATA0.FM4 database and the assumptions used for the CRA-2019 DPA actinide solubility calculations. EPA recalculated the baseline dissolved actinide solubilities in GWB and ERDA-6 brines using PHREEQC and the EPA-revised WIPP database (DATA0FM_EPA.dat). Some degree of calcite oversaturation will likely persist in WIPP repository brines because of the presence of known inhibitors such as magnesium and sulfate, so EPA assumed aragonite would form instead of calcite in these calculations. Because of database

issues associated with iron and lead, EPA did not include these constituents in the recalculation of the baseline actinide solubilities.

The results of these calculations are compared to previous WIPP PA results for the organic ligand concentrations associated with the minimum brine volume in Table 7-4. The mass of solvent water for GWB was 0.869 kg and for ERDA-6 was 1.004 kg. Both of these results are higher than the masses of solvent water calculated for the CRA-2019 DPA, which were 0.61 kg for GWB and 0.168 kg for ERDA-6 (Domski 2019c). The increased mass of water in the sensitivity calculations is the result of a smaller amount of $CaCO_3$(s) precipitation and less dissolution of hydromagnesite, which limited Phase 5 precipitation from GWB and eliminated Phase 5 precipitation from ERDA-6. The sensitivity calculations had calcite saturation indices of 0.05 to 0.08 in GWB, and 0.19 in ERDA-6. These slightly positive saturation indices are consistent with a small degree of calcite oversaturation, which is reasonable for a low temperature aqueous solution that contains multiple potential calcite precipitation inhibitors. The brine pcH values, CO_2 fugacity, and total carbon concentrations are only slightly affected by the use of the $CaCO_3$(s) polymorph aragonite instead of calcite (Table 7-4).

The Th(IV) and Np(V) dissolved concentrations calculated using the revised database and assumptions increased only slightly from the CRA-2019 DPA concentrations (Table 7-4). However, the predicted Am(III) concentrations in the minimum brine volume increased by about an order of magnitude in the sensitivity calculations relative to the CRA-2019 DPA results. At EPA's request, DOE revised the DATA0.FM4 EQ3/6 database to include the same changes as the PHREEQC database (DATA0FM_EPA.dat). DOE then reproduced the EPA actinide solubility sensitivity calculations (Domski 2021). The results of the EQ3/6 sensitivity calculations are consistent with the PHREEQC calculation results, producing Am(III), Th(IV), and Np(V) concentrations that were only slightly higher than the PHREEQC results with the equivalent database changes.

Solubility results for Am(III) from the PHREEQC and EQ3/6 sensitivity calculations for all brine volumes are compared to the CRA-2019 DPA Am(III) solubility results in Table 7-9. Because the modified DATA0FM_EPA.dat (PHREEQC) and DATA0.EP2 (EQ3/6) databases include a higher $AmEDTA^{2-}$ stability constant and lower stability constants for $CaEDTA^{2-}$ and $MgEDTA^{2-}$ than DATA0.FM4, these calculations predict a more significant effect of EDTA on total dissolved Am(III) concentrations for all brine volumes. For all of the solubility calculations, the Am(III) concentration decreases with brine volume because of dilution of the EDTA in the WIPP inventory. Other differences in the calculations, including substitution of aragonite for calcite as a potential reaction product and the omission of iron and lead phases, have been shown to have smaller effects on actinide solubilities.

Table 7-9. Am(III) Solubilities Calculated for the CRA-2019 DPA, EPA PHREEQC Calculations with Revised Database, and Revised DOE EQ3/6 Calculations

Brine and Brine Volume	CRA-2019 DPA (M)[a]	EPA PHREEQC Calculations (M)[b]	Revised DOE EQ3/6 Calculations (M)[c]
GWB 1×	1.63×10^{-7}	2.14×10^{-6}	2.77×10^{-6}
GWB 2×	1.58×10^{-7}	1.09×10^{-6}	1.39×10^{-6}
GWB 3×	1.56×10^{-7}	7.74×10^{-7}	9.63×10^{7}

GWB 4×	1.55×10^{-7}	6.19×10^{-7}	7.59×10^{-7}
GWB 5×	1.54×10^{-7}	5.28×10^{-7}	6.38×10^{-7}
ERDA-6 1×	1.78×10^{-7}	1.43×10^{-6}	1.70×10^{-6}
ERDA-6 2×	1.63×10^{-7}	7.26×10^{-7}	8.54×10^{-7}
ERDA-6 3×	1.58×10^{-7}	5.16×10^{-7}	6.01×10^{7}
ERDA-6 4×	1.54×10^{-7}	4.16×10^{-7}	4.80×10^{-7}
ERDA-6 5×	1.52×10^{-7}	3.56×10^{-7}	4.09×10^{-7}

a – Domski and Sisk-Scott (2019)
b – EPA calculations
c – Domski (2021)

7.4.11 Actinide Solubility Uncertainties

Domski (2019d) developed the CRA-2019 DPA uncertainty distributions for the +III and +IV actinide solubilities using the same approach as for previous WIPP PAs. Domski (2019d) used the same set of experimental data specified for the CRA14_SEN4, except for the exclusion of solubility data from Khalili et al. (1994). Domski (2019d) used the DATA0.FM4 EQ3/6 database to calculate model-predicted solubilities based on the experimental conditions for each measured solubility. None of the experiments used to calculate the difference values for the uncertainty distribution contained organic ligands. Consequently, revisions made to DATA0.FM1 to produce DATA0.FM4 did not change the solubilities calculated for the uncertainty distributions. This is illustrated by the uncertainty distribution for Th(IV), which was the same for the CRA14_SEN4 and CRA-2019 DPA (Table 7-6).

During a technical exchange meeting in September 2018, DOE and EPA agreed that the Khalili et al. (1994) data included in the CRA14_SEN4 evaluation did not meet the selection criteria and that these data should be excluded from the +III actinide solubility uncertainty distribution calculation for the CRA-2019 DPA. Removing the Khalili et al. (1994) data had no effect on the maximum and minimum difference values for the +III dissolved actinide solubility uncertainty distribution, but both the mean and median difference values increased (Table 7-5). The solubility data (82 values) used to calculate the CRA-2019 DPA +III actinide uncertainty distribution were obtained from three publications: 11 $Am(OH)_3$(s) solubilities from Runde and Kim (1994), 15 $NaNd(CO_3)_2$•$6H_2O$(cr) solubilities from Rao et al. 1999, and 56 microcrystalline $Nd(OH)_3$(s) solubilities from Neck et al. (2009). The distributions of these difference values are illustrated in Figures 7-1 and 7-2.

The difference values in Figure 7-1 fall into two groups that can be separated by the median value of 0.516. Many of the lowest difference values (Figure 7-2) were calculated using 11 solubility values from Runde and Kim (1994) for $Am(OH)_3$(s) and 15 $NaNd(CO_3)_2$•$6H_2O$(cr) solubility values from Rao et al. (1999). Runde and Kim (1994) used materials that were x-ray amorphous after 4 months of aging, but an NEA-TDB review determined that their measured solubilities were more consistent with the $Am(OH)_3$(cr) solubility (Guillaumont et al. 2003). The NEA-TDB review concluded that the crystallinity of the solid phase used by Runde and Kim (1994) is not definitely known (Guillaumont et al. 2003). The difference values calculated for the Runde and Kim (1994) experimental data are reasonably close to zero, indicating that $Am(OH)_3$(s) solubility data in the DATA0.FM4 database is consistent with the solubility of $Am(OH)_3$(cr). The $NaNd(CO_3)_2$•$6H_2O$(cr) solid in the Rao et al. (1999) investigation is relatively

unlikely to form in the WIPP repository because of the low CO_2 fugacity maintained by the MgO backfill (Section 4.0). The remaining difference values below the median were calculated from some of the $Nd(OH)_3(s)$ solubilities reported by Neck et al. (2009) (Figure 7-2).

The +III actinide solubility difference values greater than the median of 0.516 (Figure 7-2) were all obtained using data from Neck et al. (2009). The $Nd(OH)_3(s)$ used in the Neck et al. (2009) solubility experiments was aged for three months and exhibited the XRD pattern characteristic of $Nd(OH)_3(cr)$. Neck et al. (2009) concluded that their solubility data are representative of a less-crystalline solid $Nd(OH)_3(s)$ consisting of small particles. The combined CRA-2019 DPA +III actinide solubility uncertainty distribution appears to be relatively equally distributed into two groups (Figure 7-1): lower difference values consisting of data from Runde and Kim (1994) and Rao et al. (1999), and the lower-range Neck et al. (2009) solubility data that appear reasonably representative of $Am(OH)_3(cr)$ solubility, and higher difference values from Neck et al. (2009) that are more representative of less-crystalline, fine-grained $Am(OH)_3(s)$.

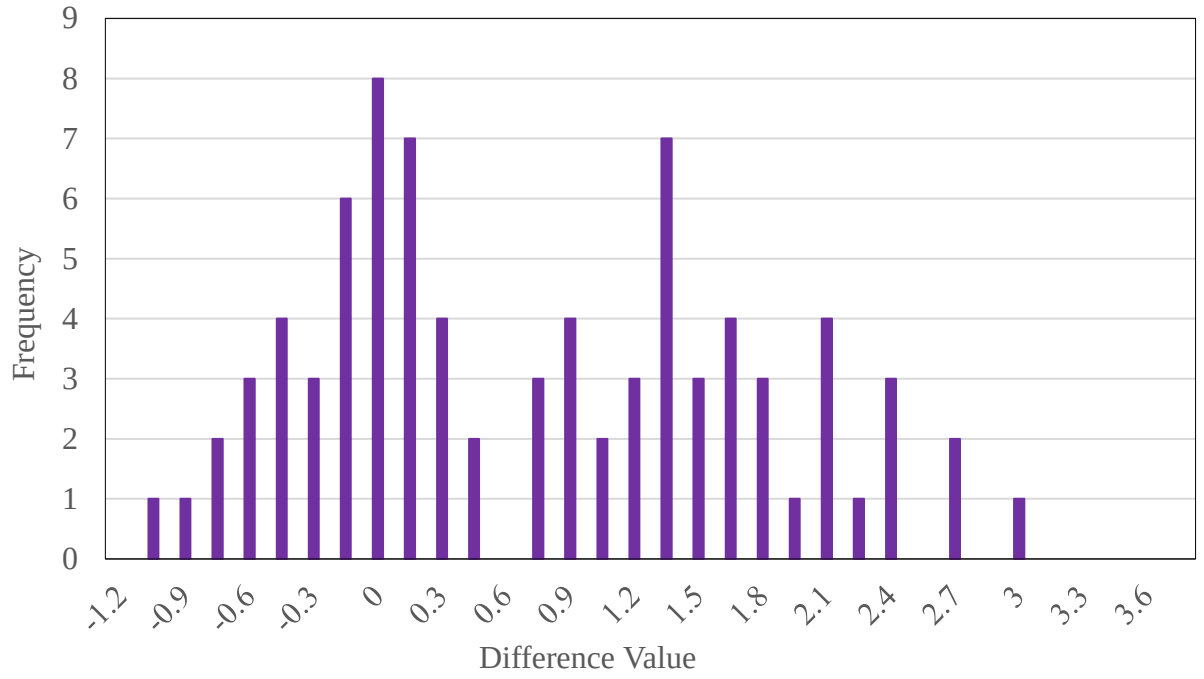

Figure 7-1. CRA-2019 DPA +III Actinide Solubility Difference Values (Domski 2019d)

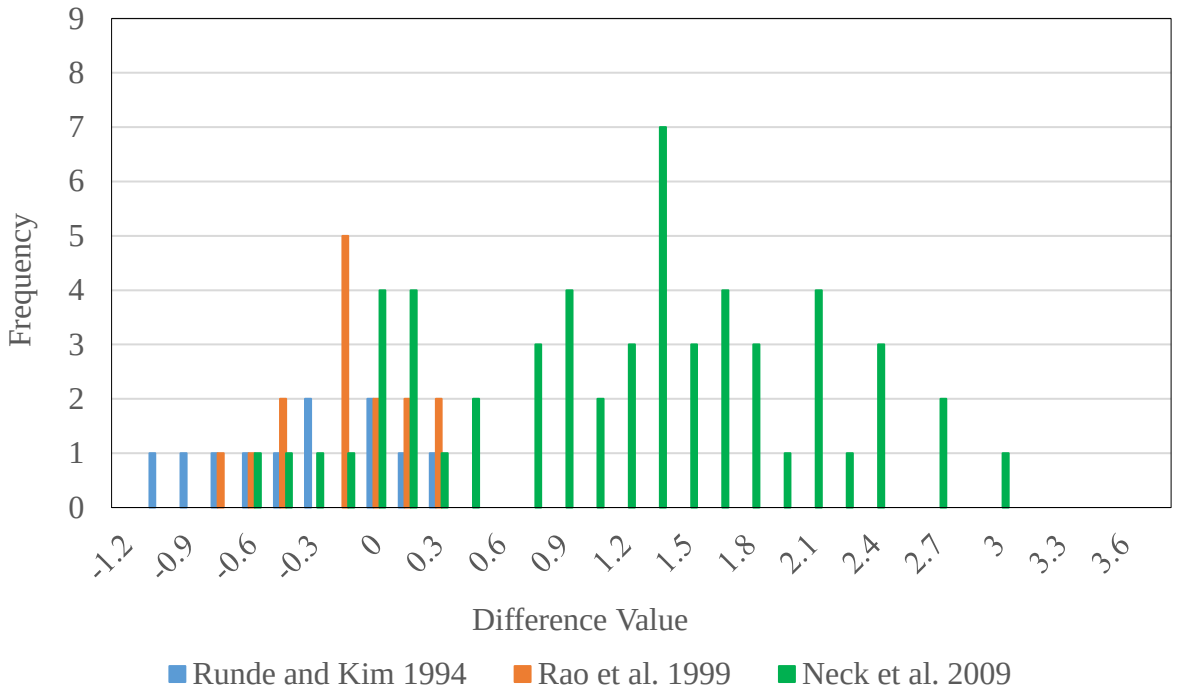

Figure 7-2. CRA-2019 DPA +III Actinide Solubility Difference Values from Runde and Kim (1994), Rao et al. (1999), and Neck et al. (2009)

The degree of crystallinity of the $Am(OH)_3(s)$ phase that will control aqueous Am(III) solubility in the long-term WIPP repository brines is uncertain. Solids in contact with aqueous solutions usually exhibit increased crystallinity and grain size over time, resulting in decreased solubility. However, self-radiolysis of $Am(OH)_3(s)$, particularly from ^{241}Am early in the repository regulatory period, could decrease the crystallinity of the solid and increase its solubility (Guillaumont et al. 2003). Because the crystallinity of $Am(OH)_3(s)$ in the long-term WIPP repository is uncertain, the +III actinide solubility uncertainty distribution should incorporate the effects related to varying degrees of crystallinity on +III actinide solubilities. The CRA-2019 DPA +III actinide solubility uncertainty distribution appears relatively evenly distributed between results consistent with crystalline Am(III) solids and microcrystalline to amorphous solids. This uncertainty distribution therefore seems to adequately represent the range of $Am(OH)_3(s)$ solubilities that may occur in the WIPP repository because of the uncertainty associated with the $Am(OH)_3(s)$ crystallinity and solubility over the 10,000-year regulatory period.

The experimental data selected for the CRA-2019 DPA uncertainty evaluation had a publication cutoff date of October 31, 2011. EPA (Peake 2020a, Comment CC1-GEOCHEM-1) requested that DOE identify any additional +III and +IV experimental solubility data appropriate for inclusion in the uncertainty distributions using a Criterion G1 cutoff date of December 2018 along with the other criteria EPA (2017d) established for selection of experimental solubility data (Section 7.2.6). EPA also requested that DOE calculate the difference values for the additional data that met the criteria and modified cutoff date and provide an assessment of the effects of the revised actinide solubility uncertainty distributions on PA results. DOE (Sosson

2020a) stated that the data used to develop the +III and +IV actinide solubility uncertainty distributions for the CRA-2019 DPA remained unchanged from the CRA14_SEN4 PA because DOE had interpreted the outcome of the September 2018 technical exchange to mean that EPA had specified this approach, except for excluding the experimental results from Khalili et al. (1994). DOE later agreed to provide the requested evaluation that would include more recent +III and +IV actinide solubility data (Santillan 2020).

Knerr (2021f) provided the results of a literature search for Th(IV), Am(III), Cm(III), and Nd(III) solubility data published through December 2020 that were not included in the CRA-2019 DPA uncertainty distribution. Seven Th(IV) publications were identified for more in-depth consideration, but none of these Th(IV) studies met all of the selection criteria.

Three $Nd(OH)_3(s)$ solubility studies published before the CRA-2019 were identified that warranted more detailed evaluation: Herm et al. (2015), Hinz et al. (2015), and Xiong et al. (2017). Herm et al. (2015) investigated the effects of nitrate on $Nd(OH)_3(s)$ solubility in concentrated NaCl, $MgCl_2$, and $CaCl_2$ solutions. Because DATA0.FM4 does not include Am(III)-nitrate aqueous species, Knerr (2021f) excluded data from nitrate-containing experiments from the evaluation. The Herm et al. (2015) data also included results obtained in NaCl, $MgCl_2$, and $CaCl_2$ solutions without nitrate. The results obtained in the $CaCl_2$ solutions did not meet the selection criteria, so Knerr (2021f) excluded the $CaCl_2$ data from the evaluation. Some of the NaCl and $MgCl_2$ data were obtained from experiments that met the selection criteria and Knerr (2021f) included these data in the evaluation. Knerr (2021f) calculated difference values for four 5.61 m NaCl samples, three 1.04 m $MgCl_2$ samples, and three 2.80 m $MgCl_2$ samples (Figure 7-3) (10 samples total). The difference values ranged from -0.13 to 3.30, with mean and median values of 1.9.

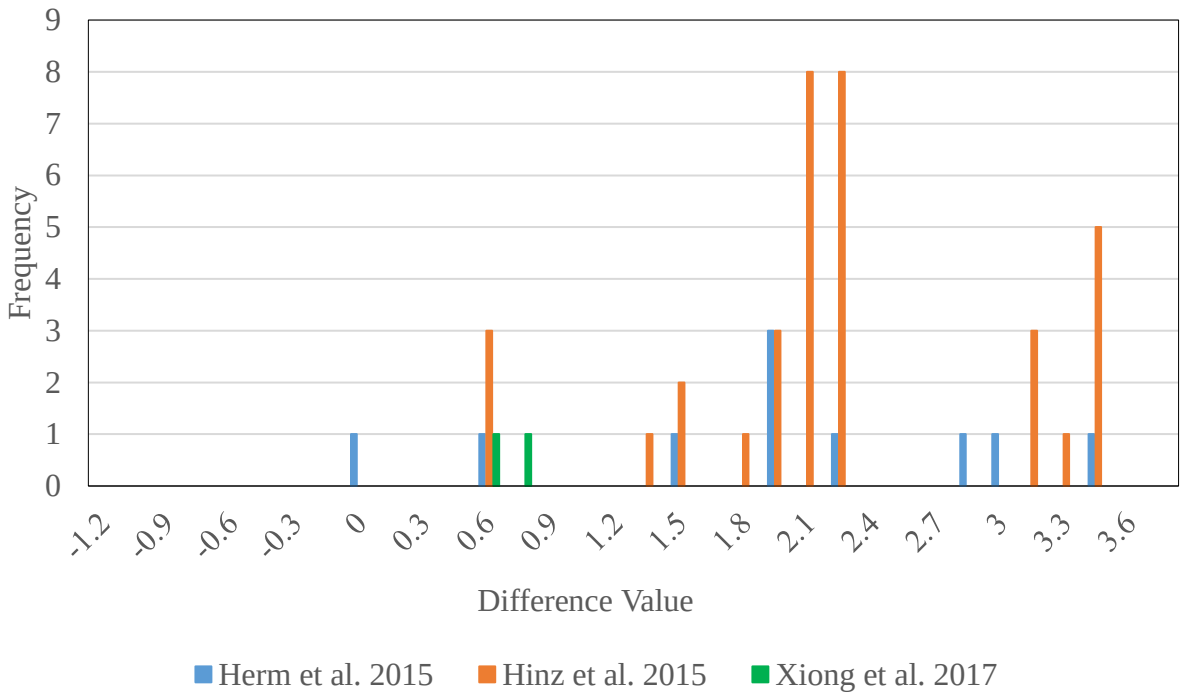

Figure 7-3. +III Actinide Solubility Difference Values for Microcrystalline $Nd(OH)_3(s)$ from Herm et al. (2015), Hinz et al. (2015), and Xiong et al. (2017)

Hinz et al. (2015) performed experiments to evaluate the effects of borate on $Nd(OH)_3(s)$ solubility in dilute and concentrated salt solutions. At borate concentrations of 0.04 M or higher in 5 M NaCl and 1.0 M $MgCl_2$, Hinz et al. (2015) observed formation of a Nd(III)-borate solid. Hinz et al. (2015) did not observe formation of a Nd(III)-borate solid phase in 1.0 M $CaCl_2$ solutions at borate concentrations of 0.004 M or 0.04 M. Knerr (2021f) appropriately selected solubility data obtained with 0.004 M borate concentrations in 5 M NaCl and 1.0 M $MgCl_2$ to maintain consistency with selection criteria G7, because Am-borate solid solubility data are not included in the WIPP thermodynamic database. Knerr (2021f) also included data obtained in 1.0 M $CaCl_2$ with borate concentrations of 0.004 M and 0.04 M. In total, Knerr (2021f) included 35 samples from Hinz et al. (2015). The difference values calculated using the Hinz et al. (2015) data ranged from a minimum of 0.57 to a maximum of 3.44, with mean and median values of 2.19 and 2.10, respectively. Knerr (2021f) included these data on a conditional basis because of the reported amorphous nature of the neodymium solid phase.

Hinz et al. (2015) reported that the solid phase in their experiments was $Nd(OH)_3(am)$. However, XRD peaks were reported for this solid (Figure 3 of Hinz et al. 2015), and Hinz et al. (2015) compared their data to the microcrystalline $Nd(OH)_3(s)$ solubility data of Neck et al. (2009). It is therefore reasonable to believe that the $Nd(OH)_3(s)$ used by Hinz et al. (2015) was similar to the microcrystalline/less crystalline solids used by Neck et al. (2009) and Herm et al. (2015). The difference values calculated using the Hinz et al. (2015) data (Figure 7-3) are consistent with values calculated using other solubility data from microcrystalline material (Figures 7-2 and 7-3), although the Hinz et al. (2015) data are mostly at the higher end of the range observed by Neck et al. (2009), possibly because of the effects of borate on +III actinide solubilities. Consequently, these data could reasonably be included in the uncertainty distribution.

Xiong et al. (2017) measured the solubility of microcrystalline $Nd(OH)_3(s)$ from undersaturation in 4.4 m and 5.0 m NaCl solutions. The experiments were sampled over time periods ranging from 1 day to 1,146 days and exhibited minimal pmH or total Nd(III) concentration changes over time. Knerr (2021f) averaged the data from each of these two experiments because the data represented successive samples from one experiment at each NaCl concentration. The difference values calculated using the Xiong et al. (2017) results were 0.73 and 0.53, indicating the measured solubilities slightly exceeded the concentrations predicted using the WIPP thermodynamic model.

Knerr (2021f) compared the CRA-2019 DPA +III actinide solubility uncertainty distribution statistics to the statistics calculated if the CRA-2019 DPA distribution is combined with the difference values from each of the three additional studies (Herm et al. 2015, Hinz et al. 2015, and Xiong et al. 2017), and if the CRA-2019 DPA distribution is combined with the difference values from all three studies. The combined distribution for all data (Table 7-5) has higher mean, median, and maximum values. Figure 7-4 illustrates the range and distribution of the combined difference values calculated for the +III actinide solubility uncertainties.

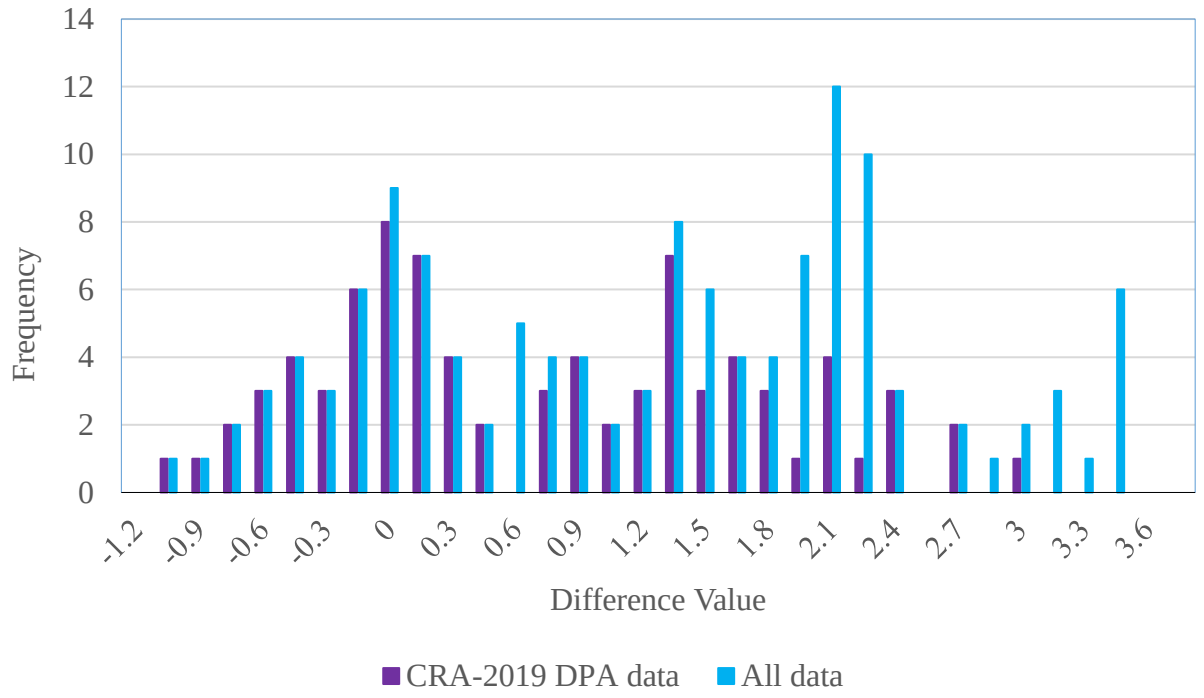

Figure 7-4. CRA-2019 DPA Difference Values Compared to All +III Actinide Solubility Difference Values (Knerr 2021f)

Combining the difference values from the additional investigations (Herm et al. 2015, Hinz et al. 2015, and Xiong et al. 2017) with the difference values used in the CRA-2019 DPA +III actinide solubility uncertainty distribution increases the representation of microcrystalline solubility data (Figure 7-4). The majority of the added difference values are strongly positive and appear to represent highly soluble microcrystalline material. Consequently, addition of these difference values to the +III actinide solubility distribution may overestimate the persistence of less-crystalline, more-soluble $Am(OH)_3(s)$ in the long-term WIPP repository. In contrast, the CRA-2019 DPA +III actinide solubility uncertainty appears to be more consistent with an equal likelihood of crystalline or microcrystalline $Am(OH)_3(s)$ formation.

DOE's approach for developing the uncertainty distributions for the +III and +IV actinide solubility uncertainty distributions includes the calculation of a difference value for each solubility experiment reported in the literature. The resulting uncertainty distribution consequently contains more values from publications with numerous solubility experiments than from publications that reported results from relatively few experiments. For example, there are 56 difference values calculated from the solubilities measured by Neck et al. (2009) using microcrystalline $Nd(OH)_3(s)$, compared to 11 difference values calculated from the solubilities from Runde and Kim (1994) that appear consistent with $Am(OH)_3(cr)$ solubility. Because the difference values for the CRA-2019 DPA and the updated distribution provided by Knerr (2021f) are calculated mostly from solubility data obtained with microcrystalline solids, the revised +III actinide solubility uncertainty distribution may provide an overly conservative estimate of the uncertainty associated with the baseline +III actinide solubilities. The effects of the revised +III

actinide solubility uncertainty distribution on predicted repository releases are addressed in Section 13.4.2.

The published solubility data used to develop the +III actinide solubility uncertainty distribution for the CRA-2019 DPA did not include organic ligands (Domski, 2019d, Knerr 2021f). Only Am(III)-organic ligands data were modified to produce EPA's revised database (DATA0FM_EPA.dat, Section 7.4.5), so these revisions would not affect the solubilities calculated for the +III actinide solubility uncertainty distributions. Consequently, the CRA-2019 DPA +III actinide solubility uncertainty distribution and the revised distribution from Knerr (2021f) can be used with baseline actinide solubilities recalculated with EPA's PHREEQC database when assessing the sensitivity of total mobilized +III actinides in WIPP brines to WIPP parameter changes (Section 12.3) and for sensitivity calculations of repository releases (Section 13.2.2).

Calculations of the solubility uncertainty distributions for the +III and +IV actinides for WIPP PA have evolved since the CCA PAVT, including the development of separate distributions for the +III and +IV oxidation states instead of a single distribution for all actinides, the development of clearly stated selection criteria for including data in the calculations, and the availability of additional published solubility data. The availability of more +III actinide solubility data for microcrystalline solids than for crystalline solids may overemphasize higher solubilities associated with the persistence of less-crystalline +III actinide solids in the long-term WIPP repository. EPA expects DOE to consider whether the availability of more actinide solubility data for some conditions may bias the resulting actinide uncertainty distributions, and whether a defensible approach is available to address this potential effect. DOE may also consider conducting solubility experiments with crystalline +III actinide solids or their analogues to increase the balance between available crystalline and microcrystalline to amorphous solid solubility data. Although the current approach used for WIPP PA appears to provide uncertainty distributions that adequately represent the potential ranges of dissolved actinide solubilities, EPA suggests that a review of other possible approaches and the relative advantages and disadvantages of these alternatives would provide additional support for the current approach for addressing +III and +IV actinide solubility uncertainties.

7.5 DISSOLVED ACTINIDE SOURCE TERM SUMMARY AND CONCLUSIONS

Calculations of the baseline dissolved actinide concentrations are based on the Dissolved Actinide Source Term and Chemical Conditions conceptual models. The baseline dissolved actinide concentrations and associated uncertainties determine the dissolved actinide concentrations and the concentrations of actinide humic and microbial colloids in WIPP repository brines (Section 8.0). Actinide concentrations mobilized in WIPP brines affect releases from the repository through DBRs and by transport through the Culebra.

EPA has reviewed the CRA-2019 DPA EQ3/6 database and calculations of the dissolved actinide source term and concludes:

- DOE calculated the revised hydromagnesite solubility in DATA0.FM4 from the free energy of formation data reported by Robie and Hemingway (1973) and the standard chemical potential data of Harvie et al. (1984). The revised hydromagnesite solubility in

DATA0.FM4 is more defensible than the DATA0.FM1 value because it is internally consistent with other thermodynamic data in the DATA0.FM4 database.

- Issues in the revised EQ3/6 database (DATA0.FM4) related to the aqueous stability constants for $CaEDTA^{2-}$, $MgEDTA^{2-}$, and $AmEDTA^{-}$, and to the derivation and testing of some of the $EDTA^{4-}$ Pitzer parameters caused significant underpredictions of the CRA-2019 DPA baseline dissolved Am(III) concentrations. EPA expects DOE to correct these data for future WIPP PAs.
- During the CRA-2009 and CRA-2014 reviews, EPA (2010b, 2017d) stated that DOE should update the Th(IV)-carbonate speciation in the database to account for data from Altmaier et al. (2005, 2006). DOE did not update the EQ3/6 thermodynamic database to account for these data. As discussed in Attachment B, EPA expects DOE to address this issue for future WIPP PAs.
- Potential internal inconsistencies were identified in the WIPP Am(III) model that was derived from Könnecke et al. (1997), which could affect the log β^0 values for $AmCl^{2+}$ and $AmCl_2^{+}$ and some of the Pitzer parameters (Oakes et al. 2021). EPA expects DOE to evaluate these possible inconsistencies for future WIPP PAs.
- Issues were identified with some of the revised citrate, oxalate, and acetate data, but these issues are not expected to have significant effects on the baseline solubilities calculated for Am(III) and Th(IV).
- The iron data added to DATA0.FM4 are adequately documented and acceptable, except for the omission of the Fe^{2+}-sulfate Pitzer parameters and solids solubilities, which should be added to the database.
- The lead data do not include Pitzer parameters, so EPA expects DOE to omit lead from WIPP actinide solubility calculations until a Pitzer model is developed and the model is adequately tested against available high ionic strength experimental data.
- Dissolved iron and lead concentrations in WIPP brines could be significantly affected by precipitation of sulfide and phosphate solids; if DOE adds iron and lead interactions with organic ligands to the database, the effects of sulfide and phosphate should also be considered.
- DOE calculated organic ligand concentrations as a function of the brine volume and used these concentrations to calculate baseline actinide solubilities. This approach was first used for the CRA-2014 PA, accounts for possible dilution of the organic ligands in larger brine volumes, and is adequately justified. This approach for calculating the organic ligand concentrations mainly affects calculations of dissolved concentrations of +III actinides.
- The assumption that calcite precipitated to saturation in the CRA-2019 DPA baseline actinide solubility calculations resulted in large amounts of Phase 5 precipitation and water consumption, but actinide solubilities were not greatly affected by these processes. EPA expects DOE to assume in future WIPP PA calculations that calcite remains slightly oversaturated because of the presence of known calcite precipitation inhibitors in WIPP repository brines.
- EPA recommends that DOE evaluate the Phase 5 solubility constant for future WIPP PAs to determine if an excessively low solubility contributed to the precipitation of large amounts of Phase 5 and water consumption in the CRA-2019 DPA actinide solubility calculations.

- Polyhalite dissolution could increase Phase 5 precipitation and water consumption in WIPP actinide solubility calculations. EPA has identified information that shows the percentage of polyhalite in the Salado Formation at the repository horizon is likely overestimated and should be reevaluated.
- The cement inventory will not significantly affect brine pH based on the results of EQ3/6 modeling calculations performed by DOE.
- Borate in WIPP brines is unlikely to significantly increase Am(III) concentrations under WIPP repository conditions (Hinz et al. 2015), but borate may have small effects on Am(III) aqueous speciation and solubility.
- EPA expects that for all future WIPP PAs, the cutoff date for publications used to develop the +III and +IV actinide solubility uncertainty distributions will be the latest date that can be implemented.
- EPA expects DOE to consider whether the availability of more actinide solubility data for some conditions (e.g., less-crystalline solid phases) could bias the resulting actinide solubility uncertainty distributions, and whether a defensible approach is available to counter this potential effect.
- An evaluation of the relative advantages and disadvantages of other approaches for addressing +III and +IV actinide solubility uncertainties may improve confidence in the current approach.

.

8.0 COLLOIDAL ACTINIDE SOURCE TERM

The Colloidal Actinide Source Term conceptual model was peer reviewed prior to the CCA PA and PAVT and found to be adequate, if somewhat conservative (Wilson et al. 1996a). This conceptual model and its implementation have remained unchanged since the CCA PAVT. The colloidal actinide source term parameters remained constant from the CCA PAVT through the PABC09, but some parameters were revised for the CRA-2014 PA and CRA-2019 DPA.

It is assumed that four types of colloids can form in the WIPP repository and influence the actinide concentrations mobilized in WIPP repository brines:

- Mineral fragment colloids,
- Intrinsic colloids,
- Humic colloids, and
- Microbial colloids.

DOE described these four types of colloids in the CCA (DOE 1996, Appendix SOTERM). Intrinsic colloids are hydrophilic actinide macromolecules that may in some cases mature into larger hydrophobic mineral fragment colloids. Mineral fragment colloids are hydrophobic, hard-sphere amorphous or crystalline solids. Mineral fragment colloids may act as substrates for actinide sorption or may consist of precipitated or coprecipitated actinide solids. Humic colloids are formed by complexation of actinides with humic substances, which are relatively small organic compounds (less than 100,000 atomic mass units) that are often powerful substrates for uptake of metal cations. Microbial colloids may act as substrates for actinide sorption, or they may intracellularly bioaccumulate actinides.

The concentrations of mineral fragment colloids and intrinsic actinide colloids used in WIPP PA are constant values and are represented by the parameters CONCMIN and CONCINT, respectively. The CONCMIN and CONCINT parameters are defined on an elemental basis rather than on the basis of the actinide oxidation state. For example, DOE uses the same PU:CONCINT value for both Pu(III) and Pu(IV) oxidation states in WIPP PA.

Actinide concentrations associated with humic substances are calculated by multiplying the total dissolved actinide concentration by a proportionality constant (parameters PHUMSIM for Salado brine and PHUMCIM for Castile brine), with the total humic colloid actinide concentration limited by a maximum value (parameter CAPHUM). Actinide concentrations associated with microbial colloids are also based on proportionality constants (parameter PROPMIC), with assigned upper limits on the actinide concentrations associated with microbial colloids (parameter CAPMIC). The humic colloid and microbial colloid parameters are defined for each actinide on an elemental basis rather than on the basis of the actinide oxidation state.

8.1 MINERAL FRAGMENT AND INTRINSIC COLLOIDS

DOE (1996) did not explicitly state a size range for mineral fragment colloids, but did assume a diameter range of 1 nm to 1 μm during particle surface area calculations used to derive the mineral fragment colloid concentrations used in PA (DOE 1996, Appendix SOTERM). Reed et al. (2013, 2019) performed experiments to update mineral fragment and intrinsic colloid

parameter values. In these experiments, Reed et al. (2013, 2019) defined each type of colloid based on the filtrate from sequential filtration experiments using the following size ranges:

- Mineral fragment colloids are 10 nm to 0.45 μm,
- Intrinsic colloids are approximately 2.5 nm to 10 nm, and
- Solution concentrations after filtration through approximately 2.5 nm filters represent dissolved material

These defined size ranges are reasonable operational assumptions for determining colloidal and dissolved concentrations from experimental data based on available filter sizes. These ranges fill in the gaps from the original CCA definition and are necessary to update colloid concentrations using experimental data.

During review of the CRA-2019 DPA, EPA requested additional information regarding sequential filtration data from Pu(III) - iron experiments (Peake 2020d, Comment CC4-SOTERM-8) and Th(IV) sequential filtration data used by Reed et al. (2019) to assess mineral fragment and intrinsic colloid concentration parameters (Peake 2020d, Comment CC4-SOTERM-11). Mineral fragment and intrinsic colloids were also discussed in an EPA-DOE technical exchange meeting (DOE 2020a), and EPA requested additional information from DOE regarding Nd(III) filtration data (Rosencrantz 2021, FC1-CCR-SOTERM-8, -9, -10).

8.1.1 CCA Mineral Fragment Colloid Concentrations Used in WIPP PA

Mineral fragment colloid parameters (CONCMIN) have not changed from the original CCA PAVT values of 2.6×10^{-8} M for all actinides. The concentrations of actinides associated with mineral fragment colloids, also called pseudocolloids, were determined for the CCA PAVT from experiments that measured their kinetic stability in WIPP-relevant brines combined with estimates of adsorption site densities. These experiments examined colloid formation using actinides sorbed onto a variety of minerals or materials such as clays and iron oxides (Papenguth 1996a). MgO backfill was not included in the initial repository design, so formation of mineral fragment colloids from MgO and its reaction products was not investigated. Papenguth (1996a) developed a distribution for mineral fragment colloid concentrations, and DOE used the maximum value of 2.6×10^{-8} M from this distribution for all actinides (DOE 1996, Appendix SOTERM).

8.1.2 Mineral Fragment Colloid Formation by MgO Hydration and Carbonation Products

Altmaier et al. (2004) observed formation of Th(IV) pseudocolloids in concentrated $MgCl_2$ solutions saturated with respect to $Mg_2Cl(OH)_3 \cdot 4H_2O$(cr). EPA (2010b) found during review of the CRA-2009 that DOE had not adequately evaluated the potential formation of mineral fragment colloids by MgO and its hydration and carbonation products under WIPP-relevant conditions.

DOE investigated the potential formation of magnesium-hydroxychloride colloids in WIPP brines using samples from long-term Martin Marietta MgO hydration and carbonation experiments performed with WIPP brines (Xiong 2017). These experiments did not contain

actinides or actinide analogues. In the first approach used in the investigation, brine samples from the experiments were sequentially filtered at pore sizes ranging from 2 to 200 nm, with the filtrates analyzed for magnesium to determine if significant magnesium-bearing colloids could be detected. Magnesium colloids were not identified using this method, although its sensitivity for detecting relatively small concentrations of magnesium hydroxychloride colloids is unclear.

The second approach involved adding a CsCl tracer to aliquots of brine from the long-term MgO hydration and carbonation experiments and subjecting these solutions to sequential filtration. A decrease in the cesium concentration with decreasing pore size would indicate the presence of cesium-adsorbing colloids (Xiong 2017). This approach depends on the assumption that cesium is strongly adsorbed by MgO colloids, although the investigations cited in support of this assumption used silica gel (Bascetin et al. 2003) and colloidal material derived from Hanford sediments, which likely contained clays and other silicates (Chen et al. 2005). It is uncertain whether adsorption of actinides on magnesium hydroxychloride colloids is equivalent to adsorption of cesium on silica-bearing colloids.

Formation of magnesium hydroxychloride colloids with the composition $Mg_2Cl(OH)_3 \cdot 4H_2O$ observed by Altmaier et al. (2004) is unlikely under WIPP repository conditions because a different magnesium-hydroxychloride solid [$Mg_3Cl(OH)_5 \cdot 4H_2O$(cr), Phase 5] has been observed in experiments with WIPP brines (Section 4.1), and because of differences in the brines used in the Altmaier et al. (2004) experiments and WIPP brines. To address uncertainty of pseudocolloid formation from MgO hydration and carbonation products under WIPP repository conditions, EPA recommends that DOE perform sequential filtration experiments with brine samples from the MgO hydration and carbonation experiments after spiking the solution aliquots with Th(IV) and a +III actinide or analogue such as Nd(III).

8.1.3 Plutonium Mineral Fragment and Intrinsic Colloids

The concentrations of intrinsic Pu(IV) colloids were determined for the CCA PAVT based on the results of experimental investigations carried out with Pu(IV) (DOE 1996, Appendix SOTERM; Papenguth and Behl 1996). Intrinsic Pu(IV) colloids were detected in NaCl brines at pcH values of approximately 4 and 7, but at pcH values of approximately 8 and higher, intrinsic Pu(IV) colloid concentrations in the experiments were below the analytical detection limit of 10^{-9} M (DOE 1996, Appendix SOTERM). Because the expected pcH of the repository was approximately 9.3, Papenguth and Behl (1996) used the analytical detection limit for the CCA PAVT plutonium intrinsic colloid concentration (Table 8-1). A literature review did not provide evidence of the formation of other actinide intrinsic colloids, so DOE assumed concentrations of thorium, uranium, neptunium, and americium intrinsic colloids equal to zero (DOE 1996, Appendix SOTERM).

Table 8-1. Actinide Concentrations Associated with Intrinsic Colloids (Parameter CONCINT)

Actinide	CCA PAVT, PABC04 and PABC09	CRA-2014 PA	CRA-2019 DPA	CRA-2019 Sensitivity Calculations
Th(IV) (M)	0.0	2×10^{-8}	4.3×10^{-8}	4.8×10^{-7}

U(IV) (M)	0.0	3×10^{-8}	1.4×10^{-6}	1.4×10^{-6}
U(VI) (M)	0.0	3×10^{-8}	1.4×10^{-6}	1.4×10^{-6}
Np(IV) (M)	0.0	2×10^{-8}	4.3×10^{-8}	4.3×10^{-8}
Np(V) (M)	0.0	2×10^{-8}	4.3×10^{-8}	4.3×10^{-8}
Pu(III) (M)	0.0	2×10^{-8}	4.3×10^{-8}	4.3×10^{-8}
Pu(IV) (M)	1.0×10^{-9}	2×10^{-8}	4.3×10^{-8}	4.3×10^{-8}
Am(III) (M)	0.0	4×10^{-9}	9.5×10^{-9}	6.7×10^{-7}

Abdel-Fattah et al. (2013) experimentally investigated the dispersion stability, electrokinetic properties, and transport of Pu(IV) colloids. This investigation showed that the energy barrier to Pu(IV) colloid aggregation decreases to zero at ionic strengths on the order of 0.1 M. These results indicate that mineral fragment colloids composed of Pu(IV) macromolecules might be unstable in high ionic strength WIPP brines. Abdel-Fattah et al. (2013) also carried out column transport experiments with native groundwater colloids composed primarily of smectite clay with added Pu(IV) colloids. These experiments showed that Pu(IV) colloids strongly associated with the groundwater colloids and were transported through packed columns as relatively stable pseudocolloids.

DOE (Reed et al. 2013) reported the results of long-term experiments that investigated Pu(VI) reduction to Pu(III) in WIPP brine by iron coupons or magnetite. After approximately six years of reaction, filtration of the brines showed that in pcH 9.1 to 9.5 ERDA-6 brine, the mineral-fragment colloid Pu(III) concentration ranged from 8.6×10^{-9} M to 2.3×10^{-8} M. Because this concentration range is bounded by the 2.6×10^{-8} M concentration originally established for the CCA PAVT (Table 8-1), the value of CONCMIN remained unchanged for the CRA-2014 PA. Reed et al. (2019) re-evaluated the Pu(III)-iron filtration data for the CRA-2019 DPA and found that the mineral fragment colloid concentrations of 2.6×10^{-8} M used in WIPP PA remained appropriate.

Reed (2020) provided more detailed filtration data from the Pu(III)-iron experiments in response to an EPA request (Peake 2020d, Comment CC4-SOTERM-8). Two Pu(III)-iron solution sequential filtration series were performed for each experiment. In the first series, the sample was sequentially passed through 0.45 μm, 0.22 μm, 10 nm, and 2.5 nm filters, with aliquots removed and analyzed for plutonium after each filtration step. In the second series, another sample was passed through a 10 nm filter and then a 2.5 nm filter with solution analysis carried out after each filtration step. Subtraction of the plutonium concentration in the 10-nm filtrate from the 0.45-μm filtrate plutonium concentration yields the plutonium concentration associated with mineral fragment colloids. The Pu(III) mineral fragment colloid concentrations calculated from the averaged replicate data reported by Reed (2020) are illustrated in Figure 8-1 and compared with the CRA-2019 DPA PU:CONCMIN value. The mineral fragment concentrations at pcH 7.7 slightly exceed the PU:CONCMIN value used in the CRA-2019 DPA, but the pcH is less than the expected pcH range of 8 to 10 in repository brines. One mineral fragment colloid concentration at pcH 8.3 (3.0×10^{-8} M) is slightly higher than the PU:CONCMIN value of 2.6×10^{-8} M, but this small concentration difference will not significantly affect calculated plutonium releases from the repository. EPA believes that the CRA-2019 DPA PU:CONCMIN value is reasonable because it is equal to or greater than more than 96% of the data in the pcH range from

8 to 10. These data indicate that the PU:CONCMIN value of 2.6×10^{-8} M used in the CRA-2019 DPA adequately bounds the Pu(III)-iron mineral fragment colloid data.

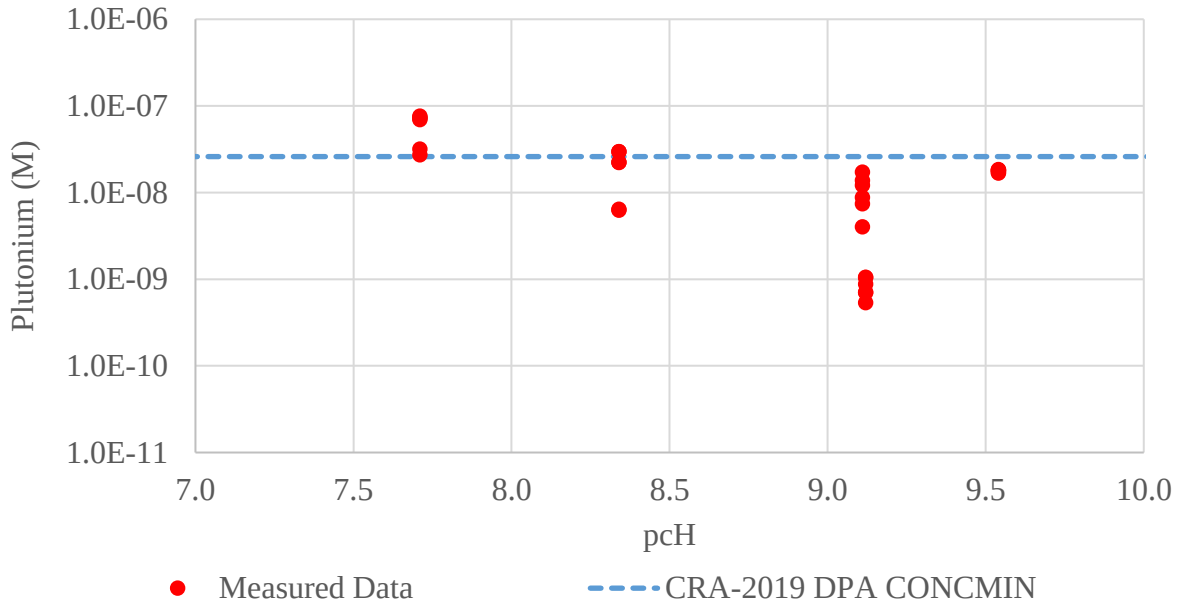

Figure 8-1. Pu(III) Mineral Fragment Colloid Concentrations Calculated from Reed (2020) Data with CRA-2019 DPA Parameter PU:CONCMIN

For the CRA-2014 PA, the PU:CONCINT parameter value used for Pu(III) and Pu(IV) intrinsic colloids was 2×10^{-8} M. This parameter value was increased to 4.3×10^{-8} M for the CRA-2019 DPA (Reed et al. 2019, DOE 2019). The Pu(III) intrinsic colloid concentrations calculated from the averaged replicate 10-nm filtered and 2.5-nm filtered data reported by Reed (2020) are illustrated in Figure 8-2 and compared with the CRA-2019 DPA PU:CONCINT value. The measured Pu(III) intrinsic colloid concentrations are adequately bounded by the PU:CONCINT value within the pcH range of 8 – 10 expected for WIPP repository brines.

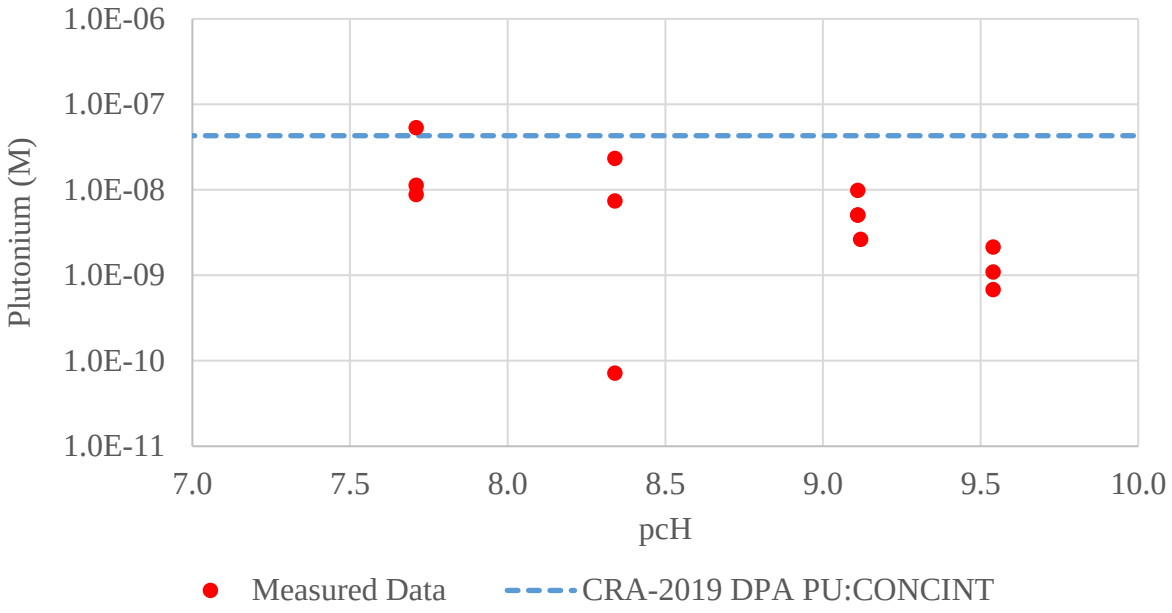

Figure 8-2. Pu(III) Intrinsic Colloid Concentrations Calculated from Reed (2020) Data with CRA-2019 DPA Parameter PU:CONCINT

8.1.4 Neodymium(III) Mineral Fragment and Intrinsic Colloids

Reed et al. (2013, Figure 4-2) presented results of a sequential filtration investigation carried out with samples from long-term Nd(III) solubility experiments. The Nd(III) experiments were performed as analogues for Am(III) and were carried out from oversaturation and undersaturation. The data were attributed to Borkowski et al. (2010), including four solubility experiments in GWB and two solubility experiments in ERDA-6. EPA noted differences in reported data between Figure 4-2 of Reed et al. (2013) and information in Borkowski et al. (2010). After a technical exchange with DOE (DOE 2020a), EPA requested that DOE provide additional information to resolve the apparent inconsistencies (Rosencrantz 2021, FC1-CCR-SOTERM-8, -9, -10).

EPA noted that Borkowski et al. (2010) used filter pore sizes of 5 nm, 30 nm, and 220 nm, which are not the same as the 2 nm and 10 nm filters cited by Reed et al. (2013, 2019). In addition, Borkowski et al. (2010) stated that colloids were not identified in their experiments and a different number of sequential filtration series were provided by Reed et al. (2013, 2019) than were provided by Borkowski et al. (2010).

In response, DOE explained that the filters used by Borkowski et al. (2010) are now understood to represent approximately 10 nm, approximately 20 nm, and approximately 220 nm pore sizes (Knerr 2021d). DOE also clarified that new samples from these experiments were analyzed by sequential filtration for the Reed et al. (2013) report.

Comparison of the 0.45 μm and 10 nm Nd(III) filtration data in Figure 4-2 of Reed et al. (2013) indicates that most experiments showed no effect of filtration between these two pore sizes, a

result that is consistent with the Borkowski et al. (2010) data. Very small differences were observed between the 0.45 µm and 10 nm filtrates in the two ERDA-6 experiments, but the concentrations of mineral fragment colloids calculated from these two experiments are below the 2.6×10^{-8} M concentration currently used for AM:CONCMIN in the CRA-2019 DPA. Consequently, the 2.6×10^{-8} M value for parameter AM:CONCMIN remains appropriate.

Figure 4-2 from Reed et al. (2013) showed that 2.5 nm and 10 nm filtration affected Nd(III) concentrations, indicating the presence of intrinsic colloids. All but one of the measured intrinsic colloid Nd(III) concentrations are higher than the CRA-2019 DPA parameter AM:CONCINT of 9.5×10^{-9} M (Figure 8-3). For the EPA sensitivity calculations (Sections 12.3 and 13.2), the selected AM:CONCINT concentration was set equal to the highest Nd(III) concentration from the dataset (6.7×10^{-7} M). This concentration was selected to provide an upper bound for the Nd(III) experimental data. A more realistic value for AM:CONCINT may be the mean intrinsic colloid concentration from the six samples (1.7×10^{-7} M), which exceeds all but the single highest measured value (Figure 8-3).

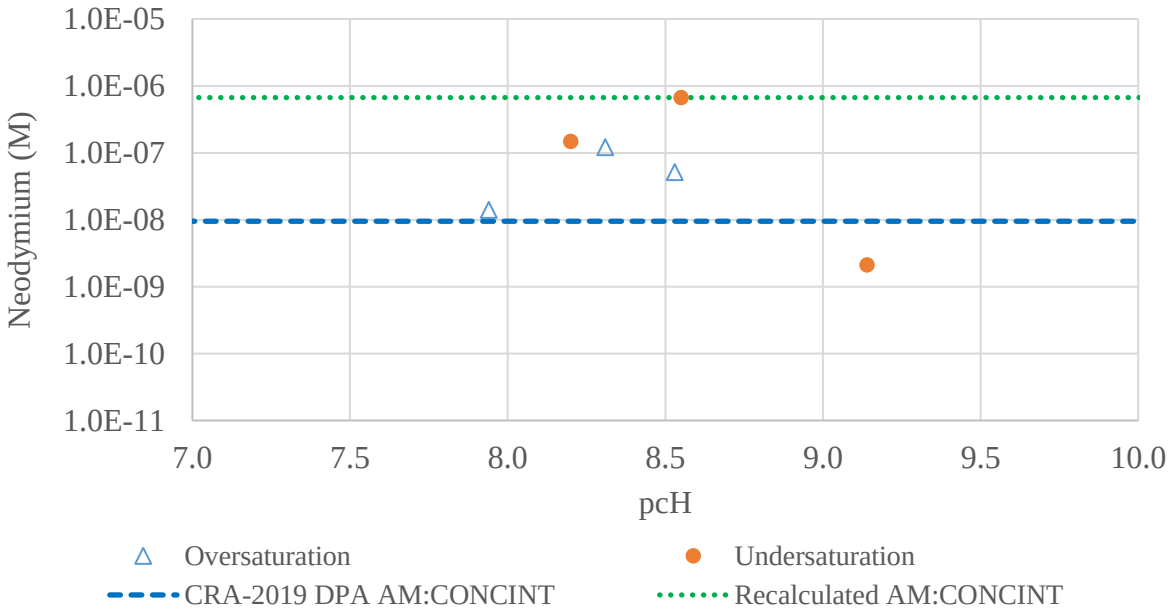

Figure 8-3. Nd(III) Intrinsic Colloid Concentrations Calculated from Reed et al. (2013) Data with CRA-2019 DPA Parameter AM:CONCINT

8.1.5 Thorium(IV) Mineral Fragment and Intrinsic Colloids

Investigations performed since the CCA PAVT have identified the formation of intrinsic Th(IV) colloids in dilute solutions and in brines. Neck et al. (2002) found that intrinsic Th(IV) colloids were present at low ionic strength based on ultracentrifugation of sampled solutions. Bitea et al. (2003) investigated the formation and stability of Th(IV) colloids in 0.5 M NaCl and found that these colloids remained stable over the course of 400 days without exhibiting agglomeration or precipitation. Results reported by Altmaier et al. (2004) indicated that intrinsic Th(IV) colloids can form and remain stable in NaCl solutions with concentrations ranging from 0.5 to 5 M, with

dissolved plus intrinsic colloidal Th(IV) concentrations of approximately 5×10^{-7} M. EPA (2010b) reviewed the literature data, found the evidence of Th(IV) intrinsic colloids to be credible, and recommended that DOE revise future calculations of Th(IV) intrinsic colloid concentrations.

Reed et al. (2013) evaluated sequential filtration data from Th(IV) solubility experiments carried out in WIPP brines from Borkowski et al. (2012) and Borkowski (2012b) from oversaturation and undersaturation experiments. Out of these eight samples, Reed et al. (2013) selected only two samples with pcH 9.1, reasoning that samples at this pcH were likely to be most relevant to WIPP brines. During review of the CRA-2014, EPA (2017d) stated that all Th(IV) sequential filtration data within the wider range of pcH values anticipated in WIPP repository brines should be considered. Reed et al. (2019, Appendix A) evaluated Th(IV) sequential filtration data from the Borkowski et al. (2012) solubility experiments conducted at pcH values from 8.13 to 9.18. However, data presented in Reed et al (2019) Table A-1 for 10 nm filtration were actually 5 nm filtration data (Peake 2020d, Comment CC4-SOTERM-9). The full dataset of mineral and intrinsic colloid concentrations calculated from the Th(IV) sequential filtration data reported by Borkowski (2012b) are illustrated in Figures 8-4 and 8-5.

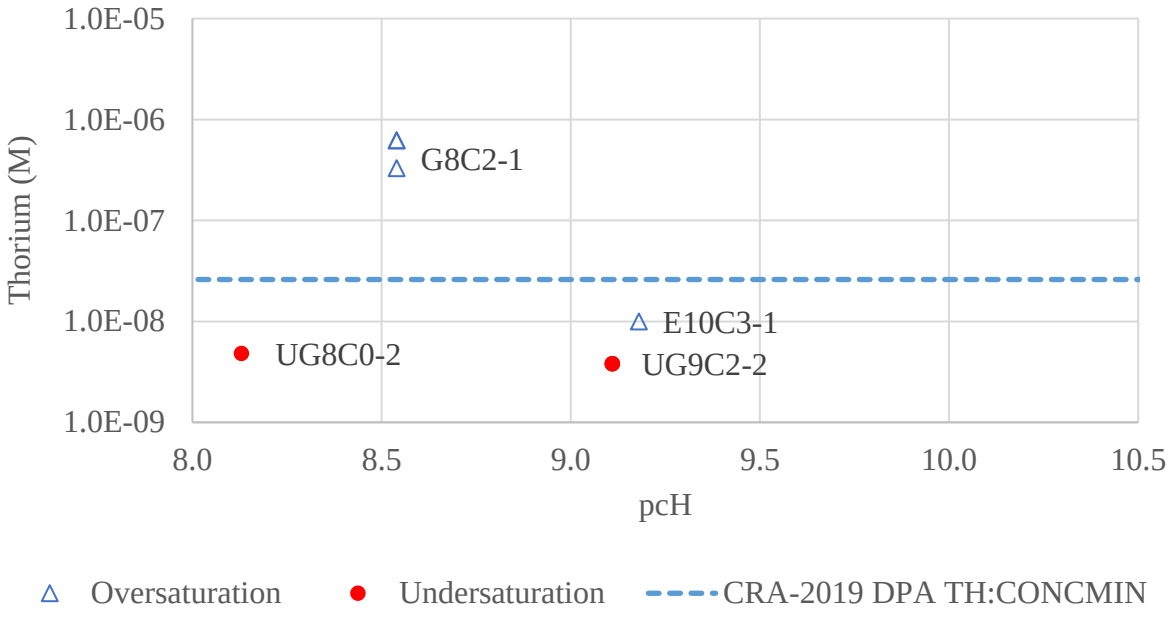

Figure 8-4. Th(IV) Mineral Fragment Colloid Concentrations Calculated from Borkowski (2012b) Data with CRA-2019 DPA Parameter TH:CONCMIN

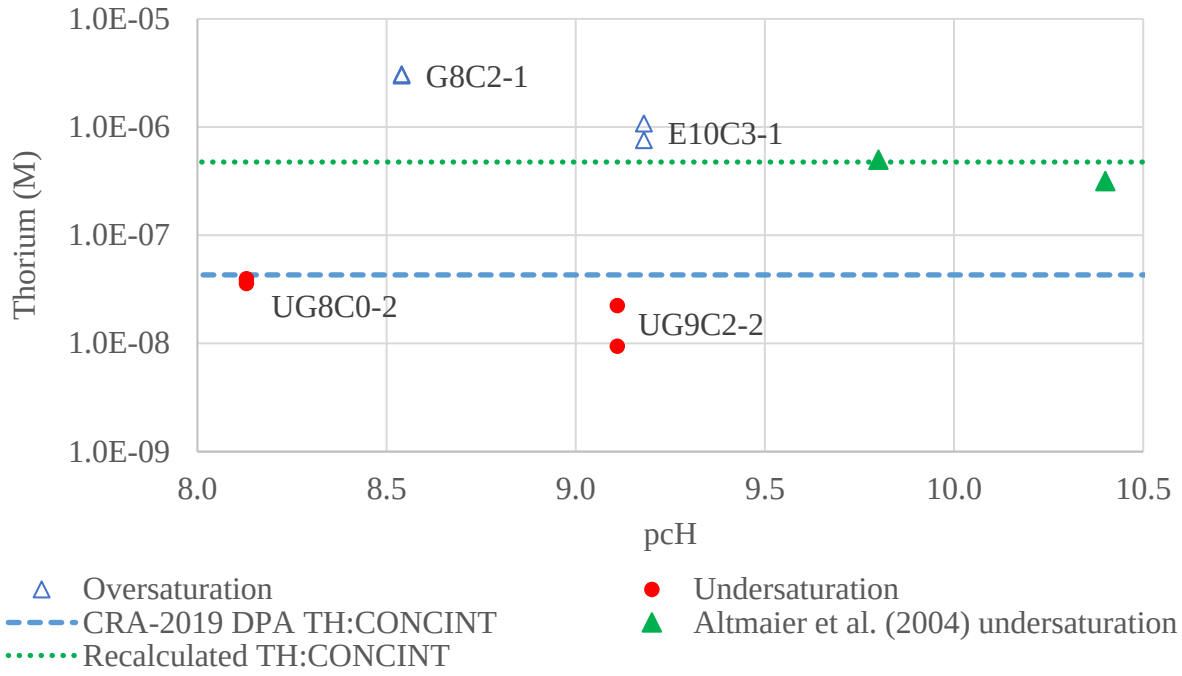

Figure 8-5. Th(IV) Intrinsic Colloid Concentrations Calculated from Borkowski (2012b) Data with CRA-2019 DPA Parameter TH:CONCINT and Data from Altmaier et al. (2004) in 5 M NaCl

Relatively high dissolved Th(IV) concentrations (2.5 nm filtration) in the replicate samples from experiment E10C3-1 (ERDA-6 brine, oversaturation) indicated that this experiment had not reached equilibrium. The remaining three experiments were conducted with GWB brine from undersaturation (UG8C0-2 and UG9C2-2) and oversaturation conditions (G8C2-1). Two sets of sequential filtration data were obtained from each of these experiments. The Th(IV) concentrations in 2.5-nm filtered samples from these experiments are consistent with the expected solubility of ThO_2(am) in WIPP brines.

Relatively low concentrations of mineral fragment colloids were determined by sequential filtration of samples from the undersaturation experiments. However, much higher mineral fragment colloid concentrations were calculated using filtration data from the oversaturated G8C2-1 experiment (Figure 8-4). EPA asked DOE to consider the effects of increasing the Th(IV) mineral fragment colloid concentration to the highest measured intrinsic colloid concentration (6.20×10^{-7} M) (Peake 2020d, Comment CC4-SOTERM-11). In response, DOE stated that there was hysteresis in experiments approached from either undersaturation or oversaturation (Knerr 2020c). EPA agrees that it is more reasonable to establish a mineral fragment colloid concentration parameter that falls between the results from the oversaturation experiment and undersaturation experiments, rather than the highest observed concentration from the oversaturation experiments. Because results from the GWB experiments from oversaturation and undersaturation bracket the CRA-2019 DPA TH:CONCMIN value of 2.6×10^{-8} M (Figure 8-4), the TH:CONCMIN concentration is reasonable.

EPA asked DOE to consider the effects of increasing the Th(IV) intrinsic colloid concentration to the highest measured intrinsic colloid concentration (3.08×10^{-6} M) (Peake 2020d, Comment

CC4-SOTERM-9). In response, DOE stated that there was hysteresis in the Th(IV) experiments approached from either undersaturation or oversaturation (Knerr 2020c). The oversaturated GWB experiment (G8C2-1) contained a significantly higher concentration of intrinsic thorium colloids than the undersaturated GWB experiments (UG8C0-2 and UG9C2-2, Figure 8-5). Intrinsic thorium colloid concentrations in the E10C3-1 experiment were also elevated, but this experiment is disregarded because the dissolved thorium concentration was significantly higher than the equilibrium solubility concentration.

The CRA-2019 DPA TH:CONCINT parameter value falls at the low end of the range bounded by the oversaturation and undersaturation GWB experiments. Altmaier et al. (2004) evaluated total thorium concentration data obtained in 0.5 and 5 M NaCl solutions and 0.25 and 2.5 M $MgCl_2$ at pH greater than 7 and determined that all solutions had total Th(IV) concentrations (colloidal plus dissolved) of approximately 5×10^{-7} M regardless of ionic strength. By subtracting the CRA-2019 DPA TH:CONCMIN concentration of 2.6×10^{-8} M from the Altmaier total thorium concentration, EPA calculated an intrinsic colloid concentration value of 4.8×10^{-7} M (Figure 8-5). This recalculated intrinsic colloid concentration for Th(IV) has the advantage of bisecting the range bracketed by the GWB undersaturation and oversaturation data and, when combined with the CRA-2019 DPA Th(IV) mineral fragment colloid concentration, it is consistent with the total thorium concentration data determined by Altmaier et al. (2004). DOE should use this higher intrinsic colloid concentration for future WIPP PAs to be consistent with the WIPP-specific and Altmaier et al. (2004) data.

8.1.6 Actinide(IV) – Silica Colloids

Prior to the CRA-2014, only a few publications addressed the formation of colloids containing structural U(IV) or Th(IV) and silica (Dreissig et al. 2011, Hennig et al. 2013, Kozai et al. 2013). Since the CRA-2014, additional publications have described formation of colloids that include structural +IV actinides and silica (Husar et al. 2015, Zänker et al. 2016, Neill et al. 2018) or stabilization of U(IV) nanoparticles by silica coatings (Neill et al. 2019). The possible formation of these colloids under WIPP repository conditions was not addressed in the CRA-2019, so EPA requested that DOE evaluate the potential formation of these types of colloids under WIPP repository conditions (Peake 2020d, Comment CC4-SOTERM-12).

Knerr (2020b) responded with a brief review of Zänker et al. (2016), Neill et al. (2018), and Neill et al. 2019). DOE concluded that it is currently impossible to determine the effects of actinide(IV)-silica colloids in WIPP repository brines because the potential effects of factors such as high ionic strength, organic complexation, and silica concentrations have not been established. Knerr (2020b) stated that silica has not been previously considered an important waste characteristic or component because silica is not a component in WIPP brine and the amount of silica that could dissolve in WIPP brine from transuranic waste is likely small. DOE acknowledged that recent data regarding actinide(IV)-silica colloid formation indicated that formation of these colloids under WIPP repository conditions could merit further investigation.

EPA agrees that actinide mobilization by actinide(IV)-silica colloids in the WIPP repository requires additional evaluation. Silica is present in WIPP waste, for example in clays and silica polymorphs such as quartz [SiO_2(s)] in waste soils. Silica has not been included as a constituent in synthetic Salado brine or Castile brines, probably because silica was omitted from the

constituents analyzed during some brine characterization investigations. For example, Stein and Krumhansl (1986) and Krumhansl et al. (1991) did not list silica as an analyte. On the other hand, Abitz et al. (1990) detected silica concentrations up to 11 mg SiO_2/L in Salado brines and Popielak et al. (1983) measured silica concentrations in five ERDA-6 (Castile brine) samples that averaged 45 mg SiO_2/L. Silica concentrations in repository brines might increase under the alkaline conditions induced by the MgO backfill, because of increased silica dissolution from waste soils and other TRU wastes that contain silica, and from silicate minerals present in the Salado Formation. DOE should evaluate the potential formation of actinide(IV)-silica colloids under WIPP repository conditions for future WIPP PAs.

8.1.7 Uranium(VI) Mineral Fragment and Intrinsic Colloids

Reed et al. (2013) reported sequential filtration data from U(VI) solubility experiment solution samples from Lucchini et al. (2013a) and found no evidence of mineral fragment colloids in these solutions. Accordingly, the U:CONCMIN parameter remained unchanged from the CCA PAVT value of 2.6×10^{-8} M. Reed et al. (2019) did not identify additional data related to U(VI) mineral fragment colloids, and the U:CONCMIN parameter remained at its original value for the CRA-2019 DPA.

Reed et al. (2013) calculated the U(VI) intrinsic colloid concentration of 3×10^{-8} M by averaging U(VI) sequential filtration results from experiments carried out in CO_2-free ERDA-6 brines at pcH values of 9.3 and 9.8. Reed et al. (2019) expanded the pcH range to include additional data obtained at pcH values of 8.6 and 8.9, removed one value at pcH 8.9 that appeared to be an outlier, then selected the highest remaining concentration of 1.4×10^{-6} M. Because a lower U(IV) intrinsic colloid concentration was estimated by analogy with Th(IV), Reed et al. (2013) used the U(VI) intrinsic colloid concentration for U:CONCINT. This value of U:CONCINT is not expected to significantly affect PA results, because actinide releases are relatively insensitive to uranium, and the 1×10^{-3} M U(VI) aqueous solubility assumed for PA is significantly greater than the intrinsic colloid concentration.

8.1.8 Neptunium(V) Mineral Fragment and Intrinsic Colloids

For the CCA PAVT, DOE (1996) set the mineral fragment colloid concentration for Np(IV) and Np(V) equal to 2.6×10^{-8} M. Additional data regarding neptunium mineral fragment colloids have not been identified since the CCA PAVT, so this value of NP:CONCMIN has remained constant for all WIPP PAs.

DOE (1996) assumed a neptunium intrinsic colloid concentration of zero for the CCA PAVT, because data that demonstrated formation of significant amounts of neptunium intrinsic colloids were not identified. DOE used a value of 2×10^{-8} M for NP:CONCINT for the CRA-2014 PA, by analogy with Th(IV). DOE increased this concentration to 4.3×10^{-8} M for the CRA-2019 DPA because of the increased TH:CONCINT value. There is little evidence that neptunium will form intrinsic colloids to the extent observed for thorium, and dissolved or colloidal neptunium concentrations have insignificant effects on PA because of the relatively low WIPP inventory of neptunium. Consequently, the NP:CONCINT value of 4.8×10^{-8} M is adequate for WIPP PA.

8.1.9 EPA Evaluation of Mineral Fragment and Intrinsic Colloid Parameters

The mineral fragment colloid parameters have remained constant at 2.6×10^{-8} M for all WIPP PAs. Evaluation of new sequential filtration data indicates that this concentration is adequate for the parameters AM:CONCMIN, NP:CONCMIN, PU:CONCMIN, TH:CONCMIN, and U:CONCMIN.

For intrinsic colloids, evaluation of the sequential filtration data for Pu(III)-iron experiments indicates that the PU:CONCINT concentration used in the CRA-2019 DPA is consistent with the high end of the measured Pu(III) intrinsic colloid concentrations. Examination of the Nd(III) sequential filtration data from Borkowski (2012a), however, indicates that the AM:CONCINT concentration used in PA should be increased from 9.5×10^{-9} M to 6.7×10^{-7} M to provide an upper bound for the data. The Th:CONCINT value should be increased from 4.3×10^{-8} M to 4.7×10^{-7} M to be consistent with the available sequential filtration data obtained in WIPP experiments and with the intrinsic colloid concentrations observed by Altmaier et al. (2004) in NaCl solutions. The NP:CONCINT and U:CONCINT parameter values used for the CRA-2019 DPA are not expected to have significant effects on total actinide releases from the repository and are acceptable for use in PA.

The TH:CONCINT and U:CONCINT intrinsic colloid parameters selected for the sensitivity calculations exceed the PU:CONCINT intrinsic colloid parameter (Table 8-1). The U:CONCINT intrinsic colloid concentration is derived from U(VI) solubility experiments, so it is unrealistic to assume this concentration for Pu(IV) intrinsic colloids based on an oxidation-state analogy between Pu(IV) and U(IV). The TH:CONCINT intrinsic colloid parameter should not be applied to Pu(IV) because CCA experiments indicated much lower Pu(IV) intrinsic colloid concentrations (DOE 1996 Appendix SOTERM Section 6.3.2.3, Papenguth and Behl 1996) and Abdel-Fattah et al. (2013) has shown that Pu(IV) will be transported by association with mineral fragment colloids rather than as intrinsic colloids. Because EPA believes Pu(III) will be the predominant plutonium oxidation state in WIPP repository brines (Section 6.3.2), it is appropriate to use the intrinsic colloid concentration in Table 8-1 that was obtained with Pu(III) for the PU:CONCINT parameter for the sensitivity calculations in Section 13.0.

8.2 HUMIC COLLOIDS

Humic substances are high-molecular-weight organic compounds introduced into natural waters as products of plant and animal tissue decomposition. In the WIPP repository, humic substances may be present in waste soils and in the organic components of Castile or Salado brines, or may form in the repository from condensation reactions between microbial metabolites (e.g., carboxylic acids), cellulosic degradation products, and the EPS associated with microbes (Papenguth 1996b). Humic substances, mainly humic acids and fulvic acids, are important to WIPP PA because of their ability to complex metal cations, including actinides, and because they can increase mobile actinide concentrations.

8.2.1 Humic Colloid Concentrations for the CCA PAVT through CRA-2014 PA

Actinide concentrations associated with humic substances are calculated for WIPP PA using proportionality constants (Table 8-2). For the CCA PAVT, proportionality constants determined

for Th(IV) were extended to U(IV), Np(IV), and Pu(IV), and proportionality constants developed for Am(III) were extended to Pu(III). Proportionality constants for Np(V) and U(VI) were based on data for these oxidation states (DOE 1996, Appendix SOTERM).

Table 8-2. Proportionality Constants and Maximum Concentrations for Humic Colloids

	Proportionality Constant Humic Colloids in Salado Brine[a] (Parameter PHUMSIM)		Proportionality Constant Humic Colloids in Castile Brine[a] (Parameter PHUMCIM)		Maximum Sorbed on Humics (M) (Parameter CAPHUM)
Actinide	CCA PAVT, PABC04, PABC09, and CRA-2014 PA	CRA-2019 DPA	CCA PAVT, PABC04, PABC09, and CRA-2014 PA	CRA-2019 DPA	CCA PAVT, PABC04, PABC09, CRA-2014 PA, and CRA-2019 DPA
Th(IV)	6.3	0.01	6.3	0.01	1.1×10^{-5}
U(IV)	6.3	0.01	6.3	0.01	1.1×10^{-5}
U(VI)	0.12	0.12	0.51	0.51	1.1×10^{-5}
Np(IV)	6.3	0.01	6.3	0.01	1.1×10^{-5}
Np(V)	9.1×10^{-4}	9.1×10^{-4}	7.4×10^{-3}	7.4×10^{-3}	1.1×10^{-5}
Pu(III)	0.19[b]	0.20	1.1[b]	0.20	1.1×10^{-5}
Pu(IV)	6.3	0.01	6.3	0.01	1.1×10^{-5}
Am(III)	0.19[b]	0.20	1.1[b]	0.20	1.1×10^{-5}

a – Units of moles colloidal actinide per mole total dissolved actinide

b – For Castile brine, a cumulative distribution from 0.065 to 1.60 with a mean value of 1.1 and a median of 1.37 was sampled for PA prior to the CRA-2019 DPA

Sources: DOE (2014, Appendix SOTERM, Table SOTERM-21); DOE (2019, Appendix GEOCHEM, Table GEOCHEM-61)

Papenguth (1996b) identified the information necessary for calculating the actinide concentrations associated with humic colloids:

- Solubility of humic substances in WIPP brines;
- Binding capacity of the humic substances;
- Complexation constants for humic substances with the actinides, Ca^{2+}, and Mg^{2+}; and
- Concentrations of actinide ions in the aqueous phase.

The solubility of humic substances was measured in simulated WIPP brines at various Ca^{2+} and Mg^{2+} concentrations to evaluate the effects of these constituents on solubility. These experiments were performed using four different humic and fulvic substances, with an upper limiting value of 2 mg/L selected from the results (Papenguth 1996b). The binding capacities of two humic substances were measured by titration, and these data were supplemented with literature values. A relatively high value of 5.56 meq OH^-/g was selected for the site-binding capacity of humic substances in WIPP PA, from the range of 3 to 6 meq OH^-/g determined in the experiments and identified in the literature.

Complexation constants were determined from experiments with Am(III) and U(VI) and three humic substances in 3 m and 6 m NaCl solutions. The experiments were performed at pH 4.8 and 6, conditions at which humic substances are highly deprotonated and americium and uranium ions have not undergone hydrolysis, which should have maximized complexation between the humic substances and the metal ions compared to the higher pH conditions in the WIPP repository. Papenguth (1996b) selected the 6 m complexation constants as the most relevant to

repository conditions. Th(IV) stability constants with humic and fulvic acids were available only at low pH, but not at higher WIPP-relevant pH values where Th(IV) would be present as the $Th(OH)_4(aq)$ species. Papenguth (1996b) used published results that established a ratio of dissolved to colloidal Th(IV) in seawater at a pH of 6.349 (Baskaran et al. 1992) for the Th(IV) proportionality constant. For Np(V), a log stability constant of 3.67 measured at pH 9 was selected. Because stability constants were not identified for plutonium with humic substances, Papenguth (1996b) used oxidation state analogies to establish proportionality constants for Pu(III) and Pu(IV).

Papenguth (1996b) used the total concentrations of actinides from actinide solubility calculations in the humic colloid calculations for the CCA PAVT. Because the uncomplexed concentrations would be significantly lower than the total dissolved concentrations that contained both uncomplexed and complexed actinides, this represented a significant source of conservatism in the CCA PAVT proportionality constants. The maximum value used in PA (CAPHUM, Table 8-2) represents the theoretical maximum concentration of actinides that can be bound by a humic substance, assuming a solubility limit of 2 mg/L, the highest site-binding capacity for fulvic acids of 5.56 meq OH^-/g, and the limiting case of a monovalent actinide species (DOE 1996, Appendix SOTERM). The approach used to calculate the effects of humic colloids was peer reviewed and approved for the CCA PA (Wilson et al. 1996a, 1996b).

Wall and Mathews (2005) evaluated the solubility of humic acids in GWB and ERDA-6 brines and the effects of MgO on the quantities of humic acids in WIPP brines. Wall and Mathews (2005) found that GWB and ERDA-6 brine promoted coagulation of the humic acid, although complete humic acid removal was not observed. Humic acids were completely removed from the brines in the presence of either reagent-grade MgO or Premier MgO, which was the backfill material being emplaced in WIPP at the time of the experiments (Section 4.2). These results indicate that the concentrations of actinides associated with humic colloids may be overestimated in WIPP PA because humic substances will be less soluble in the relatively high pH repository brines.

8.2.2 Humic Colloid Concentrations for the CRA-2019 DPA

DOE (2019) revised the CRA-2019 DPA proportionality constants (PHUMSIM and PHUMCIM, Table 8-2) for the +IV and +III actinides based on revised calculations in Mariner (2016, 2018, 2019) for the Am(III) and Th(IV) actinides. These revised proportionality constants were then applied to Pu(III), Pu(IV), U(IV), and Np(IV) using the oxidation state analogy. Mariner (2019) used the same overall approach described by Papenguth (1996b) for the +III, +V, and +VI actinides to recalculate the humic colloid proportionality constants for the +III and +IV actinides, with updated input values for the calculations. The Np(V) and U(VI) proportionality constants were not recalculated because these radionuclides do not significantly contribute to repository releases.

The updated calculations for the humic colloid proportionality constants included a revised approach for deriving the Th(IV) proportionality constant. Papenguth (1996b) previously used the ratio of dissolved to colloidal Th(IV) in seawater to determine the Th(IV) proportionality constants because of a lack of complexation constant data for Th(IV) with humic substances at higher pH values. For the CRA-2019 DPA, Mariner (2016, 2019) identified stability constant

data for Th(IV)-humic complexes that were measured from pH 3.3 to 6.9 in 0.1 M ionic strength solutions that included EDTA (Stern et al. 2014). Mariner (2016, 2019) then used the geochemical modeling code PHREEQC with thermodynamic data from DATA0.FM4 to extrapolate the Th(IV)-humic complexation stability constant to zero ionic strength, and this value was used to calculate the Th(IV)-humic colloid proportionality constant for the CRA-2019 DPA.

For Am(III) complexation, Mariner (2018, 2019) used Eu(III)-humic substance complexation constant data (Sonke and Salters 2006) as an analogue. Mariner (2018, 2019) extrapolated the conditional stability constant data to zero ionic strength using PHREEQC and thermodynamic data from DATA0.FM4. This stability constant value was significantly greater than the value used by Papenguth (1996b), which would increase the calculated proportionality constant values.

Mariner (2019) also revised the complexation constants for humic substances with Ca^{2+} and Mg^{2+} from the value of 10^2 used by Papenguth (1996b) to 10^3 based on a review of literature values obtained at ionic strengths up to 5 m. The revised complexation constants are reasonable because they are consistent with the available data. This revision decreases calculated +III and +IV proportionality constants by about an order of magnitude.

Mariner (2019) used the concentrations of the Am^{3+} and Th^{4+} aqueous species in GWB and ERDA-6 brines from the CRA-2019 DPA actinide solubility calculations (Domski and Sisk-Scott 2019) to calculate the +III and +IV actinide humic colloids proportionality constants. This represents an improvement over the calculations performed by Papenguth (1996b), who used the total dissolved Am(III), Np(V), and U(VI) concentrations calculated by Novak and Moore (1996) instead of the uncomplexed aqueous species.

There are some uncertainties related to the input values used by Mariner (2016, 2018, 2019) to recalculate the humic colloid proportionality constants. EPA has identified necessary revisions to the $AmEDTA^-$, ThEDTA(aq), and $CaEDTA^{2-}$ stability constants and some EDTA Pitzer parameters in the DATA0.FM4 database (Attachment B). These revisions to the EQ3/6 database may affect the proportionality constants calculated for humic colloids, because the association constants used for the +III and +IV actinides were determined from experiments that contained EDTA (Sonke and Salters 2006, Stern et al. 2014). The calculated proportionality constants for the +III and +IV actinides would additionally be affected by these EQ3/6 database changes because the total actinide solubilities used in the proportionality constant calculations will be affected. The effects of these EQ3/6 database revisions on the humic colloid proportionality constants would likely be small.

Another potential source of uncertainty is the assumption that that the Ca- Mg-, and actinide-humic complexation constants can be used to model reactions in WIPP brines without adjustment for ionic strength. Mariner (2016, 2018) justified this assumption by noting that log β_1 for the Ca-humic complexation constant decreases with increasing ionic strength from 0.1 to 5 m NaCl, so the assumption of a constant association constant with increasing ionic strength would conservatively overpredict the humic colloid proportionality constant. Because there is no evidence that the association constants will increase significantly with increasing ionic strength, this assumption is reasonable.

The effects of these uncertainties related to the EDTA aqueous speciation and Pitzer parameters in the DATA0.FM4 database and the assumption that association constants are constant with increased ionic strength on the PHUMCIM and PHUMSIM parameters are likely to be fairly small. Mariner (2019) accounted for possible uncertainties by choosing parameter values larger than the calculated +III and +IV proportionality constants. The calculated proportionality constant values of 0.11 and 0.12 for +III actinides in GWB and ERDA-6 brine were rounded up to 0.20, and the values of 7.1×10^{-4} and 1.6×10^{-3} for +IV actinides in GWB and ERDA-6 brine were rounded up to 0.01, adding conservatism to the proportionality constants used in the CRA-2019 DPA.

The CAPHUM values used in the CRA-2019 DPA did not change from the previous values (Table 8-2). Mariner (2019) retained the 2 mg/L solubility used by Papenguth (1996b) for humic substances, although the study by Wall and Mathews (2005) indicated that the solubility may be lower in WIPP repository brines in contact with MgO backfill. The binding capacity for actinides on humic colloids was also not revised. The solubility of humic substances in the presence of MgO backfill may be less than assumed for PA, so the CAPHUM values are likely to be conservative upper bounding values.

The changes to the humic colloid proportionality constants will affect the total mobilized concentrations of the +IV actinides in both Salado and Castile brines and the total mobilized concentrations of Am(III) and Pu(III) in Castile brines (Table 8-2). The parameter changes have been adequately justified by DOE, and the humic colloid parameters used for the CRA-2019 provide conservative estimates of actinides concentrations associated with humic colloids. EPA recommends that DOE make appropriate corrections to the EDTA stability constants and Pitzer parameters in the EQ3/6 database for future WIPP PAs and recalculate the humic colloid proportionality constants based on revised actinide solubility calculations.

8.3 MICROBIAL COLLOIDS

Actinide concentrations associated with microbial colloids in WIPP PA are based on proportionality constants (Table 8-3). WIPP PA calculations also include a maximum concentration for microbially associated actinides.

8.3.1 Microbial Colloids from the CCA PAVT to PABC09

DOE (1996) developed the CCA PA microbial colloids proportionality constants (PROPMIC) for each element. DOE used experimental data on the mobile concentrations of microbes and bioaccumulation and toxicity experiments to develop the proportionality constants (Papenguth 1996c; DOE 1996, Appendix SOTERM). The experiments used a bacterium isolated from WIPP environs (*Halomonas* sp. WIPP-1A) and an uncharacterized mixed culture which presumably contained largely archaea (BAB). DOE (1996) established upper limits for the concentrations of actinides for microbial colloids (CAPMIC) based on the concentration at which no growth was observed (Table 8-3). Because the high radiation levels of Am(III) prevented increasing concentrations until toxicity effects were observed, DOE (1996) did not determine a maximum concentration value for Am(III). The limited data prevented the development of distributions for the proportionality constants or the maximum concentrations for microbial colloids. As a result, DOE (1996) used single values in PA.

Table 8-3. Proportionality Constants and Maximum Concentrations for Microbial Colloids

	Proportionality Constant Microbes[a] (Parameter PROPMIC)				Maximum Sorbed by Microbes (M, Parameter CAPMIC)			
Actinide	CCA PAVT, PABC04, and PABC09	CRA-2014 PA and CRA14_SEN4	CRA-2019 DPA	CRA-2019 Sensitivity Calculations	CCA PAVT, PABC04 and PABC09	CRA-2014 PA and CRA14_ SEN4	CRA-2019 DPA	CRA-2019 Sensitivity Calculations
Th(IV)	3.1	1.76	0.21	3.1	0.0019	2.3×10^{-6}	3.8×10^{-8}	2.12×10^{-2}
U(IV)	0.0021	1.76	0.21	0.0021	0.0021	2.3×10^{-6}	3.8×10^{-8}	8.14
U(VI)	0.0021	1.76	0.21	0.0021	0.0023	2.3×10^{-6}	3.8×10^{-8}	8.14
Np(IV)	12.0	1.76	0.21	12.0	0.0027	2.3×10^{-6}	3.8×10^{-8}	1.27×10^{-4}
Np(V)	12.0	1.76	0.21	12.0	0.0027	2.3×10^{-6}	3.8×10^{-8}	1.27×10^{-4}
Pu(III)	0.3	1.76	0.21	2.18	6.8×10^{-5}	2.3×10^{-6}	3.8×10^{-8}	2.18×10^{-5}
Pu(IV)	0.3	1.76	0.21	2.18	6.8×10^{-5}	2.3×10^{-6}	3.8×10^{-8}	2.18×10^{-5}
Am(III)	3.6	0.32	0.03	3.6	NA[b]	3.1×10^{-8}	2.3×10^{-9}	6.28×10^{-6}

a – Units of moles colloidal actinide per mole dissolved actinide
b – Not applicable
Sources: DOE (1996, Appendix SOTERM, Table SOTERM-14), DOE (2014, Appendix SOTERM, Table SOTERM-21), DOE (2019, Appendix SOTERM, Table SOTERM-9)

8.3.2 Microbial Colloids for CRA-2014 PA

DOE updated the microbial colloid parameters for CRA-2014 based on new experiments that used pure cultures of a representative bacterium and a representative archaeon, both isolated from the WIPP environment (Reed et al. 2013, Ams et al. 2013). These experiments investigated biosorption of Nd(III) and Th(IV) on *Chromohalobacter* sp. and *Halobacterium noricense* in four simulated WIPP brines at 90% saturation and with varied concentrations of EDTA. Biosorption was tested using different pcH values and two-hour incubations. Samples were then filtered using 100 kDa (~20 nm) filters and were also centrifuged. Filtrates and supernatants were analyzed to determine the amount of actinide or analog remaining in solution to account for the actinide associated with microorganisms. Samples were also compared to abiotic control experiments to account for the possible loss of Nd(III) or Th(IV).

Based on these experiments, Reed et al. (2013) generated oxidation-state specific recommendations for PROPMIC parameters for archaea and for bacteria for +IV [Th(IV), U(IV) and Pu(IV)] and for +III [Am(III) and Pu(III)] actinides. Reed et al. (2013) proposed a PROPMIC parameter for Np(V) based on the results of Ams et al. (2013) using *Chromohalobacter* sp in 2 M and 4 M $NaClO_4$ solutions. Reed et al. (2013) also developed PROPMIC parameters on an element-by-element basis, assuming the highest PROPMIC values developed for the different oxidation states of each element. For example, the oxidation-state-specific PROPMIC parameters proposed for Pu(III) were less than the proposed Pu(IV) parameters, so Reed et al. (2013) recommended the Pu(IV) parameters for both plutonium oxidation states.

Reed et al. (2013) also recommended revision of the CAPMIC parameters to correspond with the actinide concentrations per cell reported by Francis (1998) and a measured biomass value of 10^9 cells/ml from Reed et al. (2013). This approach differs markedly from the CCA CAPMIC

approach, which used the actinide concentration at which microbial growth was no longer observed. Because the WIPP PA model only allows for a single set of microbial colloid parameters, Roselle (2013b) selected the higher of the PROPMIC and CAPMIC parameter values developed by Reed et al. (2013) for archaea and for bacteria for the CRA-2014 PA. The selected PROPMIC values were from the bacterium because this had a higher sorption than the archaeon. After reviewing this update, EPA concluded that this new approach was a significant departure from the original conceptual model.

The CRA-2014 PA PROPMIC parameters increased for U(IV), U(VI), Pu(III), and Pu(IV) and decreased for Th(IV), Np(IV), Np(V), and Am(III). Additionally, the CAPMIC concentrations decreased for all elements (Table 8-3). EPA and DOE had multiple discussions to clarify DOE's new approach for the microbial colloids update (Economy 2016, Patterson 2016a, Patterson 2016b).

EPA (2017d) noted that the CRA-2014 PA PROPMIC parameters were based on short-term testing that likely reflected only biosorption and not bioaccumulation or biomineralization. EPA (2017d) found that this approach represents a conceptual model change because previous WIPP PAs included biosorption, bioaccumulation, and biomineralization that would be observed in longer-term experiments (Papenguth 1996c; DOE 1996, Appendix SOTERM). EPA (2017d) also noted that DOE had not adequately justified changing the basis for the CAPMIC parameters from the concentration at which no microbial growth occurred to the concentration calculated from an assumed maximum cell concentration multiplied by the moles of actinides per cell. Furthermore, EPA (2017d) found that measurements for microbial colloid experiments with Th(IV) did not appear to account for thorium intrinsic colloids in the supernatant and filtrate, resulting in a possible underestimation of microbial colloids. EPA (2017d) rejected the updated CRA-2014 PROPMIC and CAPMIC parameters with the expectation that DOE would either update the microbial colloid model for the CRA-2019 or use the parameters originally calculated for the CCA.

8.3.3 Microbial Colloids for the CRA-2019 DPA

For the development of the CRA-2019 DPA PROPMIC and CAPMIC values, DOE continued to follow its CRA-2014 approach but significantly decreased these parameter values (DOE 2019, Appendix SOTERM; Reed et al. 2019). DOE (2019) decreased PROPMIC values for Th(IV), U(IV), U(VI), Np(IV), Np(V), Pu(III), and Pu(IV) from the CRA-2014 values by a factor of 8. The Am(III) PROPMIC value decreased by a factor of 10. Similarly, DOE (2019) reduced CAPMIC values 60-fold for Th(IV), U(IV), U(VI), Np(IV), Np(V), Pu(III), and Pu(IV), and by an order of magnitude for Am(III) (Table 8-3).

DOE (2019, Appendix SOTERM) calculated the CRA-2019 DPA microbial colloid parameters using archaeal, rather than the bacterial data used in the CRA-2014 PA. The Am(III) archaeal data came from experiments described in Swanson (2019). For plutonium, uranium, and neptunium, DOE used archaeal data from experiments described in Reed et al. (2013). DOE (2019) chose archaeal data with the rationale that under WIPP conditions, archaeal survival is more realistic than bacterial survival as there have been no anaerobic, extreme halophilic bacteria that have been isolated from the WIPP halite. DOE further stipulated that haloarchaeal longevity in subterranean halite has been well documented (Reed et al. 2019).

DOE (2019) updated the Am(III) PROPMIC parameters using a series of experiments outlined in Swanson (2019). In these experiments, Swanson (2019) examined microbe-actinide interactions using the Am(III) analog Nd(III) and the archaeon *Halobacterium* sp. Experiments were performed in a 3.42 M NaCl simplified brine as well as 90% ERDA-6 or GWB brines over the course of 1 to 2 months. Swanson (2019) quantified biomass from experiments either through direct cell counts, by weighing cells, or through the use of optical density measurements. Cells were harvested through centrifugation and dissolved Nd(III) concentrations were measured after passing samples through a 100 kD filter.

Swanson (2019) noted several trends in the PROPMIC update experiments. In NaCl solutions, the extent of Nd(III) removed from solution was biomass dependent (Swanson 2019, Figures 1 and 2). At the recommended 10^9 cells/ml biomass value used to calculate CAPMIC, up to 100% of the Nd(III) from experiments was removed from solution. Another trend Swanson (2019) noted was that in experiments where concentrations varied between 2 to 14 µM, the extent of Nd(III) removal was greater in higher concentration solutions, though after 1 month of exposure, Nd(III) was completely removed in all samples (Swanson 2019, Figures 6 and 7). Cases where 100% of the Nd(III) was removed could be treated as minimum PROPMIC values for future calculations.

In WIPP brines, Swanson (2019) noted that very little Nd(III) biomass association occurred in GWB while most of the Nd(III) gradually became bioassociated in ERDA-6. At the experimental pcH values (8.4 for GWB and 8.8 for ERDA-6), Nd(III) should exist in solution as the hydrolysis species $NdOH^{2+}$, $Nd(OH)_2^{+}$ and $Nd(OH)_3$ (aq). Swanson (2019) hypothesized that the low bioassociation occurring in the GWB brines was due to the relatively high Mg^{2+} content competing for bioassociation with the microorganism. The addition of 10^{-4} M EDTA to brine experiments resulted in no Nd(III) bioassociation. DOE calculated the Am(III) PROPMIC value of 0.03 from *Halobacterium* culture (archaeal) experiments in ERDA-6 incubated with Nd(III) and EDTA for one month (Swanson, 2019; Reed et al. 2019, Table B-1). DOE calculated the CRA-2019 DPA Am(III) CAPMIC value by multiplying the measured moles of Am(III) per cell by the biomass concentration (Reed et al. 2019).

The thorium, uranium, neptunium, and plutonium PROPMIC values were updated using the archaeal Th(IV) experiments with 2-hour incubations from Reed et al. (2013). DOE calculated the CRA-2019 DPA thorium, uranium, neptunium, and plutonium CAPMIC values by multiplying the measured moles of actinides per cell by the biomass concentration (Reed et al. 2019).

In addition to updating the PROPMIC and CAPMIC parameters, DOE corrected an error in the PANEL PA code used to calculate CAPMIC (Sarathi 2019b). Although DOE had changed the definition of CAPMIC from a toxicity-based approach to a biomass-based approach in CRA-2014, the PANEL code continued to reflect a toxicity-based approach in the calculations. This meant that when total mobile actinide concentrations (i.e., dissolved + humic + intrinsic + mineral fragment + microbial) were less than CAPMIC, microbial colloid concentrations were allowed to increase. However, once total mobile actinide concentrations were greater than CAPMIC, the microbial colloid contribution became zero (i.e., the concentration at which growth no longer occurred), resulting in no microbial colloid contribution to the source term past the CAPMIC value. The result of this error was an underprediction of DBR releases by 2%. For

the CRA-2019 DPA, DOE updated the code to be consistent with the biomass-based definition. In this case, the microbial colloid concentration will increase until it reaches the CAPMIC value. After that point, the microbial colloid concentration remains constant at the CAPMIC value.

8.3.4 EPA Study of the PROPMIC and CAPMIC Parameter

EPA has had multiple unresolved concerns over the new approaches DOE has taken for calculating both PROPMIC and CAPMIC parameter values since the CRA-2014. EPA and DOE held a series of technical exchanges prior to CRA-2019 to determine a path forward on microbial colloids where EPA can accept DOE's updated parameters (EPA 2018a, EPA 2018b). DOE provided further information on its experimental approach to updating PROPMIC and highlighted that the CCA CAPMIC values represented an unreasonably high biomass concentration in the subsurface (EPA 2018b). As a path towards resolution, EPA asked DOE to address remaining issues with the PROPMIC and CAPMIC parameters in the CRA-2019 documentation (Peake 2018). The Agency asked that DOE:

- Identify the expected range of cell counts anticipated in WIPP based on the cell sizes and types of microbes;
- Determine whether the cell counts used in the biomass approach were representative of expected cell counts in the WIPP environment including microorganisms associated with brine, Salado halite, wastes, and waste containers; microorganisms introduced by operations and air circulation; and microorganisms in potential seepage from surficial groundwater.
- Consider whether the effects of non-viable cells were adequately addressed, including the potential effects of sorption, passive uptake, and stimulation of nucleation and actinide mineral formation by non-viable cells;
- Explain whether DOE's CRA-2014 PA approach addressed all aspects of the original microbial colloids conceptual model discussed in the CCA (i.e., sorption, uptake, and mineralization); and
- Provide additional information regarding how biouptake of actinides affects the microbial parameters, possible actinide mineralization stimulated by phosphate groups on microbial surfaces, and the effects of actinide oxidation states on the microbial parameters.

The longer experimental times used to derive the CCA values meant that biosorption, bioaccumulation, and biomineralization discussed in the conceptual model were all addressed. In contrast, the two-hour experimental times used to develop the CRA-2014 PA parameters appear solely to address biosorption. Although longer experimental times for the Am(III) PROPMIC update in the CRA-2019 DPA are more reasonable, the thorium, plutonium, neptunium, and uranium values were obtained from two-hour experiments from Reed et al. (2013) and are difficult to defend.

In the CRA-2014 microbial colloids approach, Reed et al. (2013) also interpreted the microbial colloidal conceptual model to assume cells in the subsurface are viable. While this interpretation

is important from the perspective of gas generation, the original colloids conceptual model highlights the uncertainty regarding microbial viability at the WIPP. A new approach assuming cell viability also ignores the possibility that dead or non-viable cells native to WIPP brine or introduced into the repository environment can potentially act as material to create microbial colloids. Experiments used to update the colloidal parameters did not address the potential persistence of dead or non-viable cells in the repository and their effect on microbial colloids.

Moreover, EPA has concerns over the updated biomass approach towards CAPMIC. While EPA agrees that the previous approach may unrealistically portray an extremely high subsurface biomass, the choice of 10^9 cells/ml for the biomass-based approach was not fully justified by DOE and the Agency needs evidence that this value is reasonably representative of biomass counts under WIPP conditions.

During the CRA-2019 review, EPA requested additional information from DOE to help assess the effects of DOE's revised CAPMIC approach on repository releases. EPA requested that DOE recalculate the CAPMIC parameters using the biomass-based approach with 10^9 cells/ml and the CCA bioassociation data (Papenguth 1996c), because the CCA data were collected over longer experimental times and likely included biosorption, bioaccumulation, and biomineralization (Peake 2020d, Comment CC4-SOTERM-6(a)). EPA also requested that DOE compare repository releases predicted for the CRA-2019 DPA to predicted repository releases using the CCA PROPMIC parameters and recalculated CCA CAPMIC parameters (Peake 2020d, Comment CC4-SOTERM-6(b)). The Agency found the calculations in DOE's response (Knerr 2020c) to be incomplete, and the Agency therefore recalculated the CAPMIC values as described below in Section 8.3.4.2. The Agency also performed calculations to assess the effects of the revised PROPMIC and CAPMIC parameters on predicted repository releases (Section 13.2.3).

Given EPA's concerns over the updated microbial colloid parameters, the Agency undertook an independent study to understand how the new microbial colloid parameters compare to the broader literature. The goals of the study were to: 1) evaluate whether the new PROPMIC parameters adequately address all aspects of the original microbial colloids conceptual model (biosorption, bioaccumulation, and biomineralization); 2) determine the effects that dead or non-viable cells have on microbial colloids; and 3) understand how cell counts used in the biomass-based CAPMIC compare to biomass in WIPP-similar environments.

Due to the lack of data on actinide association with microbial colloids (i.e., PROPMIC) in the specific WIPP environment, EPA chose to perform a very broad literature search to understand how the various geochemical parameters in the WIPP environment (e.g., salinity, alkaline pH, high actinide concentration) and possible microbial ecology (e.g., type of organism, live vs. dead cells, or amount of biomass) may influence PROPMIC. Literature chosen specifically examined experiments and studies of microbial associations with actinides (e.g., uranium, thorium, plutonium, americium, etc.) and analogs (e.g., rare earth elements like neodymium, europium, etc.) over a very wide range of salinities, pH values, and other geochemical parameters. A PROPMIC value was calculated from data extracted from the literature following DOE's formula (Equation 33):

$$PROPMIC = \frac{[Actinide\ or\ Analog\ Sorbed]}{[Dissolved\ Actinide\ or\ Analog]} \quad \textbf{(33)}$$

A CAPMIC value from the data was also calculated for an actinide concentration in a solution containing 10^9 cells/ml following DOE's formulas (Equations 34 and 35):

$$moles\ actinide/cell = \frac{[moles\ "microbe-bound"\ actinide/L]}{[cells/L]} \quad \textbf{(34)}$$

$$CAPMIC = \frac{moles\ actinide}{cell} \times \frac{10^{12} cells}{L} \quad \textbf{(35)}$$

For an assessment of the biomass values used to calculate CAPMIC, EPA obtained cell counts from multiple subsurface environments including alkaline springs, actinide-contaminated shallow subsurface environments, radioactive waste repositories in crystalline rock, produced water from hydraulic fracturing, hypersaline environments, and salt deposits. EPA also examined cell counts that could be found in radioactive waste, similar to what will likely be stored at the WIPP.

The pH values in EPA's study ranged between 6 to 12.7, temperatures ranged from 10.2 to 50ºC, subsurface depths ranged from 0.2 to up to 2,600 m, and salinities ranged from 49 to nearly 720,000 mg/L. These cell counts were also compared to WIPP cell counts from various studies (Dodge et al. 1998, Swanson et al. 2012, Vreeland et al. 1998, and Wang and Francis 2005) and were used to help calculate CAPMIC and PROPMIC values. Results from this investigation are discussed below and are shown in Figures 8-6 to 8-13.

8.3.4.1 Actinide Bioassociation (PROPMIC)

DOE has noted multiple studies showing the extent of actinide bioassociation in hypersaline environments similar to WIPP (e.g., Swanson and Reed 2018, Swanson 2019). These studies, while very relevant, also highlight the lack of data in WIPP-specific conditions needed to develop the context to determine an appropriate PROPMIC value. As such, EPA expanded its literature survey beyond saline environments to parse out the impact of various WIPP geochemical parameters on PROPMIC. Figure 8-6 shows PROPMIC values calculated from data obtained from EPA's literature survey by oxidation state for studies greater than 2 hours. Notable in the figure is the wide variability in calculated PROPMIC values. Most values (i.e., close to 75%) appear bounded by the Th(IV) and Am(III) PROPMIC values used in the CCA (blue dashed lines), and are reasonably consistent with the Pu(III) and Pu(IV) CCA values (green dashed line). However, the CRA-2019 PROPMIC values (red dashed lines) are significantly lower than most of the literature PROPMIC values in Figure 8-6.

Figure 8-7 presents the PROPMIC values by actinide and shows that CCA values bound PROPMIC values for most actinides, with the notable exception of plutonium. A PROPMIC value of 2.18 bounds approximately 75% of the plutonium data. The plutonium data shown in Figure 8-7 include studies on bioassociation for Pu(IV) and Pu(V) and have several PROPMIC outliers that range between 99 to 500 from Sasaki et al. (2002) and Francis et al. (1998). These

two studies looked at plutonium associations with microbial consortia and may also include bioassociations with extracellular polymeric substances (EPS) that have been shown to strongly bioassociate with actinides (e.g., Boggs et al. 2016). Many of the experiments were also performed in conditions that may have favored bioassociation, such as dilute solutions and neutral pH values. Consequently, many of the values may be a conservative overestimate of bioassociation. However, in the absence of a more extensive dataset in WIPP-specific conditions, EPA believes these high values are defensible until more data can be generated.

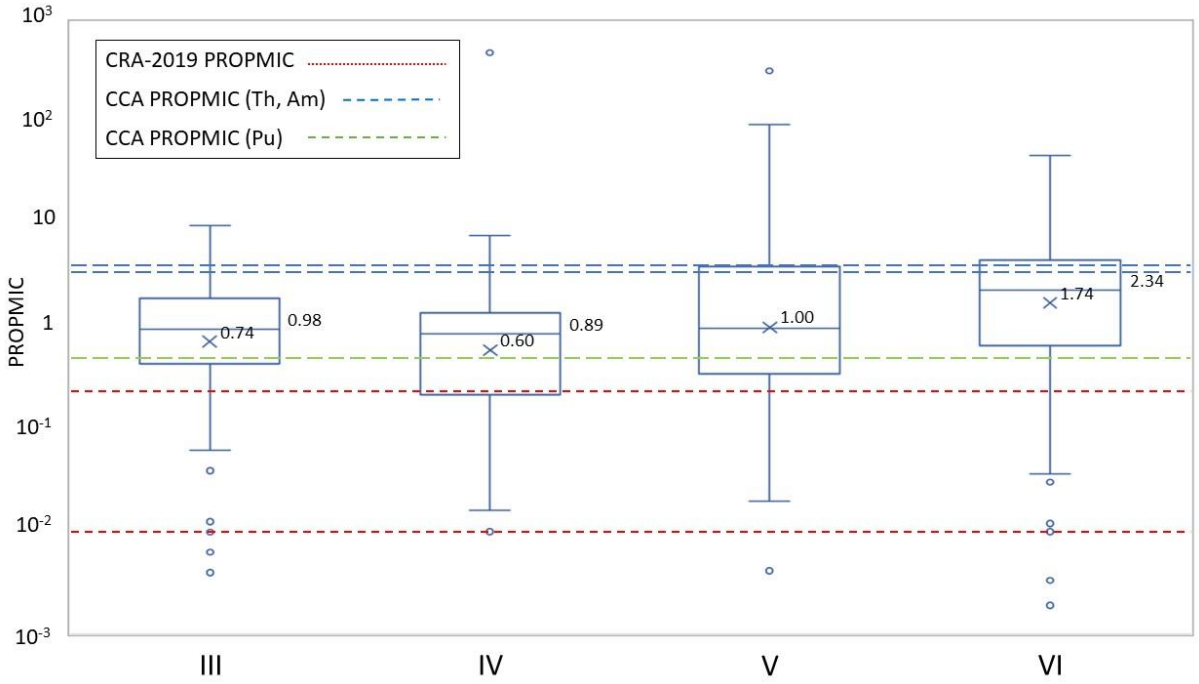

Figure 8-6. Calculated PROPMIC Values from the Literature by Oxidation State

Similarly, the uranium CCA (0.0021) and CRA-2019 (0.21) PROPMIC values fall below the range of PROPMIC values calculated from the literature (CCA and CRA-2019 PROPMIC values are not shown in Figure 8-7). Because uranium will only provide a minor contribution to repository releases, EPA believes the CCA uranium PROPMIC values are acceptable until more data are generated.

Figure 8-7 also provides the approximate calculated PROPMIC range from the Swanson (2019) based on the document's figures. The maximum values from this study far exceed the PROPMIC maxima of the other actinides in EPA's studies, particularly because Swanson (2019) noted nearly 100% removal of Nd(III) from cultures in NaCl. Only approximately half of the data points from the study are bounded by the CCA Am(III) PROPMIC. While samples measured in GWB and ERDA-6 brines are likely more representative of WIPP processes, it is important to note that extremely high PROPMIC values may be a real possibility in the WIPP, especially if organisms are capable of removing up to 100% of dissolved actinides from solution.

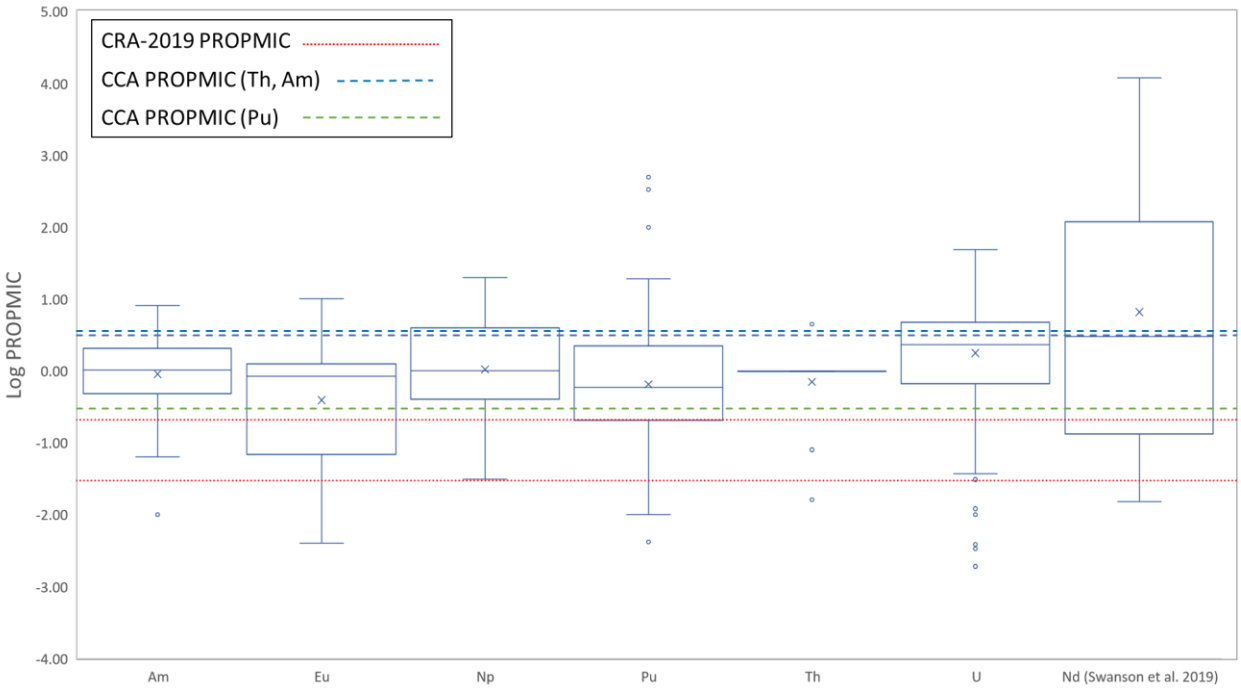

Figure 8-7. Calculated PROPMIC Values from the Literature by Actinide, Including Swanson (2019)

Swanson (2019) noted that both an indigenous and an introduced population can be initially present at the WIPP but that over the repository's lifetime, the energetic costs of surviving WIPP salinity will select for the halotolerant or halophilic organisms. Documented cases of microbial survival in similar environments favor haloarchaea rather than bacteria, though many bacteria isolated from WIPP environs have been shown to survive for several weeks when grown in the salinity of WIPP brine. Although microbial viability in the long-term WIPP environment may be uncertain, multiple studies have noted bioassociation with dead and inactive cells (Bengtsson et al. 1995, Ding et al. 2014, Haas et al. 2001, Pang et al. 2011), and note that sorption may be independent of cellular functions (Andres et al. 1993) or may even surpass live cells in their ability to sequester actinides (Sar and D'Souza 2001). Studies also document the longevity of microorganisms, whether viable or otherwise, in ancient halite fluid inclusions (e.g., Swanson 2019, Schubert et al. 2009). The mere presence of a dead or inactive introduced microorganism will likely have impacts to subsurface geochemistry and microbial colloids. Figure 8-8 highlights the differences in PROPMIC calculated between dead/inactive cell cultures in comparison to live cells and stationary-phase cultures (i.e., a mixture of live, dead, and inactive cells) in studies that provide the information. Figure 8-8 shows that mean literature PROPMIC values are lower in dead and inactive cells than live cells. However, the dead/inactive cell PROPMIC values are still more consistent with the CCA PROPMIC values than the CRA-2019 DPA PROPMIC values.

Prior to its closure, the WIPP will be a relatively open system, with many different organisms being introduced into the facility through the waste, ventilation shafts, and mining activity. Many of these organisms have been identified on halite in open panels (Swanson et al. 2012) or in the WIPP waste (Swanson et al. 2015, Swanson et al. 2021) and the identified organisms include archaea, bacteria, and fungi. It is important to note how PROPMIC may vary among the potential

types of organisms because different organisms will have varying degrees of bioassociation (e.g., Ams et al. 2013, Bader et al. 2017, Bader et al. 2018a, Bader et al. 2019).

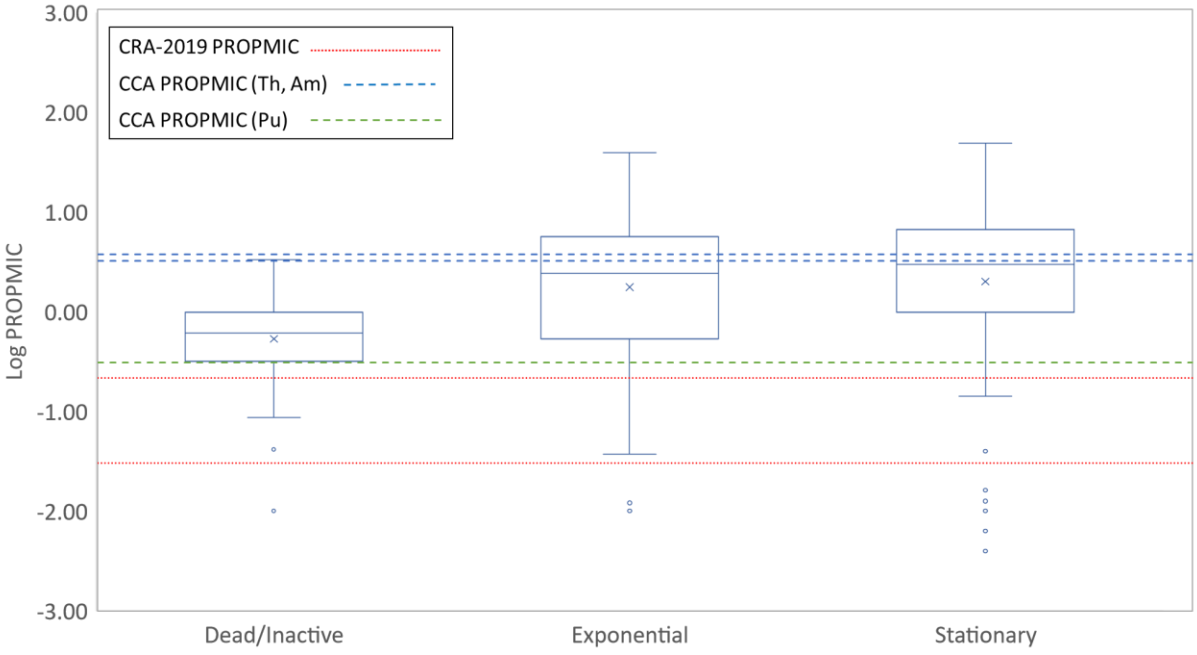

Figure 8-8. Calculated PROPMIC Values from the Literature by Cell Life Cycle

Figure 8-9 shows the PROPMIC variability when broken down by domain. The mean archaeal and eukaryal PROPMIC values are higher than the mean value for bacterial pure cultures. Archaeal data are confined to the +VI actinides and contain data only from the *Halobacterium* genus (Bader et al. 2017, Bader et al. 2018a, Bader et al. 2018b, Bader et al. 2019, Francis et al. 2004, Gillow et al. 2000, Ozaki et al. 2004). These archaea were all examined under high ionic strength and in conditions that appear relevant towards WIPP. However, the use of only one archaeal genus as well as +VI actinides makes this dataset extremely limited and does not provide any sense of the possible variability in nature. Data from the Eukarya domain are also limited to the +VI actinides but come from a variety of organisms. This includes data from yeasts which have been shown to be extremely effective at bioassociating with actinides (Zheng et al. 2018). Mixed cultures, cultures comprised of all three domains, had the lowest mean and median PROPMIC values, but the widest range, and are likely more relevant to WIPP. These are represented by three sets of cultures, two of them coming from WIPP-relevant environments (Francis 1998, Gillow et al. 2000). The exact composition of these cultures is not clearly specified in the literature and the degree of variability may stem from the fact that the mixed cultures contained EPS which, as discussed earlier, have been shown to strongly sorb actinides. Regardless of domain, mean and median PROPMIC values are bounded by the Th(IV) and Am(III) CCA PROPMIC values. On the other hand, the Pu(III) and Pu(IV) CCA PROPMIC value is less than 75% of the PROPMIC values for all domains except the mixed cultures.

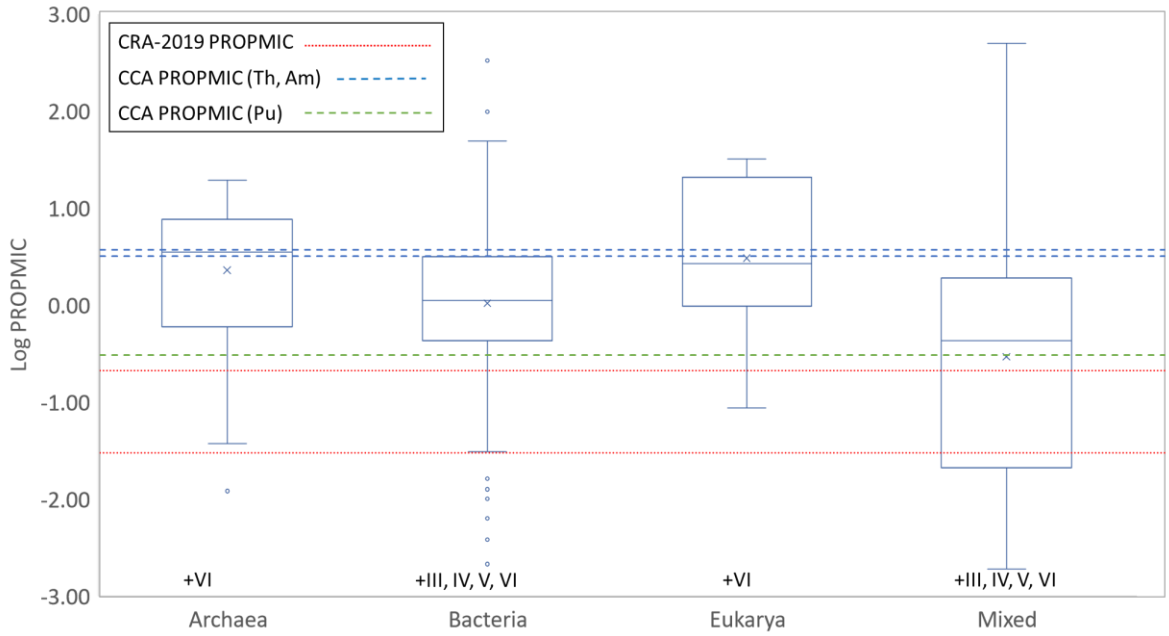

Figure 8-9. Calculated PROPMIC Values from the Literature by Domain

According to the WIPP conceptual model, microbial colloids are created through three processes: biosorption, bioaccumulation, and biomineralization. EPA's literature survey shows that most studies on bioassociation do not explicitly state these processes and often use the terms "uptake" and "sorption" interchangeably, making it difficult to parse out how PROPMIC values differ by bioassociation process. However, studies in general also note that actinide exposure time may impact the degree of bioassociation. This is because sorption will happen relatively quickly upon microbial exposure to actinides. Following sorption is bioaccumulation, which happens slowly and will also increase bioassociation values. Biomineralization appears to occur both on short and long timescales, depending on the organism and the precipitate (e.g., Bader et al. 2017, Bader et al. 2019, Zheng et al. 2018). These bioassociation patterns have been noted in many studies in EPA's dataset including Anderson et al. (2011), Bader et al. (2017), Bader et al. (2018a), Bader et al. (2018b), Bader et al. (2019), Bengtsson et al. (1995), Boggs et al. (2016), Ding et al. (2014), Erkaya et al. (2014), Francis (1998), Liu et al. (2002), Luk'yanova et al. (2008), Nazina et al. (2010), Panak and Nitsche (2001), Theodorakopoulos et al. (2015), and Zheng et al. (2018).

Figure 8-10 shows all PROPMIC values plotted against time for each actinide studied. There may be a correlation between time and PROPMIC for all values, but this correlation is extremely weak and does not sufficiently explain the variability in the dataset. This highlights the fact that the extent of bioassociation will be affected by a wide variety of factors beyond just exposure time, such as microbial type, salinity, pH, and many other factors.

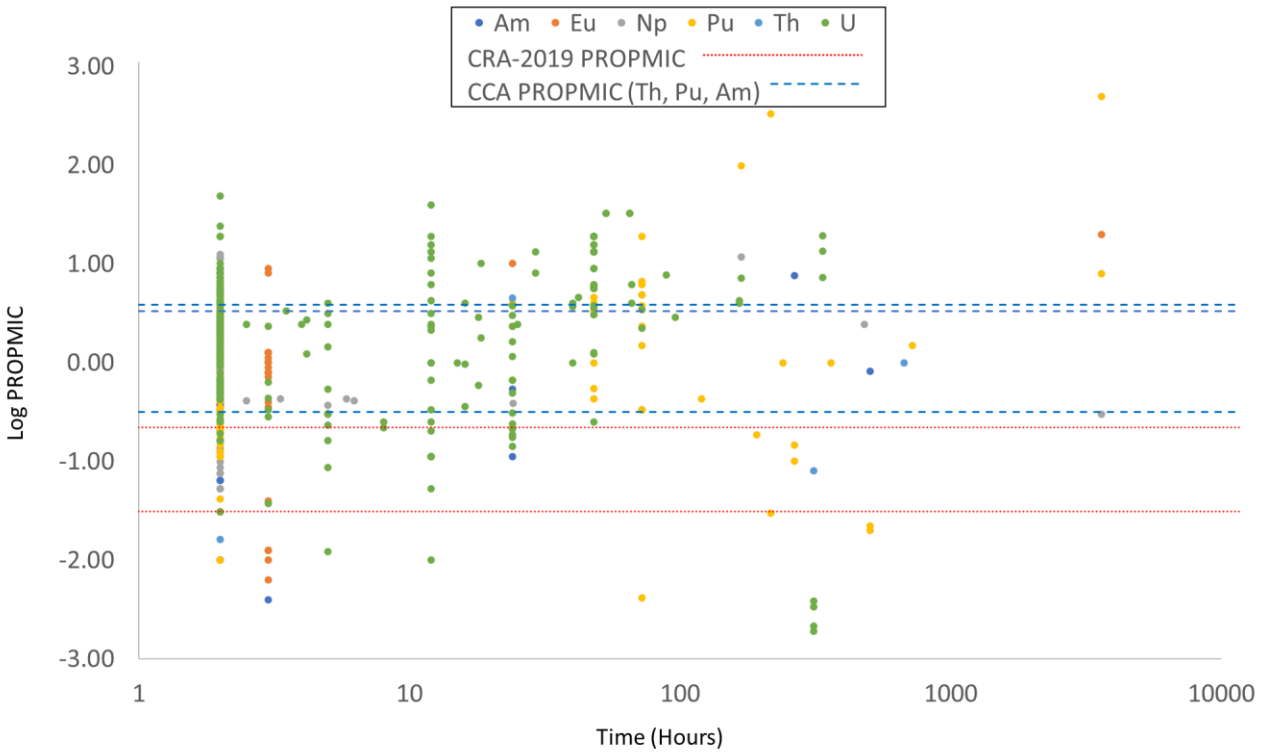

Figure 8-10. Literature PROPMIC Values vs. Experimental Time

8.3.4.2 Biomass in the Subsurface (CAPMIC)

Cell counts in EPA's survey did not exceed the 10^9 cells/ml value used to calculate CAPMIC (Figure 8-11). The lowest cell counts were 37 cells/ml in deep subsurface crystalline rock in the Aspo Hard Rock Laboratory in Sweden (Wu et al. 2016). Actinide-contaminated soils, which will be present in WIPP waste, had total counts ranging between 10^5 to 10^7 cells/g (Francis 2007, Lin et al. 2012). In contrast, cell counts in WIPP brines have been found to be less than 10^5 cells/ml in field samples and on the order of 10^9 cells/ml in cultures (Dodge et al. 1998, Gillow et al. 2000, Swanson et al. 2012, Swanson 2019). Of the data providing viable cell counts, produced water from the Triassic Stuttgart Formation contained the highest biomass count, with 5×10^6 cells/ml (Morozova et al. 2010).

Figure 8-11 provides a comparison of total and viable cell counts against total dissolved solids (TDS), a proxy for salinity. There is a weak trend between increasing TDS and decreasing total and viable cell counts ($r^2 = 0.40$ and 0.18, respectively). These trends suggest that some of the variability in cell counts can be explained by the impacts of salinity on cells, partially corroborating DOE assertions that salinity is a stressor that will limit microbial growth and survival at the WIPP.

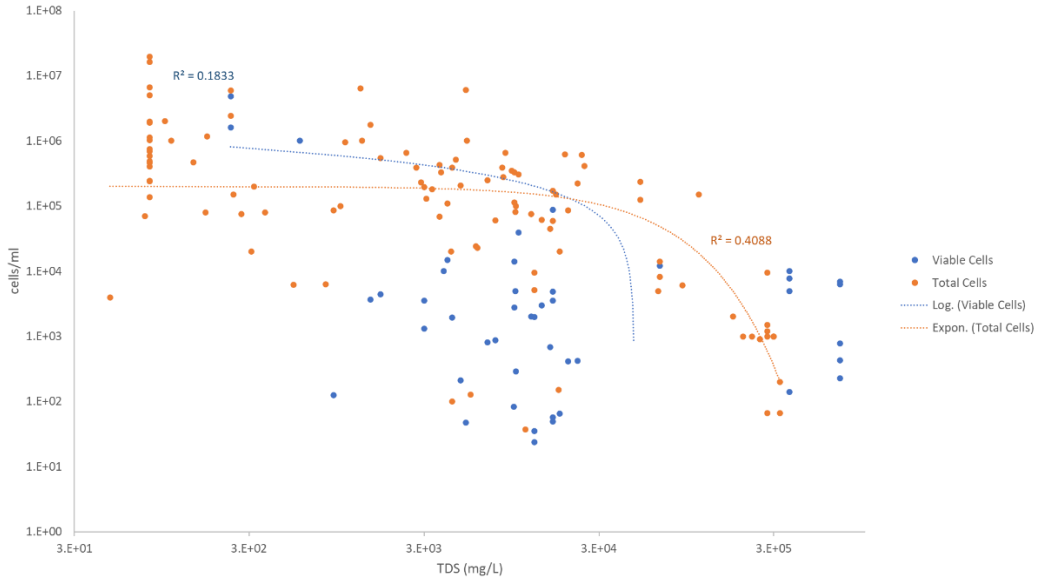

Figure 8-11. Viable and Total Cell Counts in WIPP-related Environments vs. TDS as a Proxy for Salinity

DOE states that haloarchaeal longevity has been noted in fluid inclusions from subterranean halites (Swanson 2019). EPA has also identified data on microbial longevity in halite fluid inclusions from Death Valley, California, USA (Schubert et al. 2009), though the types of cells and their viability are unknown. Cells counted from these samples are on the order of 10^7 cells/ml, two orders of magnitude lower than the value used to calculate CAPMIC, showing that this value bounds analogous hypersaline environments.

Using the 10^9 cells/ml biomass value and data from EPA's literature review, EPA calculated CAPMIC values by determining the amount of actinide associated with cells and calculating the values for 10^9 cells/ml (i.e., 10^{12} cells/L, Equation 35). For comparison, EPA also recalculated CAPMIC values from CCA data, using data from Table 2 of Papenguth (1996c). For the Papenguth (1996c) experiments without measured cell counts, cell count was estimated from a linear correlation between the reported cell counts and final optical densities. For the Papenguth (1996c) plutonium, neptunium, and uranium data, CAPMIC values were calculated from samples with direct cell counts. Americium and thorium CAPMIC values were taken from cell counts extrapolated from optical density measurements. Two uranium datapoints were discarded as cell counts and extrapolated cell counts from optical density measurements deviated significantly. CAPMIC values from EPA's study and from Papenguth (1996c) are presented by actinide in Figure 8-12 and by oxidation state in Figure 8-13.

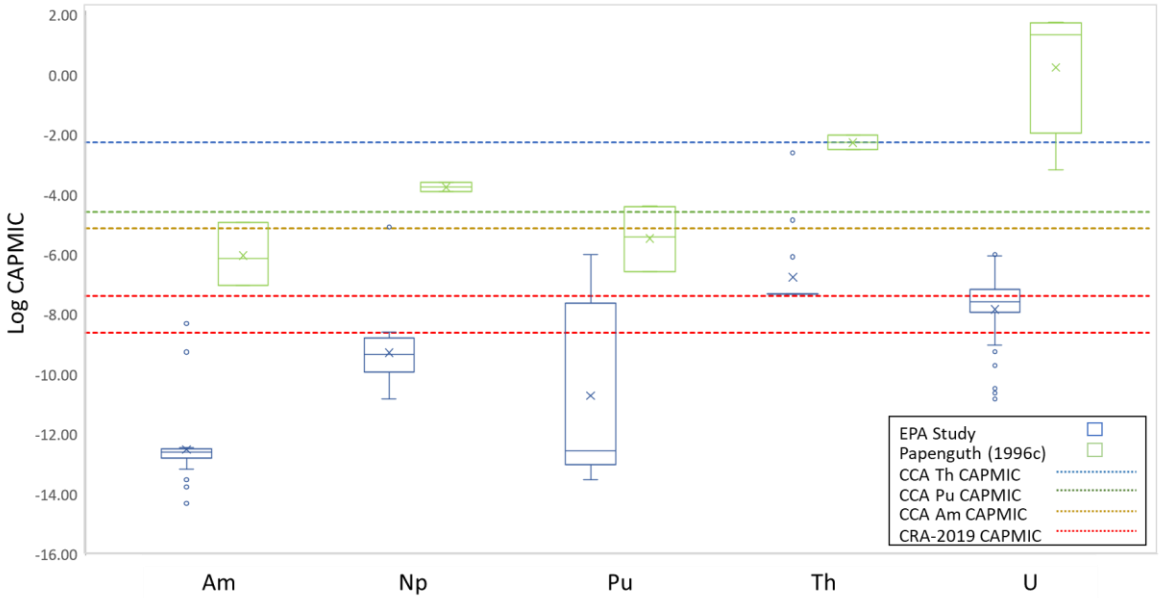

Figure 8-12. Calculated CAPMIC Values from the Literature by Actinide, Including Data from Papenguth (1996c) and recalculated CCA CAPMIC

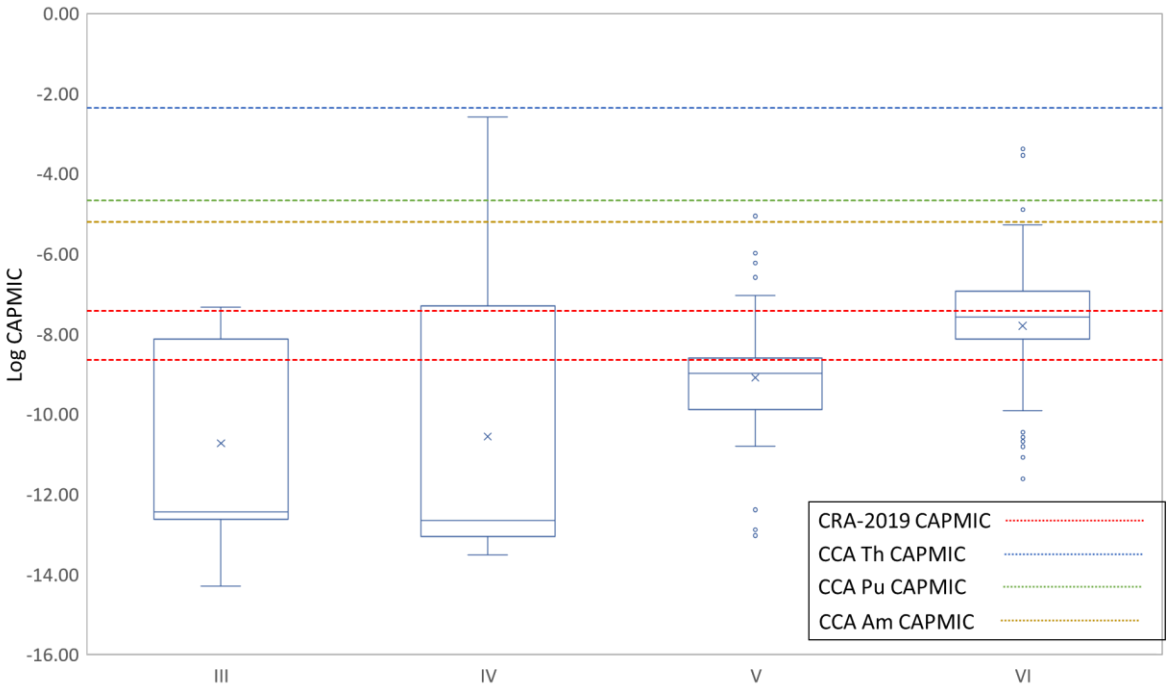

Figure 8-13. Calculated Literature CAPMIC Values by Oxidation State Compared to CRA-2019 DPA CAPMIC Values and Recalculated CCA CAPMIC

The results presented in Figures 8-12 and 8-13 show a wide range of CAPMIC values, spanning up to 12 orders of magnitude. CAPMIC values used for the CRA-2019 DPA do appear to bound the values EPA has observed in the literature (Figure 8-12). Mean literature thorium CAPMIC values appear to fall above the CRA-2019 DPA values, but thorium data still appear to align with

CRA-2019 DPA values. Much of the data available in the literature to calculate CAPMIC were limited as many studies did not provide sufficient data to determine the amount of actinide associated with a cell. For example, Luk'yanova et al. (2008) provided a lot of bioassociation data for plutonium, americium, neptunium, and uranium but provided biomass counts in mg/L of protein which do not readily provide a calculable value that could be scaled to 10^9 cells/ml. Furthermore, the pH range and timescales examined in the dataset limited the number of studies available to use for a CAPMIC calculation.

CAPMIC values recalculated from Papenguth (1996c) bound values from the literature and are several orders of magnitude higher than the CRA-2019 DPA CAPMIC parameters. Organisms from this study likely overrepresent surficial microorganisms but are performed in WIPP environments and likely provide conservative results. However, the Papenguth (1996c) values address the issues of timescale and microbial diversity that EPA believes are necessary to defend the updated CAPMIC parameter values. Because the data collected for the CRA-2019 DPA CAPMIC values are bounded by the recalculated CCA values, EPA believes recalculated CCA CAPMIC values remain appropriate until DOE can perform additional experiments to address uncertainties related to timescales and organisms described above.

8.3.5 EPA Evaluation of PROPMIC and CAPMIC

After a series of technical exchange meetings, EPA provided DOE with a list of follow-up questions regarding the CRA-2014 microbial colloids parameters (Peake 2018). In response, Swanson (2019) provided a range of bioassociation values from various studies conducted at high ionic strength to compare to the CRA-2019 DPA PROPMIC values. Because there are so few studies in high ionic strength environments from which to draw more PROPMIC values, EPA notes that one takeaway from the report is the paucity of data on bioassociation in WIPP-specific environments, creating knowledge gaps and uncertainties. For example, very few studies exist that examine long term +III actinide bioassociation with archaea in WIPP-related environments. Similarly, very few studies exist looking at bacterial and eukaryal actinide bioassociation at high ionic strength. Because of these data gaps, EPA believes it is justified to draw from a larger set of studies on bioassociation beyond the WIPP-specific environment. The CCA PROPMIC values adequately bound this more extensive dataset, whereas the CRA-2019 DPA PROPMIC values are consistently lower than the literature values for all actinides examined by EPA. In light of all the uncertainties and knowledge gaps, EPA does not believe a decrease in PROPMIC from the CCA values is currently justified.

One lingering uncertainty is the long-term presence and durability of inactive, nonviable, or dead cells in brine that have been introduced into the repository or that are already present. These cells may not be limited to the archaea but may also include bacteria and eukaryotes that have been introduced, such as bacterial spores (Swanson et al. 2021) which will have different degrees of bioassociation than the archaea. Many dead and inactive cells may persist in the repository over 10,000 years (e.g., Schubert et al. 2009). EPA's review suggests dead and inactive cells will bioassociate less than live cells, but that these values will need to be considered in the overall PROPMIC selection.

EPA notes that DOE has begun performing calculations that quantify the possible range of microbial cell counts introduced into the WIPP. For example, Swanson et al. (2021) performed a

rough calculation estimating the number of *Bacillus* spores that could be introduced through waste, ranging between 10^5 to 10^8 spores/ml of brine. Significant quantities of microbial cells can be associated with waste and other repository solid materials. For example, Wang and Francis (2005) identified total bacterial cell counts up to 6.29×10^{11} cells/g in bentonite meant for nuclear waste disposal and fungi up to 2.46×10^4 cells/g in waste soils, and Szponar (2012) reported 1.25×10^9 cells/g in mineral deposits formed by discharge from alkaline springs. DOE should perform calculations similar to those of Swanson et al. (2021) with other representative organisms, including bacteria and fungi in the waste and archaea in brine, to provide a clearer picture of which organisms will likely dominate the 10^9 cells/ml biomass in the post-closure repository environment. These calculations will provide information on which value for PROPMIC would be most representative and bounding.

In the experiments to update the Am(III) CRA-2019 parameters, Swanson (2019) adequately addressed the impact of experimental time and its implications to biosorption, bioaccumulation, and biomineralization towards PROPMIC by extending the length of experiments over the course of two months. EPA believes that the approach DOE has taken in these experiments provides a defensible path forward towards updating future parameters, though more organisms will need to be examined to address variability in PROPMIC calculated from the literature data. Because the current Am(III) PROPMIC parameter is derived from a single organism, EPA disagrees with the value chosen at this time. However, the Agency believes the experimental timeframe and approach used to derive the value were appropriate. EPA does not find the updated thorium, neptunium, plutonium, and uranium values appropriate as these values were derived from 2-hour experiments previously considered and rejected during the Agency's review of the CRA-2014 PA.

For its sensitivity calculations (Sections 12.3 and 13.2.3), and for future WIPP PAs, EPA recommends using the americium, thorium, neptunium, and uranium CCA PROPMIC values, because these values bound the variability found in the literature. For Pu(III) and Pu(IV), EPA recommends a PROPMIC value of 2.18 as this bounds 75% of the data in the literature and omits outliers that were discussed earlier. Recommended values are provided in Table 8-3.

Based on the data collected from EPA's independent evaluation, DOE's use of the 10^9 cells/ml value for its biomass-based CAPMIC approach appears to be reasonable. However, EPA continues to find the CRA-2019 CAPMIC parameter values to be uncertain because the revised values are based solely on a single organism. For future WIPP PAs, EPA recommends the use of the recalculated CCA CAPMIC values from Papenguth (1996c) experimental data, listed in Table 8-3. These values should be used in future WIPP PAs until more experiments similar to Swanson (2019) are performed that address the issues discussed above regarding experimental timescale and the effects of different organisms.

8.4 COLLOIDS SUMMARY AND CONCLUSIONS

Review of the colloid parameters used in the CRA-2019 DPA has shown:

- Parameter values reflecting mineral fragment colloids (CONCMIN) have remained unchanged since the CCA PAVT, and these parameter values are consistent with the available data.

- DOE investigated whether mineral fragment colloids might form during reaction of MgO in WIPP brines and transport actinides. EPA suggests that DOE could resolve remaining uncertainties regarding formation of pseudocolloids from MgO hydration and carbonation products by performing sequential filtration experiments with brine samples from the MgO hydration and carbonation experiments after spiking the solution aliquots with Th(IV) and a +III actinide or analogue such as Nd(III).
- The intrinsic colloid parameter for plutonium (PU:CONCINT) is adequately bounding for the available Pu(III) sequential filtration data.
- The CRA-2019 DPA intrinsic colloid parameter for americium (AM:CONCINT) is less than most of the concentrations calculated from sequential filtration data for Nd(III). EPA expects DOE to increase the AM:CONCINT concentration to 1.7×10^{-7} M to adequately represent the Nd(III) experimental data.
- EPA expects that the intrinsic colloid parameter for thorium (TH:CONCINT) will be increased to 4.8×10^{-7} M to adequately account for the results of oversaturation experiments and total Th(IV) colloids detected in concentrated NaCl solutions by Altmaier et al. (2004).
- DOE should evaluate the potential effects of the formation of structural silica colloids with +IV actinide species, including evaluating the effects of high ionic strength and high pcH on silica solubilities in repository brines.
- Humic colloid parameters were revised for the CRA-2019 DPA, and these parameters provide a reasonable upper bound on the concentrations of actinides associated with humic colloids. Because the humic colloid experiments were conducted in solutions that contained EDTA, EPA recommends that DOE confirm the adequacy of these parameters by making appropriate corrections to the EDTA stability constants and Pitzer parameters in the EQ3/6 database and recalculating the humic colloid proportionality constants for future WIPP PAs.
- DOE significantly decreased the proportionality constant (PROPMIC) used to calculate microbial colloids as well as its upper bound (CAPMIC) for the CRA-2019 DPA. Values were changed to reflect data from experiments on *Halobacterium* sp. using data from Swanson (2019) for Am(III) and Reed et al. (2013) for all other actinides. The CAPMIC approach continues to be based on the CRA-2014 assumption that the CAPMIC is the maximum cell concentration (10^9 cells/ml) multiplied by the moles of actinides per cell.
- Experiments used to update thorium, uranium, neptunium, and plutonium PROPMIC and CAPMIC parameter values continue to reflect 2-hour experiments and do not adequately address all aspects of microbial colloids including biosorption, bioaccumulation, and biomineralization.
- EPA conducted an independent study to investigate the potential ranges of PROPMIC and CAPMIC values in the literature. Results show that the CRA-2019 DPA parameters do not reflect the large variability in the literature because these values only draw from a single organism. However, PROPMIC values from the CCA and from EPA's independent study, as well as recalculated CAPMIC values from Table 2 of Papenguth (1996c), appear to bound most values from the literature. EPA expects DOE to use the CCA PROPMIC values and recalculated CCA CAPMIC values from the EPA sensitivity calculations (Table 8-3) until more data can be collected in WIPP-specific environments.

- EPA's literature review finds that the 10^9 cells/ml value used to calculate a biomass-based CAPMIC is appropriate as it bounds biomass in most natural subsurface and radioactive waste repository environments.
- DOE should calculate the possible range of microbial cell counts of representative organisms in addition to *Bacillus* spores (such as bacteria and fungi) similar to the calculation performed in Swanson et al. (2021). These calculations should include various organisms that could be introduced into WIPP through waste and archaea that could be introduced in brine to provide a clearer picture of which organisms will likely dominate the 10^9 cells/ml biomass in the post-closure environment. These calculations will provide information on which PROPMIC values would be most representative and bounding.
- Experiments performed by Swanson (2019) appropriately addressed EPA concerns regarding all aspects of bioassociation, including biosorption, bioaccumulation, and biomineralization as the experimental timeframes are on the order of two months. While EPA disagrees with the ultimate Am(III) PROPMIC value chosen because the value does not adequately bound the literature data or the account for variety of organisms that may be present, the Agency believes similar experiments on multiple organisms and actinides provide a path forward towards defensibly updating PROPMIC and CAPMIC.

9.0 CULEBRA DOLOMITE DISTRIBUTION COEFFICIENTS

Radionuclides may reach the Culebra Dolomite Member of the Rustler Formation via brine flow through boreholes that intersect the repository (DOE 2019, Appendix PA). Radionuclides introduced into the Culebra Dolomite may be transported through natural groundwater flow to the land withdrawal boundary (LWB). Predictions of radionuclide transport and release through the Culebra Dolomite are affected by sorption onto minerals along this potential pathway. Accordingly, DOE developed distribution coefficients (K_ds) to express a linear relationship between sorbed and aqueous concentrations of the radionuclides (DOE 2004).

9.1 DISTRIBUTION COEFFICIENTS USED IN THE CCA PA AND PAVT

The distribution coefficients used in the CCA PA and PAVT were developed using data from experiments carried out at LANL and SNL:

- Sorption studies carried out with 'dolomite-rich Culebra rock' by Triay and coworkers,
- Sorption studies performed using pure dolomite from Norway and synthetic NaCl solutions by Brady and coworkers, and
- Transport studies using intact core samples of Culebra rock by Lucero and coworkers.

Brush (1996) compiled and evaluated sorption data from these sources, and DOE used the selected K_d values in the CCA PA and CCA PAVT (Table 9-1). Brush and Storz (1996) subsequently updated these values because of slight errors in the calculated K_d values. Brush (1996) and Brush and Storz (1996) provided K_d values for actinide elements for both deep (Castile and Salado) brines and Culebra brines. For conservatism, DOE used only the ranges of K_ds for the brine having the smaller mean value in PA. A uniform distribution was used for all K_d ranges in the CCA PA (Brush 1996; Brush and Storz 1996). Sorption experiments were conducted in the presence of organic ligands, but DOE did not revise the ranges of K_ds to include the potential effects of organic ligands because it assumed that metals present in the waste (such as iron and nickel) would compete with actinides for the organic ligands and would limit the effects of ligands on actinide sorption (Brush 1996, Brush and Storz 1996).

EPA (1998b) evaluated the ranges and distributions of K_d values used in the CCA PA. EPA accepted the ranges used in the CCA PA, but disagreed with the uniform distribution for these ranges. EPA instead specified a log-uniform distribution for the K_d ranges for use in the PAVT.

9.2 DISTRIBUTION COEFFICIENTS USED IN THE CRA-2004 PA, PABC04, AND CRA-2009 PA

The CRA-2004 PA, PABC04, and CRA-2009 PA used the revised K_d ranges from Brush and Storz (1996) (Table 9-1). During the review of the CRA-2004 PA and PABC04, EPA (2006c) evaluated the K_d ranges and log-uniform distribution of the data. Aqueous speciation data and modeling calculations available from the CRA-2004 (EPA 2006c) indicated that solubilities of the +III and +V actinides could be affected by organic ligands. Consequently, EPA (2006c) re-examined the K_d values measured in brines with organic ligands (Brush and Storz 1996).

Table 9-1. Comparison of Matrix K_d Values

K_d Range [m^3/kg]	CCA PA and PAVT (Brush 1996)	CRA-2004 PA, PABC04 and CRA-2009 PA (Brush and Storz 1996)	High Concentration Organics (Brush and Storz 1996)[a]	PABC09, CRA-2014 PA, and CRA-2019 DPA (Clayton 2009)[b]
Am(III)	0.02–0.5	0.02–0.4	0.00505–0.00740	0.005–0.4
Pu(III)	0.02–0.5	0.02–0.4	--	0.005–0.4
Th(IV)	0.9–20	0.7–10	0.000467–0.00469	0.0005–10
U(IV)	0.9–20	0.7–10	--	0.0005–10
Np(IV)	0.9–20	0.7–10	--	0.0005–10
Pu(IV)	0.9–20	0.7–10	--	0.0005–10
Np(V)	0.001–0.2	0.001–0.2	0.00–0.00249	0.00003–0.2
U(VI)	0.00003–0.03	0.00003–0.02	0.00–0.0101	0.00003–0.02

a – SPC brine (Salado) with 0.0489 M acetate, 0.003417 M citrate, 1.1×10^{-5} M EDTA, and 0.00288 M lactate; H-17 brine (Culebra) and ERDA-6 brine (Castile) with 0.0195 M acetate, 0.00340 M citrate, 1.46×10^{-5} M EDTA, and 0.00076 M lactate

b – Log-uniform distribution

Comparison of the K_d ranges used in the CCA PA and PAVT with the ranges used in the CRA-2004 PA, PABC04, and CRA-2009 PA indicated that the differences were small (Table 9-1). Furthermore, these revised K_d ranges are more conservative because the lower K_d values should result in less sorption. EPA (2006c) determined that the revised K_d ranges used in the CRA-2004 PA and PABC04 were acceptable, because no new experimental sorption data were available, the changes to the K_d ranges were minor and conservative and these changes had been previously reviewed and found acceptable by EPA (1998a).

9.3 DISTRIBUTION COEFFICIENTS USED IN THE PABC09 AND CRA-2014 PA

The CRA-2009 PA used the same ranges of K_d values and distributions as the CRA-2004 PA and PABC04 (DOE 2009, Appendix PA). However, higher organic ligand concentrations were predicted for the PABC09 than for previous PAs (Table 7-2). EPA (2010b) found that the predicted acetate and citrate concentrations for the PABC09 were similar to concentrations in the high-ligand-concentration experiments Brush and Storz (1996) reported, and the predicted EDTA concentration exceeded the concentrations reported for the high-ligand-concentration experiments. EPA (2010b) concluded that the effects of organic ligands on the transport of Np(V) or U(VI) through the Culebra are not likely to be significant for PA. However, EPA (2010b) observed that the Am(III) and Th(IV) K_d ranges measured in experiments with high concentrations of organic ligands were significantly lower than the K_d ranges used in the CCA PAVT, PABC04, and CRA-2009 PA calculations. EPA consequently requested additional information from DOE regarding the possible effects of increased ligand concentrations and lower K_d values on +III and +IV actinide releases by transport through the Culebra (Cotsworth 2009b).

DOE re-evaluated the range of K_d values used to assess retardation of actinides during transport through the Culebra (Clayton 2009, Moody 2010). There was no evidence that the upper bound should be changed. Consequently, the upper bounds for the K_d ranges were maintained, but the lower bounds were reduced for the PABC09 to account for the possibility of higher organic ligand concentrations (Table 9-1).

The K_d ranges sampled for the PABC09 were also used for the CRA-2014 PA (DOE 2014, Appendix PA, Table PA-1). During review of the CRA-2014, EPA requested that DOE assess the possible effects on the K_d ranges of changed organic ligand concentrations since the PABC09 (Edwards 2014) and DOE responded with an assessment of the organic ligand inventory changes (Franco 2015a). The acetate, citrate and EDTA concentrations calculated for the CRA-2014 PA were consistent with the concentrations used for the PABC09 (Table 7-2). Oxalate concentrations for all brine volumes were higher in the CRA-2014 PA than in the PABC09. However, because aqueous speciation calculations indicate that oxalate is likely to precipitate as the Ca-oxalate solid whewellite and is unlikely to affect actinide speciation in WIPP brines (Brush and Domski 2013b), oxalate is not expected to significantly affect sorption in the Culebra. Additionally, the lower bounds of the sampled K_d ranges are quite low (Table 9-1), which would maximize Culebra transport.

9.4 DISTRIBUTION COEFFICIENTS USED IN THE CRA-2019 DPA

The K_d ranges sampled for the PABC09 were also used for the CRA-2019 DPA (Kim and Feng 2019). Because the CRA-2019 DPA concentrations of acetate, citrate, and EDTA in WIPP repository brines (Table 7-2) are consistent with the high-organic-ligand concentrations used in the Brush and Storz (1996) experiments, the K_d ranges sampled for the PABC09 and CRA-2014 PA continue to be appropriate for the CRA-2019 DPA.

Emerson et al. (2018) evaluated the effects of ionic strength on Nd(III) retention by Culebra Dolomite. Batch adsorption and column experiments were conducted from 0.01 M to 5 M NaCl. Experimental results indicated that adsorption may not be affected by ionic strength and resulted in K_d values of greater than 3,000 ml/g (3 m^3/kg). The K_d values measured by Emerson et al. (2018) were higher than the 0.005–0.4 m^3/kg range sampled for Am(III) for the CRA-2019 DPA. However, the experiments did not evaluate the possible effects of organic ligands such as EDTA, and EPA agrees that the K_d values calculated from these experiments should not be used in PA calculations.

9.5 CULEBRA DOLOMITE DISTRIBUTION COEFFICIENTS CONCLUSIONS

Radionuclides may reach the Culebra Dolomite, the most transmissive member of the Rustler Formation through brine flow up a borehole. After brine containing radionuclides enters the Culebra Dolomite, the radionuclide concentrations will be affected by sorption onto the minerals during flow along the pathway to the LWB.

Sorption data were collected from experiments using Culebra Dolomite and used to calculate K_d values for simulations of transport through the Culebra Dolomite. The K_d values used in the CRA-2019 DPA remain the same as those used in the PABC09 and CRA-2014 PA and reflect the effects of higher organic ligands concentrations on actinide sorption. These K_d values likely provide a conservative assessment of actinide transport and continue to remain appropriate.

10.0 HETEROGENEOUS WASTE LOADING

WIPP PA calculations include the assumption that waste will be homogeneously loaded in the repository. At the time of the CCA, no information was available regarding the potential patterns of waste loading that might occur, and this assumption was appropriate. However, EPA noted during its review of the CRA-2004 PA that Panel 1 waste loading information showed that the assumption of homogeneity was incorrect. Because shipments of waste placed in Panel 1 included an intensive campaign of waste shipments from the Rocky Flats site, 54% of the waste in Panel 1 was from that site (Leigh 2003).

EPA (2006c) evaluated the potential effects of waste heterogeneity on the results of PA. This evaluation included the potential effects on actinide solubility calculations and the MgO excess factor (EF) calculations (see Section 4.6.1). As described in Section 4.6.6, DOE accounts for the effects of heterogeneous waste loading on the MgO EF by implementing an approved emplacement plan that ensures the required minimum EF is maintained. Klein (2018) provided data showing that as of the inventory cutoff date of December 31, 2017, the EF values in all waste rooms exceeded the required minimum value of 1.2.

During review of the CRA-2004 PA, EPA requested additional information from DOE regarding the potential effects of heterogeneous waste loading on the assumption of homogeneous chemical conditions throughout the entire repository (Cotsworth 2004a). DOE responded with an assessment of the potential effects of higher amounts of plutonium in Panel 1 than would be expected from homogeneous emplacement throughout a 10-panel repository (Detwiler 2004c). DOE stated that the only likely effect of this higher-than-expected loading of plutonium in Panel 1 would be increased radiolysis. However, because of microbial consumption of CPR and the amounts of metallic iron in the repository, DOE stated that reducing conditions and lower plutonium oxidation states would still be maintained in Panel 1.

The panel closures are expected to have extremely low permeabilities (Camphouse et al. 2012) and will effectively limit the contact of brine between panels. Heterogeneous waste loading is unlikely to affect actinide solubilities if a relatively high proportion of the actinide inventory is present in a single panel, because of the assumption of chemical equilibrium with respect to the solubilities of actinide solid phases. However, the placement of waste with a high proportion of the organic ligand inventory in a panel could affect actinide solubilities. DOE has accounted for this possibility in the actinide solubility calculations by assuming the entire organic ligand inventory is dissolved in the amount of brine released from the repository (Brush and Domski 2013a). This approach ensures that the effects of heterogeneous waste placement are adequately accounted for in the actinide solubility calculations, provided that the inventory of organic ligands is bounded.

RH waste disposal in shielded containers will increase the steel and lead inventories in panels filled after EPA's approval was received (Edwards 2011, 2013). The total CRA-2019 DPA scaled number of shielded containers in the repository at closure is 31,942 (LANL-CO 2018). Because only nine shielded containers were placed in WIPP as of December 31, 2017 (Knerr 2021g), almost all shielded containers will be placed in the remaining unfilled panels. The mass of steel per shielded container is relatively high compared to other waste containers, but the steel surface area to tare weight ratio is relatively low (Day 2015), which will limit increased gas

generation due to anoxic steel corrosion in panels with higher numbers of shielded containers. The increased mass of lead associated with the shielded containers was found to be an insignificant contributor to overall gas generation rates compared to steel corrosion, because of the lower lead corrosion rate and surface area (Section 3.2.1). Consequently, it is reasonable to assume that segregation of the shielded containers into a few panels will not significantly affect overall gas generation rates in those panels due to increased lead and steel corrosion.

The SR-KAC-PuOx waste stream is plutonium that has been declared as excess to U.S. needs and includes surplus weapons-grade plutonium that will be blended and packaged for disposal at WIPP. The projected final form volume of SR-KAC-PuOx is about 3.5% of the total WIPP waste volume, but this waste stream contains about 29% of the total EPA units at the time of repository closure, and about 42% of the total EPA units at 10,000 years post-closure (Zeitler et al. 2019). At the time of the CRA-2019, SR-KAC-PuOx was projected waste, meaning it had not yet been generated but was estimated to be generated through calendar year 2033. This waste will therefore be placed in the remaining unfilled panels, and because it is a single waste stream, it may be placed in a small number of panels. The radionuclides ^{241}Am, ^{238}Pu, ^{239}Pu, ^{240}Pu, and ^{242}Pu represent greater than 96% of the decay heat in the WIPP inventory and are expected to represent the most important contributors to radiolytic gas generation (Kicker 2019b). SR-KAC-PuOx will contain approximately 30% of the total 2033 inventory (in Ci) of these five radionuclides, so a significant fraction of the modeled radiolytic brine consumption and gas generation could occur in relatively few panels, which may significantly affect DBRs and spallings releases from these panels. For future WIPP PAs, EPA expects DOE to evaluate whether the PA calculations adequately address the effects on releases of placement of this waste stream in a limited number of panels.

In summary:

- The effects of heterogenous waste loading are unlikely to significantly affect actinide solubilities because of the assumption of chemical equilibrium between brine and actinide solid phases.
- DOE accounts for organic ligands by dissolving the entire inventory in the amount of brine released from the repository.
- Because a large number of shielded containers will be emplaced in currently unfilled panels, these panels will contain relatively large inventories of lead and steel. Because the steel surface area to tare weight ratio is relatively low for shielded containers, the increased mass of steel in these panels is unlikely to significantly increase gas generation rates. Relatively low lead corrosion rates and a low surface area to mass ratio for lead in the shielded containers will also limit the effects of lead corrosion on gas generation rates in panels with large numbers of shielded containers.
- The SR-KAC-PuOx waste stream contains approximately 30% of the radionuclides that account for radiolytic gas generation and brine consumption in WIPP PA. This waste stream represents about 3.5% of the total waste volume and could be placed in a limited number of panels. EPA expects DOE to evaluate whether the current PA calculations

adequately address the effects on repository releases if this waste form is placed in a limited number of panels.

11.0 EFFECTS OF CHEMICAL PROCESSES ON REPOSITORY WATER BALANCE

Chemical processes that may affect the quantity of water in the repository include microbial degradation of CPR, MgO hydration to form brucite or hydromagnesite, dehydration of hydromagnesite to form magnesite, anoxic corrosion of iron-based metal or other metals, and brine radiolysis. For the CCA PAVT, PABC04, and PABC09, brine consumption from anoxic corrosion of iron-based metal was the only chemical process included in the repository water balance. SC&A (2008b) qualitatively evaluated the possible effects of various chemical processes on brine generation and consumption, and concluded that the potential importance of CPR degradation, MgO hydration and carbonation, and FeS precipitation on the repository water balance warranted additional evaluation.

EPA observed during its review of the CRA-2009 (DOE 2009) that the potential effects of processes other than anoxic corrosion on the repository water balance had not been addressed (Cotsworth 2009a). EPA requested additional information from DOE regarding whether production of water by CPR degradation and consumption of water by brucite hydration and hydromagnesite persistence might significantly affect predicted repository performance. DOE acknowledged the potential for water consumption or production with reactions involving magnesium-based minerals and microbial degradation of CPR (Moody 2009a). DOE concluded that although it would be appropriate to include all water balance considerations in future WIPP PA calculations, the uncertainties associated with water balance changes caused by brucite hydration, hydromagnesite persistence in the repository, and production of water by CPR degradation precluded adding these processes to the repository water balance calculations at that time. EPA (2010b) agreed that this conclusion was reasonable, but recommended DOE continue evaluating the effects of chemical processes on the repository water balance for the CRA-2014.

For the CRA-2014 PA, DOE (2014) modified the repository water balance to include multiple chemical processes. In addition to the flow of water in and out of the repository, the chemical processes in the revised water balance included brine consumption by anoxic corrosion of iron-based metals, brine production by sulfidation of iron-based metals, brine production by microbial degradation of CPR materials, brine consumption by MgO hydration, and brine production by hydromagnesite conversion to magnesite. Camphouse (2013b) summarized the reactions included in the water balance and Clayton (2013) provided justification for the implementation and stoichiometric coefficients for the water balance. During review of the CRA-2014, Bryson (2015) found that repository releases were not sensitive to water balance calculation changes.

Brine consumption and production in the CRA-2019 DPA is addressed in Appendix GEOCHEM (DOE 2019). Brine consumption by radiolysis was included in the water balance calculations for the CRA-2019 DPA in addition to brine consumption by anoxic corrosion of iron-based metals, brine production by microbial degradation of CPR materials, brine consumption by MgO hydration, and brine production by hydromagnesite conversion to magnesite. Brine production by sulfidation of iron-based metals was not included in the CRA-2019 DPA in response to EPA comments during review of the CRA-2014 (Section 3.1.3). Gas generation and brine consumption by lead corrosion continues to be screened out for the CRA-2019 DPA (Section 3.2.1).

11.1 ANOXIC CORROSION AND SULFIDATION OF IRON-BASED METALS

Anoxic corrosion consumes water, which has been accounted for in all WIPP PAs. Brine consumption through anoxic corrosion occurs via the reaction:

$$Fe(s) + 2\ H_2O(l) \rightarrow Fe(OH)_2(s) + H_2(g) \quad \textbf{(36)}$$

Reaction (36) results in the consumption of two moles of water for each mole of iron consumed. The rates of this anoxic corrosion reaction in humid and inundated conditions are based on sampled parameters (Section 3.1.2). The brine consumption rates from anoxic corrosion of iron-based metals were increased relative to the CRA-2014 PA because the inundated corrosion rate was increased to account for the effects of high gas pressures (Section 3.1.2).

For the CRA-2014 PA, DOE assumed that H_2S created by CPR degradation [reaction (12)] preferentially reacts with iron hydroxide [reaction (7)] versus metallic iron [reaction (2)]. The assumption that H_2S preferentially reacts with $Fe(OH)_2(s)$ increases brine production and decreases gas production compared to the assumption that all or some of the H_2S reacts with metallic iron. After discussion with EPA during review of the CRA-2014 PA, DOE agreed to remove reactions (2) and (7) from calculations of the water balance and gas production in PA (Section 3.1.3). DOE removed the iron sulfidation reactions (2) and (7) by setting the stoichiometric parameters REFCON:STCO_31 and REFCON:STCO_32 to zero (DOE 2019 Appendix PA Section PA-1.1.9, Kim and Feng 2019). Removing reaction (7) from PA calculations increases the amount of gas in the repository and decreases the amount of brine.

Water Balance Reactions

$Fe(s) + H_2S(g) \leftrightharpoons FeS(s) + H_2(g)$	(2)
$Fe(OH)_2(s) + H_2S(g) \leftrightharpoons FeS(s) + 2\ H_2O(l)$	(7)
$Pb(s) + H_2O(l) \leftrightharpoons PbO(s) + H_2(g)$	(10)
$C_6H_{10}O_5 + 4.8\ H^+ + 4.8\ NO_3^- \rightarrow 7.4\ H_2O(l) + 6\ CO_2(g) + 2.4\ N_2(g)$	(11)
$C_6H_{10}O_5 + 6\ H^+ + 3\ SO_4^{2-} \rightarrow 5\ H_2O(l) + 6\ CO_2(g) + 3\ H_2S(g)$	(12)
$MgO(s) + H_2O(l) \leftrightharpoons Mg(OH)_2(s)$	(18)
$3\ MgO(s) + 6\ H_2O(l) + H^+ + Cl^- \leftrightharpoons Mg_3(OH)_5Cl{\bullet}4H_2O(s)$	(19)
$Mg_5(CO_3)_4(OH)_2{\bullet}4H_2O(s) + CO_2(g) \leftrightharpoons 5\ MgCO_3(s) + 5\ H_2O(l)$	(25)
$Fe(s) + 2\ H_2O(l) \rightarrow Fe(OH)_2(s) + H_2(g)$	(36)

11.2 LEAD CORROSION

EPA requested additional information related to effects of the increased CRA-2019 DPA lead inventory from shielded RH waste containers on gas generation and the water balance (Peake 2020e, Comment CC5-SCR-9). DOE's response to this comment (Knerr 2021c) is discussed in

detail as part of the gas generation evaluation (Section 3.2.1). The calculations provided by Knerr (2021c) showed that gas generation from lead corrosion, and by extension brine consumption via reaction (10), would be small relative to other processes including iron corrosion.

11.3 MICROBIAL DEGRADATION OF CPR

DOE used the CPR microbial degradation reactions (11) and (12) and rate parameters used to calculate gas generation for the CRA-2019 DPA (Tables 3-5 and 3-6) to calculate the production of water by CPR degradation (DOE 2019, Appendix GEOCHEM). Because the moles of water produced differs for reaction (11) and reaction (12), DOE uses the average stoichiometry model (Wang and Brush 1996) to calculate the production of gas and water by CPR degradation:

$$[C_6H_{10}O_5]/6 + \text{microbes} \rightarrow y\ H_2(g) + z\ H_2O(l) + \text{unknowns} \quad \textbf{(37)}$$

Clayton (2013) describes the calculation of y and z in equation (37) using the maximum amount of CPR that can be degraded within 10,000 years in a particular vector and the potential amounts of CPR that can be degraded by denitrification reaction (11) and sulfate reduction reaction (12). This approach adequately incorporates the effects of CPR degradation on water balance.

11.4 BACKFILL REACTIONS

The MgO backfill reactions included in the water balance are: 1) MgO hydration to form brucite, reaction (18), which consumes water; 2) the carbonation of brucite to form hydromagnesite, reaction (23), which does not consume or produce water; and 3) conversion of hydromagnesite to magnesite, reaction (25), which produces water (DOE 2019, Appendix GEOCHEM). Formation of Phase 5 from MgO, reaction (19), is not included in the CRA-2019 DPA water balance.

11.4.1 MgO Hydration Rate

The CRA-2019 DPA parameters used to represent the rate of MgO hydration to brucite, reaction (18), were WAS_AREA:BRUCITEC in ERDA-6 brine, WAS_AREA:BRUCITES in GWB brine, and WAS_AREA:BRUCITEH under humid conditions. Clayton (2013) developed these parameters using MgO hydration rates and associated uncertainties for each brine type developed by Nowak and Clayton (2007). The MgO hydration rate data were based on experiments conducted with Premier MgO, whereas MgO in the repository has been provided by three vendors, with a relatively small amount from National Magnesia Chemicals and larger amounts from Premier Chemicals and Martin Marietta Magnesia. Martin Marietta MgO represents the largest fraction of the MgO currently emplaced in the repository and the proportion of this material has become more significant over time because Martin Marietta is the current MgO supplier.

Preliminary tests with Martin Marietta MgO showed that it reacted to form brucite faster than Premier MgO (Wall 2005), so using a hydration rate obtained only with Premier MgO underestimates the MgO hydration rate and overestimates the amount of brine in the repository. Deng et al. (2009) reported initial results of Martin Marietta MgO hydration experiments, but further results from these experiments have not been reported. Sensitivity analyses performed for

the CRA-2014 PA indicated that repository releases were not sensitive to the MgO hydration rates (Kirchner 2013). However, it is possible that higher MgO hydration rates consistent with the presence of Martin Marietta MgO could affect the amounts of brine in the repository and affect repository performance under some conditions.

After a discussion of the status of the Martin Marietta MgO hydration rate experiments at an EPA/DOE technical exchange meeting, DOE committed to combining Martin Marietta MgO hydration rate data with Premier MgO hydration rate data for use in future WIPP PAs (Shrader 2016). This update to the MgO hydration rate was not included in the CRA-2019 DPA, and DOE used the CRA-2014 PA MgO hydration rate parameters to calculate the repository water balance.

MgO hydration to produce Phase 5 has been observed in experiments with GWB brine, and its precipitation was predicted from GWB and ERDA-6 brines in the CRA-2019 DPA actinide solubility calculations (Table 7-4). Precipitation of Phase 5 instead of brucite consumes twice as much water per mole of MgO via reactions (18) and (19), so formation of significant amounts of Phase 5 instead of brucite would increase brine consumption. DOE should address the possible formation of significant quantities of Phase 5 by re-evaluating its solubility as well as investigating its formation in Martin Marietta MgO hydration experiments.

11.4.2 MgO and Brucite Carbonation Rates

The reaction rates for the MgO and brucite carbonation reactions are defined by the sampled CPR degradation rate because the available CO_2 is produced by CPR degradation. The Gas Generation conceptual model includes the assumption that essentially all CO_2 is rapidly consumed by reaction with the MgO backfill (SC&A 2008b). DOE assumed for the CRA-2014 PA and CRA-2019 DPA that CO_2 preferentially reacts with brucite instead of unreacted MgO.

For the stoichiometric coefficients used in PA, the brucite carbonation reaction was normalized by Clayton (2013) to the moles of CO_2:

$$1.25\ Mg(OH)_2(s) + CO_2(g) \rightarrow 0.25\ Mg_5(CO_3)_4(OH)_2{\bullet}4H_2O(s) \quad \textbf{(38)}$$

EPA observed that assuming CO_2 preferentially reacts with brucite instead of with MgO:

$$1.25\ MgO(s) + CO_2(g) + 1.25\ H_2O(l) \rightarrow 0.25\ Mg_5(CO_3)_4(OH)_2{\bullet}4H_2O(s) \quad \textbf{(39)}$$

increases brine in the repository because more brine is consumed by reaction (39) than by reaction (38). In response, DOE cited WIPP-specific experiments that support the assumption that brucite to hydromagnesite is the reasonably expected pathway for carbonation (EPA 2017d).

Clayton (2013) also assumed that if CO_2 generation occurs in the repository but brucite is not available in BRAGFLO simulations, MgO will be converted directly to magnesite. EPA (2017d) questioned this assumption because magnesite is not expected to form directly from MgO in the WIPP repository (Section 4.1). DOE showed in its response that the maximum potential decrease in water is 0.081 m^3, which is insignificant to the overall water balance (EPA 2017d).

11.4.3 Hydromagnesite Conversion Rate

DOE (Clayton 2013) formulated the conversion reaction from hydromagnesite to magnesite for inclusion in the BRAGFLO calculations as:

$$Mg_5(CO_3)_4(OH)_2{\bullet}4H_2O(s) \rightarrow 4\ MgCO_3(s) + Mg(OH)_2(s) + 4\ H_2O(l) \quad \textbf{(40)}$$

Clayton (2013) calculated the range for the hydromagnesite conversion rate used in the CRA-2014 PA using reaction times of 100 years to 10,000 years (Table 11-1). EPA (2017d) reviewed the available experimental and natural analogue data and found that the rate of hydromagnesite to magnesite conversion in WIPP could be sufficiently slow to cause the persistence of hydromagnesite throughout all of the 10,000-year regulatory period. EPA (2017d) determined that the sampled hydromagnesite conversion rate range should be established assuming that the most rapid conversion would result in complete conversion in 200 years, and ranging to no conversion during the 10,000-year regulatory period. DOE used these rates, which are summarized in Table 11-1, in the CRA-2019 DPA with a sampled uniform distribution (DOE 2019, Appendix GEOCHEM; Kim and Feng 2019).

Table 11-1. Hydromagnesite Conversion Rates (parameter WAS_AREA:HYMAGCON)

Minimum Rate (mol kg^{-1} sec^{-1})	Maximum Rate (mol kg^{-1} sec^{-1})	Reaction Time (years)	Source
6.8×10^{-12}	6.8×10^{-10}	100 – 10,000	CRA-2014 PA (Clayton 2013)
0	3.4×10^{-10}	200 – infinite	CRA-2019 DPA (EPA 2017d)

11.5 BRINE RADIOLYSIS

As discussed in Section 3.6, brine radiolysis by wetted solid, dissolved, and colloidal radionuclides on gas generation was included in the CRA-2019 DPA. Gas generation through brine radiolysis consumes water and produces $H_2(g)$, and the moles of H_2O consumed are approximately equal to the moles of H_2 produced. DOE discussed the effects of radiolysis on gas generation rates in the CRA-2019 DPA, but did not address the effects of radiolysis on brine consumption (DOE 2019, Appendix GEOCHEM). Day (2019b) and Zeitler et al. (2019) discussed the parameters GLOBAL:GDEPFAC, GLOBAL:DECAYNRG, and GLOBAL:GH2AVG for calculating $H_2(g)$ generation rates through brine radiolysis, but Day (2019b) only parenthetically mentioned brine consumption and Zeitler et al. (2019) did not discuss radiolytic brine consumption. EPA requested that DOE clarify whether brine consumption through radiolysis was included in CRA-2019 DPA calculations of brine volumes (Peake 2020f, Comment CC6-GEOCHEM-35).

Knerr (2021b) confirmed that radiolytic brine consumption was included in CRA-2019 DPA brine volume calculations, and that the amount of H_2O consumed was equal to the amount of $H_2(g)$ produced. A revised equation describing the modeled rates of brine production and consumption was also provided to replace the equation that omitted radiolytic brine consumption (DOE 2019, Appendix GEOCHEM).

11.6 TOTAL BRINE CONSUMPTION RATE

Multiple chemical processes affect the amount of brine in the WIPP repository. Processes that produce brine include conversion of hydromagnesite to magnesite and microbial degradation of CPR. Brine is consumed by anoxic corrosion of iron-based metals, hydration of MgO to brucite and Phase 5, and brine radiolysis. Knerr (2021b) provided a revised equation that summarizes the effects of these processes on the total brine production rate (q_{rb}):

$$q_{rb} = q_{rbc} + q_{rbs} + q_{rbm} + q_{rbh} + q_{rbhc} + q_{rbr} \quad \textbf{(41)}$$

This equation accounts for the rates of brine consumption and production by corrosion of iron-based metals (q_{rbc}), iron sulfidation reactions (q_{rbs}), microbial degradation of CPR materials (q_{rbm}), MgO hydration (q_{rbh}), hydromagnesite conversion to magnesite (q_{rbhc}), and brine radiolysis (q_{rbr}).

11.7 WATER BALANCE SUMMARY AND CONCLUSIONS

Changes made to the water balance calculations since the CRA-2014 PA in response to EPA comments include elimination of brine production by sulfidation of iron-based metals, increased inundated anoxic steel corrosion rates, and a revised sampled range for the hydromagnesite conversion rate. Brine consumption by radiolysis was added to the CRA-2019 DPA calculations because of the expected effects of the increased CRA-2019 DPA radionuclide inventory.

Conclusions reached during EPA review of the water balance calculations include:

- The MgO hydration rates used in the water balance calculations are based on data from Premier MgO, which is present in smaller quantities than Martin Marietta MgO and also hydrates more slowly. Because higher MgO hydration rates might affect the amounts of brine in the repository and its performance, it would be appropriate for DOE to develop hydration rates using Martin Marietta MgO and use these rates with Premier MgO hydration rates in future WIPP PA water balance calculations.
- MgO hydration to produce Phase 5 consumes more water than MgO hydration to brucite. DOE should assess the possible formation of significant quantities of Phase 5 and the effects on water balance by evaluating the Phase 5 solubility data and investigating its formation in Martin Marietta MgO hydration experiments.
- EPA expects DOE to evaluate the potential for gas generation by radiolysis of adsorbed water for future WIPP PAs. EPA also expects that if this process is found to be a potentially significant source of gas generation, its effects on brine consumption will also be considered in calculations for future WIPP PAs.

A sensitivity study performed during review of the CRA-2014 indicated that repository releases are minimally affected by changes in the water balance calculations (Bryson 2015). The issues identified by EPA with the CRA-2019 DPA water balance are therefore expected to have reasonably small effects on repository performance.

12.0 TOTAL MOBILIZED ACTINIDE CALCULATIONS FOR PA

The total mobilized actinide concentration in WIPP brines is defined for PA as the sum of the dissolved actinide concentrations and the colloidal actinide concentrations. DOE (2019, Appendix PA) summarized the information required to calculate the dissolved and colloidal actinide concentrations for each PA realization:

- Whether the scenario uses the Salado or Castile end-member brine composition;
- The baseline dissolved concentrations of +III, +IV, +V, and +VI actinides in the brine;
- Sampled uncertainty values for the +III and +IV actinide solubilities;[9]
- Whether actinides with multiple possible oxidation states are present in their relatively reduced [U(IV), Np(IV), and Pu(III)] or relatively oxidized [U(VI), Np(V), and Pu(IV)] oxidation states;
- The constant concentrations of intrinsic and mineral-fragment colloids;
- The proportionality constants and maximum concentrations of humic and microbial colloid actinides; and
- The total inventory of the actinide.

EPA has identified issues related to some of the CRA-2019 DPA chemistry parameters. The effects of these parameter changes on the calculation of mean total mobilized actinides are evaluated to determine whether these parameters could significantly affect predicted repository performance.

12.1 CRA-2014 PA AND CRA-2019 DPA TOTAL MOBILIZED ACTINIDES

DOE (2019, Appendix PA) discusses the actinide source term calculations and provides example calculations of actinide solubility and colloidal actinides for the CRA-2019 DPA. Table SOTERM-32 (DOE 2019, Appendix SOTERM) summarizes dissolved and colloidal actinide concentrations calculated using median parameter values for the CRA-2019 DPA. The dissolved, colloidal, and total mobilized actinides calculated using median parameter values are also compared for the CCA PAVT, PABC04, PABC09, CRA-2014 PA, and CRA-2019 DPA in Table SOTERM-33.

Sarathi (2019a) provides additional information regarding calculations of actinide mobilization for the CRA-2019 DPA. Changes between the CRA-2014 PA and CRA-2019 DPA that affected actinide solubilities and colloidal actinide concentrations included:

- Updated organic ligands inventory,
- EQ3/6 database revisions,
- Updated +III and +IV actinide solubility uncertainty distributions,

[9] Neptunium, which is the only actinide predicted in repository brines in the +V state, does not have a significant effect on PA because of its low number of curies in the inventory (see Section 5.0). An upper-limit concentration is used for U(VI), which is the only +VI actinide predicted in WIPP brines. Consequently, uncertainty distributions for Np(V) and U(VI) were not developed or sampled for the CRA-2019 DPA.

- Revised intrinsic colloid concentrations,
- Revised proportionality constants for humic colloids,
- Revised proportionality constants and maximum concentration limits for microbial colloids, and
- Modified equation used to calculate the concentration limit for actinides associated with mobile microbial colloids to be consistent with current basis for this parameter.

Sarathi (2019a, Figure 14) compares total actinide mobilization by element for the CRA-2014 PA and CRA-2019 DPA, with total actinide mobilization separated according to redox conditions in Figure 15. Am(III), Pu(III), and Pu(IV) median and mean total mobilized concentrations decreased in the CRA-2019 DPA relative to the CRA-2014 PA, and overall total mobile radioactivity concentrations decreased (Sarathi 2019a).

During the CRA-2019 DPA review, EPA calculated the mean total mobilized actinide concentrations using DOE's CRA-2019 DPA parameters, including DOE's EQ3/6-calculated baseline dissolved actinide concentrations for the minimum brine volume (Domski and Sisk-Scott 2019), mean values for the +III and +IV actinide uncertainty distributions (Domski 2019d), mineral fragment and intrinsic colloid concentrations, and humic and microbial colloidal actinide concentrations calculated using the baseline solubilities and mean actinide solubility uncertainties, colloidal proportionality constants, and maximum colloidal concentrations. The results of EPA's calculations using the CRA-2019 DPA parameters are summarized in Table 12-1. In GWB and ERDA-6 brine, mean total mobilized Am(III) and Pu(III) concentrations are dominated by dissolved species, with the next-largest concentrations associated with humic colloids. For both GWB and ERDA-6 brine, Am(III) and Pu(III) concentrations associated with microbial colloids are limited by the maximum concentration.

Dissolved Th(IV), Np(IV), and Pu(IV) concentrations represent 40% of the CRA-2019 DPA mean total mobilized concentrations for these oxidation states (Table 12-1). For these actinide oxidation states, intrinsic colloids contribute 32% of the mean total mobilized actinide concentrations, with smaller contributions from mineral fragment colloids (19%) and microbial colloids (8%). The mean total mobilized concentration of U(IV) is primarily attributed to intrinsic colloids. Mean total mobilized Np(V) is dominated by dissolved species, with smaller contributions from intrinsic, mineral fragment, and microbial colloids. The total mobilized U(VI) concentration is dominated by dissolved species.

Table 12-2 provides the mean dissolved, colloidal, and total mobilized actinide concentrations calculated by EPA for the CRA-2014 PA. CRA-2019 DPA mean total mobilized Am(III) concentrations increased slightly relative to CRA-2014 PA results because of the increased mean solubility uncertainty parameter (SOLVAR), which offset decreased baseline solubilities and microbial colloid concentrations in the CRA-2019 DPA. CRA-2019 DPA mean total mobilized Pu(III) concentrations decreased slightly compared to the CRA-2014 PA because of the decreased microbial colloid concentration limit (PU:CAPMIC).

CRA-2019 DPA mean total mobilized +IV actinide concentrations decreased relative to the CRA-2014 PA concentrations because of a significant decrease in the mean +IV actinide solubility uncertainty parameter (SOLVAR) and decreased humic colloid proportionality constants (PHUMSIM and PHUMCIM). The decrease in the mean total mobilized U(IV)

concentrations was smaller than for the other +IV actinides because of the increased CRA-2019 DPA intrinsic colloid concentration for uranium. CRA-2019 DPA mean total mobilized Np(V) actinide concentrations decreased relative to the CRA-2014 PA concentrations because of a decreased proportionality constant for microbial colloids (PROPMIC).

Sarathi (2019a) observed that the inventory screening process for including radionuclides in PA calculations is appropriate for solids releases. However, there may be circumstances in which radionuclides that comprise a small portion of the total inventory may comprise a large portion of the radioactivity in contaminated brine because of differences in solubilities of the radionuclides. Sarathi (2019a) performed a screening calculation for DBR that assumed that the entire unaccounted-for inventory at year 100 of 2.8 EPA units dissolves in the minimum brine volume necessary for a DBR and the maximum DBR volume of 200 m^3. The unaccounted DBR release was calculated to be approximately 0.02 EPA units per DBR occurrence, which is unlikely to significantly affect the demonstration of compliance. Sarathi (2019a) noted that the effects of the unaccounted-for inventory on releases through the Culebra are more complex, and stated that an upcoming memo would address this potential issue.

12.2 EPA RECALCULATIONS OF TOTAL MOBILIZED ACTINIDES

EPA identified issues related to the CRA-2019 DPA baseline actinide solubility parameters (Section 7.4.10), Th(IV) and Am(III) intrinsic colloid parameters, and microbial colloid parameters (Sections 8.1.9 and 8.3.5). To evaluate the sensitivity of the mean total mobilized actinides to these parameters, EPA recalculated mean total mobilized actinides (Table 12-3) using baseline actinide solubilities that were recalculated to account for DATA0.FM4 issues (Section 7.4.10) and EPA's revised intrinsic and microbial colloid parameters (Sections 8.1.9 and 8.3.5). The results of these calculations demonstrate the effects of these parameter changes on predicted actinide concentrations mobilized in WIPP brines, and indicates whether these changes are likely to affect predicted repository releases. The sensitivity of predicted repository releases to these parameter changes is addressed in Section 13.0.

Total mobilized Am(III) and Pu(III) concentrations are significantly increased in the EPA calculations (Table 12-3) by higher mean solubilities compared to the CRA-2019 DPA (Table 12-1). The higher mean dissolved +III actinide concentrations in the EPA calculations contribute to increased humic colloid and microbial colloid concentrations. The microbial colloid concentrations for Am(III) and Pu(III) are also higher in the EPA calculations because of increased microbial colloid proportionality constants (PROPMIC) and concentration limits (CAPMIC). The results of the EPA calculations show that Am(III) and Pu(III) are mostly mobilized as dissolved species and microbial colloids (Table 12-3). Because of the importance of americium and plutonium isotopes to repository releases, the +III baseline solubility and microbial colloid parameters are likely to affect predicted repository releases.

The total mobilized Th(IV) concentration in the EPA calculations (Table 12-3) is increased relative to the CRA-2019 DPA (Table 12-1) by higher concentrations associated with intrinsic and microbial colloids. The higher Th(IV) microbial colloid concentration is caused by a higher Th(IV) proportionality constant for microbial colloids in the EPA calculations. Th(IV) is primarily mobilized as intrinsic and microbial colloids in the EPA calculations.

Table 12-1. CRA-2019 DPA Mean Dissolved, Colloidal, and Total Mobilized Actinides

Radionuclide and Oxidation State	Brine	Baseline Dissolved Concentration (M)	Mean SOLVAR (Domski 2019d)	Mean Solubility (M)	Mineral Fragment Colloids (M)	Intrinsic Colloids (M)	Humic Colloids (M)	Microbial Colloids (M)	Total Colloidal (M)	Total Mobilized (M)
Am(III)	GWB	1.63×10^{-7}	0.651	7.30×10^{-7} (80%)	2.60×10^{-8}	9.50×10^{-9}	1.46×10^{-7}	2.30×10^{-9} [c]	1.84×10^{-7} (20%)	9.14×10^{-7}
Pu(III)	GWB	1.63×10^{-7}	0.651	7.30×10^{-7} (74%)	2.60×10^{-8}	4.30×10^{-8}	1.46×10^{-7}	3.80×10^{-8} [c]	2.53×10^{-7} (26%)	9.83×10^{-7}
Th(IV)	GWB	5.45×10^{-8}	-0.011	5.31×10^{-8} (40%)	2.60×10^{-8}	4.30×10^{-8}	5.31×10^{-10}	1.12×10^{-8}	8.07×10^{-8} (60%)	1.34×10^{-7}
U(IV)	GWB	5.45×10^{-8}	-0.011	5.31×10^{-8} (4%)	2.60×10^{-8}	1.40×10^{-6}	5.31×10^{-10}	1.12×10^{-8}	1.44×10^{-6} (96%)	1.49×10^{-6}
Np(IV)	GWB	5.45×10^{-8}	-0.011	5.31×10^{-8} (40%)	2.60×10^{-8}	4.30×10^{-8}	5.31×10^{-10}	1.12×10^{-8}	8.07×10^{-8} (60%)	1.34×10^{-7}
Pu(IV)	GWB	5.45×10^{-8}	-0.011	5.31×10^{-8} (40%)	2.60×10^{-8}	4.30×10^{-8}	5.31×10^{-10}	1.12×10^{-8}	8.07×10^{-8} (60%)	1.34×10^{-7}
Np(V)	GWB	4.02×10^{-7}	--[a]	4.02×10^{-7} (83%)	2.60×10^{-8}	4.30×10^{-8}	3.66×10^{-10}	1.12×10^{-8}	8.05×10^{-8} (17%)	4.83×10^{-7}
U(VI)	GWB	1.00×10^{-3}	--[a]	1.00×10^{-3} (99%)	2.60×10^{-8}	1.40×10^{-6}	1.10×10^{-5} [b]	3.80×10^{-8} [c]	1.25×10^{-5} (1%)	1.01×10^{-3}
Am(III)	ERDA-6	1.78×10^{-7}	0.651	7.97×10^{-7} (80%)	2.60×10^{-8}	9.50×10^{-9}	1.59×10^{-7}	2.30×10^{-9} [c]	1.97×10^{-7} (20%)	9.94×10^{-7}
Pu(III)	ERDA-6	1.78×10^{-7}	0.651	7.97×10^{-7} (75%)	2.60×10^{-8}	4.30×10^{-8}	1.59×10^{-7}	3.80×10^{-8} [c]	2.66×10^{-7} (25%)	1.06×10^{-6}
Th(IV)	ERDA-6	5.44×10^{-8}	-0.011	5.30×10^{-8} (40%)	2.60×10^{-8}	4.30×10^{-8}	5.30×10^{-10}	1.11×10^{-8}	8.07×10^{-8} (60%)	1.34×10^{-7}
U(IV)	ERDA-6	5.44×10^{-8}	-0.011	5.30×10^{-8} (4%)	2.60×10^{-8}	1.40×10^{-6}	5.30×10^{-10}	1.11×10^{-8}	1.44×10^{-6} (96%)	1.49×10^{-6}
Np(IV)	ERDA-6	5.44×10^{-8}	-0.011	5.30×10^{-8} (40%)	2.60×10^{-8}	4.30×10^{-8}	5.30×10^{-10}	1.11×10^{-8}	8.07×10^{-8} (60%)	1.34×10^{-7}
Pu(IV)	ERDA-6	5.44×10^{-8}	-0.011	5.30×10^{-8} (40%)	2.60×10^{-8}	4.30×10^{-8}	5.30×10^{-10}	1.11×10^{-8}	8.07×10^{-8} (60%)	1.34×10^{-7}
Np(V)	ERDA-6	1.20×10^{-6}	--[a]	1.20×10^{-6} (93%)	2.60×10^{-8}	4.30×10^{-8}	8.88×10^{-9}	1.11×10^{-8}	8.90×10^{-8} (7%)	1.29×10^{-6}
U(VI)	ERDA-6	1.00×10^{-3}	--[a]	1.00×10^{-3} (99%)	2.60×10^{-8}	1.40×10^{-6}	1.10×10^{-5} [b]	3.80×10^{-8} [c]	1.25×10^{-5} (1%)	1.01×10^{-3}

a – Np(V) and U(VI) solubility uncertainty parameters are not sampled for PA
c – CAPHUM value
d – CAPMIC value

Table 12-2. CRA-2014 PA Mean Dissolved, Colloidal, and Total Mobilized Actinides

Radionuclide and Oxidation State	Brine	Baseline Dissolved Concentration (M)	Mean SOLVAR (Brush and Domski 2013c)	Mean Solubility (M)	Mineral Fragment Colloids (M)	Intrinsic Colloids (M)	Humic Colloids (M)	Microbial Colloids (M)	Total Colloidal (M)	Total Mobilized (M)
Am(III)	GWB	2.59×10^{-6}	-0.678	5.44×10^{-7} (77%)	2.60×10^{-8}	4.00×10^{-9}	1.03×10^{-7}	3.10×10^{-8} [d]	1.64×10^{-7} (23%)	7.08×10^{-7}
Pu(III)	GWB	2.59×10^{-6}	-0.678	5.44×10^{-7} (33%)	2.60×10^{-8}	2.00×10^{-8}	1.03×10^{-7}	9.57×10^{-7}	1.11×10^{-6} (67%)	1.65×10^{-6}
Th(IV)	GWB	6.05×10^{-8}	0.673	2.85×10^{-7} (11%)	2.60×10^{-8}	2.00×10^{-8}	1.80×10^{-6}	5.01×10^{-7}	2.34×10^{-6} (89%)	2.63×10^{-6}
U(IV)	GWB	6.05×10^{-8}	0.673	2.85×10^{-7} (11%)	2.60×10^{-8}	2.00×10^{-8}	1.80×10^{-6}	5.01×10^{-7}	2.34×10^{-6} (89%)	2.63×10^{-6}
Np(IV)	GWB	6.05×10^{-8}	0.673	2.85×10^{-7} (11%)	2.60×10^{-8}	2.00×10^{-8}	1.80×10^{-6}	5.01×10^{-7}	2.34×10^{-6} (89%)	2.63×10^{-6}
Pu(IV)	GWB	6.05×10^{-8}	0.673	2.85×10^{-7} (11%)	2.60×10^{-8}	2.00×10^{-8}	1.80×10^{-6}	5.01×10^{-7}	2.34×10^{-6} (89%)	2.63×10^{-6}
Np(V)	GWB	2.77×10^{-7}	--[a]	2.77×10^{-7} (35%)	2.60×10^{-8}	--[b]	2.52×10^{-10}	4.88×10^{-7}	5.14×10^{-7} (65%)	7.91×10^{-7}
U(VI)	GWB	1.00×10^{-3}	--[a]	1.00×10^{-3} (99%)	2.60×10^{-8}	3.00×10^{-8}	1.10×10^{-5} [c]	2.30×10^{-6} [d]	1.34×10^{-5} (1%)	1.01×10^{-3}
Am(III)	ERDA-6	1.48×10^{-6}	-0.678	3.11×10^{-7} (44%)	2.60×10^{-8}	4.00×10^{-9}	3.42×10^{-7}	3.10×10^{-8} [d]	4.03×10^{-7} (56%)	7.13×10^{-7}
Pu(III)	ERDA-6	1.48×10^{-6}	-0.678	3.11×10^{-7} (25%)	2.60×10^{-8}	2.00×10^{-8}	3.42×10^{-7}	5.47×10^{-7}	9.34×10^{-7} (75%)	1.25×10^{-6}
Th(IV)	ERDA-6	7.02×10^{-8}	0.673	3.31×10^{-7} (11%)	2.60×10^{-8}	2.00×10^{-8}	2.08×10^{-6}	5.82×10^{-7}	2.71×10^{-6} (89%)	3.04×10^{-6}
U(IV)	ERDA-6	7.02×10^{-8}	0.673	3.31×10^{-7} (11%)	2.60×10^{-8}	2.00×10^{-8}	2.08×10^{-6}	5.82×10^{-7}	2.71×10^{-6} (89%)	3.04×10^{-6}
Np(IV)	ERDA-6	7.02×10^{-8}	0.673	3.31×10^{-7} (11%)	2.60×10^{-8}	2.00×10^{-8}	2.08×10^{-6}	5.82×10^{-7}	2.71×10^{-6} (89%)	3.04×10^{-6}
Pu(IV)	ERDA-6	7.02×10^{-8}	0.673	3.31×10^{-7} (11%)	2.60×10^{-8}	2.00×10^{-8}	2.08×10^{-6}	5.82×10^{-7}	2.71×10^{-6} (89%)	3.04×10^{-6}
Np(V)	ERDA-6	8.76×10^{-7}	--[a]	8.76×10^{-7} (36%)	2.60×10^{-8}	--[b]	6.48×10^{-9}	1.54×10^{-6}	1.57×10^{-6} (64%)	2.45×10^{-6}
U(VI)	ERDA-6	1.00×10^{-3}	--[a]	1.00×10^{-3} (99%)	2.60×10^{-8}	3.00×10^{-8}	1.10×10^{-5} [c]	2.30×10^{-6} [d]	1.34×10^{-5} (1%)	1.01×10^{-3}

a – Np(V) and U(VI) solubility uncertainty parameters are not sampled for PA
b – Np(V) intrinsic colloids are not included in the PA calculations
c – CAPHUM value
d – CAPMIC value

Table 12-3. EPA CRA-2019 Sensitivity Calculation Mean Dissolved. Colloidal, and Total Mobilized Actinides

Radionuclide and Oxidation State	Brine	Baseline Dissolved Concentration (M)	Mean SOLVAR (Domski 2019d)	Mean Solubility (M)	Mineral Fragment Colloids (M)	Intrinsic Colloids (M)	Humic Colloids (M)	Microbial Colloids (M)	Total Colloidal (M)	Total Mobilized (M)
Am(III)	GWB	2.14×10^{-6}	0.651	9.58×10^{-6} (52%)	2.60×10^{-8}	6.70×10^{-7}	1.92×10^{-6}	6.28×10^{-6} [b]	1.32×10^{-5} (48%)	1.85×10^{-5}
Pu(III)	GWB	2.14×10^{-6}	0.651	9.58×10^{-6} (30%)	2.60×10^{-8}	4.30×10^{-8}	1.92×10^{-6}	2.09×10^{-5}	2.81×10^{-5} (70%)	3.25×10^{-5}
Th(IV)	GWB	5.50×10^{-8}	-0.011	5.36×10^{-8} (7%)	2.60×10^{-8}	4.80×10^{-7}	5.36×10^{-10}	1.66×10^{-7}	6.73×10^{-7} (93%)	7.26×10^{-7}
U(IV)	GWB	5.50×10^{-8}	-0.011	5.36×10^{-8} (4%)	2.60×10^{-8}	1.40×10^{-6}	5.36×10^{-10}	1.13×10^{-10}	1.43×10^{-6} (96%)	1.48×10^{-6}
Np(IV)	GWB	5.50×10^{-8}	-0.011	5.36×10^{-8} (7%)	2.60×10^{-8}	4.30×10^{-8}	5.36×10^{-10}	6.43×10^{-7}	7.13×10^{-7} (93%)	7.67×10^{-7}
Pu(IV)	GWB	5.50×10^{-8}	-0.011	5.36×10^{-8} (22%)	2.60×10^{-8}	4.30×10^{-8}	5.36×10^{-10}	1.17×10^{-7}	1.86×10^{-7} (78%)	2.40×10^{-7}
Np(V)	GWB	4.38×10^{-7}	--[a]	4.38×10^{-7} (8%)	2.60×10^{-8}	4.30×10^{-8}	3.99×10^{-10}	5.26×10^{-6}	5.33×10^{-6} (92%)	5.76×10^{-6}
U(VI)	GWB	1.00×10^{-3}	--[a]	1.00×10^{-3} (99%)	2.60×10^{-8}	1.40×10^{-6}	1.10×10^{-5} [c]	2.10×10^{-6}	1.45×10^{-5} (1%)	1.01×10^{-3}
Am(III)	ERDA-6	1.43×10^{-6}	0.651	6.40×10^{-6} (29%)	2.60×10^{-8}	6.70×10^{-7}	1.28×10^{-6}	6.28×10^{-6} [b]	1.11×10^{-5} (56%)	1.47×10^{-5}
Pu(III)	ERDA-6	1.43×10^{-6}	0.651	2.07×10^{-5} (44%)	2.60×10^{-8}	4.30×10^{-8}	1.28×10^{-6}	2.09×10^{-5}	2.60×10^{-5} (71%)	2.17×10^{-5}
Th(IV)	ERDA-6	5.84×10^{-8}	-0.011	5.69×10^{-8} (8%)	2.60×10^{-8}	4.80×10^{-7}	5.69×10^{-10}	1.77×10^{-7}	6.83×10^{-7} (92%)	7.40×10^{-7}
U(IV)	ERDA-6	5.84×10^{-8}	-0.011	5.69×10^{-8} (4%)	2.60×10^{-8}	1.40×10^{-6}	5.69×10^{-10}	1.20×10^{-10}	1.43×10^{-6} (96%)	1.48×10^{-6}
Np(IV)	ERDA-6	5.84×10^{-8}	-0.011	5.69×10^{-8} (7%)	2.60×10^{-8}	4.30×10^{-8}	5.69×10^{-10}	6.83×10^{-7}	7.53×10^{-7} (93%)	8.10×10^{-7}
Pu(IV)	ERDA-6	5.84×10^{-8}	-0.011	5.69×10^{-8} (23%)	2.60×10^{-8}	4.30×10^{-8}	5.69×10^{-10}	1.24×10^{-7}	1.94×10^{-7} (77%)	2.51×10^{-7}
Np(V)	ERDA-6	1.82×10^{-6}	--[a]	1.82×10^{67} (8%)	2.60×10^{-8}	4.30×10^{-8}	1.35×10^{-8}	2.18×10^{-5}	2.19×10^{-5} (92%)	2.37×10^{-5}
U(VI)	ERDA-6	1.00×10^{-3}	--[a]	1.00×10^{-3} (99%)	2.60×10^{-8}	1.40×10^{-6}	1.10×10^{-5} [c]	2.10×10^{-6}	1.45×10^{-5} (1%)	1.01×10^{-3}

a – Np(V) and U(VI) solubility uncertainty parameters are not sampled for PA
b – CAPMIC value

U(IV) concentrations were not significantly affected by the parameter changes in the EPA calculations, with the mean total mobilized U(IV) concentrations in both the EPA calculations and CRA-2019 DPA dominated by intrinsic colloids. The Np(IV) and Pu(IV) total mobilized concentrations increased in the EPA calculations because of increased proportionality constants and maximum concentrations for microbial colloids. Because of the importance of plutonium to predicted repository releases, these results provide additional evidence that plutonium microbial colloid parameters are likely to significantly affect predicted repository releases.

12.3 EPA EVALUATION OF THE SENSITIVITY OF TOTAL MOBILIZED ACTINIDE CONCENTRATIONS TO PA PARAMETERS

The total mobilized actinide concentrations calculated in ERDA-6 brine using mean parameter values for the PABC09, CRA-2014 PA, CRA-2019 DPA, and EPA's CRA-2019 recalculation are compared in Table 12-4. EPA's recalculated plutonium concentration includes the assumption that Pu(III) will be the dominant plutonium oxidation state (Section 6.3.2). For americium and plutonium, which are the actinides that most significantly affect repository releases, the mean total mobilized concentrations are highest in the EPA's CRA-2019 recalculations.

Table 12-4. Mean Total Mobilized Concentrations in ERDA-6 Brine for the PABC09, CRA-2014 PA, CRA-2019 DPA, and CRA-2019 EPA Calculations

Radionuclide Oxidation State	PABC09 (M)	CRA-2014 PA (M)	CRA-2019 DPA (M)	EPA's CRA-2019 Recalculation (M)
Am(III)	6.23×10^{-6}	7.13×10^{-7}	9.94×10^{-7}	1.47×10^{-5}
Pu(III)	2.64×10^{-6}	1.25×10^{-6}	1.06×10^{-6}	Pu(III): 2.17×10^{-5}
Pu(IV)	2.66×10^{-7}	3.04×10^{-6}	1.34×10^{-7}	
Th(IV)	3.53×10^{-7}	3.04×10^{-6}	1.34×10^{-7}	7.40×10^{-7}
U(IV)	2.56×10^{-7}	3.04×10^{-6}	1.49×10^{-6}	U(IV): 1.48×10^{-6}
U(VI)	1.01×10^{-3}	1.01×10^{-3}	1.01×10^{-3}	
Np(IV)	6.33×10^{-7}	3.04×10^{-6}	1.34×10^{-7}	Np(IV): 8.10×10^{-7}
Np(V)	1.14×10^{-5}	2.45×10^{-6}	1.29×10^{-6}	

EPA (2017c, 2017d) evaluated the sensitivity of total mobilized actinide concentrations to PA parameters during review of the CRA-2014 PA. EPA (2017d) found that the +III actinide solubility uncertainty distribution parameters and microbial colloid proportionality and maximum concentration limit parameters significantly affected total mobilized actinide concentrations. EPA's CRA-2019 calculations also show that these parameters have significant effects on total +III actinide mobilization. Issues with DATA0.FM4 that significantly affected +III actinide baseline solubilities affected the total mobilized +III actinide concentrations used in the CRA-2019 DPA.

Consideration of the effects of parameter changes on total mobilized actinide concentrations for the PABC09, CRA-2014 PA, CRA-2019 DPA, and EPA's CRA-2019 recalculations using the mean parameters from these PAs has demonstrated:

- The baseline +III actinide solubilities, which EPA's review has shown were underestimated for the CRA-2019 DPA, significantly affect total mobilized +III actinide concentrations.
- Intrinsic colloids contribute significantly to mobilization of the +IV actinides.
- Mineral fragment colloids constitute a small fraction of total mobilized +IV actinide concentrations.
- Humic colloids have small effects on +III actinide mobilization and little effect on +IV actinide mobilization using the proportionality constants and maximum concentration limits updated for the CRA-2019 DPA.
- Total mobilized actinide concentrations are sensitive to the proportionality constants and maximum concentration limits for actinides associated with microbial colloids, demonstrating the importance of establishing defensible values for these parameters.

The effects of EPA's identified parameter changes on predicted repository releases are addressed in Section 13.0.

13.0 SENSITIVITY OF REPOSITORY RELEASES TO CHEMISTRY PARAMETERS

DOE evaluated the sensitivity of repository releases to the CRA-2019 DPA chemistry parameters using two approaches. DOE (2019) used a stepwise linear regression analysis to evaluate the sensitivity of releases to sampled parameters (Zeitler 2019b). This evaluation, while useful, does not provide information on the sensitivity of modeled repository releases to all PA parameters because many PA parameters, such as baseline actinide solubilities and intrinsic and mineral fragment colloids, are not sampled. DOE (2019) provided additional information regarding the effects of PA parameters on repository releases by comparing releases calculated for the CRA-2014 PA and CRA-2019 DPA and identifying the parameter changes that contributed to the observed differences (Brunell 2019, Zeitler et al. 2019).

EPA developed additional information regarding the sensitivity of releases to chemistry parameters from sensitivity calculations performed during EPA's reviews of the CRA-2014 and CRA-2019. The CRA14_SEN4 PA calculation, which was performed during the CRA-2014 review, included some chemistry parameter changes along with other parameter revisions. EPA performed additional sensitivity calculations during the CRA-2019 review to evaluate the effects of individual chemistry parameters and the combined effects of chemistry parameter changes on predicted repository releases.

13.1 DOE EVALUATION OF THE SENSITIVITY OF CRA-2019 DPA REPOSITORY RELEASES TO CHEMISTRY PARAMETERS

Zeitler (2019b) evaluated the sensitivity of repository releases to sampled parameters for the CRA-2019 DPA, and compared these results to the CRA-2014 PA results. For the CRA-2019 DPA, the actinide solubility uncertainty for the +III actinides (SOLMOD3:SOLVAR) was the dominant parameter contributing to variability in total releases in two out of three replicates, and was of equal importance to the parameter BH_SAND:PRMX_LOG[10] in the third replicate. For the CRA-2014 PA, SOLMOD3:SOLVAR was the second-most dominant parameter contributing to variability in total releases in all three replicates, with the actinide oxidation state parameter (GLOBAL:OXSTAT) appearing as the third-most dominant parameter in one out of three replicates. The SOLMOD3:SOLVAR and GLOBAL:OXSTAT parameters affect the concentrations of total mobilized Am(III), Pu(III), and Pu(IV). Because repository releases are dominated by americium and plutonium isotopes, it is reasonable that these sampled parameters significantly influence the results of repository release calculations.

Brunell (2019) determined that average and maximum DBR volumes increased in the CRA-2019 DPA compared to the CRA-2014 PA, which resulted in increased CRA-2019 DPA actinide releases through DBRs. The larger DBR volumes occurred because of increased repository pressure and saturation conditions, which were related to changes in the inundated and humid

[10] BH_SAND:PRMX_LOG is the logarithm of the x-direction intrinsic permeability of a borehole filled with silty sand

steel corrosion rates, addition of gas generation from brine radiolysis, and removal of iron sulfidation reactions for the CRA-2019 DPA (Brunell 2019).

13.2 EPA EVALUATION OF THE SENSITIVY OF REPOSITORY RELEASES TO CHEMISTRY PARAMETERS

EPA performed a series of calculations to examine the effects of chemistry parameter changes on repository releases. The calculations demonstrated the effects of individual parameter changes as well as the combined effects of parameter changes on repository releases. The revised baseline actinide solubility parameters were included in all sensitivity calculations because of the relatively large effects of the underpredicted CRA-2019 DPA +III baseline actinide solubilities on releases, and because actinide solubilities also affect humic and microbial colloid concentrations. Four calculations were performed to assess the sensitivity of repository releases to chemistry parameter revisions identified during EPA's review:

- GCHM_S0: EPA-recalculated baseline solubility parameters (Section 7.4.10);
- GCHM_S1: EPA-recalculated baseline solubility parameters and the updated +III actinide uncertainty solubility distribution (Knerr 2021f) that includes data from recent solubility investigations (Section 7.4.11);
- GCHM_S2: revised baseline actinide solubility parameters, revised intrinsic colloid parameters (Section 8.1.9), and revised microbial colloid proportionality constants and maximum concentration limits (Section 8.3.5); and
- GCHM_S3: revised baseline actinide solubility parameters, revised intrinsic and microbial colloid parameters, and revised actinide oxidation state parameter to include Pu(III), Np(IV), and U(IV) oxidation states in all realizations (Section 6.3).

The revised parameter values used in the sensitivity calculations are summarized in Attachment C. The sensitivity analyses were fully qualified under the Agency's QAPP, allowing the results to be used in supporting regulatory decisions. A detailed description of EPA's analysis and documentation of compliance with the requirements of EPA's QAPP are provided Attachment D. A copy of the EPA's QAPP is archived in Docket EPA-HQ-OAR-2019-0534.

The chemistry parameter changes implemented in these calculations only affect mobilization of actinides in brine, so the predicted CRA-2019 DPA spallings releases and cuttings and cavings releases remained unchanged. Although total mobilized actinides could influence releases through the Culebra Member of the Rustler Formation, releases through the Culebra do not contribute significantly to modeled total releases. Because repository releases are dominated by americium and plutonium, changes in total mobilized neptunium and uranium concentrations do not significantly affect DBRs or total repository releases. The effects of the chemistry parameter changes on repository releases therefore are discussed below in terms of americium and plutonium concentrations in WIPP brines, and the effects of these concentration changes on DBRs and total releases.

13.2.1 Sensitivity to Baseline Actinide Solubilities (GCHM_S0)

As discussed in Section 7.4.10, EPA's review of the CRA-2019 DPA baseline actinide solubility calculations indicated that the +III actinide baseline solubilities were significantly

underestimated (Table 7-9). For example, assuming the minimum ERDA-6 brine volume, EPA calculated a +III actinide baseline solubility of 2.14×10^{-6} M, which exceeds the CRA-2019 DPA concentration of 1.63×10^{-7} M by about an order of magnitude. EPA performed the GCHM_S0 calculation to determine the effects of the increased Am(III) and Pu(III) baseline solubilities on predicted repository releases. The effects of these increased baseline solubilities on mean DBRs and mean total releases are illustrated in Figures 13-1 and 13-2, respectively. The increased Am(III) and Pu(III) baseline solubilities increased mean DBRs compared to the CRA-2019 DPA (Figure 13-1) nearly twofold at the 0.1 probability compliance point and 1.7-fold at the 0.01 compliance point. Mean total releases increased approximately 1.6-fold relative to the CRA-2019 DPA at low probabilities (Figure 13-2) because total releases are dominated by cuttings and cavings at higher probabilities. These results show that because DOE underpredicted baseline +III actinide solubilities relative to the EPA-calculated concentrations, CRA-2019 DPA DBRs and total repository releases were less than EPA-predicted releases. However, mean total repository releases calculated with the increased Am(III) and Pu(III) baseline solubilities remained below regulatory limits (Figure 13-2).

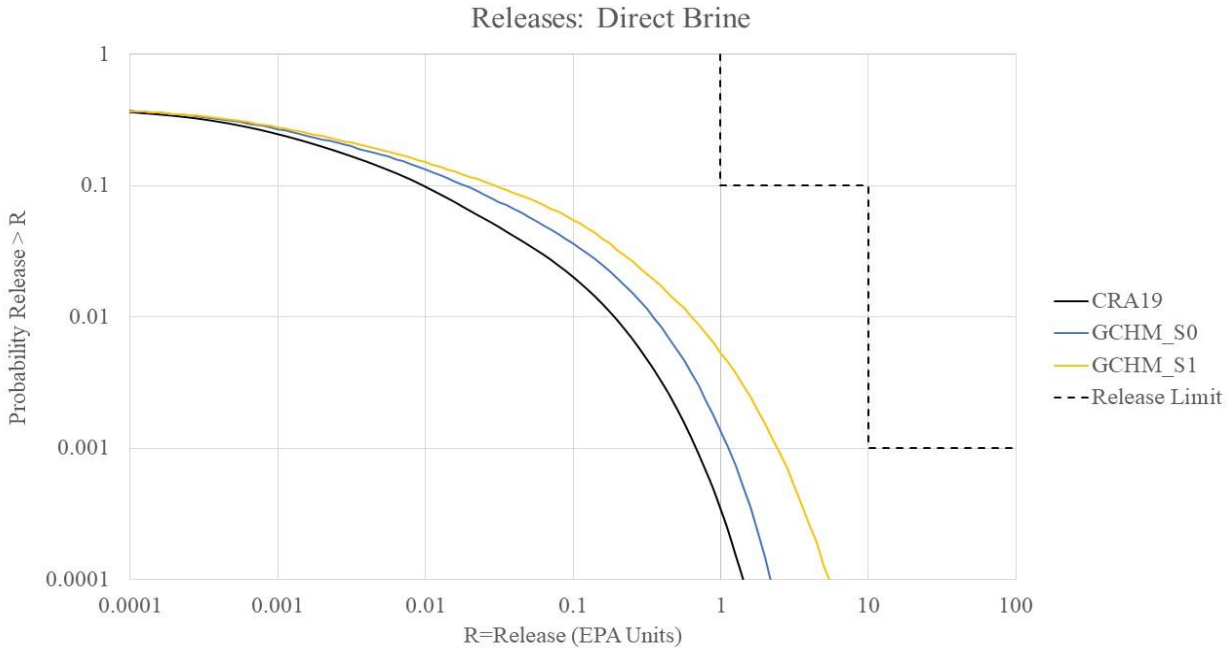

Figure 13-1. Mean DBRs Calculated for the CRA-2019 DPA (CRA19), the Baseline Actinide Solubility Sensitivity Calculation (GCHM_S0), and the Baseline Actinide Solubility plus +III Actinide Solubility Uncertainty Sensitivity Calculation (GCHM_S1)

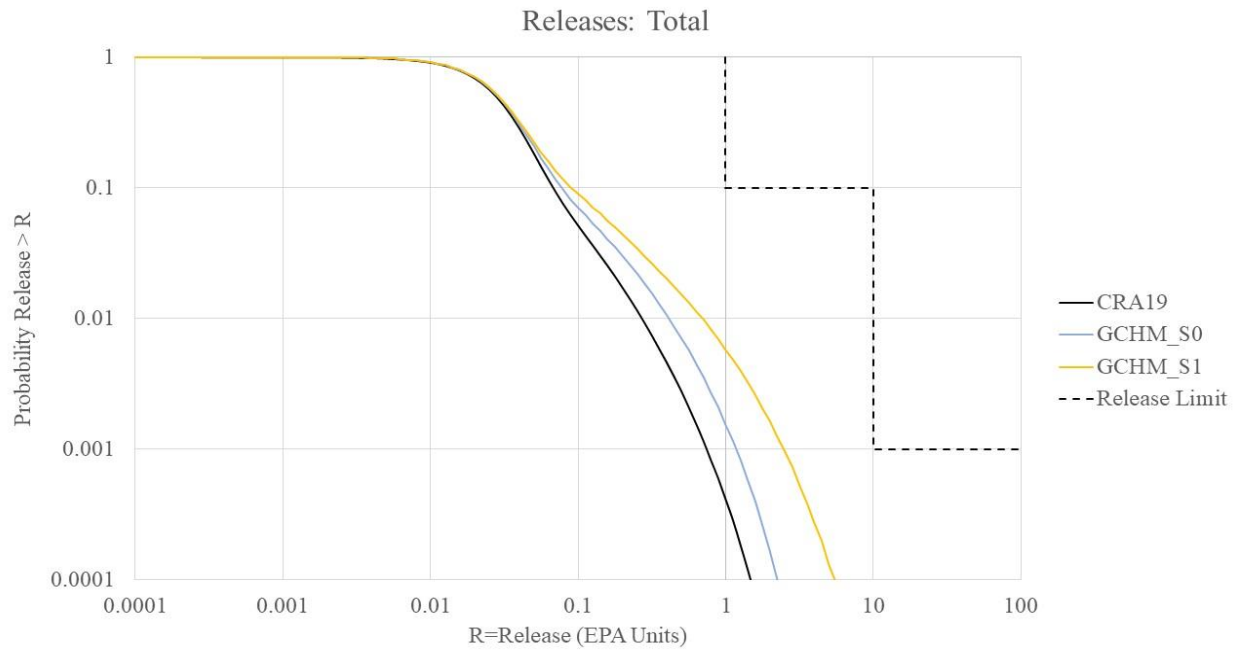

Figure 13-2. Mean Total Releases Calculated for the CRA-2019 DPA (CRA19), the Baseline Actinide Solubility Sensitivity Calculation (GCHM_S0), and the Baseline Actinide Solubility plus +III Actinide Solubility Uncertainty Sensitivity Calculation (GCHM_S1)

13.2.2 Sensitivity to Baseline Actinide Solubilities and the Revised +III Actinide Solubility Uncertainty Distribution (GCHM_S1)

In response to a request from EPA, Knerr (2021f) developed an updated +III actinide solubility uncertainty distribution that combined difference values from three recent investigations with difference values included in the CRA-2019 DPA uncertainty distribution (Section 7.4.11). EPA performed calculation GCHM_S1 to evaluate the effects on repository releases of combining the increased baseline actinide solubilities with the revised +III actinide solubility uncertainty distribution (Figures 13-1 and 13-2). EPA does not recommend including the updated +III actinide solubility uncertainty distribution in future WIPP PAs, because the revised uncertainty distribution includes a relatively high proportion of difference values calculated with more-soluble, microcrystalline solids, and likely provides an overly conservative estimate of the uncertainty associated with the baseline +III actinide solubilities (Section 7.4.11). However, EPA has included these release calculations to demonstrate the sensitivity of calculated releases to the +III actinide solubility uncertainty distribution.

Comparison of the GCHM_S1 results to the GCHM_S0 results show that DBRs and total releases are significantly increased by the revised +III actinide solubility uncertainty distribution. DBRs increased significantly compared to the CRA-2019 DPA (Figure 13-1) because of relatively large increases in the mean Am(III) and Pu(III) solubilities that resulted from the increased baseline solubilities and +III actinide solubility distribution. The increased DBR releases calculated for GCHM_S1 increase mean total releases at low probabilities (Figure 13-2), approximately 3.6-fold at the 0.01 probability compliance point. However, predicted total

releases remain below regulatory limits. The results in Figures 13-1 and 13-2 illustrate the sensitivity of DBRs and total releases to the +III actinide solubility uncertainty distribution. This result is consistent with the sensitivity evaluation of repository releases to sampled parameters for the CRA-2019 DPA (Zeitler 2019b) (Section 13.1).

13.2.3 Sensitivity to Baseline Actinide Solubilities and Revised Colloid Parameters (GCHM_S2)

EPA determined that increased concentrations are more defensible for the Am(III) and Th(IV) intrinsic colloid parameters (Section 8.1.9). EPA also found that revised PROPMIC parameter values and recalculated CAPMIC values would be more defensible in future WIPP PAs until more data can be collected in WIPP-specific experiments (Section 8.3.5). The GCHM_S2 calculation combines these intrinsic and microbial colloid parameter changes with the increased baseline actinide solubilities used in the GCHM_S0 calculation (Figures 13-3 and 13-4). Comparison of the DBR results for these EPA calculations shows that addition of the intrinsic and microbial colloid parameter changes to increased solubilities affects DBRs at probabilities greater than 0.001 (3.1-fold increase at 0.1 probability and a 3.6-fold increase at 0.01 probability), with negligible effects at lower probabilities (Figure 13-3). The minimal effects on DBRs at lower probabilities are likely caused by the actinide concentrations associated with microbial colloids reaching the maximum (CAPMIC) concentrations and by the decreasing importance of the constant intrinsic colloid concentrations for the +III actinides for higher sampled +III actinide uncertainty values.

The combination of colloid parameter changes with higher baseline solubilities does not affect total releases at high probabilities, where releases are dominated by cuttings and cavings (Figure 13-4). The colloid parameter changes incorporated in the GCHM_S2 calculation slightly increase releases in the probability range from 0.001 to ~ 0.5.

13.2.4 Effects of Combined Parameter Changes (GCHM_S3)

EPA calculated higher baseline +III actinide solubilities (Section 7.4.10), Am(III) and Th(IV) intrinsic colloid concentrations (Section 8.1.9), and revised microbial colloid proportionality constants and maximum concentration parameters (Section 8.3.5). EPA also determined that plutonium, neptunium, and uranium most likely would be present in WIPP repository brines and solids only in their most reduced oxidation states, which affects the PA parameter GLOBAL:OXSTAT (Section 6.3). These chemistry parameter changes identified by EPA were combined in EPA's GCHM_S3 calculation.

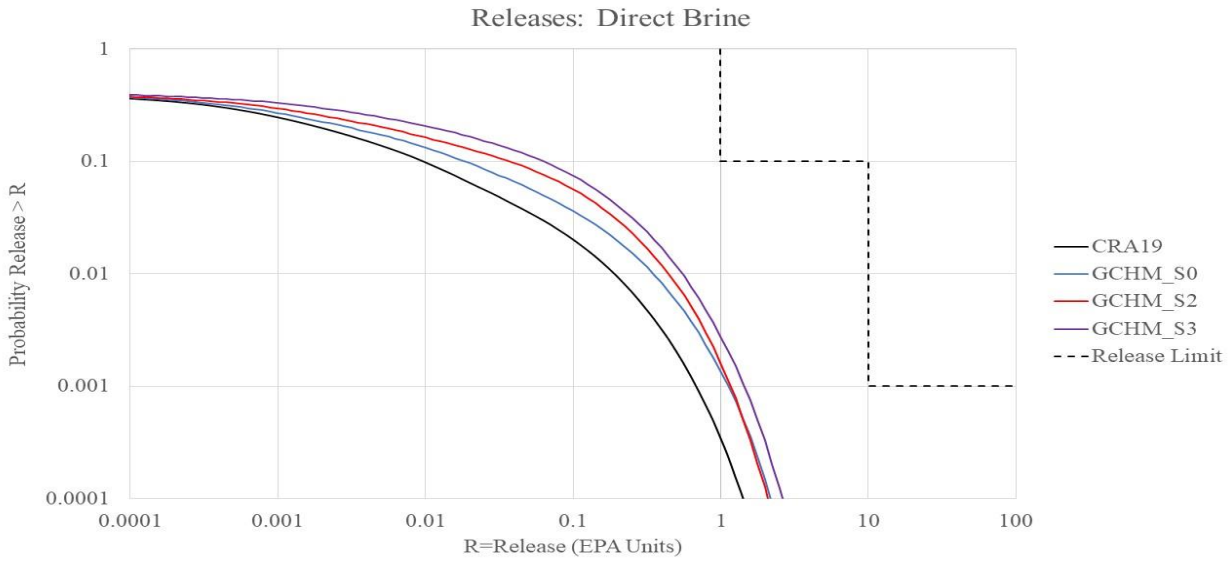

Figure 13-3. Mean DBRs Calculated for the CRA-2019 DPA (CRA19); the Baseline Actinide Solubility Sensitivity Calculation (GCHM_S0); the Baseline Actinide Solubility plus Intrinsic and Microbial Colloid Sensitivity Calculation (GCHM_S2); and the Sensitivity Calculation Combining Revised Baseline Actinide Solubility, Revised Intrinsic and Microbial Colloid, and Revised Actinide Oxidation State Parameters (GCHM_S3)

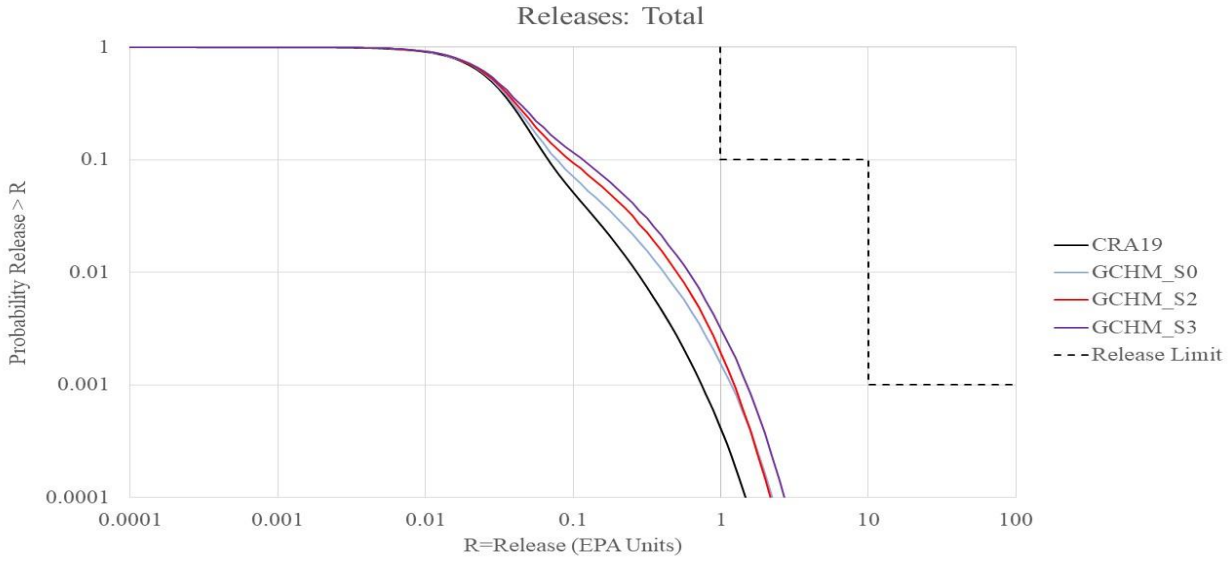

Figure 13-4. Mean Total Repository Releases Calculated for the CRA-2019 DPA (CRA19); the Baseline Actinide Solubility Sensitivity Calculation (GCHM_S0); the Baseline Actinide Solubility plus Intrinsic and Microbial Colloid Sensitivity Calculation (GCHM_S2); and the Sensitivity Calculation Combining Revised Baseline Actinide Solubility, Revised Intrinsic and Microbial Colloid, and Revised Actinide Oxidation State Parameters (GCHM_S3)

Comparison of the GCHM_S2 and GCHM_S3 results show that DBRs increased as a result of the changed oxidation state assumption (Figure 13-3). These increased DBRs are caused by the higher revised total mobilized Pu(III) concentrations compared to the revised total mobilized Pu(IV) concentrations (Table 12-3). The combined chemistry parameter changes resulted in increased mean DBRs at all probabilities (Figure 13-3) and increased mean total releases at low probabilities (Figure 13-4). At the 0.1 probability compliance point, increases were 6.5-fold from CRA-2019 values while at the 0.01 probability compliance point, releases were 2.1-fold higher. However, mean total repository releases remained below the regulatory limits in all of EPA's calculations.

13.3 CHEMISTRY PARAMETERS LIKELY TO AFFECT CALCULATED REPOSITORY RELEASES

Understanding the sensitivity of repository releases to PA parameters is important for prioritizing issues that require additional investigation for future WIPP PAs. DOE's evaluations of the sensitivity of repository releases to PA parameters (Zeitler 2019b, Brunell 2019) and calculations performed by EPA show that some chemistry-related parameters can significantly affect repository releases.

Parameters that affect the total mobilized americium and plutonium concentrations in brine can significantly affect DBRs. The most important chemistry parameters affecting total mobilized americium and plutonium concentrations include:

- Baseline actinide solubilities for the +III and +IV actinides,
- +III and +IV actinide solubility uncertainty distributions,
- Actinide oxidation state parameter,
- Microbial colloid proportionality constants and maximum concentrations for the +III and +IV actinides,
- Humic colloid proportionality constants for the +III actinides, and
- Intrinsic colloid parameters for the +IV actinides.

EPA's review of the CRA-2019 DPA has identified issues with the baseline +III actinide solubility parameters, development of the actinide uncertainty distributions, actinide oxidation state assumption, microbial colloid parameters, and the intrinsic colloid parameters for Am(III) and Th(IV) used in the CRA-2019 DPA. The sensitivity calculations indicate that the actinide oxidation state, baseline actinide solubilities, and actinide solubility uncertainty distributions have the greatest effects on predicted actinide releases.

Parameters that affect repository brine saturation and pressures may significantly affect DBRs and spallings releases by changing the frequencies and volumes of DBRs and spallings releases. The most significant of these parameters, based on review of the CRA-2019 DPA include:

- Microbial gas generation parameters,
- Inundated and humid steel corrosion parameters,
- Stoichiometric parameters for inclusion of steel sulfidation reactions, and
- Brine radiolysis parameters.

The microbial gas generation, steel corrosion, and iron sulfidation stoichiometric parameters are consistent with currently available data and do not require additional investigation at this time. Processes that were not evaluated in the CRA-2019 DPA that may affect brine saturation and repository pressure include radiolysis of water adsorbed on waste and CPR radiolysis. EPA expects DOE to continue to evaluate the effects of these processes in addition to brine radiolysis by dissolved, colloidal, and wetted radionuclide solids for future WIPP PAs.

14.0 SUMMARY AND CONCLUSIONS

This TSD summarizes EPA's review of chemistry-related CRA-2019 DPA parameters, assumptions, calculations, and documentation. The Agency identified some CRA-2019 DPA chemistry parameters that appear to be inconsistent with currently available data. However, the results of the Agency's review and additional calculations show that predicted repository releases will remain within regulatory limits if the chemistry parameters in question are revised. EPA expects DOE to address the issues identified in this TSD for future WIPP PAs to minimize uncertainties associated with the PA results.

14.1 GAS GENERATION

The conceptual model and implementation of gas generation from anoxic corrosion of iron-based metals used for the CRA-2019 DPA are supported by the available data. Iron corrosion rates for the CRA-2014 PA were lower than previous WIPP PAs based on new project-specific investigations of humid and inundated iron corrosion rates. For the CRA-2019 DPA, DOE increased the inundated iron corrosion rate distribution to account for the presence of low CO_2 concentrations in the repository and the higher inundated corrosion rate measured at high pressure. Humid steel corrosion rates were zero in previous WIPP PAs. For the CRA-2019 DPA, DOE sampled a cumulative distribution function for the humid iron corrosion rate that was developed using project-specific data. Both the inundated and humid iron corrosion rates used in the CRA-2019 DPA are well-documented, consistent with the available experimental data, and appropriate for use in WIPP PA.

For the CRA-2014 PA, DOE assumed that all H_2S generated by CPR degradation would instantaneously react with iron metal and $Fe(OH)_2(s)$. This assumption was inconsistent with project-specific data that show H_2S may passivate iron. The reaction of H_2S with $Fe(OH)_2(s)$ can result in lower gas pressures, reduce spallings releases, and reduce DBRs. EPA requested that DOE eliminate the iron sulfidation reactions from the CRA-2019 DPA to account for H_2S passivation of iron metal, and DOE complied by setting the appropriate stoichiometric coefficients to zero.

The gas generation rate caused by anoxic corrosion of iron-based metal in the repository is proportional to the steel surface area per unit disposal volume (D_s). Calculations of D_s depend on the proportions of different wastes and waste containers in the repository, particularly the surface area to tare weight ratios of the waste containers. The steel inventory increased significantly between the CRA-2014 PA and CRA-2019 DPA because of increased planned use of RH shielded containers. EPA found that the D_s value used in the CRA-2019 DPA and in previous WIPP PAs is consistent with the current emplacement data. EPA expects DOE to calculate the likely D_s value range for future WIPP PAs based on the waste inventory and the emplaced, stored, and scaled anticipated container counts in the WIPP inventory.

Metals and alloys other than iron-based materials in WIPP waste or packaging materials, such as aluminum and lead, may generate gas through anoxic corrosion. The CRA-2019 DPA lead inventory increased significantly from the CRA-2014 PA inventory because of changes in the estimated final form container types for some RH waste streams from RH canisters to shielded containers. Bounding calculations performed by DOE demonstrated that gas generation from

lead corrosion will be a negligible fraction of overall gas generation rates. CRA-2019 DPA inventories of waste aluminum-based metals and alloys and other metals and alloys remain very low compared to lead packaging and iron-based waste and packaging inventories, so corrosion of waste aluminum and other metals will have negligible effects on repository gas generation rates.

Implementation of microbial gas generation remained unchanged for the CRA-2019 DPA from the CRA-2014 PA. The microbial gas generation rates used for the CRA-2019 DPA are suitable for modeling gas generation rates from degradation of cellulosic materials, but may overestimate gas generation rates from the degradation of plastics and rubber. DOE accounts for uncertainties regarding the rates of plastic and rubber degradation in the WIPP repository environment by assuming plastic and rubber degradation occurs in only 25% of the realizations. Based on the available data, the current approach for modeling microbial gas generation rates is appropriate.

The effects of gas generation by alpha radiolysis of brine were included in the CRA-2019 DPA. Brine radiolysis by dissolved and colloidal actinides and by wetted radionuclide solids was included in the calculations. Alpha radiolysis of brines is known to produce H_2(g), O_2(g), and oxidizing ionic species. Oxidizing ionic species and O_2(g) are expected to rapidly react with metallic iron or other reductants in the repository, so only radiolytic H_2(g) production is expected to affect repository conditions. DOE demonstrated that the approach and parameters used to calculate H_2(g) generation rates from brine radiolysis by dissolved, colloidal, and wetted radionuclide solids were reasonable. In response to an EPA request, DOE also evaluated the potential significance of gas generation by radiolysis of water adsorbed on waste in the WIPP repository and provided reasonable justification for omitting this gas generation process from the CRA-2019 DPA. However, EPA expects DOE to further evaluate gas generation by adsorbed water radiolysis to determine whether it should be included in gas generation rate calculations for future WIPP PAs because: 1) DOE's preliminary evaluation showed that this gas generation rate may equal or exceed the rates of gas generation by microbial degradation of CPR and radiolysis of brine by dissolved, colloidal, and wetted radionuclide solids; and 2) the timing of gas generation by adsorbed water radiolysis might differ significantly from the timing of other gas-generation processes and affect repository performance because of potentially higher gas-generation rates early in the repository performance period.

Calculations performed by DOE indicate that gas generation from CPR radiolysis may be similar in magnitude to gas generation from brine radiolysis by dissolved, colloidal, and wetted radionuclide solids and by microbial degradation of CPR under some repository conditions. DOE has demonstrated for the CRA-2019 DPA that CPR radiolysis is unlikely to significantly affect WIPP repository performance because gas generation is dominated by anoxic corrosion of iron, the CPR inventory may be a limiting factor in some PA vectors, and the results of bounding gas generation calculations demonstrated that gas generation through CPR radiolysis will have relatively small effects on repository releases. Because changes in gas generation rates can have complex effects on repository releases, EPA expects DOE to include additional consideration of the importance of CPR radiolysis in its evaluation of radiolytic gas generation processes for the next PA, especially the effects of higher gas generation rates during the first 1,000 years after repository closure.

Radiolytic gas generation has been reported for waste materials other than CPR in the WIPP inventory, including hydrated minerals, solidified inorganic wastes, solidified organic wastes,

and cements. DOE has demonstrated that radiolysis of these other wastes will have little effect on overall repository gas generation rates.

14.2 BACKFILL EFFICACY

The available data indicate that the MgO backfill will adequately control brine pH and CO_2 fugacity, and thereby limit actinide solubilities in WIPP brines under inundated conditions. Because the rate at which hydromagnesite will convert to magnesite in the repository environment is uncertain, PA calculations of actinide solubilities include the assumption that the brucite-hydromagnesite reaction will buffer CO_2 fugacity at low levels consistent with relatively low actinide solubilities under inundated conditions. Calculation of the minimum amount of emplaced MgO on a room-by-room basis appropriately accounts for the uncertainties associated with the rate of hydromagnesite conversion to magnesite and the chemical composition of the MgO. The current MgO emplacement plan ensures that a sufficient quantity of MgO is emplaced in each room of the repository. The MgO reactivity testing procedure and test results provided by DOE demonstrate that the current backfill material contains a sufficient percentage of reactive periclase plus lime to control chemical conditions in the repository, and that the current testing procedure would detect any MgO shipments with inadequate reactive material percentages.

14.3 ACTINIDE OXIDATION STATES

Assumptions related to actinide oxidation states in the WIPP repository have remained unchanged since the CCA. DOE assumes for PA that Th(IV), Am(III), and Cm(III) are the only oxidation states of these actinides that will be present in the WIPP repository. DOE assumes that neptunium may be present in the Np(IV) or Np(V) oxidation states and uranium may be present in the U(IV) or U(VI) oxidation states. Because extremely reducing conditions will be established in the repository shortly after closure, inclusion of the higher and more soluble oxidation states for neptunium and uranium in the total mobilized actinide calculations is conservative. Because neptunium and uranium do not significantly contribute to repository releases, inclusion of the higher oxidation states for these radionuclides has little to no effect on PA results.

For all WIPP PAs, DOE has assumed equal probabilities that aqueous and solid-phase plutonium will be present in either the Pu(III) or Pu(IV) oxidation states. This assumption affects repository releases because total mobilized Pu(III) concentrations in WIPP brines are higher than total mobilized Pu(IV) concentrations. EPA has evaluated the available data and concludes that there is a high likelihood that plutonium concentrations in WIPP brines will be controlled by the solubility of Pu(III) solids in equilibrium with Pu(III) aqueous species. Because the assumed plutonium oxidation state will significantly influence total mobilized plutonium in PA, EPA believes that assuming the solubility of Pu(III) solids controls dissolved plutonium concentrations in repository brines will provide more defensible predictions of total mobilized plutonium concentrations in WIPP brines.

14.4 DISSOLVED ACTINIDE SOURCE TERM

DOE calculated the baseline dissolved actinide solubilities for the CRA-2019 DPA using the EQ3/6 modeling code, the DATA0.FM4 database, and organic ligands concentrations based on

the CRA-2019 DPA inventory and brine volumes equal to 1-, 2-, 3-, 4-, and 5-times the minimum brine volume required for a DBR.

EPA identified issues with DATA0.FM4 that should be addressed by DOE prior to performing future WIPP PAs:

- Calculations were not provided to demonstrate Phase 5 experimental solubilities can be adequately predicted using DATA0.FM4.
- EDTA aqueous speciation data appear to be erroneous, including the stability constants for $AmEDTA^-$, ThEDTA(aq), and NpO_2EDTA^{3-}.
- The $CaEDTA^{2-}$ aqueous stability constant should be revised from 12.69 to 12.36, because the latter value was calculated using the Pitzer ion interaction model instead of the SIT model.
- Discrepancies between measured and assumed EDTA concentration data in the $Ca_2EDTA \cdot 7H_2O(s)$ experiments indicate the solubility data and the $Na^+/CaEDTA^{2-}$, $Mg^{2+}/CaEDTA^{2-}$, $Mg^{2+}/MgEDTA^{2-}$, and $Ca^{2+}/EDTA^{4-}$ Pitzer parameters are unreliable.
- Parameter fitting checks were not reported for the Pitzer interaction parameters for the $Mg^{2+}/CaEDTA^{2-}$, $Mg^{2+}/MgEDTA^{2-}$, and $Ca^{2+}/EDTA^{4-}$ ion pairs.
- $Am(Citrate)_2^{3-}$, $Th(Citrate)_2^{2-}$, and earlandite were omitted.
- $Ca(Oxalate)_2^{2-}$, $Am(Oxalate)_2^-$, $Th(Oxalate)_2(aq)$, and $NpO_2(Oxalate)_2^{3-}$ were omitted.
- The evaluation of Am(III)-acetate and Th(IV)-acetate speciation data was incomplete.
- Fe(II)-sulfate solids and Pitzer parameters were omitted.
- Lead data do not include Pitzer parameters and DOE did not demonstrate that DATA0.FM4 can be used to adequately model high ionic strength solubilities of lead solid phases.
- DOE did not provide an evaluation of lead solid phases likely to form in the repository environment based on natural analogues or other data, and omitted potentially significant lead solids such as hydrocerussite.
- DOE should evaluate possible inconsistencies that have been reported in Pitzer parameters from Könnecke et al. (1997).
- The Th(IV)-carbonate speciation should be updated.

DOE recalculated the log K_s^0 for hydromagnesite using data from Robie and Hemingway (1973). This recalculated solubility is internally consistent with other data in the database, and is therefore more defensible than the previous DATA0.FM1 value.

DOE has not developed an aqueous speciation and solubility model for U(VI) and continues to use a fixed concentration of 1.0×10^{-3} M for the dissolved concentration. U(VI) is unlikely to persist in the WIPP repository because of the extremely reducing conditions that will develop shortly after closure.

Unlike previous WIPP PAs, actinide solubility calculations for the CRA-2019 DPA included iron and lead aqueous species and solid phases and calcite precipitation was allowed to reach equilibrium. Precipitated solids included large amounts of Phase 5 in both GWB and ERDA-6 brine, and a large fraction of solvent water was consumed by Phase 5 precipitation in the ERDA-6 brine calculations. EPA questions these results, because significant water consumption by

Phase 5 precipitation is not included in the repository water balance, Phase 5 precipitation has not been observed in MgO hydration experiments in ERDA-6, and formation of large amounts of Phase 5 could form impermeable masses of MgO reaction products that limit the ability of the MgO backfill to control CO_2 fugacity. Slight oversaturation with respect to calcite is more likely in the WIPP environment because numerous brine constituents are known to inhibit calcite precipitation, for example, Mg^{2+}, SO_4^{2-}, and organic ligands. DOE performed additional actinide solubility calculations demonstrating that the calculated actinide solubilities were not greatly affected by the degree of calcite oversaturation or initial iron and lead solid phases (Domski 2019c). Additional calculations performed by DOE at the Agency's request demonstrated that maintaining a small amount of calcite oversaturation limited Phase 5 precipitation in GWB and eliminated it in ERDA-6, resulting in the consumption of smaller amounts of solvent water. The results obtained with slight calcite oversaturation are more realistic and DOE should consider maintaining a small degree of calcite oversaturation in future dissolved actinide solubility calculations. Calculations demonstrating that Phase 5 solubility is adequately parameterized in DATA0.FM4 were not available. Excessive Phase 5 precipitation would be predicted if the solubility of Phase 5 is too low, which may contribute to calculations of excess water consumption. EPA expects DOE to provide an evaluation of the Phase 5 solubility data for future WIPP PAs.

Actinide solubility calculations performed by DOE showed that inclusion of iron and lead phases did not greatly affect calculated actinide solubilities. The lead data should be removed from the database, however, because it does not include Pitzer parameters and has not been tested using available high ionic strength experimental data. If DOE adds iron or lead interactions with organic ligands to the database, the effects of iron or lead precipitation as sulfide and phosphate solids should also be considered.

DOE performed dissolved actinide solubility calculations to evaluate the potential effects of cements in the waste inventory and polyhalite in the Salado Formation on the actinide solubility calculations. The results of calculations that included portlandite from cement indicated that the quantity of cement in the WIPP inventory will not significantly affect brine chemistry or actinide solubilities. Inclusion of polyhalite in the actinide solubility calculations resulted in the precipitation of large amounts of Phase 5 and water consumption. However, Salado Formation mineralogy data indicate that the amount of polyhalite has been overestimated, and EPA recommends that DOE re-evaluate the available mineralogy data to provide a more realistic estimate of the amount of polyhalite that may be available for reaction.

EPA performed actinide solubility calculations using PHREEQC and a converted version of the DATA0.FM4 database to assess the sensitivity of the results to issues identified by EPA during review of the DATA0.FM4 database and to the assumptions used for the CRA-2019 DPA actinide solubility calculations. EPA performed calculations with slight oversaturation with respect to calcite, without iron or lead phases, and with DATA0.FM4 revisions to address identified database issues. Results of these calculations showed that correction of issues related to EDTA in DATA0.FM4 significantly increased modeled +III dissolved actinide solubilities compared to the CRA-2019 DPA.

DOE used the CRA14_SEN4 PA actinide solubility uncertainty distributions for the CRA-2019 DPA, with the exception of removing one dataset from the +III actinide distribution. The cutoff

date for publications used to develop these distributions was October 31, 2011. As requested by EPA, DOE evaluated data from publications that became available between the CRA-2014 and CRA-2019. Additional data that met the screening criteria were not identified for the +IV actinides, but three investigations provided additional data for the +III actinide solubility uncertainty distribution. Inclusion of these data increased the mean, median, and maximum values in the +III actinide distribution, and would increase total mobilized +III actinide concentrations calculated for WIPP PA. EPA expects that for all future WIPP PAs, the cutoff date for publications used to develop the +III and +IV actinide solubility uncertainty distributions will be the latest date that can be implemented. DOE should consider whether the availability of more actinide solubility data for some conditions (e.g., less-crystalline solid phases) may bias the resulting actinide uncertainty distributions, and whether a defensible approach is available to counter this potential effect, such as performing more experiments examining the solubility of crystalline +III actinides or an analogue such as crystalline Nd(III). EPA also suggests that a review of other possible approaches for estimating the actinide solubility uncertainties and the relative advantages and disadvantages of these alternatives would provide additional support for the approach currently used to characterize +III and +IV actinide solubility uncertainties.

14.5 COLLOIDAL ACTINIDE SOURCE TERM

The mineral fragment colloid parameters for the CRA-2019 DPA have remained unchanged since the CCA PAVT, and these parameters remain consistent with the available data. The humic colloid parameters were revised for the CRA-2019 DPA based on revised calculations and provide reasonable upper bounds on the actinide concentrations associated with humic colloids. Because the humic colloid experiments were conducted in solutions that contained EDTA, EPA expects that for future WIPP PAs, DOE will make appropriate corrections to the EDTA stability constants and Pitzer parameters in the EQ3/6 database and recalculate the humic colloid proportionality constants.

The intrinsic colloid parameter for plutonium (PU:CONCINT) is adequately bounding for the available data. The neptunium and uranium intrinsic colloid parameters (NP:CONCINT and U:CONCINT) values used for the CRA-2019 DPA are acceptable for use in PA and are unlikely to significantly affect repository performance. The intrinsic colloid parameter for Th(IV) (Th:CONCINT) should be increased from its CRA-2019 DPA value to be consistent with sequential filtration data from WIPP experiments and with the Th(IV) intrinsic colloid concentrations observed by Altmaier et al. (2004). Nd(III) sequential filtration data indicate that the Am(III) intrinsic colloid parameter (AM:CONCINT) concentration used in the CRA-2019 DPA should be increased to provide an appropriate upper bound for the data. EPA expects DOE to address the Th(IV) and Am(III) intrinsic colloid parameters for future WIPP PAs.

DOE revised the microbial colloid proportionality constant parameters (PROPMIC) and parameters for the maximum actinide concentrations associated with microbial colloids (CAPMIC) for the CRA-2019 DPA. As a result of these modifications and the decreased baseline dissolved +III actinide concentrations, CRA-2019 DPA actinide concentrations associated with microbial colloids were less than CRA-2014 PA concentrations. EPA evaluated the data provided by DOE and surveyed the available scientific literature to determine the potential ranges of the PROPMIC and CAPMIC parameter values. Based on this review, EPA

believes DOE's revised approach to calculating CAPMIC is reasonable, but the values chosen for the CRA-2019 DPA do not address uncertainty in the literature. Similarly, DOE's approach to updating the Am(III) PROPMIC appears reasonable, but significant uncertainties remain. EPA concludes that the CRA-2019 DPA parameters do not reflect the large variability in the literature, because the CRA-2019 DPA values were determined using a single organism. PROPMIC values from the CCA and from EPA's investigation, as well as CAPMIC values recalculated from data reported by Papenguth (1996c), appear to bound most values from the literature. DOE should use the CCA PROPMIC values and recalculated CAPMIC values until more data applicable to the WIPP environment are collected.

14.6 CULEBRA DOLOMITE DISTRIBUTION COEFFICIENTS

Distribution coefficients used to model actinide transport through the Culebra to the LWB for the CRA-2019 DPA are consistent with the estimated organic ligand concentrations based on the CRA-2019 DPA inventory for these compounds. These K_d values are likely to provide a conservative assessment of actinide transport through the Culebra.

14.7 HETEROGENEOUS WASTE LOADING

Heterogeneous waste loading is unlikely to significantly affect actinide solubilities because of the assumption of chemical equilibrium between brine and actinide solid phases, and because DOE assumes the entire inventory of organic ligands dissolves in the amount of brine released from the repository. Most shielded containers that will be used at WIPP will be placed in currently unfilled panels. Consequently, these panels will contain relatively large inventories of steel and lead packaging materials. Because the steel surface area to tare weight ratio for shielded containers is relatively low, the increased mass of steel is unlikely to significantly increase gas generation rates in panels with large numbers of shielded containers. Relatively low lead corrosion rates and a low surface area to mass ratio for lead in the shielded containers will limit the effects of lead corrosion on gas generation rates in panels with large numbers of shielded containers.

The SR-KAC-PuOx waste stream represents about 3.5% of the total WIPP waste volume, but contains approximately 30% of the radionuclides that cause radiolytic gas generation and brine consumption in WIPP PA. If this waste stream is emplaced in a limited number of panels, these panels may exhibit higher gas generation rates and greater brine consumption than other panels. EPA expects DOE to evaluate for future WIPP PAs whether the PA calculations adequately address the potential effects of segregation of this waste stream in a limited number of panels on brine consumption, gas generation, and repository releases.

14.8 REPOSITORY WATER BALANCE

The only chemical process included in the water balance calculations for the CCA PAVT, PABC04, and PABC09 was the consumption of water by anoxic corrosion. DOE modified the water balance for the CRA-2014 PA by adding water production by microbial degradation of CPR, water consumption by the MgO hydration reaction, and water produced by conversion of hydromagnesite to magnesite. For the CRA-2019 DPA, DOE also included brine consumption by radiolysis from dissolved or colloidal radionuclides in WIPP brines, and from wetted

radionuclide solids. Incorporation of these chemical processes in addition to anoxic corrosion in the water balance represents a significant improvement in the water balance calculations for WIPP PA.

The MgO hydration rates used in the water balance calculations are based on data from Premier MgO, which is present in smaller quantities than Martin Marietta MgO and also hydrates more slowly. EPA recommends that DOE develop hydration rates using Martin Marietta MgO and incorporate these hydration rates in water balance calculations for future WIPP PAs. EPA also expects DOE to evaluate the potential for significant brine consumption by radiolysis of water adsorbed on waste materials for future WIPP PAs. MgO hydration to produce Phase 5 consumes more water than MgO hydration to brucite, but the formation of Phase 5 is not included in the CRA-2019 DPA water balance. DOE should assess whether formation of significant quantities of Phase 5 in the backfill may occur and whether it should be included in the water balance for future WIPP PAs. DOE should also consider whether radiolysis of water adsorbed on waste can consume significant quantities of water for future WIPP PAs.

14.9 ACTINIDE MOBILIZATION IN WIPP BRINES

Americium and plutonium isotopes are the most important contributors to releases from the WIPP repository. Results of total mobile actinide source term calculations using mean CRA-2019 DPA parameter values indicate that total mobile Am(III) and Pu(III) concentrations consist mainly of dissolved species, with smaller concentrations mobilized as humic colloids. Total mobilized Pu(IV) concentrations calculated using mean parameter values for the CRA-2019 DPA were dominated by dissolved Pu(IV) and Pu(IV) associated with intrinsic and mineral fragment colloids. Using the mean CRA-2019 DPA parameter values, the total mobilized Pu(III) concentrations for GWB and ERDA-6 brine exceed the total mobilized Pu(IV) concentrations by a factor of 7 to 8.

EPA performed sensitivity calculations to determine the effects of increased dissolved Am(III) and Pu(III) concentrations resulting from the assumption that all actinides would be in their more reduced oxidation state, revisions to the EDTA data in the EQ3/6 thermodynamic database, changes to the Am(III) and Th(IV) intrinsic colloid parameters, revisions to the microbial colloid proportionality constants, and revised microbial colloid maximum concentration limits. Compared to the CRA-2019 DPA, total mobilized Am(III) and Pu(III) concentrations increased by more than an order of magnitude as a result of these changes. EPA sensitivity calculations demonstrated that these increased Am(III) and Pu(III) concentrations significantly increased DBRs and also increased mean total releases at low probabilities, but mean total repository releases remained below regulatory limits.

14.10 PRIORITIZATION OF CHEMISTRY-RELATED ISSUES

EPA's review of the CRA-2019 DPA chemistry-related models and parameters has identified issues that require additional evaluation. EPA believes the following should be prioritized for future WIPP PAs, because these issues might significantly affect predicted repository releases. These issues include, in approximate order of their priority:

- Revise the EQ3/6 database, especially to resolve issues related to the EDTA data, possible inconsistencies in Am(III) stability constants and Pitzer parameters, Th(IV)-carbonate aqueous speciation, Phase 5 solubility, addition of missing iron-sulfate data, and removal of lead data, but including all issues identified in Attachment B;
- Assume Pu(III), Np(IV), and U(IV) will be the dominant oxidation states for actinide solubility and mobilization calculations;
- Evaluate the potential effects on repository releases of placing waste stream SR-KAC-PuOx in a limited number of panels;
- Continue investigating radiolytic gas generation and brine consumption, including the relative importance and timing of radiolysis of brine by dissolved, colloidal, and wetted radionuclide solids, radiolysis of water adsorbed on waste, and CPR radiolysis;
- For future WIPP PAs, update the cutoff date for publications used to develop the +III and +IV actinide solubility uncertainty distributions to the most recent date that can be implemented;
- Determine whether the availability of more actinide solubility data for some conditions (e.g., less-crystalline solid phases) may bias the resulting actinide uncertainty distributions, and whether an alternative defensible approach is available to counter this potential effect;
- Revise parameters used to calculate actinide concentrations associated with microbial colloids (PROPMIC and CAPMIC) to be consistent with the available literature and project-specific data;
- Revise Th(IV) and Am(III) intrinsic colloid parameters to be consistent with the available literature and project-specific data;
- Assume a reasonable degree of calcite oversaturation in actinide solubility calculations to prevent unrealistic amounts of Phase 5 precipitation and solvent water consumption;
- Determine whether Phase 5 formation could affect the water balance calculations after re-evaluating its solubility and investigating its formation in Martin Marietta MgO hydration experiments; and
- Remove lead data in DATA0.FM4, which are incomplete and should not be used in WIPP actinide solubility calculations.

There are additional issues that should be addressed to minimize uncertainty in future WIPP PAs. These issues, listed in the order in which they are considered in this TSD include:

- Calculate D_s using projected total container counts at closure from DOE's inventory calculations and bounding estimates for iron-based waste;
- Evaluate MgO hydration rates using Martin Marietta MgO to improve the water balance;
- Use the appropriate brine volumes to calculate the initial solid phases in the 2-, 3-, 4-, and 5-times minimum brine volume actinide solubility calculations;
- Evaluate the potential effects of sulfides and phosphates on lead and iron solubilities, if lead or iron interactions with organic ligands are added to the actinide solubility calculations;
- Continue evaluating the potential effects of borate on actinide aqueous speciation and solid phase solubilities;
- Re-evaluate the available mineralogy data to provide a more realistic estimate of polyhalite concentrations in the Salado Formation;

- Review other possible approaches for evaluating actinide solubility uncertainties and the relative advantages and disadvantages of these alternatives to provide additional support for the current approach for addressing +III and +IV actinide solubility uncertainties;
- Resolve remaining uncertainties regarding formation of pseudocolloids from MgO hydration and carbonation products by performing sequential filtration experiments with brine samples from the MgO hydration and carbonation experiments after spiking the solution aliquots with Th(IV) and a +III actinide or analogue such as Nd(III);
- Investigate the effects of revised EDTA data in the EQ3/6 database on humic colloid parameters;
- Investigate the effects of silica aqueous species, solid phases, and formation of silica colloids with +IV actinides;
- Calculate the possible range of microbial cell counts of representative organisms in addition to *Bacillus* spores, such as bacteria and fungi, that could be introduced into WIPP through waste and archaea in brine, to provide a clearer picture of which organisms will likely dominate the 10^9 cells/ml biomass in the post-closure environment. This will provide information on which value for PROPMIC would be most representative and bounding.

EPA's review included sensitivity calculations performed using various combinations of chemistry parameters that were revised to address the identified issues. The results of the Agency's review and these sensitivity calculations show that there is a reasonable expectation that repository releases will remain within regulatory numerical release limits (40 CFR 191.13) if the chemistry parameters in question are revised.

15.0 REFERENCES

Abdel-Fattah, A.I, D. Zhou, H. Boukhalfa, S. Tarimala, S.D. Ware, and A.A. Keller. 2013. Dispersion stability and electrokinetic properties of intrinsic plutonium colloids: implications for subsurface transport. *Environmental Science and Technology* 47:5626-5634.

Abitz, R., J. Myers, P. Drez, and D. Deal. 1990. Geochemistry of Salado Formation brines from the Waste Isolation Pilot Plant (WIPP). *Waste Management '90. Tucson, AZ (USA)*. 25 February - 1 March 1990, CONF-900210-63.

AlMahamid, I., K.A. Becraft, N.L. Hakem, R.C. Gatti, and H. Nitsche. 1996. Stability of various plutonium valence states in the presence of NTA and EDTA. *Radiochimica Acta* 74:129-134.

Altmaier, M., and H. Geckeis. 2011. Plutonium and actinide chemistry in saline solutions. *Plutonium Futures, Actinide Research Quarterly* 2:29-32.

Altmaier, M., V. Neck and T. Fanghänel. 2004. Solubility and colloid formation of Th(IV) in concentrated NaCl and $MgCl_2$ solution. *Radiochimica Acta* 92:537-543.

Altmaier, M., V. Neck, R. Müller, and T. Fanghänel. 2005. Solubility of $ThO_2 \cdot xH_2O$ in carbonate solution and the formation of ternary Th(IV) hydroxide-carbonate complexes. *Radiochimica Acta* 93:83-92.

Altmaier, M., V. Neck, M.A. Denecke, R. Yin, and T. Fanghänel. 2006. Solubility of $ThO_2 \cdot xH_2O$ and the formation of ternary Th(IV) hydroxide-carbonate complexes in $NaHCO_3$-Na_2CO_3 solutions containing 0-4 M NaCl. *Radiochimica Acta* 94:495-500.

Altmaier, M., V. Neck, and T. Fanghänel. 2008. Solubility of Zr(IV), Th(IV) and Pu(IV) hydrous oxides in $CaCl_2$ solutions and the formation of ternary Ca-M(IV)-OH complexes. *Radiochimica Acta* 96:541-550.

Altmaier, M., V. Neck, J. Lützenkirchen, and T. Fanghänel. 2009. Solubility of plutonium in $MgCl_2$ and $CaCl_2$ solutions in contact with metallic iron. *Radiochimica Acta* 97:187-192.

Altmaier, M., D. Fellhauer, X. Gaona, and E. Yalcintas. 2017. *Assessment of Np(IV) and U(IV) as Improved Analogs for Pu(IV) in High Ionic-Strength Brine Systems*. KIT/INE Report, Karlsruhe, Germany.

Ams, D.A., J.S. Swanson, J.E.S. Szymanowski, J.B. Fein, M. Richmann, and D.T. Reed. 2013. The effect of high ionic strength on neptunium (V) adsorption to a halophilic bacterium. *Geochimica et Cosmochimica Acta* 110:45-57.

Anderson, B.L., M.K. Sheaffer, and L.E. Fischer. 2000. *Hydrogen Generation in TRU Waste Transportation Packages.* Prepared for the Spent Fuel Project Office, Office of Nuclear Materials Safety and Safeguards, U.S. Nuclear Regulatory Commission, Washington D.C. Prepared by Lawrence Livermore National Laboratory, Livermore, California.

Anderson, C., A. Johnsson, H. Moll, and K. Pedersen. 2011. Radionuclide geomicrobiology of the deep biosphere. *Geomicrobiology Journal* 38:540-561.

André, C., and G.R. Choppin. 2000. Reduction of Pu(V) by humic acid. *Radiochimica Acta* 88:613-616.

Andres, Y., H. J. MacCordick, and J.-C. Hubert. 1993. Adsorption of several actinide (Th, U) and lanthanide (La, Eu, Yb) ions by *Mycobacterium smegmatis*. *Applied Microbiology Biotechnology* 39:413-417.

ANL (Argonne National Laboratory). 1997. *Actinide Stability/Solubility Studies in Support of the Waste Isolation Pilot Plant*. Chemical Technology Division Annual Technical Report 1997. ANL-98/13, pp. 50-52.

Babb, S.C. 1996. *NONLIN, Ver. 2.00 User's Manual.* Sandia National Laboratories, Albuquerque, New Mexico, January 31, ERMS 230740.

Bader, M., K. Müller, H. Foerstendorf, B. Drobot, M. Schmidt, N. Musat, J.S. Swanson, D.T. Reed, T. Stumpf, and A. Cherkouk. 2017. Multistage bioassociation of uranium onto an extremely halophilic archaeon revealed by a unique combination of spectroscopic and microscopic techniques. *Journal of Hazardous Materials* 327:225-232.

Bader, M., K. Müller, H. Foerstendorf, M. Schmidt, K. Simmons, J. S. Swanson, D.T. Reed, T. Stumpf, and A. Cherkouk. 2018a. Comparative analysis of uranium bioassociation with halophilic bacteria and archaea. *PLOS One*, 13(1).

Bader, M., A. Rossberg, R. Steudtner, B. Drobot, K. Großmann, M. Schmidt, N. Musat, T. Stumpf, A. Ikeda-Ohno, and A. Cherkouk. 2018b. Impact of Haloarchaea on speciation of uranium—a multispectroscopic approach. *Environmental Science and Technology* 52:12895-12904.

Bader, M., H. Moll, R. Steudtner, H. Lösch, B. Drobot, T. Stumpf, and A. Cherkouk. 2019. Association of Eu (III) and Cm (III) onto an extremely halophilic archaeon. *Environmental Science and Pollution Research* 26:9352-9364.

Banaszak, J.E., S.M. Webb, B.E. Rittmann, J.-F. Gaillard, and D.T. Reed. 1999. Fate of Neptunium in Anaerobic, Methanogenic Microcosm. *Scientific Basis for Nuclear Waste Management XXII* 556:1141–1149.

Banik, N. 2006. *Speciation of Tetravalent Plutonium in Contact with Humic Substances and Kaolinite Under Environmental Conditions.* PhD thesis, Johannes Gutenberg-University Mainz.

Barber, D.B., K.P. Carney, P.R. Hart, D.G. Cummings, M.T. Sayer, D.L. Hendrix, K.T. Shirley, and J.C. Demirgian. 2001. The determination of the rate of hydrogen generation from transuranic 003 type organic sludge. *Waste Management Conference 2001*, Tucson, Arizona.

Bascetin, E., H. Haznedaroglu, and A.Y. Erkol. 2003. The adsorption behavior of cesium on silica gel. *Applied Radiation and Isotopes* 59:5-9.

Baskaran, M., P.H. Santschi, G. Benoit, and B.D. Honeyman. 1992. Scavenging of thorium isotopes by colloids in seawater of the Gulf of Mexico. *Geochimica et Cosmochimica Acta* 56:3375-3388.

Batchelder, T. 2018. *Reactivity Test for MgO*. Nuclear Waste Partnership LLC, Email to Y. Xiong, Sandia National Laboratories, Carlsbad, New Mexico, January 31, 2018, ERMS 569318.

Behrens, R.G., E.C. Buck, N.L. Dietz, J.K. Bates, E. Van Deventer, and D.J. Chaiko. 1995. *Characterization of Plutonium-Bearing Wastes by Chemical Analysis and Analytical Electron Microscopy.* Argonne National Laboratory, Argonne, Illinois, ANL-95/35.

Bellot-Gurlet, L., D. Neff, S. Réguer, J. Monnier, M. Saheb, and P. Dillmann. 2009. Raman studies of corrosion layers formed on archaeological irons in various media. *Journal of Nano Research* 8:147-156.

Bengtsson, L., B. Johansson, T. Hackett, L. McHale, and A. McHale. 1995. Studies on the biosorption of uranium by *Talaromyces emersonii* CBS 814.70 biomass. *Applied Microbiology Biotechnology* 42:807-811.

Berninger, U.-N., G. Jordan, J. Schott, and E.H. Oelkers. 2014. The experimental determination of hydromagnesite precipitation rates at 22.5 – 75ºC. *Mineralogical Magazine* 78:1405-1416.

Bitea, C., R. Müller, V. Neck, C. Walther, and J.I. Kim. 2003. Study of the generation and stability of thorium(IV) colloids by LIBD combined with ultrafiltration. *Colloids and Surfaces A: Physicochem. Eng. Aspects* 217:63-70.

Boggs, M.A., Y. Jiao, Z. Dai, M. Zavarin, and A.B. Kersting. 2016. Interactions of plutonium with Pseudomonas sp. strain EPS-1W and its extracellular polymeric substances. *Applied and Environmental Microbiology* 82:7093-7101.

Bolton, H., D. Rai, and L Xun. 2006. Biotransformation of Pu-EDTA: implications to Pu immobilization. *DOE-BER Environmental Remediation Sciences Project #1010283*. Richland, WA.

Bone, S., S. Kozimor, and D.T. Reed. 2019. *WIPP Pu Data: SSRL Beam Lin 11-2; March 2016.* Los Alamos National Laboratory. Carlsbad NM. Los Alamos Report LA-UR-19-27778.

Borkowski, M. 2010. *Numerical Values for Graphs Presented in the Report LCO-ACP-08, Rev. 0 Entitled: "Actinide (III) Solubility in WIPP Brine: Data Summary and Recommendations."* LANL-CO ACRSP ACP-1002-05-17-01, Los Alamos National Laboratory, Carlsbad, New Mexico.

Borkowski, M. 2012a. *Numerical Values for Graphs Presented in Report LCO-ACP-08, Rev. 0, Entitled Actinide(III) Solubility in WIPP Brine: Data Summary and Recommendations.* LA-UR-10-00898; LANL-CO ACRSP ACP-1002-05-17-01. Los Alamos National Laboratory, Carlsbad, New Mexico.

Borkowski, M. 2012b. *Numerical Values for Graphs Presented in Report LCO-ACP-08, Rev. 0, Entitled Solubility of An(IV) in WIPP Brine: Thorium Analog Studies in WIPP Simulated Brine, and for Graphs Published in Borkowski, M., et al. Radiochimica Acta 98 (9-11), 577-582 (2010).* LA-UR- 12-26640; LANL-CO ACRSP ACP-01/2012, Rev. 0. Los Alamos National Laboratory, Carlsbad, New Mexico.

Borkowski, M., J.F. Lucchini, M.K. Richmann, and D.T. Reed. 2009. *Actinide (III) Solubility in WIPP Brine: Data Summary and Recommendations*. LCO-ACP-08. LANL\ACRSP Report. Los Alamos National Laboratory, Los Alamos, New Mexico. Cited by DOE (2009) as Borkowski et al. (2008).

Borkowski, M, M. Richmann, D.T. Reed, and Y. Xiong. 2010. Complexation of Nd(III) with tetraborate ion and its effect on actinide(III) solubility in WIPP brine. *Radiochimica Acta* 98:577-582.

Borkowski, M, M. Richmann, and J.F. Lucchini. 2012. *Solubility of An(IV) in WIPP Brine: Thorium Analog Studies in WIPP Simulated Brine.* LA-UR 12-24417. Los Alamos National Laboratory, Carlsbad, New Mexico.

Bots, P., A. van Veelen, J.F.W. Mosselmans, C. Muryn, R.A. Wogelius, and K. Morris. 2019. Neptunium(V) and uranium(VI) reactions at the magnetite (111) surface. *Geosciences* 9:81.

Boukhalfa, H., S. Reilly, W. Smith, and M. Neu. 2003. Stability and redox behavior of plutonium-EDTA and Mixed Pu(IV)-EDTA-L (L= Hydroxide, Carbonate, Citrate) Complexes. *AIP Conference Proceedings* 673:238.

Boukhalfa, H., S. Reilly, W. Smith, and M. Neu. 2004. EDTA and mixed-ligand complexes of tetravalent and trivalent plutonium. *Inorganic Chemistry* 43:5816-5823.

Boukhalfa, H., G.A. Icopini, S.D. Reilly, and M.P. Neu. 2007. Plutonium(IV) retention by the metal-reducing bacteria *Geobacter metallireducens* GS15 and *Shewanella oneidensis* MR1. *Applied and Environmental Microbiology* 73:5897-5903.

Bouniol, P., and E. Bjergbakke. 2008. A comprehensive model to describe radiolytic processes in cement medium. *Journal of Nuclear Materials* 372:1-15.

Brendebach, B., M. Altmaier, J. Rothe, V. Neck, and M.A. Denecke. 2007. EXAFS study of aqueous Zr^{IV} and Th^{IV} complexes in alkaline $CaCl_2$ solutions: $Ca_3[Zr(OH)_6]^{4+}$ and $Ca_4[Th(OH)_8]^{4+}$. *Inorganic Chemistry* 46:6804-6810.

Brooks, S.C., J.K. Fredrickson, S.L. Carroll, D.W. Kennedy, J.M. Zachara, A.E. Plymale, S.D. Kelly, K.M. Kemner, and S. Fendorf. 2003. Inhibition of bacterial U(VI) reduction by calcium. *Environmental Science and Technology* 37:1850-1858.

Brunell, S. 2019. *Analysis Package for Normalized Releases in the 2019 Compliance Recertification Application Performance Assessment (CRA-2019 PA).* Sandia National Laboratories, Carlsbad, New Mexico, ERMS 571373.

Brush, L.H. 1990. *Test Plan for Laboratory and Modeling Studies of Repository and Radionuclide Chemistry for the Waste Isolation Pilot Plant*. SAND90-0266. Sandia National Laboratories, Albuquerque, New Mexico.

Brush, L.H. 1996. *Ranges and Probability Distributions of K_ds for Dissolved Pu, Am, U, Th and Np in the Culebra for the PA calculations to Support the WIPP CCA*. Memorandum to M.S. Tierney, Sandia National Laboratories, Albuquerque, New Mexico, June 10, 1996, ERMS 238801.

Brush, L.H., and P.S. Domski. 2013a. *Calculation of Organic Ligand Concentrations for the WIPP CRA-2014 PA.* Sandia National Laboratories, Carlsbad, New Mexico, ERMS 559005.

Brush, L.H., and P.S. Domski. 2013b. *Prediction of Baseline Actinide Solubilities for the WIPP CRA-2014 PA.* Sandia National Laboratories, Carlsbad, New Mexico, ERMS 559138.

Brush, L.H., and P.S. Domski. 2013c. *Uncertainty Analysis of Actinide Solubilities for the WIPP CRA-2014 PA, Rev. 1. Supersedes ERMS 559278.* Sandia National Laboratories, Carlsbad, New Mexico, ERMS 559712.

Brush, L.H., and L.J. Storz. 1996. *Revised Ranges and Probability Distributions of K_ds for Dissolved Pu, Am, U, Th and Np in the Culebra for the PA calculations to Support the WIPP CCA*. Memorandum to M.S. Tierney, Sandia National Laboratories, Albuquerque, New Mexico, July 24, 1996, ERMS 241561.

Brush, L.H., and Y. Xiong. 2003a. *Calculation of Actinide Solubilities for the WIPP Compliance Recertification Application*. Sandia National Laboratories Carlsbad Programs Group, Carlsbad, New Mexico, May 8, 2003, ERMS 529131.

Brush, L.H., and Y. Xiong. 2003b. *Calculation of Organic Ligand Concentrations for the WIPP Compliance Recertification Application*. Sandia National Laboratories, Carlsbad, New Mexico, ERMS 527567.

Brush, L.H., and Y. Xiong. 2003c. *Calculation of Organic Ligand Concentrations for the WIPP Compliance Recertification Application and for Evaluating Assumptions of Homogeneity in WIPP PA*. Sandia National Laboratories, Carlsbad, New Mexico, ERMS 531488.

Brush, L.H., and Y. Xiong. 2005. *Calculation of Organic-Ligand Concentrations for the WIPP Performance-Assessment Baseline Calculations*. Sandia National Laboratories, Carlsbad, New Mexico, ERMS 539635.

Brush, L.H. and Y. Xiong. 2009. *Calculation of Organic-Ligand Concentrations for the WIPP CRA-2009 PABC*. Sandia National Laboratories, Carlsbad, New Mexico, ERMS 551481.

Brush, L.H., Y. Xiong, J.W. Garner, A. Ismail, and G.T. Roselle. 2006. *Consumption of Carbon Dioxide by Precipitation of Carbonate Minerals Resulting from Dissolution of Sulfate Minerals in the Salado Formation in Response to Microbial Sulfate Reduction in the WIPP*. Sandia National Laboratories, Carlsbad, New Mexico, ERMS 544785.

Brush, L.H., Y. Xiong, J.W. Garner, T.B. Kirchner and J.J. Long. 2008. *Sensitivity of the Long-Term Performance of the WIPP to EDTA*. Sandia National Laboratories, Carlsbad, New Mexico, ERMS 548398.

Brush, L.H., Y. Xiong, and J.J. Long. 2009. *Results of the Calculations of Actinide Solubilities for the WIPP CRA-2009 PABC*. Sandia National Laboratories, Carlsbad, New Mexico, ERMS 552201.

Brush, L.H., P.S. Domski and Y.-L. Xiong. 2011. *Predictions of the Compositions of Standard WIPP Brines as a Function of pcH for Laboratory Studies of the Speciation and Solubilities of Actinides.* Sandia National Laboratories, Carlsbad, New Mexico, ERMS 555727.

Bryan, C.R., and A.C. Snider. 2001a. *MgO Hydration and Carbonation at SNL/Carlsbad, Sandia National Laboratories Technical Baseline Reports, WBS 1.3.5.4, Repository Investigations, Milestone RI010, January 31, 2001*. Sandia National Laboratories, Carlsbad, New Mexico, ERMS 516749, pp. 66 to 83.

Bryan, C.R., and A.C. Snider. 2001b. MgO Experimental Work Conducted at SNL/CB: Continuing Investigations with Premier Chemicals MgO, *Sandia National Laboratories Technical Baseline Reports, WBS 1.3.5.4, Repository Investigations, Milestone RI020, July 31, 2001*.

Bryson, D.C. 2015. *Response to the U.S. Environmental Protection Agency Letters Dated February 27, 2015 and June 5, 2015 Regarding the 2014 Compliance Recertification Application.* Letter to J.D. Edwards, U.S. Environmental Protection Agency, July 15, 2015.

Bynum, R.V. 1997. *Confirmation of the Ability of a Designed Backfill to Control the Chemical Environment in the WIPP*. DOE Test Plan TP 97-01, Rev. 0, Sandia National Laboratories, Albuquerque, New Mexico.

Camphouse, R.C. 2013a. *Analysis Package for Salado Flow Modeling Done in the 2014 Compliance Recertification Application Performance Assessment (CRA-2014 PA).* Sandia National Laboratories, Carlsbad, New Mexico.

Camphouse, R.C. 2013b. *Analysis Plan for the 2014 WIPP Compliance Recertification Application Performance Assessment.* AP-164, Sandia National Laboratories, Carlsbad, New Mexico.

Camphouse, R.C., M. Gross, C.G. Herrick, D.C. Kicker, and B. Thompson. 2012. *Recommendations and Justifications of Parameter Values for the Run-of-Mine Salt Panel Closure System Design Modeled in the PCS-2012 PA.* Sandia National Laboratories, Carlsbad, New Mexico, ERMS 557396.

Cevirim-Papaioannou, N., E. Yalcintas, X. Gaona, K. Dardenne, M. Altmaier, and M.H. Geckeis. 2018. Redox chemistry of uranium in reducing, dilute to concentrated NaCl solutions. *Applied Geochemistry* 98:286-300.

Chen, G., M. Flury, J.B. Harsh, and P.C. Lichtner. 2005. Colloid-facilitated transport of cesium in variably saturated Hanford Sediments. *Environmental Science and Technology* 39:3435-3442.

Cheng, W., and Z. Li. 2010. Controlled supersaturation precipitation of hydromagnesite for the $MgCl_2 – Na_2CO_3$ system at elevated temperatures: chemical modeling and experiment. *Industrial & Engineering Chemistry Research* 49:1964-1974.

Cho, H.-R., Y.-S. Youn, E.C. Jung, and W. Cha. 2016. Hydrolysis of trivalent plutonium and solubility of Pu(OH)3 (am) under electrolytic reducing conditions. *Dalton Transactions* 45: 19449-19457.

Choppin, G.R. 1991. Redox Speciation of Plutonium in Natural Waters. *Journal of Radioanalytical and Nuclear Chemistry Articles*, 147:109-116.

Choppin, G.R., A.H. Bond, M. Borkowski, M. Bronikowski, J.-F. Chen, S. Lis, J. Mizera, O.S. Pokrovsky, N.A. Wall, Y.X. Xia, and R.C. Moore. 2001. *Waste Isolation Pilot Plant Actinide Source Term Test Program: Solubility Studies and Development of Modeling Parameters*. Sandia National Laboratories, Albuquerque, New Mexico, April 2001, SAND99-0943.

Clayton, D. 2008. *Update to the Calculation of the Minimum Brine Volume for a Direct Brine Release.* Memorandum to L. Brush, Sandia National Laboratories, Carlsbad, New Mexico, April 2, 2008.

Clayton, D. 2009. *Update to the K_d Values for the PABC-2009. S*andia National Laboratories, Carlsbad, New Mexico, ERMS 552395.

Clayton, D.J. 2013. *Justification of Chemistry Parameters for Use in BRAGFLO for AP-164, Rev. 1.* Sandia National Laboratories, Carlsbad, New Mexico, ERMS 559466.

Cotsworth, E. 2004a. *CRA Completeness Comments - 3rd set - August 2004*. U.S. Environmental Protection Agency Office of Radiation and Indoor Air, Washington DC, letter (with enclosure) to R. Paul Detwiler, U.S. Department of Energy Carlsbad Field Office, September 2, 2004.

Cotsworth, E. 2004b. *First Set of CRA Comments (with enclosure).* U.S. Environmental Protection Agency Office of Radiation and Indoor Air, Washington DC, letter to R. Paul Detwiler, U.S. Department of Energy Carlsbad Field Office, May 20, 2004.

Cotsworth, E. 2005. *EPA Letter on Conducting the Performance Assessment Baseline Change (PABC) Verification Test.* Environmental Protection Agency Office of Radiation and Indoor Air, Washington DC., letter (with enclosure) to Inés Triay, U.S. Department of Energy, Carlsbad Field Office. March 4, 2005, ERMS 538858. Docket A-98-49, Item II-B3-80.

Cotsworth, E. 2009a. *CRA-2009 First (1) Completeness Letter.* U.S. Environmental Protection Agency Office of Radiation and Indoor Air, letter to D. Moody, U.S. Department of Energy Carlsbad Field Office, May 21, 2009.

Cotsworth, E. 2009b. *CRA-2009 Third Completeness Letter*. U.S. Environmental Protection Agency Office of Radiation and Indoor Air, letter to D. Moody, U.S. Department of Energy Carlsbad Field Office, October 19, 2009.

Crane R.A., and T.B. Scott. 2014. The removal of uranium onto nanoscale zero-valent iron particles in anoxic batch systems. *Journal of Nanomaterials* Article ID 956360.

Crane R.A., H. Pullin, and T.B. Scott. 2015. the influence of calcium, sodium and bicarbonate on the uptake of uranium onto nanoscale zero-valent iron particles. *Chemical Engineering Journal* 277:252–259.

Crawford, B., D. Guerin, S. Lott, B. McInroy, J. McTaggart, and G. Van Soest. 2009. *Performance Assessment Inventory Report – 2008.* INV-PA-08, Revision 0, Los Alamos National Laboratory Carlsbad Operations, LA-UR-09-02260, April 23, 2009.

Day, B. 2015. *Review of the Technical Basis for REFCON:ASDRUM, DRROOM, and VROOM Performance Assessment Analysis Parameters with Comparison to the Currently Emplaced Steel Surface Area per Unit Volume in the WIPP Repository.* Sandia National Laboratories, Carlsbad, New Mexico. ERMS 564670.

Day, B. 2019a. *Analysis Package For Salado Flow in the 2019 Compliance Recertification Application Performance Assessment (CRA-2019 PA).* Sandia National Laboratories, Carlsbad, New Mexico. ERMS 571368.

Day, B. 2019b. *Reassessment of Need and Parameter Justification for Modeling Gas Generation due to Radiolysis of Brine and Cellulose/Plastic/Rubber in WIPP for CRA-2019*. Sandia National Laboratories, Carlsbad, New Mexico. ERMS 570873.

Deng, H., S. Johnsen, Y. Xiong, G.T. Roselle, and M. Nemer. 2006. *Analysis of Martin Marietta MagChem® 10 WTS-60 MgO.* Sandia National Laboratories, Carlsbad, New Mexico. ERMS 544712.

Deng, H., M.B. Nemer, and Y. Xiong. 2007. *Experimental Study of MgO Reaction Pathways and Kinetics (Rev. 1, January 10)*. TP 06-03, Sandia National Laboratories, Carlsbad, New Mexico, ERMS 545182.

Deng, H., Y. Xiong, M. Nemer, and S. Johnsen. 2009. *Experimental Work Conducted on MgO Long-Term Hydration, 2008 Milestone Report. S*andia National Laboratories, Carlsbad, New Mexico, ERMS 551421.

Detwiler, R.P. 2004a. *MgO Emplacement.* U.S. Department of Energy Carlsbad Field Office, letter to Elizabeth Cotsworth, U.S. Environmental Protection Agency Office of Radiation and Indoor Air, Washington DC, October 20, 2004.

Detwiler, R.P. 2004b. *Partial Response to Environmental Protection Agency (EPA) May 20, 2004 Letter on CRA, Enclosure 1.* U.S. Department of Energy Carlsbad Field Office, Letter to Elizabeth Cotsworth, U.S. Environmental Protection Agency Office of Radiation and Indoor Air, Washington, DC, August 16, 2004.

Detwiler, R.P. 2004c. *Partial Response to Environmental Protection Agency (EPA) September 2, 2004, Letter on Compliance Recertification Application.* U.S. Department of Energy Carlsbad Field Office, Letter to Elizabeth Cotsworth, U.S. Environmental Protection Agency Office of Radiation and Indoor Air, Washington, DC, December 23, 2004.

Detwiler, R.P. 2004d. *Response to EPA May 20, 2004, Letter on CRA.* U.S. Department of Energy Carlsbad Field Office, letter to Elizabeth Cotsworth, U.S. Environmental Protection Agency Office of Radiation and Indoor Air, Washington, DC, September 29, 2004.

Ding, M., J.L. Conca, C. den Auwer, R.I. Gabitov, N.J. Hess, P. Paviet-Hartmann, P.D. Palmer, V. LoPresti, and S.D. Conradson. 2006. Chemical speciation of heterogeneously reduced Pu in synthetic brines. *Radiochimica Acta* 94:249-259.

Ding, C., S. Feng, W. Cheng, J. Zhang, X. Li, J. Liao, Y. Yang, Z. An, S. Luo, J. Yang, J. Tang, and N. Liu. 2014. Biosorption behavior and mechanism of thorium on *Streptomyces sporoverrucosus* dwc-3. *Journal of Radioanalytical Nuclear Chemistry,* 301:237-245.

Dodge, C. J., M. Dunn, A.J. Francis, J.B. Gillow, K. Mantione, M.E. Pansoy-Hjelvik, and H.W. Papenguth. 1998. *Role of Microbes as Biocolloids in the Transport of Actinides from a Deep Underground Radioactive Waste Repository.* SAND98-0370J, Sandia National Laboratories, Albuquerque, New Mexico.

Dodge, C.J., A.J. Francis, J.B. Gillow, G.P. Halada, C. Eng, and C.R. Clayton. 2002. Association of uranium with iron oxides typically formed on corroding steel surfaces. *Environmental Science and Technology* 36:3504–3511.

DOE (U.S. Department of Energy). 1996. *Title 40 CFR Part 191 Compliance Certification Application for the Waste Isolation Pilot Plant*, DOE/CAO-1996-2184, October 1996, Carlsbad Field Office, Carlsbad, New Mexico.

DOE (U.S. Department of Energy). 2004. *Title 40 CFR 191 Parts B and C Compliance Recertification Application*. U.S. Department of Energy Carlsbad Field Office, March 2004.

DOE (U.S. Department of Energy). 2009. *Title 40 CFR 191 Parts B and C Compliance Recertification Application*. U.S. Department of Energy Carlsbad Field Office, March 2009.

DOE (U.S. Department of Energy). 2012a. *Annual Transuranic Waste Inventory Report – 2012. Revision 0.* U.S. Department of Energy, Carlsbad Field Office, DOE/CBFO-94-1012.

DOE (U.S. Department of Energy). 2012b. *CH-TRU Payload Appendices, Rev. 3.* December 2012. Carlsbad, NM.

DOE (U.S. Department of Energy). 2014. *Title 40 CFR 191 Parts B and C Compliance Recertification Application*. U.S. Department of Energy Carlsbad Field Office, March 2014.

DOE (U.S. Department of Energy). 2017. *Annual Transuranic Waste Inventory Report – 2017. Revision 0.* U.S. Department of Energy, Carlsbad Field Office, DOE/TRU-18-3425.

DOE (U.S. Department of Energy). 2018. *Annual Transuranic Waste Inventory Report – 2018. Revision 0.* U.S. Department of Energy, Carlsbad Field Office, DOE/TRU-18-3425.

DOE (U.S. Department of Energy). 2019. *Title 40 CFR 191 Parts B and C Compliance Recertification Application*. U.S. Department of Energy Carlsbad Field Office, March 2019.

DOE (U.S. Department of Energy). 2020a. *EPA/DOE Technical Exchange on CRA-2019 Colloids, December 21, 2020 Notes*. U.S. Department of Energy Carlsbad Field Office, DOE RLSO 1-26-20.

DOE (U.S. Department of Energy). 2020b. *Transuranic Waste Acceptance Criteria for the Waste Isolation Pilot Plant, Revision 10*. U.S. Department of Energy Carlsbad Field Office, August 2020, DOE/WIPP-02-3122.

Domski, P.S. 2019a. *An Update to the EQ3/6 Pitzer Thermodynamic Database DATA0.FM1 with the Creation of DATA0.FM4*. Sandia National Laboratories. Carlsbad, New Mexico. ERMS 571052.

Domski, P.S. 2019b. *Correction of a Binary Pitzer Parameter in DATA0.FM4, PPR 2019-003.* Sandia National Laboratories, Carlsbad, New Mexico. ERMS 572172.

Domski, P.S. 2019c. *Technical Aspects of the Baseline Solubility Model for the CRA-2019 PA.* Sandia National Laboratories, Carlsbad, New Mexico, ERMS 571535.

Domski, P.S. 2019d. *Uncertainty Analysis of Actinide Solubilities for the CRA-2019 PA.* Sandia National Laboratories, Carlsbad, New Mexico, ERMS 571179.

Domski, P.S. 2020. *Correction of the α_1 Terms of Three Binary Pitzer Parameter Blocks in DATA0.FM4, PPR 2019-004 through 2019-013*. Sandia National Laboratories, Carlsbad, New Mexico, ERMS 572559.

Domski, P.S. 2021. *EPA Requested Changes to the CRA-2019 DPA Thermodynamic Database and Baseline Actinide Solubility Model*. Sandia National Laboratories, Carlsbad, New Mexico, ERMS 576365.

Domski, P.S., and C. Sisk-Scott. 2019. *Prediction of Baseline Actinide Solubilities for CRA 2019 with an Updated EQ3/6 Pitzer Thermodynamic Database, DATA0.FM4*. Sandia National Laboratories, Carlsbad, New Mexico, ERMS 571178.

Domski, P.S., and Y. Xiong. 2015a. *Analysis Plan for the Compilation and Testing of Selected Parameters from AP-134, Revision 3, AP-154, Revision 2 and AP-155, Revision 3 for Incorporation in a New QA EQ3/6 Thermodynamic Database.* Sandia National Laboratories, Carlsbad, New Mexico, ERMS 564585

Domski, P.S., and Y. Xiong. 2015b. *Prediction of Baseline Actinide Solubilities with an Updated EQ3/6 Thermodynamic Database (DATA0.FM2) in Response to EPA Completeness Comment 3-C-3 For CRA 2014.* Sandia National Laboratories, Carlsbad, New Mexico, ERMS 565032.

Dreissig, I. S. Weiss, C. Hennig, G. Bernhard, and H. Zänker. 2011. Formation of uranium(IV)-silica colloids at near-neutral pH. *Geochimica et Cosmochimica Acta* 75:352-367.

Du, A., B. Boonchayaanant, W.-M. Wu, S. Fendorf, J. Bargar, and C.S. Criddle. 2011. Reduction of uranium(V) by soluble iron(II) conforms with thermodynamic predictions. *Environmental Science and Technology* 45:4718-4725.

Dumas, T., D. Fellhauer, D. Schild, X. Gaona, M. Altmaier, and A. Scheinost. 2019. Plutonium retention mechanisms by magnetite under anoxic conditions: entrapment versus sorption. *ACS Earth and Space Chemistry* 3:2197-2206.

Duro, L., S. El Aamrani, M. Rovira, J. de Pablo, and J. Bruno. 2008. Study of the interaction between U(VI) and the anoxic corrosion products of carbon steel. *Applied Geochemistry* 23:1094-1100.

Eckerman, K., and A. Endo. 2008. ICRP (International Commission on Radiological Protection) Publication 107. 2008. Nuclear Decay Data for Dosimetric Calculations. *Annals of the ICRP* 38:7-96.

Economy, K. 2016. *High Order Chemistry Discussion Points.* U.S. Environmental Protection Agency, Email to R. Patterson, U.S. Department of Energy, July 28, 2016.

Edwards, J.D. 2011. U.S. Environmental Protection Agency, Office of Air and Radiation, to E. Ziemianski, U.S. Department of Energy, Carlsbad Field Office, August 8, 2011.

Edwards, J.D. 2013. U.S. Environmental Protection Agency, Office of Air and Radiation, to J. Franco, U.S. Department of Energy, Carlsbad Field Office, September 3, 2013.

Edwards, J.D. 2014. *First Set of EPA Completeness Comments for CRA 2014.* U.S. Environmental Protection Agency, Letter to J.R. Franco, U.S. DOE Carlsbad Field Office, December 17, 2014.

Edwards, J.D. 2015a. *Fourth Set of EPA Completeness Questions.* U.S. Environmental Protection Agency, Letter to J.R. Franco, U.S. DOE Carlsbad Field Office, July 30, 2015.

Edwards, J.D. 2015b. *Second Set of EPA Completeness Questions.* U.S. Environmental Protection Agency, Letter to J.R. Franco, U.S. DOE Carlsbad Field Office, February 27, 2015.

Edwards, J.D. 2015c. *Third Set of EPA Completeness Questions.* U.S. Environmental Protection Agency, Letter to J.R. Franco, U.S. DOE Carlsbad Field Office, June 5, 2015.

Emerson, H.P., F. Zengotita, M. Richmann, Y. Katsenovich, D.T. Reed, and T.M. Dittrich. 2018. Retention of neodymium by dolomite at variable ionic strength as probed by batch and column experiments. *Journal of Environmental Radioactivity* 190-191:89-96.

Emmerich, M., A. Bhansali, T. Lösekann-Behrens, C. Schröder, A. Kappler, and S. Behrens. 2012. Abundance, distribution, and activity of Fe(II)-oxidizing and Fe(III)-reducing

microorganisms in hypersaline sediments of Lake Kasin, Southern Russia. *Applied and Environmental Microbiology* 78:4386–4399.

EPA (Environmental Protection Agency). 1997a. *Compliance Application Review Documents for the Criteria for the Certification and Recertification of the Waste Isolation Pilot Plant's Compliance with the 40 CFR Part 191 Disposal Regulations: Final Certification Decision CARD 24: Waste Characterization.* U.S. Environmental Protection Agency Office of Radiation and Indoor Air. Washington, DC. Docket A-93-02 Item V-B-2.

EPA (U.S. Environmental Protection Agency). 1997b. *Compliance Application Review Documents for the Criteria for the Certification and Recertification of the Waste Isolation Pilot Plant's Compliance with the 40 CFR Part 191 Disposal Regulations: Final Certification Decision. CARD 44: Engineered Barrier*. EPA Air Docket A-93-02-V-B-2. U.S. Environmental Protection Agency Office of Radiation and Indoor Air. Washington, DC.

EPA (U.S. Environmental Protection Agency). 1998a. *Technical Support Document for Section 194.14: Assessment of K_ds used in the CCA*. U.S. Environmental Protection Agency Office of Radiation and Indoor Air, Washington DC. Docket A-93-02 Item V-B-4.

EPA (U.S. Environmental Protection Agency). 1998b. *Technical Support Document for Section 194.23: Parameter Justification Report.* Environmental Protection Agency Office of Radiation and Indoor Air, Washington, DC. Docket A-93-02 Item V-B-14.

EPA (U.S. Environmental Protection Agency). 1998c. *Technical Support Document for Section 194.24: EPA's Evaluation of DOE's Actinide Source Term.* Environmental Protection Agency Office of Radiation and Indoor Air, Washington, DC. Docket A-93-02 Item V-B-17.

EPA (U.S. Environmental Protection Agency). 2001a. *Approval of Elimination of Minisacks*. Environmental Protection Agency Office of Radiation and Indoor Air, Washington, DC. Docket A-98-49, II-B-3, Item 15.

EPA (U.S. Environmental Protection Agency). 2001b. *MgO Minisack Review*. U.S. Environmental Protection Agency Office of Radiation and Indoor Air, Washington, DC. ERMS 519362 (US EPA 2001a, enclosure).

EPA (U.S. Environmental Protection Agency). 2006a. *Criteria for the Certification and Recertification of the Waste Isolation Pilot Plant's Compliance With the Disposal Regulations: Recertification Decision*. *Federal Register* 71:18010-18021, April 10.

EPA (U.S. Environmental Protection Agency). 2006b. *Technical Support Document for Section 194.23: Review of the 2004 Compliance Recertification Performance Assessment Baseline Calculation*. Office of Radiation and Indoor Air, Docket No. A-98-49, Item II-B1-3, March 2006.

EPA (U.S. Environmental Protection Agency). 2006c. *Technical Support Document for Section 194.24: Evaluation of the Compliance Recertification Actinide Source Term and Culebra Dolomite Distribution Coefficient Values*. Office of Radiation and Indoor Air, Docket No. A-98-49, Item II-B1-16, March 2006.

EPA (U.S. Environmental Protection Agency). 2010a. *Criteria for the Certification and Recertification of the Waste Isolation Pilot Plant's Compliance With the Disposal Regulations: Recertification Decision*. *Federal Register* 75:70584-70595, November 18.

EPA (U.S. Environmental Protection Agency). 2010b. *Technical Support Document for Section 194.24: Evaluation of the Compliance Recertification Actinide Source Term, Backfill Efficacy and Culebra Dolomite Distribution Coefficient Values (Revision 1)*. Office of Radiation and Indoor Air, Docket No. A-98-49, Item II-B1-25, November 2010.

EPA (U.S. Environmental Protection Agency). 2017a. *Criteria for the Certification and Recertification of the Waste Isolation Pilot Plant's Compliance With the Disposal Regulations: Recertification Decision*. *Federal Register* 82:33106-33122, July 19.

EPA (U.S. Environmental Protection Agency). 2017b. *Probability of Encountering Castile Brine beneath the WIPP Waste Panels Using the TDEM Block Method*. Docket EPA-HQ-OAR-2014-0609. U.S. Environmental Protection Agency. Washington, DC.

EPA (U.S. Environmental Protection Agency). 2017c. *Review of EPA Sensitivity Studies of the DOE CRA-2014 WIPP Compliance Recertification Performance Assessment*. Docket EPA-HQ-OAR-2014-0609. U.S. Environmental Protection Agency. Washington, DC.

EPA (U.S. Environmental Protection Agency). 2017d. *Technical Support Document for Section 194.24: Evaluation of the Compliance Recertification Actinide Source Term, Gas Generation, Backfill Efficacy, Water Balance and Culebra Dolomite Distribution Coefficient Values*. Office of Radiation and Indoor Air, Docket No. EPA-HQ-OAR-2014-0609, June 2017.

EPA (U.S. Environmental Protection Agency). 2018a. *Technical Exchange Meeting February 13-15, 2018*. Albuquerque, New Mexico

EPA (U.S. Environmental Protection Agency). 2018b. *Technical Exchange Meeting September 25-27, 2018*. Albuquerque, New Mexico

Erkaya, I.A., M.Y. Arica, A. Akbulut, and G. Bayramoglu. 2014. Biosorption of uranium(VI) by free and entrapped Chlamydomonas reinhardtii: kinetic, equilibrium and thermodynamic studies. *Journal of Radioanalytical and Nuclear Chemistry* 299:1993-2003.

Felicione, F.S., K.P. Carney, and C.C. Dwight. 2001. Results from the Gas Generation Experiments at Argonne National Laboratory-West. *Sandia National Laboratories Technical Baseline Reports, WBS 1.3.5.4, Repository Investigations Milestone R1020, July 31, 2001*. Sandia National Laboratories, Carlsbad, New Mexico, ERMS 518970, pp. 2-1 to 2-5.

Felmy, A.R., and M.J. Mason. 2003. An Aqueous Thermodynamic Model for the Complexation of Sodium and Strontium with Organic Chelates Valid to High Ionic Strength. I. Ethylenedinitrilotetraacetic Acid (EDTA). *Journal of Solution Chemistry*. 32:283-300.

Felmy, A.R., and J.H. Weare. 1986. The prediction of borate mineral equilibria in natural waters: application to Searles Lake, California. *Geochimica et Cosmochimica Acta* 0:2771-2783.

Felmy, A.R., D. Rai, J.A. Schramke, and J.L. Ryan. 1989. The solubility of plutonium hydroxide in dilute solutions and in high-ionic-strength chloride brines. *Radiochimica Acta* 48:29-35.

Felmy, A.R., D. Rai and M.J. Mason. 1991. The solubility of hydrous thorium(IV) oxide in chloride media: development of an aqueous ion-interaction model. *Radiochimica Acta*55:177-185.

Felmy, A.R., D. Rai, M.S. Sterner, M.J. Mason, N.J. Hess and S.D. Conradson. 1997. Thermodynamic models for highly charged aqueous species: solubility of Th(1V) hydrous oxide in concentrated $NaHCO_3$ and Na_2CO_3 solutions. *Journal of Solution Chemistry* 26:233-248.

Felmy, A.R., D.A. Moore, K.M. Rosso, O. Qafoku, D. Rai, E.C. Buck and E.S. Ilton. 2011. Heterogeneous reduction of PuO_2 with Fe(II): importance of the Fe(III) reaction product. *Environmental Science and Technology* 45:3952-3958.

Felmy, A.R., D.A. Moore, C.I. Pearce, S.D. Conradson, O. Qafoku, E.C. Buck, K.M. Rosso, and E.S. Ilton. 2012. Controls on soluble Pu concentrations in PuO_2/magnetite suspensions. *Environmental Science and Technology* 46:11610-11617.

Fiedor, J.N., W.D. Bostick, R.J. Jarabek, and J. Farrell. 1998. Understanding the mechanism of uranium removal from groundwater by zero-valent iron using x-ray photoelectron spectroscopy. *Environmental Science and Technology* 32:1466-1473.

Fox, B. 2008. *Parameter Summary Report for the CRA-2009.* Rev. 0, Sandia National Laboratories, Carlsbad, New Mexico, ERMS 549747.

Fourdrin, C., H. Aarrachi, C. Latrille, S. Esnouf, F. Bergaya and S. Le Caer. 2013. Water radiolysis in exchanged-montmorillonites: the H_2 production mechanisms. *Environmental Science and Technology* 47:9530-9537

Francis, A.J. 1998. Biotransformation of uranium and other actinides in radioactive wastes. *Journal of Alloys and Compounds* 271–273:78–84.

Francis, A.J. 2007. Microbial mobilization and immobilization of plutonium. *Journal of Alloys and Compounds* 444 – 445:500 – 505.

Francis, A.J., and C.J. Dodge. 2008. Bioreduction of uranium(VI) complexed with citric acid by *clostridia* affects its structure and solubility. *Environmental Science and Technology* 42:8277-8282.

Francis, A.J., and J.B. Gillow. 1994. *Effects of Microbial Processes on Gas Generation Under Expected Waste Isolation Pilot Plant Repository Conditions. Progress Report through 1992.* Sandia National Laboratories, Albuquerque, New Mexico, SAND93-7036, WPO 26555.

Francis, A.J., and J.B. Gillow. 2000. *Progress Report: Microbial Gas Generation Program.* Unpublished memorandum to Y. Wang, January 6, 2000. Brookhaven National Laboratory, Upton, New York, ERMS 509352.

Francis A.J., J.B. Gillow, and M.R. Giles. 1997. *Microbial Gas Generation Under Expected Waste Isolation Pilot Plant Repository Conditions*. Sandia National Laboratories, Albuquerque, New Mexico, SAND96-2582.

Francis, A.J., J.B. Gillow, C.J. Dodge, M. Dunn, K. Mantione, B.A. Strietelmeier, M.E. Pansoy-Hjelvik, and H.W. Papenguth. 1998. Role of bacteria as biocolloids in the transport of actinides from a deep underground radioactive waste repository. *Radiochimica Acta*, 82, 347-354.

Francis, A.J., J. Gillow, C.J. Dodge, R. Harris, T. Beveridge, and H. Papenguth, 2004. Uranium association with halophilic and non-halophilic bacteria and archaea. *Radiochimica Acta*, 92:481-488.

Francis, A.J., C.J. Dodge, J.B. Gillow, and H.W. Papenguth. 2000. Biotransformation of uranium compounds in high ionic strength brine by a halophilic bacterium under denitrifying conditions. *Environmental Science and Technology* 34:2311-2317.

Francis, A.J., C.J. Dodge, and T. Ohnuki. 2007. Microbial transformations of plutonium. *Journal of Nuclear and Radiochemical Sciences* 8:121-126.

Franco, J.R. 2012. *Planned Change Notice for Placement of Magnesium Oxide Supersacks.* U.S. Department of Energy Letter to A. Perrin, U.S. Environmental Protection Agency, February 14, 2012.

Franco, J.R. 2015a. *Response to Environmental Protection Agency Letter Dated December 17, 2014 Regarding the 2014 Compliance Recertification Application.* U.S. Department of Energy Letter to J.D. Edwards, U.S. Environmental Protection Agency, March 18, 2015.

Franco, J.R. 2015b. *Response to Environmental Protection Agency Letters Dated December 17, 2014 and February 27, 2015 Regarding the 2014 Compliance Recertification Application.* U.S. Department of Energy Letter to J.D. Edwards, U.S. Environmental Protection Agency, May 29, 2015.

Frederickson, J.K., J.M. Zachara, D.W. Kennedy, M.C. Duff, Y.A. Gorby, S.-M. W. Li, and K. Krupka. 2000. Reduction of U(VI) in goethite (α-FeOOH) suspensions by a dissimilatory metal-reducing bacterium. *Geochimica et Cosmochimica Acta* 64:3085-3098.

Gallegos, T.J., C.C. Fuller, S.M. Webb, and W. Betterton. 2013. Uranium(VI) interactions with mackinawite in the presence and absence of bicarbonate and oxygen. *Environmental Science and Technology* 47:7357-7364.

Giambalvo, E.R. 2002a. *Recommended Parameter Values for Modeling An(III) Solubility in WIPP Brines*. Memorandum to L.H. Brush, July 25, 2002, ERMS 522982.

Giambalvo, E.R. 2002b. *Recommended Parameter Values for Modeling Organic Ligands in WIPP Brines*. Memorandum to L.H. Brush, July 25, 2002, ERMS 522981.

Giambalvo, E.R. 2002c. *Recommended Parameter Values for Modeling An(IV) Solubility in WIPP Brines*. Memorandum to L.H. Brush, July 26, 2002, ERMS 522986.

Giambalvo, E.R. 2002d. *Recommended Parameter Values for Modeling An(V) Solubility in WIPP Brines*. Memorandum to L.H. Brush, July 26, 2002, ERMS 522990.

Giambalvo, E.R. 2002e. *Recommended μ^0/RT Values for Modeling the Solubility of Oxalate Solids in WIPP Brines.* Memorandum to L.H. Brush, July 31, 2002, ERMS 523057.

Giambalvo, E.R. 2003. *Release of FMT Database FMT_021120.CHEMDAT*. Memorandum to L.H. Brush, March 10, 2003, ERMS 526372.

Gillow, J.B., and A.J. Francis. 2001a. Re-evaluation of Microbial Gas Generation Under Expected Waste Isolation Pilot Plant Conditions: Data Summary Report, January 24, 2001, *Sandia National Laboratories Technical Baseline Reports, WBS 1.3.5.4, Repository Investigations Milestone RI010, January 31, 2001.* Sandia National Laboratories, Carlsbad, New Mexico, ERMS 516749, pp. 19–46.

Gillow, J.B., and A.J. Francis. 2001b. Re-evaluation of Microbial Gas Generation Under Expected Waste Isolation Pilot Plant Conditions: Data Summary and Progress Report (February 1 - July 13, 2001), *Sandia National Laboratories Technical Baseline Reports, WBS 1.3.5.4, Repository Investigations Milestone R1020, July 31, 2001.* Sandia National Laboratories. Carlsbad, New Mexico, ERMS 518970, pp. 3-1 to 3-21.

Gillow J.B., and A.J. Francis. 2002a. Re-evaluation of Microbial Gas Generation Under Expected Waste Isolation Pilot Plant Conditions: Data Summary and Progress Report (July 14, 2001 - January 31, 2002), January 22, 2002. *Sandia National Laboratories Technical Baseline Reports, WBS 1.3.5.3, Compliance Monitoring; WBS 1.3.5.4, Repository Investigations, Milestone RI110, January 31, 2002.* Sandia National Laboratories, Carlsbad, New Mexico, ERMS 520467, pp. 2.1-1 to 2.1-26.

Gillow, J.B., and A.J. Francis. 2002b. Re-evaluation of Microbial Gas Generation Under Expected Waste Isolation Pilot Plant Conditions: Data Summary and Progress Report (February 1–July 15, 2002), January 18, 2002. *Sandia National Laboratories Technical Baseline Reports, WBS 1.3.5.3, Compliance Monitoring; WBS 1.3.5.4, Repository Investigations, Milestone RI130, July 31, 2002.* Sandia National Laboratories, Carlsbad, New Mexico, ERMS 523189, pp. 3.1-1 to 3.1-A10.

Gillow, J., and A.J. Francis. 2003. *Microbial Gas Generation Under Expected Waste Isolation Pilot Plant Repository Conditions.* Final Report, Revision 0, October 6 Draft, ERMS 532877.

Gillow, J., M. Dunn, A.J. Francis, D. Lucero, and H. Papenguth. 2000. The potential of subterranean microbes in facilitating actinide migration at the Grimsel Test Site and Waste Isolation Pilot Plant. *Radiochimica Acta*, 88:769-775.

Gitlin, B.C. 2006. U.S. Environmental Protection Agency, Office of Air and Radiation, Washington, DC. Letter to D.C. Moody, U.S. Department of Energy, Carlsbad Field Office, Carlsbad, New Mexico. April 28, 2006.

Grambow, B., E. Smailos, H. Geckeis, R. Müller, and H. Hentschel. 1996. Sorption and reduction of uranium(VI) on iron corrosion products under reducing saline conditions. *Radiochimica Acta* 74:149 154.

Gray, W.J., and S.A. Simonson. 1984. *Gamma and Alpha Radiolysis of Salt Brines*. PNL-SA-12746, 1984 Fall Meeting of the Materials Research Society in Boston, Mass., November 1984.

Grenthe, I., X. Gaona, A.V. Plyasunov, L. Rao, W.H. Runde, B. Grambow, R.J.M. Konings, A.L. Smith, and E.E. Moore. 2020. *Second Update on the Chemical Thermodynamics of Uranium Neptunium Plutonium Americium and Technetium*. OECD Nuclear Energy Agency Data Bank, Eds., OECD Publications, Boulogne-Billancourt, France.

Gu, B., L. Liang, M.J. Dickey, X. Yin, and S. Dai. 1998. Reductive precipitation of uranium (VI) by zero-valent iron. *Environmental Science and Technology* 32:3366–3373.

Guillaumont, R., T. Fanghänel, V. Neck, J. Fuger, D.A. Palmer, I. Grenthe, and M.H. Rand. 2003. *Update on the Chemical Thermodynamics of Uranium, Neptunium, Plutonium, Americium and Technetium.* OECD Nuclear Energy Agency Data Bank, Eds., OECD Publications, Issy-les-Moulineaux, France.

Haas, J. R., T.J. Dichristina, and R. Wade Jr. 2001. Thermodynamics of U (VI) sorption onto *Shewanella putrefaciens. Chemical Geology* 180:33-54.

Hansen, C.W., L.H. Brush, M.B. Gross, F.D. Hansen, B. Thompson, J.S. Stein, and B-Y Park 2003a. *Effects of Supercompacted Waste and Heterogeneous Waste Emplacement on Repository Performance, Rev. 0.* Sandia National Laboratories Carlsbad Programs Group, Carlsbad, New Mexico, October 7, 2003. ERMS 532326

Hansen, C.W., L.H. Brush, M.B. Gross, F.D. Hansen, B-Y Park, J.S. Stein, and B. Thompson 2003b. *Effects of Supercompacted Waste and Heterogeneous Waste Emplacement on Repository Performance, Rev. 1.* Sandia National Laboratories Carlsbad Programs Group, Carlsbad, New Mexico, October 17, 2003, ERMS 532475.

Harvie, C.F., N. Møller, and J.H. Weare. 1984. The prediction of mineral solubilities in natural waters: The Na-K-Mg-Ca-H-Cl-SO4-OH-HCO_3-CO_3-CO_2-H_2O system to high ionic strengths at 25°C *Geochimica Cosmochimica Acta* 48:723-751.

Haschke, J.M., T.H. Allen, and L.A. Morales. 2000. Reaction of Plutonium Dioxide with Water: Formation and Properties of PuO_{2+x}. *Science* 287:285-287.

Hennig, C. S. Weiss, D. Banerjee, E. Brendler, V. Honkimäki, G. Cuello, A. Ikeda-Ohno, A.C. Scheinost, and H. Zänker. 2013 Solid-state properties and colloidal stability of thorium(IV)–silica nanoparticles. *Geochimica Cosmochimica Acta* 103:197-212.

Herm, M., X. Gaona, T. Rabung, D. Fellhauer, C. Crepin, K. Dardenne, M. Altmaier, and H. Geckeis. 2015. Solubility and spectroscopic study of An^{III}/Ln^{III} in dilute to concentrated Na-Mg-Ca-Cl-NO_3 solutions. *Pure and Applied Chemistry* 87:487-502.

Hinz, K., M. Altmaier, X. Gaona, T. Rabung, D. Schild, M. Richmann, D. Reed, E. Alekseev, and H. Geckeis. 2015. Interaction of Nd(III) and Cm(III) with borate in dilute to concentrated alkaline NaCl, $MgCl_2$ and $CaCl_2$ solutions: solubility and TRLFS studies. *New Journal of Chemistry* 39:849-859.

Hobart, D.E., and R.C. Moore. 1996. *Analysis of Uranium (VI) Solubility Data for WIPP Performance Assessment WBS 1.1.10.1.1.* Sandia National Laboratories, May 28, 1996, ERMS 239856.

Hopkins, A.M., C. Sutter, G. Julse, and J. Teal. 2003. Disposal of TRU waste from the Plutonium Finishing Plant in Pipe Overpack Contains to WIPP including new security requirements. *WM '03 Conference*, February 23-27, Tucson, Arizona.

Hua, B., J. Xu, J. Terry, and B. Deng. 2006. Kinetics of uranium(VI) reduction by hydrogen sulfide in anoxic aqueous systems. *Environmental Science and Technology* 40:4666-4671.

Hua, Y., W. Wand, X. Huang, T. Gu, D. Ding, L. Ling, and W Zhang. 2018. Effect of bicarbonate on aging and reactivity of nanoscale zerovalent iron (nZVI) toward uranium removal. *Chemosphere* 201:603-611.

Huber, F., D. Schild, T. Vitova, J. Rothe, R. Kirsch, and T. Schäfer. 2012. U(VI) removal kinetics in presence of synthetic magnetite nanoparticles. *Geochimica et Cosmochimica Acta* 96:154-173.

Hummel, W., G. Anderegg, L. Rao, I. Puigdomènech and O. Tochiyama. 2005. *Chemical Thermodynamics of Compounds and Complexes of U, Np, Pu, Am, Tc, Se, Ni and Zr with Selected Organic Ligands.* OECD Nuclear Energy Agency Data Bank, Eds., OECD Publications, Issy-les-Moulineaux, France.

Husar, R., S. Weiss, C. Henig, R. Hűbner, A. Ikeda-Ohno, and H. Zänker. 2015. Formation of neptunium(IV)–silica colloids at near-neutral and slightly alkaline pH. *Environmental Science and Technology* 49:665-671.

Hyun, S.P., J.A. Davis, K. Sun and K.F. Hayes. 2012. Uranium(VI) reduction by iron(II) monosulfide mackinawite. *Environmental Science and Technology* 46:3369-3376.

Icopini, G.A., J. Boukhalfa, and M.P. Neu. 2007. Biological reduction of Np(V) and Np(V) citrate by metal-reducing bacteria. *Environmental Science and Technology* 41:2764–69.

Icopini, G.A., J.G. Lack, L.E. Hersman, M.P. Neu, and H. Boukhalfa. 2009. Plutonium(V/VI) reduction by the metal-reducing bacteria *Geobacter metallireducens* GS-15 and *Shewanella oneidensis* MR-1. *Applied and Environmental Microbiology* 75:3641-3647.

INEEL (Idaho National Engineering and Environmental Laboratory). 1999. *TRUPACT-II Matrix Depletion Program Final Report*. Prepared for the U.S. Department of Energy, Idaho Falls, Idaho, INEL/EXT-98-00987.

Ismail, A.E., J. Deng. J.-H. Jang, and T.J. Wolery. 2009. *Verification of FMT Database and Conversion to EQ3/6 Format.* Sandia National Laboratories, Carlsbad, New Mexico, ERMS 550689.

Jenks, G.H. 1972. *Radiolysis and Hydrolysis is Salt-Mine-Brines.* ORNL-TM-3717, Oak Ridge National Laboratories, Oak Ridge, Tennessee, March 1972.

Kanney, J.F., A.C. Snider, T.W. Thompson, and L.H. Brush. 2004. *Effect of Naturally Occurring Sulfate on the MgO Safety Factor in the Presence of Supercompacted Waste and Heterogeneous Waste Emplacement.* Sandia National Laboratories Carlsbad Programs Group, Carlsbad, New Mexico, March 5, 2004.

Kanney, J.F., and E.D. Vugrin, 2006. *Updated Analysis of Characteristic Time and Length Scales for Mixing Processes in the WIPP Repository to Reflect the CRA-2004 PABC Technical Baseline and the Impact of Supercompacted Mixed Waste and Heterogeneous Waste Emplacement.* Memorandum to D.S. Kessel, Sandia National Laboratories, Carlsbad, New Mexico, August 31, 2006.

Katz, J.L., M.R. Reick, R.E. Herzog, and K.I. Parsiegla. 1993. Calcite growth inhibition by iron. *Langmuir* 9:1423-1430.

Kelm, M., I. Pashlidis, and J.I. Kim. 1999. Spectroscopic investigation on the formation of hypochlorite by alpha radiolysis in concentrated NaCl solutions. *Applied Radiation and Isotopes* 51:637-642.

Khalili, F.K., V. Symeopoulos, J.F. Chen, and G.R. Choppin. 1994. Solubility of Nd in brine. *Radiochimica Acta* 66/67:51-54.

Kicker, D.C. 2019a. *Analysis Package for Cuttings, Cavings, and Spallings in the 2019 Compliance Recertification Application Performance Assessment (CRA-2019 PA). Revision 0.* Sandia National Laboratories, Carlsbad, New Mexico, ERMS 571369.

Kicker, D.C. 2019b. *Radionuclide Inventory Screening Analysis for the 2019 Compliance Recertification Application Performance Assessment. (CRA-2019 DPA). Revision 1.* Sandia National Laboratories, Carlsbad, New Mexico, ERMS 571659.

Kicker, D.C, and C.G. Herrick. 2013. *Parameter Summary Report for the Compliance Recertification Application, Rev. 0*. Sandia National Laboratories, Carlsbad, New Mexico, ERMS 560298.

Kim, S., and L.M. Feng. 2019. *Input Parameter Report for the 2019 Compliance Recertification Application Performance Assessment (CRA-2019 DPA), Revision 0.* Sandia National Laboratories, Carlsbad, New Mexico, ERMS 571377.

Kirchner, T. 2008. *Generation of the LHS Samples for the AP-137 Revision 0 (CRA09) PA Calculations.* Sandia National Laboratories, Carlsbad, New Mexico, ERMS 547971.

Kirchner, T. 2013. *Sensitivity of the CRA-2014 Performance Assessment Releases to Parameters.* Sandia National Laboratories, Carlsbad, New Mexico, ERMS 560043.

Kirkes, L. 2019. *Lead Inventory Impact on Gas Generation*. Sandia National Laboratories. Carlsbad, New Mexico, ERMS 571255.

Klein, T. 2018. *Re: MgO Emplacement Factor as of December 31, 2017.* Nuclear Waste Partnership LLC, Email to Y. Xiong, January 22, 2018, Sandia National Laboratories, Carlsbad, New Mexico, ERMS 569317.

Knerr, R. 2020a. *Response 3 to U.S. Environmental Protection Agency's 2019 Compliance Recertification Application Completeness Comments Letter dated March 23, 2020 and May 6, 2020 from Tom Peake to Mike Brown*. U.S. Department of Energy, Carlsbad Field Office, Carlsbad, New Mexico. Letter to L.B. Veal, U.S. Environmental Protection Agency Radiation Protection Division, Washington, D.C. August 13, 2020.

Knerr, R. 2020b. *Response 6 to U.S. Environmental Protection Agency's 2019 Compliance Recertification Application Completeness Comments Letter dated March 23, 2020, May 8, 2020, June 12, 2020, and July 17, 2020 from Tom Peake to Mike Brown*. U.S. Department of Energy, Carlsbad Field Office, Carlsbad, New Mexico. Letter to L.B. Veal, U.S. Environmental Protection Agency Radiation Protection Division, Washington, D.C. October 26, 2020.

Knerr, R. 2020c. *Response 7 to U.S. Environmental Protection Agency's 2019 Compliance Recertification Application Completeness Comments Letters dated May 6, 2020, June 12, 2020, July 17, 2020 and September 11, 2020 from Tom Peake to Mike Brown*. U.S. Department of Energy, Carlsbad Field Office, Carlsbad, New Mexico. Letter to L.B. Veal, U.S. Environmental Protection Agency Radiation Protection Division, Washington, D.C. December 1, 2020.

Knerr, R. 2021a. *Response 8 to U.S. Environmental Protection Agency's 2019 Compliance Recertification Application Completeness Comments Letter dated September 11, 2020 and November 13, 2020 from Tom Peake to Mike Brown*. U.S. Department of Energy, Carlsbad Field Office, Carlsbad, New Mexico. Letter to L.B. Veal, U.S. Environmental Protection Agency Radiation Protection Division, Washington, D.C. January 13, 2021.

Knerr, R. 2021b. *Response 9 to U.S. Environmental Protection Agency's 2019 Compliance Recertification Application Completeness Comments Letter dated September 11, 2020 and November 13, 2020 from Tom Peake to Mike Brown*. U.S. Department of Energy, Carlsbad Field Office, Carlsbad, New Mexico. Letter to L.B. Veal, U.S. Environmental Protection Agency Radiation Protection Division, Washington, D.C. March 4, 2021.

Knerr, R. 2021c. *Response 10 to U.S. Environmental Protection Agency's 2019 Compliance Recertification Application Completeness Comments Letter dated September 11, 2020 and November 13, 2020 from Tom Peake to Mike Brown*. U.S. Department of Energy, Carlsbad Field Office, Carlsbad, New Mexico. Letter to L.B. Veal, U.S. Environmental Protection Agency Radiation Protection Division, Washington, D.C. March 30, 2021.

Knerr, R. 2021d. *Response 11 to U.S. Environmental Protection Agency's 2019 Compliance Recertification Application Completeness Comments Letter dated September 11, 2020 and*

November 13, 2020 from Tom Peake to Mike Brown and Email Dated January 7, 2021 from Ingrid Rosencrantz to Anderson Ward. U.S. Department of Energy, Carlsbad Field Office, Carlsbad, New Mexico. Letter to L.B. Veal, U.S. Environmental Protection Agency Radiation Protection Division, Washington, D.C. April 23, 2021.

Knerr, R. 2021e. *Response 12 to U.S. Environmental Protection Agency's 2019 Compliance Recertification Application Completeness Comments Letter dated September 11, 2020 and November 13, 2020 from Tom Peake to Mike Brown*. U.S. Department of Energy, Carlsbad Field Office, Carlsbad, New Mexico. Letter to L.B. Veal, U.S. Environmental Protection Agency Radiation Protection Division, Washington, D.C. May 27, 2021.

Knerr, R. 2021f. *Supplementary Information as Requested by U.S. Environmental Protection Agency During Technical Exchange Meeting on June 22, 2020*. U.S. Department of Energy, Carlsbad Field Office, Carlsbad, New Mexico. Letter to L.B. Veal, U.S. Environmental Protection Agency Radiation Protection Division, Washington, D.C. July 8, 2021.

Knerr, R. 2021g. *Carlsbad Field Office Response 13 to U.S. Environmental Protection Agency's 2019 Compliance Recertification Application Follow-up Completeness Comment*. U.S. Department of Energy, Carlsbad Field Office, Carlsbad, New Mexico. Letter to L.B. Veal, U.S. Environmental Protection Agency Radiation Protection Division, Washington, D.C. May 18, 2021.

Knerr, R. 2022. *Submission of Materials Completing Action Items Agreed Upon in the December 14, 2021 Classified Briefing for EPA by NNSA and DOE-CBFO*. U.S. Department of Energy, Carlsbad Field Office, Carlsbad, New Mexico. Letter to L.B. Veal, U.S. Environmental Protection Agency Radiation Protection Division, Washington, D.C. January 26, 2022.

Kouba, S. 2013. *Re: MgO Emplacement Factor as of December 31, 2012; Attachment: CBFO_Emplacement_Statistics-12-31-2012.txt.* Nuclear Waste Partnership LLC, Email to L. Brush, October 8, 2013, Sandia National Laboratories, Carlsbad, New Mexico.

Kozai, N., T. Ohnuki, and T. Iwatsuki, 2013. Characterization of saline groundwater at Horonobe, Hokkaido, Japan by SEC-UV-ICP-MS: Speciation of uranium and iodine. *Water Research* 47:1570-1584.

Krumhansl, J.L., K.M. Kimball, and C.L. Stein. 1991. *Intergranular Fluid Compositions from the Waste Isolation Pilot Plant (WIPP), Southeastern New Mexico*. Sandia National Laboratories, Albuquerque, New Mexico, SAND90-0584, March 1991.

Krumhansl, J.L., Kelly, J.W., Papenguth, H.W., and R.V. Bynum. 1997. *MgO Acceptance Criteria*. Unpublished memorandum to E.J. Nowak, December 10, 1997. Sandia National Laboratories, Albuquerque, New Mexico, ERMS 248997.

Le Caër, S. 2011. Water radiolysis: influence of oxide surfaces on H_2 production under ionizing radiation. *Water* 3:235-253.

Lambert, S.J. 1992. Geochemistry of the Waste Isolation Pilot Plant (WIPP) site, southeastern New Mexico, USA. *Applied Geochemistry* 7:513-531.

Langmuir, D. 1997. *Aqueous Environmental Chemistry.* Prentice Hall, Upper Saddle River, New Jersey.

LANL-CO 2018. *Estimation of Cellulose, Plastic, and Rubber Emplacement and Operational Materials in the Waste Isolation Pilot Plant (WIPP).* LANL-CO. INV-SAR-51, Revision 0, December 13, 2018. LANL-CO Record ID# INV-1812-05-01-01.

Larson, K.W. 1996. *Brine-Waste Contact Volume for Scoping Analysis of Organic Ligand Concentration*. Unpublished memorandum to R.V. Bynum, Sandia National Laboratories, Albuquerque, New Mexico, March 13, 1996, ERMS 236044.

Latta, D.E., C.A. Gorski, M.I Boyanov, E. J. O'Loughlin, K.M. Kemner, and M.M. Scherer. 2012. Influence of magnetite stoichiometry on U^{VI} reduction. *Environmental Science and Technology* 46:778-786.

LaVerne, J.A., and L. Tandon. 2003. H_2 production in the radiolysis of water on UO_2 and other oxides. *Journal of Physical Chemistry B* 107:13623-13628.

Lebron I., and D.L. Suarez. 1996. Calcite nucleation and precipitation kinetics as affected by dissolved organic matter at 25C and pH > 7.5. *Geochimica et Cosmochimica Acta* 60:2765-2776.

Leigh, C. 2003. *Estimate of Cellulosics, Plastics, and Rubbers in a Single Panel in the WIPP Repository in Support of AP-107, Supersedes ERMS 530959*. Unpublished Analysis Report. Sandia National Laboratories, Carlsbad, New Mexico, ERMS 531324.

Leigh, C.D. 2005. *Organic Ligand Masses TRU Waste Streams from TWBID Revision 2.1 Version 3.13 Data Version D4.15, Revision 1*. Memorandum to L.H. Brush, April 18, 2005, Sandia National Laboratories, Carlsbad, New Mexico, ERMS 539550.

Leigh, C., J. Kanney, L. Brush, J. Garner, R. Kirkes, T. Lowry, M. Nemer, J. Stein, E. Vugrin, S. Wagner, and T. Kirchner. 2005. *2004 Compliance Recertification Application Performance Assessment Baseline Calculation*. Sandia National Laboratories, Carlsbad, New Mexico, ERMS 541521.

Li Z., L. Wang, L. Yuan, C. Xiao, L. Mei, L. Zheng, J. Zhang, J. Yang, Y. Zhao, Z. Zhu, Z. Chai, and W. Shi. 2015. Efficient removal of uranium from aqueous solution by zero-valent iron nanoparticle and its graphene composite. *Journal of Hazardous Materials* 290:26–33.

Lin, X., D. Kennedy, J. Frederickson, B. Bjornstad, and A. Konopka. 2012. Vertical stratification of subsurface microbial community composition across geological formations at the Hanford Site. *Environmental Microbiology*, 14:414-425.

Liu, N., Y. Yang, S. Luo, T. Zhang, J. Jin, J. Liao, and X. Hua. 2002. Biosorption of 241Am by Rhizopus arrihizus: preliminary investigation and evaluation. *Applied Radiation Isotopes*, 57: 139-143.

Lovley, D.R., and E.J.P. Phillips. 1992. Reduction of uranium by *Desulfovibrio desulfuricans*. A*pplied and Environmental Microbiology* 58:850-856.

Lucchini, J.F., H. Khaing, M. Borkowski, M.K. Richmann, and D.T. Reed. 2010. *Actinide (VI) Solubility in Carbonate-free WIPP Brine: Data Summary and Recommendations.* LCO-ACP-10, LANL\ACRSP Report. Los Alamos National Laboratory, Los Alamos, New Mexico. Cited in the text of DOE (2009) as Lucchini et al. 2009 and as Lucchini et al. 2008 in the reference list.

Lucchini J.F, D.T. Reed, M.K. Richmann, and M. Borkowski. 2013a. *Actinide (VI) Solubility in Carbonate-free WIPP Brine: Data Summary and Recommendations*. LANL/ACRSP Report LCO-ACP-14, LA-UR 13-20786. Carlsbad, NM: Los Alamos National Laboratory.

Lucchini, J.F., M. Borkowski, H. Khaing, M.K. Richmann, J.S. Swanson, K. Simmons, and D.T. Reed. 2013b. *WIPP Actinide-Relevant Brine Chemistry.* Los Alamos National Laboratory, Carlsbad, New Mexico, LA-UR 13-20620.

Luk'yanova, E.A., E.V. Zakharova, L.I. Konstantinova, and T.N. Nazina. 2008. Sorption of radionuclides by microorganisms from a deep repository of liquid low-level waste. *Radiochemistry* 50:85-90.

Marcinowski, F. 2004. U.S. Environmental Protection Agency Office of Radiation and Indoor Air, Washington DC, Letter to R. Paul Detwiler, U.S. Department of Energy Carlsbad Field Office, March 26, 2004.

Mariner, P.E. 2016. *Actinide(IV)-Humic Complexation in the WIPP Performance Assessment.* Sandia National Laboratories, Albuquerque, New Mexico, ERMS 569599.

Mariner, P.E. 2018. *Actinide(III)-Humic Complexation in the WIPP Performance Assessment.* Sandia National Laboratories, Albuquerque, New Mexico, ERMS 567222.

Mariner, P.E. 2019. *A Summary of Humic Colloid Parameter Values to be Implemented in the CRA-2019 Deferred Performance Assessment.* Sandia National Laboratories, Albuquerque, New Mexico, ERMS 571250.

Marquardt, C.M., A. Seibert, R. Artinger, M.A. Denecke, B. Kuczewski, D. Schild, and T. Fanghänel. 2004. The redox behavior of plutonium in humic rich groundwater. *Radiochimica Acta* 92:617-623.

Marquardt, C.M., N.L. Banik, N Shcherbina, and H. Geckeis. 2008. Redox behavior of plutonium and neptunium in aqueous solution containing humic substances or hydroquinone. *NRC7 – Seventh International Conference on Nuclear and Radiochemistry.* Hungary, August 24 – 28, 2008.

McAlhany. S. 2018. *Surplus Plutonium Disposition – Dilute and Dispose Approach*. National Nuclear Security Administration, M3-SR-18-0012, Revision 0. February 23, 2018.

Meinrath, D., and J.I. Kim. 1991. Solubility products of different Am(III) and Nd(III) carbonates. *European Journal of Solid State and Inorganic Chemistry* 28:383-388.

Meinrath, D., and H. Takeishi. 1993. Solid-liquid equilibria of Nd^{3+} in carbonate solutions. *Journal of Alloys and Compounds* 194:93-99.

MFG. 2000. *Evaluation of the Reported Presence of Oxidized Plutonium in the STTP Experiments and in Plutonium Oxide Solid.* Prepared for the U.S. Environmental Protection Agency Office of Radiation and Indoor Air by MFG Inc., Boulder, Colorado, in association with TechLaw Inc., Lakewood, Colorado and Monitor Scientific, Denver, Colorado.

Molecke, M.A. 1979. Gas Generation from Transuranic Waste Degradation. SAND79-091. Sandia National Laboratories, Albuquerque, New Mexico. WPO 28093.

Moody, D.C. 2006. U.S. Department of Energy, Carlsbad Field Office, Letter to E.A. Cotsworth, U.S. Environmental Protection Agency, requesting a reduction in the MgO EF from 1.67 to 1.2. April 10, 2006. ERMS 543262.

Moody, D.C. 2009a. *Response to Environmental Protection Agency Letter dated May 21, 2009 Regarding Compliance Recertification Application*. U.S. Department of Energy, Carlsbad Field Office, Letter to E. Cotsworth, August 24, 2009, Office of Radiation and Indoor Air, Environmental Protection Agency.

Moody, D.C. 2009b. *Response to Environmental Protection Agency May 21, 2009 and July 16, 2009 Letters on the 2009 Compliance Recertification Application*. U.S. Department of Energy, Carlsbad Field Office, Letter to E. Cotsworth, Office of Radiation and Indoor Air, Environmental Protection Agency, November 25, 2009.

Moody, D.C. 2010. Response *to Environmental Protection Agency October 19, 2009 Letter on the 2009 Compliance Recertification Application*. U.S. Department of Energy, Carlsbad Field Office, Letter to E. Cotsworth, Office of Radiation and Indoor Air, Environmental Protection Agency, February 19, 2010.

Morozova, D., M. Wandrey, M. Alawi, M. Zimmer, A. Vieth, M. Zettlitzer, and H. Würdemann. 2010. Monitoring of the microbial community composition in saline aquifers during CO_2 storage by fluorescence in situ hybridisation. *International Journal of Greenhouse Gas Control* 4:981-989.

Myllykylä, E., and K. Ollila. 2011. *Interaction Between U(VI) and Fe(II) in Aqueous Solution Under Anaerobic Conditions – Closed System Experiments*. Posiva OY Working Report 2011-06, Eurojoki, Finland.

Narlesky, J.E., M.A. Stroud, P.H. Smith, D. M. Wayne, R. E. Mason, and L.A Worl, 2012. *Characterization of Representative Materials in Support of Safe, Long Term Storage of Surplus Plutonium in DOE-STD-3013 Containers*, LA-UR-12-23790, Los Alamos National Laboratory, Los Alamos, New Mexico.

Nazina, T.N., E.A. Luk'yanova, E. V. Zakharova, L.I. Konstantinova, S.N. Kalmykov, A.B. Poltaraus, and A.A. Zubkov. 2010. Microorganisms in a disposal site for liquid radioactive wastes and their influence on radionuclides. *Geomicrobiology Journal* 27:473-486.

Neck, V., R. Müller, M. Bouby, M. Altmaier, J. Rothe, M.A. Denecke, and J.I. Kim. 2002. Solubility of Amorphous Th(IV) Hydroxide-Application of LIBD to Determine the Solubility Product and EXAFS for Aqueous Speciation. *Radiochimica Acta* 90:485-494.

Neck, V., M. Altmaier, and T. Fanghänel. 2007. Solubility of plutonium hydroxides/hydrous oxides under reducing conditions and in the presence of oxygen. *Comptes Rendus Chimie* 10:959-977.

Neck, V., M. Altmaier, T. Rabung, J. Lützenkirchen, and T. Fanghänel. 2009. Thermodynamics of trivalent actinides and neodymium in NaCl, $MgCl_2$, and $CaCl_2$ solutions: solubility, hydrolysis, and ternary Ca-M(III)-OH complexes. *Pure and Applied Chemistry* 81:1555-1568.

Neff, D., P. Dillman, L. Bellot-Gurlet, and G. Beranger. 2005. Corrosion of iron archaeological artefacts in soil: characterization of the corrosion system. *Corrosion Science* 47:515-535.

Neill, T.M., K. Morris, C.I. Pearce, N.K. Sherriff, M.G. Burke, P.A. Chater, A. Janssen, L. Natrajan, and S. Shaw. 2018. Stability, composition, and core-shell particle structure of uranium(IV)-silicate colloids. *Environmental Science and Technology* 52:9118-9127.

Neill, T.M., K. Morris, C.I. Pearce, L. Abrahamsen-Mills, L. Kovarik, S. Kellet, B. Rigby, T. Vitova, B. Schacherl, and S. Shaw. 2019. Silicate stabilization of colloidal UO_2 produced by uranium metal corrosion. *Journal of Nuclear Materials* 526.

Neiss, J., B.D. Stewart, P.S. Nico, and S. Fendorf. 2007. Speciation-dependent microbial reduction of uranium within iron-coated sands. *Environmental Science and Technology* 41:7343-7348.

Nemer, M. 2005. *Updated Value of WAS_AREA:PROBDEG*. Memorandum to D.S. Kessel, April 20, 2005, Sandia National Laboratories, Carlsbad, New Mexico, ERMS 539441.

Nemer, M. 2008. *Procedure for Testing for the Periclase + Lime Content in Martin Marietta MgO Rev. 1*. November 17, 2008, Sandia National Laboratories, Carlsbad, New Mexico, ERMS 550455.

Nemer, M. 2009. *Adequacy of MgO Reactivity Test (EPA Re-Certification Question 1-C-2) and Interpreting MgO Reactivity Test Results Above 96 Mol %.* Sandia National Laboratories, Carlsbad, New Mexico, ERMS 551892.

Nemer, M., and D. Clayton. 2008. *Analysis Package for Salado Flow Modeling: 2009 Compliance Recertification Application Calculation.* Sandia National Laboratories, Carlsbad, New Mexico, ERMS 548607.

Nemer, M., and J. Stein. 2005. *Analysis Package for BRAGFLO: 2004 Compliance Recertification Application Performance Assessment Baseline Calculation*. Sandia National Laboratories, Carlsbad, New Mexico, ERMS 540527.

Nemer, M., J. Stein, and W. Zelinski. 2005. *Analysis Report for BRAGFLO Preliminary Modeling Results With New Gas Generation Rates Based Upon Recent Experimental Results*. Analysis Report, Sandia National Laboratories, Carlsbad, New Mexico, ERMS 539437.

Nemer, M., Y. Xiong, A.E. Ismail, and J. Jang. 2011. Solubility of $Fe_2(OH)_3Cl$ (pure-iron end-member of hibbingite) in NaCl and Na_2SO_4 brines. *Chemical Geology* 280:26-32.

Novak, C.F. and R.C. Moore. 1996. *Estimates of Dissolved Concentrations for +III, +IV, +V, and +VI Actinides in a Salado and a Castile Brine under Anticipated Repository Conditions*. Memo to M.D. Siegel, March 28, 1996, Sandia National Laboratories, Albuquerque, New Mexico, CCA Ref. No. 479.

Nowak, E.J., and D.J. Clayton. 2007. *Analysis of MgO Hydration Laboratory Results and Calculation of Extent of Hydration and Resulting Water Uptake Versus Time Under Postulated WIPP Conditions.* Sandia National Laboratories, Carlsbad, New Mexico, ERMS 546769.

Oakes, C.S., A.L. Ward, N. Chugunov, and J. Icenhower. 2021. A speciated, conventional Pitzer ion-interaction model for the aqueous Nd^{3+} - H^{+} - Na^{+} - K^{+} - Ca^{2+} - Cl^{-} - OH^{-} system at 298 K and 0.1 MPa. *Geochimica Cosmochimica Acta* 297:308-327.

O'Donnell, J.H. 1991. Chemistry of radiation degradation of polymers. *Radiation Effects on Polymers.* ACS Symposium Series 475, American Chemical Society, Washington, DC, pp. 402–413.

Offner, S. 2018. *Re: MgO Data for CRA-2019.* Nuclear Waste Partnership LLC, Email to Y. Xiong, February 7, 2018, Sandia National Laboratories, Carlsbad, New Mexico, ERMS 569319.

Ohnuki, T., T. Yoshida, T. Ozaki, N. Kozai, F. Sakamoto, T. Nankawa, Y. Suzuki and A.J. Francis. 2007. Chemical speciation and association of plutonium with bacteria, kaolinite clay, and their mixture. *Environmental Science and Technology* 41:3134-3139.

O'Loughlin, E.J., S.D. Kelly, R.E. Cook, R. Csencsits, and K.M. Kemner. 2003. Reduction of uranium(VI) by mixed iron(II)/iron(III) hydroxide (green rust): formation of UO_2 nanoparticles. *Environmental Science and Technology* 37:721–727.

Ozaki, T., J. Gillow, T. Kimura, T. Ohnuki, Z. Yoshida, and A.J. Francis. 2004. Sorption behavior of europium (III) and curium (III) on the cell surfaces of microorganisms. *Radiochimica Acta* 92:741-748.

Panak, P., and H. Nitsche. 2001. Interaction of aerobic soil bacteria with plutonium(VI). *Radiochimica Acta* 89:499-504.

Pang, C., Y.-H. Liu, X.-H. Cao, M. Li, G.-L. Huang, R. Hua, C.-X. Wang, Y.-T. Liu, and X.-F. An. 2011. Biosorption of uranium (VI) from aqueous solution by dead fungal biomass of *Penicillium citrinum. Chemical Engineering Journal* 170:1-6.

Papenguth, H.W. 1996a. *Parameter Record Package for Colloidal Actinide Source Term Parameters. Mobile-Colloidal-Actinide Source Term. 1. Mineral Fragment Colloids.* Memorandum to C.T. Stockman, May 7, 1996, Sandia National Laboratories, Albuquerque, New Mexico, ERMS 235850.

Papenguth, H.W. 1996b. *Parameter Record Package for Colloidal Actinide Source Term Parameters. Mobile-Colloidal-Actinide Source Term. 3. Humic Substances.* Memorandum to C.T. Stockman, May 7, 1996, Sandia National Laboratories, Albuquerque, New Mexico, ERMS 235855.

Papenguth, H.W. 1996c. *Parameter Record Package for Colloidal Actinide Source Term Parameters. Mobile-Colloidal-Actinide Source Term. 4. Microbes.* Memorandum to C.T. Stockman, May 7, 1996, Sandia National Laboratories, Albuquerque, New Mexico, ERMS 235856.

Papenguth, H.W., and Y.K. Behl. 1996. *Test Plan for Evaluation of Colloid-Facilitated Actinide Transport at the Waste Isolation Pilot Plant.* TP 96-01, Sandia National Laboratories, Albuquerque, New Mexico.

Parkhurst, D.L. and C.A.J. Appelo. 2013. Description of input and examples for PHREEQC version 3 – A computer program for speciation, batch-reaction, one-dimensional transport and inverse geochemical calculations. *U.S. Geological Survey Techniques and Methods, Book 6. Chapter A43*. http://pubs.usgs.gov/tm/06/a43.

Patterson, R. 2016a. *Pu Oxidation State Implementation.* U.S. Department of Energy Email to T. Peake and K. Economy, U.S. Environmental Protection Agency, September 8, 2016.

Patterson, R. 2016b. *Response to the U.S. Environmental Protection Agency Email Dated July 28, 2016 Regarding Chemistry Questions on the 2014 Compliance Recertification Application.* U.S. Department of Energy, Letter to T. Peake, U.S. Environmental Protection Agency, October 6, 2016.

Peake, T. 2012. *Magnesium Oxide Supersack Size Reduction and Alternative Emplacement Plan.* U.S. Environmental Protection Agency, email to R. Patterson, U.S. Department of Energy, July 13, 2012.

Peake, T. 2016. *Changes to Actinide References Used in the Calculation of Actinide Solubility Uncertainty.* U.S. Environmental Protection Agency, email to S. Dunagan, U.S. Department of Energy, Carlsbad, New Mexico, September 30, 2016.

Peake, T. 2018. Letter to M. Brown, US Department of Energy, Carlsbad, New Mexico, December 17, 2018.

Peake, T. 2020a. *First Set of EPA Completeness Comments and Questions for Compliance Recertification Application 2019 (CRA-2019).* U.S. Environmental Protection Agency, Center for Waste Management and Regulation, Washington, D.C. Letter to M. Brown, U.S. Department of Energy, Carlsbad Field Office, Carlsbad, New Mexico, March 23, 2020.

Peake, T. 2020b. *Second Set of EPA Completeness Comments and Questions for Compliance Recertification Application 2019 (CRA-2019).* U.S. Environmental Protection Agency, Center for Waste Management and Regulation, Washington, D.C. Letter to M. Brown, U.S. Department of Energy, Carlsbad Field Office, Carlsbad, New Mexico, May 6, 2020.

Peake, T. 2020c. *Third Set of EPA Completeness Comments and Questions for Compliance Recertification Application 2019 (CRA-2019).* U.S. Environmental Protection Agency, Center for Waste Management and Regulation, Washington, D.C. Letter to M. Brown, U.S. Department of Energy, Carlsbad Field Office, Carlsbad, New Mexico, June 12, 2020.

Peake, T. 2020d. *Fourth Set of EPA Completeness Comments and Questions for Compliance Recertification Application 2019 (CRA-2019).* U.S. Environmental Protection Agency, Center for Waste Management and Regulation, Washington, D.C. Letter to M. Brown, U.S. Department of Energy, Carlsbad Field Office, Carlsbad, New Mexico, July 17, 2020.

Peake, T. 2020e. *Fifth Set of EPA Completeness Comments and Questions for Compliance Recertification Application 2019 (CRA-2019).* U.S. Environmental Protection Agency, Center for Waste Management and Regulation, Washington, D.C. Letter to M. Brown, U.S. Department of Energy, Carlsbad Field Office, Carlsbad, New Mexico, September 11, 2020.

Peake, T. 2020f. *Sixth Set of EPA Completeness Comments and Questions for Compliance Recertification Application 2019 (CRA-2019).* U.S. Environmental Protection Agency, Center for Waste Management and Regulation, Washington, D.C. Letter to M. Brown, U.S. Department of Energy, Carlsbad Field Office, Carlsbad, New Mexico, November 13, 2020.

Peake, T. 2021. U.S. Environmental Protection Agency, Center for Waste Management and Regulation, Washington, D.C. Letter to M. Brown, U.S. Department of Energy, Carlsbad Field Office, Carlsbad, New Mexico, February 19, 2021.

Plymale, A.E., V.L. Bailey, J.K. Fredrickson, S.M. Heald, L. Shi, Z. Wang, C.T. Resch, D.A. Moore, and H. Bolton. 2012. Biotic and abiotic reduction and solubilization of $Pu(IV)O_2 \bullet xH_2O$(am) as affected by anthraquinone-2,6-disulfonate (AQDS) and ethylenediaminetetraacetate (EDTA). *Environmental Science and Technology* 46:2132-2140.

Popielak, R.S., R.L. Beauheim, S.R. Black, W.E. Coons, C.T. Ellingson, and R.L. Olsen. 1983. Brine Reservoirs in the Castile Formation, Waste Isolation Pilot Plant (WIPP) Project, Southeastern New Mexico, TME 3153, Prepared for U.S. DOE by D'Appolonia Consulting Engineers, Inc. Albuquerque, NM. ERMS 242085.

Rai, D., and J.L. Ryan. 1982. Crystallinity and solubility of Pu(IV) oxide and hydrous oxide in aged aqueous suspensions. *Radiochimica Acta* 30:213-216.

Rai, D., and J.L. Ryan. 1985. Neptunium(IV) hydrous oxide solubility under reducing and carbonate conditions. *Inorganic Chemistry* 24: 247–251.

Rai, D., A.R. Felmy, D.A. Moore and M.J. Mason. 1995. The solubility of Th(IV) and U(IV) hydrous oxides in concentrated $NaHCO_3$ and Na_2CO_3 aqueous solutions. *Scientific Basis for Nuclear Waste Management XVIII.* Kyoto, Japan, pp. 1143–1150.

Rai, D., Y.A. Gorby, J.K. Frederickson, D.A. Moore and M. Yui. 2002. Reductive dissolution of PuO_2(am): the effect of Fe(II) and hydroquinone. *Journal of Solution Chemistry* 31:433-453.

Rai, D., D.A. Moore, K.M. Rosso, A.R. Felmy, and H. Bolton. 2008. Environmental mobility of Pu(IV) in the presence of ethylenediaminetetraacetic acid: Myth or reality? *Journal of Solution Chemistry* 37:957-986.

Rao, L.F., D. Rai, and A.R. Felmy. 1996a. Solubility of $Nd(OH)_3$(c) in 0.1 M NaCl aqueous solution at 25°C and 90°C. *Radiochimica Acta* 72:151-155.

Rao, L.F., D. Rai, A.R. Felmy, R.W. Fulton, and C.F. Novak. 1996b. Solubility of $NaNd(CO_3)_3 \cdot 6H_2O(c)$ in concentrated Na_2CO_3 and $NaHCO_3$ solutions at 25°C and 90°C. *Radiochimica Acta* 75:141-147.

Rao, L., D. Rai, A.R. Felmy and C.F. Novak. 1999. Solubility of $NaNd(CO_3)_3 \cdot 6H_2O(c)$ in mixed electrolyte ($Na\text{-}Cl\text{-}CO_3\text{-}HCO_3$) and synthetic brine solutions. In *Actinide Speciation in High Ionic Strength Media: Experimental and Modeling Approaches to Predicting Actinide Speciation and Migration in the Subsurface.* Proceedings of an American Chemical Society Symposium on Experimental and Modeling Studies of Actinide Speciation in Non-Ideal Systems. Held August 26-28, 1996 in Orlando, Florida. Eds. D.T. Reed, S.B. Clark and L. Rao. Kluwer Academic/Plenum Publishers, pp. 153-169.

Reed, D.R. 2020. *Supporting Document Justification for the Pu(III) Intrinsic Colloid Parameter (CONCINT) Based on Plutonium Filtration Data.* LA-UR 20-29679, Los Alamos National Laboratory, Carlsbad, New Mexico.

Reed, D.T., S. Okajima, L.H. Brush, and M.A. Molecke. 1993. Radiolytically-Induced Gas Production in Plutonium-Spiked WIPP Brine, Scientific Basis for Nuclear Waste Management XVL Materials Research Society Symposium Proceedings, Boston, MA, November 30 - December 4, 1992. C.G. Interrante and R.T. Pabalan, eds., Materials Research Society, Pittsburgh, PA. Vol. 294, pp. 431--438. SAND92-7283C, ERMS 228637.

Reed, D. T., D.G. Wygmans, and M.K. Richmann. 1996. *Stability of Pu(VI), Np(VI), and U(VI) in Simulated WIPP Brine*. Argonne National Laboratory Interim Report.

Reed, D.T., D.R. Wygmans, S.B. Aase, and J.E. Banaszak. 1997. *Reduction of Np(VI) and Pu(VI) by Organic Chelating Agents*. Sandia National Laboratories, SAND97-2845C.

Reed, D.T., D.G. Wygmans, S.B. Aase, and J.E. Banaszak. 1998. Reduction of Np(VI) and Pu(VI) by organic chelating agents. *Radiochimica Acta* 82:109-114.

Reed, D.T., J.F. Lucchini, S.B. Aase, and A.J. Kropf. 2006. Reduction of plutonium(VI) in brine under subsurface conditions. *Radiochimica Acta* 94:591-597.

Reed, D.T., S.E. Pepper, M.K. Richmann, G. Smith, R. Deo, and B.E. Rittmann. 2007. Subsurface bio-mediated reduction of higher-valent uranium and plutonium. *Journal of Alloys and Compounds* 444/445:376–382.

Reed, D.T., J.F. Lucchini, M. Borkowski, and M.K. Richmann. 2010. *Reduction of Higher-Valent Plutonium by Iron under Waste Isolation Pilot Plant (WIPP)-Relevant Conditions: Data Summary and Recommendations*. LCO-ACP-09, Rev. 0, LANL\ACRSP Report, Los Alamos National Laboratory, Los Alamos, New Mexico.

Reed, D.R., M. Borkowski, J. Swanson, M. Richmann, H. Khaing, J.F. Lucchini, and D. Ams. 2011. Redox-controlling processes for multivalent metals and actinides in the WIPP. in *Redox Phenomena Controlling Systems*, M. Altmaier, B. Kienzler, L. Duro, M. Grivé, and V. Montoya (eds.) 3rd Annual Workshop Proceedings, 7th EC Recosy Cooperative Project, Karlsruhe Institute for Technology, March 2011.

Reed, D.T., J.S. Swanson, J.F. Lucchini, and M.K. Richmann. 2013. *Intrinsic, Mineral and Microbial Colloid Enhancement Parameters for the WIPP Actinide Source Term.* LCO-ACP-18, Revision 0, Los Alamos National Laboratory, Carlsbad, New Mexico.

Reed, D.T., J.S. Swanson, and F. Stanley. 2019. *LANL/ACRSP Parameter Recommendations for the CRA-2019 Deferred Performance Assessment*. LCO-ACP-24, Revision 1, Los Alamos National Laboratory, Carlsbad, New Mexico, ERMS 571296.

Regenspurg, S., D. Schild, T. Schäfer, F. Huber and M. Malmström. 2009. Removal of uranium(VI) from the aqueous phase by iron(II) minerals in the presence of bicarbonate. *Applied Geochemistry* 24:1617-1625.

Réguer, S., P. Dillman and F. Mirambet. 2007. Buried iron archaeological artefacts: Corrosion mechanisms related to the presence of Cl-containing phases. *Corrosion Science* 49:2726-2744.

Rémazeilles, C., D. Neff, F. Kergourlay, E. Foy, E. Conforto, S. Réguer, P. Refait and P. Dillmann. 2009. Mechanisms of long-term anaerobic corrosion of iron archaeological artefacts in seawater. *Corrosion Science* 51:2932-2041.

Reyes, J. 2008. U.S. Environmental Protection Agency, Office of Air and Radiation, Washington DC, letter to D. Moody, U.S. Department of Energy Carlsbad Field Office, February 11, 2009.

Rittmann, B.E., J.E. Banaszak, and D.T. Reed. 2002. Reduction of Np(V) and precipitation of Np(IV) by an anaerobic microbial consortium. *Biodegradation* 13:329–342.

Roberts, H.E., K. Morris, J.F.W. Mosselmans, G.T.W. Law, and S. Shaw. 2019. Neptunium reactivity during co-precipitation and oxidation of Fe(II)/Fe(III) (oxyhydr)oxides. *Geosciences* 9:27

Robie, R.A. and B.S. Hemingway. 1973. The enthalpies of formation of nesquehonite, $MgCO_3 \cdot 3H_2O$, and hydromagnesite, $5MgO \cdot 4CO_2 \cdot 5H_2O$. *Journal of Research of the U.S. Geological Survey* 1:543-547.

Roselle, G.T. 2009. *Iron and Lead Corrosion in WIPP-Relevant Conditions: Six Month Results.* Sandia National Laboratories, Carlsbad, New Mexico, ERMS 546084.

Roselle, G.T. 2010. *Iron and Lead Corrosion in WIPP-Relevant Conditions: 12 Month Results.* Sandia National Laboratories, Carlsbad, New Mexico, ERMS 554383.

Roselle, G.T. 2011a. *Iron and Lead Corrosion in WIPP-Relevant Conditions: 18 Month Results.* Sandia National Laboratories, Carlsbad, New Mexico, ERMS 554715.

Roselle, G.T. 2011b. *Iron and Lead Corrosion in WIPP-Relevant Conditions: 24 Month Results.* Sandia National Laboratories, Carlsbad, New Mexico, ERMS 555246.

Roselle, G.T. 2013a. *Determination of Corrosion Rates from Iron/Lead Corrosion Experiments to be Used for Gas Generation Calculations, Revision 1.* Analysis Report, Sandia National Laboratories, Carlsbad, New Mexico, ERMS 559077.

Roselle, G. T. 2013b. *Summary of Colloid Parameters to be Implemented in the CRA-2014 PA*. Letter from G. Roselle to S. Dunagan. February 15, 2013. Sandia National Laboratories. Carlsbad, New Mexico

Rosencrantz, I. 2021. *Nd(III) Colloids.* U.S. Environmental Protection Agency, email to A. Ward, U.S. Department of Energy, January 7, 2021.

Rothe, J., M.A. Denecke, V. Neck, R. Müller, and J.I. Kim. 2002. XAFS investigation of the structure of aqueous thorium(IV) species, colloids and solid thorium(IV) oxide/hydroxide. *Inorganic Chemistry* 41:249-258.

RSI (Institute for Regulatory Science). 2006. *Application of Magnesium Oxide as an Engineered Barrier at Waste Isolation Pilot Plant, Report of the Expert Panel*. RSI-06-01.

Runde, W., and J.I. Kim. 1994. *Untersuchungen der Übertragbarkeit von Labordaten Natürliche Verhältnisse: Chemisches Verhalten von Drei- und Fünfwertigem Americium in Salinen NaCl-Lösungen (Study of the Extrapolability of Laboratory Data to Natural Conditions: Chemical Behavior of Trivalent and Pentavalent Americium in Saline NaCl Solutions).* RCM-01094, Institute for Radiochemistry, Technical University of Munich, Munich, Federal Republic of German, ERMS 241862.

Rusin, P.A., L. Quintana, J.R. Brainard, B.A. Strietelmeir, C.D. Trait, S.A. Ekberg, P.D. Palmer, T.W. Newton, and D.L Clark. 1994. Solubilization of plutonium hydrous oxide by iron-reducing bacteria. *Environmental Science and Technology* 28:1686-1690.

Saheb, M., D. Neff, P. Dillmann, H. Matthiesen, E. Foy, and L. Bellot-Gurlet. 2009. Multisecular corrosion behaviour of low carbon steel in anoxic soils: characterization of corrosion system on archaeological artefacts. *Materials and Corrosion* 60:99-105.

Saheb, M., D. Neff, J. Demory, E. Foy, and P. Dillman. 2010. Characterisation of corrosion layers formed on ferrous archaeological artefacts buried in anoxic media. *Corrosion Eng. Sci. Technol*. 45:381-387.

Santillan, E.F. 2020. *Follow Up to 6/22 Phone Call.* U.S. Environmental Protection Agency, email to R. Patterson, U.S. Department of Energy, Carlsbad, New Mexico, June 23, 2020.

Sar, P., and D'Souza, S. F. 2001. Biosorptive uranium uptake by a Pseudomonas strain: characterization and equilibrium studies. *Journal of Chemical Technology Biotechnology*, 76(12), 1286-1294.

Sarathi, R. 2019a. *Analysis Package for Actinide Mobilization and Salado Transport in the 2019 Compliance Recertification Application Performance Assessment (CRA-2019 PA).* Sandia National Laboratories, Carlsbad, New Mexico, ERMS 571371.

Sarathi, R., 2019b. *Explanation of CAPMIC Definition and Usage in PA Calculations*. January 14, 2019. Memo to R.C. Camphouse. Sandia National Laboratories, Carlsbad, New Mexico. ERMS 570685

Sasaki, T., T. Kubota, S. Mito, T. Kauri, and A. Kudo. 2002. Radionuclide sorption to a mixture of anaerobic bacteria in the repository environment. *Journal of Nuclear Science and Technology* 39:954-957.

SC&A (S. Cohen & Associates). 2006. *Preliminary Review of the Degradation of Cellulosic, Plastic and Rubber Materials in the Waste isolation Pilot Plant, and Possible Effects on Magnesium Oxide Safety Factor.* Prepared for the U.S. Environmental Protection Agency Office of Radiation and Indoor Air, August 21.

SC&A (S. Cohen & Associates). 2008a. *Review of MgO-Related Uncertainties in the Waste Isolation Pilot Plant.* Prepared for the U.S. Environmental Protection Agency Office of Radiation and Indoor Air, January 24.

SC&A (S. Cohen & Associates). 2008b. *Verification of the Waste Isolation Pilot Plant Chemistry Conceptual Models.* Prepared for the U.S. Environmental Protection Agency Office of Radiation and Indoor Air, September 19.

SC&A (S. Cohen and Associates). 2011. *EQ3/6 Computer Code Evaluation*. Prepared for U.S. Environmental Protection Agency Office of Radiation and Indoor Air. Draft March 2011.

Scheinost, A., R. Steudtner, R. Hűbner, S. Weiss, and F. Bok. 2016. Neptunium^{V} retention by siderite under anoxic conditions: Precipitation of NpO_2-like nanoparticles and of Np^{IV} pentacarbonate. *Environmental Science and Technology* 50:10413-10420.

Schramke, J.A., E.F.U. Santillan, and R.T. Peake. 2020. Plutonium oxidation states in the Waste Isolation Pilot Plant repository. *Applied Geochemistry* 116:1-15.

Schubert, B. A., T.K. Lowenstein, and M.N. Timofeeff. 2009. Microscopic identification of prokaryotes in modern and ancient halite, Saline Valley and Death Valley, California. *Astrobiology* 9:467-482.

Scott, T.B., G.C. Allen, P.J. Heard, and M.G. Randell. 2005. Reduction of U(VI) to U(IV) on the surface of magnetite. *Geochimica et Cosmochimica Acta* 69:5639-5646.

Selwyn, L. 2004. Overview of archaeological iron: the corrosion problem, key factors affecting treatment, and gaps in current knowledge. In: Ashton, J., Hallam, D. (Eds.), *Metal 04: Proceedings of the International Conference on Metals Conservation*. National Museum of Australia, Canberra, pp. 294–306.

Sheng, G., X. Shao, Y. Li, J. Li, H. Dong, W. Cheng, X. Gao, and Y. Huang. 2014. Enhanced removal of uranium(VI) by nanoscale zerovalent iron supported on Na−bentonite and an investigation of mechanism. *Journal of Physical Chemistry* 118:2952−2958.

Shrader, T. 2015. *Response to the U.S. Environmental Protection Agency Letters Dated June 5, 2015 and July 30, 2015 Regarding the 2014 Compliance Recertification Application.* U.S. Department of Energy Letter to J.D. Edwards, U.S. Environmental Protection Agency, December 8, 2015.

Shrader, T. 2016. *Response to the U.S. Environmental Protection Agency Letters Dated June 5, 2015, July 30, 2015 and February 26, 2016 Regarding the 2014 Compliance Recertification Application.* U.S. Department of Energy Letter to J.D. Edwards, U.S. Environmental Protection Agency, May 25, 2016.

Silva, R.J. 1982. *The Solubilities of Crystalline Neodymium and Americium Trihydroxides.* LBL-15055. Lawrence Berkeley National Laboratory, Berkeley, California.

Singer, D.M., S.M. Chatman, E.S. Ilton, K.M. Rosso, J.F. Banfield, and G.A. Waychunas. 2012a. Identification of simultaneous U(VI) sorption complexes and U(IV) nanoprecipitates on the magnetite (III) surface. *Environmental Science and Technology* 46:3811-3820.

Singer, D.M., S.M. Chatman, E.S. Ilton, K.M. Rosso, J.F. Banfield, and G.A. Waychunas. 2012b. U(VI) sorption and reduction kinetics on the magnetite (111) surface. *Environmental Science and Technology* 46:3821-3830.

Slater, S.A., D.B. Chamberlain, S.A. Base, B.D. Babcock, C. Conner, J. Sedlet, and G.F. Vandegrift. 1997. Optimization of Magnetite Carrier Precipitation Process for Plutonium Waste Reduction. *Separation Science and Technology* 32:127-147.

Snider, A.C. 2001. MgO Hydration Experiments Conducted at SNL/ABQ. *Sandia National Laboratories Technical Baseline Reports, WBS 1.3.5.4, Repository Investigations, Milestone RI020, July 31, 2001*. Sandia National Laboratories, Carlsbad, New Mexico. ERMS 518970, pp. 4-1 to 4-3.

Snider, A.C. 2002. MgO Studies: Experimental Work Conducted at SNL/Carlsbad. Efficacy of Premier Chemicals MgO as an Engineered Barrier, *Sandia National Laboratories Technical Baseline Reports, WBS 1.3.5.3, Compliance Monitoring; WBS 1.3.5.4, Repository Investigations, Milestone RI110, January 31, 2002.* Sandia National Laboratories, Carlsbad, New Mexico. ERMS 520467, pp. 3.1-1 to 3.1-18.

Snider, A.C. 2003a. Hydration of Magnesium Oxide in the Waste Isolation Pilot Plant, *Sandia National Laboratories Technical Baseline Reports, WBS 1.3.5.3, Compliance Monitoring; WBS 1.3.5.4, Repository Investigations, Milestone RI 03-210, January 31, 2003.* Sandia National Laboratories, Carlsbad, New Mexico, ERMS 526049, pp. 4.2-1 to 4.2-6.

Snider, A.C. 2003b. *Verification of the Definition of Generic Weep Brine and the Development of a Recipe for this Brine*. Unpublished Analysis Report, Sandia National Laboratories, Carlsbad, New Mexico, April 8, 2003, ERMS 527505.

Snider, A.C., and Y.L. Xiong. 2002. Carbonation of Magnesium Oxide, *Sandia National Laboratories Technical Baseline Reports, WBS 1.3.5.3, Compliance Monitoring; WBS 1.3.5.4, Repository Investigations, Milestone RI130, July 31, 2002.* Sandia National Laboratories, Carlsbad, New Mexico, ERMS 523189, pp. 4.1-1 to 4.1-28.

Snider, A.C., and Y.L. Xiong. 2004. *Continuing Investigations of the Hydration and Carbonation of Premier Chemical MgO.* Sandia National Laboratories, Carlsbad, New Mexico, ERMS 537188.

SNL (Sandia National Laboratories). 1997. *Chemical Conditions Model: Results of the MgO Backfill Efficacy Investigation.* Prepared for the U.S. Department of Energy, Carlsbad Area Office, April 23, 1997. Docket No. A-93-02, II-A-39.

Sonke, J.E., and V.J.M. Salters. 2006. Lanthanide–humic substances complexation. I. Experimental evidence for a lanthanide contraction effect. *Geochimica Cosmochimica Acta* 70:1495-1506.

Sosson, G. 2019. *Deferred Performance Assessment for the Compliance Recertification Application 2019.* U.S. Department of Energy, Carlsbad Field Office, Carlsbad, New Mexico. Letter to L.B. Veal, U.S. Environmental Protection Agency Radiation Protection Division, Washington, D.C. December 20, 2019.

Sosson, G. 2020a. *Response 1 to U.S. Environmental Protection Agency's 2019 Compliance Recertification Application Completeness Comments Letter dated March 23, 2020 from Tom Peake to Mike Brown*. U.S. Department of Energy, Carlsbad Field Office, Carlsbad, New Mexico. Letter to L.B. Veal, U.S. Environmental Protection Agency Radiation Protection Division, Washington, D.C. June 11, 2020.

Sosson, G. 2020b. *Response 2 to U.S. Environmental Protection Agency's 2019 Compliance Recertification Application Completeness Comments Letter dated March 23, 2020 from Tom Peake to Mike Brown*. U.S. Department of Energy, Carlsbad Field Office, Carlsbad, New Mexico. Letter to L.B. Veal, U.S. Environmental Protection Agency Radiation Protection Division, Washington, D.C. July 9, 2020.

Stein, C.L. 1985. *Mineralogy in the Waste Isolation Pilot Plant (WIPP) Facility Stratigraphic Horizon*. SAND-85-0321, Sandia National Laboratories, Albuquerque, New Mexico, September 1985.

Stein, J. 2005. *Estimate of Volume of Brine in Repository That Leads to a Brine Release*. Memorandum to L.H. Brush, April 13, Sandia National Laboratories, Carlsbad, New Mexico, ERMS 539372.

Stein, C.L., and J.L. Krumhansl. 1986. *Chemistry of Brines in Salt from the Waste Isolation Pilot Plant (WIPP), Southeastern New Mexico: A Preliminary Investigation*. SAND-85-0897, Sandia National Laboratories, Albuquerque, New Mexico, March 1986.

Stein, J., and M. Nemer. 2005. *Analysis Plan for Updating the Microbial Degradation Rates for Performance Assessment*. AP-116, Sandia National Laboratories, Carlsbad, New Mexico, ERMS 538596.

Stern, J.C., D.L. Foustoukos, J.E. Sonke, and V.J.M. Salters. 2014. Humic acid complexation of Th, Hf and Zr in ligand competition experiments: Metal loading and pH effects. *Chemical Geology* 363:241-249.

Storz, L. 1996. *Estimate of the Amount of $Ca(OH)_2$ Contained in the Portland Cement Fraction of the Waste for Disposal in the WIPP*. Memorandum to Y. Wang, June 24, 1996, Sandia National Laboratories, Albuquerque, New Mexico, ERMS 240351.

Suzuki, Y., S.D. Kelly, K.M. Kemner, and J.F. Banfield. 2003. Microbial populations stimulated for hexavalent uranium reduction in uranium mine sediment. *Applied and Environmental Microbiology* 69:1337-1346.

Swanson, J. 2019. *Review of the Microbial Colloid Contribution to the WIPP Actinide Source Term*. Los Alamos Report LA-UR-19-22310, Los Alamos National Laboratory, New Mexico.

Swanson, J. and D. Reed. 2018. *Biomass-Based Approach to Determine the CAPMIC Biocolloid Parameter for the WIPP*. Los Alamos National Laboratory; Carlsbad, NM. LA-UR-18-22808

Swanson, J.S., D.T. Reed, D.A. Ams, D.M. Norden, and K.A. Simmons. 2012. *Status Report on the Microbial Characterization of Halite and Groundwater Samples from the WIPP*. Report LCO-ACP-12, LA-UR 12-22824. Los Alamos National Laboratory, Carlsbad, New Mexico.

Swanson, J., D. Reed, M. Richmann, and D. Cleveland. 2015. Investigation into the post-excavation sources of methane from INL TRU waste drums. (No. LA-UR-15-26657). Los Alamos National Laboratory, Carlsbad, New Mexico.

Swanson, J., A. Navarrette, C. Hazelton, M. Richmann, and F. Stanley. 2021. Biomass and salt-dependent effects of Bacillus spores on radionuclide migration from the Waste Isolation Pilot Plant. *Chemosphere* 280:130680.

Szponar, N. 2012. *Carbon Cycling at a Site of Present Day Serpentinization: the Tables, Gros Morne National Park*. Masters Thesis, Memorial University of Newfoundland.

Tasi, A., X. Gaona, D. Fellhauer, M. Böttle, J. Rothe, K. Dardenne, D. Schild, M. Grivé, E. Colàs, J. Bruno, K. Källström, M. Altmaier, and H. Geckeis. 2018. Redox behavior and solubility of plutonium under alkaline, reducing conditions. *Radiochimica Acta* 106:259-279.

TEA (Trinity Engineering Associates). 2004. *Review of Effects of Supercompacted Waste and Heterogeneous Waste Emplacement on WIPP Repository Performance. Final Report*. Prepared for U.S. Environmental Protection Agency, Office of Radiation and Indoor Air, Washington, DC, March 17, 2004.

Telander, M.R., and R.E. Westerman. 1993. *Hydrogen Generation by Metal Corrosion in Simulated Waste Isolation Pilot Plant Environments: Progress Report for the Period November 1989 through December 1992*. SAND92-7347, Sandia National Laboratories, Albuquerque, New Mexico, ERMS 223456.

Telander, M.R., and R.E. Westerman. 1997. *Hydrogen Generation by Metal Corrosion in Simulated Waste Isolation Pilot Plant Environments.* SAND96-2538, Prepared for Sandia National Laboratories, Albuquerque, New Mexico by Pacific Northwest National Laboratory, Richland, Washington.

Theodorakopoulos, N., V. Chapon, F. Coppin, M. Floriani, T. Vercouter, C. Sergeant, V. Camilleri, C. Berthomieu, and L. Février. 2015. Use of combined microscopic and spectroscopic techniques to reveal interactions between uranium and Microbacterium sp. A9, a strain isolated from the Chernobyl exclusion zone. *Journal of Hazardous Materials* 285:285-293.

Triay, I.R. 2005. *Partial Response to Environmental Protection Agency (EPA) September 2, 2004, Letter on Compliance Recertification Application.* U.S. Department of Energy Carlsbad Field Office, letter to Elizabeth Cotsworth, U.S. Environmental Protection Agency Office of Radiation and Indoor Air, Washington, DC, January 19, 2005.

Trueman, B.F., and G.A. Gagnon. 2016. Understanding the role of particulate iron in lead release to drinking water. *Environmental Science and Technology* 50:9053-9060.

Trueman, B.F., G.A. Sweet, M.D. Harding, H. Estabrook, D.P. Bishop, and G.A. Gagnon. 2017. Galvanic corrosion of lead by iron (oxyhydr)oxides: potential impacts on drinking water quality. *Environmental Science and Technology* 51:6812-6820.

Tsarev, S., T.D. Waite, and R.N. Collins. 2016. Uranium reduction by Fe(II) in the presence of montmorillonite and nontronite. *Environmental Science and Technology* 50:8223-8230.

Van Soest, G.D. 2012. *Performance Assessment Inventory Report – 2012*. Los Alamos National Laboratory Carlsbad Operations INV-PA-12, Revision 0, LA-UR-12-26643.

Van Soest, G.D. 2018. *Performance Assessment Inventory Report – 2018*. Los Alamos National Laboratory Carlsbad Operations INV-PA-18, Revision 0, December 12, 2018.

Veirs, D.K., J.M. Berg, and M.L. Crowder. 2012. *The Effect of Plutonium Dioxide Water Surface Coverage on the Generation of Hydrogen and Oxygen*. Los Alamos National Laboratory, Los Alamos, New Mexico, LA-UR-12-22377.

Villareal, R., J.M. Bergquist, and S.L. Leonard. 2001. *The Actinide Source Term Waste Test Program (STTP) Final Report*, Volume I. Los Alamos National Laboratory, LA UR 01 6822.

Vreeland, R.H., A.F. Piselli Jr., S. McDonnough, and S.S. Meyers. 1998. Distribution and diversity of halophilic bacteria in a subsurface salt formation. *Extremophiles* 2:321-331

Vugrin, E.D., M.B. Nemer, and S. Wagner, 2006. *Uncertainties Affecting MgO Effectiveness and Calculation of the MgO Effective Excess Factor*. Revision 0, Sandia National Laboratories, Carlsbad, New Mexico.

Vugrin, E.D., M.B. Nemer, and S. Wagner, 2007. *Uncertainties Affecting MgO Effectiveness and Calculation of the MgO Effective Excess Factor*. Revision 1, Sandia National Laboratories, Carlsbad, New Mexico. ERMS 546377.

Wade, D. 2021. *Central Characterization Program Acceptable Knowledge Summary Report for Savannah River Site Waste Stream: SR-KAC-PuOx, Revision 1.* Nuclear Waste Partnership, Carlsbad, New Mexico. CCP-AK-SRS-23.

Wall, N.A. 2005. *Preliminary Results for the Evaluation of Potential New MgO*. Sandia National Laboratories, Carlsbad, New Mexico. ERMS 538514.

Wall, N.A., and S.A. Mathews. 2005. Sustainability of humic acids in the presence of magnesium oxide. *Applied Geochemistry* 20:1704-1713.

Wang, Y., and LH. Brush. 1996. *Estimates of Gas-Generation Parameters for the Long-Term WIPP Performance Assessment*. Unpublished memorandum to M.S. Tierney, Sandia National Laboratories, Albuquerque, New Mexico, January 26, 1996, WPO 31943.

Wang, Y., and A. J. Francis. 2005. Evaluation of microbial activity for long-term performance assessments of deep geologic nuclear waste repositories. *Journal of Nuclear and Radiochemical Sciences*, 6:43-50.

Wang, Y., L.H. Brush, H. Gao, and J.S. Stein. 2003. Re-evaluation of Microbial Gas Generation Rates for Long-Term WIPP Performance Assessment. *Sandia National Laboratories Technical Baseline Reports, WBS 1.3.5.3, Compliance Monitoring; WBS 1.3.5.4, Repository Investigations, Milestone RI 03-210, January 31, 2003*. Sandia National Laboratories, Carlsbad, New Mexico, pp. 3.1-1 to 3.1-12.

Weiner, R.F. 1996. *Oxidation State Distribution in the WIPP*. Presentation at Technical Exchange Meeting on June 27, 1996, Sandia National Laboratory, Albuquerque, New Mexico.

Werner, J.R. 2016. U.S. Environmental Protection Agency. Letter to S. Dunagan, U.S. Department of Energy, Carlsbad New Mexico, November 4, 2016.

Wilson, C., D. Porter, J. Gibbons, E. Oswald, G. Sjoblom, and F. Caporuscio. 1996a. *Conceptual Models Peer Review Report*, Prepared for the U.S. Department of Energy, Carlsbad, New Mexico, July 1996, Docket No. A-93-02 Item II-G-1.

Wilson, C., D. Porter, J. Gibbons, E. Oswald, G. Sjoblom, and F. Caporuscio. 1996b. *Conceptual Models Supplementary Peer Review Report*, Prepared for the U.S. Department of Energy, Carlsbad, New Mexico, December 1996, Docket No. A-93-02 Item II-G-12.

Wilson, C., D. Porter, J. Gibbons, E. Oswald, G. Sjoblom, and F. Caporuscio. 1997a. *Conceptual Models Second Supplementary Peer Review Report*, Prepared for the U.S. Department of Energy, Carlsbad, New Mexico, January 1997, Docket No. A-93-02 Item II-G-21.

Wilson, C., D. Porter, J. Gibbons, E. Oswald, G. Sjoblom, and F. Caporuscio. 1997b. *Conceptual Models Third Supplementary Peer Review Report*, Prepared for the U.S. Department of Energy, Carlsbad, New Mexico, April 1997, Docket No. A-93-02 Item II-G-22.

Wilson, D.L., M.L. Baker, B.R. Hart, J.E. Marra, J.M. Schwantes, and P.E. Shoemaker. 2015. *Waste Isolation Pilot Plant Technical Assessment Team Report.* U.S. Department of Energy, SRNL-RP-2014-01198.

Wolery, T.J., Y.-L. Xiong, and J.J. Long. 2010. *Verification and Validation Plan/Validation Document for EQ3/6 Version 8.0a for Actinide Chemistry, Document Version 8.10.* Sandia National Laboratories, Carlsbad, New Mexico, ERMS 550239.

WTS (Washington TRU Solutions LLC). 2003. *Specification for Prepackaged MgO Backfill.* Unpublished Specification, D-0101, Rev. 5. Washington TRU Solutions LLC, Carlsbad, New Mexico.

WTS (Washington TRU Solutions). 2009a. *Engineering Change Order (ECO) 12137.* January 2009.

WTS (Washington TRU Solutions). 2009b. *Specifications for Prepackaged MgO Backfill*. Waste Isolation Pilot Plant Procedure D-0101, Revision 8, February 2009.

Wu, X., K. Holmfeldt, V. Hubalek, D. Lundin, M. Åström, S. Bertilsson, and M. Dopson 2016. Microbial metagenomes from three aquifers in the Fennoscandian shield terrestrial deep biosphere reveal metabolic partitioning among populations. *The ISME Journal* 10:1192-1203.

Xia, Y., L. Rao, A.R. Felmy, and D. Rai. 2001. Determining the Distribution of Pu, Np, and U Oxidation States in Dilute NaCl and Synthetic Brine Solutions. *Journal of Radioanalytical and Nuclear Chemistry* 250:27-37.

Xiong, Y. 2009. *Release of FMT_090720.CHEMDAT.* E-mail to Jennifer Long, July 22, 2009, Sandia National Laboratories, Carlsbad, New Mexico, ERMS 539304.

Xiong, Y. 2011. *Release of EQ3/6 Database DATA0.FM1.* Email to J.J. Long, March 9, 2011, Sandia National Laboratories, Carlsbad, New Mexico.

Xiong, Y.L. 2017. *Absence of Mineral Colloids in High Ionic Strength Solutions Associated with Salt Formations: Experimental Determination and Applications to Nuclear Waste Management.* Sandia National Laboratories, Carlsbad, New Mexico, ERMS 568244.

Xiong, Y., and P.S. Domski. 2016a. *Uncertainty Analysis of Actinide Solubilities for CRA 2014 Sensitivity Investigation Number 4 (CRA 2014_SEN4).* Sandia National Laboratories, Carlsbad, New Mexico, ERMS 567306.

Xiong, Y., and P.S. Domski. 2016b. *Updating the WIPP Thermodynamic Database, Revision 1, Supersedes ERMS 565730.* Sandia National Laboratories, Carlsbad, New Mexico, ERMS 566047.

Xiong, Y., and A.S. Lord. 2008. Experimental investigations of the reaction path in the MgO-CO_2-H_2O system in solutions with various ionic strengths, and their applications to nuclear waste isolation. *Applied Geochemistry* 23:1634-1659.

Xiong, Y., and A.C. Snider. 2003. *Carbonation Rates of the Magnesium Oxide Hydration Product Brucite in Various Solutions. Sandia National Laboratories Technical Baseline Reports, WBS 1.3.5.4, Repository Investigations, Milestone RI 03-210, January 31, 2003.* Sandia National Laboratories, Carlsbad, New Mexico, ERMS 526049, pp. 4.3-1 to 4.3-11.

Xiong, Y., E.J. Nowak, and L.H. Brush. 2004. *Updated Uncertainty Analysis of Actinide Solubilities for the Response to EPA Comment C-23-16.* Sandia National Laboratories, Carlsbad, New Mexico, ERMS 538219.

Xiong, Y., E.J. Nowak, and L.H. Brush. 2005. *Updated Uncertainty Analysis of Actinide Solubilities for the Response to EPA Comment C-23-16, Rev. 1 (Supersedes ERMS 538219).* Sandia National Laboratories, Carlsbad, New Mexico, ERMS 539595.

Xiong, Y. L.H., Brush, A. Ismail, and J.J. Long. 2009. *Uncertainty Analysis of Actinide Solubilities for the WIPP CRA-2009 PABC.* Sandia National Laboratories, Carlsbad, New Mexico, ERMS 552500.

Xiong, Y., H. Deng, M. Nemer, and S. Johnsen. 2010. Experimental determination of the solubility constant for magnesium chloride hydroxide hydrate ($Mg_3Cl(OH)_5•4H_2O$, Phase 5) at room temperature, and its importance to nuclear waste isolation in geological repositories in salt formations. *Geochimica et Cosmochimica Acta* 74:4605-4611.

Xiong, Y.L., L. Kirkes, and C. Marrs. 2017. Long-term experimental determination of solubilities of micro-crystalline Nd(III) hydroxide in high ionic strength solutions: applications to nuclear waste management. *Aquatic Geochemistry* 23:359-375.

Xu, J., Y. Li, C. Jing, H. Zhang, and Y. Ning. 2014. Removal of uranium from aqueous solution using montmorillonite-supported nanoscale zero-valent iron. *Journal of Radioanalytical and Nuclear Chemistry* 299: 329–336.

Yan S., Y. Chen, W. Xiang, Z. Bao, C. Liu, and B. Deng. 2014. Uranium(VI) reduction by nanoscale zero-valent iron in anoxic batch systems: The role of Fe(II) and Fe(III). *Chemosphere* 117:625–630.

Yang, H., D. Cui, D. Grolimund, V.V. Rondinella, R. Brűtsch, M. Amme, C. Kutahyali, A.T. Wiss, A. Puranen, and K. Spahiu. 2017. Reductive precipitation of neptunium on iron surfaces under anaerobic conditions. *Journal of Nuclear Materials* 496:109-116.

Zänker, H. S. Weiss, C. Henning, V. Brendler, and A. Ikeda-Ohno. 2016. Oxyhydroxy silicate colloids: a new type of waterborne actinide(IV) colloids. *ChemistryOpen* 5:174-182.

Zavarin, M., and H.E. Doner. 2005. Effect of P and Se(IV) on calcite precipitation inhibition. *Soil Science* 170:612-623.

Zeitler, T.R. 2018. *Bounding Calculation of the Cumulative Distribution for STEEL:HUMCORR.* Sandia National Laboratories, Carlsbad New Mexico, ERMS 569807.

Zeitler, T.R. 2019a. *Analysis Package for Parameter Sampling in the 2019 Compliance Recertification Application Performance Assessment (CRA-2019 DPA) Revision 0.* Sandia National Laboratories, Carlsbad, New Mexico, ERMS 571367.

Zeitler, T.R. 2019b. *Analysis Package for the Sensitivity of Releases to Input Parameters in the 2019 Compliance Recertification Application Performance Assessment (CRA-2019 DPA) Revision 0.* Sandia National Laboratories, Carlsbad, New Mexico, ERMS 571374.

Zeitler, T.R., and B. Day. 2016. *CRA14_SEN4 Sensitivity Study Revision 1.* Sandia National Laboratories, Carlsbad, New Mexico, ERMS 567505.

Zeitler, T.R., and C. Hansen. 2015a. *Cumulative Distribution for STEEL:CORRMCO2*. Sandia National Laboratories, Carlsbad, New Mexico, ERMS 565005.

Zeitler, T. R., and C. Hansen. 2015b. *Cumulative Distribution for STEEL:HUMCORR*. Sandia National Laboratories, Carlsbad, New Mexico, ERMS 565009.

Zeitler, T. R., and C. Hansen. 2015c. *Updated Calculation of the Cumulative Distribution for STEEL:HUMCORR*. Sandia National Laboratories, Carlsbad, New Mexico, ERMS 565108.

Zeitler, T.R., J. Bethune, S. Brunell, D. Kicker, and J. Long. 2019. *Summary Report for the 2019 Compliance Recertification Application Performance Assessment (CRA-2019 DPA).* Sandia National Laboratories, Carlsbad, New Mexico, ERMS 571376.

Zerwekh, A. 1979. *Gas Generation from Radiolytic Attack of TRU-Contaminated Hydrogenous Waste*. Los Alamos National Laboratory, Los Alamos, New Mexico, LA-7674-MS.

Zhang, P., J. Hardesty, and H. Papenguth. 2001. *MgO Hydration Experiments Conducted at SNL-ABQ. Sandia National Laboratories Technical Baseline Reports, WBS 1.3.5.4, Compliance Monitoring; WBS 1.3.5.4, Repository Investigations, Milestone RI010, January 31, 2001.* Sandia National Laboratories, Carlsbad, New Mexico, ERMS 516749, pp. 55-65.

Zhang Z., J. Liu, X. Cao, X. Luo, R. Hua, Y. Liu, X. Yu, L. He, and Y. Liu. 2015. Comparison of U(VI) adsorption onto nanoscale zero-valent iron and red soil in the presence of U(VI)-CO_3/Ca–U(VI)–CO_3 Complexes. *Journal of Hazardous Materials* 300:633–642.

Zheng, X., Shen, Y., Wang, X., and Wang, T. 2018. Effect of pH on uranium (VI) biosorption and biomineralization by *Saccharomyces cerevisiae*. *Chemosphere*, 203, 109-116.

Attachment A: EPA Completeness Questions

During their CRA-2019 review, EPA requested additional information from DOE (Peake 2020a-2020f). Most of these completeness comments are addressed in the main body of this TSD (Table A-1). The resolution of other EPA review comments, such as errata, requests for supporting computer code input and output files, and requests for cited documentation, are summarized by comment number below. The complete text of all comments, DOE's responses, and EPA's evaluation of these responses are included in Appendix A of EPA (2021).

CC1-GEOCHEM-3 Inaccurate Statement Regarding Sampling of MgO Hydration Rate Parameters

DOE (2019, Appendix GEOCHEM-2019, page GEOCHEM-29, lines 6-9) stated that constant values would be assumed for CRA-2019 MgO hydration rates in inundated and humid conditions. However, Kim and Feng (2019) listed the MgO hydration rate parameters WAS_AREA:BRUCITEC, WAS_AREA:BRUCITEH, and WAS_AREA:BRUCITES as LHS sampled parameters for the CRA-2019 DPA in their Tables 1 and 4, and provided summaries of the sampled values in their Tables A.25, A.26, and A.27. EPA requested confirmation from DOE that the MgO hydration rates were sampled for the CRA-2019 DPA (Peake 2020a). Sosson (2020) confirmed that these rates were sampled for the CRA-2019 and included the Appendix GEOCHEM-2019 misstatement in errata tracking for the CRA-2019.

CC1-GEOCHEM-4 Typographical Error

Peake (2020a) noted that when discussing the process models for the dissolved actinide source term in Section GEOCHEM-4.4.2, DOE (2019) listed the dissolved +IV actinide model twice and the +VI actinide model was not listed. Sosson (2020) acknowledged this typographical error, and the appropriate change was incorporated in errata tracking for the CRA-2019.

CC1-GEOCHEM-5 Typographical Error

Peake (2020a) noted a typographic error in Appendix GEOCHEM-2019, Section GEOCHEM-4.4.2.1, where DOE (2019) used An(IV) (+IV oxidation state actinide) instead of An(III) (+III oxidation state actinide) during a discussion of the process model uncertainty for dissolved An(III). Sosson (2020) acknowledged this typographical error, and the appropriate change was incorporated in errata tracking for the CRA-2019.

CC1-GEOCHEM-6 Missing Discussion of Conceptual Model Uncertainty for Dissolved An(III)

Peake (2020a) noted that Appendix GEOCHEM-2019, Section GEOCHEM-4.4.1 provided a discussion of the uncertainties associated with the conceptual models for the dissolved +IV, +V, and +VI actinides, but DOE (2019) did not provide a discussion of conceptual model uncertainties for dissolved +III actinides. Peake (2020a) requested a discussion of the uncertainties associated with the conceptual model for the +III actinides, which was provided by Sosson (2020).

Table A-1. Summary Table of Completeness Questions and DOE Responses in this TSD

Question	Topic	DOE Response Set[a]	Evaluation/Resolution	Discussion/ Documentation
APPENDIX GEOCHEM-RELATED QUESTIONS				
CC1-GEOCHEM-1 a-c	Cutoff dates actinide solubility	#1 (6/10/20) & Supplementary Information (7/8/21)	postponed in first response, DOE later provided satisfactory calculations	Section 7.4.11
CC1-GEOCHEM-2	BIOGENFC inaccurate statement	#1 (6/10/20)	satisfactory, acknowledged in errata	Section 3.4.7
CC1-GEOCHEM-3	MgO hydration rate inaccurate statement	#1 (6/10/20)	satisfactory, acknowledged in errata	Attachment A
CC1-GEOCHEM-4	Typographic error	#1 (6/10/20)	satisfactory, acknowledged in errata	Attachment A
CC1-GEOCHEM-5	Typographic error	#1 (6/10/20)	satisfactory, acknowledged in errata	Attachment A
CC1-GEOCHEM-6	Missing discussion An(III)	#1 (6/10/20)	satisfactory, additional information provided	Attachment A
CC2-GEOCHEM-7	Missing Reference	#3 (8/13/20)	satisfactory, references provided	Attachment A
CC2-GEOCHEM-8 a-c	Clarification of data source information in Domski (2019)	#6 (10/26/20)	satisfactory, data source and documentation identified	Attachment B 4.1.3, 4.3.2, 5.0
CC2-GEOCHEM-9	Typographical Errors in Table GEOCHEM-21	#3 (8/13/20)	satisfactory, acknowledged in errata	Attachment A
CC2-GEOCHEM-10 a-g	Testing of revised EDTA stability constants and Pitzer ion-interaction parameters	#4 (9/15/20)	adequate response, additional investigation required for future PAs	Attachment B 4.1.1, 4.1.4
CC2-GEOCHEM-11 a-c	Data used to derive $Ca_2EDTA{\cdot}7H_2O(s)$ solubility product and evaluation	#3 (a) #5 (b,c)	satisfactory (a); adequate response (b,c), $Ca_2EDTA{\cdot}7H_2O(s)$ solubility product rejected by EPA	Attachment B 4.1.3, 4.1.4
CC2-GEOCHEM-12 a-f	Evaluation of revised citrate equilibrium constants	#4 (9/15/20)	adequate response, additional investigation required for future PAs	Attachment B 4.2.1, 4.2.2, 4.2.3, 4.2.4
CC2-GEOCHEM-13	Omission of earlandite from DATA0.FM4	#6 (10/26/20)	acknowledged omission; DOE calculations demonstrated no effects on actinide solubility modeling results	Attachment B 4.2.6

Question	Topic	DOE Response Set[a]	Evaluation/Resolution	Discussion/ Documentation
CC2-GEOCHEM-14	Supporting files for actinide solubility calculations	#3 (8/13/20)	satisfactory, files provided	Section 7.4.4
CC2-GEOCHEM-15	Effects of selected G value for H_2(g) production by brine radiolysis	#7 (12/1/20)	satisfactory	Section 3.6.1
CC2-GEOCHEM-16	Omission of RH waste gamma irradiation from radiolysis evaluation	#7 (12/1/20)	satisfactory	Section 3.6.5
CC3-GEOCHEM-17 a-d	Plutonium particle sizes used in radiolytic gas generation calculations	#7 (12/1/20)	satisfactory	Section 3.1.4, 3.6.1
CC3-GEOCHEM-18	Reference request	#5 (10/19/20)	satisfactory; reference provided	Attachment A
CC3-GEOCHEM-19 a-b	Evaluation of matrix depletion and radiolytic gas generation for cellulosics, plastics, and rubber radiolysis	#7 (12/1/20)	satisfactory, additional investigation required for future PAs	Section 3.6.3
CC3-GEOCHEM-20	Gas generation in unsaturated repository	#7 (12/1/20)	satisfactory, additional investigation required for future PAs	Section 3.6.2
CC3-GEOCHEM-21	Gas generation by radiolysis of non-CPR waste materials	#7 (12/1/20)	satisfactory	Section 3.6.4
CC4-GEOCHEM-22	Appendix GEOCHEM colloid parameter table	#7 (12/1/20)	satisfactory, acknowledged in errata	Attachment A
CC5-GEOCHEM-23	Humic colloid PHREEQC input, output, and database files	#7 (12/1/20)	satisfactory, files provided	Attachment A
CC5-GEOCHEM-24	Inclusion of calcite precipitation in EQ3/6 calculations	#8 (1/13/21) & #12 (5/27/21)	satisfactory; follow up call held with DOE February 2021	Section 7.4.4, 7.4.6
CC5-GEOCHEM-25	Effects of polyhalite on modeled brine chemistry	#8 (1/13/21) & #12 (5/27/21)	satisfactory; follow up call held with DOE February 2021	Section 7.4.4, 7.4.8
CC5-GEOCHEM-26	Effects of cements on brine chemistry	#8 (1/13/21) & #12 (5/27/21)	satisfactory; follow up call held with DOE February 2021	Section 7.4.4, 7.4.9

Question	Topic	DOE Response Set[a]	Evaluation/Resolution	Discussion/ Documentation
CC5-GEOCHEM-27 a-d	Incomplete documentation related to Pitzer parameter errors in DATA0.FM4	#8 (1/13/21)	satisfactory, requested data provided	Attachment B 4.1.8
CC6-GEOCHEM-28	Iron-sulfate Pitzer parameters and solid phases not in DATA0.FM4	#10 (3/30/21)	adequate response, omitted data should be added to database for future PAs	Attachment B 5.0
CC6-GEOCHEM-29	Adequacy of lead parameterization in DATA0.FM4	#10 (3/30/21)	adequate response, lead data rejected by EPA	Attachment B 6.0
CC6-GEOCHEM-30	Jang and Kim (2016) report request	#9 (3/4/21)	satisfactory, reference provided	Attachment A
CC6-GEOCHEM-31	Comparison of modeled and experimental glushinskite data	#10 (3/30/21)	satisfactory	Attachment B 4.3.2
CC6-GEOCHEM-32	Effects of shielded containers on steel surface area per unit volume	#9 (3/4/21)	adequate response	Section 3.1.4
CC6-GEOCHEM-33	Humid steel corrosion parameter	#9 (3/4/21)	satisfactory	Section 3.1.2
CC6-GEOCHEM-34	Incorrect units for gas generation and brine production rates	#9 (3/4/21)	satisfactory, acknowledged in errata	Attachment A
CC6-GEOCHEM-35	Omission of brine radiolysis effects from Appendix GEOCHEM discussions of radiolysis and the brine production model	#9 (3/4/21)	satisfactory, acknowledged in errata	Section 3.7
FC2-CCR-GEOCHEM-32	Steel surface area (number of shielded containers)	#13 (5/18/21)	satisfactory	Section 10.0
APPENDIX SOTERM-RELATED QUESTIONS				
CC1-SOTERM-1	Document request. LANL-CO (2018a) and LANL-CO (2018b)	#1 (6/10/20)	satisfactory, reference provided	Inventory TSD* Attachment A
CC1-SOTERM-2	Borate aqueous speciation	#6 (10/26/20)	satisfactory	Attachment B 7.5

Question	Topic	DOE Response Set[a]	Evaluation/Resolution	Discussion/ Documentation
CC1-SOTERM-3	Am(III) aqueous speciation	SOTERM 3 (5/20/21)	satisfactory	Attachment B 7.1
CC1-SOTERM-4	Th(IV) aqueous speciation	#6 (10/26/20)	satisfactory	Attachment B 8.0
CC1-SOTERM-5	Incomplete iron inventory data	#1 (6/10/20)	satisfactory, acknowledged in errata	Attachment A
CC4-SOTERM-6 a-b	Comparison of PROPMIC values to literature values	#7 (12/1/20)	incomplete response, technical exchange held December 2020, calculations and data comparisons performed by EPA	Section 8.3.4
CC4-SOTERM-7	Missing reference	#6 (10/26/20)	satisfactory; reference provided	Attachment A
CC4-SOTERM-8 a-c	Pu(III) intrinsic colloid concentrations	#7 (12/1/20)	adequate response, technical exchange held December 2020	Section 8.1, 8.1.3, 8.1.4
CC4-SOTERM-9	Th(IV) intrinsic colloid concentrations error	#7 (12/1/20)	partially adequate response, technical exchange held December 2020, EPA performed additional assessment	Section 8.1.5
CC4-SOTERM-10	Th(IV) concentration data revisions	#7 (12/1/20)	satisfactory	Attachment A
CC4-SOTERM-11	Th(IV) mineral fragment colloid parameter	#7 (12/1/20)	satisfactory	Section 8.1, 8.1.5
CC4-SOTERM-12	Actinide(IV)-silica colloids	#6 (10/26/20)	partially adequate response; technical exchange held December 2020, additional investigation required for future PAs	Section 8.1.6
FC1-CCR-SOTERM-8	Nd (III) colloids data	#11 (4/23/21)	satisfactory	Section 8.1, Section 8.1.4
FC1-CCR-SOTERM-9	Nd (III) colloids data	#11 (4/23/21)	satisfactory	Section 8.1, Section 8.1.4
FC1-CCR-SOTERM-10	Nd (III) colloids data	#11 (4/23/21)	satisfactory	Section 8.1, Section 8.1.4
APPENDIX SCR-RELATED QUESTIONS				
CC5-SCR-8	Screening argument for galvanic coupling within the repository (FEP W50)	#10 (3/30/21)	satisfactory	Section 3.3; FEPs TSD

Question	Topic	DOE Response Set[a]	Evaluation/Resolution	Discussion/ Documentation
CC5-SCR-9	Screening decision for gas generation by lead corrosion (FEPs W5 and W49)	#10 (3/30/21)	satisfactory	Section 3.2.1, 11.2; FEPs TSD

a – Response #1: Sosson (2020)
Response #3: Knerr (2020a)
Response #4: Knerr (2020b)
Response #5: Knerr (2020c)
Response #6: Knerr (2020d)
Response #7: Knerr (2020e)
Response #8: Knerr (2021a)
Response #9: Knerr (2021b)
Response #10: Knerr (2021c)
Response #11: Knerr (2021d)
Response #12: Knerr (2021e)
Response SOTERM 3: Knerr (2021f)
Supplementary Information: Knerr (2021g)

CC1-SOTERM-1 Document Request from Van Soest (2018)

Peake (2020a) requested copies of two reports cited by Van Soest (2018):

> LANL 2018c. *Chemical and Cement Components 2017 Inventory Estimates*. LANL-CO. INV-SAR-50, Revision 0, December 13, 2018.
>
> LANL 2018d. *Estimation of Cellulose, Plastic, and Rubber Emplacement and Operational Materials in the Waste Isolation Pilot Plant*. LANLCO. INV-SAR-51, Revision 0, December 13, 2018.

Sosson (2020) provided these reports, which are included in the reference list below as LANL-CO (2018a) and LANL-CO (2018b), respectively.

CC1-SOTERM-5 Incomplete Iron Inventory Data in Table SOTERM-3

Peake (2020a) asked DOE to note that the iron inventory data in Appendix SOTERM Table SOTERM-3 includes only waste materials and does not include steel packaging materials. Sosson (2020) acknowledged this omission and provided a modified table and text that is included by reference in the errata list for the CRA-2019.

CC2-GEOCHEM-7: Missing Reference Xiong, Y.-L. 2018.

EPA requested a copy of the following document (Peake 2020b):

> Xiong, Y.-L. 2018. Experimental Determination of Solubilities of Lead Oxalate (PbC_2O_4), Di-Calcium Ethylenediaminetetraacetic Acid Hydrate ($Ca_2EDTA•7H_2O(s)$) in $MgC1_2$-H_2O System, and Earlandite ($Ca_3[C_3H_5O(COO)_3]_2•4H_2O$) in NaCl-$H_2O$ and $MgC1_2$-H_2O Systems, and Their Respective Pitzer Interaction Parameters, Revision 3, Supersedes ERMS 567810. Carlsbad, NM: Sandia National Laboratories. ERMS 570088.

Knerr (2020a) provided a copy of this report.

CC2-GEOCHEM-9 Typographical Errors in Table GEOCHEM-21

Peake (2020b) pointed out typographical errors in equations provided in Table GEOCHEM-21. Knerr (2020a) provided the corrected equations, which are included in in errata tracking for the CRA-2019.

CC3-GEOCHEM-18 Reference Request

Peake (2020c) requested a report cited by Day (2019):

> U.S. DOE. 2012. CH-TRU Payload Appendices, Rev. 3, December 2012. Carlsbad, NM.

This report was provided by Knerr (2020b).

CC4-GEOCHEM-22 Appendix GEOCHEM Colloid Parameter Table

EPA (Peake 2020d) noted apparent discrepancies between some colloid parameters listed in Appendix GEOCHEM-19 Table GEOCHEM-61 (DOE 2019) and the parameters used in the

CRA-2014 PA (Kicker and Herrick 2013) and the CRA-2019 DPA (Kim and Feng 2019). DOE addressed this comment by including a clarifying footnote and modifying the title of Table GEOCHEM-61. Both of these changes were added to the CRA-2019 errata tracking list maintained by DOE (Knerr 2020e).

CC4-SOTERM-7 Missing Reference

EPA (Peake 2020d) requested clarification from DOE, because DOE (2019) referenced Nishikava et al. (2018) on page SOTERM-57 (Section 5.4.2) but this citation does not appear in the reference list and the author's name appeared to have been misspelled. Knerr (2020d) provided the following reference:

> Nishikawa, S., T. Kobayashi, T. Sasaki, and I. Takagi. 2018. Solubilities and solubility products of thorium hydroxide under moderate temperature conditions. *Radiochimica Acta* 106:655-667.

DOE added the changes to their errata list for the CRA-2019.

CC4-SOTERM-10 Th(IV) Concentration Revisions

Peake (2020d) requested clarification regarding differences in Th(IV) intrinsic colloid and dissolved Th(IV) concentrations between Borkowski (2012) and Reed et al. (2013). Knerr (2020e) pointed out that EPA had reversed two columns, which created the discrepancy.

CC5-GEOCHEM-23: Humic Colloid PHREEQC Input, Output, and Database Files

EPA (Peake 2020e) requested copies of the PHREEQC input, output, and database (ymp_r2.dat) files used by Mariner (2019) to calculate the CRA-2019 DPA humic colloid parameters. Knerr (2020e) provided electronic copies of these files.

CC6-GEOCHEM-30: Jang and Kim (2016) Report Request

EPA (Peake 2020f) requested a report cited by Domski (2019), Jang (2019), and Sisk-Scott (2019):

> Jang, J.-H. and S. Kim. 2016. *Derivation of Pitzer Interaction Parameters and Thermodynamic Properties for the Aqueous Species of Ferrous Iron and Their Pairs*, Revision 2. Sandia National Laboratories, Carlsbad, NM.

Knerr (2021b) provided this document to EPA.

CC6-GEOCHEM-34: Incorrect Units for Gas Generation and Brine Production Rates

DOE (2019) states that the rate of total gas production in Appendix GEOCHEM Section GEOCHEM-2.2 is in terms of "unit volume of waste." However, DOE (2019) provides the component rates on the right-hand side of Equation GEOCHEM.2 in terms of "unit disposal volume." EPA requested that DOE correct this editorial error (Peake 2020f). Knerr (2021a) clarified that the correctly stated units should be "gas production per unit volume of waste in the model grid," and included this change in errata tracking for the CRA-2019. DOE confirmed that PA calculations were not affected by the description of disposal units.

References

Borkowski, M. 2012. *Numerical Values for Graphs Presented in Report LCO-ACP-08, Rev. 0, Entitled Solubility of An(IV) in WIPP Brine: Thorium Analog Studies in WIPP Simulated Brine, and for Graphs Published in Borkowski, M., et al. Radiochimica Acta 98 (9-11), 577-582 (2010).* LA-UR- 12-26640; LANL-CO ACRSP ACP-01/2012, Rev. 0. Los Alamos National Laboratory, Carlsbad, New Mexico.

Day, B. 2019. *Reassessment of Need and Parameter Justification for Modeling Gas Generation due to Radiolysis of Brine and Cellulose/Plastic/Rubber in WIPP for CRA-2019*. Sandia National Laboratories, Carlsbad, New Mexico. ERMS 570873.

DOE (U.S. Department of Energy). 2012. *CH-TRU Payload Appendices, Rev. 3.* Carlsbad, New Mexico, December 2012.

DOE (U.S. Department of Energy). 2019. *Title 40 CFR 191 Parts B and C Compliance Recertification Application*. U.S. Department of Energy Carlsbad Field Office, March 2019.

Domski, P.S. 2019. *An Update to the EQ3/6 Pitzer Thermodynamic Database DATA0.FM1 with the Creation of DATA0.FM4*. Sandia National Laboratories. Carlsbad, New Mexico. ERMS 571052.

EPA (U.S. Environmental Protection Agency) 2021. *Overview of EPA Review of U.S. Department of Energy 2019 WIPP Compliance Recertification Application Performance Assessment*. Office of Radiation and Indoor Air, Docket No. EPA-HQ-OAR-2019-0534.

Jang, J.J. 2019. *AP-182, Analysis Plan for Derivation and Addition of Equilibrium Constants and Pitzer Interaction Parameters to the WIPP Geochemical Thermodynamic Database*. Sandia National Laboratories, Carlsbad, New Mexico,

Jang, J.-H., and S. Kim. 2016. *Derivation of Pitzer Interaction Parameters and Thermodynamic Properties for the Aqueous Species of Ferrous Iron and Their Pairs*, Revision 2. Sandia National Laboratories, Carlsbad, New Mexico,

Kicker, D.C, and C.G. Herrick. 2013. *Parameter Summary Report for the Compliance Recertification Application, Rev. 0*. Sandia National Laboratories, Carlsbad, New Mexico, ERMS 560298.

Kim, S., and L.M. Feng. 2019. *Input Parameter Report for the 2019 Compliance Recertification Application Performance Assessment (CRA-2019 DPA), Revision 0.* Sandia National Laboratories, Carlsbad, New Mexico, ERMS 571377.

Knerr, R. 2020a. *Response 3 to U.S. Environmental Protection Agency's 2019 Compliance Recertification Application Completeness Comments Letter dated March 23, 2020 and May 6, 2020 from Tom Peake to Mike Brown*. U.S. Department of Energy, Carlsbad Field Office, Carlsbad, New Mexico. Letter to L.B. Veal, U.S. Environmental Protection Agency Radiation Protection Division, Washington, D.C. August 13, 2020.

Knerr, R. 2020b. *Response 4 to U.S. Environmental Protection Agency's 2019 Compliance Recertification Application Completeness Comments Letter dated March 23, 2020 from Tom Peake to Mike Brown*. U.S. Department of Energy, Carlsbad Field Office, Carlsbad, New Mexico. Letter to L.B. Veal, U.S. Environmental Protection Agency Radiation Protection Division, Washington, D.C. September 15, 2020.

Knerr, R. 2020c. *Response 5 to U.S. Environmental Protection Agency's 2019 Compliance Recertification Application Completeness Comments Letter dated May 6, 2020 and June 12 2020 from Tom Peake to Mike Brown*. U.S. Department of Energy, Carlsbad Field Office, Carlsbad, New Mexico. Letter to L.B. Veal, U.S. Environmental Protection Agency Radiation Protection Division, Washington, D.C. October 19, 2020.

Knerr, R. 2020d. *Response 6 to U.S. Environmental Protection Agency's 2019 Compliance Recertification Application Completeness Comments Letter dated March 23, 2020, May 8, 2020, June 12, 2020, and July 17, 2020 from Tom Peake to Mike Brown*. U.S. Department of Energy, Carlsbad Field Office, Carlsbad, New Mexico. Letter to L.B. Veal, U.S. Environmental Protection Agency Radiation Protection Division, Washington, D.C. October 26, 2020.

Knerr, R. 2020e. *Response 7 to U.S. Environmental Protection Agency's 2019 Compliance Recertification Application Completeness Comments Letters dated May 6, 2020, June 12, 2020, July 17, 2020 and September 11, 2020 from Tom Peake to Mike Brown*. U.S. Department of Energy, Carlsbad Field Office, Carlsbad, New Mexico. Letter to L.B. Veal, U.S. Environmental Protection Agency Radiation Protection Division, Washington, D.C. December 1, 2020.

Knerr, R. 2021a. *Response 8 to U.S. Environmental Protection Agency's 2019 Compliance Recertification Application Completeness Comments Letter dated September 11, 2020 and November 13, 2020 from Tom Peake to Mike Brown*. U.S. Department of Energy, Carlsbad Field Office, Carlsbad, New Mexico. Letter to L.B. Veal, U.S. Environmental Protection Agency Radiation Protection Division, Washington, D.C. January 13, 2021.

Knerr, R. 2021b. *Response 9 to U.S. Environmental Protection Agency's 2019 Compliance Recertification Application Completeness Comments Letter dated September 11, 2020 and November 13, 2020 from Tom Peake to Mike Brown*. U.S. Department of Energy, Carlsbad Field Office, Carlsbad, New Mexico. Letter to L.B. Veal, U.S. Environmental Protection Agency Radiation Protection Division, Washington, D.C. March 4, 2021.

Knerr, R. 2021c. *Response 10 to U.S. Environmental Protection Agency's 2019 Compliance Recertification Application Completeness Comments Letter dated September 11, 2020 and November 13, 2020 from Tom Peake to Mike Brown*. U.S. Department of Energy, Carlsbad Field Office, Carlsbad, New Mexico. Letter to L.B. Veal, U.S. Environmental Protection Agency Radiation Protection Division, Washington, D.C. March 30, 2021.

Knerr, R. 2021d. *Response 11 to U.S. Environmental Protection Agency's 2019 Compliance Recertification Application Completeness Comments Letter dated September 11, 2020 and November 13, 2020 from Tom Peake to Mike Brown and Email Dated January 7, 2021 from Ingrid Rosencrantz to Anderson Ward*. U.S. Department of Energy, Carlsbad Field Office,

Carlsbad, New Mexico. Letter to L.B. Veal, U.S. Environmental Protection Agency Radiation Protection Division, Washington, D.C. April 23, 2021.

Knerr, R. 2021e. *Response 12 to U.S. Environmental Protection Agency's 2019 Compliance Recertification Application Completeness Comments Letter dated September 11, 2020 and November 13, 2020 from Tom Peake to Mike Brown*. U.S. Department of Energy, Carlsbad Field Office, Carlsbad, New Mexico. Letter to L.B. Veal, U.S. Environmental Protection Agency Radiation Protection Division, Washington, D.C. May 27, 2021.

Knerr, R. 2021f. *Response SOTERM 3 to U.S. Environmental Protection Agency's 2019 Compliance Recertification Application Completeness Comments Letter dated March 23, 2020, from Tom Peake to Mike Brown.* U.S. Department of Energy, Carlsbad Field Office, Carlsbad, New Mexico. Letter to L.B. Veal, U.S. Environmental Protection Agency Radiation Protection Division, Washington, D.C. May 20, 2021.

Knerr, R. 2021g. *Supplementary Information as Requested by U.S. Environmental Protection Agency During Technical Exchange Meeting on June 22, 2020*. U.S. Department of Energy, Carlsbad Field Office, Carlsbad, New Mexico. Letter to L.B. Veal, U.S. Environmental Protection Agency Radiation Protection Division, Washington, D.C. July 8, 2021.

LANL-CO. 2018a. *Chemical and Cement Components 2017 Inventory Estimates*. LANL-CO. INV-SAR-50, Revision 0, December 13, 2018.

LANL-CO. 2018b. *Estimation of Cellulose, Plastic, and Rubber Emplacement and Operational Materials in the Waste Isolation Pilot Plant*. LANLCO. INV-SAR-51, Revision 0, December 13, 2018.

Mariner, P.E. 2019. *A Summary of Humic Colloid Parameter Values to be Implemented in the CRA-2019 Deferred Performance Assessment.* Sandia National Laboratories, Albuquerque, New Mexico, ERMS 571250.

Nishikawa, S., T. Kobayashi, T. Sasaki, and I. Takagi. 2018. Solubilities and solubility products of thorium hydroxide under moderate temperature conditions. *Radiochimica Acta* 106:655-667.

Peake, T. 2020a. *First Set of EPA Completeness Comments and Questions for Compliance Recertification Application 2019 (CRA-2019).* U.S. Environmental Protection Agency, Center for Waste Management and Regulation, Washington, D.C. Letter to M. Brown, U.S. Department of Energy, Carlsbad Field Office, Carlsbad, New Mexico, March 23, 2020.

Peake, T. 2020b. *Second Set of EPA Completeness Comments and Questions for Compliance Recertification Application 2019 (CRA-2019).* U.S. Environmental Protection Agency, Center for Waste Management and Regulation, Washington, D.C. Letter to M. Brown, U.S. Department of Energy, Carlsbad Field Office, Carlsbad, New Mexico, May 6, 2020.

Peake, T. 2020c. *Third Set of EPA Completeness Comments and Questions for Compliance Recertification Application 2019 (CRA-2019).* U.S. Environmental Protection Agency, Center for Waste Management and Regulation, Washington, D.C. Letter to M. Brown, U.S. Department of Energy, Carlsbad Field Office, Carlsbad, New Mexico, June 12, 2020.

Peake, T. 2020d. *Fourth Set of EPA Completeness Comments and Questions for Compliance Recertification Application 2019 (CRA-2019).* U.S. Environmental Protection Agency, Center for Waste Management and Regulation, Washington, D.C. Letter to M. Brown, U.S. Department of Energy, Carlsbad Field Office, Carlsbad, New Mexico, July 17, 2020.

Peake, T. 2020e. *Fifth Set of EPA Completeness Comments and Questions for Compliance Recertification Application 2019 (CRA-2019).* U.S. Environmental Protection Agency, Center for Waste Management and Regulation, Washington, D.C. Letter to M. Brown, U.S. Department of Energy, Carlsbad Field Office, Carlsbad, New Mexico, September 11, 2020.

Peake, T. 2020f. *Sixth Set of EPA Completeness Comments and Questions for Compliance Recertification Application 2019 (CRA-2019).* U.S. Environmental Protection Agency, Center for Waste Management and Regulation, Washington, D.C. Letter to M. Brown, U.S. Department of Energy, Carlsbad Field Office, Carlsbad, New Mexico, November 13, 2020.

Reed, D.T., J.S. Swanson, J.F. Lucchini and M.K. Richmann. 2013. *Intrinsic, Mineral and Microbial Colloid Enhancement Parameters for the WIPP Actinide Source Term.* LCO-ACP-18, Revision 0, Los Alamos National Laboratory, Carlsbad, New Mexico.

Sisk-Scott, C. 2019. *AP-183, Analysis Plan to Update the WIPP Geochemical Thermodynamic Database (DATA0.FM1) to DATA0.FM4 for CRA-2019*. Revision 1, Carlsbad, NM Sandia National Laboratories.

Sosson, G. 2020. *Response 1 to U.S. Environmental Protection Agency's 2019 Compliance Recertification Application Completeness Comments Letter dated March 23, 2020 from Tom Peake to Mike Brown*. U.S. Department of Energy, Carlsbad Field Office, Carlsbad, New Mexico. Letter to L.B. Veal, U.S. Environmental Protection Agency Radiation Protection Division, Washington, D.C. June 11, 2020.

Van Soest, G.D. 2018. *Performance Assessment Inventory Report – 2018*. Los Alamos National Laboratory Carlsbad Operations INV-PA-18, Revision 0, December 12, 2018.

Xiong, Y.-L. 2018. *Experimental Determination of Solubilities of Lead Oxalate (PbC_2O_4), Di-Calcium Ethylenediaminetetraacetic Acid Hydrate ($Ca_2EDTA•7H_2O(s)$) in $MgC1_2$-H_2O System, and Earlandite ($Ca_3[C_3H_5O(COO)_3]_2•4H_2O$) in NaCl-$H_2O$ and $MgC1_2$-H_2O Systems, and Their Respective Pitzer Interaction Parameters*. Revision 3, Supersedes ERMS 567810. Sandia National Laboratories. Carlsbad, New Mexico ERMS 570088.

Attachment B: DATA0.FM4 Database Review

CONTENTS

Tables ii
Figures iii
Acronyms and Symbols iv
1.0 Introduction 1
2.0 Database Documentation 3
3.0 Brine Constituents and Magnesium Minerals 5
3.1 Hydromagnesite 5
3.2 Phase 5 5
4.0 Organic Ligands 8
4.1 EDTA 8
4.1.1 H_4EDTA(aq) Acid Dissociation Constants 10
4.1.2 Sodium and Potassium 11
4.1.3 Calcium 13
4.1.4 Magnesium 16
4.1.5 Americium(III) 18
4.1.6 Thorium(IV) 20
4.1.7 Neptunium(V) 21
4.1.8 DATA0.FM4 Parameter Problem Reports 22
4.1.9 EDTA Summary 23
4.2 Citrate 25
4.2.1 H_3Citrate(aq) Acid Dissociation Constants 27
4.2.2 Magnesium and Calcium 27
4.2.3 Americium(III) 29
4.2.4 Thorium(IV) 29
4.2.5 Neptunium(V) 30
4.2.6 Earlandite 30
4.2.7 Citrate Summary 31
4.3 Oxalate 32
4.3.1 H_2Oxalate(aq) Acid Dissociation Constants 32
4.3.2 Magnesium and Calcium 33
4.3.3 Americium(III) 34
4.3.4 Thorium(IV) 35
4.3.5 Neptunium(V) 35
4.3.6 Oxalate Summary 36
4.4 Acetate 36

5.0 Iron(II) 38
6.0 Lead(II) 41
7.0 Americium(III) 43
7.1 Americium(III) Hydrolysis 43
7.2 Pitzer Parameters 44
7.3 $Am(OH)_3$ Solids 44
7.4 Americium(III)-Carbonate Aqueous Species and Solids 46
7.5 Americium(III)-Borate Aqueous Species and Solids 47
7.6 Americium(III) Summary 48
8.0 Thorium(IV) 49
8.1 Thorium(IV) Hydrous Oxide Solid and Hydrolysis 49
8.2 Thorium(IV)-Carbonate Speciation 51
8.3 Thorium(IV)-Sulfate Solids and Aqueous Species 51
8.4 Thorium(IV) Summary 51
9.0 Neptunium(V) and Uranium(VI) 53
10.0 Summary and Conclusions 54
11.0 References 58

TABLES

Table 1-1. WIPP Geochemical Modeling Codes and Databases 1
Table 2-1. DATA0.FM4 Documentation 3
Table 4-1. EDTA Aqueous Speciation Data From Giambalvo (2002b) and Hummel et al. (2005) 9
Table 4-2. EDTA Pitzer Parameter Changes Between DATA0.FM1 and DATA0.FM4 12
Table 4-3. Correction of Choppin et al. (2001) ThEDTA(aq) Apparent Stability Constants for $NaEDTA^{3-}$ 20
Table 4-4. Citrate Aqueous Speciation Data From Giambalvo (2002b) and Hummel et al. (2005) 26
Table 4-5. Oxalate Aqueous Speciation and Solids Solubility Data from Giambalvo (2002b, 2002e) and Hummel et al. (2005) 33
Table 4-6. Actinide-Acetate Aqueous Speciation 37
Table 5-1. Iron(II) Solids Solubility Data from Sisk-Scott (2019) and Domski (2019a) 38
Table 5-2. Iron(II) Aqueous Speciation Data from Sisk-Scott (2019) and Domski (2019a) 38
Table 5-3. Iron(II) Cation-Anion Interaction Parameters 38
Table 5-4. Iron(II) Cation-Cation Interaction Parameters (Moog et al. 2004) 38
Table 5-5. Iron(II) Cation-Cation-Anion Interaction Parameters (Moog et al. 2004) 39
Table 7-1. Standard State Stability Constants for Am(III) Hydrolysis Species 44

Table 7-2. Reported Solubility Data for $Am(OH)_3$(cr), $Am(OH)_3$(am), $Nd(OH)_3$(cr), and $Nd(OH)_3$(am) 45
Table 7-3. Stability Data for Am(III)-Carbonate Species 46
Table 7-4. Solubility Data for Am(III)-Carbonate Solids 47
Table 8-1. Solubility Data for ThO_2(am) Solids 49
Table 8-2. Stability Data for $Th(OH)_4$(aq) 50
Table 10-1. DATA0.FM4 Issues Summary 54

FIGURES

Figure 3-1. Reported Hydromagnesite Solubility Constants 6
Figure 4-1. Experimentally Measured and Calculated H_4EDTA(aq) Apparent pK_a Values, Including Experimental Values Recalculated from Choppin et al. (2001) Data by Hummel et al. (2005) 11
Figure 4-2. Experimentally Measured and Calculated $MgEDTA^{2-}$ Apparent Log β Values, Including Experimental Values Recalculated by Hummel et al. (2005) 17
Figure 4-3. Experimentally Measured and Calculated $AmEDTA^-$ Apparent Log β Values, Including Corrected Experimental Values from Hummel et al. (2005) 19
Figure 4-4. Experimentally Measured and Calculated ThEDTA(aq) Apparent Log β Values, Including Experimental Values Recalculated to Account for $NaEDTA^{3-}$ Species 21
Figure 4-5. Experimentally Measured and Calculated $MgCitrate^-$ Apparent Log β_{101} Values, and Experimentally Measured and Calculated MgHCitrate(aq) Log β_{111} Values 28

ACRONYMS AND SYMBOLS

α_1, α_2	Pitzer cation – anion interaction parameters
β	Apparent stability constant
β^0	Standard state stability constant
$\beta^{(0)}, \beta^{(1)}$	Pitzer cation – anion interaction parameters
C^{φ}	Pitzer cation – anion interaction parameters
CCA	Compliance Certification Application
CRA	Compliance Recertification Application
CRA-2004	First Compliance Recertification Application, March 2004
CRA-2009	Second Compliance Recertification Application, March 2009
CRA-2014	Third Compliance Recertification Application, March 2014
CRA-2019	Fourth Compliance Recertification Application, March 2019
CRA-2019 DPA	Deferred PA for the CRA-2019, December 2019
DATA0.FM1	Database used for CRA-2014 PA
DATA0.FM4	Database used for CRA-2019 DPA
DOE	U.S. Department of Energy
EDTA	Ethylenediaminetetraacetic acid
EPA	U.S. Environmental Protection Agency
EQ3/6	Geochemical modeling code used for CRA-2014 PA and CRA-2019 DPA
ERDA-6	Simulated Castile brine formulation
FMT	Fracture Matrix Transport geochemical modeling code
FMT_050405.CHEMDAT	FMT database used for PABC04 and PABC09
GWB	Generic Weep Brine, simulated Salado brine formulation
K_a	
K_s^0	Standard state solubility constant
μ^0/RT	Standard state chemical potential (dimensionless)
NEA	Nuclear Energy Agency
NEA-TDB	Nuclear Energy Agency Thermochemical Database
PA	Performance assessment
PABC04	CRA-2004 Performance Assessment Baseline Calculations
PABC09	CRA-2009 Performance Assessment Baseline Calculations
PAVT	Performance Assessment Verification Testing
pcH	Negative logarithm of the hydrogen ion concentration, molar units
pH	Negative logarithm of the hydrogen ion activity
PHREEQC	Geochemical modeling code developed by the U.S. Geological Survey

ACRONYMS AND SYMBOLS

pK_a	Negative logarithm of the apparent acid dissociation constant
pK_a^0	Negative logarithm of the standard-state acid dissociation constant
pmH	Negative logarithm of the hydrogen ion concentration, molal units
ψ_{ijk}	Pitzer cation – cation – anion interaction parameter
θ_{cc}	Pitzer cation – cation interaction parameter
SIT	Specific Ion Interaction Theory
TRLFS	Time-resolved laser fluorescence spectroscopy
WIPP	Waste Isolation Pilot Plant
XRD	X-ray diffraction

1.0 INTRODUCTION

DOE calculates baseline actinide solubilities for Waste Isolation Pilot Plant (WIPP) performance assessments (PAs) using geochemical modeling codes. These codes use an associated database that contains the solid phase solubility, aqueous speciation, and Pitzer parameter data needed for the calculations. DOE used the FMT code for the Compliance Certification Application Performance Assessment Verification Testing (CCA PAVT), the 2004 Performance Assessment Baseline Calculation (PABC04), and the 2009 Performance Assessment Baseline Calculation (PABC09) actinide solubility calculations (Table 1-1). DOE replaced the FMT code with the EQ3/6 code beginning with the 2014 Compliance Recertification Application Performance Assessment (CRA-2014 PA).

Table 1-1. WIPP Geochemical Modeling Codes and Databases

Performance Assessment	Code	Database
CCA PAVT	FMT	HMW-3456-960318.CHEMDAT[11]
PABC04	FMT	FMT_050405.CHEMDAT
PABC09	FMT	FMT_050405.CHEMDAT
CRA-2014 PA	EQ3/6	DATA0.FM1
CRA-2019 DPA	EQ3/6	DATA0.FM4

DOE produced each database listed in Table 1-1 by revising the previous database version. DOE performed significant revisions to the CCA PAVT database to produce the FMT_050405.CHEMDAT database. DOE later reformatted the FMT_050405.CHEMDAT database and included a few changes to create DATA0.FM1, the EQ3/6 database used to perform the CRA-2014 PA actinide solubility calculations (SC&A 2011, DOE 2014). DATA0.FM1 included a correction of the Pitzer parameter A^{ϕ} from 0.39 to 0.392 and a correction of the Pitzer parameter $\beta^{(1)}$ for NaCl from 0.2644 to 0.2664. DOE also added the equilibrium constant for Phase 5 to DATA0.FM1 (Xiong 2011).

DOE revised DATA0.FM1 to produce DATA0.FM4, which DOE used for the Compliance Recertification Application Deferred Performance Assessment (CRA-2019 DPA) baseline actinide solubility calculations.

EPA reviewed the DATA0.FM4 database and its supporting documentation to determine whether the database complies with 40CFR 194.15, which requires updated geochemical information in each CRA. This review included the DATA0.FM4 data for the major elements, organic ligands, iron, lead, and actinides. During this review, EPA assessed the technical acceptability and internal consistency of the database parameters, along with the adequacy of the database documentation.

[11] Version identified by Novak and Moore (1996); EPA (1998) discussed the uncertainty regarding the exact database version used for the compliance certification application. Giambalvo (2002b) identified the CCA PAVT database as FMT_970407.CHEMDAT.

EPA's DATA0.FM4 review identified a number of database issues. The most important issues are associated with EDTA aqueous speciation and Pitzer parameters, which significantly affected calculations of the baseline dissolved +III actinide solubilities for the CRA-2019 DPA. Because of these issues, the baseline +III actinide solubilities that DOE used in the CRA-2019 DPA were significantly underestimated. The other identified database issues included omission of possible aqueous species without adequate demonstration of possible effects on actinide solubilities, inadvertent omission of data from the database, parameter entry errors, and parameterizations of the Am(III) and Th(IV) solubility models that DOE has not adequately updated as required by 40CFR 194.15. Section 10.0 summarizes EPA's DATA0.FM4 database concerns.

2.0 DATABASE DOCUMENTATION

Table 2-1 lists documents that describe the processes followed to update DATA0.FM1 to DATA0.FM4. Additional analysis reports that describe the derivation of specific thermodynamic data are addressed later in this document as part of the reviews of database additions and revisions.

DATA0.FM4 includes parameters derived under analysis plans AP-154, AP-176, and AP-182 (Domski 2019a). Changes made to DATA0.FM1 to produce DATA0.FM4 include revision of the hydromagnesite solubility constant, modification and addition of organic ligands data, and the addition of iron and lead data (Sisk-Scott 2019, Domski 2019a).

Table 2-1. DATA0.FM4 Documentation

Document	Description
Xiong (2013a)	AP-154, Rev. 2: Analysis plan for deriving thermodynamic data for Fe(II), lead, and sulfide species
Jang and Domski (2016)	AP-176: Analysis plan for deriving thermodynamic data for Fe(II)
Jang (2019)	AP-182: Analysis plan for deriving or importing new thermodynamic data into the existing WIPP geochemical modeling database
Sisk-Scott (2019)	AP-183: Analysis plan for updating DATA0.FM1 to DATA0.FM4, addressing organic ligands and solids, MgO solids, iron data, and lead data
Domski (2019a)	Analysis report documenting the steps used to create the DATA0.FM4 database under AP-183

The AP-154, AP-176, and AP-183 analysis plans outline the procedures for selecting and deriving thermodynamic data during revision of the WIPP EQ3/6 database. Xiong (2013a) includes some observations regarding the approach for calculating thermodynamic data and for demonstrating the acceptability of fitted parameters:

- If the thermodynamic quantities of the experimental system at reference state are well known, the experimental data will be modeled as a function of ionic strength to derive Pitzer parameter(s) only.
- The fitted values of the Pitzer parameters should be of a similar magnitude to those in the peer-reviewed literature for comparable interaction types, and the reference to literature values should be cited in documents reporting the results.
- The differences between the measured data and the modeled predictions should form a curve that has a well-defined minimum when plotted versus the parameter values.
- Graphs showing comparisons of modeled and experimental data should be included in documents reporting the results.

AP-183 (Sisk-Scott 2019) listed the thermodynamic parameters to be included in the DATA0.FM4 database and the steps to be followed when adding or revising the parameters to create DATA0.FM4. Sisk-Scott (2019) referred to CRA-2019 Appendix GEOCHEM (DOE

2019) for parameter review and selection. The approach used to create DATA0.FM4 was to first prepare a provisional database that contained all revised parameters. Testing of this preliminary database was performed by running a Python minimization script coupled with EQ3/6 calculations to adjust the target parameter to minimize the differences between experimental values and calculated values. These minimization routines were performed on parameters previously determined from WIPP experimental data to establish whether the parameter value was significantly altered if re-evaluated using the preliminary database. Testing was not carried out on thermodynamic parameters obtained from the literature (Sisk-Scott 2019, Domski 2019a).

Sisk-Scott (2019) and Domski (2019a) did not provide justification for the lack of testing for literature data. Much of the literature data introduced during creation of DATA0.FM4 was extrapolated to the reference state of zero ionic strength using the Specific Ion Interaction Theory (SIT) method to calculate ion activity coefficients at high ionic strength. However, these reference state data are then used with ion activity coefficients calculated with the Pitzer approach. The use of different methods of calculating the ion activity coefficients introduces uncertainty with respect to this literature data. Comparison of experimental data to data modeled using literature-derived parameters could identify instances where the different methods of calculating ion activity coefficients (SIT and Pitzer) cause significant divergence between modeled and measured data. In addition, such comparisons could identify internal inconsistencies in the database that should be rectified.

3.0 BRINE CONSTITUENTS AND MAGNESIUM MINERALS

All WIPP thermodynamic databases have included the Harvie et al. (1984) parameterization of the Na^+-K^+-Mg^{2+}-Ca^{2+}-Cl^--SO_4^{2-}-CO_3^{2-}-H_2O system using the Pitzer model, and extension of this parameterization to borate-containing systems by Felmy and Weare (1986). Solubilities were obtained from Harvie et al. (1984) for a number of minerals important for WIPP solubility calculations, including halite, brucite, calcite, anhydrite, polyhalite, portlandite, and other minerals. Phosphate aqueous species and the solubility of $AmPO_4$(cr) were included based on data from Rai et al. (1992).

3.1 HYDROMAGNESITE

Hydromagnesite [$Mg_5(CO_3)_4(OH)_2 \bullet 4H_2O$(s)] solubility is important for WIPP actinide solubility calculations because the brucite-hydromagnesite reaction controls predicted CO_2 fugacities in WIPP brines. The solubility of hydromagnesite in the WIPP thermodynamic database versions through DATA0.FM1 was derived from calorimetric measurements by Robie and Hemingway (1973). However, Robie and Hemingway (1973) reported both a free energy of formation for hydromagnesite and a solubility constant (log K_s^0). The DATA0.FM1 hydromagnesite log K_s^0 value of 32.25 was apparently calculated from the log K_s^0 value reported by Robie and Hemingway (1973). Domski (2019a) calculated a log K_s^0 value for hydromagnesite of 31.49 from the free energy of formation data reported by Robie and Hemingway (1973) and the standard chemical potential data of Harvie et al. (1984). The revised log K_s^0 value of 31.49 in DATA0.FM4 is an improvement over the previous value because it was calculated using the Harvie et al. (1984) chemical potential data for auxiliary species and is therefore internally consistent with other thermodynamic data in DATA0.FM4.

During the CRA-2014 review, DOE proposed a hydromagnesite log K_s^0 value of 29.33 based on solubility measurements by Xiong (2015c). However, EPA (2017) determined that the proposed solubility was too low compared to other experimental solubility data (Figure 3-1) and found that the hydromagnesite solubility based on Robie and Hemingway (1973) appears to be the most acceptable value. The DATA0.FM4 hydromagnesite log K_s^0 is reasonably consistent with the solubilities reported by Berninger et al. (2014) and Gautier et al. (2014), which were also found to be acceptable by EPA (2017). Consequently, the recalculated hydromagnesite solubility in DATA0.FM4 is appropriate for use in WIPP PA.

The effects of the slightly decreased hydromagnesite solubility in DATA0.FM4 relative to DATA0.FM1 will be a small decrease in predicted CO_2 fugacity. Lower CO_2 fugacity can decrease the actinide solubilities calculated for WIPP PA because of decreased formation of actinide-carbonate aqueous species.

3.2 PHASE 5

The solubility of Phase 3 [$Mg_2(OH)_3Cl \bullet 4H_2O$(s)] in DATA0.FM1 (Harvie et al. 1984) has been included in all thermodynamic database versions used for WIPP PA. Formation of Phase 3 has not been observed in experiments with WIPP brines and MgO backfill materials. However, precipitation of another magnesium hydroxychloride solid, Phase 5 [$Mg_3(OH)_5Cl \bullet 4H_2O$(s)], was observed in MgO(s) hydration experiments with GWB brine (Snider 2002, Deng et al. 2009).

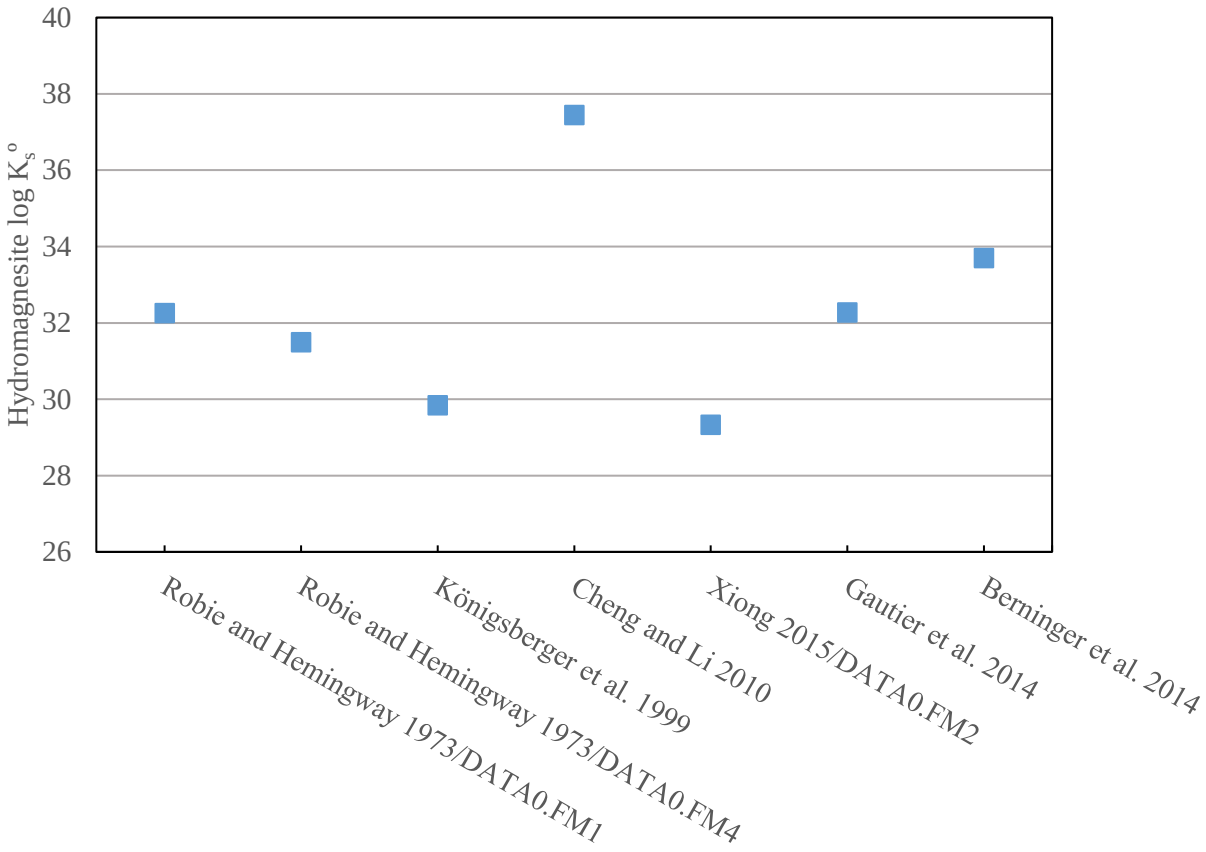

Figure 3-1. Reported Hydromagnesite Solubility Constants

Phase 5 solubility (Xiong 2009, Xiong et al. 2009, Xiong et al. 2010) was added to the database during development of DATA0.FM1 (Xiong 2011). Xiong et al. (2009, 2010) performed solubility experiments with Phase 5 solids in a series of $MgCl_2$ - NaCl mixtures and used measured pmH, magnesium concentrations, and chloride concentrations from these experiments to calculate the solubility of Phase 5 in the experimental solutions. Xiong et al. (2010) used the Pitzer approach to extrapolate these data to obtain a log K_s^0 value for Phase 5 at zero ionic strength. This Phase 5 log K_s^0 value was included in DATA0.FM1 for the CRA-2014 PA and in DATA0.FM4 for the CRA-2019 DPA.

Actinide solubility calculations performed for the CRA-2014 PA predicted that Phase 5 would be in equilibrium with GWB brine under repository conditions but would not precipitate from ERDA-6 brine, which is consistent with the available experimental data (EPA 2017). On the other hand, actinide solubility calculations performed for the CRA-2019 DPA predicted significant Phase 5 precipitation from both GWB and ERDA-6 brines (Domski 2019n). Phase 5 precipitation from ERDA-6 brine is inconsistent with the reported experimental results with ERDA-6 brine and MgO(s) (Snider 2002, Deng et al. 2009).

DOE has not provided calculations demonstrating that the DATA0.FM4 database can be used to accurately model the experimental solubility data for Phase 5. Figure 5 in Xiong et al. (2009)

appears to show that the calculated solubility of Phase 5 is consistently less than the measured values in simplified GWB brine. Precipitation of Phase 5 from ERDA-6 in the CRA-2019 PA may be a consequence of the modeling assumptions used in the actinide solubility calculations. However, if the Phase 5 log K_s^0 value is too low, the stability of Phase 5 and its precipitation would be overestimated. Consequently, EPA expects DOE to perform calculations demonstrating that the Phase 5 log K_s^0 value in the DATA0.FM4 database is consistent with the measured data.

4.0 ORGANIC LIGANDS

The FMT database used for the CCA PAVT did not include organic ligands. DOE reviewed the available literature for the CRA-2004 and recommended parameter values for modeling the interaction of organic species with Am^{3+}, Th^{4+}, NpO_2^+, Mg^{2+}, Ca^+, Na^+, K^+, H^+, and Cl^- (Giambalvo 2002b). The recommended parameters were mainly derived from Choppin et al. (2001) and other studies obtained from the same WIPP experimental program (Pokrovsky et al. 1998, Mizera et al. 1999, Moore et al. 1999, Borkowski et al. 2001). These parameters, including aqueous speciation and Pitzer parameters, were added to the WIPP thermodynamic database for the PABC04 (FMT_050405.CHEMDAT). Data were added for acetate, citrate, EDTA, oxalate, and lactate. However, lactate is not included in the inventory estimates of organic ligands (Van Soest 2018) or actinide solubility calculations. In addition to the data from Giambalvo (2002b), a few changes were made to the organic ligands data in the FMT database prior to the PABC04 actinide solubility calculations. These changes include data related to acetate (Xiong 2004a) and oxalate (Xiong 2004b). DATA0.FM1 contained the same organic ligands data as FMT_050405.CHEMDAT.

Thermodynamic data related to organic ligands were updated during development of DATA0.FM4. Between DATA0.FM1 and DATA0.FM4, some of the EDTA, citrate, and oxalate data were revised, and other data for these organic ligands were added. No modifications were made to parameters related to acetate between DATA0.FM1 and DATA0.FM4.

4.1 EDTA

EDTA (ethylenediaminetetraacetic acid, $C_{10}H_{16}N_2O_8$) is important to WIPP PA baseline actinide solubility calculations because of its ability to form stable aqueous complexes with Am(III), Cm(III), and Pu(III), and increase dissolved actinide source term concentrations. The parameter changes in the DATA0.FM4 database include revised standard-state stability constants ($\log \beta^0$) for aqueous EDTA species, addition of three aqueous EDTA species, addition of a calcium-EDTA solid phase, and revised Pitzer parameters.

Giambalvo (2002b) reviewed WIPP experimental data (Pokrovsky et al. 1998, Mizera et al. 1999, Choppin et al. 2001) and included derived EDTA parameters in the DATA0.FM1 database (Table 4-1). These parameters were based on measurements in solutions ranging from 0.3 to 5.0 m NaCl. Acid dissociation constants (K_a) for $H_4EDTA(aq)$ and the $\log \beta^0$ for $MgEDTA^{2-}$ were measured potentiometrically. Complexation of Ca^{2+} by $EDTA^{4-}$ was not measured, so the $\log \beta^0$ for this species was assumed equal to the $MgEDTA^{2-}$ $\log \beta^0$. The apparent stability constants ($\log \beta$) for Am(III)-EDTA, Th(IV)-EDTA, and Np(V)-EDTA complexes as a function of ionic strength were determined using a solvent extraction method.

Giambalvo (2002b) extrapolated the $\log \beta$ data summarized by Choppin et al. (2001) to zero ionic strength using Pitzer parameters. Choppin et al. (2001) provided $\log \beta$ values as a function of ionic strength for both the $MgEDTA^{2-}$ and $MgHEDTA^-$ aqueous species, but Giambalvo (2002b) evaluated only the $MgEDTA^{2-}$ species and $MgHEDTA^-$ was not included in DATA0.FM1.

Table 4-1. EDTA Aqueous Speciation Data From Giambalvo (2002b) and Hummel et al. (2005)

Reaction	pK_a^0 and log β^0	
	Giambalvo (2002b) DATA0.FM1	Hummel et al. (2005) DATA0.FM4 (except where noted)
(a) $EDTA^{4-} + 4\ H^+ \leftrightarrow H_4EDTA(aq)$	23.04	23.42
(b) $EDTA^{4-} + 3\ H^+ \leftrightarrow H_3EDTA^-$	20.54	21.19
(c) $EDTA^{4-} + 2\ H^+ \leftrightarrow H_2EDTA^{2-}$	17.45	18.04
(d) $EDTA^{4-} + H^+ \leftrightarrow HEDTA^{3-}$	10.57	11.24
(e) $Na^+ + EDTA^{4-} \leftrightarrow NaEDTA^{3-}$	--[a]	2.80
(f) $Mg^{2+} + EDTA^{4-} \leftrightarrow MgEDTA^{2-}$	10.13	10.90
(g) $H^+ + Mg^{2+} + EDTA^{4-} \leftrightarrow MgHEDTA^-$	--[a]	15.40
(h) $Ca^{2+} + EDTA^{4-} \leftrightarrow CaEDTA^{2-}$	10.13[b]	12.69
(i) $H+ + Ca^{2+} + EDTA^{4-} \leftrightarrow CaHEDTA^-$	--[a]	16.23
(j) $Am^{3+} + EDTA^{4-} \leftrightarrow AmEDTA^-$	18.97	19.67[c]
(k) $Th^{4+} + EDTA^{4-} \leftrightarrow ThEDTA(aq)$	23.557	--[c,d]
(l) $NpO_2^+ + EDTA^{4-} \leftrightarrow NpO_2EDTA^{3-}$	8.5352	9.23[c]
(m) $NpO_2^+ + H^+ + EDTA^{4-} \leftrightarrow NpO_2HEDTA^{2-}$	15.5464	17.06[c]
(n) $NpO_2^+ + 2H^+ + EDTA^{4-} \leftrightarrow NpO_2H_2EDTA^-$	20.8648	22.51[c]

a – species not included in DATA0.FM1

b – $CaEDTA^{2-}$ log β^0 assumed equal to $MgEDTA^{2-}$ value

c – Giambalvo (2002b) log β^0 values for Am(III)-, Th(IV)-, and Np(V)-EDTA complexes were retained in DATA0.FM4

d – thorium complexation with EDTA not reviewed by Hummel et al. (2005)

The Nuclear Energy Agency (NEA) performed a critical review of available EDTA data in Hummel et al. (2005), compiled a set of accepted data obtained over a range of ionic strengths, and extrapolated the accepted data to zero ionic strength using the SIT model. The data used by Hummel et al. (2005) included the NaCl solution data from the WIPP program (Pokrovsky et al. 1998, Mizera et al. 1999, Choppin et al. 2001) as well as data from other investigations conducted in different background electrolyte solutions.

Sisk-Scott (2019) states that the WIPP EDTA thermodynamic data were reviewed, and the decision was made to revise most of the thermodynamic data to be consistent with Hummel et al. (2005). The aqueous speciation data for EDTA were updated in DATA0.FM4 by replacing the DATA0.FM1 $H_4EDTA(aq)$ acid dissociation constants (pK_a^0), $MgEDTA^{2-}$ log β^0, and $CaEDTA^{2-}$ log β^0 with pK_a^0 and log β^0 values from Hummel et al. (2005) (Table 4-1). Log β^0 values were also added for the aqueous species $NaEDTA^{3-}$, $MgHEDTA^-$, and $CaHEDTA^-$. No changes were made to the $AmEDTA^-$, ThEDTA(aq), NpO_2EDTA^{3-}, NpO_2HEDTA^{2-}, and $NpO_2H_2EDTA^-$ log β^0 values between DATA0.FM1 and DATA0.FM4.

Addition of the $NaEDTA^{3-}$ aqueous species to DATA0.FM4 is supported by the available data, as discussed by Felmy and Mason (2003). Including this species in DATA0.FM4 requires reevaluation of other EDTA log β^0 values, because the $NaEDTA^{3-}$ species will affect the results of parameter fitting to the experimental data. Hummel et al. (2005) accounted for the $NaEDTA^{3-}$ species when fitting the experimental data for their recommended parameters that are included in DATA0.FM4. Parameters that remained unchanged in the DATA0.FM4 database include the $AmEDTA^-$, ThEDTA(aq), NpO_2EDTA^{3-}, NpO_2HEDTA^{2-}, and $NpO_2H_2EDTA^-$ log β^0 values. Consequently, these log β^0 values must be evaluated to determine if including the $NaEDTA^{3-}$ species in DATA0.FM4 causes significant differences between the modeled and measured concentrations of these aqueous EDTA species.

4.1.1 H_4EDTA(aq) Acid Dissociation Constants

The Hummel et al. (2005) pK_a^0 values for H_4EDTA(aq) are compared to the DATA0.FM1 values in Table 4-1 [reactions (a) – (d)]. EPA requested that DOE provide a comparison of the apparent pK_a values measured as a function of ionic strength by Choppin et al. (2001) and the apparent pK_a values calculated using DATA0.FM1 and DATA0.FM4 [Peake 2020b, Comment CC2-GEOCHEM-10(a) – (f)] as part of a series of verification calculations for DATA0.FM4. These comparisons are necessary to determine whether the DATA0.FM4 database used for the CRA-2019 PA actinide solubility calculations provides aqueous speciation results consistent with the available high-ionic-strength data for aqueous EDTA species (Mizera et al. 1999, Choppin et al. 2001). Figure 1 of Knerr (2020b) illustrates the results of DOE's calculations and is reproduced in Figure 4-1. The calculations provided by Knerr (2020b) show that for reactions (a) – (c), speciation calculations performed using either DATA0.FM1 or DATA0.FM4 are in good agreement with the experimentally measured data. However, for reaction (d), the pK_a value calculated using DATA0.FM4 departed significantly from the measured values. DOE suggested in their response that the deviation was likely caused by factors that included addition of the $NaEDTA^{3-}$ aqueous species, mixing of values obtained using SIT-based analysis and Pitzer-based analysis, and Pitzer interaction parameter changes that were incorporated in DATA0.FM4.

Hummel et al. (2005, Table VIII-8-a) recalculated the apparent pK_a values for H_4EDTA(aq) at 25°C in NaCl solutions using the Mizera et al. (1999) and Choppin et al. (2001) data by accounting for the $NaEDTA^{3-}$ species. Comparison of these recalculated apparent pK_a values with the values calculated using DATA0.FM4 shows that these values agree quite well (Figure 4-1). Because the DATA0.FM4 acid dissociation constants adequately reproduce the Choppin et al. (2001) data after accounting for the $NaEDTA^{3-}$ aqueous species, the revised H_4EDTA(aq) acid dissociation data are acceptable for use in WIPP PA.

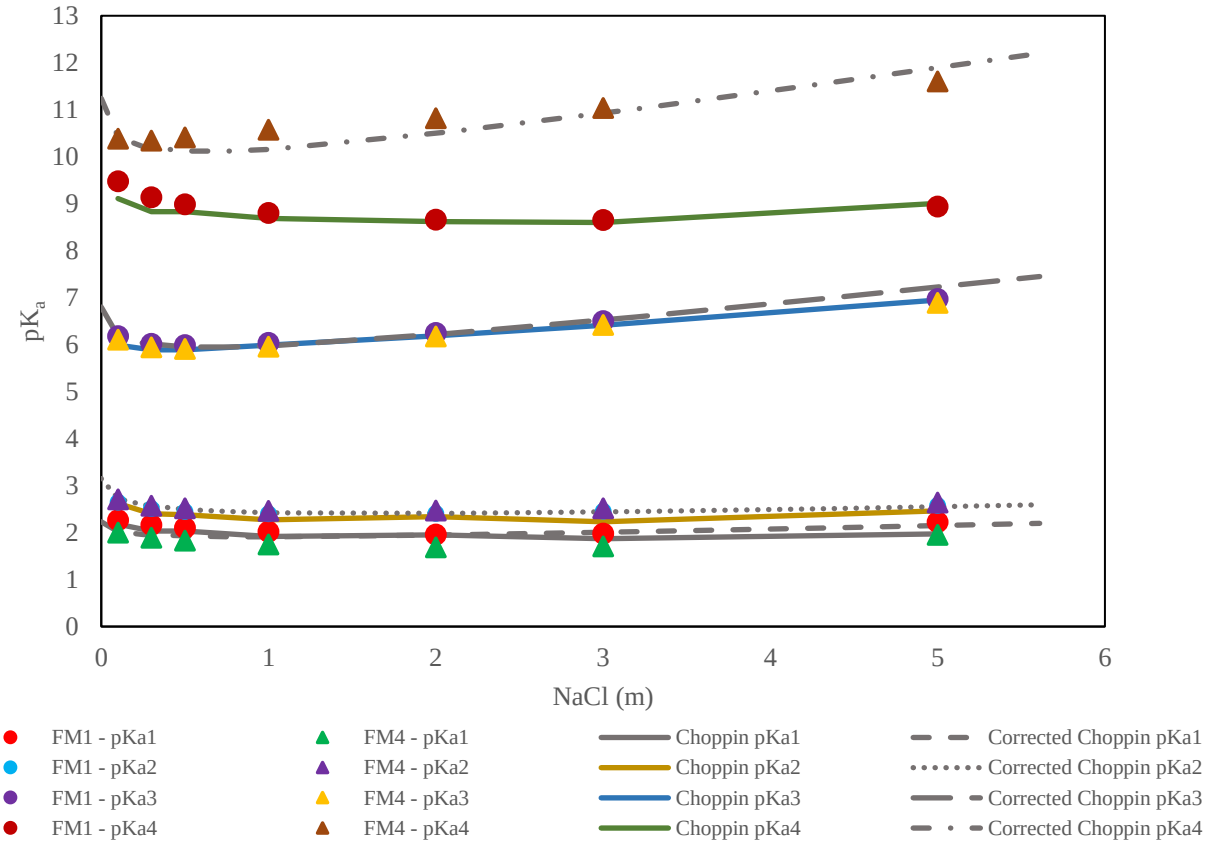

Figure 4-1. Experimentally Measured and Calculated $H_4EDTA(aq)$ Apparent pK_a Values, Including Experimental Values Recalculated from Choppin et al. (2001) Data by Hummel et al. (2005)

4.1.2 Sodium and Potassium

Choppin et al. (2001) did not include formation of the $NaEDTA^{3-}$ aqueous species during their data evaluation, and this species was not included in DATA0.FM1. Pitzer parameters for interaction of $EDTA^{4-}/Na^{+}$ were included in DATA0.FM1 from Choppin et al. (2001), and these parameters were extended to $EDTA^{4-}/K^{+}$ ion interactions (Table 4-2).

Hummel et al. (2005) included the $NaEDTA^{3-}$ species in their data evaluation [Table 4-1, reaction (e)]. The Hummel et al. (2005) log β^0 value of 2.80 is consistent with the Felmy and Mason (2003) value of 2.70 determined using the Pitzer approach and titration data in high ionic strength NaCl solutions (Mizera et al. 1999, Choppin et al. 2001). The $NaEDTA^{3-}$ aqueous species and the Hummel et al. (2005) log β^0 value were added to the DATA0.FM4 database. Because this aqueous species was not included in prior evaluations of the Choppin et al. (2001) data, other log β^0 values for EDTA species that were used in DATA0.FM1 must be recalculated.

Table 4-2. EDTA Pitzer Parameter Changes Between DATA0.FM1 and DATA0.FM4

i	j	α1/α2	$\beta^{(0)}$	$\beta^{(1)}$	C^{φ}	Database	Source
$EDTA^{4-}$	Na^{+}	2.0/12.0	1.02	11.6	0.001	DATA0.FM1	Giambalvo (2002b)
		2.0/12.0	1.10	15.6	0.001	DATA0.FM4	Felmy and Mason (2003)
$EDTA^{4-}$	K^{+}	2.0/12.0	1.02	11.6	0.001	DATA0.FM1	Giambalvo (2002b) by analogy with Na^{+}
		2.0/12.0	1.10	15.6	0.001	DATA0.FM4	Felmy and Mason (2003) by analogy with Na^{+}
$NaEDTA^{3-}$	Na^{+}	2.0/12.0	0.59	5.39	0	DATA0.FM4	Felmy and Mason (2003) new parameter
$EDTA^{4-}$	Ca^{2+}	2.0[a]/12.0	5.39[b]	0	0	DATA0.FM4	Domski (2018b) new parameter
$CaEDTA^{2-}$	Na^{+}	2.0/12.0	0.213	1.74	0.0087	DATA0.FM1	Giambalvo (2002b)
		2.0/12.0	0.185	2.41	0	DATA0.FM4	Domski (2018a)
$CaEDTA^{2-}$	K^{+}	2.0/12.0	0.213	1.74	0.0087	DATA0.FM1	Giambalvo (2002b)
		2.0/12.0	0.185	2.41	0	DATA0.FM4	Domski (2018a) by analogy with Na^{+}
$CaEDTA^{2-}$	Mg^{2+}	2.0[a]/12.0	0	7.21	0	DATA0.FM4	Domski (2018b) new parameter
$MgEDTA^{2-}$	Mg^{2+}	2.0[a]/12.0	0	7.27	0	DATA0.FM4	Domski (2018b) new parameter
$MgEDTA^{2-}$	Na^{+}	2.0/12.0	0.213	1.74	0.0087	DATA0.FM1	Giambalvo (2002b) deleted parameter
$MgEDTA^{2-}$	K^{+}	2.0/12.0	0.213	1.74	0.0087	DATA0.FM1	Giambalvo (2002b) deleted parameter

a – The α_1 parameter value of 2.0 for the $Ca^{2+}/EDTA^{4-}$, $Mg^{2+}/CaEDTA^{2-}$, and $Mg^{2+}/MgEDTA^{2-}$ ion pairs in DATA0.FM4 is incorrect; the correct α_1 parameter value for these ion pairs is 1.4 (Section 4.1.7)

b – The $\beta^{(0)}$ parameter value of 5.39 for the $Ca^{2+}/EDTA^{4-}$ ion pair in DATA0.FM4 is incorrect; the correct $\beta^{(0)}$ parameter value for this ion pair is 2.48 (Section 4.1.7)

Felmy and Mason (2003) developed a thermodynamic model using the Pitzer approach for the Na^+-Sr^{2+}-$EDTA^{4-}$-NO_3^--CO_3^{2-}-H_2O system to ionic strengths up to about 9 molal. During development of this model, Felmy and Mason (2003) calculated Pitzer parameters for $Na^+/NaEDTA^{3-}$ and $Na^+/EDTA^{4-}$ interactions using titration data in concentrated NaCl (Mizera et al. 1999, Choppin et al. 2001), and a pK_a^0 for $HEDTA^{3-}$ of 10.57 from Choppin et al. (2001) [Table 4-1, reaction (d)]. Addition of the $Na^+/NaEDTA^{3-}$ and $Na^+/EDTA^{4-}$ Pitzer parameters to DATA0.FM4 is reasonable because they were calculated using high-ionic-strength NaCl data. However, DATA0.FM4 includes Pitzer parameters for $Na^+/NaEDTA^{3-}$ and $Na^+/EDTA^{4-}$ interactions with a different pK_a^0 for $HEDTA^{3-}$ (11.24 instead of 10.57), creating an internal inconsistency that might affect modeling results. However, this combination of the Felmy and Mason (2003) $Na^+/NaEDTA^{3-}$ and $Na^+/EDTA^{4-}$ Pitzer parameters with the different pK_a^0 for $HEDTA^{3-}$ does not appear to have significantly affected the fit of the apparent pK_a values calculated with DATA0.FM4 to the experimental values recalculated by Hummel et al. (2005) (Figure 4-1). Consequently, the Pitzer parameters for $Na^+/NaEDTA^{3-}$ and $Na^+/EDTA^{4-}$ interactions and the $NaEDTA^{3-}$ log β^0 value appear to be adequate despite the inconsistency in the $HEDTA^{3-}$ pK_a^0.

4.1.3 Calcium

Choppin et al. (2001) provided apparent log β values for magnesium complexation by EDTA as a function of ionic strength. Giambalvo (2002b) used these data to calculate the standard chemical potential and Pitzer parameters for the $MgEDTA^{2-}$ aqueous species. No log β^0 values or Pitzer parameters were available for the $CaEDTA^{2-}$ aqueous species, so these parameters were assumed equal to the Giambalvo (2002b) $MgEDTA^{2-}$ parameter values.

The $CaEDTA^{2-}$ and $CaHEDTA^-$ log β^0 values in DATA0.FM4 are from Hummel et al. (2005) [Table 4-1, reactions (h) and (i)]. The log β^0 values for these species are based on extrapolations of experimental data to zero ionic strength using SIT. The increased log β^0 value for $CaEDTA^{2-}$ will increase calcium-EDTA complexation relative to calculations performed with DATA0.FM1, potentially decreasing EDTA complexation of actinides and calculated actinide solubilities. Addition of the $CaHEDTA^-$ aqueous species to the database should have small effects, if any, on actinide solubility calculations under WIPP repository conditions because this species is much less important than $CaEDTA^{2-}$ and $NaEDTA^{3-}$ species under repository pH conditions (Hummel et al. 2005, Figure VIII-18).

The DATA0.FM4 log β^0 value of 12.69 for $CaEDTA^{2-}$ was determined using SIT and relatively low-ionic-strength data (Hummel et al. 2005). However, WIPP database consistency is improved if equilibrium constants evaluated using the Pitzer model are favored for inclusion in the WIPP database over other models such as SIT, as noted in Analysis Plan AP-176 (Jang and Domski 2016). Experimental data are available from two studies for the $CaEDTA^{2-}$ log β^0 value that were obtained at higher ionic strength, with the Pitzer model of ion interactions used to extrapolate to zero ionic strength (Xiong 2018, Felmy and Mason 2003). Xiong (2018) used experimental $Ca_2EDTA•7H_2O(s)$ solubility data obtained in high ionic strength NaCl solutions to simultaneously fit Pitzer parameters, the $Ca_2EDTA•7H_2O(s)$ log K_s^0 value, and the $CaEDTA^{2-}$ log β^0 value, and obtained a $CaEDTA^{2-}$ log β^0 value of 12.14 ± 0.05. The aqueous species $NaEDTA^{3-}$ was not included in these calculations, which would affect the calculated log K_s^0

value. In addition, the simultaneous fitting of multiple parameters by Xiong (2018) results in relatively large uncertainties in these parameters.

Felmy and Mason (2003) used the Pitzer ion interaction model and experimental data obtained in high-ionic-strength Na^+-Sr^{2+}-$EDTA^{4-}$-NO_3^--CO_3^{2-}-H_2O solutions, and derived a log β^0 value of 12.36 for $CaEDTA^{2-}$ at 22 – 23°C. The log β^0 values from either Xiong (2018) or Felmy and Mason (2003) would result in less complexation of EDTA by Ca^{2+} than the current DATA0.FM4 value and may increase EDTA complexation of actinides.

DOE should adopt the $CaEDTA^{2-}$ log β^0 value from Felmy and Mason (2003) because it was calculated using higher-ionic-strength data than the Hummel et al. (2005) value, included the $NaEDTA^{3-}$ aqueous species that was not considered by Xiong (2018), and the data were extrapolated to zero ionic strength using Pitzer parameters for sodium and EDTA species that are included in DATA0.FM4. Changing the $CaEDTA^{2-}$ log β^0 value to 12.36 is expected to decrease predicted formation of the $CaEDTA^{2-}$ aqueous species relative to calculations with DATA0.FM4, which could increase predicted actinide complexation by EDTA.

DOE fit $Ca_2EDTA•7H_2O$(s) solubility data obtained in NaCl solutions (Xiong 2018, Table 4) to calculate the log K_s^0 value for $Ca_2EDTA•7H_2O$(s) and Pitzer interaction parameters for Na^+/$CaEDTA^{2-}$ (Domski 2018a). For these calculations, Domski (2018a) used DATA0.FM1 with some modifications, including updated EDTA acid dissociation constants, an updated log β^0 for the $CaEDTA^{2-}$, and addition of the $NaEDTA^{3-}$ species to be consistent with the values in DATA0.FM4. Domski (2018a) also included revised Pitzer parameters for Na^+/$EDTA^{4-}$ and Na^+/$HEDTA^{3-}$ interactions citing Felmy (2003) as the source of these data. The revised Na^+/$EDTA^{4-}$ Pitzer parameters are from Felmy and Mason (2003) and are included in DATA0.FM4.

The source of the Na^+/$HEDTA^{3-}$ interaction parameters used by Domski (2018a) are unclear, because Felmy and Mason (2003) used the parameters developed by Mizera et al. (1999) that were also used by Giambalvo (2002b). DATA0.FM4 includes the original Giambalvo (2002b) values for the Na^+/$HEDTA^{3-}$ interaction parameters instead of the parameters used by Domski (2018a), which is a possible source of database inconsistency. Omission of Pitzer parameters for Na^+/$NaEDTA^{3-}$ from the Domski (2018a) parameter fitting calculations is another potential source of inconsistency, because these Pitzer parameters are included in DATA0.FM4. However, the net effects of these Pitzer parameter differences appear to be small because parameter fitting carried out for the Na^+-Ca^{2+}-Cl^--$EDTA^{4-}$ system (Domski 2019a) confirmed the log K_s^0 for $Ca_2EDTA•7H_2O$(s) and Pitzer interaction parameters for Na^+/$CaEDTA^{2-}$ derived by Domski (2018a).

In response to questions from EPA [Peake 2020b, Comment CC2-GEOCHEM-8(a) and Comment CC2-GEOCHEM-11(a)], DOE confirmed that the data used to derive the solubility product for $Ca_2EDTA•H_2O$(s) and the $\beta^{(0)}$ and $\beta^{(1)}$ Pitzer parameters for the $CaEDTA^{2-}$/Na^+ ion pair were from Table 4 of Xiong (2018), and that the EDTA concentrations were assumed equal to half of the measured calcium concentrations (Knerr 2020a). Domski (2019a) tested the ability of the final version of DATA0.FM4 to reproduce the fitted parameter values using the Na^+-Ca^{2+}-Cl^--$EDTA^{4-}$ system data and the same values were calculated for the solubility of $Ca_2EDTA•H_2O$(s) and the $\beta^{(0)}$ and $\beta^{(1)}$ Pitzer parameters for the $CaEDTA^{2-}$/Na^+ ion pair.

The $Ca_2EDTA•7H_2O(s)$ solubility results in NaCl solutions in Xiong (2018) were reported by Kirkes et al. (2014). The $Ca_2EDTA•7H_2O(s)$ solubility experiments were performed by adding the solid to NaCl solutions. Because $Ca_2EDTA•7H_2O(s)$ was the only source of calcium and EDTA in the experiments, the stoichiometry of this solid and maintenance of charge balance requires that the total EDTA concentration in solution samples must be equal to 50% of the calcium concentration (in molal units). The total EDTA concentrations reported by Kirkes et al. (2014) are consistently about 40% higher than the concentrations calculated from the calcium concentration. The cause of this discrepancy was not identified. Because these data are physically unrealistic, they are not acceptable for use in WIPP PA.

EPA requested additional information comparing calculated apparent log K_s values for $Ca_2EDTA•7H_2O(s)$ to the experimentally measured log K_s values as a function of NaCl concentration, using the data from Kirkes et al. (2014) [Peake 2020b, Comment CC2-GEOCHEM-11(b)]. The standard state solubility constant for $Ca_2EDTA•7H_2O(s)$ is defined using the activities of Ca^{2+} and $EDTA^{4-}$:

$$K_s^0 = \{Ca^{2+}\}^2 \times \{EDTA^{4-}\}$$

The total concentrations of calcium $[Ca_T]$ and $[EDTA_T]$ are used to calculate the apparent solubility constant:

$$K_s = [Ca_T]^2 \times [EDTA_T]$$

The apparent log K_s values calculated with DATA0.FM4 can be directly compared to apparent log K_s values calculated from the concentrations measured in the experiments to evaluate the reliability of modeled concentrations.

Knerr (2020c) provided the results of these calculations, including apparent log K_s values calculated using both the measured EDTA concentrations (Kirkes et al. 2014) and using EDTA concentrations equal to half the measured calcium concentrations. The results show that the measured and calculated apparent log K_s values are consistent if it is assumed that EDTA concentrations are 50% of the calcium concentrations, because these are the data used by Domski (2018a) to calculate the solubility of $Ca_2EDTA•7H_2O(s)$ in NaCl solutions. However, using the measured EDTA concentration from Kirkes et al. (2014) resulted in calculated apparent log K_s values that are lower than the measured apparent log K_s values. Because $Ca_2EDTA•7H_2O(s)$ is quite soluble and very unlikely to form in the WIPP repository, the differences between the Domski (2018a) and Xiong (2018) log K_s^0 values are not expected to affect actinide solubilities calculated for WIPP PA (Knerr 2020c).

The discrepancies between EDTA concentrations measured in the Kirkes et al. (2014) experiments and concentrations calculated from the measured calcium concentrations render the $Ca_2EDTA•7H_2O(s)$ log K_s^0 and the Pitzer interaction coefficients for $Na^+/CaEDTA^{2-}$ unacceptable for use in WIPP PA calculations. Additional uncertainty is introduced by simultaneous fitting of the $Ca_2EDTA•7H_2O(s)$ log K_s^0 value and Pitzer interaction parameters for $Na^+/CaEDTA^{2-}$ to the experimental data. A well-established log K_s^0 value is not available for $Ca_2EDTA•7H_2O(s)$ and fitting both the $Ca_2EDTA•7H_2O(s)$ log K_s^0 and the Pitzer interaction

coefficients for $Na^+/CaEDTA^{2-}$ results in significant uncertainty in the Pitzer interaction coefficients for $Na^+/CaEDTA^{2-}$.

4.1.4 Magnesium

Choppin et al. (2001) provided apparent log β values for magnesium complexation by EDTA as a function of ionic strength. Giambalvo (2002b) used these data to calculate the standard chemical potential and Pitzer parameters for the $MgEDTA^{2-}$ aqueous species. These data were included in DATA0.FM1. Giambalvo (2002b, Figure 3d) demonstrated that the experimentally measured and calculated $MgEDTA^{2-}$ apparent log β values were in good agreement. Although Choppin et al. (2001) provided apparent log β values as a function of ionic strength for the $MgHEDTA^-$ species, DOE did not include this species in DATA0.FM1.

The DATA0.FM4 $MgEDTA^{2-}$ and $MgHEDTA^-$ species and log β^0 data are from Hummel et al. (2005) [Table 4-1, reactions (f) and (g)]. The log β^0 values are based on extrapolations of experimental data to zero ionic strength using SIT. The change in the $MgEDTA^{2-}$ log β^0 value increases EDTA complexation by magnesium relative to DATA0.FM1. Addition of the $MgHEDTA^-$ aqueous species to DATA0.FM4 should have relatively small effects, if any, on actinide solubility calculations under WIPP repository conditions because this species is much less important than $MgEDTA^{2-}$ and $NaEDTA^{3-}$ species under repository conditions (Hummel et al. 2005, Figure VIII-18).

EPA requested an evaluation from DOE that compared the apparent $MgEDTA^{2-}$ log β values measured as a function of ionic strength in NaCl solutions by Choppin et al. (2001) and the apparent log β values calculated using DATA0.FM1 and DATA0.FM4 [Peake 2020b, Comment CC2-GEOCHEM-10(g)]. Figure 4 in the response to this request (Knerr 2020b) is reproduced below as Figure 4-2. The results in this figure show that the Choppin et al. (2001) experimentally measured apparent log β values are reproduced quite well by the DATA0.FM1 calculations.

The apparent log β values originally determined by Choppin et al. (2001) do not account for the $NaEDTA^{3-}$ aqueous species that is included in DATA0.FM4. Hummel et al. (2005, Table VIII-17) corrected these measured apparent log β values as a function of ionic strength by accounting for the formation of the $NaEDTA^{3-}$ aqueous species. As shown in Figure 4-2, correcting the measured apparent log β values decreases the differences between the measured values and values predicted using DATA0.FM4. However, the DATA0.FM4 apparent log β values still significantly exceed measured values.

Knerr (2020b) stated that part of the difference between the measured $MgEDTA^{2-}$ log β values and the values calculated using DATA0.FM4 is due to the cumulative effects of Pitzer parameter changes. The Pitzer parameter changes for the interactions of EDTA with WIPP brine constituents are summarized in Table 4-2. These changes included modifications of parameters in DATA0.FM1, addition of new interaction parameters, and deletion of interaction parameters.

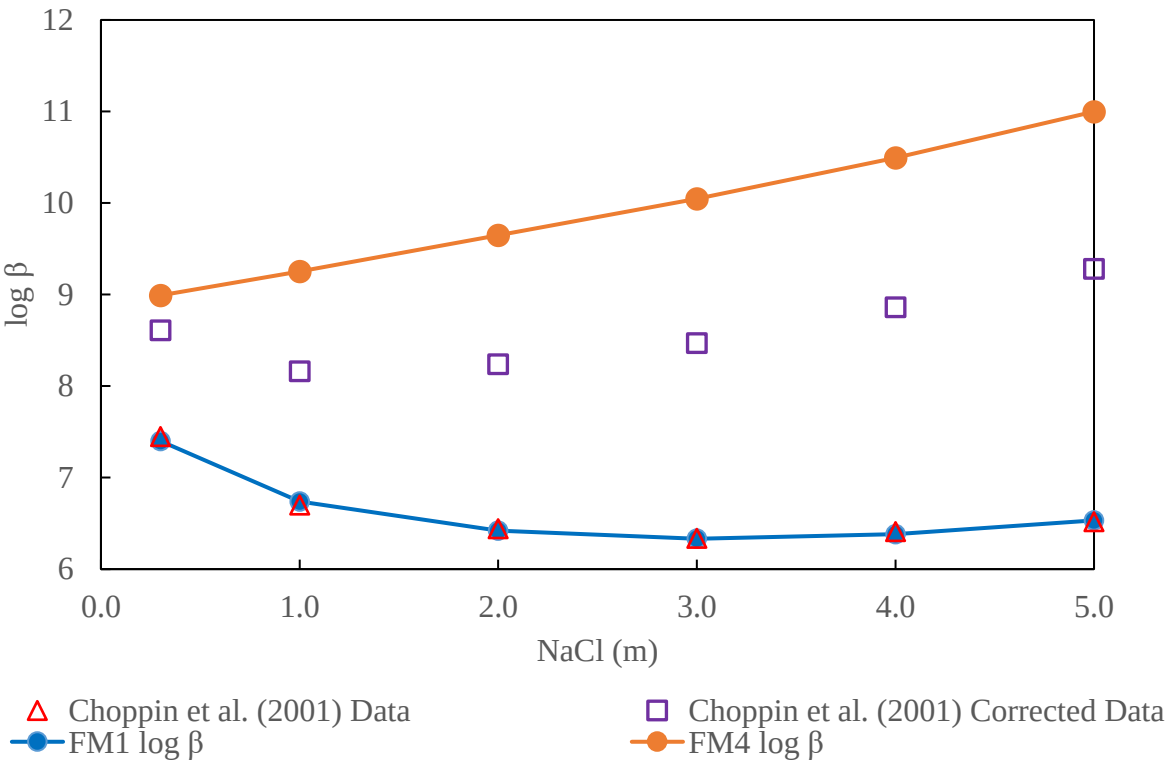

Figure 4-2. Experimentally Measured and Calculated $MgEDTA^{2-}$ Apparent Log β Values, Including Experimental Values Recalculated by Hummel et al. (2005)

Domski (2018b) fit $Ca_2EDTA•7H_2O(s)$ solubility data obtained in $MgCl_2$ solutions (Xiong 2018, Table 3) to derive new Pitzer parameters for interactions between $Mg^{2+}/CaEDTA^{2-}$, $Mg^{2+}/MgEDTA^{2-}$, and $Ca^{2+}/EDTA^{4-}$. Domski (2018b) was unable to achieve convergence with the EQ3/6 code using the 2.5 M $MgCl_2$ solution data, so these experimental results were omitted from the evaluation. For the fitting calculations, Domski (2018a) used DATA0.FM1 with some modifications, including updated EDTA acid dissociation constants, an updated log β^0 for the $CaEDTA^{2-}$, and addition of the $Ca_2EDTA•7H_2O(s)$ log K_s^0 value from Domski (2018a) to be consistent with the values in DATA0.FM4. However, the log β^0 value for the $MgEDTA^{2-}$ aqueous species does not appear to have been updated from the DATA0.FM1 value of 10.13 to the DATA0.FM4 value of 10.90. In addition, log β^0 values for $MgHEDTA^-$ and $CaHEDTA^-$ were apparently not added to be consistent with DATA0.FM4. These log β^0 value differences are potential causes of the discrepancies between measured and predicted apparent log β values for $MgEDTA^{2-}$. Because of the greater importance of the $MgEDTA^{2-}$ species compared to $MgHEDTA^-$ and $CaHEDTA^-$, the inconsistent $MgEDTA^{2-}$ log β^0 values are most likely to have affected the calculation of the $Mg^{2+}/CaEDTA^{2-}$, $Mg^{2+}/MgEDTA^{2-}$, and $Ca^{2+}/EDTA^{4-}$ Pitzer parameters.

After all changes were incorporated to create DATA0.FM4, AP-183 specifies that parameter fitting checks should be performed (Sisk-Scott 2019). Parameter fitting checks were not reported by Domski (2019a) for the Pitzer parameters for interactions between $Mg^{2+}/CaEDTA^{2-}$,

Mg^{2+}/$MgEDTA^{2-}$, and Ca^{2+}/$EDTA^{4-}$ (Domski 2018b). Consequently, whether the discrepancies in the log β^0 value for $MgEDTA^{2-}$ used by Domski (2018b) and omission of data for $MgHEDTA^{-}$ and $CaHEDTA^{-}$ species caused significant errors in the Mg^{2+}/$CaEDTA^{2-}$, Mg^{2+}/$MgEDTA^{2-}$, and Ca^{2+}/$EDTA^{4-}$ Pitzer parameters cannot be determined based on the available information. EPA expects DOE will investigate whether these Pitzer parameters are the cause of the discrepancies between calculated and measured apparent log β values for $MgEDTA^{2-}$.

EPA requested additional calculations comparing calculated apparent log K_s values for $Ca_2EDTA•7H_2O(s)$ to the experimentally measured values as a function of $MgCl_2$ concentration, using the data from Kirkes et al. (2014) [Peake 2020b, Comment CC2-GEOCHEM-11(c)]. Knerr (2020c) provided the results of these calculations, which parallel the calculations described in Section 4.1.3 for NaCl solutions. The results of these calculations (Knerr 2020c, Figure 11-2) showed that the apparent log K_s values calculated with DATA0.FM4 were inconsistent with the apparent log K_s values calculated using either the measured EDTA concentrations or the EDTA concentrations calculated from the measured calcium concentrations. The inability to reproduce the experimental data demonstrates that the Pitzer parameters for Mg^{2+}/$CaEDTA^{2-}$, Mg^{2+}/$MgEDTA^{2-}$, and Ca^{2+}/$EDTA^{4-}$ unacceptable for use in WIPP PA.

The results reported for the $Ca_2EDTA•7H_2O(s)$ solubility experiments in $MgCl_2$ solutions have measured EDTA concentrations that are approximately 40% higher than the concentrations that are calculated assuming the EDTA concentrations are half of the measured calcium concentrations. Because the experimental data are physically unrealistic, they are not acceptable for use in WIPP PA. The use of physically unrealistic data to calculate the Pitzer parameters for Mg^{2+}/$CaEDTA^{2-}$, Mg^{2+}/$MgEDTA^{2-}$, and Ca^{2+}/$EDTA^{4-}$ is an additional reason for rejecting these parameters for use in WIPP PA.

The current parameterization of DATA0.FM4 overpredicts the amount of EDTA that will be complexed by magnesium. This overprediction would cause underprediction of the complexation of actinides by EDTA and decrease predicted actinide releases.

4.1.5 Americium(III)

The DATA0.FM1 log β^0 value for $AmEDTA^{-}$ was based on the experimental data from Choppin et al. (2001). DOE did not change the log β^0 value or Pitzer parameters for the $AmEDTA^{-}$ species for DATA0.FM4. However, DATA0.FM4 includes the $NaEDTA^{3-}$ aqueous species, so DOE should have revised the log β^0 value for the $AmEDTA^{-}$ species for inclusion in DATA0.FM4.

EPA requested that DOE compare the $AmEDTA^{-}$ apparent log β values measured by Choppin et al. (2001) as a function of ionic strength to the values calculated using DATA0.FM1 and DATA0.FM4 [Peake 2020b, Comment CC2-GEOCHEM10(f)]. Figure 3 in the response to this request (Knerr 2020b) is reproduced below as Figure 4-3. The results show that the Choppin et al. (2001) experimentally measured apparent log β values are consistent with the values calculated with DATA0.FM1.

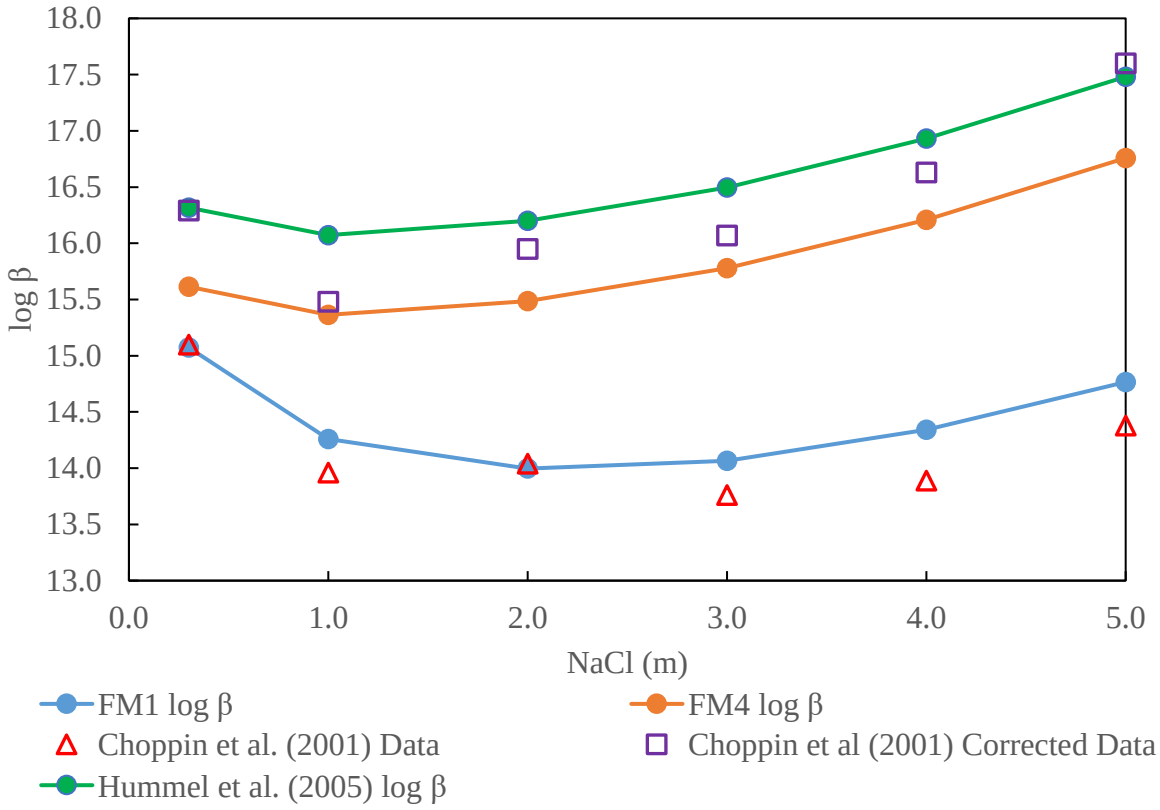

Figure 4-3. Experimentally Measured and Calculated $AmEDTA^-$ Apparent Log β Values, Including Corrected Experimental Values from Hummel et al. (2005)

The apparent log β values originally calculated by Choppin et al. (2001) do not account for the formation of the $NaEDTA^{3-}$ aqueous species. Hummel et al. (2005, Table VIII-41) recalculated the apparent log β values for the $AmEDTA^-$ species from the Choppin et al. (2001) data by including the $NaEDTA^{3-}$, $AmCl^{2+}$, and $AmCl_2^+$ species (Figure 4-3). Hummel et al. (2005) used these data to extrapolate a log β^0 for $AmEDTA^-$ of 19.67 at zero ionic strength, compared to the DATA0.FM4 value of 18.97. As shown in Figure 4-3, correcting the measured apparent log β values to account for $NaEDTA^{3-}$ decreases the differences between the measured values and values predicted using DATA0.FM4. However, the DATA0.FM4 apparent log β values are still significantly less than the measured values, particularly at high ionic strength. These results demonstrate that Am(III) complexation by EDTA is underpredicted using the DATA0.FM4 database.

EPA recalculated the apparent log β values for $AmEDTA^-$ using the DATA0.FM4 database converted for use with the PHREEQC geochemical modeling code (Parkhurst and Appelo 2013), and a revised $AmEDTA^-$ log β^0 value of 19.67 from Hummel et al. (2005). The recalculated apparent log β values are consistent with the corrected Choppin et al. (2001) data (Figure 4-3). These results show that revising the $AmEDTA^-$ log β^0 value to 19.67 in the DATA0.FM4 database will improve the fit of the model to the available experimental data and increase the

predicted complexation of Am(III) by EDTA. EPA expects DOE to revise the $AmEDTA^-$ log β^0 value to 19.67 to accurately model the complexation of Am(III) by EDTA in WIPP dissolved actinide solubility calculations.

4.1.6 Thorium(IV)

The DATA0.FM1 log β^0 value for ThEDTA(aq) was based on the experimental data from Choppin et al. (2001) and DOE did not change the log β^0 value or Pitzer parameters for this species for DATA0.FM4. However, because DATA0.FM4 includes the $NaEDTA^{3-}$ aqueous species, the log β^0 value for the ThEDTA(aq) species must be recalculated. Hummel et al. (2005) did not include thorium in their review, but correction factors that address the presence of the $NaEDTA^{3-}$ aqueous species were provided for the ionic strengths of interest (Table 4-3).

EPA requested that DOE compare the ThEDTA(aq) log β values measured by Choppin et al. (2001) as a function of ionic strength to the values calculated using the DATA0.FM1 and DATA0.FM4 databases [Peake 2020b, Comment CC2-GEOCHEM10(e)]. Figure 2 in the response to this request (Knerr 2020b) is reproduced below in Figure 4-4. The results show that the Choppin et al. (2001) experimentally measured apparent log β values are consistent with the values calculated with DATA0.FM1.

The DATA0.FM4 apparent log β values are less than the apparent log β values recalculated from the Choppin et al. (2001) values to account for the $NaEDTA^{3-}$ species. These results indicate the log β^0 value for ThEDTA(aq) should be redetermined by extrapolating the Choppin et al. (2001) data to zero ionic strength, which is likely to result in a log β^0 value that is increased by approximately an order of magnitude (to approximately 24.6). Calculations with DATA0.FM4 underestimate the complexation of thorium by EDTA. However, because thorium speciation is strongly dominated by $Th(OH)_4(aq)$ and thorium carbonate species under WIPP repository conditions, revising the ThEDTA(aq) log β^0 value will likely have negligible effects on repository releases.

Table 4-3. Correction of Choppin et al. (2001) ThEDTA(aq) Apparent Stability Constants for $NaEDTA^{3-}$

Ionic Strength	Apparent Log β[a]	$K_{Na+}[Na+]$[b]	Corrected Apparent Log β
0.3	16.15	13.6	17.28
0.3	16.32	13.6	17.45
1	15.37	27.6	16.81
1	15.58	27.6	17.02
2	15.55	62.5	17.35
3	15.73	133.8	17.86
4	16.18	279.0	18.63
5	16.94	572.0	19.70

a – Choppin et al. 2001
b – Hummel et al. 2005, Table A-28

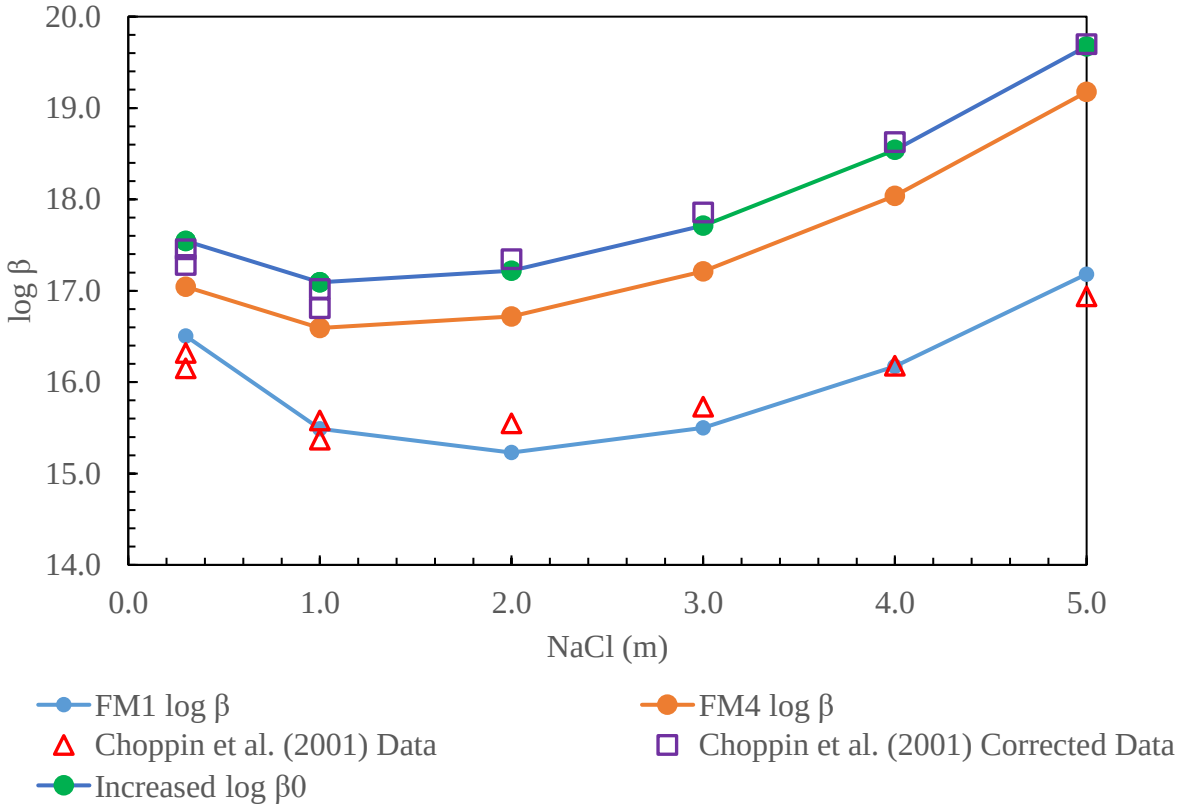

Figure 4-4. Experimentally Measured and Calculated ThEDTA(aq) Apparent Log β Values, Including Experimental Values Recalculated to Account for $NaEDTA^{3-}$ Species

4.1.7 Neptunium(V)

The DATA0.FM1 log β^0 values for NpO_2EDTA^{3-}, NpO_2HEDTA^{2-}, and $NpO_2H_2EDTA^{-}$ were based on the experimental data from Choppin et al. (2001) and no changes were made to the log β^0 values or Pitzer parameters for this species for DATA0.FM4. However, because DATA0.FM4 includes the $NaEDTA^{3-}$ aqueous species, the log β^0 values for the Np(V)-EDTA species should have been recalculated.

Hummel et al. (2005) revised the Choppin et al. (2001) apparent log β values for the Np(V)-EDTA species to account for the $NaEDTA^{3-}$ species and used SIT to extrapolate the corrected data to zero ionic strength (Table 4-1). The Hummel et al. (2005) log β^0 values for NpO_2EDTA^{3-}, NpO_2HEDTA^{2-}, and $NpO_2H_2EDTA^{-}$ indicate that retaining the DATA0.FM1 log β^0 values results in an underprediction of Np(V) complexation by EDTA. DOE should replace the Np(V)-EDTA log β^0 values for with the Hummel et al. (2005) values. However, because Np(V) is not strongly complexed by EDTA and Np(V) contributes little to repository releases, these database issues are not expected to significantly affect repository releases.

4.1.8 DATA0.FM4 Parameter Problem Reports

Pitzer parameter α_1 and α_2 values for cation-anion pairs are assigned based on the charges of the aqueous species. Pitzer and Silvester (1978) determined $\alpha_1 = 2.0$ and that the α_2 parameter could be omitted for cation-anion pairs that include a univalent ion. Pitzer and Silvester (1978) determined $\alpha_1 = 1.4$ and $\alpha_2 = 12.0$ for 2:2 cation-anion pairs, and $\alpha_1 = 2.0$ and $\alpha_2 = 50.0$ for 3:2 and 4:2 ion pairs.

WIPP calculations of Pitzer activity coefficients are based on equations and Na-K-Ca-Mg-H-Cl-SO_4-CO_2-$B(OH)_4$-H_2O data provided by Harvie et al. (1984) and Felmy and Weare (1986) (Babb and Novak 1995). Both Harvie et al. (1984) and Felmy and Weare (1986) assumed a default α_1 value of 1.4 for 2:2 or higher ion pairs. Harvie et al. (1984) and Felmy and Weare (1986) also assumed a default α_2 value of 12.0 for all electrolytes. Babb and Novak (1995) assumed for the WIPP thermodynamic database, that $\alpha_1 = 2.0$ and $\alpha_2 = 12.0$ for ion pairs containing a univalent cation or anion, $\alpha_1 = 1.4$ and $\alpha_2 = 12.0$ for 2:2 cation-anion pairs, and $\alpha_1 = 1.4$ and $\alpha_2 = 50.0$ for 3:2 and 4:2 ion pairs. WIPP thermodynamic databases since the CCA have included these Babb and Novak (1995) α_1 and α_2 values.

Incorrect α_1 Pitzer parameter values were included in the DATA0.FM4 database for the Ca^{2+}/$EDTA^{4-}$, Mg^{2+}/$MgEDTA^{2-}$ and Mg^{2+}/$CaEDTA^{2-}$ ion pairs. An incorrect α_1 value of 2.0 was entered in the database instead of the correct value of 1.4 for these three ion pairs. In a series of Parameter Problem Reports (PPRs), Domski (2019d - 2019m) stated that the incorrect Pitzer parameters affected the parameter values for +III actinide solubilities in GWB and ERDA-6 brines used in PA, but PA modeling with these updated +III actinide solubility parameters resulted in no impact to the CCDFGF plots of total +III actinides released from the repository. EPA requested additional information to assess the magnitude and importance of the actinide solubility errors caused by the incorrect Pitzer parameters [Peake 2020c, Comment CC5-GEOCHEM-27(a)-(d)].

Peake [2020c, Comment CC5-GEOCHEM-27(a)-(b)] requested the +III actinide solubilities in GWB and ERDA-6 brines that were calculated using the corrected α_1 Pitzer parameter values for the Ca^{2+}/$EDTA^{4-}$, Mg^{2+}/$MgEDTA^{2-}$, and Mg^{2+}/$CaEDTA^{2-}$ ion pairs. To assist in the evaluation of the significance of the recalculated actinide solubilities to modeled actinide releases, EPA also requested documentation describing the revised PA calculations performed to establish that the corrected +III actinide solubilities did not significantly affect PA results, and a copy of Domski (2020). Knerr (2021b) provided an Excel spreadsheet with the calculated actinide solubilities and an evaluation of the effects of the α_1 Pitzer parameter errors on calculated actinide solubilities (Domski 2020).

Domski (2020) created a version of DATA0.FM4 with the corrected α_1 Pitzer parameters and used this database to recalculate the baseline actinide solubilities in GWB and ERDA-6 brines using the entire range of organic ligand concentrations (1 to 5 times the minimum brine volume necessary for a brine release). Domski (2020) identified changes to the modeled Am(III) concentrations for both brines at the five brine volumes compared to the CRA-2019 DPA concentrations (Domski and Sisk-Scott 2019). The Am(III) concentration changes were small, and concentration changes for other brine constituents or actinides were not observed. Kim et al.

(2020) evaluated the effects of the corrected Am(III) baseline solubilities on PA results and found that there is no effect of these changes on the actinide releases from the WIPP repository.

Domski (2019d - 2019m) noted that issues related to the $Ca^{2+}/EDTA^{4-}$, $Mg^{2+}/MgEDTA^{2-}$ and $Mg^{2+}/CaEDTA^{2-}$ Pitzer parameters were discovered during an evaluation triggered by PPR 2019-003, so EPA also requested a copy of this document [Peake 2020c, Comment CC5-GEOCHEM-27(c)]. Knerr (2021a) provided the requested PPR 2019-003 (Domski 2019c), and a memo summarizing an analysis of the effects of the parameter error (Domski 2019b). PPR 2019-003 documented that an incorrect $\beta^{(0)}$ Pitzer parameter was included in DATA0.FM4 for the $Ca^{2+}/EDTA^{4-}$ ion pair. An incorrect value of 5.39 was entered into the database, but the correct value is 2.48 (Domski 2018b). Domski (2019b) evaluated the effects of this error by creating a corrected version of DATA0.FM4 and repeating the actinide solubility calculations for GWB brine and ERDA-6 with the highest concentrations of organic ligands (calculated with the minimum brine volume for a release). Comparison of the results of the actinide solubility calculations using the original and corrected versions of DATA0.FM4 showed that the different values of the $\beta^{(0)}$ Pitzer parameter for the $Ca^{2+}/EDTA^{4-}$ ion pair did not affect calculated actinide solubilities (Domski 2019b). Because the actinide solubilities are the only PA parameters produced using DATA0.FM4, the error described by PPR 2019-003 has been demonstrated to have no effect on PA results. In addition to the incorrect α_1 and $\beta^{(0)}$ parameters for the $Ca^{2+}/EDTA^{4-}$ ion pair, EPA notes that α_2 for this 4:2 ion pair should be 50.0 (Babb and Novak 1995) instead of the value of 12.0 included in DATA0.FM4. This α_2 error was not addressed in the parameter problem reports.

Peake [2020c, Comment CC5-GEOCHEM-27(d)] observed that the ion pair $Ca^{2+}/MgEDTA^{2-}$ was identified instead of the correct ion pair $Mg^{2+}/CaEDTA^{2-}$ in the parameter problem reports (Domski 2019d – 2019m). This error has no effect on PA results, because the correct ion pair is included in the DATA0.FM4 database and its supporting documentation (Domski 2018b, Domski 2019a). Knerr (2021b) stated that a memorandum of correction noting this error (Domski 2020) was added to the records for PPRs 2019-004 through 2019-013 (Domski 2019d - 2019m).

DOE has demonstrated that the DATA0.FM4 α_1 Pitzer parameter errors described by PPR 2019-003 through PPR 2019-013 had no significant effects on WIPP PA results. Domski (2020) reported that a QA version of the database has been created with the corrected $\beta^{(0)}$ Pitzer parameter for the $Ca^{2+}/EDTA^{4-}$ ion pair and α_1 Pitzer parameter values for the $Ca^{2+}/EDTA^{4-}$, $Mg^{2+}/MgEDTA^{2-}$, and $Mg^{2+}/CaEDTA^{2-}$ ion pairs. However, EPA does not accept the $Ca^{2+}/EDTA^{4-}$, $Mg^{2+}/MgEDTA^{2-}$, and $Mg^{2+}/CaEDTA^{2-}$ Pitzer parameters for use in WIPP PA for the reasons summarized above in Section 4.1.4. If DOE corrects the $Ca^{2+}/EDTA^{4-}$ Pitzer parameters, they should revise the α_2 parameter for this 4:2 ion pair from 12.0 to 50.0 to maintain consistency with the values adopted by Babb and Novak (1995).

4.1.9 EDTA Summary

The EDTA data in DATA0.FM4 were reviewed to determine whether the data are adequately documented, internally consistent, and accurately reproduce the available experimental data. Conclusions reached during this review include:

- Calculations performed with DATA0.FM4, which contains the Hummel et al. (2005) pK_a^0 values for $H_4EDTA(aq)$, produce predicted apparent log β values as a function of ionic strength that are consistent with the experimental data of Choppin et al. (2001) after the apparent log β values are corrected for the formation of the $NaEDTA^{3-}$ aqueous species.

- The log β^0 value of 2.80 for the $NaEDTA^{3-}$ aqueous species determined by Hummel et al. (2005) using SIT is supported by its consistency with the log β^0 value of 2.70 determined by Felmy and Mason (2003) using the Pitzer model of ion interactions.

- DATA0.FM4 includes Pitzer parameters for $Na^+/NaEDTA^{3-}$ and $Na^+/EDTA^{4-}$ interactions determined by Felmy and Mason (2003) using the titration data of Mizera et al. (1999) in concentrated NaCl solutions and an pK_a^0 for $HEDTA^{3-}$ of 10.57 (Mizera et al. 1999, Choppin et al. 2001). DATA0.FM4 includes these $Na^+/NaEDTA^{3-}$ and $Na^+/EDTA^{4-}$ Pitzer parameters and a different $HEDTA^{3-}$ pK_a^0 of 11.24, creating an internal inconsistency in the DATA0.FM4 database. However, this inconsistency did not affect prediction of pK_a values for $H_4EDTA(aq)$ as a function of ionic strength, so it is unlikely to significantly affect dissolved actinide solubility modeling results.

- The $CaEDTA^{2-}$ log β^0 value of 12.69 in DATA0.FM4 was determined using low-ionic-strength data extrapolated to zero ionic strength using SIT. The $CaEDTA^{2-}$ log β^0 value should be revised to 12.36 (Felmy and Mason 2003) because the latter value was determined using high-ionic-strength data, and the extrapolation to zero ionic strength used Pitzer parameters for sodium and EDTA species that are included in DATA0.FM4.

- Calculations performed using DATA0.FM4 significantly overpredict the stability of $MgEDTA^{2-}$ based on comparisons with measured data. A possible cause of this overprediction is the determination of the $Mg^{2+}/CaEDTA^{2-}$, $Mg^{2+}/MgEDTA^{2-}$, and $Ca^{2+}/EDTA^{4-}$ Pitzer parameters with the log β^0 value for $MgEDTA^{2-}$ of 10.13 from DATA0.FM1 instead of the log β^0 value of 10.90 from DATA0.FM4. In addition, these parameters were fit to solubility data with significant discrepancies between measured and calculated EDTA concentrations. Parameter fitting checks were not reported for the $Mg^{2+}/CaEDTA^{2-}$, $Mg^{2+}/MgEDTA^{2-}$, and $Ca^{2+}/EDTA^{4-}$ Pitzer parameters, so the validity of these parameters cannot be determined based on the available information and EPA does not accept these parameters for use in WIPP PA. EPA expects DOE to resolve the discrepancies between calculated and measured apparent log β values for $MgEDTA^{2-}$. Overprediction of magnesium complexation by EDTA is expected to result in underprediction of actinide complexation by EDTA.

- The $AmEDTA^-$ log β^0 value of 18.97 in DATA0.FM4 underpredicts Am(III) complexation by EDTA because this value does not account for formation of the $NaEDTA^{3-}$ aqueous species. This underprediction will result in the underestimation of the dissolved +III actinide concentrations calculated for WIPP PA. EPA expects DOE to include the $AmEDTA^-$ log β^0 value of 19.67 (Hummel et al. 2005) in the WIPP thermodynamic database because it has been demonstrated to significantly improve the

agreement between calculated and experimentally measured apparent log β values for $AmEDTA^-$.

- The ThEDTA(aq) log β^0 value of 23.557 in DATA0.FM4 underpredicts thorium complexation by EDTA because this value does not account for formation of the $NaEDTA^{3-}$ aqueous species. The corrected log β^0 value should be increased by approximately an order of magnitude. EPA expects DOE to recalculate the ThEDTA(aq) log β^0 value using the experimentally measured apparent log β values corrected for the formation of the $NaEDTA^{3-}$ aqueous species.

- The DATA0.FM4 log β^0 values for NpO_2EDTA^{3-}, NpO_2HEDTA^{2-}, and $NpO_2H_2EDTA^-$ result in the underprediction of the complexation of Np(V) by EDTA because these values do not account for the formation of the $NaEDTA^{3-}$ aqueous species. Hummel et al. (2005) revised the log β^0 values for these Np(V)-EDTA species by accounting for the formation of the $NaEDTA^{3-}$ aqueous species, and EPA expects DOE to include these revised log β^0 values in the WIPP thermodynamic database.

- DOE has demonstrated that the DATA0.FM4 Pitzer parameter errors described by PPR 2019-003 through PPR 2019-013 had no significant effects on WIPP PA results. However, EPA does not accept the affected $Mg^{2+}/CaEDTA^{2-}$, $Mg^{2+}/MgEDTA^{2-}$, and $Ca^{2+}/EDTA^{4-}$ Pitzer interaction parameters for reasons that include using physically unrealistic experimental data to derive the parameters, using an inconsistent log β^0 value for $MgEDTA^{2-}$, and omission of data for $MgHEDTA^-$ and $CaHEDTA^-$ species during the parameter-fitting calculations.

- DOE derived some DATA0.FM4 parameters by simultaneously fitting multiple parameters to a single data set. For example, Xiong (2018) used experimental $Ca_2EDTA•7H_2O(s)$ solubility data obtained in high ionic strength NaCl solutions to simultaneously fit Pitzer parameters, the $Ca_2EDTA•7H_2O(s)$ log K_s^0 value, and the $CaEDTA^{2-}$ log β^0 value. Simultaneously fitting multiple parameters to a single data set results in relatively large uncertainties in these parameters.

4.2 CITRATE

Citrate ($C_6H_5O_7^{3-}$) can form relatively strong complexes with actinides, but has not been predicted to significantly increase dissolved actinide concentrations in repository brines at the concentrations predicted in the WIPP inventory. Giambalvo (2002b) used data obtained in 0.3 - 5 m NaCl (Mizera et al. 1999, Choppin et al. 2001) to determine the aqueous speciation for citrate in DATA0.FM1. Giambalvo (2002b) calculated log β^0 values using the Mizera et al. (1999) and Choppin et al. (2001) Pitzer parameters for acid dissociation of $H_3Citrate(aq)$, and for citrate complexation of Am(III), Th(IV), Np(V), magnesium, and calcium.

In Hummel et al. (2005), the NEA reviewed available citrate data, compiled a set of accepted data over a range of ionic strengths, and extrapolated the accepted data to zero ionic strength using the SIT model of ion interactions. The Hummel et al. (2005) evaluation included the NaCl solution data from Mizera et al. (1999) and Choppin et al. (2001) and additional data from other

investigations conducted in a variety of background electrolytes. Hummel et al. (2005) provided the aqueous speciation, pK_a^0 values for $H_3Citrate(aq)$ acid dissociation, and log β^0 values for citrate complexation of Am(III), Np(V), magnesium, and calcium. Hummel et al. (2005) did not review data for thorium-citrate complex formation. Hummel et al. (2005) reviewed the available data for aqueous citrate complex formation with sodium and potassium, and concluded that the complexes, if formed, are weak. Consequently, Hummel et al. (2005) did not provide recommended log β^0 values for the formation of sodium-citrate and potassium-citrate complexes.

The aqueous speciation data for citrate were updated in DATA0.FM4 by replacing the DATA0.FM1 pK_a^0 values for $H_3Citrate(aq)$ and the log β^0 values for $MgCitrate^-$ and $CaCitrate^-$ with the respective values from Hummel et al. (2005) (Table 4-4). Data were also included in DATA0.FM4 for the additional aqueous species MgHCitrate(aq), $MgH_2Citrate^+$, CaHCitrate(aq), and $CaH_2Citrate^+$. The log β^0 values for AmCitrate(aq), $ThCitrate^+$, and $NpO_2Citrate^{2-}$ in DATA0.FM1 were retained in DATA0.FM4.

Table 4-4. Citrate Aqueous Speciation Data From Giambalvo (2002b) and Hummel et al. (2005)

Reaction	pK_a^0 and Log β^0	
	Giambalvo (2002b) DATA0.FM1	**Hummel et al. (2005) DATA0.FM4 (except where noted)**
(a) $Citrate^{3-} + 3\ H^+ \leftrightarrow H_3Citrate(aq)$	14.5098	14.27
(b) $Citrate^{3-} + 2\ H^+ \leftrightarrow H_2Citrate^-$	11.2630	11.14
(c) $Citrate^{3-} + H^+ \leftrightarrow HCitrate^{2-}$	6.4232	6.36
(d) $Mg^{2+} + Citrate^{3-} \leftrightarrow MgCitrate^-$	5.2997	4.81
(e) $Mg^{2+} + H^+ + Citrate^{3-} \leftrightarrow MgHCitrate(aq)$	--[a]	8.96
(f) $Mg^{2+} + 2\ H^+ + Citrate^{3-} \leftrightarrow MgH_2Citrate^+$	--[a]	12.45
(g) $Ca^{2+} + Citrate^{3-} \leftrightarrow CaCitrate^-$	5.2997[b]	4.80
(h) $Ca^{2+} + H^+ + Citrate^{3-} \leftrightarrow CaHCitrate(aq)$	--[a]	9.28
(i) $Ca^{2+} + 2\ H^+ + Citrate^{3-} \leftrightarrow CaH_2Citrate^+$	--[a]	12.67
(j) $Am^{3+} + Citrate^{3-} \leftrightarrow AmCitrate(aq)$	8.7984	8.55[c]
(k) $Am^{3+} + 2\ Citrate^{3-} \leftrightarrow Am(Citrate)_2^{3-}$	--[a]	13.90[d]
(l) $Am^{3+} + H^+ + Cit^{3-} \leftrightarrow AmHCitrate^+$	--[a]	12.36[d]
(m) $Am^{3+} + 2\ H^+ + 2\ Cit^{2-} \leftrightarrow Am(HCitrate)_2^-$	--[a]	23.52[d]
(n) $Th^{4+} + Citrate^{3-} \leftrightarrow ThCitrate^+$	15.2355	--[c,e]
(o) $NpO_2^+ + Citrate^{3-} \leftrightarrow NpO_2Citrate^{2-}$	3.4969	3.68[c]

a – species not included in DATA0.FM1

b – $CaCitrate^-$ log β^0 assumed equal to $MgCitrate^-$ value

c – Giambalvo (2002b) log β^0 values for AmCitrate(aq), $ThCitrate^+$, and $NpO_2Citrate^{2-}$ were retained in DATA0.FM4

d – species not included in DATA0.FM4

e – thorium complexation with citrate not included in Hummel et al. (2005) review

4.2.1 H_3Citrate(aq) Acid Dissociation Constants

The pK_a^0 values for H_3Citrate(aq) provided by Hummel et al. (2005) are compared to the DATA0.FM1 values in Table 4-4 [reactions (a) – (c)]. EPA requested that DOE provide a comparison of the apparent pK_a values measured as a function of ionic strength by Choppin et al. (2001) and the apparent pK_a values calculated using DATA0.FM1 and DATA0.FM4 [Peake 2020b, Comment CC2-GEOCHEM-12(a)-(c)]. These comparisons demonstrate whether the DATA0.FM4 database used for the CRA-2019 PA actinide solubility calculations provides speciation results consistent with the available high-ionic-strength data for aqueous citrate species from Choppin et al. (2001).

Figure 12-1 of Knerr (2020b) illustrates the results of these calculations. These calculations show that for reactions (a) – (c), speciation calculations performed using either DATA0.FM1 or DATA0.FM4 are in good agreement with the experimentally measured data. This result is reasonable, because of the small differences in the pK_a^0 values between DATA0.FM1 and DATA0.FM4 (Table 4-4).

4.2.2 Magnesium and Calcium

Choppin et al. (2001) provided apparent log β values for the $MgCitrate^-$ and MgHCitrate(aq) aqueous species, but Giambalvo (2002b) did not calculate a log β^0 value for MgHCitrate(aq), and only the $MgCitrate^-$ aqueous species was included in DATA0.FM1. Giambalvo (2002b) used the data to calculate the standard chemical potential for the $MgCitrate^-$ aqueous species and binary Pitzer parameters for $Na^+/MgCitrate^-$ interactions. Giambalvo (2002b, Figure 3c) demonstrated that the experimentally measured and calculated $MgCitrate^-$ apparent log β values were in reasonable agreement. Giambalvo (2002b) did not provide justification for omitting the MgHCitrate(aq) species from DATA0.FM1.

Hummel et al. (2005) reviewed the data regarding magnesium-citrate aqueous speciation and found that the formation of $MgCitrate^-$ and MgHCitrate(aq) was commonly accepted, and that the weak complex $MgH_2Citrate^+$ may also form. Modifications to the magnesium-citrate data in DATA0.FM4 include revision of the log β^0_{101} value for $MgCitrate^-$ and addition of log β^0_{111} and log β^0_{121} values for MgHCitrate(aq) and $MgH_2Citrate^+$, respectively. No changes or additions were made to the Pitzer interaction parameters for magnesium-citrate aqueous species. EPA requested that DOE provide a comparison of the apparent log β_{101} values for $MgCitrate^-$ measured as a function of ionic strength by Choppin et al. (2001) and log β_{101} values calculated using DATA0.FM1 and DATA0.FM4 [Peake 2020b, Comment CC2-GEOCHEM-12(f)].

Figure 12-4 from Knerr (2020b), illustrating the results of the requested magnesium-citrate calculations, is reproduced in Figure 4-5. These results confirm that the DATA0.FM1 calculations accurately reproduce the measured apparent log β_{101} value for $MgCitrate^-$ as previously shown by Giambalvo (2002b, Figure 3c), and as expected because the log β^0_{101} and binary Pitzer parameters for $Na^+/MgCitrate^-$ interactions were obtained by fitting these data. The calculations performed using DATA0.FM4 yield apparent log β_{101} values that are slightly less than the DATA0.FM1 values because of the smaller log β^0_{101} value used in DATA0.FM4.

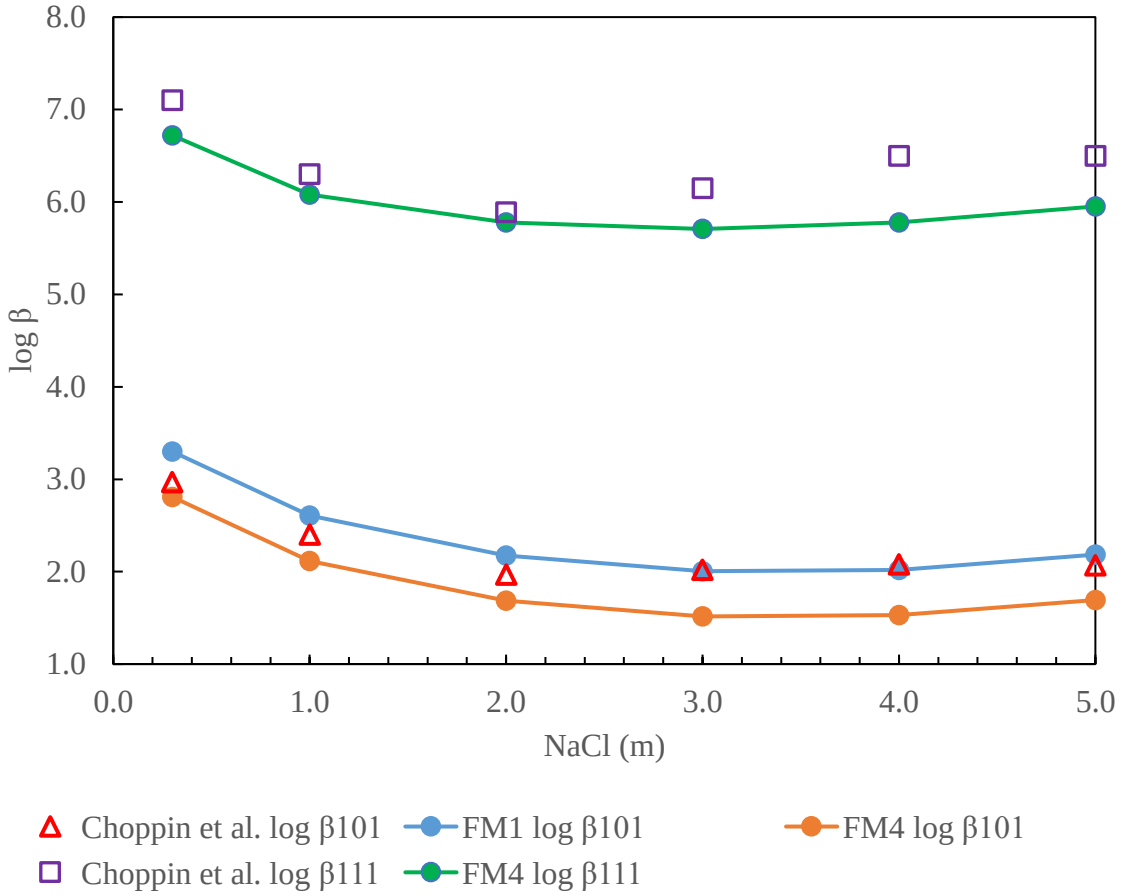

Figure 4-5. Experimentally Measured and Calculated $MgCitrate^-$ Apparent Log β_{101} Values, and Experimentally Measured and Calculated MgHCitrate(aq) Log β_{111} Values

Knerr (2020b) also provided the data necessary to calculate the apparent log β_{111} values for MgHCitrate(aq), which are compared to the measured values in Figure 4-5. These results show that the DATA0.FM4 calculations underpredict the formation of both $MgCitrate^-$ and MgHCitrate(aq). However, underprediction of $MgCitrate^-$ and MgHCitrate(aq) species formation using DATA0.FM4 would increase the availability of citrate to complex actinide species. Consequently, the differences between the calculated and measured apparent log β values are not expected to result in underestimated repository releases. DOE should consider revising the $MgCitrate^-$ log β^0 value back to the Giambalvo (2002b) value of 5.30, which would improve the agreement between the modeled and experimental data at high ionic strength. Revisions to the MgHCitrate(aq) and $MgH_2Citrate^+$ log β^0 values may also be considered, but these aqueous species are expected to be present in insignificant concentrations at the moderately alkaline conditions of WIPP repository brines.

Choppin et al. (2001) did not perform experiments investigating the complexation of calcium by citrate, so Giambalvo (2002b) assumed that the log β^0_{101} for $CaCitrate^-$ and the Pitzer binary

interaction parameters for Na^+/$CaCitrate^-$ interactions were equal to the values calculated for magnesium. Hummel et al. (2005) evaluated data from solutions with ionic strengths up to 0.5 m and determined log β^0 values for $CaCitrate^-$, CaHCitrate(aq), and $CaH_2Citrate^+$ using SIT to extrapolate measured apparent log β values to zero ionic strength. The Hummel et al. (2005) log β^0 values for $CaCitrate^-$, CaHCitrate(aq), and $CaH_2Citrate^+$ are included in DATA0.FM4 and the Pitzer parameters for Na^+/$CaCitrate^-$ interactions continue to be equal to the magnesium values calculated by Giambalvo (2002b). The log β^0_{101} value for $CaCitrate^-$ in DATA0.FM4 is essentially the same as the log β^0_{101} value for $MgCitrate^-$. Because of the relatively low calcium concentrations in repository brines compared to magnesium concentrations, formation of $CaCitrate^-$ is unlikely to significantly affect predicted actinide solubilities.

4.2.3 Americium(III)

Choppin et al. (2001) and Wall et al. (2002) provided apparent log β values for AmCitrate(aq). Choppin et al. (2001) also provided neutral ion Pitzer parameters for AmCitrate(aq)/Cl^- interactions. Giambalvo (2002b) used these data to derive a log β^0 value for AmCitrate(aq). These AmCitrate(aq) data were included in DATA0.FM1 and were not revised in DATA0.FM4.

Hummel et al. (2005) reviewed the available data regarding the complexation of Am(III) by citrate and identified disagreements between various studies regarding aqueous speciation. Hummel et al. (2005) identified $AmHCitrate^{2+}$, $Am(HCitrate)_2^-$, AmCitrate(aq), and $Am(Citrate)_2^{3-}$ as the most plausible species. The $AmHCitrate^{2+}$ and $Am(HCitrate)_2^-$ aqueous species are only likely to form in significant quantities in low pH solutions (Hummel et al. 2005, Figure VII-33), so AmCitrate(aq) and $Am(Citrate)_2^{3-}$ are expected to be the most significant aqueous species under the moderately alkaline conditions in WIPP repository brines. The formation of $Am(Citrate)_2^{3-}$ has been identified in subsequent investigations, including Mathur et al. (2007), Thakur et al. (2012), and Brown et al. (2014).

EPA requested that DOE provide a comparison of the AmCitrate(aq) apparent log β values measured as a function of ionic strength by Choppin et al. (2001) and Wall et al. (2002) with the apparent log β values calculated using DATA0.FM1 and DATA0.FM4 [Peake 2020b, Comment CC2-GEOCHEM-12(e)]. Knerr (2020b) provided this comparison and showed that the apparent log β values calculated using DATA0.FM1 and DATA0.FM4 were virtually identical, and overestimated AmCitrate(aq) formation at ionic strengths greater than about 3 m.

A number of investigations have shown that under the mildly alkaline conditions in WIPP repository brines, both AmCitrate(aq) and $Am(Citrate)_2^{3-}$ species may form. Consequently, EPA recommends including the log β^0 for $Am(Citrate)_2^{3-}$ from Hummel et al. (2005) (Table 4-4) in future WIPP database versions.

4.2.4 Thorium(IV)

Choppin et al. (2001) provided apparent log β values as a function of ionic strength for the $ThCitrate^+$ and $Th(Citrate)_2^{2-}$ aqueous species. Choppin et al. (2001) also provided binary Pitzer parameters for $ThCitrate^+$/Cl^- interactions. Giambalvo (2002b) used the Choppin et al. (2001) apparent log β values and Pitzer parameters to calculate a log β^0 value for $ThCitrate^+$, but did not address the formation of the $Th(Citrate)_2^{2-}$ aqueous species. The log β^0 for $ThCitrate^+$ and Pitzer

parameters for $ThCitrate^{+}/Cl^{-}$ interactions in DATA0.FM1 and DATA0.FM4 are the values recommended by Giambalvo (2002b).

Different aqueous Th(IV)-citrate species have been identified by subsequent investigations. Felmy et al. (2006) identified aqueous species with citrate to Th(IV) ratios from 2 to 3 under neutral to alkaline conditions over a range of ionic strengths. Felmy et al. (2006) proposed several potential Th-OH-citrate aqueous species that are consistent with their experimental data [e.g., $Th(OH)_3(Citrate)_3^{8-}$]. Bonin et al. (2008) used the $ThCitrate^{+}$ and $Th(Citrate)_2^{2-}$ aqueous species to evaluate spectrophotometric data.

EPA requested that DOE provide a comparison of the $ThCitrate^{+}$ apparent log β values measured as a function of ionic strength by Choppin et al. (2001) with the apparent log β values calculated using DATA0.FM1 and DATA0.FM4 [Peake 2020b, Comment CC2-GEOCHEM-12(d)]. Knerr (2020b) provided this comparison and showed that the apparent log β values calculated using DATA0.FM1 and DATA0.FM4 were virtually identical, and the calculated apparent log β values significantly underestimated $ThCitrate^{+}$ formation at ionic strengths of 3 m or greater.

Underprediction of Th(IV)-citrate complexation in repository brines is likely to have relatively small effects on calculated dissolved Th(IV) concentrations in WIPP repository brines because the dominant aqueous Th(IV) species are likely to be $Th(OH)_4(aq)$ and Th(IV)-carbonate species. To address the uncertainty associated with the ability of citrate to mobilize Th(IV), DOE should re-evaluate the experimentally measured apparent log β values for $ThCitrate^{+}$ (Choppin et al. 2001). DOE should also add the $Th(Citrate)_2^{2-}$ aqueous species to the database based on the apparent log β values from Choppin et al. (2001).

4.2.5 Neptunium(V)

The only reported Np(V)-citrate aqueous species is $NpO_2Citrate^{2-}$ (Hummel et al. 2005). Giambalvo (2002b) used the apparent log β values reported by Choppin et al. (2001) to calculate the log β^0 value for $NpO_2Citrate^{2-}$ and binary Pitzer parameters for $Na^{+}/ NpO_2Citrate^{2-}$ interactions. Hummel et al. (2005) used apparent log β values obtained from 0.1 to 5 m NaCl experiments (Bronikowski et al. 1999, Choppin et al. 2001) and apparent log β values obtained in 0.1 to 5 m $NaClO_4$ experiments (Rizkalla et al 1990, Pokrovsky and Choppin 1997) and the SIT model of ion interactions to calculate a log β^0 value for $NpO_2Citrate^{2-}$. The log β^0 values calculated by Giambalvo (2002b) and Hummel et al. (2005) are similar, with a slightly higher value calculated by Hummel et al. (2005) (Table 4-4). The log β^0 value for $NpO_2Citrate^{2-}$ calculated by Giambalvo (2002b) was included in both DATA0.FM1 and DATA0.FM4 and remains acceptable.

4.2.6 Earlandite

Both the DATA0.FM4 analysis plan (Sisk-Scott 2019) and analysis report (Domski 2019a) described the addition of earlandite [$Ca_3(Citrate) \bullet 4H_2O(s)$] solubility data to DATA0.FM4. However, earlandite is missing from DATA0.FM4 (Peake 2020b, Comment CC2-GEOCHEM-13). DOE acknowledged that earlandite was omitted from the database and performed calculations to determine if this omission affected the CRA-2019 DPA actinide solubility modeling results (Knerr 2020d). The results showed that earlandite was undersaturated in the

modeled brines and would not precipitate under the modeled conditions. DOE therefore demonstrated that the omission of earlandite from DATA0.FM4 had no effect on the CRA-2019 DPA actinide solubility modeling results.

4.2.7 Citrate Summary

EPA reviewed the citrate data in DATA0.FM4 to determine whether the data are adequately documented, internally consistent, and accurately reproduce the available experimental data. EPA's conclusions include:

- The pK_a values for $H_3Citrate(aq)$ were slightly modified from DATA0.FM1 to the values selected in a Nuclear Energy Agency Thermochemical Database (NEA-TDB) review by Hummel et al. (2005). Speciation calculations performed using the DATA0.FM4 database demonstrated that the revised acid dissociation constants adequately reproduced the apparent pK_a values measured as a function of ionic strength by Choppin et al. (2001).

- The magnesium-citrate aqueous species and associated log β^0 values in DATA0.FM1 were revised in DATA0.FM4 to be consistent with the aqueous speciation and log β^0 values from Hummel et al. (2005). Comparison of the Choppin et al. (2001) measured apparent log β values as a function of ionic strength to the values calculated using DATA0.FM4 showed that the calculated values underpredicted the formation of both $MgCitrate^-$ and MgHCitrate(aq). These results indicate that actinide solubility calculations with DATA0.FM4 could slightly overpredict actinide mobilization by citrate, but these effects would be small and would not be expected to significantly affect repository release predictions.

- Comparison of apparent log β values measured by Choppin et al. (2001) for AmCitrate(aq) and values calculated using DATA0.FM4 indicated that the calculated values overestimated AmCitrate(aq) formation at ionic strengths greater than about 3 molal. Because predicted dissolved Am(III) concentrations are more significantly affected by EDTA complexation than by citrate, this overprediction would not significantly affect repository release predictions.

- Formation of the $Am(Citrate)_2^{3-}$ species has been identified by Hummel et al. (2005) and several subsequent investigations, but this species is not included in DATA0.FM4.

- Choppin et al. (2001) provided apparent log β values as a function of ionic strength for the $ThCitrate^+$ and $Th(Citrate)_2^{2-}$ aqueous species. However, only the $ThCitrate^+$ aqueous species was included in DATA0.FM1 and DATA0.FM4.

- Comparison of the measured apparent log β values for $ThCitrate^+$ (Choppin et al. 2001) and apparent log β values calculated using DATA0.FM4 showed that $ThCitrate^+$ formation was underpredicted at ionic strengths of 3 molal or greater. Because Th(IV) speciation is expected to be dominated by $Th(OH)_4(aq)$ and Th(IV)-carbonate species, the

underprediction of $ThCitrate^{+}$ formation is likely to have insignificant effects on predicted repository releases.

- Solubility data for the solid phase earlandite was reportedly added to DATA0.FM4, but this phase was omitted from the database. DOE has demonstrated that this omission had no effects on dissolved actinide solubility calculations for the CRA-2019 PA, because this phase remained undersaturated in the modeled repository brines.

- No changes were made to the $NpO_2Citrate^{2-}$ log β^0 or Pitzer interaction parameters between DATA0.FM1 and DATA0.FM4.

4.3 OXALATE

Oxalate ($C_2O_4^{2-}$) can form relatively strong complexes with actinides but does not significantly increase predicted actinide solubilities in repository brines at the oxalate concentrations in the WIPP inventory. Giambalvo (2002b) used data obtained in 0.3 – 5 m NaCl (Mizera et al. 1999, Choppin et al. 2001, Borkowski et al. 2001) to determine oxalate aqueous speciation (Table 4-5) and Pitzer parameters in DATA0.FM1. Giambalvo (2002b) calculated pK_a values for $H_2Oxalate(aq)$, and log β^0 values for oxalate complexation of Am(III), Th(IV), Np(V), and magnesium. Calcium-oxalate aqueous speciation and Pitzer parameter data were unavailable, so calcium-oxalate log β^0 values and Pitzer parameters were assumed equal to magnesium values. Giambalvo (2002e) also calculated log K_s^0 values for three oxalate solids [Table 4-5, reactions (m)-(o)]. DATA0.FM1 oxalate data also included a correction to the molecular weight of oxalate and the addition of whewellite [$CaOxalate•H_2O(s)$] solubility (Xiong 2004b).

Hummel et al. (2005) reviewed the available oxalate data, including the data summarized by Choppin et al. (2001). Their selected log β^0 values for many aqueous species are very similar to the values in DATA0.FM1 (Table 4-5). Hummel et al. (2005) did not find evidence supporting the formation of oxalate aqueous species with sodium, which is consistent with the aqueous speciation used in DATA0.FM1 and DATA0.FM4.

Changes made to the oxalate aqueous speciation and solubility data between DATA0.FM1 and DATA0.FM4 included addition of the $Mg(Oxalate)_2^{4-}$ aqueous species and the solubility of glushinskite [$MgOxalate•2H_2O(s)$] (Sisk-Scott 2019, Domski 2019a). Pitzer parameters for oxalate were also added during the development of DATA0.FM4.

4.3.1 H_2Oxalate(aq) Acid Dissociation Constants

The pK_a^0 values calculated by Giambalvo (2002b) were based on extrapolation of data obtained in high-ionic-strength NaCl (Choppin et al. 2001) to zero ionic strength using the Pitzer model of ion interactions. Hummel et al. (2005) used the SIT model to extrapolate data obtained over a wide range of ionic strengths in various ionic media. The results of the two evaluations of the pK_a^0 values for $H_2Oxalate(aq)$ are essentially the same (Table 4-5), showing that these values are well established.

4.3.2 Magnesium and Calcium

Choppin et al. (2001) reported apparent log β values for MgOxalate(aq) and $Mg(Oxalate)_2^{2-}$. Giambalvo (2002b) used these data to calculate a log β^0 value for MgOxalate(aq) and a Pitzer neutral ion interaction parameter ($\lambda = 0.189$) for MgOxalate(aq)/Cl^- interactions. Calculated and measured apparent log β values were compared and found to be in good agreement (Giambalvo 2002b, Figure 3b). No explanation was provided for omission of the $Mg(Oxalate)_2^{2-}$ aqueous species. The MgOxalate(aq) log β^0 value and Pitzer parameter were extended to the calcium-oxalate aqueous species.

Table 4-5. Oxalate Aqueous Speciation and Solids Solubility Data from Giambalvo (2002b, 2002e) and Hummel et al. (2005)

Reaction	Log β^0		
	Giambalvo (2002b, 2002e) DATA0.FM1	**Hummel et al. (2005)**	**DATA0.FM4 (from DATA0.FM1 unless otherwise noted)**
(a) $Oxalate^{2-} + 2\ H^+ \leftrightarrow H_2Oxalate(aq)$	5.6532	5.65	5.6532
(b) $Oxalate^{2-} + H^+ \leftrightarrow HOxalate^-$	4.2596	4.25	4.2596
(c) $Mg^{2+} + Oxalate^{2-} \leftrightarrow MgOxalate(aq)$	3.7931	3.56	3.7931
(d) $Mg^{2+} + 2\ Oxalate^{2-} \leftrightarrow Mg(Oxalate)_2^{2-}$	--[a]	5.17	5.24[b]
(e) $Ca^{2+} + Oxalate^{2-} \leftrightarrow CaOxalate(aq)$	3.7931[c]	3.19	3.7931[c]
(f) $Ca^{2+} + 2\ Oxalate^{2-} \leftrightarrow Ca(Oxalate)_2^{2-}$	--[a]	4.02	--[d]
(g) $Am^{3+} + Oxalate^{2-} \leftrightarrow AmOxalate^+$	6.1556	6.51	6.1556
(h) $Am^{3+} + 2\ Oxalate^{2-} \leftrightarrow Am(Oxalate)_2^-$	--[a]	10.71	--[d]
(i) $Am^{3+} + 3\ Oxalate^{2-} \leftrightarrow Am(Oxalate)_3^{3-}$	--[a]	13.00	--[d]
(j) $Th^{4+} + Oxalate^{2-} \leftrightarrow ThOxalate^{2+}$	11.3863	--[e]	11.3863
(k) $NpO_2^+ + Oxalate^{2-} \leftrightarrow NpO_2Oxalate^-$	4.24	3.90	4.24
(l) $NpO_2^+ + 2\ Oxalate^{2-} \leftrightarrow NpO_2(Oxalate)_2^{3-}$	--[a]	5.80	--[d]
(m) $H_2Oxalate{\bullet}2H_2O(s) \leftrightarrow 2\ H^+ + Oxalate^{2-} + 2H_2O$	-5.6615	--	-5.6615
(n) $NaHOxalate{\bullet}H_2O(s) \leftrightarrow 2\ Na^+ + Oxalate^{2-} + 2H_2O$	-6.0608	--	-6.0608
(o) $Na_2Oxalate(s) \leftrightarrow 2\ Na^+ + Oxalate^{2-}$	-2.4051	--	-2.4051
(p) $CaOxalate{\bullet}H_2O(s)$ (whewellite) $\leftrightarrow Ca^{2+} + Oxalate^{2-} + H_2O$	-8.7517	-8.73	-8.7517
(q) $MgOxalate{\bullet}2H_2O(s)$ (glushinskite) $\leftrightarrow Mg^{2+} + Oxalate^{2-} + 2\ H_2O$	--[a]	-6.4 ± 0.2[f]	-6.41

a – not included in DATA0.FM1
b – Jang (2019) from Choppin et al. (2001) data
c – CaOxalate(aq) log β^0 value assumed equal to MgOxalate(aq) value
d – species not included in DATA0.FM4
e – Th(IV) complexation with oxalate not reviewed by Hummel et al. (2005)
f – Hummel et al. (2005) did not recommend a solubility value for glushinskite because of scatter in the evaluated solubility data, but suggested a range that encompasses the reported solubilities

Hummel et al. (2005) evaluated magnesium-oxalate and calcium-oxalate aqueous speciation and selected the MgOxalate(aq), $Mg(Oxalate)_2^{2-}$, CaOxalate(aq), and $Ca(Oxalate)_2^{2-}$ aqueous species. Jang and Kim (2016) used the apparent $Mg(Oxalate)_2^{2-}$ log β values from Choppin et al. (2001) to calculate a log β^0 of 5.24, which DOE added to DATA0.FM4. This value is consistent with the recommended value from Hummel et al. (2005). The $Ca(Oxalate)_2^{2-}$ aqueous species and Hummel et al. (2005) log β^0 value of 4.02 should be added to future versions of the database to account for the potential formation of this aqueous species.

Domski (2019a) tested the ability of DATA0.FM4 to reproduce the fitted parameter values using the Na^+-Mg^{2+}-Cl^--$oxalate^{2-}$ system data and the same fitted parameters were calculated for glushinskite [MgOxalate•$2H_2O$(s)] solubility, the $\beta^{(0)}$ Pitzer parameter for the $Mg(Oxalate)_2^{2-}$/Na^+ ion pair, the λ Pitzer parameter for the MgOxalate(aq)/Mg^{2+} ion pair and the λ Pitzer parameter for the MgOxalate(aq)/Na^+ ion pair. EPA requested clarification of the data used for the parameter fitting calculations [Peake 2020b, Comment CC2-GEOCHEM-8(b)]. Knerr (2020d) explained that the original data source was Jang and Kim (2016), but the data were slightly modified by inclusion and averaging of additional measurements. Knerr (2020d) stated that these data are included in the records package for AP-182.

Jang and Kim (2016) measured glushinskite solubility in $MgCl_2$ and NaCl solutions. Jang (2019) evaluated these data using a literature value for glushinskite solubility (Table 4-5) to derive additional Pitzer parameters for the magnesium-oxalate system (Sisk-Scott 2019, Domski 2019a). Because these parameters were derived using a different version of the WIPP database, EPA requested that DOE provide figures comparing the experimentally measured glushinskite solubilities to solubilities modeled using DATA0.FM4 (Peake 2020d, Comment CC6-GEOCHEM-31). Knerr (2021c) provided figures demonstrating that calculations with DATA0.FM4 provided reasonable predictions of glushinskite solubility in NaCl and $MgCl_2$ solutions.

4.3.3 Americium(III)

Borkowski et al. (2001) and Choppin et al. (2001) reported apparent log β values for $AmOxalate^+$ and $Am(Oxalate)_2^-$ and Pitzer binary interaction parameters for $AmOxalate^+$/Cl^- interactions. Giambalvo (2002b) used these data to calculate a log β^0 value for $AmOxalate^+$. This log β^0 value and the Choppin et al. (2001) Pitzer parameters were included in DATA0.FM1. No explanation was provided for omission of the $Am(Oxalate)_2^-$ aqueous species.

Hummel et al. (2005) identified the aqueous species $AmOxalate^+$, $Am(Oxalate)_2^-$, and $Am(Oxalate)_3^{3-}$, and selected log β^0 values for these three species. Only one investigation provided reliable data for the $Am(Oxalate)_3^{3-}$ aqueous species. The log β^0 for $AmOxalate^+$ derived by Hummel et al. (2005) using the SIT model of ion interactions is reasonably consistent with the value determined by Giambalvo (2002b) (Table 4-5).

Thakur et al. (2015) re-evaluated the Am(III)-oxalate speciation data in NaCl solutions (Choppin et al. 2001) simultaneously with Am(III)-oxalate speciation data in $NaClO_4$ solutions. Thakur et al. (2015) identified both the $AmOxalate^+$ and $Am(Oxalate)_2^-$ aqueous species, and derived log β^0 values for these species of 6.30 and 10.84, respectively. The log β^0 for $AmOxalate^+$ is consistent

with the values reported by Giambalvo (2002b) and Hummel et al. (2005). The log β^0 for $Am(Oxalate)_2^-$ is consistent with the value selected by Hummel et al. (2005).

The log β^0 for $AmOxalate^+$ and binary Pitzer interaction parameters in DATA0.FM4 were not modified from the values in DATA0.FM1. Addition of the $Am(Oxalate)_2^-$ species to the WIPP database is recommended so the Am(III)-oxalate speciation in the database is consistent with the speciation identified by Choppin et al. (2001), Borkowski et al. (2001), and Thakur et al. (2015).

4.3.4 Thorium(IV)

Choppin et al. (2001) reported apparent log β values for Th(IV) complexation by oxalate, providing data for the aqueous species $ThOxalate^{2+}$ and $Th(Oxalate)_2(aq)$. Choppin et al. (2001) also provided Pitzer binary interaction parameters for $ThOxalate^{2+}/Cl^-$ interactions. Giambalvo (2002b) used the Choppin et al. (2001) data to calculate a log β^0 value for $ThOxalate^{2+}$. The log β^0 value for $ThOxalate^{2+}$ and the Choppin et al. (2001) Pitzer parameters were included in DATA0.FM1. No explanation was provided for omission of the $Th(Oxalate)_2(aq)$ aqueous species from DATA0.FM1.

No revisions were made to the Th(IV)-oxalate data between the DATA0.FM1 and DATA0.FM4 database versions. Inclusion of $Th(Oxalate)_2(aq)$ in the WIPP database is recommended to maintain consistency between Th(IV)-oxalate speciation in the database and the speciation identified by Choppin et al. (2001).

4.3.5 Neptunium(V)

Choppin et al. (2001) and Borkowski et al. (2001) reported apparent log β values for Np(V) complexation by oxalate, providing data for the aqueous species $NpO_2Oxalate^-$ and $NpO_2(Oxalate)_2^{3-}$. Choppin et al. (2001) also provided Pitzer binary interaction parameters for $NpO_2Oxalate^{2+}/Na^+$ interactions. Giambalvo (2002b) used the Choppin et al. (2001) data to calculate a log β^0 value for $NpO_2Oxalate^-$. The log β^0 value for $NpO_2Oxalate^-$ and the Choppin et al. (2001) Pitzer parameters were included in DATA0.FM1. No explanation was provided for omission of the $NpO_2(Oxalate)_2^{3-}$ aqueous species from DATA0.FM1.

Hummel et al. (2005) identified the aqueous species $NpO_2Oxalate^-$ and $NpO_2(Oxalate)_2^{3-}$ and included apparent log β values from Choppin et al. (2001) in their evaluation. Extrapolation of the available data to zero ionic strength using the SIT model of ion interactions resulted in a log β^0 value for $NpO_2Oxalate^-$ that is reasonably consistent with the value calculated by Giambalvo (2002b) using the Pitzer model (Table 4-5).

The Np(V)-oxalate data were not revised between the DATA0.FM1 and DATA0.FM4 database versions. Inclusion of $NpO_2(Oxalate)_2^{3-}$ in the WIPP database is recommended to maintain consistency between Np(V)-oxalate speciation in the database and the speciation identified by Choppin et al. (2001).

4.3.6 Oxalate Summary

Oxalate data in DATA0.FM4 were reviewed to determine whether the data are adequately documented, internally consistent, and can be used to accurately reproduce the available experimental data. Conclusions reached during this review include:

- The pK_a^0 values for H_2Oxalate(aq) are consistent with the available experimental data and appear to be well established.
- The magnesium-oxalate speciation was updated in DATA0.FM4 to include $Mg(Oxalate)_2^{2-}$, which was identified by Choppin et al (2001) but was omitted from previous WIPP database versions. Addition of this species to the database was appropriate.
- The updated Pitzer parameters and glushinskite solubility added to DATA0.FM4 were appropriately documented and have been shown to reproduce the experimental data.
- The aqueous species $Ca(Oxalate)_2^{2-}$, $Am(Oxalate)_2^{-}$, $Th(Oxalate)_2$(aq), and $NpO_2(Oxalate)_2^{3-}$ have been identified in the literature, and Choppin et al. (2001) provided experimentally derived apparent log β values for all of these species except $Ca(Oxalate)_2^{2-}$. These species should be added to the WIPP database to maintain consistency with the speciation identified by Choppin et al. (2001) and other investigations.

4.4 ACETATE

Acetate ($C_2H_3O_2^-$) can form relatively strong complexes with actinides. At the inventory concentrations predicted for the CRA 2019 DPA, acetate complexation is predicted to increase the dissolved Np(V) concentration in WIPP brines released from the repository (Domski and Sisk-Scott 2019). No changes were made to the acetate data between DATA0.FM1 and DATA0.FM4 (Domski 2019a).

The acetate aqueous speciation, log β^0 values, and Pitzer interaction parameters in DATA0.FM4 are based on data from Choppin et al. (2001). Giambalvo (2002b) calculated pK_a^0 values for acid dissociation of HAcetate(aq) and log β^0 values for acetate complexation of Am(III), Th(IV), Np(V), and magnesium. Calcium-acetate aqueous speciation and Pitzer parameter data were unavailable, so Giambalvo (2002b) assumed calcium log β^0 values and Pitzer parameters were equal to the values determined for magnesium. Xiong (2004a) revised the NpO_2Acetate(aq) standard chemical potential prior to the development of DATA0.FM1 based on a recalculation by Giambalvo (2003).

The aqueous acetate speciation used by Choppin et al. (2001) was included in DATA0.FM4 (Table 4-6). Choppin et al. (2001) reported data for the single $AmAcetate^{2+}$ aqueous species, but more recent publications have identified the formation of three Am(III)-acetate species (Table 4-6). DOE should assess the available data and determine if the additional Am(III) acetate species should be added to the database before the next WIPP PA.

Choppin et al. (2001) provided data for the $ThAcetate^{3+}$ and $Th(Acetate)_2^{2+}$ aqueous species. However, five Th(IV)-acetate species have been identified by other studies (Rao et al. 2005, Willberger et al. 2019). Willberger et al. (2019) also evaluated NpO_2^+ complexation by acetate and confirmed the formation of the single $NpO_2Acetate(aq)$ species that is included in DATA0.FM4. DOE should address whether the Th(IV)-acetate speciation in DATA0.FM4 should be revised based on the results of these investigations for the WIPP PA.

Table 4-6. Actinide-Acetate Aqueous Speciation

DATA0.FM4 Choppin et al. (2001)	**Rao et al. (2005)[a]**	**Fröhlich et al. (2015)**	**Willberger et al. (2019)**
$AmAcetate^{2+}$	$AmAcetate^{2+}$ $Am(Acetate)_2^+$ $Am(Acetate)_3(aq)$	$AmAcetate^{2+}$ $Am(Acetate)_2^+$ $Am(Acetate)_3(aq)$.	$AmAcetate^{2+}$ $Am(Acetate)_2^+$ $Am(Acetate)_3(aq)$.
$ThAcetate^{3+}$ $Th(Acetate)_2^{2+}$	$ThAcetate^{3+}$ $Th(Acetate)_2^{2+}$ $Th(Acetate)_3^+$ $Th(Acetate)_4(aq)$ $Th(Acetate)_5^-$	--[b]	$ThAcetate^{3+}$ $Th(Acetate)_2^{2+}$ $Th(Acetate)_3^+$ $Th(Acetate)_4(aq)$ $Th(Acetate)_5^-$
$NpO_2Acetate(aq)$	--[b]	--[b]	$NpO_2Acetate(aq)$

a – Nd(III) analogue for Am(III)
b – not investigated in this study

5.0 IRON(II)

DATA0.FM4 is the first version of the WIPP geochemical modeling database to include Fe(II) data. Sisk-Scott (2019), Domski (2019a), and DOE (2019, Appendix GEOCHEM-2019) document the solids solubility data (Table 5-1), aqueous speciation data (Table 5-2), and Pitzer interaction coefficients (Tables 5-3 through 5-5) in DATA0.FM4. Both Section GEOCHEM-3.2.8 (DOE 2019) and Sisk-Scott (2019) state that the DATA0.FM4 includes eight iron-bearing solids, but only four solids were added. Only Fe^{2+} hydrolysis and carbonate aqueous species and solid phases are included in DATA0.FM4. Data are not included for modeling of the effects of organic ligands, sulfate, sulfide, or phosphate on Fe(II) aqueous speciation or solid phase precipitation.

Table 5-1. Iron(II) Solids Solubility Data from Sisk-Scott (2019) and Domski (2019a)

Reaction	Log K_s^0	Data source
$Fe(OH)_2$-hex(s) + 2 H^+ = Fe^{2+} + 2 H_2O	12.89	Kim et al. (2017)
$Fe_2Cl(OH)_3$(s) (oxychloride-Fe-3) + 3 H^+ = 2 Fe^{2+} + Cl^- + 3 H_2O	17.08	Kim et al. (2017)
$FeCO_3$(s) + H^+ = Fe^{2+} + HCO_3^- (siderite)	-0.12	Stumm and Morgan (1996)
$Fe_2CO_3(OH)_2$(s) (chukanovite) + 3 H^+ = 2 Fe^{2+} + HCO_3^- + 2 H_2O	12.32	Kim et al. (2017)

Table 5-2. Iron(II) Aqueous Speciation Data from Sisk-Scott (2019) and Domski (2019a)

Reaction	Log β^0	Data source
$FeOH^+$ + H^+ = Fe^{2+} + H_2O	9.31	Shock et al. (1997)
$Fe(OH)_2$(aq) + 2 H^+ = Fe^{2+} + 2 H_2O	20.82[a]	Stumm and Morgan (1996)
$Fe(OH)_3^-$ + 3 H^+ = Fe^{2+} + 3 H_2O	31.0	Baes and Mesmer (1976)
$FeCO_3$(aq) + H^+ = Fe^{2+} + HCO_3^-	4.83	Bruno et al. (1992)
$Fe(CO_3)_2^{2-}$ + 2 H^+ = Fe^{2+} + 2 HCO_3^-	13.89	Kim et al. (2017)

a – this value was not located in Stumm and Morgan (1996), and may be from Baes and Mesmer (1976)

Table 5-3. Iron(II) Cation-Anion Interaction Parameters

i	j	α_1/α_2	$\beta^{(0)}$	$\beta^{(1)}$	$\beta^{(2)}$	C^φ	Source
Fe^{2+}	Cl^-	2.0/12.0	0.37324	1.13499	0	-0.02152	Moog et al. (2004)
Na^+	$Fe(CO_3)_2^{2-}$	2.0/12.0	-0.23	6.26	0	0.0	Kim et al. (2017)

Table 5-4. Iron(II) Cation-Cation Interaction Parameters (Moog et al. 2004)

i	j	θ_{cc}
Na^+	Fe^{2+}	0.10945
Mg^{2+}	Fe^{2+}	0.145
K^+	Fe^{2+}	0.0274
Ca^{2+}	Fe^{2+}	0.0811

Table 5-5. Iron(II) Cation-Cation-Anion Interaction Parameters (Moog et al. 2004)

i	j	k	ψ_{ijk}
Fe^{2+}	Na^{+}	Cl^{-}	-0.01605
Fe^{2+}	K^{+}	Cl^{-}	-0.0252
Fe^{2+}	Mg^{2+}	Cl^{-}	-0.0299
Fe^{2+}	Ca^{2+}	Cl^{-}	-0.0160

The Fe(II) data included in DATA0.FM4 are from a DOE evaluation of the experimentally determined solubilities of four Fe(II) solids (Table 5-1) in concentrated NaCl, Na_2SO_4, and Na_2CO_3 solutions (Kim et al. 2017). Kim et al. (2017) evaluated solubility data for ferrous hydroxide [$Fe(OH)_2$-hex(s)] and $Fe_2Cl(OH)_3$(s) (oxychloride-Fe-3 in DATA0.FM4, also referred to as hibbingite) from Nemer et al. (2011) and additional solubility data for siderite [$FeCO_3$(s)] and chukanovite [$Fe_2CO_3(OH)_2$(s)]. Kim et al. (2017) maintained consistency with the existing aqueous speciation and Pitzer parameter data in DATA0.FM1 and used Fe(II) aqueous speciation and log β^0 data (Table 5-2) that are well-established in the literature. Kim et al. (2017) also demonstrated adequate fitting results to the experimental data. Consequently, the Fe(II) solids solubility, aqueous speciation, and Pitzer parameters developed by Kim et al. (2017) are sufficiently documented for addition to the WIPP database.

Jang (2017) summarized the data from Kim et al. (2017) that would be added to the WIPP database. Additional Pitzer parameters were included for Mg^{2+}, K^{+}, and Ca^{2+} interactions with Fe^{2+} (Tables 5-3 to 5-5) based on isopiestic data from Moog et al. (2004). Jang (2017) stated that confirmatory calculations should be performed using the revised database to demonstrate that the fitted parameters are consistent with the $Fe_2Cl(OH)_3$(s) solubility data from Nemer et al. (2011), and with the solubility data for siderite and chukanovite from Kim et al. (2017). Domski (2019a) provided these confirmatory calculations.

Iron(II)-sulfate solid solubility data, Pitzer parameters for interactions of Fe(II) and sulfate species, and the log β^0 for the $Fe(OH)_4^{2-}$ aqueous species from Kim et al. (2017) were summarized by Jang (2017) for inclusion in the WIPP database. However, these data were not discussed in DOE documentation by Sisk-Scott (2019) or Domski (2019a), and were not included in DATA0.FM4. EPA asked DOE to explain the omission of these data (Peake 2020d, Comment CC6-GEOCHEM-28). EPA also asked DOE to evaluate the potential effects of omitting the $Fe(OH)_4^{2-}$ aqueous species, Pitzer parameters, and solid solubilities on the actinide solubility calculations for the CRA-2019 DPA.

The omission of the Fe(II)-sulfate solids solubility and Pitzer parameters was unintentional, and Knerr (2021c) stated that these data will be included in future versions of the WIPP database. Because sulfate forms weak aqueous complexes with the +III and +IV actinides, DOE expected negligible effects on the CRA-2019 DPA actinide solubility calculations. Knerr (2021c) did not address the omission of the $Fe(OH)_4^{2-}$ aqueous species, but Sisk-Scott (2019) stated that this species was rejected because an aqueous speciation diagram had indicated that it would not form under WIPP conditions. This conclusion is reasonable, because there is little to no evidence supporting the existence of the $Fe(OH)_4^{2-}$ aqueous species (Lemire et al. 2013).

Domski (2019a) performed parameter fitting tests for the solubilities of $Fe_2Cl(OH)_3$(s) and $Fe(OH)_2$-hex(s) (Table 5-1), the log β^0 for the $Fe(CO_3)_2^{2-}$ aqueous species (Table 5-2), and the Pitzer parameters for $Fe(CO_3)_2^{2-}/Na^+$ interactions (Table 5-3). Only a very small difference was observed for the solubility of $Fe(OH)_2$-hex(s) and all other parameters evaluated with DATA0.FM4 were identical to the parameters from Kim et al. (2017). EPA requested confirmation of the source of the data used by Domski (2019a) to perform the parameter fitting [Peake 2020b, Comment CC2-GEOCHEM-8(c)]. DOE stated that the data were obtained from Kim et al. (2017, Table 5) (Knerr 2020d). DOE has adequately documented the addition of the Fe^{2+}- CO_2 - H_2O - Na^+- Cl^- system to DATA0.FM4. After addition of the Fe(II)-sulfate solids solubility data and Pitzer parameters, EPA expects that DOE will perform parameter fitting tests for the Pitzer parameters for Fe^{2+}-sulfate interactions (Jang 2017).

WIPP repository brines are expected to contain sulfide from microbial sulfate reduction and phosphates from the waste inventory. Because reduced iron can form relatively insoluble sulfide and phosphate solid phases, geochemical modeling performed without accounting for the effects of sulfide and phosphate could overpredict Fe^{2+} concentrations. Elevated Fe^{2+} concentrations would increase the competition for organic ligands, leading to the potential underprediction of actinide complexation by organic ligands. Therefore, inclusion of Fe(II) interactions with organic ligands in WIPP actinide solubility calculations will also require consideration of the effects of phosphate and sulfide.

6.0 LEAD(II)

DOE lists experimental studies performed with lead for the WIPP program in Sisk-Scott (2019). These investigations provide data related to the solubilities of cerussite [$PbCO_3$(s)] and Pb(II) oxalate [PbOxalate(s)], and Pitzer interaction parameters for Pb(II)-EDTA, Pb(II)-citrate, and Pb(II)-oxalate in NaCl and $MgCl_2$ solutions. The studies include Xiong (2013b, 2014a, 2014b, 2015a, 2015b, 2018). Characterization of solid phases from the cerussite solubility experiments identified abellaite [$NaPb_2(CO_3)_2(OH)$(s)] in addition to cerussite (Sisk-Scott 2019). In addition, recent DOE analysis of the solids from experiments with PbO(s) starting materials (Kirkes et al. 2014, Xiong 2018) indicated the presence of lead solid phases in addition to α-PbO(s). DOE determined that the presence of solid phases in the experiments would require additional evaluation of the data, so DOE decided to use data from Powell et al. (2009) in the parameterization of the Pb(II) model for DATA0.FM4. DOE did not include any Pitzer parameters for aqueous species.

Powell et al. (2009) reviewed Pb(II) aqueous speciation and solids solubility data for the inorganic ligands OH^-, Cl^-, CO_3^{2-}, SO_4^{2-}, and PO_4^{3-}. This review included evaluation of the reliability of the stability constants and related publications, use of SIT to extrapolate the stability constants to an ionic strength of zero, and recommendation of aqueous speciation and log β^0 values at 25°C and zero ionic strength. There are many limitations of the Pb(II) parameterization in DATA0.FM4 (Peake 2020d, Comment CC6-GEOCHEM-29):

- There are no predicted effects of ionic strength due to the lack of Pitzer parameters;
- Solid phases that can form during corrosion of lead objects in marine environments were omitted, including laurionite [Pb(OH)Cl(s)], hydrocerussite [$Pb_3(CO_3)_2(OH)_2$(s)], mendipite [$Pb_3O_2Cl_2$(s)], cotunnite [$PbCl_2$(s)], and galena [PbS(s)];
- Solid phases formed during experiments with WIPP brines were omitted, including $KCl•2PbCl_2$(cr) and caracolite [$NaCl•Na_2SO_4•2PbSO_4$(cr)]; and
- Phosphate data and sulfide data were omitted from the database.

Use of the Pitzer activity coefficient model to predict the solubilities of actinides in highly concentrated WIPP brines is an important part of the actinide source term conceptual model (Wilson et al. 1996, SC&A 2008). For this reason, the lead data added to DATA0.FM4 are inconsistent with the actinide source term conceptual model. DOE has not discussed whether Pb(II) Pitzer parameters developed for the WIPP program by Felmy et al. (2000) were considered for inclusion in DATA0.FM4. Considerable uncertainty is associated with the calculated aqueous Pb(II) concentrations and solid phase stabilities because the Pitzer model was not used to account for the effects of high ionic strength in WIPP brines. The magnitude of these uncertainties cannot be assessed because DOE did not provide the results of validation calculations with the Pb(II) data in DATA0.FM4.

DATA0.FM4 contains solubility data for Pb(II) oxide [litharge, α-PbO(s, red)], Pb(II) carbonates [cerussite and phosgenite, $Pb_2CO_3Cl_2$(s)], and Pb(II) sulfate [anglesite, $PbSO_4$(s)] that were selected by Powell et al. (2009). DOE has not provided an evaluation of the solid phases that are likely to form in the WIPP repository. Investigations of lead corrosion products in seawater environments have indicated other phases may form, including hydrocerussite, laurionite, cotunnite, massicot, mendipite, and galena (North and MacLeod 1987, MacLeod 1991). Felmy et al. (2000) also observed

precipitation of $KCl•2PbCl_2(cr)$ and caracolite [$NaCl•Na_2SO_4•2PbSO_4(cr)$] from experiments with carbonate-free Salado (G-Seep) and Castile (ERDA-6) brines. DOE should evaluate the solids likely to form in the WIPP repository environment based on the available natural analogue and laboratory experimental data. Using the results of this evaluation, DOE should include solubility data for potentially important Pb(II) solid phases in the EQ3/6 database.

As previously noted for Fe(II) (Section 5.0), WIPP repository brines are expected to contain sulfide from microbial activity and phosphates from the waste inventory. Lead(II) can form galena, which is an insoluble sulfide. Lead(II) is also known to form insoluble phosphate solid phases such as pyromorphite [$Pb_5(PO_4)_3OH(s)$]. Geochemical modeling without accounting for the effects of sulfide and phosphate could overpredict Pb^{2+} concentrations and the competition for organic ligands. This overprediction would lead to the possible underprediction of actinide complexation by organic ligands. Therefore, inclusion of Pb(II) interactions with organic ligands in WIPP actinide solubility calculations will also require consideration of the effects of phosphate and sulfide on Pb(II) solid phase formation.

The Pb(II) data in DATA0.FM4 are incomplete and should not be included in WIPP PA calculations because DATA0.FM4 lacks Pitzer parameters for lead species, it may not include all solids that could form in the WIPP repository environment, and because DOE has not demonstrated that the DATA0.FM4 can be used to accurately simulate available experimental solubility data in high ionic strength solutions. Until DOE has addressed these issues, EPA expects DOE to omit Pb(II) aqueous species and solid phases from the actinide solubility calculations.

7.0 AMERICIUM(III)

This section addresses the inorganic Am(III) solid phase data, aqueous speciation data, and Pitzer parameters in DATA0.FM4. Complexation of Am(III) by acetate, citrate, EDTA, and oxalate and the related Pitzer parameters for organic ligands are addressed in Section 4.0. Americium(III) data in DATA0.FM4 are based on an evaluation by Giambalvo (2002a, 2002b) and these data have not been updated since the PABC04. Much of the Am(III) data in DATA0.FM4 were obtained from Fanghänel et al. (1994) and Könnecke et al. (1997).

DOE (2019, Appendix SOTERM) provided a summary of Am(III) chemistry, including solids solubilities and aqueous speciation. However, this summary did not include an assessment of the DATA0.FM4 thermodynamic data. For example, log β^0 values for $AmOH^{2+}$, $Am(OH)_2^+$, and $Am(OH)_3(aq)$ from various studies were listed in Table SOTERM-23, but the log β^0 values in DATA0.FM4 were not listed or compared to the other data. EPA requested additional information regarding Am(III) aqueous speciation and solubility data, noting that recent publications (e.g., Xiong et al. 2017b, Kim et al. 2018) were not discussed in Appendix SOTERM (DOE 2019) (Peake 2020a, Comment CC1-SOTERM-3). EPA also asked DOE to address whether data published since the last revision of the Am(III) aqueous speciation and solubility data in the EQ3/6 database (Giambalvo 2002a) have significant implications for modeling predictions of WIPP repository brine chemistry. Knerr (2021d) provided the requested information, which is addressed in the following discussion.

Modeling of dissolved actinide solubilities for WIPP PA has shown that under WIPP repository conditions, the most important Am(III) aqueous species will be Am(III) hydrolysis species and aqueous Am(III) complexes with EDTA and carbonate. Solid phases most likely to form under repository conditions are expected to be $Am(OH)_3(s)$ and possibly Am(III)-carbonate solids. Relatively recent publications have indicated that borate in WIPP brines may also affect dissolved Am(III) concentrations.

7.1 AMERICIUM(III) HYDROLYSIS

The NEA reviewed Am(III) and Cm(III) hydrolysis data in Guillaumont et al. (2003), including data from experiments in solutions up to 6.2 m NaCl (Runde and Kim 1994, Fanghänel et al. 1994). The log β^0 values were determined by extrapolating to zero ionic strength using SIT (Table 7-1). NEA provided an update of this review in Grenthe et al. (2020), and retained the Am(III) hydrolysis constants recommended by Guillaumont et al. (2003). The DATA0.FM4 Am(III) hydrolysis constants are consistent with the Guillaumont et al. (2003) values within the stated uncertainties.

Two recent studies have calculated Am(III) hydrolysis constants. Kim et al. (2018) evaluated the first hydrolysis constant of Eu(III) as an analogue for Am(III) using time-resolved laser fluorescence spectroscopy (TRLFS). The measurements were performed in 0.1 M $NaClO_4$, and the results were extrapolated to zero ionic strength using SIT. The resulting log β^0 of 7.87 ± 0.22 is outside the uncertainty range for the value selected by Guillaumont et al. (2003), and is higher than the DATA0.FM4 value (Table 7-1). Oakes et al. (2021) obtained hydrolysis constants for $AmOH^{2+}$ and $Am(OH)_2^+$ (Table 7-1) that are also higher than the DATA0.FM4 hydrolysis constants by fitting a Pitzer model to $Am(OH)_3(cr)$ solubility data from Rao et al. (1996a) and

Silva (1982). The hydrolysis constants in DATA0.FM4 (Table 7-1) are reasonable because they fall within the range of values established by NEA-TDB and Oakes et al. (2021).

Table 7-1. Standard State Stability Constants for Am(III) Hydrolysis Species

$AmOH^{2+}$	$Am(OH)_2^+$	$Am(OH)_3(aq)$	Reference
7.5556	15.6915	25.6905	DATA0.FM4 (Giambalvo 2002a) from Fanghänel et al. (1994) and Könnecke et al. (1997)
7.2 ± 0.5	15.1 ± 0.7	26.2 ± 0.5	NEA-TDB, Guillaumont et al. (2003), Grenthe et al. (2020)
7.87 ± 0.22	--[a]	--[a]	Kim et al. (2018), Eu(III) analogue study
8.03	16.2	22.45	Oakes et al. (2021)

a – not evaluated in this study

7.2 PITZER PARAMETERS

Giambalvo (2002a, Table 2) cited Könnecke et al. (1997) as the source of a value of -0.016 kg^2/mol^2 for the Am^{3+}- Cl^- C^ϕ parameter. However, the Am^{3+}- Cl^- C^ϕ parameter value in DATA0.FM4 is instead -0.0166 kg^2/mol^2. DOE should resolve this inconsistency.

7.3 $AM(OH)_3$ SOLIDS

The log K_s^0 for $Am(OH)_3$(s) in DATA0.FM4 (Table 7-2) is from Morss and Williams (1994), based on their compilation of literature values. DOE (Giambalvo 2002a) noted that Könnecke et al. (1997) successfully used this log K_s^0 value to simulate $Am(OH)_3$(s) solubility data in 5 M NaCl from Runde and Kim (1994). Giambalvo (2002a) demonstrated that the Am(III) solubility, aqueous speciation, and Pitzer parameter data in the WIPP database accurately modeled the Runde and Kim (1994) solubility data.

The NEA reviewed Am(III) solids solubility data (Guillaumont et al. 2003), and extrapolated the $Am(OH)_3$(s) solubilities to zero ionic strength using SIT. Guillaumont et al. (2003) differentiated between solubilities measured using crystalline, aged $Am(OH)_3$(cr) and solubilities determined with X-ray amorphous $Am(OH)_3$(am) (Table 7-2). Guillaumont et al. (2003) noted that the $Am(OH)_3$(am) solubility measured by Runde and Kim (1994) is more consistent with $Am(OH)_3$(cr) and concluded that the crystallinity of this solid phase is uncertain. Guillaumont et al. (2003) recommended log K_s^0 values for crystalline and amorphous $Am(OH)_3$(s) (Table 7-2). The solubilities recommended by Guillaumont et al. (2003) were retained in the updated NEA-TDB review by Grenthe et al. (2020).

Neck et al. (2009) measured the solubility of $Nd(OH)_3$(s) as an analogue for $Am(OH)_3$(s) in concentrated NaCl, $MgCl_2$, and $CaCl_2$ solutions. Based on these solubility measurements and considerations regarding the crystallinity and aging of the solid phases, Neck et al. (2009) recommended retention of the $Am(OH)_3$(cr) and $Am(OH)_3$(am) log K_s^0 values selected by Guillaumont et al. (2003).

Table 7-2. Reported Solubility Data for $Am(OH)_3$(cr), $Am(OH)_3$(am), $Nd(OH)_3$(cr), and $Nd(OH)_3$(am)

Log K_s^0	Solid	Reference
15.9 ± 0.4	$Am(OH)_3$(cr)	Silva (1982)
16.0 ± 0.2	$Nd(OH)_3$(cr)	Silva (1982)
14.96	$Nd(OH)_3$(cr)	Rao et al. (1996a)
14.49[a]	$Am(OH)_3$(s)	Könnecke et al. (1997) from Morss and Williams (1994)
15.6 ± 0.6	$Am(OH)_3$(cr)	Guillaumont et al. (2003), Grenthe et al. (2020)
16.9 ± 0.6	$Am(OH)_3$(am)	Guillaumont et al. (2003), Grenthe et al. (2020)
17.2 ± 0.4	$Nd(OH)_3$(cr, fine-grained)	Neck et al. (2009)
16.85 ± 0.2	$Nd(OH)_3$(am)	Xiong et al. (2017b)
14.946	$Nd(OH)_3$(cr)	Oakes et al. (2021)
17.18	$Nd(OH)_3$(am)	Oakes et al. (2021)

a – log K_s^0 value in DATA0.FM1 and DATA0.FM4

Xiong et al. (2017b) reported the results of long-term solubility experiments using fine-grained $Nd(OH)_3$(cr) in 4.4 m and 5.0 m NaCl solutions. All experiments were carried out from undersaturation. As noted by Knerr (2021d), solution samples from the experiments were filtered using 0.2 μm filters, so these samples may have contained colloidal material, which would increase the measured solubilities. Xiong et al. (2017b) found that their experimentally determined $Nd(OH)_3$(cr) solubilities were in good agreement with $Am(OH)_3$(s) solubilities calculated using the WIPP thermodynamic model. The experimental results from Xiong et al. (2017b) were reasonably consistent with the data from Runde and Kim (1994), showing that the solubilities measured in the latter study may have represented microcrystalline material. Xiong et al. (2017b) used the WIPP model to calculate a log K_s^0 value for $Nd(OH)_3$(am) of 16.85 using the solubility data of Neck et al. (2009), which agrees with the value selected by Guillaumont et al. (2003) for $Am(OH)_3$(am).

Oakes et al. (2021) evaluated the available +III actinide data, and had difficulty reproducing some of the figures from Könnecke et al. (1997). Oakes et al. (2021) concluded that there are potential internal inconsistencies in the WIPP Am(III) model that was derived from Könnecke et al. (1997), which could affect the log β^0 values for $AmCl^{2+}$ and $AmCl_2^+$ and some of the Pitzer parameters. DOE should evaluate these possible inconsistencies prior to the next WIPP PA.

Oakes et al. (2021) used the solids solubility data from Rao et al. (1996a) and Silva (1982) and the Pitzer model of ion interactions to calculate a log K_s^0 for $Nd(OH)_3$(cr) that is consistent with the Pitzer-extrapolated solubilities calculated by Rao et al. (1996a) and slightly lower than the SIT-extrapolated value from Guillaumont et al. (2003) (Table 7-2). The log K_s^0 calculated for finely crystalline to amorphous material calculated by Oakes et al. (2021) is consistent with the log K_s^0 values from Neck et al. (2009) and Guillaumont et al. (2003).

Guillaumont et al. (2003) addressed issues associated with using X-ray diffraction (XRD) to characterize the crystallinity of the bulk $Am(OH)_3$(s) phase in solubility experiments, noting that the bulk crystallinity of a solid may differ from the surface properties that control aqueous solubility. Surface properties that differ from the bulk solid phase may explain the relatively high

solubility measured by Neck et al. (2009) using fine-grained crystalline solids and the relatively low solubility measured by Runde and Kim (1994) using XRD-amorphous material.

The degree of crystallinity, and hence solubility, of $Am(OH)_3(s)$ that will form in the long-term WIPP repository and control solubilities is uncertain. Over long time periods, it is reasonable to expect that the grain size and crystallinity of a solid will increase. However, α-radiolysis damage to the crystal structure, particularly from short-lived radionuclides such as ^{241}Am, may reduce the crystallinity and increase the solubility of $Am(OH)_3(s)$ in the repository.

The $Am(OH)_3(s)$ log K_s^0 in DATA0.FM4 is equal to the lowest value reported in the recent literature (Table 7-2). As acknowledged by Knerr (2021d), this log K_s^0 value results in underprediction of baseline dissolved Am(III) concentrations in WIPP PA calculations. This very low solubility in DATA0.FM4 results in an actinide solubility uncertainty distribution that is biased towards positive values (Domski 2019o). Revising the $Am(OH)_3(s)$ log K_s^0 to be consistent with the solubility of $Am(OH)_3(am)$ would not significantly change PA results, because the associated +III actinide solubility uncertainty distribution would also change. Consequently, the $Am(OH)_3(s)$ solubility data in DATA0.FM4 and associated CRA-2019 DPA +III actinide solubility uncertainty distribution adequately account for the uncertainty regarding the crystallinity and solubility of $Am(OH)_3(s)$ in the WIPP repository. However, EPA expects DOE to consider revising the $Am(OH)_3(s)$ solubility data to be consistent with the NEA-TDB values (Guillaumont et al. 2003), to improve consistency of the thermodynamic database with the available literature data.

7.4 AMERICIUM(III)-CARBONATE AQUEOUS SPECIES AND SOLIDS

Giambalvo (2002a) determined the Am(III)-carbonate aqueous speciation (Table 7-3) and solids solubility data (Table 7-4) in DATA0.FM4 based on investigations by Rao et al. (1996b) and Felmy et al. (1990). Guillaumont (2003) included additional data from other investigations, and used SIT to extrapolate the apparent log K_s values to zero ionic strength. An updated NEA-TDB review (Grenthe et al. 2020) resulted in a minor change to the $Am(CO_3)_3^{3-}$ log β^0 value (Table 7-3). The log β^0 values for the Am(III)-carbonate aqueous species and the log K_s^0 values in DATA0.FM4 are reasonable because they are within the ranges of the uncertainties provided by Guillaumont et al. (2003) and Grenthe et al. (2020).

Ternary complexes of the +III actinides have been identified with calcium and hydroxide ion that were assumed to be $Ca[Cm(OH)_3]^{2+}$, $Ca_2[Cm(OH)_4]^{3+}$ and $Ca_3[Cm(OH)_6]^{3+}$ (Neck et al. 2009, Rabung et al. 2008). These ternary species are unlikely to be important under WIPP repository conditions because they affect the solubility of the +III actinides only at pcH greater than about 11 and at relatively high calcium concentrations, and these conditions are not anticipated in the WIPP repository environment.

Table 7-3. Stability Data for Am(III)-Carbonate Species

$AmCO_3^+$	$Am(CO_3)_2^-$	$Am(CO_3)_3^{3-}$	Reference
2.24	7.68	15.8	DATA0.FM4 (Giambalvo 2002a)
2.3 ± 0.4	7.8 ± 0.5	16.0 ± 0.8	Guillaumont et al. (2003)
2.3 ± 0.4	7.8 ± 0.5	16.02 ± 0.5	Grenthe et al. (2020)

Table 7-4. Solubility Data for Am(III)-Carbonate Solids

Log K_s^0	Solid[a]	Reference
1.64	$AmOHCO_3$(s)	DATA0.FM4 (Giambalvo 2002a)
1.94 ± 1.0	$AmOHCO_3 \cdot 0.5H_2O$ (s)	Guillaumont et al. (2003)
-0.71	$NaAm(CO_3)_2 \cdot 6H_2O$(s)[a]	DATA0.FM4 (Giambalvo 2002a)
-0.56 ± 0.5	$NaAm(CO_3)_2 \cdot 5H_2O$(s)[a]	Guillaumont et al. (2003)

a – the waters of hydration in these solids differ, but have no effect on the log K_s^0 values

7.5 AMERICIUM(III)-BORATE AQUEOUS SPECIES AND SOLIDS

EPA (2017) reviewed available data regarding the possible complexation of +III actinides by borate species and precipitation of borate solid phases and found that additional studies related to Am(III)-borate complexation and Am-borate solid phase precipitation had been published since the CRA-2014 (e.g., Xiong 2017, Xiong et al. 2017a). In response to an EPA request for additional information regarding the effects of borate on the mobilization of +III actinides (Peake 2020a, Comment CC1-SOTERM-2), DOE provided a more comprehensive evaluation of the available data (Knerr 2020d).

Knerr (2020d) differentiated between the effects of borate on Am(III) speciation at low concentrations and the effects at higher concentrations (> 0.10 M). Initial total borate concentrations in WIPP brines range from 0.063 to 0.158 M. After equilibration with Salado minerals and MgO backfill hydration and carbonation products, CRA-2019 DPA dissolved actinide solubility calculations resulted in total borate concentrations ranging from 0.224 M to 0.283 M (Domski and Sisk-Scott 2019). However, lower borate concentrations were predicted by the CRA-2014 PA actinide solubility calculations (0.0623 M - 0.186 M).

Hinz et al. (2015) saw no significant effect of total borate concentrations ≤ 0.004 M in Nd(III) solubility experiments in neutral to slightly alkaline concentrated NaCl and $MgCl_2$ solutions. At pcH 8 with borate concentrations greater than 0.16 M, TRLFS showed that aqueous Cm(III)-borate species become predominant (Hinz et al. 2015). Experimental results of solubility experiments with $Nd(OH)_3$(am) performed in NaCl solutions with up to 0.4 M borate showed that Nd(III) concentrations decreased between pcH 6 and 9 because of the formation of a borate-containing Nd(III) solid phase (Hinz et al. (2015). Although these results indicate that borate is unlikely to significantly increase Am(III) concentrations under WIPP repository conditions, borate may have small effects on Am(III) aqueous speciation and solubility.

Xiong et al. (2017a) conducted $Nd(OH)_3$(am) solubility experiments in NaCl solutions in equilibrium with borax [$Na_2B_4O_7 \cdot 10H_2O$(s)] to evaluate the effects of relatively high borate concentrations on Am(III) solubilities. Xiong et al. (2017a) found that at pmH 9 and the higher ionic strength (5.6 m) relevant to WIPP conditions, borate did not increase Nd(III) concentrations. Xiong (2017) summarized the results of fitting calculations performed with data from Borkowski et al. (2010) to determine the log β^0 value for $AmHB_4O_7^{2+}$, the log K_s^0 for $AmB_9O_{13}(OH)_4$(cr), and Pitzer interaction parameters for the $AmHB_4O_7^{2+}/Cl^-$ ion pair. DOE has not added these parameters to the WIPP database, and insufficient information is presented by Xiong (2017) to enable a complete review of the parameters at this time.

7.6 AMERICIUM(III) SUMMARY

The results of this overview of Am(III) aqueous speciation and solids solubility data indicate that the DATA0.FM4 Am(III) aqueous speciation and solids solubility data are reasonably representative of the solubility of $Am(OH)_3$(cr). Formation of $Am(OH)_3$(am) in the repository may occur because of α-radiolysis damage to the crystal structure. The possible effects of $Am(OH)_3$(am) on dissolved +III actinide solubilities are addressed by including microcrystalline $Am(OH)_3$(s) solubility data in the +III actinide solubility uncertainty distribution. DOE should consider revising the $Am(OH)_3$(s) solubility data to be more consistent with the NEA-TDB values (Guillaumont et al. 2003).

Oakes et al. (2021) found potential internal inconsistencies in the WIPP Am(III) model, which could affect the log β^0 values for $AmCl^{2+}$ and $AmCl_2^+$ and some of the Pitzer parameters. DOE should evaluate these possible inconsistencies prior to the next WIPP PA.

Continued evaluation of the potential effects of borate on the dissolved concentrations of Am(III) is also recommended if additional information becomes available. The Am(III)-carbonate aqueous speciation and solids solubilities in DATA0.FM4 are consistent with the available data.

8.0 THORIUM(IV)

The Th(IV) data in DATA0.FM4 are based on evaluations by Giambalvo (2002b, 2002c) and Nowak (2005), and these data have not been updated since the PABC04. This section addresses the inorganic Th(IV) species and solid phases. Complexation of Th(IV) by acetate, citrate, EDTA, and oxalate is addressed in Section 4.0.

EPA requested additional information regarding the expected effects of the currently available WIPP-relevant Th(IV) aqueous speciation and solubility data on modeling predictions of WIPP repository brine chemistry (Peake 2020a, Comment CC1-SOTERM-4). Knerr (2020d) provided an evaluation of the available data and its potential effects on modeling dissolved Th(IV) concentrations for WIPP PA, and this information is included in the discussion below.

8.1 THORIUM(IV) HYDROUS OXIDE SOLID AND HYDROLYSIS

Felmy et al. (1991) measured the solubility of ThO_2(am) in 0.6 M to 3 M NaCl and in 0.6 M KCl and used the Pitzer model to evaluate the data. Preparation of the ThO_2(am) solids used in the experiments did not include aging or drying. Phase separation was carried out for aqueous samples using 1.8 nm filtration. Solubility data in solutions with pH less than 7 were used to derive the log K_s^0 value for ThO_2(am) in the DATA0.FM1 database (Table 8-1), because Th(IV) hydrolysis does not affect total Th(IV) in this pH range. Felmy et al. (1991) found that their log K_s^0 was consistent with the experimental data of Ryan and Rai (1987) in 0.1 M $NaClO_4$.

Rai et al. (2000) performed ThO_2(am) solubility experiments in 0.1 M NaCl for up to 22 days, and performed phase separation using 1.8 nm filtration. The relatively high log K_s^0 from this study (Table 8-1) is likely related to the short duration of these experiments and consequent lack of aging of the amorphous solid.

Table 8-1. Solubility Data for ThO_2(am) Solids

Solid	Log K_s^0	Reference
ThO_2(am)	10.5	Felmy et al. (1991)
ThO_2(am)	11.1	Rai et al. (2000)
ThO_2(am)	10.4865	DATA0.FM4 (Giambalvo 2002c, Nowak 2005)
ThO_2(am)	8.19	Neck et al. (2002), Altmaier et al. (2004)
ThO_2(am, hydrous, fresh)	9.29 ± 0.9	Rand et al. (2008)
ThO_2(am, hydrous, aged)	8.49 ± 0.9	Rand et al. (2008)

Neck et al. (2002) evaluated the solubility of $ThO_2 \cdot xH_2O$(am) in 0.5 M NaCl solutions, and Altmaier et al. (2004) conducted $ThO_2 \cdot xH_2O$(am) solubility experiments in concentrated NaCl and $MgCl_2$ solutions. The ThO_2(am) solids in these investigations were dried at room temperature for one week in a vacuum desiccator. Both investigations used ultracentrifugation to remove colloids from the solution samples. Neck et al. (2002) extrapolated their solubility data to zero ionic strength using SIT and established a lower log K_s^0 value for ThO_2(am) (Table 8-1) than Felmy et al. (1991).

Rand et al. (2008) concluded that different reported ThO_2(am) solubilities may reflect differences in the solid phase, including chemical composition, water content, and degree of crystallinity. Rand et al. (2008) also found that different reported solubilities may be related to separation of colloids from dissolved Th(IV), including insufficient removal of colloids or sorption on filter materials. Felmy et al. (1991) and Rai et al. (2000) used 1.8 nm filtration to separate dissolved and colloidal Th(IV), whereas Neck et al. (2002) and Altmaier et al. (2004) used ultracentrifugation. Lower concentrations measured in the investigations in which solutions were ultracentrifuged rather than filtered may be related to more effective removal of colloids and polymeric Th(IV) by ultracentrifugation. Because ~2 nm filtration has been used to separate Th(IV) colloids from dissolved Th(IV) in intrinsic colloid studies for WIPP PA, the higher reported dissolved Th(IV) concentrations measured by Felmy et al. (1991) and Rai et al. (2000) may be more consistent with the Th(IV) mineral fragment and intrinsic colloid parameters currently used for WIPP PA.

Rand et al. (2008) provided recommended log K_s^0 values for fresh and aged hydrous ThO_2(am) based on the recalculated log K_s^0 values from Felmy et al. (1991) and other investigations (Table 8-1). Rand et al. (2008, Table VII-19) developed these recommended log K_s^0 values by extrapolating experimental solubilities reported in the literature to zero ionic strength using SIT and the Th(IV) aqueous speciation selected in their review. This recalculation of the log K_s^0 values using SIT significantly decreased the log K_s^0 value from Felmy et al. (1991), from 10.5 using the Pitzer model to a range of 9.2 to 9.4 using SIT (Rand et al. 2008, Table VII-19). This difference between the Felmy et al. (1991) and Rand et al. (2008) log K_s^0 values indicates that the SIT model of ion interactions produces significantly different results for the Th(IV)-Na^+-K^+-Cl^--H_2O system than the Pitzer model. Consequently, if a log K_s^0 value from Rand et al. (2008) is substituted into the WIPP database, calculations demonstrating agreement between modeled and experimental Th(IV) concentrations would be required.

$Th(OH)_4$(aq) is the only hydrolysis species included in DATA0.FM4, and the log β^0 value from Neck et al. (2002) is included in DATA0.FM4 (Table 8-2). Exclusion of other Th^{4+} hydrolysis species, such as $Th(OH)_2^{2+}$, has no effect on actinide solubility calculations for WIPP PA because $Th(OH)_4$(aq) is the predominant hydrolysis species in the pcH range anticipated in repository brines. Rand et al. (2008) calculated a similar log β^0 value (Table 8-2) from solubility experiments carried out from pH 6 to 14, assuming a ThO_2(am) solubility of 8.5. Rand et al. (2008) noted that this is an "operational" log β^0 value, because the aqueous Th(IV) in the experiments may have included small polymeric species in addition to $Th(OH)_4$(aq).

Table 8-2. Stability Data for $Th(OH)_4$(aq)

Log β^0	Reference
17.5002	DATA0.FM4 Giambalvo (2002c), Nowak (2005), Xiong (2005)
17.49	Neck et al. (2002)
17.4 ± 0.7	Rand et al. (2008)

8.2 THORIUM(IV)-CARBONATE SPECIATION

The Th(IV)-carbonate aqueous species $Th(CO_3)_5^{6-}$ and $Th(OH)_3CO_3^-$ are included in DATA0.FM4. DOE documented inclusion of these species in Giambalvo (2002c) based on an evaluation by Novak (1996) of solubility data from Felmy et al. (1991, 1997). The $Th(CO_3)_5^{6-}$ aqueous species is not a significant contributor to total Th(IV) dissolved concentrations calculated for WIPP PA because of the relatively low carbonate concentrations in WIPP repository brines.

Two studies have subsequently examined $ThO_2 \cdot xH_2O$(am) solubility and Th(IV)-carbonate complexation in 0.5 M NaCl (Altmaier et al. 2005) and in 0 to 4 M NaCl solutions (Altmaier et al. 2006). These studies found the aqueous speciation of Th(IV) was dominated by $Th(OH)_4$(aq) and the Th(IV) species $ThOH(CO_3)_4^{5-}$ and $Th(OH)_2(CO_3)_2^{2-}$, with additional minor contributions from $Th(OH)_2CO_3$(aq), and $Th(OH)_3CO_3^-$ at pH values less than 11. EPA (2017, Section 6.7.4) compared Th(IV) concentrations predicted using the WIPP actinide solubility model to the Altmaier et al. (2006) measured concentrations and found that the model underpredicted the measured Th(IV) concentrations by approximately a factor of two. Because of the relatively low carbonate concentrations in WIPP repository brines, EPA (2017) concluded that carbonate complexation of Th(IV) is likely to have relatively small effects on total Th(IV) concentrations under WIPP repository conditions and the different Th(IV)-carbonate aqueous speciation is not expected to significantly affect total Th(IV) solubilities calculated for WIPP PA. However, DOE should update the Th(IV)-carbonate aqueous speciation data for the next WIPP PA to be consistent with currently available literature data and to minimize uncertainty associated with this issue.

Brendebach et al. (2007) identified the formation of Ca-Th(IV)-hydroxide complexes that resulted in high solubilities of Th(IV) hydrous oxides in alkaline $CaCl_2$ solutions. Under the investigated conditions, pcH 11 to 12 and $CaCl_2$ concentrations greater than 0.5 M, the dominant aqueous Th(IV) species was identified as $Ca_4[Th(OH)_8]^{4+}$. Although formation of the $Ca_4[Th(OH)_8]^{4+}$ species could result in relatively high Th(IV) concentrations under pcH and calcium concentrations controlled by the interaction of cementitious waste forms with brine, these high pcH and high calcium concentration conditions are not predicted to occur in the WIPP repository environment.

8.3 THORIUM(IV)-SULFATE SOLIDS AND AQUEOUS SPECIES

DATA0.FM4 includes additional Th(IV)-sulfate solids solubility and aqueous speciation data based on an investigation by Felmy and Rai (1992). Th(IV) is not strongly complexed by sulfate under WIPP repository conditions, and the Th(IV)-sulfate solids are relatively soluble. Consequently, the Th(IV)-sulfate data do not affect calculated total Th(IV) solubilities for WIPP PA.

8.4 THORIUM(IV) SUMMARY

The ThO_2(s) log K_s^0 in DATA0.FM4 is relatively high compared to values calculated for either fresh or aged/dried solid materials by Rand et al. (2008). These differences may be caused by different aging or crystal size of the ThO_2(am) solid. However, these differences may also result

from use of SIT by Rand et al. (2008) to recalculate reported log K_s^0 values and the different solution concentrations that may be produced by 1.8 nm filtration compared to ultracentrifugation. Modification of the ThO_2(s) log K_s^0 value in the WIPP database would require consideration of these issues and comparison of modeled and experimentally measured Th(IV) solubilities at high ionic strength. EPA (2017, Section 6.7.5) found that the current model for ThO_2(am) solubility agrees with the Felmy et al. (1991) data obtained in 3 M NaCl. Agreement of the dissolved Th(IV) model with these data is important because the Felmy et al. (1991) data were obtained using 1.8 nm filtration, which is consistent with the methods used to parameterize the Th(IV) intrinsic colloids for WIPP PA. The $Th(OH)_4$(aq) log β^0 value in DATA0.FM4 is consistent with the value determined by Rand et al. (2008) from solubility studies performed from pH 6 to 14.

EPA (2017, Section 6.7.5) found that the current WIPP model for Th(IV) underpredicted the measured Th(IV) concentrations in experiments with carbonate because the current speciation has not been updated to be consistent with currently available data. Carbonate complexation of Th(IV) is likely to have relatively small effects on total Th(IV) concentrations under WIPP repository conditions. Consequently, the different Th(IV)-carbonate aqueous speciation is not expected to significantly affect total Th(IV) solubilities calculated for WIPP PA. However, DOE should update the Th(IV)-carbonate aqueous speciation data for the next WIPP PA to be consistent with currently available literature data and to minimize uncertainty associated with this issue.

9.0 NEPTUNIUM(V) AND URANIUM(VI)

The Np(V) data in DATA0.FM4 have changed little since the CCA PAVT (Giambalvo 2002d), except for the addition of Np(V) complexation with organic ligands (Section 4.0). The data include Np(V) hydrous oxide and carbonate solids and Np(VI) hydrolysis and carbonate species, as well as complexes formed with the organic ligands acetate, citrate, EDTA, lactate, and oxalate. Because Np(V) does not significantly contribute to total radionuclide releases from the repository, the Np(V) data have not been a priority for review and revision by DOE.

Because DOE has not developed a model for calculating the solubility of U(VI), a fixed bounding concentration of 10^{-3} M is assumed for PA.

10.0 SUMMARY AND CONCLUSIONS

Domski and Sisk-Scott (2019) used the DATA0.FM4 database with the EQ3/6 geochemical modeling code to calculate baseline dissolved Am(III), Th(IV), and Np(V) solubility parameters for the CRA-2019 DPA. EPA reviewed the DATA0.FM4 database and found that the recalculated log K_s^0 for hydromagnesite in DATA0.FM4 is more internally consistent with other data in the database than the previous DATA0.FM1 value and is acceptable for use in WIPP PA calculations. DOE has also adequately documented addition of the Fe^{2+}- CO_2 - H_2O - Na^+- Cl^- system to DATA0.FM4.

EPA has identified a number of issues related to the DATA0.FM4 database and its supporting documentation (Table 10-1). DOE has already acknowledged and acted to resolve some of these issues. EPA expects that DOE will address the remaining issues in Table 10-1 before the next WIPP PA. Issues related to the EDTA system, particularly Issues 2 through 8, are the highest priority because of their effects on calculations of dissolved +III actinide concentrations for WIPP PA. The solubility of $Am(OH)_3(am)$ (Issue 29) is also high priority to ensure the dissolved +III actinide concentrations used in WIPP PA are consistent with the currently available literature data.

EPA expects to use Table 10-1 as a starting point for future WIPP EQ3/6 database reviews. EPA believes the number of issues identified during this review is associated with the length of time since the last substantive revision of the WIPP thermodynamic database for the PABC04. More frequent updates to the EQ3/6 database, and more frequent communication with EPA as updates are in progress, will result in improved compliance with the requirements of 40 CFR194.15 and expedite the review process for future CRAs.

Table 10-1. DATA0.FM4 Issues Summary

Parameter	Issue	Potential Resolution	Report Section
Phase 5 log K_s^0	1	Perform calculations demonstrating that Phase 5 solubilities calculated with DATA0.FM4 database are consistent with measured data	3.2
$CaEDTA^{2-}$ log β^0	2	Revise to 12.36 (Felmy and Mason 2003)	4.1.3
$Ca_2EDTA•7H_2O(s)$ log K_s^0	3	Unacceptable because of experimental data discrepancies	4.1.3
$Na^+/CaEDTA^{2-}$ Pitzer parameters	4	Unacceptable because of experimental data discrepancies	4.1.3
$Mg^{2+}/CaEDTA^{2-}$ Pitzer parameters	5	Unacceptable because of experimental data discrepancies	4.1.4
$Mg^{2+}/MgEDTA^{2-}$ Pitzer parameters	6	Unacceptable because of experimental data discrepancies	4.1.4
$Ca^{2+}/EDTA^{4-}$ Pitzer parameters	7	Unacceptable because of experimental data discrepancies	4.1.4
$AmEDTA^-$ log β^0	8	Revise to 19.67 (Hummel et al. 2005)	4.1.5

Parameter	Issue	Potential Resolution	Report Section
ThEDTA(aq)	9	Recalculate from Choppin et al. (2001) apparent log β values to account for the $NaEDTA^{3-}$ aqueous species	4.1.6
NpO_2EDTA^{3-} log β^0	10	Revise to 9.23 (Hummel et al. 2005)	4.1.7
NpO_2HEDTA^{2} log β^0	11	Revise to 17.06 (Hummel et al. 2005)	4.1.7
NpO_2H_2EDTA log β^0	12	Revise to 22.51 (Hummel et al. 2005)	4.1.7
$MgCitrate^-$ log β^0	13	Revise to 5.30 (Giambalvo 2002b)	4.2.2
MgHCitrate(aq) log β^0	14	Calculate using Choppin et al. (2001) apparent log β values	4.2.2
$Am(Citrate)_2^{3-}$ log β^0	15	Include Hummel et al. (2005) value of 13.90	4.2.3
$ThCitrate^+$ log β^0	16	Re-evaluate using Choppin et al. (2001) data	4.2.4
$Th(Citrate)_2^{2-}$ log β^0	17	Include based on Choppin et al. (2001) log β values	4.2.4
Earlandite log K_s^0	18	Add to database	4.2.6
$Ca(Oxalate)_2^{2-}$ log β^0	19	Add Hummel et al. (2005) value of 4.02	4.3.2
$Am(Oxalate)_2^-$ log β^0	20	Add to database	4.3.3
$Th(Oxalate)_2$(aq) log β^0	21	Add to database	4.3.4
$NpO_2(Oxalate)_2^{3-}$ log β^0	22	Add to database	4.3.5
$Am(Acetate)_2^+$ log β^0 $Am(Acetate)_3$(aq) log β^0	23	Determine whether these species should be added to the database	4.4
$Th(Acetate)_3^+$ log β^0 $Th(Acetate)_4$(aq) log β^0 $Th(Acetate)_5^-$ log β^0	24	Assess whether these species should be added to the database	4.4
Fe^{2+}-sulfate Pitzer parameters	25	Add to database, perform parameter fitting tests	5.0
Fe^{2+}-sulfate solids	26	Add to database	5.0
Pb(II) data	27	Remove from database	6.0
Am(III) Pitzer parameters	28	Resolve inconsistency in Am^{3+}- Cl^- C^ϕ Pitzer parameter from Könnecke et al. (1997)	7.2
$Am(OH)_3$(s) solubility	29	Revise to be consistent with NEA-TDB value	7.3
Am^{3+}-borate complexation and solid phase	30	Assess available data to determine if sufficient for inclusion in the WIPP database	7.4
Th(IV)-carbonate speciation and log β^0 values	31	Update to be consistent with Altmaier et al. (2006) data	8.0

EPA also noted more general database-related issues that are not included in Table 10-1. In a number of cases, there was insufficient documentation of decisions regarding WIPP database revisions. For example, the decision to revise the EDTA aqueous speciation data to align with the data in Hummel et al. (2005) was reasonable, although little explanation was provided by DOE. Use of the Hummel et al. (2005) aqueous speciation data for EDTA is justifiable because addition of the $NaEDTA^{3-}$ aqueous species is consistent with the current understanding of EDTA

speciation in concentrated NaCl solutions. However, no justification was provided for the decision to retain the $AmEDTA^-$, ThEDTA(aq), NpO_2EDTA^{3-}, NpO_2HEDTA^{2-}, and NpO_2H_2EDTA log β^0 values, even though the retained values did not account for the effects of including the $NaEDTA^{3-}$ aqueous species. These database inconsistencies, combined with issues related to the $MgEDTA^{2-}$ and $CaEDTA^{2-}$ aqueous species (Issues 2 through 12 in Table 10-1), are important because they caused significant underprediction of the baseline +III actinide solubilities calculated for the CRA-2019 DPA.

The lack of testing of literature solubility constants, aqueous speciation constants, or Pitzer interaction parameters in the database against experimentally measured data is another concern. Testing may not be necessary in the case of well-established literature values, such as the log K_s^0 for cerussite. However, for less well-established data, and for data extrapolated to zero ionic strength using SIT, it is necessary to demonstrate that reliable results are provided using the Pitzer model combined with SIT-calculated log K_s^0 and log β^0 values. In the case of the Hummel et al. (2005) organic ligands data, much of the high-ionic-strength data was obtained by Choppin et al. (2001) in NaCl solutions, and comparisons of modeled and experimentally measured apparent log β values agreed reasonably well in a number of cases, e.g., the H_4EDTA acid dissociation constants (Section 4.1.1). However, there may be other instances in which using log K_s^0 and log β^0 values calculated with SIT combined with the Pitzer model for ion interactions results in divergence between experimental and modeled data at high ionic strength. Testing of model-calculated results against experimental data is also an important quality control check, as shown by the results of calculations requested by EPA related to $MgEDTA^{2-}$ during the DATA0.FM4 review (Section 4.1.4). For future EQ3/6 database updates, EPA expects DOE to provide a reasonable justification if testing of literature values is not performed.

AP-154 (Xiong 2013a) provided a methodology and acceptance criteria for developing thermodynamic data. The AP-154 acceptance criteria included a requirement that Pitzer parameters should have magnitudes similar to literature values for comparable interaction types. However, this information was not provided in the CRA-2019 DPA submission to EPA. DOE should provide this information for future database updates to show that reasonable Pitzer parameters were calculated. AP-154 also states that modeled data should be compared to experimentally measured data, but these comparisons were absent in many cases. Including this information in supporting documentation for future database updates would expedite the review process.

Lead aqueous species and solid phases were added to DATA0.FM4 from a review by Powell et al. (2009). DOE did not evaluate the likely solid phases that may form in the WIPP environment based on natural analogues or other considerations, and potentially important lead solid phases, such as hydrocerussite, were not included in the database. Powell et al. (2009) used the SIT model of ion interactions to extrapolate the available data to zero ionic strength. These data for lead aqueous species and solid phases were added to DATA0.FM4 without Pitzer parameters. DOE did not provide calculations to demonstrate the adequacy of this model at high ionic strength. DOE also did not provide the reasons for selecting the Powell et al. (2009) compilation when a Pitzer-based WIPP project investigation of the lead thermodynamic model is available in the published literature (Felmy et al. 2000). Use of the Pitzer model for modeling high ionic strength solutions is an important element of the WIPP Dissolved Actinide Source Term

conceptual model (SC&A 2008). Consequently, the DATA0.FM4 lead system data in its present form must not be used in WIPP PA calculations.

Because of the large quantities of lead and iron in the CRA-2019 DPA inventory (Van Soest 2018), addition of these constituents to the WIPP thermodynamic database is reasonable. However, because of the potential importance of precipitation of iron and lead sulfides and phosphates solids, EPA expects DOE to consider the effects of sulfides and phosphates in addition to organic ligand interactions if iron and lead are included in dissolved actinide source term calculations.

Pitzer parameter entry errors were identified by DOE for the EDTA system data (Section 4.1.8). In addition, the solubility of earlandite and the Fe^{2+}-sulfate data were inadvertently omitted from DATA0.FM4. EPA expects DOE to improve the database revision process to better prevent parameter entry errors and omissions. These errors and omissions likely had insignificant effects on the calculation of the baseline actinide solubility parameters for the CRA-2019 DPA, but cast doubt on the thoroughness of the DOE process for producing a quality-assured database.

11.0 REFERENCES

Altmaier, M., V. Neck, and T. Fanghänel. 2004. Solubility and colloid formation of Th(IV) in concentrated NaCl and $MgCl_2$ solution. *Radiochimica Acta* 92:537-543.

Altmaier, M., V. Neck, R. Müller, and T. Fanghänel. 2005. Solubility of $ThO_2 \cdot xH_2O$ in carbonate solution and the formation of ternary Th(IV) hydroxide-carbonate complexes. *Radiochimica Acta* 93:83-92.

Altmaier, M., V. Neck, M.A. Denecke, R. Yin and T. Fanghänel. 2006. Solubility of $ThO_2 \cdot xH_2O$ and the formation of ternary Th(IV) hydroxide-carbonate complexes in $NaHCO_3$-Na_2CO_3 solutions containing 0-4 M NaCl. *Radiochimica Acta* 94:495-500.

Babb, S.C., and C.F. Novak. 1995. *Users Manual for FMT, Version 2.0.* Sandia National Laboratories, Carlsbad, New Mexico. ERMS 228119.

Baes, C.F., and R.E. Mesmer. 1976. *The Hydrolysis of Cations*. Wiley-Interscience, New York.

Berninger, U.-N., G. Jordan, J. Schott, and E.H. Oelkers. 2014. The experimental determination of hydromagnesite precipitation rates at 22.5 – 75ºC. *Mineralogical Magazine* 78:1405-1416.

Bonin, L., G. Cote, and P. Moisy. 2008. Speciation of An(IV) (Pu, Np, U and Th) in citrate media. *Radiochimica Acta* 96:145-152.

Borkowski, M., R.C. Moore, M. Bronikowski, J.-F. Chen, O.S. Pokrovsky, Y.X. Xia and G.R. Choppin. 2001. Thermodynamic modeling of actinide complexation with oxalate at high ionic strength. *Journal of Radioanalytical and Nuclear Chemistry* 248:467-471.

Borkowski, M, M. Richmann, D.T. Reed and Y. Xiong. 2010. Complexation of Nd(III) with tetraborate ion and its effect on actinide(III) solubility in WIPP brine. *Radiochimica Acta* 98:577-582.

Brendebach, B., M. Altmaier, J. Rothe, V. Neck and M.A. Denecke. 2007. EXAFS study of aqueous Zr^{IV} and Th^{IV} complexes in alkaline $CaCl_2$ solutions: $Ca_3[Zr(OH)_6]^{4+}$ and $Ca_4[Th(OH)_8]^{4+}$. *Inorganic Chemistry* 46:6804-6810.

Bronikowski, M., O.S. Pokrovsky, M. Borkowski, and G.R. Choppin. 1999. UO_2^{2+} and NpO_2^{+} complexation with citrate in brine solutions. In: Reed D.T., S.B. Clark. And L. Rao (eds.) *Actinide Speciation in High Ionic Strength Media*. Springer, Boston, MA.

Brown, M.A., A.J. Kropf, A. Paulenova, and A.V. Gelis. 2014. Aqueous complexation of citrate with neodymium(III) and americium(III): a study by potentiometry, absorption spectrophotometry, microcalorimetry, and XAFS. *Dalton Transactions* 43:6446-6454.

Bruno, J., P. Wersin, and W. Stumm. 1992. On the influence of carbonate in mineral dissolution: II. The solubility of $FeCO_3$(s) at 25°C and 1 atm total pressure. *Geochimica Cosmochimica Acta* 56:1149-1155.

Cheng, W. and Z. Li. 2010. Controlled supersaturation precipitation of hydromagnesite for the $MgCl_2$ – Na_2CO_3 system at elevated temperatures: chemical modeling and experiment. *Industrial & Engineering Chemistry Research* 49:1964-1974.

Choppin, G.R., A.H. Bond, M. Borkowski, M. Bronikowski, J.-F. Chen, S. Lis, J. Mizera, O.S. Pokrovsky, N.A. Wall, Y.X. Xia, and R.C. Moore. 2001. *Waste Isolation Pilot Plant Actinide Source Term Test Program: Solubility Studies and Development of Modeling Parameters*. Sandia National Laboratories, Albuquerque, New Mexico, April 2001, SAND99-0943.

Deng, H., Y. Xiong, M. Nemer, and S. Johnsen. 2009. *Experimental Work Conducted on MgO Long-Term Hydration, 2008 Milestone Report. S*andia National Laboratories, Carlsbad, New Mexico, ERMS 551421.

DOE (U.S. Department of Energy). 2014. *Title 40 CFR 191 Parts B and C Compliance Recertification Application*. U.S. Department of Energy Carlsbad Field Office, March 2014.

DOE (U.S. Department of Energy). 2019. *Title 40 CFR 191 Parts B and C Compliance Recertification Application*. U.S. Department of Energy Carlsbad Field Office, March 2019.

Domski, P.S. 2018a. *Memo on the Estimation of the Solubility Product (Log Ksp) for $Ca_2EDTA.7H_2O$, and Pitzer Parameters for the $Na^+/CaEDTA^{2-}$ Pair.* Sandia National Laboratories, Carlsbad, New Mexico, ERMS 570202 Carlsbad, NM: Sandia National Laboratories.

Domski, P.S. 2018b. *Memo on the Estimation of Pitzer Parameters for the $Mg^{2+}/CaEDTA^{2-}$ $Mg^{2+}/MgEDTA^{2-}$, and $Ca^{2+}/EDTA^{4-}$ Pairs*. Carlsbad, NM Sandia National Laboratories. ERMS 570855.

Domski, P.S. 2019a. *An Update to the EQ3/6 Pitzer Thermodynamic Database DATA0.FM1 with the Creation of DATA0.FM4*. Sandia National Laboratories. Carlsbad, New Mexico. ERMS 571052.

Domski, P.S. 2019b. *Correction of a Binary Pitzer Parameter in DATA0.FM4, PPR 2019-003.* Sandia National Laboratories, Carlsbad, New Mexico. ERMS 572172.

Domski, P.S. 2019c. *Parameter Problem Report (PPR) 2019-003*. Sandia National Laboratories, Carlsbad, New Mexico. ERMS 572265.

Domski, P.S. 2019d. *Parameter Problem Report (PPR) 2019-004*. Sandia National Laboratories, Carlsbad, New Mexico. ERMS 572492.

Domski, P.S. 2019e. *Parameter Problem Report (PPR) 2019-005*. Sandia National Laboratories, Carlsbad, New Mexico. ERMS 572493.

Domski, P.S. 2019f. *Parameter Problem Report (PPR) 2019-006*. Sandia National Laboratories, Carlsbad, New Mexico. ERMS 572494.

Domski, P.S. 2019g. *Parameter Problem Report (PPR) 2019-007*. Sandia National Laboratories, Carlsbad, New Mexico. ERMS 572495.

Domski, P.S. 2019h. *Parameter Problem Report (PPR) 2019-008*. Sandia National Laboratories, Carlsbad, New Mexico. ERMS 572496.

Domski, P.S. 2019i. *Parameter Problem Report (PPR) 2019-009*. Sandia National Laboratories, Carlsbad, New Mexico. ERMS 572497.

Domski, P.S. 2019j. *Parameter Problem Report (PPR) 2019-010*. Sandia National Laboratories, Carlsbad, New Mexico. ERMS 572498.

Domski, P.S. 2019k. *Parameter Problem Report (PPR) 2019-011*. Sandia National Laboratories, Carlsbad, New Mexico. ERMS 572499.

Domski, P.S. 2019l. *Parameter Problem Report (PPR) 2019-012*. Sandia National Laboratories, Carlsbad, New Mexico. ERMS 572500.

Domski, P.S. 2019m. *Parameter Problem Report (PPR) 2019-013*. Sandia National Laboratories, Carlsbad, New Mexico. ERMS 572501.

Domski, P.S. 2019n. *Technical Aspects of the Baseline Solubility Model for the CRA-2019 PA.* Sandia National Laboratories, Carlsbad, New Mexico, ERMS 571535.

Domski, P.S. 2019o. *Uncertainty Analysis of Actinide Solubilities for CRA 2019*. Sandia National Laboratories, Carlsbad, New Mexico, ERMS 571179.

Domski, P.S. 2020. *Correction of the α_1 Terms of Three Binary Pitzer Parameter Blocks in DATA0.FM4, PPR 2019-004 through 2019-013*. Sandia National Laboratories, Carlsbad, New Mexico, ERMS 572559.

Domski, P.S., and C. Sisk-Scott. 2019. *Prediction of Baseline Actinide Solubilities for CRA 2019 with an Updated EQ3/6 Pitzer Thermodynamic Database, DATA0.FM4*. Sandia National Laboratories, Carlsbad, New Mexico, ERMS 574281.

EPA (U.S. Environmental Protection Agency) 2017. *Technical Support Document for Section 194.24: Evaluation of the Compliance Recertification Actinide Source Term, Gas Generation, Backfill Efficacy, Water Balance and Culebra Dolomite Distribution Coefficient Values*. Office of Radiation and Indoor Air, Docket No. EPA-HQ-OAR-2014-0609, June 2017.

Fanghänel, T., J.I. Kim, P. Paviet, R. Klenze, and W. Hauser. 1994. Thermodynamics of radioactive trace elements in concentrated electrolyte solutions: Hydrolysis of Cm^{3+} in NaCl-solutions. *Radiochimica Acta* 66/67:81-87.

Felmy, A.R., and M.J. Mason. 2003. An Aqueous Thermodynamic Model for the Complexation of Sodium and Strontium with Organic Chelates Valid to High Ionic Strength. I. Ethylenedinitrilotetraacetic Acid (EDTA). *Journal of Solution Chemistry*. 32:283-300.

Felmy, A.R., and D. Rai. 1992. An aqueous thermodynamic model for a high valence 4:2 electrolyte Th^{4+}-SO_4^{2-} in the system Na^+-K^+-Li^+-NH_4^+-Th^{4+}-SO_4^{2-}-HSO_4^--H_2O to high concentration. *Journal of Solution Chemistry* 21:407-423.

Felmy, A.R., and J.H. Weare. 1986. The prediction of borate mineral equilibria in natural waters: application to Searles Lake, California. *Geochimica Cosmochimica Acta* 20:2771-2783.

Felmy, A.R., D. Rai and R.W. Fulton, 1990. The solubility of $AmOHCO_3$(c) and the aqueous thermodynamics of the system Na^+ - Am^{3+} - HCO_3^- - OH^- - H_2O. *Radiochimica Acta* 50:193-204.

Felmy, A.R., D. Rai and M.J. Mason. 1991. The solubility of hydrous thorium(IV) oxide in chloride media: development of an aqueous ion-interaction model. *Radiochimica Acta* 55:177-185.

Felmy, A.R., D. Rai, M.S. Sterner, M.J. Mason, N.J. Hess, and S.D. Conradson. 1997. Thermodynamic models for highly charged aqueous species: solubility of Th(1V) hydrous oxide in concentrated $NaHCO_3$ and Na_2CO_3 solutions. *Journal of Solution Chemistry* 26:233-248.

Felmy, A. R., L. M. Onishi, N. S. Foster, J. R. Rustad, D. Rai, M. J. Mason. 2000. An aqueous thermodynamic model for the Pb^{2+} - Na^+ - K^+ - Ca^{2+} - Mg^{2+} - H^+ - Cl^- - SO_4^{2-} - H_2O system to high concentration: Application to WIPP brines. *Geochimica Cosmochimica Acta* 64:3615-3628.

Felmy, A.R., H. Cho, D.A. Dixon, Y. Xia, N.J. Hess, and Z. Wang. 2006. The aqueous complexation of thorium with citrate under neutral to basic conditions. *Radiochimica Acta* 94:205-212.

Fröhlich, D. R., A. Skerencak-Frech, N. Bauer, A. Rossberg, and P.J. Panak. 2015. The pH dependence of Am(III) complexation with acetate: an EXAFS study. *Journal of Synchrotron Radiation* 22:99−104.

Gautier, Q., P. Bénézeth, V. Mavromatis and J. Schott. 2014. Hydromagnesite solubility product and growth kinetics in aqueous solution from 25 to 75ºC. *Geochimica Cosmochimica Acta* 138:1-20.

Giambalvo, E.R. 2002a. *Recommended Parameter Values for Modeling An(III) Solubility in WIPP Brines*. Memorandum to L.H. Brush, July 25, 2002, ERMS 522982.

Giambalvo, E.R. 2002b. *Recommended Parameter Values for Modeling Organic Ligands in WIPP Brines*. Memorandum to L.H. Brush, July 25, 2002, ERMS 522981.

Giambalvo, E.R. 2002c. *Recommended Parameter Values for Modeling An(IV) Solubility in WIPP Brines*. Memorandum to L.H. Brush, July 26, 2002, ERMS 522986.

Giambalvo, E.R. 2002d. *Recommended Parameter Values for Modeling An(V) Solubility in WIPP Brines*. Memorandum to L.H. Brush, July 26, 2002, ERMS 522990.

Giambalvo, E.R. 2002e. *Recommended μ^0/RT Values for Modeling the Solubility of Oxalate Solids in WIPP Brines.* Memorandum to L.H. Brush, July 31, 2002, ERMS 523057.

Giambalvo, E.R. 2003. *Release of FMT Database FMT_021120.CHEMDAT*. Memorandum to L.H. Brush, March 10, 2003, ERMS 526372.

Grenthe, I., X. Gaona, A.V. Plyasunov, L. Rao, W.H. Runde, B. Grambow, R.J.M. Konings, A.L. Smith, and E.E. Moore. 2020. *Second Update on the Chemical Thermodynamics of Uranium Neptunium Plutonium Americium and Technetium*. OECD Nuclear Energy Agency Data Bank, Eds., OECD Publications, Boulogne-Billancourt, France.

Guillaumont, R., T. Fanghänel, V. Neck, J. Fuger, D.A. Palmer, I. Grenthe and M.H. Rand. 2003. *Update on the Chemical Thermodynamics of Uranium, Neptunium, Plutonium, Americium and Technetium.* OECD Nuclear Energy Agency Data Bank, Eds., OECD Publications, Issy-les-Moulineaux, France.

Harvie, C.F., N. Møller, and J.H. Weare. 1984. The prediction of mineral solubilities in natural waters: The Na-K-Mg-Ca-H-Cl-SO4-OH-HCO_3-CO_3-CO_2-H_2O system to high ionic strengths at 25°C *Geochimica Cosmochimica Acta* 48:723-751.

Hinz, K., M. Altmaier, X. Gaona, T. Rabung, D. Schild, M. Richmann, D. Reed, E. Alekseev, and H. Geckeis. 2015. Interaction of Nd(III) and Cm(III) with borate in dilute to concentrated alkaline NaCl, $MgCl_2$ and $CaCl_2$ solutions: solubility and TRLFS studies. *New Journal of Chemistry* 39:849-859.

Hummel, W., G. Anderegg, I. Puigdomènech, L. Rao, and O. Tochiyama. 2005. *Chemical Thermodynamics of Compounds and Complexes of U, Np, Pu, Am, Tc, Zr, Ni and Se with Selected Organic Ligands*. Chemical Thermodynamics, Volume 9, OECD Nuclear Energy Agency, Data Bank, Issy-les-Moulineaux, France, Elsevier B.B. Amsterdam, The Netherlands, p. 1088.

Jang, J.-H. 2017. *Solubility Model for Ferrous Iron Hydroxide, Hibbingite, Siderite, and Chukanovite in High Saline Solutions of Sodium Chloride, Sodium Sulfate, and Sodium Carbonate*. Sandia National Laboratories, Carlsbad, New Mexico. SAND2017-12502J.

Jang, J.-H. 2019. *AP-182, Analysis Plan for Derivation and Addition of Equilibrium Constants and Pitzer Interaction Parameters to the WIPP Geochemical Thermodynamic Database*. Revision 0. Sandia National Laboratories, Carlsbad, New Mexico.

Jang, J.-H. and P.S. Domski. 2016. *AP-176, Analysis Plan for the Development of a Self-Consistent Extension of the WIPP Geochemical Thermodynamic Database that Includes Aqueous Ferrous Iron Chemistry.* Revision 0. Sandia National Laboratories, Carlsbad, New Mexico.

Jang, J.-H. and S. Kim. 2016. *Derivation of Pitzer Interaction Parameters and Thermodynamic Properties for the Aqueous Species of Ferrous Iron and Their Pairs*, Revision 2. Sandia National Laboratories, Carlsbad, NM.

Kim, S., C. Marrs, M. Nemer, and J.-H. Jang. 2017. Solubility Model for Ferrous Iron Hydroxide, Hibbingite, Siderite, and Chukanovite in High Saline Solutions of Sodium Chloride, Sodium Sulfate, and Sodium Carbonate. *ACS Earth and Space Chemistry* 1:647−663.

Kim, H.-K., S. Choi, E.C. Jung, H.-R. Cho, J.I. Yun, and W. Cha. 2018. TRLFS study of hydrolyzed Eu(III) species. *Journal of Luminescence* 202:469-474.

Kim, S., P.S. Domski, and L.M. Feng. 2020. *Impact Analysis of Corrected Actinide (Ill) Baseline Solubility Parameters on Performance Assessments.* Sandia National Laboratories, Carlsbad, New Mexico, ERMS 572507.

Kirkes, L., T. Olivas, J.-H. Jang, S. Kim, and Y. Xiong. 2014. *Third Milestone Report on Test Plan TP 08-02, Iron, Lead, Sulfide, and EDTA Solubilities*. Revision 2. Sandia National Laboratories, Carlsbad, New Mexico, ERMS 562947.

Knerr, R. 2020a. *Response 3 to U.S. Environmental Protection Agency's 2019 Compliance Recertification Application Completeness Comments Letter dated March 23, 2020 and May 6, 2020from Tom Peake to Mike Brown*. U.S. Department of Energy, Carlsbad Field Office, Carlsbad, New Mexico. Letter to L.B. Veal, U.S. Environmental Protection Agency Radiation Protection Division, Washington, D.C. August 13, 2020.

Knerr, R. 2020b. *Response 4 to U.S. Environmental Protection Agency's 2019 Compliance Recertification Application Completeness Comments Letter dated March 23, 2020 from Tom Peake to Mike Brown*. U.S. Department of Energy, Carlsbad Field Office, Carlsbad, New Mexico. Letter to L.B. Veal, U.S. Environmental Protection Agency Radiation Protection Division, Washington, D.C. September 15, 2020.

Knerr, R. 2020c. *Response 5 to U.S. Environmental Protection Agency's 2019 Compliance Recertification Application Completeness Comments Letter dated May 6, 2020 and June 12, 2020 from Tom Peake to Mike Brown*. U.S. Department of Energy, Carlsbad Field Office, Carlsbad, New Mexico. Letter to L.B. Veal, U.S. Environmental Protection Agency Radiation Protection Division, Washington, D.C. October 19, 2020.

Knerr, R. 2020d. *Response 6 to U.S. Environmental Protection Agency's 2019 Compliance Recertification Application Completeness Comments Letter dated March 23, 2020 from Tom Peake to Mike Brown*. U.S. Department of Energy, Carlsbad Field Office, Carlsbad, New Mexico. Letter to L.B. Veal, U.S. Environmental Protection Agency Radiation Protection Division, Washington, D.C. October 26, 2020.

Knerr, R. 2021a. *Response 8 to U.S. Environmental Protection Agency's 2019 Compliance Recertification Application Completeness Comments Letter dated September 11, 2020 and November 13, 2020 from Tom Peake to Mike Brown*. U.S. Department of Energy, Carlsbad Field Office, Carlsbad, New Mexico. Letter to L.B. Veal, U.S. Environmental Protection Agency Radiation Protection Division, Washington, D.C. January 13, 2020.

Knerr, R. 2021b. *Response 9 to U.S. Environmental Protection Agency's 2019 Compliance Recertification Application Completeness Comments Letter dated September 11, 2020 and November 13, 2020 from Tom Peake to Mike Brown*. U.S. Department of Energy, Carlsbad Field Office, Carlsbad, New Mexico. Letter to L.B. Veal, U.S. Environmental Protection Agency Radiation Protection Division, Washington, D.C. March 4, 2020.

Knerr, R. 2021c. *Response 10 to U.S. Environmental Protection Agency's 2019 Compliance Recertification Application Completeness Comments Letter dated September 11, 2020 and November 13, 2020 from Tom Peake to Mike Brown*. U.S. Department of Energy, Carlsbad Field Office, Carlsbad, New Mexico. Letter to L.B. Veal, U.S. Environmental Protection Agency Radiation Protection Division, Washington, D.C. March 30, 2020.

Knerr, R. 2021d. *Response SOTERM 3 to U.S. Environmental Protection Agency's 2019 Compliance Recertification Application Completeness Comments Letter dated March 23, 2020, from Tom Peake to Mike Brown*. U.S. Department of Energy, Carlsbad Field Office, Carlsbad, New Mexico. Letter to L.B. Veal, U.S. Environmental Protection Agency Radiation Protection Division, Washington, D.C. May 20, 2021.

Königsberger, E., L.-C. Königsberger, and H. Gamsjäger. 1999. Low-temperature thermodynamic model for the system Na_2CO_3 – $MgCO_3$ – $CaCO_3$ – H_2O. *Geochimica Cosmochimica Acta* 19/20:3105-3119.

Könnecke, T., T. Fanghänel and J.I. Kim. 1997. Thermodynamics of trivalent actinides in concentrated electrolyte solutions: modelling the chloride complexation of Cm(III). *Radiochimica Acta* 76:131-135.

Lemire, R.J., U. Berner, C. Musikas, D.A. Palmer, P. Taylor, and O. Tochiyama. 2013. *Chemical Thermodynamics of Iron, Part 1*. OECD Nuclear Energy Agency Data Bank, Eds., OECD Publications, Issy-les-Moulineaux, France.

MacLeod, I. 1991. Identification of corrosion products on non-ferrous metal artifacts recovered from shipwrecks. *Studies in Conservation* 36:222-234.

Mathur, J.N., K. Cernochova, and G.R. Choppin. 2007. Thermodynamics and laser luminescence spectroscopy of binary and ternary complexation of Am^{3+}, Cm^{3+} and Eu^{3+} with citric acid, and citric acid + EDTA at high ionic strength. *Inorganica Chimica Acta* 360:1785-1791.

Mizera, J., A.H. Bond, G.R. Choppin and R.C. Moore. 1999. Dissociation constants of carboxylic acids at high ionic strengths. In *Actinide Speciation in High Ionic Strength Media*, eds. Reed et al., Kluwer Academic/Plenum Publishers, New York, pp. 113-124.

Moog, H. C., and S. Hagemann. 2004. *Thermodynamic Modeling in High-Saline solutions: Data for Fe(II), Fe(III), and S(-II) and Development of a Program for the Modelling of Reactive Transport Within the Near Field of a Repository*. Volume number: GRS-195, Final report for a project funded by the Federal Ministry for Economy and Technology (BMWA), Funding number 02 E 9138.

Moore, R.C., M. Borkowski, M. Bronikowski, J.-F. Chen, O.S. Pokrovsky, Y.X. Xia and G.R. Choppin. 1999. Thermodynamic modeling of actinide complexation with acetate and lactate at high ionic strength. *Journal of Solution Chemistry* 28:521-531.

Morss, L.R. and C.W. Williams. 1994. Synthesis of crystalline americium hydroxide, $Am(OH)_3$ and determination of its enthalpy of formation; estimation of the solubility-product constants of actinide(III) hydroxides. *Radiochimica Acta* 66-67:89-94.

Neck, V., R. Müller, M. Bouby, M. Altmaier, J. Rothe, M.A. Denecke, and J.I. Kim. 2002. Solubility of Amorphous Th(IV) Hydroxide-Application of LIBD to Determine the Solubility Product and EXAFS for Aqueous Speciation. *Radiochimica Acta* 90:485-494.

Neck, V., M. Altmaier, T. Rabung, J. Lützenkirchen and T. Fanghänel. 2009. Thermodynamics of trivalent actinides and neodymium in NaCl, $MgCl_2$, and $CaCl_2$ solutions: solubility, hydrolysis, and ternary Ca-M(III)-OH complexes. *Pure and Applied Chemistry* 81:1555-1568.

Nemer, M., Y. Xiong, A.E. Ismail, and J. Jang. 2011. Solubility of $Fe_2(OH)_3Cl$ (pure-iron end-member of hibbingite) in NaCl and Na_2SO_4 brines. *Chemical Geology* 280:26-32.

North, N.A., and I.D. MacLeod. 1987. Corrosion of metals. In *Corrosion of Marine Archaeological Objects*, Ed. C. Pearson, Butterworths, London, pp. 68-98.

Novak, C.F. 1996. *Preliminary Inorganic Model for Thorium Solubility in WIPP brines, in Database File HMW_3Th5_960119.CHEMDAT*. Memo to E. J. Nowak, 19 January 1996, Albuquerque, NM.

Novak, C.F. and R.C. Moore. 1996. *Estimates of Dissolved Concentrations for +III, +IV, +V, and +VI Actinides in a Salado and a Castile Brine under Anticipated Repository Conditions*. Memo to M.D. Siegel, March 28, 1996, Sandia National Laboratories, Albuquerque, New Mexico, CCA Ref. No. 479.

Nowak, E.J. 2005. *Recommended Change in the FMT Thermodynamic Data Base.* Memorandum to L.H. Brush, April 1, Sandia National Laboratories, Carlsbad, New Mexico, ERMS 539227.

Oakes, C.S., A.L. Ward, N. Chugunov, and J. Icenhower. 2021. A speciated, conventional Pitzer ion-interaction model for the aqueous Nd^{3+} - H^+ - Na^+ - K^+ - Ca^{2+} - Cl^- - OH^- system at 298 K and 0.1 MPa. *Geochimica Cosmochimica Acta* 297:308-327.

Parkhurst, D.L., and C.A.J. Appelo. 2013. Description of input and examples for PHREEQC version 3—a computer program for speciation, batch-reaction, one-dimensional transport, and inverse geochemical calculations. *U.S. Geological Survey, Chapter 43 of Section A, Groundwater; Book 6, Modeling Techniques*. https://pubs.er.usgs.gov/publication/tm6A43

Peake, T. 2020a. *First Set of EPA Completeness Comments and Questions for Compliance Recertification Application 2019 (CRA-2019).* U.S. Environmental Protection Agency, Center for Waste Management and Regulation, Washington, D.C. Letter to M. Brown, U.S. Department of Energy, Carlsbad Field Office, Carlsbad, New Mexico, March 23, 2020.

Peake, T. 2020b. *Second Set of EPA Completeness Comments and Questions for Compliance Recertification Application 2019 (CRA-2019).* U.S. Environmental Protection Agency, Center for Waste Management and Regulation, Washington, D.C. Letter to M. Brown, U.S. Department of Energy, Carlsbad Field Office, Carlsbad, New Mexico, May 6, 2020.

Peake, T. 2020c. *Fifth Set of EPA Completeness Comments and Questions for Compliance Recertification Application 2019 (CRA-2019).* U.S. Environmental Protection Agency, Center

for Waste Management and Regulation, Washington, D.C. Letter to M. Brown, U.S. Department of Energy, Carlsbad Field Office, Carlsbad, New Mexico, September 11, 2020.

Peake, T. 2020d. *Sixth Set of EPA Completeness Comments and Questions for Compliance Recertification Application 2019 (CRA-2019).* U.S. Environmental Protection Agency, Center for Waste Management and Regulation, Washington, D.C. Letter to M. Brown, U.S. Department of Energy, Carlsbad Field Office, Carlsbad, New Mexico, November 13, 2020.

Pitzer, K.S., and L.F. Silvester. Thermodynamics of electrolytes. 11. Properties of 3:2, 4:2, and other high-valence types. *The Journal of Physical Chemistry* 82:1239-1242.

Pokrovsky, O.S., and G.R. Choppin. 1997. Neptunium(V) complexation by acetate, oxalate and citrate in $NaClO_4$ media at 25°C. *Radiochimica Acta* 79:167-171.

Pokrovsky, O.S., M. Bronikowski, R.C. Moore and G.R. Choppin. 1998. Interaction of neptunyl(V) and uranyl(V1) with EDTA in NaCl media: Experimental study and Pitzer modeling. *Radiochimica Acta* 80:23-29.

Powell, K. J., P. L. Brown, R. H. Byrne, T. Gajda, G. Hefter, A.-K Luez, S. Sjoberg, and H. Wanner. 2009. Chemical speciation of environmentally significant metals with inorganic ligands. Part 3: the Pb^{2+} + OH^-, Cl^-, CO_3^{2-}, SO_4^{2-}, and PO_4^{3-} systems (IUPAC Technical Report). *Pure and Applied Chemistry* 81:2425-2476.

Rabung, T., M. Altmaier, V. Neck and T. Fanghänel. 2008. A TRLFS study of Cm(III) hydroxide complexes in alkaline $CaCl_2$ solutions. *Radiochimica Acta* 96:551-560.

Rai, D., A.R. Felmy, and R.W. Fulton. 1992. Solubility and ion activity product of $AmPO_4 \bullet xH_2O$(am). *Radiochimica Acta* 56:7-14.

Rai, D., D.A. Moore, C.S. Oakes, and M. Yui. 2000. Thermodynamic model for the solubility of thorium dioxide in the Na^+-Cl^--OH^--H_2O system at 23°C and 90°C. *Radiochimica Acta* 88:297-306.

Rand, M., J. Fuger, I. Grenthe, V. Neck, and D. Rai. 2008. *Chemical Thermodynamics of Thorium.* OECD Nuclear Energy Agency Data Bank, Eds., OECD Publications, Issy-les-Moulineaux, France.

Rao, L.F., D. Rai and A.R. Felmy. 1996a. Solubility of $Nd(OH)_3$(c) in 0.1 M NaCl aqueous solution at 25°C and 90°C. *Radiochimica Acta* 72:151-155.

Rao, L.F., D. Rai A.R. Felmy, R.W. Fulton and C.F. Novak. 1996b. Solubility of $NaNd(CO_3)_3 \bullet 6H_2O$(c) in concentrated Na_2CO_3 and $NaHCO_3$ solutions at 25°C and 90°C. *Radiochimica Acta* 75:141-147.

Rao, L., P. Zanonato, and P. Di Bernardo. 2005. Interaction of actinides with carboxylates in solution: Complexation of U(VI), Th(IV), and Nd(III) with acetate at variable temperatures. *Journal of Nuclear and Radiochemical Sciences* 6:31−37.

Rizkalla, E.N., F. Nectoux, S. Dabos-Seignon, and M. Pagès. 1990. Complexation of neptunium(V) by halo- and hydroxycarboxylate ligands. *Radiochimica Acta* 51:113-117.

Robie, R.A. and B.S. Hemingway. 1973. The enthalpies of formation of nesquehonite, $MgCO_3 \cdot 3H_2O$, and hydromagnesite, $5MgO \cdot 4CO_2 \cdot 5H_2O$. *Journal of Research of the U.S. Geological Survey* 1:543-547.

Runde, W., and J.I. Kim. 1994. *Untersuchungen der Übertragbarkeit von Labordaten Natürliche Verhältnisse: Chemisches Verhalten von Drei- und Fünfwertigem Americium in Salinen NaCl-Lösungen (Study of the Extrapolability of Laboratory Data to Natural Conditions: Chemical Behavior of Trivalent and Pentavalent Americium in Saline NaCl Solutions).* RCM-01094, Institute for Radiochemistry, Technical University of Munich, Munich, Federal Republic of German, ERMS 241862.

Ryan J.L. and D. Rai. 1987. Thorium(IV) hydrous oxide solubility. *Inorganic Chemistry* 26:4140-4142.

SC&A (S. Cohen & Associates). 2008. *Verification of the Waste Isolation Pilot Plant Chemistry Conceptual Models*. Prepared for the U.S. Environmental Protection Agency Office of Radiation and Indoor Air, September 19, 2008.

SC&A (S. Cohen and Associates). 2011. *EQ3/6 Computer Code Evaluation*. Prepared for U.S. Environmental Protection Agency Office of Radiation and Indoor Air. Draft March 2011.

Shock, E.L., D.C. Sassani, M. Willis, and D.A. Sverjensky. 1997.Inorganic species in geologic fluids: Correlations among standard molal thermodynamic properties of aqueous ions and hydroxide complexes. *Geochimica Cosmochimica Acta*, 61 (5) 907-950.

Silva, R.J. 1982. *Thermodynamic Properties of Chemical Species in Nuclear Waste, Topical Report, The Solubilities of Crystalline Neodymium and Americium Trihydroxides*. Lawrence Berkeley Laboratory, LBL-15055.

Sisk-Scott, C. 2019. *AP-183, Analysis Plan to Update the WIPP Geochemical Thermodynamic Database (DATA0.FM1) to DATA0.FM4 for CRA-2019*. Revision 1, Carlsbad, NM Sandia National Laboratories.

Snider, A.C. 2002. MgO Studies: Experimental Work Conducted at SNL/Carlsbad. Efficacy of Premier Chemicals MgO as an Engineered Barrier, *Sandia National Laboratories Technical Baseline Reports, WBS 1.3.5.3, Compliance Monitoring; WBS 1.3.5.4, Repository Investigations, Milestone RI110, January 31, 2002.* Sandia National Laboratories, Carlsbad, New Mexico. ERMS 520467, pp. 3.1-1 to 3.1-18.

Stumm, W., and J.J. Morgan. 1996. *Aquatic Chemistry*, 3rd ed.; John Wiley and Sons.

Thakur, P., Y. Xiong, M. Borkowski, and G.R. Choppin. 2012. Thermodynamic modeling of trivalent Am, Cm and Eu-citrate complexation in concentrated $NaClO_4$ media. *Radiochimica Acta* 100:165-172.

Thakur, P., Y. Xiong, and M. Borkowski. 2015. *An Improved Thermodynamic Model for the Complexation of Trivalent Actinides and Lanthanide with Oxalic Acid Valid to High Ionic Strength*. Sandia National Laboratories, Carlsbad, New Mexico, SAND2015-6902J.

Van Soest, G.D. 2018. *Performance Assessment Inventory Report – 2018*. Los Alamos National Laboratory Carlsbad Operations INV-PA-18, Revision 0, December 12, 2018.

Wall, N.A., M. Borkowski, J.-F. Chen, and G.R. Choppin. 2002. Complexation of americium with humic, fulvic and citric acids at high ionic strength. *Radiochimica Acta* 90:563-568.

Willberger, C., D. Leichtfuβ, S. Amayri, and T. Reich. 2019. Determination of the Stability Constants of the Acetate Complexes of the Actinides Am(III), Th(IV), Np(V), and U(VI) Using Capillary Electrophoresis-Inductively Coupled Plasma Mass Spectrometry. *Inorganic Chemistry* 58:4851-4858.

Wilson, C., D. Porter, J. Gibbons, E. Oswald, G. Sjoblom, and F. Caporuscio. 1996. *Conceptual Models Peer Review Report*. Prepared for the U.S. Department of Energy, Carlsbad, New Mexico, July 1996, Docket No. A-93-02 Item II-G-1.

Xiong, Y.-L. 2004a. *A Correction of the Dimensionless Standard Chemical Potential of NpO2Ac(aq) in FMT_041116.CHEMDAT*. Memorandum to L.H. Brush, December 6, 2004, Sandia National Laboratories, Carlsbad, New Mexico, ERMS 538162.

Xiong, Y.-L. 2004b. *A Correction of the Molecular Weight of Oxalate in FMT_021120.CHEMDAT and Incorporation of Calcium Oxalate Monohydrate (Whewellite) Into CHEMDAT With Its Recommended Dimensionless Standard Chemical Potential (μ^0/RT) Value*. Memorandum to L.H. Brush, June 8, 2004, Sandia National Laboratories, Carlsbad, New Mexico, ERMS 535813.

Xiong, Y.-L. 2005. *Release of FMT_050405.CHEMDAT*. E-mail to J.F. Kanney and J.J. Long, April 5, 2005, Sandia National Laboratories, Carlsbad, New Mexico, ERMS 539304.

Xiong, Y. 2009. *Release of FMT_090720.CHEMDAT*. E-mail to J.J. Long, July 22, 2009, Sandia National Laboratories, Carlsbad, New Mexico, ERMS 539304.

Xiong, Y. 2011. *Release of EQ3/6 Database DATA0.FM1*. Email to J.J. Long, March 9, 2011, Sandia National Laboratories, Carlsbad, New Mexico, ERMS 555152.

Xiong, Y. 2013a. *AP-154, Analysis Plan for Derivation of Thermodynamic Properties Including Pitzer Parameters for Solubility Studies of Iron, Lead and EDTA*. Revision 2. Sandia National Laboratories, Carlsbad, New Mexico, ERMS 561114.

Xiong, Y. 2013b. *Experimental Determination of Solubilities of Crystalline Lead Oxalate, $PbC_2O_4(cr)$, in the NaCl-H_2O System*. Sandia National Laboratories, Carlsbad, New Mexico, ERMS 560651.

Xiong, Y. 2014a. *Experimental and Thermodynamic Modeling of $PbCit^-$ Interactions in NaCl and $MgCl_2$ Solutions*. Sandia National Laboratories, Carlsbad, New Mexico, ERMS 562836.

Xiong, Y. 2014b. *Experimental and Thermodynamic Modeling of $PbEDTA^{2-}$ Interactions in NaCl and $MgCl_2$ Solutions*. Sandia National Laboratories, Carlsbad, New Mexico, ERMS 562877.

Xiong, Y. 2015a. *Experimental and Thermodynamic Modeling Solubility of Cerussite, $PbCO_3$(s), in the Carbonate System to High Ionic Strengths.* Revision 1, Supersedes ERMS 561917 Sandia National Laboratories, Carlsbad, New Mexico, ERMS 564929.

Xiong, Y.-L. 2015b. Experimental determination of lead carbonate solubility at high ionic strengths: a Pitzer model description. *Monatshefte für Chemie* 146:1433-1443.

Xiong, Y. 2015c. *Recalculation of Solubility Constants of Synthetic Hydromagnesite(5424) Using the Pitzer Model.* Sandia National Laboratories, Carlsbad, New Mexico, ERMS 564356.

Xiong, Y. 2017. Solution chemistry for actinide borate species to high ionic strengths: Equilibrium constants for $AmHB_4O_7^{2+}$ and $AmB_9O_{13}(OH)_4$(cr) and their importance to nuclear waste management. *MRS Advances* 2:741–746.

Xiong, Y. 2018. *Experimental Determination Of Solubilities Of Lead Oxalate (PbC_2O_4), Di-calcium Ethylenediaminetetraacetic Acid Hydrate ($Ca_2EDTA•7H_2O$(s)) in $MgC1_2$-H_2O System, and Earlandite ($Ca_3[C_3H_5O(COO)_3]_2•4H_2O$) in NaCl-$H_2O$ and $MgC1_2$-H_2O systems, and Their Respective Pitzer Interaction Parameters, Revision 3,* Supersedes ERMS 567810. Carlsbad, NM: Sandia National Laboratories. ERMS 570088.

Xiong, Y., H. Deng, M.B. Nemer and S. Johnsen. 2009. *Thermodynamic Data for Phase 5 ($Mg_3Cl(OH)_5•4H_2O$) Determined from Solubility Experiments.* Memorandum to L.H. Brush, May 8, 2009, Sandia National Laboratories, Carlsbad, New Mexico, ERMS 551706.

Xiong, Y., H. Deng, M. Nemer and S. Johnsen. 2010. Experimental determination of the solubility constant for magnesium chloride hydroxide hydrate ($Mg_3Cl(OH)_5•4H_2O$, Phase 5) at room temperature, and its Importance to nuclear waste isolation in geological repositories in salt formations. *Geochimica et Cosmochimica Acta* 74:4605-4611.

Xiong, Y. L. Kirkes, C. Marrs, and J. Knox. 2017a. Am(III)/Nd(III) interactions with borate: experimental investigations of $Nd(OH)_3$(micro cr) solubility in NaCl solutions in equilibrium with borax. *6th East Asia Forum on Radwaste Management*, November 27-29, 2017, Osaka, Japan.

Xiong, Y. L. Kirkes, and C. Marrs. 2017b. Long-term experimental determination of solubilities of micro-crystalline Nd(III) hydroxide in high ionic strength solutions: applications to nuclear waste management. *Aquatic Geochemistry* 23:359-375.

Attachment C: CRA-2019 Sensitvity Calculation Parameters

EPA performed sensitivity calculations to examine the effects on repository releases of geochemistry parameter changes recommended based on the results of the CRA-2019 review (Section 13.4). The following parameters were revised in these calculations:

1. Actinide oxidation states: Pu(III), Np(IV), and U(IV) (GLOBAL:OXSTAT, Table C-1)
2. Baseline actinide solubilities: EPA-recalculated baseline solubilities (Table C-2)
3. +III actinide solubility uncertainty distribution: +III actinide solubility uncertainty distribution updated with recent data (Tables C-1 and C-3)
4. Colloid parameters: revised parameters for Am(III) intrinsic colloid concentrations, Th(IV) intrinsic colloid concentrations, microbial colloid proportionality constants, and microbial colloid maximum concentration limits (Table C-4)

Table C-1. Revised Sampled Oxidation State and Am(III) Solubility Uncertainty Parameters

Parameter	Attribute	CRA-2019 DPA	CRA-2019 Sensitivity PA
GLOBAL:OXSTAT	Distribution	Uniform	Uniform
	Maximum	1.00	0.1
	Mean	0.50	0.05
	Median	0.50	0.05
	Minimum	0.00	0.00
	Standard Deviation	0.289	0.0289
SOLMOD3:SOLVAR	Distribution	Cumulative	Cumulative
	Maximum	2.97	3.44
	Mean	0.64	1.16
	Median	0.346	1.24
	Minimum	-1.14	-1.14
	Standard Deviation	0.978	1.18

Table C-2. Revised Actinide Solubility Parameters

Actinide	Brine	Brine Volume	Parameter	CRA-2019 DPA (M)	CRA-2019 Sensitivity PA (M)
Am(III)	Salado	1×	SOLMOD3:SOLSOH	1.78×10^{-7}	2.139×10^{-6}
Am(III)	Salado	2×	SOLMOD3:SOLSOH2	1.63×10^{-7}	1.093×10^{-6}
Am(III)	Salado	3×	SOLMOD3:SOLSOH3	1.58×10^{-7}	7.736×10^{-7}
Am(III)	Salado	4×	SOLMOD3:SOLSOH4	1.54×10^{-7}	6.193×10^{-7}
Am(III)	Salado	5×	SOLMOD3:SOLSOH5	1.52×10^{-7}	5.277×10^{-7}
Am(III)	Castile	1×	SOLMOD3:SOLCOH	1.78×10^{-7}	1.429×10^{-6}
Am(III)	Castile	2×	SOLMOD3:SOLCOH2	1.63×10^{-7}	7.263×10^{-7}
Am(III)	Castile	3×	SOLMOD3:SOLCOH3	1.58×10^{-7}	5.164×10^{-7}
Am(III)	Castile	4×	SOLMOD3:SOLCOH4	1.54×10^{-7}	4.158×10^{-7}
Am(III)	Castile	5×	SOLMOD3:SOLCOH5	1.52×10^{-7}	3.563×10^{-7}
Th(IV)	Salado	1×	SOLMOD4:SOLSOH	5.45×10^{-8}	5.497×10^{-8}
Th(IV)	Salado	2×	SOLMOD4:SOLSOH2	5.45×10^{-8}	5.509×10^{-8}
Th(IV)	Salado	3×	SOLMOD4:SOLSOH3	5.45×10^{-8}	5.513×10^{-8}
Th(IV)	Salado	4×	SOLMOD4:SOLSOH4	5.45×10^{-8}	5.515×10^{-8}
Th(IV)	Salado	5×	SOLMOD4:SOLSOH5	5.45×10^{-8}	5.517×10^{-8}
Th(IV)	Castile	1×	SOLMOD4:SOLCOH	5.44×10^{-8}	5.836×10^{-8}
Th(IV)	Castile	2×	SOLMOD4:SOLCOH2	5.44×10^{-8}	5.844×10^{-8}
Th(IV)	Castile	3×	SOLMOD4:SOLCOH3	5.44×10^{-8}	5.847×10^{-8}
Th(IV)	Castile	4×	SOLMOD4:SOLCOH4	5.44×10^{-8}	5.848×10^{-8}
Th(IV)	Castile	5×	SOLMOD4:SOLCOH5	5.44×10^{-8}	5.849×10^{-8}
Np(V)	Salado	1×	SOLMOD5:SOLSOH	4.02×10^{-7}	4.375×10^{-7}
Np(V)	Salado	2×	SOLMOD5:SOLSOH2	2.83×10^{-7}	3.216×10^{-7}
Np(V)	Salado	3×	SOLMOD5:SOLSOH3	2.42×10^{-7}	2.822×10^{-7}
Np(V)	Salado	4×	SOLMOD5:SOLSOH4	2.21×10^{-7}	2.626×10^{-7}
Np(V)	Salado	5×	SOLMOD5:SOLSOH5	2.09×10^{-7}	2.507×10^{-7}
Np(V)	Castile	1×	SOLMOD5:SOLCOH	1.20×10^{-6}	1.822×10^{-6}
Np(V)	Castile	2×	SOLMOD5:SOLCOH2	7.27×10^{-7}	1.416×10^{-6}
Np(V)	Castile	3×	SOLMOD5:SOLCOH3	5.52×10^{-7}	1.278×10^{-6}
Np(V)	Castile	4×	SOLMOD5:SOLCOH4	4.61×10^{-7}	1.209×10^{-6}
Np(V)	Castile	5×	SOLMOD5:SOLCOH5	4.05×10^{-7}	1.168×10^{-6}
U(VI)	Salado	all	SOLMOD6:SOLSOH	1.00×10^{-3}	1.000×10^{-3}
U(VI)	Castile	all	SOLMOD6:SOLCOH	1.00×10^{-3}	1.000×10^{-3}

Table C-3. Revised Actinide Solubility Uncertainty Distribution Function

From AN(III)_CC1-GEOCHEM-1_Supplemental_Uncertainty.xlsx (Knerr 2021f)

D	P(D<X)
-1.1425098036	0.00645
-0.9323583436	0.01290
-0.8759538359	0.01935
-0.8056760430	0.02581
-0.6946808515	0.03226
-0.6778551785	0.03871
-0.6658045741	0.04516
-0.5665296399	0.05161
-0.5629724056	0.05806
-0.4879508573	0.06452
-0.4869709875	0.07097
-0.4426710373	0.07742
-0.4176173040	0.08387
-0.3768260745	0.09032
-0.2916416520	0.09677
-0.2321098716	0.10323
-0.2288850394	0.10968
-0.2025332927	0.11613
-0.1660768392	0.12258
-0.1605316898	0.12903
-0.1383757027	0.13548
-0.1264324499	0.14194
-0.1221784634	0.14839
-0.1147710934	0.15484
-0.1123312845	0.16129
-0.1083482987	0.16774
-0.1055148830	0.17419
-0.1000040344	0.18065
-0.0791883871	0.18710
-0.0693641105	0.19355
-0.0252010379	0.20000
0.0070303144	0.20645
0.0489933394	0.21290
0.0490385651	0.21935
0.0498063297	0.22581
0.0741358853	0.23226

D	P(D<X)
0.0741358853	0.23871
0.1060913696	0.24516
0.1556772397	0.25161
0.1603940909	0.25806
0.1829055533	0.26452
0.1938630604	0.27097
0.2150511210	0.27742
0.2406448036	0.28387
0.2543261176	0.29032
0.3130252108	0.29677
0.3300905486	0.30323
0.3383038956	0.30968
0.3463571505	0.31613
0.3562446968	0.32258
0.3833934009	0.32903
0.4242932001	0.33548
0.4631238859	0.34194
0.4818834998	0.34839
0.5083089020	0.35484
0.57034140	0.36129
0.57395140	0.36774
0.57835654	0.37419
0.6015537547	0.38065
0.6448105283	0.38710
0.6495759476	0.39355
0.6510243696	0.40000
0.6608468037	0.40645
0.6684537873	0.41290
0.6852822681	0.41935
0.7015820729	0.42581
0.7493903661	0.43226
0.7555140746	0.43871
0.7782050165	0.44516
0.7886658363	0.45161
0.8015796711	0.45806
0.8020899908	0.46452
0.8112685689	0.47097
0.8502723482	0.47742
0.8567192414	0.48387
0.8684401437	0.49032

D	P(D<X)
0.8899532533	0.49677
0.9190161285	0.50323
0.9336411831	0.50968
0.9529695408	0.51613
1.02553722	0.52258
1.0287195184	0.52903
1.0685670059	0.53548
1.0954348241	0.54194
1.1708039870	0.54839
1.2154635050	0.55484
1.2176815674	0.56129
1.2326462571	0.56774
1.2360771386	0.57419
1.2361700938	0.58065
1.26974551	0.58710
1.2859462159	0.59355
1.2952306388	0.60000
1.32749284	0.60645
1.3666032594	0.61290
1.4188595232	0.61935
1.4196737088	0.62581
1.42331141	0.63226
1.4519477124	0.63871
1.48546647	0.64516
1.5189703232	0.65161
1.5572558360	0.65806
1.5702985263	0.66452
1.6437982582	0.67097
1.6722332127	0.67742
1.7036909665	0.68387
1.77286743	0.69032
1.7925659419	0.69677
1.8304580063	0.70323
1.83487657	0.70968
1.85844875	0.71613
1.8687850907	0.72258
1.91464086	0.72903
1.9167888437	0.73548
1.9488067186	0.74194
1.9639350835	0.74839

D	P(D<X)
1.96594122	0.75484
2.0230327749	0.76129
2.02528484	0.767742
2.04899510	0.774194
2.0596522477	0.780645
2.0686151470	0.787097
2.08888928	0.793548
2.09104395	0.8
2.09124580	0.806452
2.09253811	0.812903
2.09794274	0.819355
2.10978733	0.825806
2.11060377	0.832258
2.14475899	0.83871
2.14806225	0.845161
2.16065407	0.851613
2.16127395	0.858065
2.1754390298	0.864516
2.1927200512	0.870968
2.20255008	0.877419
2.23163601	0.883871
2.2517886670	0.890323
2.3436819694	0.896774
2.3729976469	0.903226
2.6279348755	0.909677
2.6834875743	0.916129
2.8164729093	0.922581
2.9591113514	0.929032
2.9714739556	0.935484
3.06925377	0.941935
3.12137396	0.948387
3.13777928	0.954839
3.19699209	0.96129
3.3024739444	0.967742
3.32439635	0.974194
3.36185140	0.980645
3.36431423	0.987097
3.42406377	0.993548
3.43784635	1

Table C-4. Revised Intrinsic Colloid and Microbial Colloid Parameters

Parameter	Units	CRA-2019 DPA	CRA-2019 Sensitivity PA
AM:CONCINT	M	9.50E-09	6.70E-07
TH:CONCINT	M	4.30E-08	4.80E-07
AM:CAPMIC	M	2.30E-09	6.28E-06
NP:CAPMIC	M	3.80E-08	1.27E-04
PU:CAPMIC	M	3.80E-08	2.18E-05
TH:CAPMIC	M	3.80E-08	2.12E-02
U:CAPMIC	M	3.80E-08	8.14E+00
AM:PROPMIC	none	0.3	3.6
NP:PROPMIC	none	0.21	12
PU:PROPMIC	none	0.21	2.18
TH:PROPMIC	none	0.21	3.1
U:PROPMIC	none	0.21	0.0021

Attachment D: PHREEQC QA Summary Report

1.0 QA CHECKS ON DATABASE CONVERSION (TASK 4B)

1.1 SUMMARY PHREEQC DATABASE CONVERSION CHECK

Copies of the original EQ3/6 database file (data0.FM4) and the converted database file for PHREEQC (DATA0FM4.dat) were compared side by side in a text editor. At least 25 values from each of aqueous species stability constants, solids solubility constants, and Pitzer ion interaction parameters were selected at random and compared across the two files. The database file line in each, the parameter, parameter value, agreement, and reference were compiled into a spreadsheet. For the Pitzer parameters, the most impactful are alpha and beta values, so those were selected. These data tables for each along with screenshot examples follow:

Table 2. Aqueous species stability constants database comparison

EQ3/6	PHREEQ					
Line	**Line**	**Species**	**Paramete**	**Value in**	**Values**	**Reference**
5626	239	PbCl+	log_k	-1.5	Y	Powell et al., 2009 Derived with SIT Model
5780	294	Fe(CO3)2--	log_k	13.89	Y	Kim et al. 2017
5856	234	MgOH+	log_k	11.8091	Y	no ref listed
5765	274	PbSO4(aq)	log_k	-2.72	Y	Powell et al., 2009 Derived with SIT Model
5916	206	CO2(aq)	log_k	-6.3374	Y	no ref listed
5976	218	B3O3(OH)4	log_k	-20.1893	Y	no ref listed
6038	330	H3PO4(aq)	log_k	-9.3517	Y	no ref listed
6128	431	AmOH++	log_k	7.556	Y	no ref listed
6188	443	AmCl2+	log_k	0.74	Y	no ref listed
6233	446	AmSO4+	log_k	-3.2485	Y	no ref listed
6325	503	NpO2CO3-	log_k	5.3223	Y	no ref listed
6355	509	NpO2(CO3)	log_k	25.6859	Y	no ref listed
6370	512	NpO2OH(a	log_k	11.3085	Y	no ref listed
6400	334	HAcetate(aq	log_k	-4.7568	Y	no ref listed
6415	344	H3Citrate(a	log_k	-14.27	Y	Hummel et al. 2005 Derived with SIT Model
6158	437	Am(OH)3(a	log_k	25.6905	Y	no ref listed
6113	425	Am(CO3)3-	log_k	15.8157	Y	no ref listed
6068	322	PO4---	log_k	12.3426	Y	no ref listed
6053	326	H2PO4-	log_k	-7.2062	Y	no ref listed
5976	218	B3O3(OH)4	log_k	-20.1893	Y	no ref listed
5946	318	MgCO3(aq)	log_k	7.4108	Y	no ref listed
6006	226	CaB(OH)4+	log_k	-1.6503	Y	no ref listed
6022	230	MgB(OH)4	log_k	-1.3993	Y	no ref listed
5931	314	CaCO3(aq)	log_k	7.188	Y	no ref listed
6248	467	Th(CO3)5(6	log_k	24.5828	Y	no ref listed
n=	25					

*PHREEQC has reaction written reversed (association vs. dissociation reaction), so the sign of logK values are opposite of what is in EQ3/6

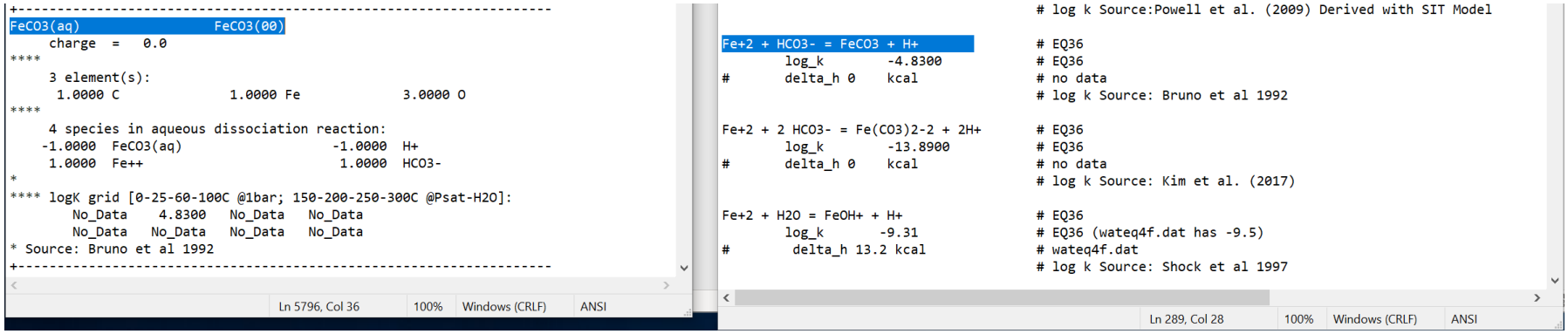

Figure 6. Screenshot of database file comparison, EQ3/6 on left, and converted file for PHREEQC on right.

Table 3. Solids solubility constants database comparison

EQ3/6	PHREE					
Line	**Line**	**Species**	**Paramete**	**Value in**	**Values**	**Reference**
7125	570	Pb2CO3Cl2(s)	log_k	0.41	Y*	Powell et al., 2009 drived with SIT Model
7210	592	MgOxalate.2H2O(s)	log_k	-6.41	Y	Glushinskite from AP-182
8597	986	Hydromagnesite4323	log_k	28.8104	Y	no ref listed
7242	600	Chukanovite	log_k	12.32	Y	Kim et al 2017
7343	624	AmPO4(c)	log_k	-12.4595	N**	no ref listed
7679	714	Arcanite	log_k	-1.7763	Y	no ref listed
8133	860	Natron	log_k	9.5145	Y	no ref listed
8414	935	Thermonatrite	log_k	10.8211	Y	no ref listed
8514	963	Na_Metaborate	log_k	0.3292	Y	no ref listed
8382	926	Tachyhydrite	log_k	17.3839	Y	no ref listed
7373	632	Th(SO4)2.9H2O(s)	log_k	-12.9982	Y	no ref listed
7272	733	Brucite	log_k	17.109	Y	no ref listed
7906	795	Halite	log_k	1.5704	Y	no ref listed
8218	883	Portlandite	log_k	22.8035	Y	no ref listed
8399	930	Thenardite	log_k	-0.2875	Y	no ref listed
8267	896	KNaCO3.6H2O	log_k	10.2233	Y	no ref listed
8101	852	Misenite	log_k	-10.8061	Y	no ref listed

8020	829	Magnesite	log_k	2.5054	Y	no ref listed
7890	790	Gypsum	log_k	-4.5805	Y	no ref listed
7970	816	Kieserite	log_k	-0.1227	Y	no ref listed
7841	776	Epsomite	log_k	-1.8811	Y	no ref listed
7986	821	Leonite	log_k	-3.979	Y	no ref listed
8184	874	Pirssonite	log_k	11.4354	Y	no ref listed
8350	916	Sylvite	log_k	0.8999	Y	no ref listed
8465	951	B(OH)3 or	log_k	-9.2694	Y	no ref listed

n= 25

*reaction written differently, so sign reversed

**EQ3/6 reaction and log_k are listed in terms of dissociation into biphosphate ion. PHREEQC dissociation uses phosphate ion

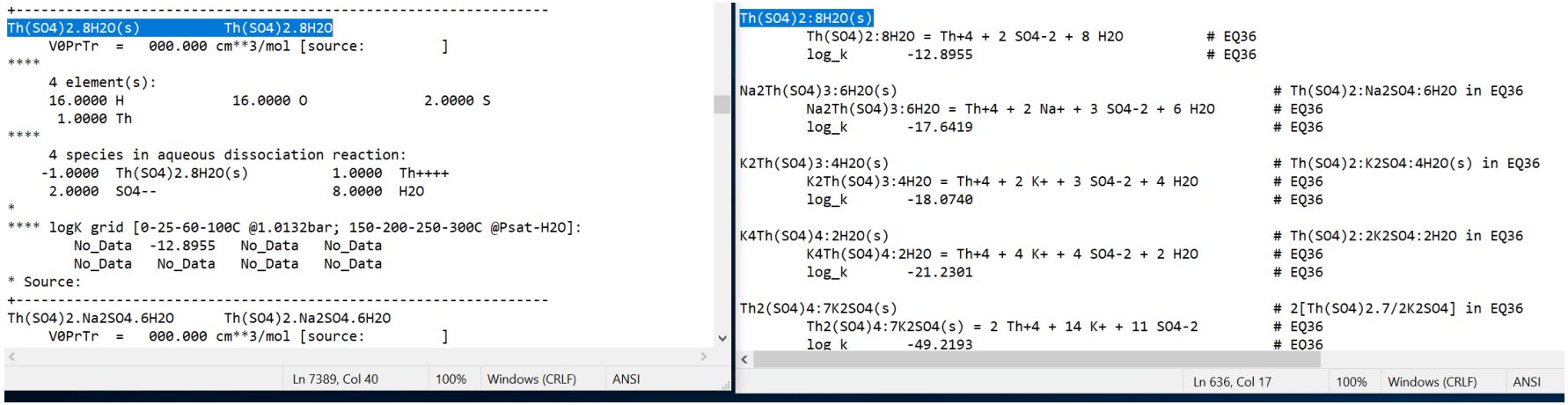

Figure 7. Database screenshot for solid species comparison, EQ3/6 on left, and converted file for PHREEQC on right.

Table 4. Pitzer ion interaction parameter database comparison.

EQ3/6	PHREEQC					
Line	**Line**	**Species**	**Parameter**	**Value in**	**Values**	**Ref Agree**
127	1003	Ca2+ EDTA-4	beta0, a1	5.39	Y	Domski 2018
127	1800	Ca2+ EDTA-4	alpha(1)	2	Y	Domski 2018
302	1010	Na+Cl-	beta0, a1	0.0765	Y	HMW84
302	1160	Na+Cl-	beta1, a1	0.2664	Y	HMW84

302	1807	Na+Cl-	alpha(2)	2	Y	HMW84
1502	1855	K+B(OH)4-	alpha(1)	2	Y	FW86
1502	1058	K+B(OH)4-	beta0, a1	0.035	Y	FW86
1502	1208	K+B(OH)4-	beta1, a1	0.14	Y	FW86
1727	1864	K+HPO4--	alpha(2)	12	Y	P91
1727	1067	K+HPO4--	beta0, a1	0.0248	Y	P91
1727	1217	K+HPO4--	beta1, a1	1.274	Y	P91
3230	1924	AmCl++Cl-	alpha(2)	2	Y	FK98/Konnecke et aal. (Cm analogue)
3230	1127	AmCl++Cl-	beta0, a1	0.593	Y	FK98/Konnecke et aal. (Cm analogue)
3230	1277	AmCl++Cl-	beta1, a1	3.15	Y	FK98/Konnecke et aal. (Cm analogue)
3430	1932	ThCitrate+Cl-	alpha(1)	2	Y	SAND99
3430	1135	ThCitrate+Cl-	beta0, a1	-0.7467	Y	SAND99
3430	1285	ThCitrate+Cl-	beta1, a1	0.29	Y	SAND99
3255	1925	NpO2+Cl-	alpha(2)	12	Y	NFRK95
3255	1128	NpO2+Cl-	beta0, a1	0.1415	Y	NFRK95
3255	1278	NpO2+Cl-	beta1, a1	0.281	Y	NFRK95
3580	1938	Th(Acetate)2++Cl-	alpha(1)	2	Y	Moore et al. 1999
3580	1141	Th(Acetate)2++Cl-	beta0, a1	0.4671	Y	Moore et al. 1999
3580	1291	Th(Acetate)2++Cl-	beta1, a1	1.74	Y	Moore et al. 1999
2605	1899	Mg++CL-	alpha(1)	2	Y	HMW84
2605	1102	Mg++CL-	beta0, a1	0.35235	Y	HMW84
2605	1252	Mg++CL-	beta1, a1	1.6815	Y	HMW84
n	26					

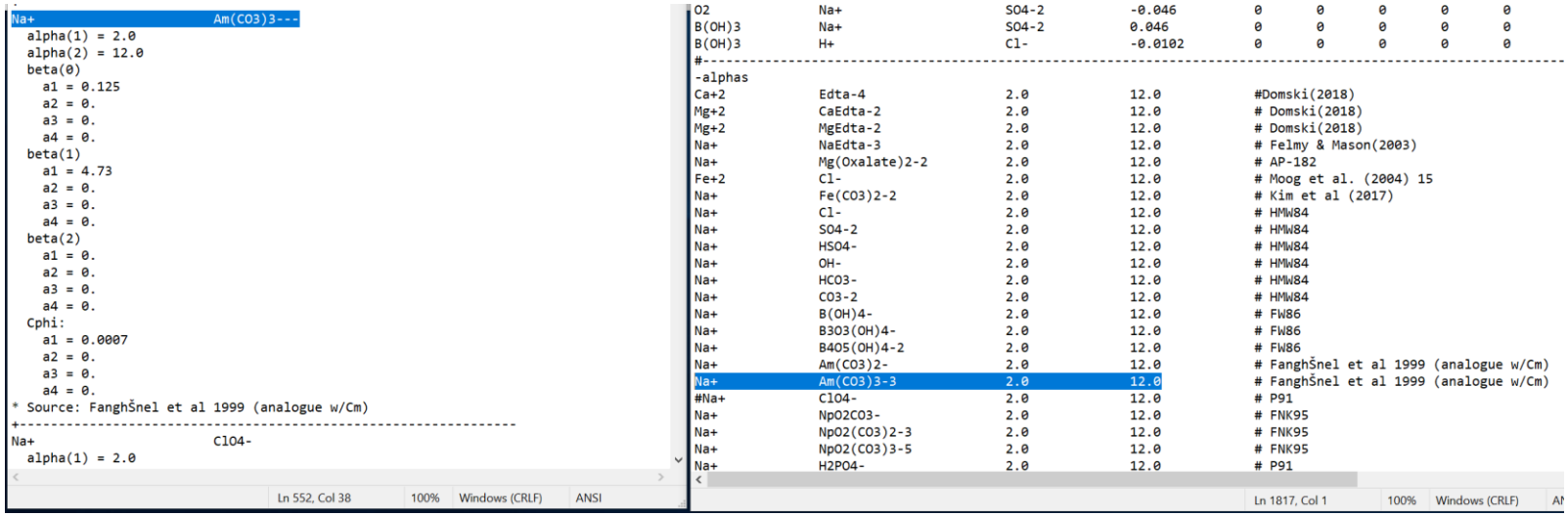

Figure 8. Database comparison screenshot of Pitzer alpha value comparison, EQ3/6 on left, and converted file for PHREEQC on right..

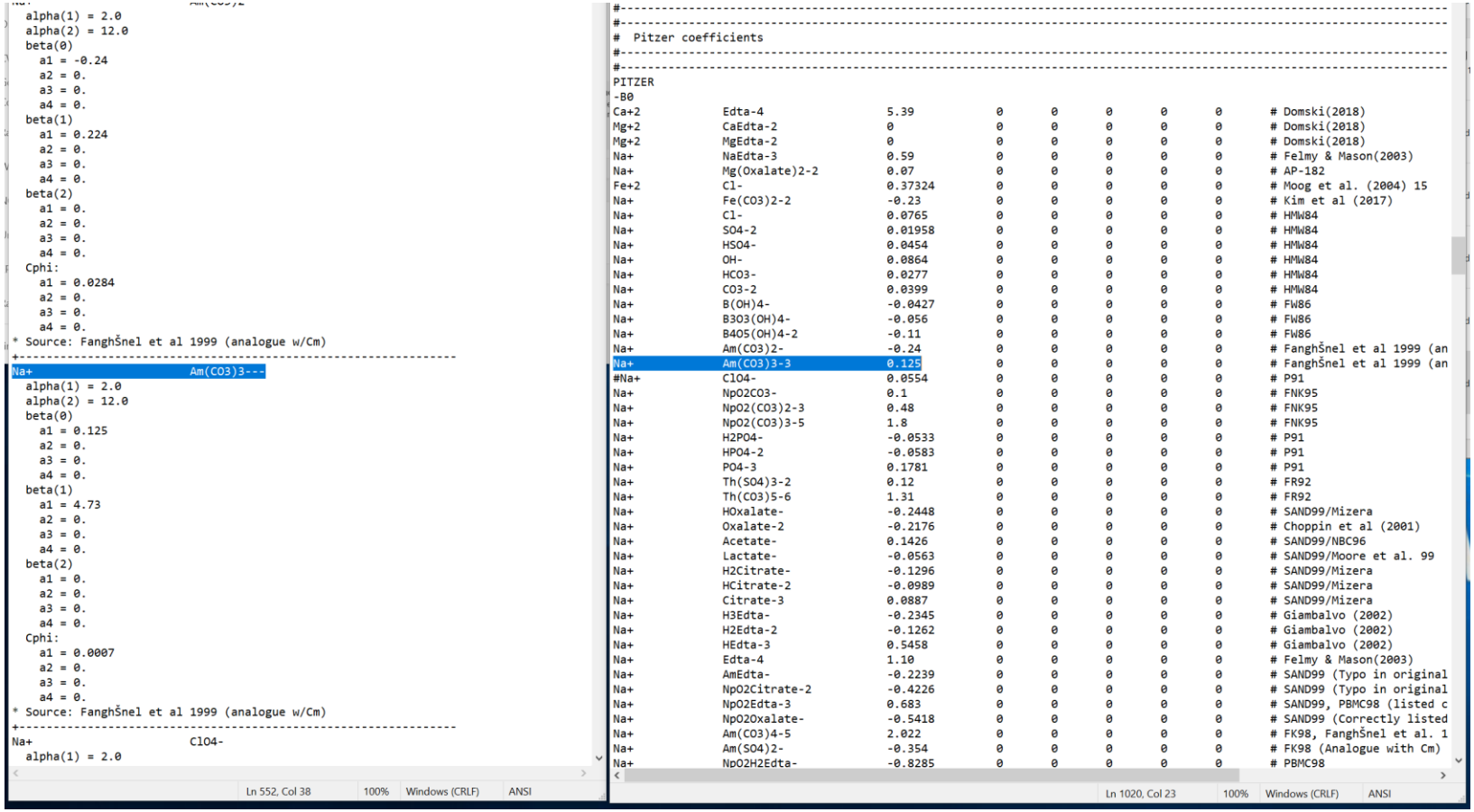

Figure 9. Database comparison screenshot of Pitzer beta value (beta 0, a1), EQ3/6 on left, and converted file for PHREEQC on right.

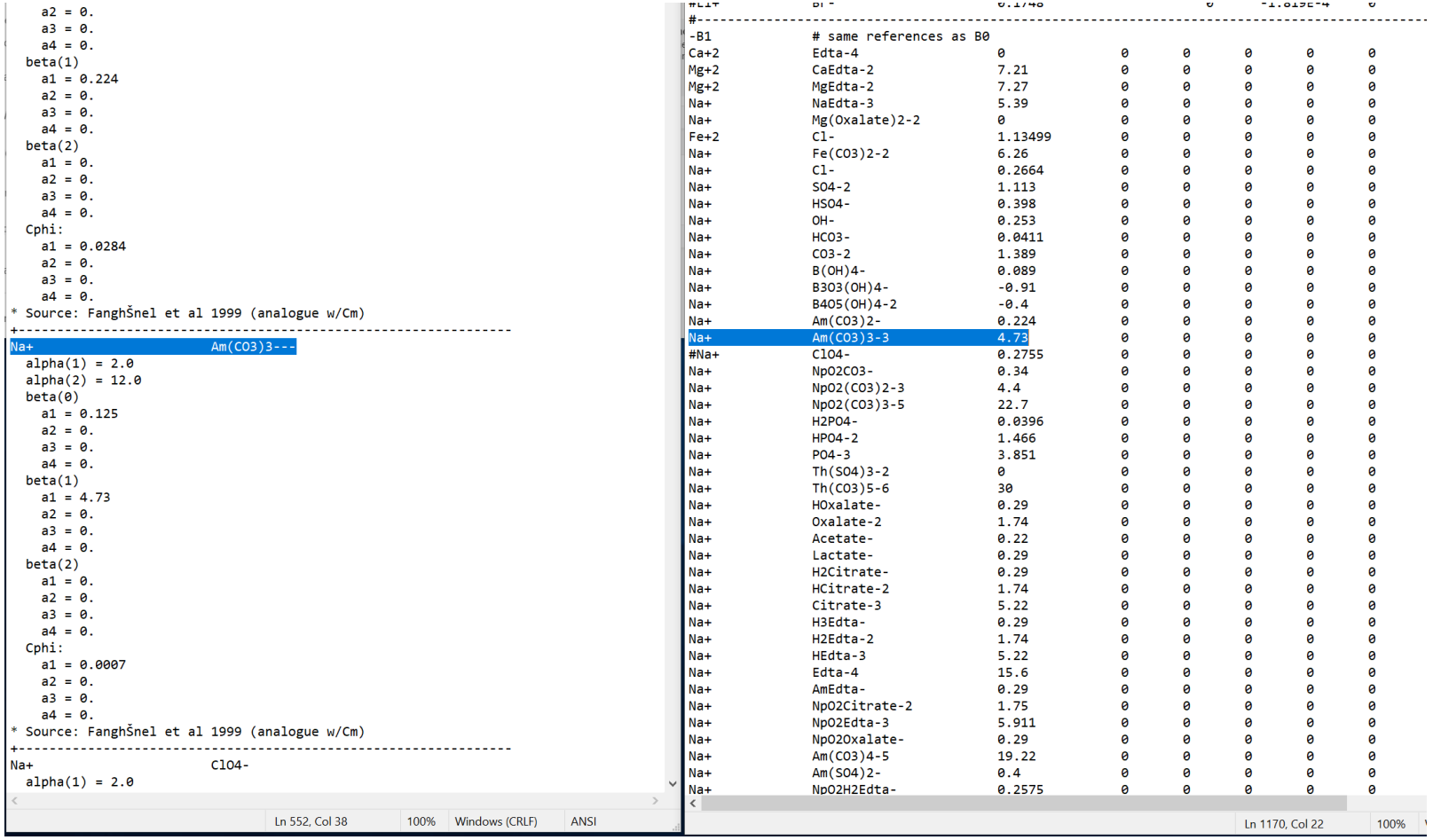

Figure 10. Database comparison screenshot of Pitzer beta value (beta 1, a1), EQ3/6 on left, and converted file for PHREEQC on right.

1.2 DISCUSSION AND CONCLUSION

Parameters, values, and references agreed across the original and converted databases in nearly all cases. The only disagreements between the databases were with positive vs. negative signs and are completely explained by how the chemical reaction is written in the database, i.e., whether it was written as an association reaction or a dissociation reaction in one or the other databases. The only other instance of disagreement between the two databases was for the log_k value of AmPO4(c) in the solids (Table 2). This can be attributed to how PHREEQC deals with the reaction in a single step instead of 2 steps in EQ3/6.

These changes are documented in the file header for the converted database:

> "#…Aqueous speciation written as association reactions so log k's are reversed
> # from EQ36 format
> # Reactions with dissolved carbonates, dissolved boron, and phosphate are re-written
> # to use CO3-2, B(OH)3, and PO4-3 as the basis species to be consistent with PHREEQC
> # format using relevant reactions. This change was done to allow direct comparisons
> # of log k's to values in PITZER.DAT but all are consistent with DATA0.FM4"

In summary, the EQ3/6 database conversion to a PHREEQC format appears to have been done correctly and any conversions or changes are adequately documented.

1.3 PHREEQC DATABASE MODIFICATION OF DATA0FM_EPA.DAT CHECK

A similar approach of comparing values in the original database file (DATA0.FM4) and EPA-modified database file (DATA0FM_EPA.dat) was used to verify the selected parameters were correctly incorporated. All of the values listed in QAPP Table 1 (Modifications to DATA0FM.dat to produce DATA0FM_EPA.dat) were checked against the two database files. The database file line in each and whether the values were in agreement were compiled into a spreadsheet (Table 5). A screenshot of the two files is also included in Figure 11.

1.4 CONCLUSION AND SUMMARY

Values agreed across the original and modified database files in nearly all cases. The only differences from the QAPP Table 1 were opposite signs as already explained in footnote a of the table. Also two of the values were not changed in the database itself, rather in the input file, as indicated by footnote b.

Table 5. Check of QAPP Table 1 agreement with database files

Data	DATA0.FM4[a]	DATA0FM_EPA.dat	Source	LINE in DATA0.FM4	LINE in DATA0_EPA.FM4	Values Match
$Am^{3+} + EDTA^{4-} = AmEDTA^{-}$ stability constant	-18.97	19.67	Hummel et al. (2005), Table III-6	458	468	Y
$NpO_2^{+} + EDTA^{4-} = NpO_2EDTA^{3-}$ stability constant	-8.5352	9.23	Hummel et al. (2005), Table III-6	524	534	Y
$NpO_2^{+} + H^{+} + EDTA^{4-} = NpO_2HEDTA^{2-}$ stability constant	-15.5464	17.06	Hummel et al. (2005), Table III-6	527	537	Y
$NpO_2^{+} + 2\ H^{+} + EDTA^{4-} = NpO_2H_2EDTA^{2-}$ stability constant	-20.8648	22.51	Hummel et al. (2005), Table III-6	530	540	Y
$Th^{4+} + EDTA^{4-} = ThEDTA(aq)$ stability constant	-23.557	24.6[b]	EPA estimate	491	501	N
$Mg^{2+} + EDTA^{4-} = MgEDTA^{2-}$ stability constant	-10.90	9.20[b]	EPA estimate	386	393	N
$Ca^{2+} + EDTA^{4-} = CaEDTA^{2-}$ stability constant	-12.69	12.36	Felmy and Mason (2003)	392	399	Y
$Ca^{2+}/EDTA^{4-}$ ion pair $\beta^{(0)}$ Pitzer parameter	5.39	2.48	Domski (2019b)	1003	1017	Y
$Ca^{2+}/EDTA^{4-}$ ion pair	2.0	1.4	Domski (2020)	1800	1814	Y

α_1 Pitzer parameter						
Mg^{2+}/$MgEDTA^{2-}$ ion pair α_1 Pitzer parameter	2.0	1.4	Domski (2020)	1802	1816	Y
Mg^{2+}/$CaEDTA^{2-}$ ion pair α_1 Pitzer parameter	2.0	1.4	Domski (2020)	1801	1815	Y
Am^{3+} + $Citrate^{3-}$ = AmCitrate(aq) stability constant	-8.7984	8.55	Hummel et al. (2005), Table III-4	456	462	Y
Am^{3+} + 2 $Citrate^{3-}$ = $Am(Citrate)_2^{3-}$ stability constant	--	13.90	Hummel et al. (2005), Table III-4	n/a	465	Y
NpO_2^+ + $Citrate^{3-}$ = $NpO_2Citrate^{2-}$ stability constant	-3.4969	3.68	Hummel et al. (2005), Table III-4	521	531	Y
$Ca_3Citrate_2$:$4H_2O$ = 3 Ca^{2+} + 2 $Citrate^{3-}$ + 4 H_2O earlandite solubility constant	--	-17.90	Hummel et al. (2005)	n/a	555	Y*

a – DATA0FM_EPA.dat aqueous speciation reactions are written as association reactions to match Hummel et al. (2005). Because the DATA0.FM4 reactions are written as dissociation reactions, the sign is changed relative to the values in Hummel et al (2005) and DATA0FM_EPA.dat

b – MgEDTA2- and ThEDTA(aq) aqueous stability constants were approximated by EPA, so they were not added to the DATA0FM_EPA.dat database. These stability constants were included in the PHREEQC calculations by adding the data blocks to the input files used in the actinide solubility calculations.

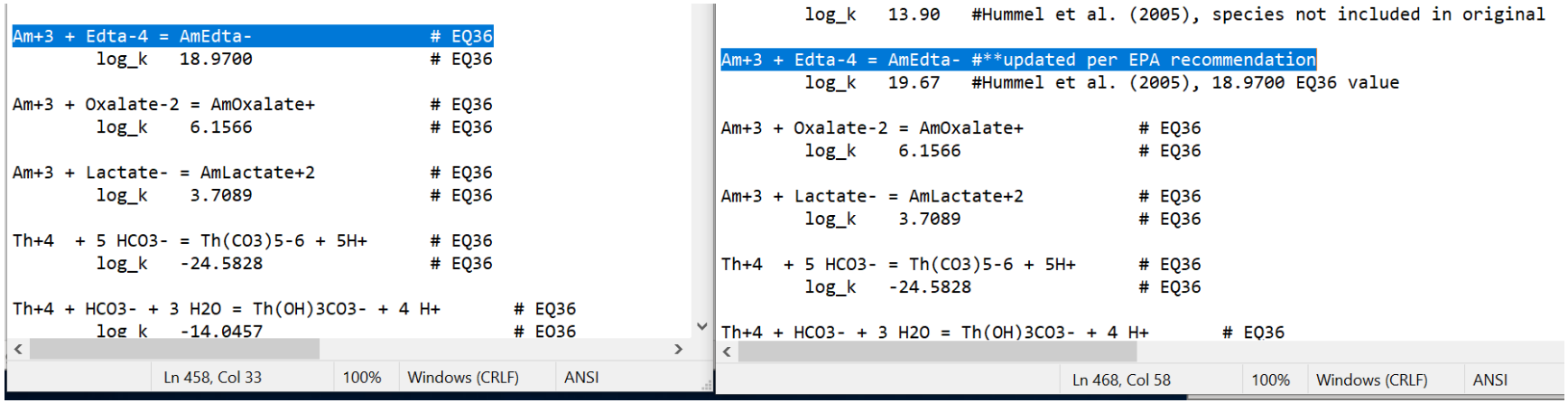

Figure 11. Screenshot of original database file (left) and updated database file (right).

2.0 QA CHECKS ON PHREEQC INPUT FILES (TASK 4C AND 4D)

2.1 SUMMARY

Examination of all input files showed no anomalous entries and that values matched the appropriate documentation cited in the QAPP. The following PHREEQC input files went through QA checks to ensure:

- Brine constituent values (e.g., pH, temperature, ion molar concentrations) matched values from DOE EQ3/6 input files and Domski and Sisk-Scott (2019) for all brines and brine volumes
- Organic ligand concentrations matched values from EQ3/6 input files and Domski and Sisk-Scott (2019) for all brines and brine volumes
- Mineral phase selection and molar values matched values from EQ3/6 input files and Domski and Sisk-Scott (2019) for all brines and brine volumes
- Calcite saturation indices of 0.03 have been appropriately applied to input files for calculations used during completeness discussions with DOE (GWB_EPADB and ERDA6_EPADB)
- Stability constants for $MgEDTA^{2-}$ and ThEDTA match EPA documentation and have been entered appropriately into input files (GWB_EPADB, ERDA6_EPADB, GWB_EPA, and ERDA6_EPA)
- Assumptions, including choice of aragonite and removal of iron and lead phases, match discussions from Knerr (2020) (for recalculation of actinide solubilities GWB_EPA and ERDA6_EPA)

Note, density will vary for each brine volume based on the varied concentrations of organic ligands present. Previous input files used to calculate values presented in the QAPP did not include variable densities and only used the value for 1x brine volume for all brine volumes. These input files have since been updated and use of these updated values have been verified in this report. DOE calculated densities for each brine volume using the spreadsheet *Conc_density_calcs_CRA-2019_PA.xlsx* (Domski and Sisk-Scott 2019) and are listed below.

Table 6 WIPP brine densities

	Density (g/cm^3)	
	GWB	**ERDA-6**
1x Volume	1.2366	1.20138
2x Volume	1.23560	1.20038
3x Volume	1.23526	1.20004
4x Volume	1.23510	1.19988

5x Volume	1.23500	1.19978

EPA will perform the calculations using the input files in the table below.

Table 7 Input files examined

Files	Purpose	QA Checks
GWB_DOE.inp ERDA6_DOE.inp	Reproduce DOE CRA-2019 DPA solubility for GWB and ERDA-6 brines	• Brine composition • Organic ligand concentrations • Mineral phase selection • Mineral phase molar values • Correct spreadsheet transcription to convert from molal to molar concentrations
GWB_EPADB.inp ERDA6_EPADB.inp	Repeat DOE CRA-2019 DPA calculations using EPA revised database and calcite saturation assumptions	• Brine composition (all brine volumes) • Organic ligands (all brine volumes) • Mineral phase selection • Mineral phase molar values • $MgEDTA^{2-}$ and ThEDTA reactions and log_k • Calcite saturation index • Correct spreadsheet transcription to convert from molal to molar concentrations
GWB_EPA.inp ERDA6_EPA.inp	Recalculate CRA-2019 solubility using EPA revised database and assumptions	• Brine composition (all brine volumes) • Organic ligands (all brine volumes) • Mineral phase selection • Mineral phase molar values • $MgEDTA^{2-}$ and ThEDTA reactions and log_k • Inclusion of aragonite • Removal of iron and lead phases • Correct spreadsheet transcription to convert from molal to molar concentrations

Lastly, QA checks have been performed to verify that output file values have been correctly transcribed onto the spreadsheet used to convert from molal to molar concentrations, which are used for the WIPP PA. Conversions are saved under the file *Actinide solubility calculations for revised PA.xlsx*.

2.2 REPRODUCTION OF CRA-2019 SOLUBILITY

The following screenshots provide objective evidence of the QA checks on the input files (GWB_DOE.inp and ERDA6_DOE.inp) used to recreate DOE CRA-2019 solubilities using the reformatted database. All values for brine composition, organic ligands, mineral selection, and mineral molar quantities match the appropriate documented values in GWB and ERDA-6 input files for all brine volumes.

Below is an example of the GWB calculation at 1x brine volume. Brine constituents entered in the PHREEQC file match the brine constituents in the EQ3 file. Actinides, Pb, and Fe differ in the input files because those concentrations in brine are determined by equilibrating minerals

Figure 39 PHREEQC (A) using DATA0FM.dat and its corresponding EQ3 (B) input files for GWB at 1x volume

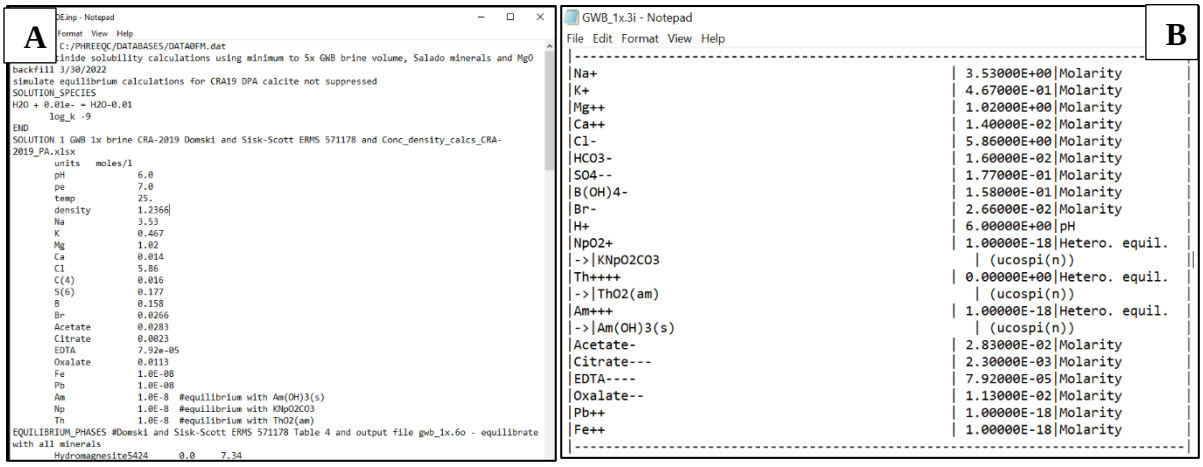

with brine and their inclusion in the initial brine composition in PHREEQC is inconsequential to the calculation. Input files for other brine volumes also match their corresponding EQ3 files.

The screenshot below provides evidence that mineral phase selection and molar quantities match DOE's EQ6 input files and QAPP documentation for GWB brine, in this case at 1x volume. In this example, hydromagnesite and brucite inputs and quantities match in both files, though the other mineral phases and quantities in PHREEQC also correspond with DOE's inputs for all brine volumes.

Figure 13 PHREEQC (A) using DATA0FM.dat and its corresponding EQ6 input files for GWB at 1x volume for hydromagnesite and brucite

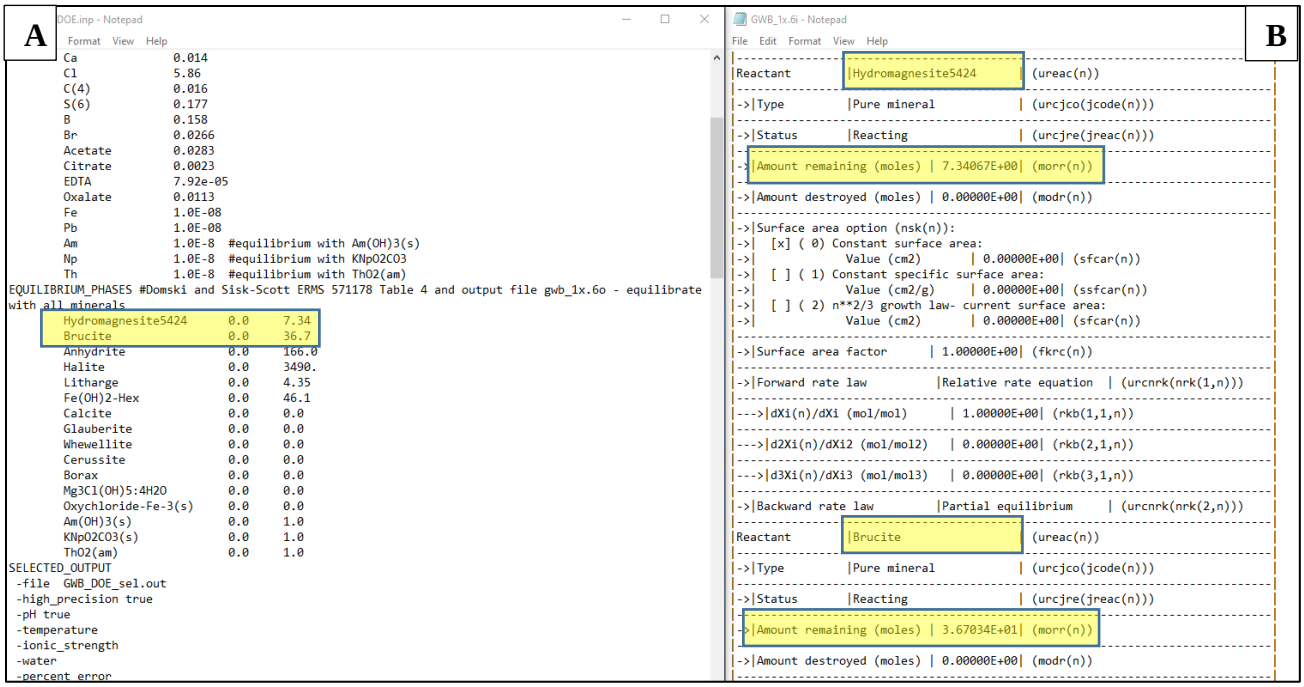

The screenshots below provide example evidence that organic ligand concentrations match DOE's input files and the appropriate cited documentation for all brine volumes for the GWB calculations corresponding to 2x volumes. Organic ligand concentrations match their corresponding brine volumes for all PHREEQC input files.

Figure 14 Portions of PHREEQC (A) using DATA0FM.dat and its corresponding EQ3 (B) input files showing organic ligand concentrations for GWB at 2x volumes

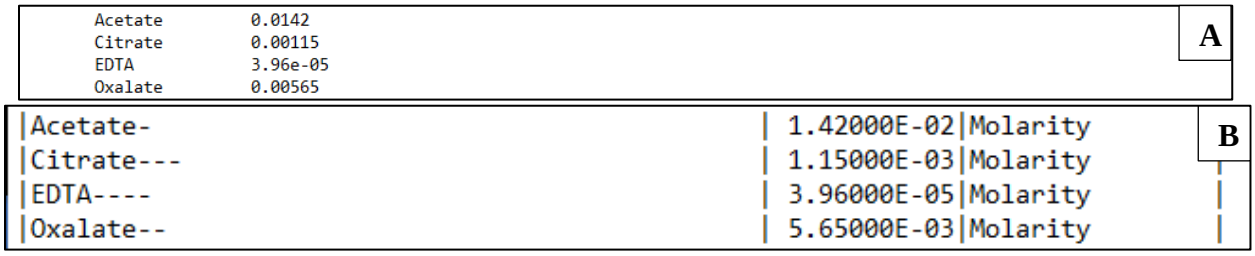

As with the GWB calculations, the screenshot below is an example of the ERDA-6 calculation, but at 3x brine volume. Brine constituents entered in the PHREEQC file match the brine constituents in the EQ3 file. Actinides, Pb, and Fe differ in the input files because those concentrations in brine are determined by equilibrating minerals with brine and their inclusion in the initial brine composition in PHREEQC is inconsequential to the calculation. Input files for other brine volumes also match their corresponding EQ3 files.

Figure 15 PHREEQC (A) using DATA0FM.dat and its corresponding EQ3 (B) input files for ERDA-6 at 3x volumes

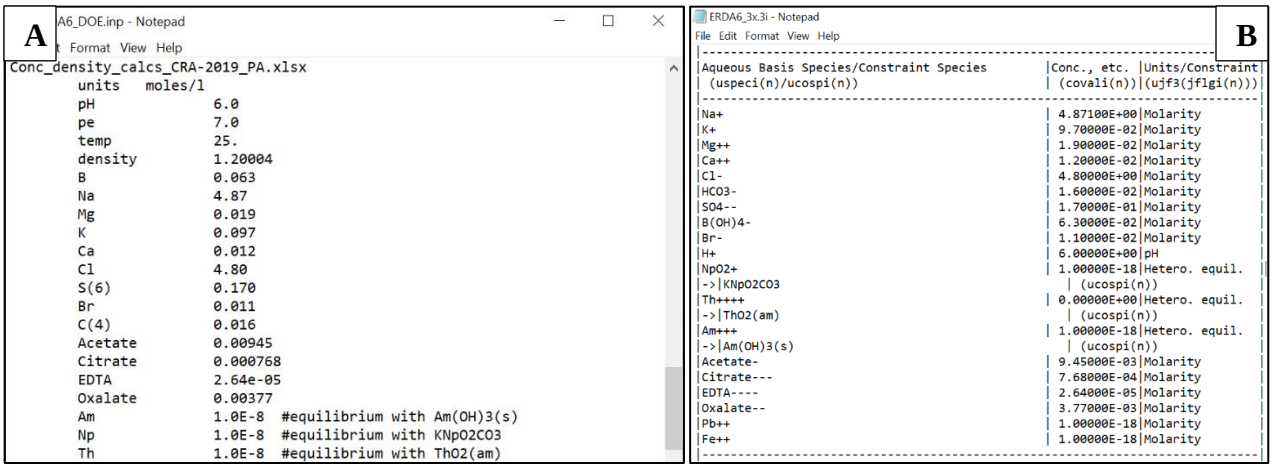

The screenshot below provides evidence that mineral phase selection and molar quantities match DOE's EQ6 input files and QAPP documentation for ERDA-6 brine, in this case at 4x volume. In this example, anhydrite and halite inputs and quantities match in both files, though the other mineral phases and quantities in PHREEQC also correspond with DOE's inputs. Other mineral phases and quantities in PHREEQC also correspond with DOE's inputs for all brine volumes.

Figure 16 PHREEQC (A) using DATA0FM.dat and its corresponding EQ6 (B) input files for ERDA-6 at 4x volume for anhydrite and halite

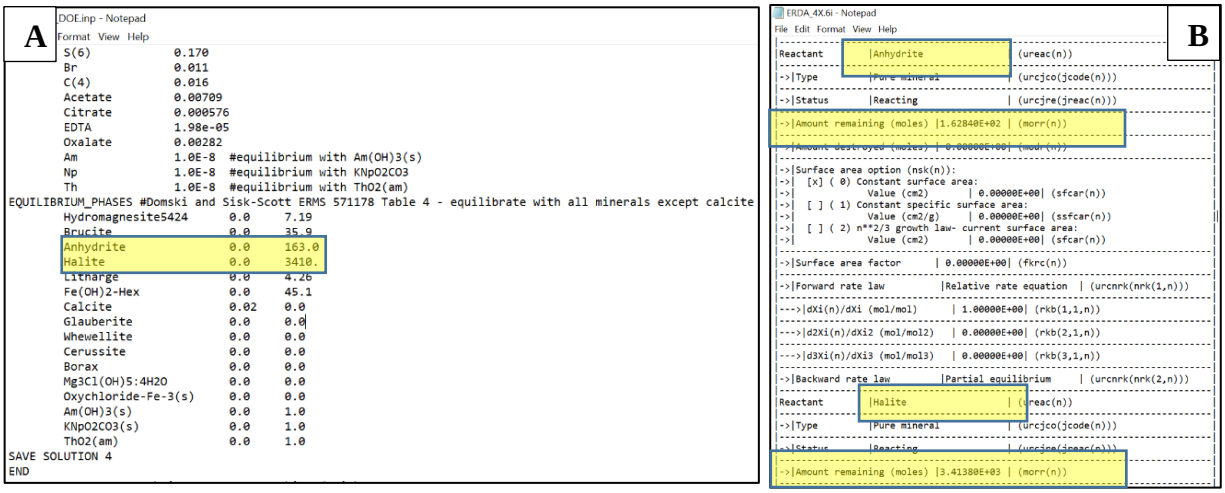

The screenshots below provide example evidence that organic ligand concentrations match DOE's input files and the appropriate cited documentation for all brine volumes for the ERDA-6 calculations corresponding to 5x ERDA-6 brine volumes. Organic ligand concentrations match their corresponding brine volumes for all PHREEQC input files.

Figure 17 Portions of PHREEQC (A) using DATA0FM.dat and its corresponding EQ3 (B) input files showing organic ligand concentrations for ERDA-6 at 5x volumes

A

Acetate	0.00567
Citrate	0.000461
EDTA	1.58e-05
Oxalate	0.00226

B

Acetate-	5.67000E-03	Molarity
Citrate---	4.61000E-04	Molarity
EDTA----	1.58000E-05	Molarity
Oxalate--	2.26000E-03	Molarity

The screenshots below demonstrate that model output results for GWB at 2x volumes were correctly input into the spreadsheet to convert from output molal concentrations to molar concentrations for use in the PA. QA checks for other GWB and ERDA-6 brine volumes also showed correct entry into the spreadsheet.

Figure 18 PHREEQC output (left) and molar spreadsheet calculator (right) for GWB at 2x volumes using DATA0FM.dat

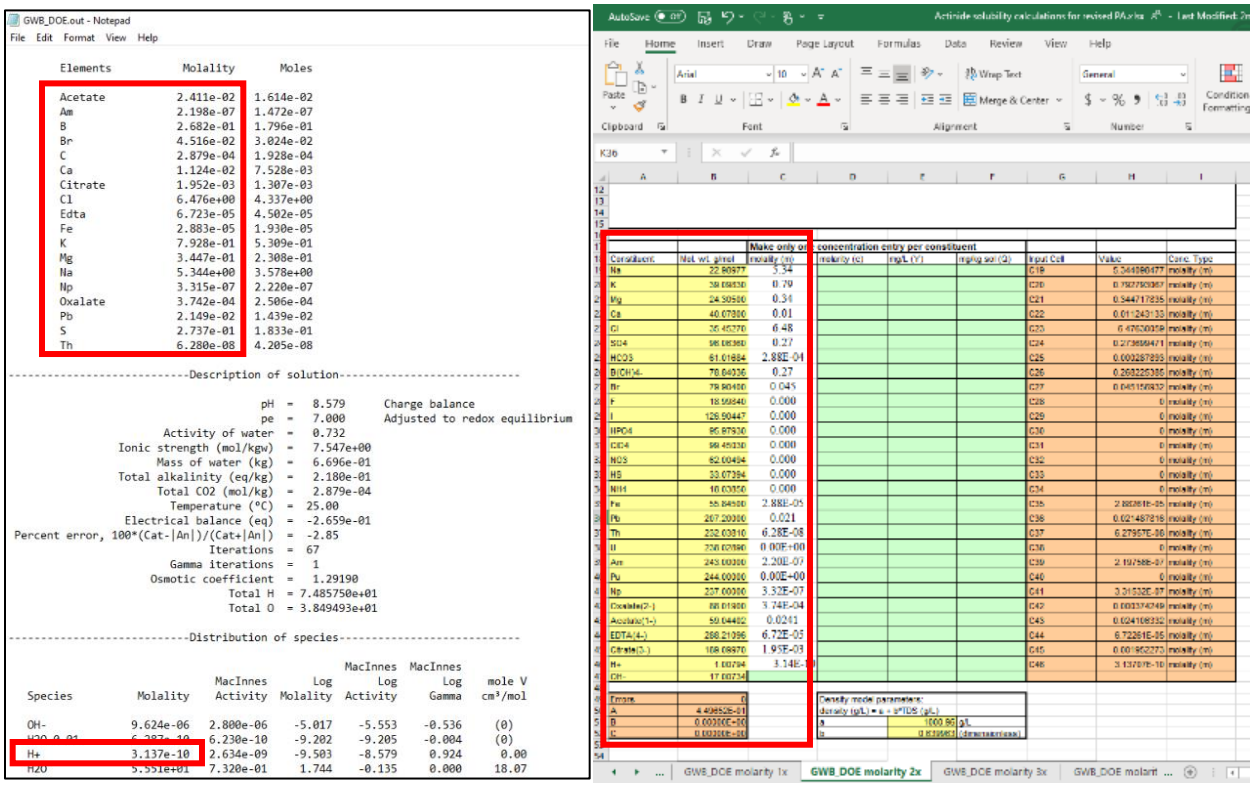

2.3 REPEAT CRA-2019 SOLUBILITY CALCULATION WITH REVISED DATABASE AND CALCITE SI

The screenshots below exhibit the results of the QA checks for input files (GWB_EPADB.inp and ERDA6_EPADB.inp) recalculating DOE solubilities featuring updates to the reformatted database and a revised calcite saturation index. All values for brine composition, organic ligands, mineral selection, mineral molar quantities, saturation indices, and stability constants match the appropriate documented values in both input files for all brine volumes.

The below image is a portion of the input file used to explore changes in solubility for 2x GWB and provides evidence that input files match QAPP documentation for all GWB calculations. Brine constituent values and equilibrium phase minerals and quantities match values previously discussed. Calcite saturation index is at 0.03 as previously discussed in EPA's completeness documentation.

Figure 19 PHREEQC input file for 2x GWB using DATA0FM_EPA.dat and revised calcite saturation index

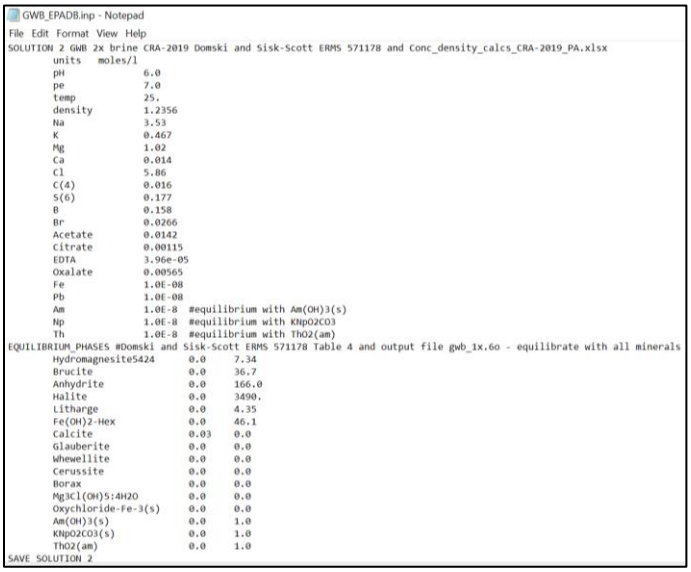

GWB_EPADB.inp - Notepad

File Edit Format View Help

```
SOLUTION 2 GWB 2x brine CRA-2019 Domski and Sisk-Scott ERMS 571178 and Conc_density_calcs_CRA-2019_PA.xlsx
        units   moles/l
        pH              6.0
        pe              7.0
        temp            25.
        density         1.2356
        Na              3.53
        K               0.467
        Mg              1.02
        Ca              0.014
        Cl              5.86
        C(4)            0.016
        S(6)            0.177
        B               0.158
        Br              0.0266
        Acetate         0.0142
        Citrate         0.00115
        EDTA            3.96e-05
        Oxalate         0.00565
        Fe              1.0E-08
        Pb              1.0E-08
        Am              1.0E-8  #equilibrium with Am(OH)3(s)
        Np              1.0E-8  #equilibrium with KNpO2CO3
        Th              1.0E-8  #equilibrium with ThO2(am)
EQUILIBRIUM_PHASES #Domski and Sisk-Scott ERMS 571178 Table 4 and output file gwb_1x.6o - equilibrate with all minerals
        Hydromagnesite5424      0.0     7.34
        Brucite                 0.0     36.7
        Anhydrite               0.0     166.0
        Halite                  0.0     3490.
        Litharge                0.0     4.35
        Fe(OH)2-Hex             0.0     46.1
        Calcite                 0.03    0.0
        Glauberite              0.0     0.0
        Whewellite              0.0     0.0
        Cerussite               0.0     0.0
        Borax                   0.0     0.0
        Mg3Cl(OH)5:4H2O         0.0     0.0
        Oxychloride-Fe-3(s)     0.0     0.0
        Am(OH)3(s)              0.0     1.0
        KNpO2CO3(s)             0.0     1.0
        ThO2(am)                0.0     1.0
SAVE SOLUTION 2
```

The screenshot below shows part of the input file used to explore changes in solubility for 5x ERDA-6 and provides evidence that input files match QAPP documentation for all ERDA-6 calculations. Input values match documentation, though Fe and Pb are absent from the brine concentrations as with previous files. This difference is insignificant as this does not impact final calculations in PHREEQC.

Figure 20 PHREEQC input file for 5x ERDA-6 using DATA0FM_EPA.dat and revised calcite saturation index

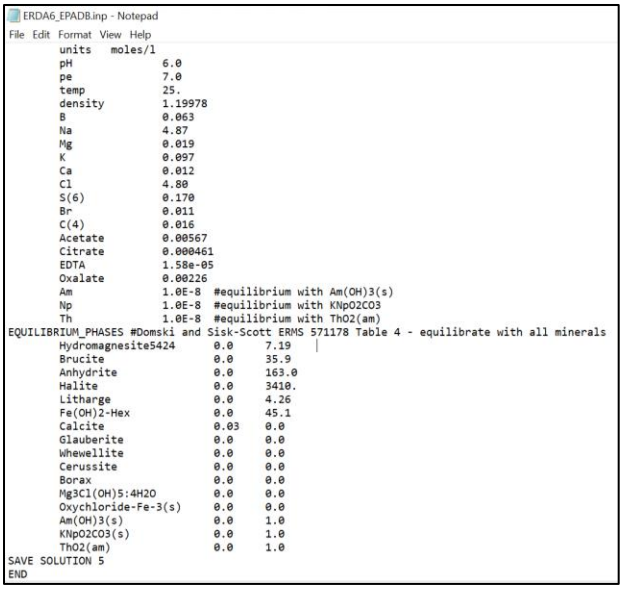

ERDA6_EPADB.inp - Notepad

File Edit Format View Help

```
        units   moles/l
        pH              6.0
        pe              7.0
        temp            25.
        density         1.19978
        B               0.063
        Na              4.87
        Mg              0.019
        K               0.097
        Ca              0.012
        Cl              4.80
        S(6)            0.170
        Br              0.011
        C(4)            0.016
        Acetate         0.00567
        Citrate         0.000461
        EDTA            1.58e-05
        Oxalate         0.00226
        Am              1.0E-8  #equilibrium with Am(OH)3(s)
        Np              1.0E-8  #equilibrium with KNpO2CO3
        Th              1.0E-8  #equilibrium with ThO2(am)
EQUILIBRIUM_PHASES #Domski and Sisk-Scott ERMS 571178 Table 4 - equilibrate with all minerals
        Hydromagnesite5424      0.0     7.19
        Brucite                 0.0     35.9
        Anhydrite               0.0     163.0
        Halite                  0.0     3410.
        Litharge                0.0     4.26
        Fe(OH)2-Hex             0.0     45.1
        Calcite                 0.03    0.0
        Glauberite              0.0     0.0
        Whewellite              0.0     0.0
        Cerussite               0.0     0.0
        Borax                   0.0     0.0
        Mg3Cl(OH)5:4H2O         0.0     0.0
        Oxychloride-Fe-3(s)     0.0     0.0
        Am(OH)3(s)              0.0     1.0
        KNpO2CO3(s)             0.0     1.0
        ThO2(am)                0.0     1.0
SAVE SOLUTION 5
END
```

An example showing objective evidence that input files correctly entered $MgEDTA^{2-}$ and ThEDTA reactions and complexation constants to correct erroneous DOE values can be found in the next section.

The screenshots below demonstrate that model output results for ERDA-6 brine at 4x volumes were correctly transcribed into the spreadsheet to convert from molal to molar concentrations. QA checks for other GWB and ERDA-6 brine volumes also showed correct entry into the spreadsheet for this set of calculations.

Figure 21 PHREEQC output (left) and molar spreadsheet calculator (right) for ERDA-6 at 4x volumes using DATA0_FM.dat and revised calcite saturation index

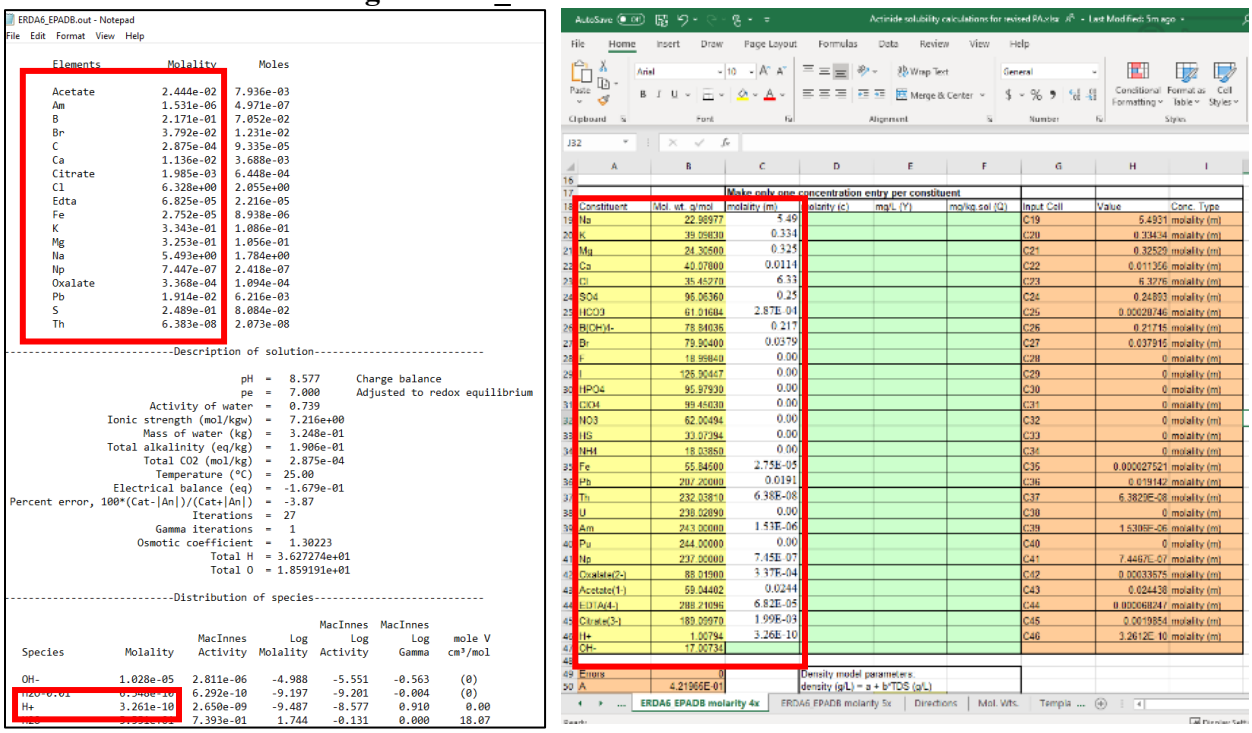

ERDA6_EPADB.out - Notepad

File Edit Format View Help

Elements	Molality	Moles
Acetate	2.444e-02	7.936e-03
Am	1.531e-06	4.971e-07
B	2.171e-01	7.052e-02
Br	3.792e-02	1.231e-02
C	2.875e-04	9.335e-05
Ca	1.136e-02	3.688e-03
Citrate	1.985e-03	6.448e-04
Cl	6.328e+00	2.055e+00
Edta	6.825e-05	2.216e-05
Fe	2.752e-05	8.938e-06
K	3.343e-01	1.086e-01
Mg	3.253e-01	1.056e-01
Na	5.493e+00	1.784e+00
Np	7.447e-07	2.418e-07
Oxalate	3.368e-04	1.094e-04
Pb	1.914e-02	6.216e-03
S	2.489e-01	8.084e-02
Th	6.383e-08	2.073e-08

----------Description of solution----------

pH	= 8.577	Charge balance
pe	= 7.000	Adjusted to redox equilibrium
Activity of water	= 0.739	
Ionic strength (mol/kgw)	= 7.216e+00	
Mass of water (kg)	= 3.248e-01	
Total alkalinity (eq/kg)	= 1.906e-01	
Total CO2 (mol/kg)	= 2.875e-04	
Temperature (°C)	= 25.00	
Electrical balance (eq)	= -1.679e-01	
Percent error, 100*(Cat-|An|)/(Cat+|An|)	= -3.87	
Iterations	= 27	
Gamma iterations	= 1	
Osmotic coefficient	= 1.30223	
Total H	= 3.627274e+01	
Total O	= 1.859191e+01	

----------Distribution of species----------

Species	Molality	MacInnes Activity	Log Molality	MacInnes Log Activity	Log Gamma	mole V cm³/mol
OH-	1.028e-05	2.811e-06	-4.988	-5.551	-0.563	(0)
H2O	5.548e+01	6.292e-10	-9.197	-9.201	-0.004	(0)
H+	3.261e-10	2.650e-09	-9.487	-8.577	0.910	0.00
[illegible]	[illegible]	7.393e-01	1.744	-0.131	0.000	18.07

Actinide solubility calculations for revised PA.xlsx - Last Modified: 5m ago

File Home Insert Draw Page Layout Formulas Data Review View Help

J32

Make only one concentration entry per constituent

Constituent	Mol. wt. g/mol	molality (m)	molarity (c)	mg/L (Y)	mg/kg sol (Q)	Input Cell	Value	Conc. Type
Na	22.98977	5.49				C19	5.4931	molality (m)
K	39.09830	0.334				C20	0.33434	molality (m)
Mg	24.30500	0.325				C21	0.32529	molality (m)
Ca	40.07800	0.0114				C22	0.011356	molality (m)
Cl	35.45270	6.33				C23	6.3276	molality (m)
SO4	96.06360	0.25				C24	0.24893	molality (m)
HCO3	61.01684	2.87E-04				C25	0.00028746	molality (m)
B(OH)4-	78.84036	0.217				C26	0.21715	molality (m)
Br	79.90400	0.0379				C27	0.037916	molality (m)
F	18.99840	0.00				C28	0	molality (m)
I	126.90447	0.00				C29	0	molality (m)
HPO4	95.97930	0.00				C30	0	molality (m)
ClO4	99.45030	0.00				C31	0	molality (m)
NO3	62.00494	0.00				C32	0	molality (m)
HS	33.07394	0.00				C33	0	molality (m)
NH4	18.03850	0.00				C34	0	molality (m)
Fe	55.84500	2.75E-05				C35	0.000027521	molality (m)
Pb	207.20000	0.0191				C36	0.019142	molality (m)
Th	232.03810	6.38E-08				C37	6.3829E-08	molality (m)
U	238.02890	0.00				C38	0	molality (m)
Am	243.00000	1.53E-06				C39	1.5308E-06	molality (m)
Pu	244.00000	0.00				C40	0	molality (m)
Np	237.00000	7.45E-07				C41	7.4467E-07	molality (m)
Oxalate(2-)	88.01900	3.37E-04				C42	0.00033675	molality (m)
Acetate(1-)	59.04402	0.0244				C43	0.024438	molality (m)
EDTA(4-)	288.21096	6.82E-05				C44	0.000068247	molality (m)
Citrate(3-)	189.09970	1.99E-03				C45	0.0019854	molality (m)
H+	1.00794	3.26E-10				C46	3.2612E-10	molality (m)
OH-	17.00734							
Errors	0							
A	4.21966E-01							

Density model parameters

density (g/L) = a + b*TDS (g/L)

ERDA6 EPADB molarity 4x | ERDA6 EPADB molarity 5x | Directions | Mol. Wts. | Templa ...

2.4 RECALCULATION OF CRA-2019 SOLUBILITY FOR SENSITIVITY STUDIES

The screenshots below show the results of the QA checks for input files (GWB_EPA.inp and ERDA6_EPA.inp) recalculating DOE solubilities that were ultimately used for the EPA sensitivity studies. These calculations feature corrections to previous DOE values and revised assumptions. All values for brine composition, organic ligands, mineral selection, mineral molar quantities, stability constants, and assumptions match the appropriate documented values in both input files for all brine volumes.

The screenshot below shows the input file for the recalculation of GWB at all volumes using updated DOE assumptions (e.g., aragonite precipitation, no iron and lead phases). The reactions and log_k values for $MgEDTA^{2-}$ and ThEDTA have been correctly entered and match the values described in Attachment B, Section 4.1.6. This is the same in the corresponding ERDA-6 recalculation input file and for the GWB_EPADB.inp and ERDA6_EPADB.inp files.

Figure 22 Portion of PHREEQC input showing the updated log_k for $MgEDTA^{2-}$ and ThEDTA complexes for GWB at all volumes for recalculated CRA-2019 solubilities

GWB_EPA.inp - Notepad

File Edit Format View Help

```
DATABASE C:/PHREEQC/DATABASES/DATA0FM_EPA.dat
TITLE Actinide solubility calculations using minimum to 5x GWB brine volume, Salado minerals and MgO backfill 3/30/2022
revised actinide solubility calculations for CRA19 DPA using EPA assumptions and database
SOLUTION_SPECIES
H2O + 0.01e- = H2O-0.01
       log_k -9
Edta-4 + Mg+2 = MgEdta-2                    # EQ36
        log_k      9.20          # original Hummel et al. (2005) value is 10.9
#modify MgEDTA-2 log beta to improve fit to Choppin et al. (2001) apparent log betas (as corrected by Hummel et al. 2005)
Th+4 + Edta-4 = ThEdta          # EQ36
        log_k      24.6         # original Hummel et al. (2005) value is 23.557
#modify ThEDTA log beta to improve fit to Choppin et al. (2001) apparent log betas (as corrected by Hummel et al. 2005)
END
```

The screenshot below exhibits part of the input file used to recalculate actinide solubilities in ERDA-6 brine at 4x volumes. Brine constituent values and equilibrium phase molar quantities match values that correspond to the values outlined in the QAPP. In addition, the assumptions of aragonite precipitation and the exclusion of iron and lead phases match previous discussions with DOE. This is also the same for the GWB brine input files.

Figure 23 PHREEQC input file for ERDA-5 at 4x volumes for recalculated CRA-2019 solubilities

ERDA6_EPA.inp - Notepad

File Edit Format View Help

```
        units   moles/l
        pH              6.0
        pe              7.0
        temp            25.
        density         1.19988
        B               0.063
        Na              4.87
        Mg              0.019
        K               0.097
        Ca              0.012
        Cl              4.80
        S(6)            0.170
        Br              0.011
        C(4)            0.016
        Acetate         0.00709
        Citrate         0.000576
        EDTA            1.98e-05
        Oxalate         0.00282
        Am              1.0E-8  #equilibrium with Am(OH)3(s)
        Np              1.0E-8  #equilibrium with KNpO2CO3
        Th              1.0E-8  #equilibrium with ThO2(am)
EQUILIBRIUM_PHASES #Domski and Sisk-Scott ERMS 571178 Table 4 - equilibrate with all minerals except calcite
        Hydromagnesite5424      0.0     7.19
        Brucite                 0.0     35.9
        Anhydrite               0.0     163.0
        Halite                  0.0     3410.
        Aragonite               0.0     0.0
        Glauberite              0.0     0.0
        Whewellite              0.0     0.0
        Borax                   0.0     0.0
        Mg3Cl(OH)5:4H2O         0.0     0.0
        Am(OH)3(s)              0.0     1.0
        KNpO2CO3(s)             0.0     1.0
        ThO2(am)                0.0     1.0
SAVE SOLUTION 4
```

The screenshots below demonstrate that model output results for GWB brine at 2x volumes were correctly input into the spreadsheet to convert from molal to molar concentrations. QA checks for other GWB brine volumes also showed correct entry into the spreadsheet.

Figure 24 PHREEQC output (left) and molar spreadsheet calculator (right) for GWB at 2x volumes for recalculated CRA-2019 solubilities

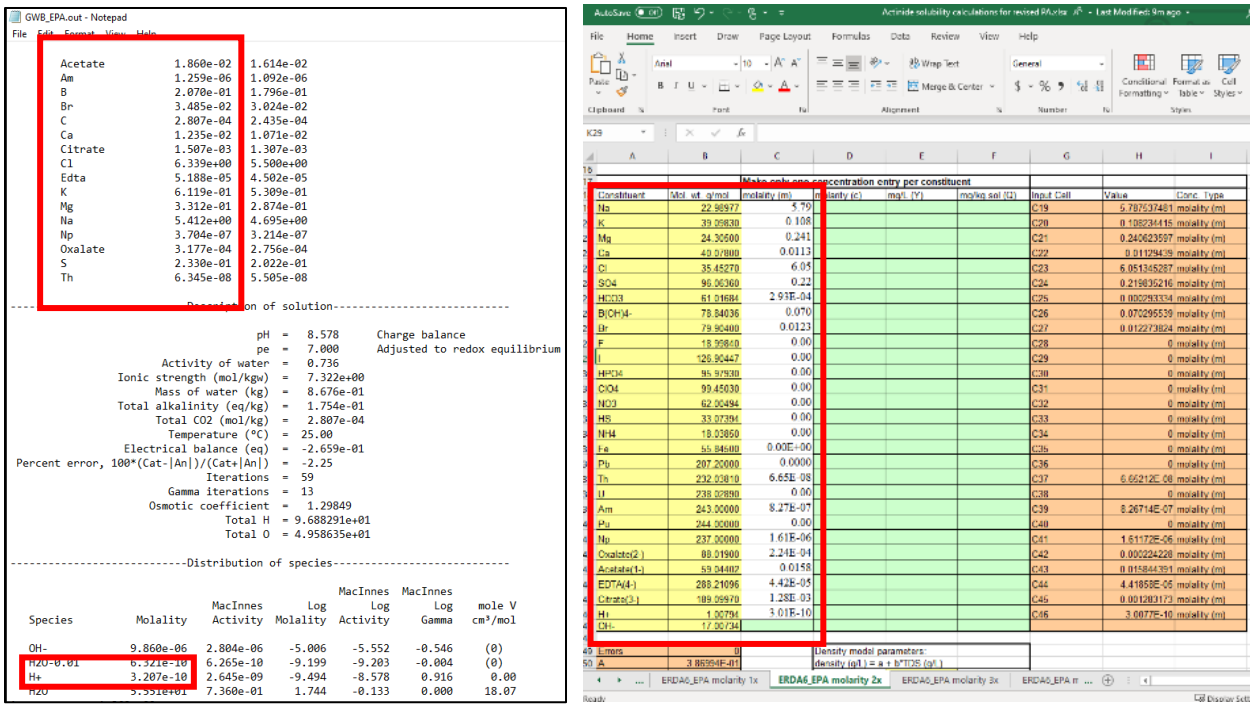

The screenshots below demonstrate that model output results for ERDA-6 brine for the recalculated solubilities that correect DOE database at 3x volumes were correctly input into the spreadsheet to convert from molal to molar concentrations. QA checks for other ERDA-6 brine volumes also showed correct entry into the spreadsheet.

Figure 25 Figure 19 PHREEQC output (left) and molar spreadsheet calculator (right) for ERDA-6 at 3x volumes for recalculated CRA-2019 solubilities

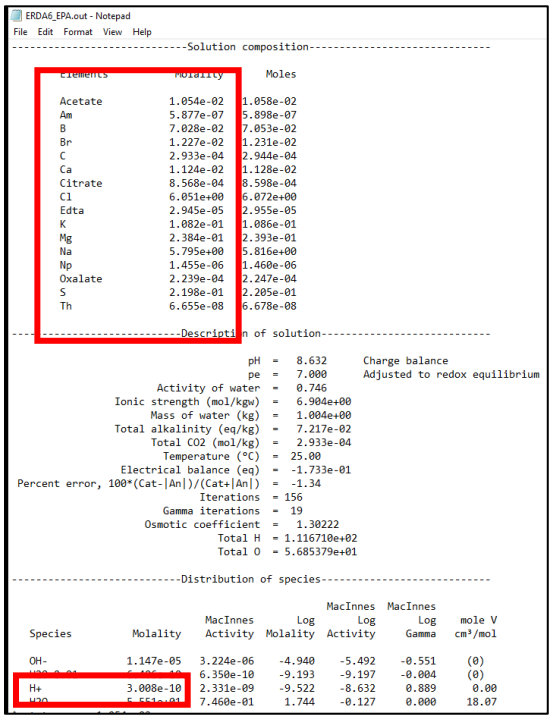
ERDA6_EPA.out - Notepad
File Edit Format View Help
Solution composition
Elements Molarity Moles
Acetate 1.054e-02 1.058e-02
Am 5.877e-07 5.898e-07
B 7.028e-02 7.053e-02
Br 1.227e-02 1.231e-02
C 2.933e-04 2.944e-04
Ca 1.124e-02 1.128e-02
Citrate 8.568e-04 8.598e-04
Cl 6.051e+00 6.072e+00
Edta 2.945e-05 2.955e-05
K 1.082e-01 1.086e-01
Mg 2.384e-01 2.393e-01
Na 5.795e+00 5.816e+00
Np 1.455e-06 1.460e-06
Oxalate 2.239e-04 2.247e-04
S 2.198e-01 2.205e-01
Th 6.655e-08 6.678e-08
Description of solution
pH = 8.632 Charge balance
pe = 7.000 Adjusted to redox equilibrium
Activity of water = 0.746
Ionic strength (mol/kgw) = 6.904e+00
Mass of water (kg) = 1.004e+00
Total alkalinity (eq/kg) = 7.217e-02
Total CO2 (mol/kg) = 2.933e-04
Temperature (°C) = 25.00
Electrical balance (eq) = -1.733e-01
Percent error, 100*(Cat-|An|)/(Cat+|An|) = -1.34
Iterations = 156
Gamma iterations = 19
Osmotic coefficient = 1.30222
Total H = 1.116710e+02
Total O = 5.685379e+01
Distribution of species
Species Molality MacInnes Activity Log Molality Log MacInnes Activity Log MacInnes Gamma mole V cm³/mol
OH- 1.147e-05 3.224e-06 -4.940 -5.492 -0.551 (0)
6.350e-10 -9.193 -9.197 -0.004 (0)
H+ 3.008e-10 2.331e-09 -9.522 -8.632 0.889 0.00
7.460e-01 1.744 -0.127 0.000 18.07

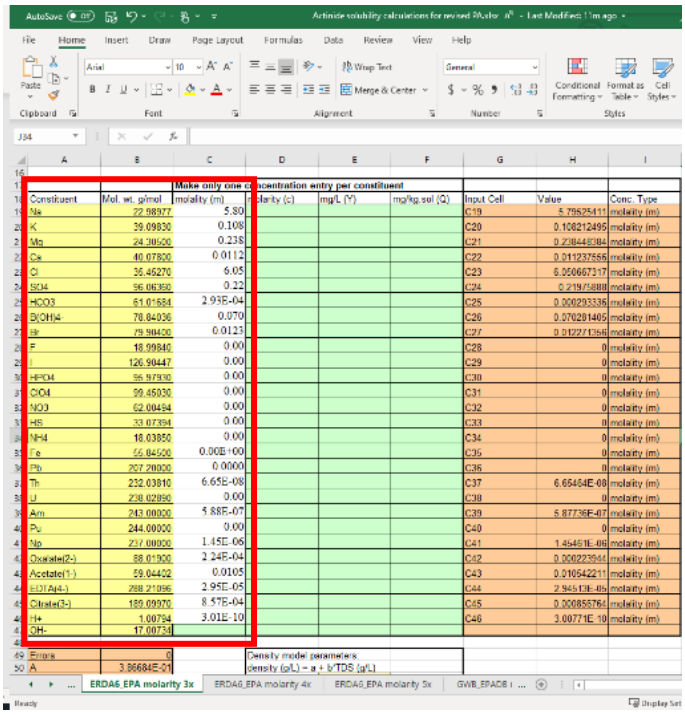

After correcting for the different brine densities in the original input files, Am(III), Th(IV), and Np(V) values used for the solubility parameters differed slightly compared to the values presented in the QAPP. However, these differences are very minor and only occur after two or three decimal places. These corrected values will be used as the SOLMOD3, SOLMOD4, and SOLMOD5 parameter values in EPA's sensitivity studies.

Table 8 Updated solubility values for EPA sensitivity study

Actinide	Parameter	QAPP Concentration (M)	Updated Concentration (M)
Am(III)	SOLMOD3:SOLSOH	2.139E-06	2.139E-06
Am(III)	SOLMOD3:SOLSOH2	1.091E-06	1.093E-06
Am(III)	SOLMOD3:SOLSOH3	7.721E-07	7.736E-07
Am(III)	SOLMOD3:SOLSOH4	6.180E-07	6.193E-07
Am(III)	SOLMOD3:SOLSOH5	5.266E-07	5.277E-07
Am(III)	SOLMOD3:SOLCOH	1.429E-06	1.429E-06
Am(III)	SOLMOD3:SOLCOH2	7.256E-07	7.263E-07
Am(III)	SOLMOD3:SOLCOH3	5.158E-07	5.164E-07
Am(III)	SOLMOD3:SOLCOH4	4.153E-07	4.158E-07

Am(III)	SOLMOD3:SOLCOH5	3.559E-07	3.563E-07
Th(IV)	SOLMOD4:SOLSOH	5.497E-08	5.497E-08
Th(IV)	SOLMOD4:SOLSOH2	5.509E-08	5.509E-08
Th(IV)	SOLMOD4:SOLSOH3	5.514E-08	5.513E-08
Th(IV)	SOLMOD4:SOLSOH4	5.516E-08	5.515E-08
Th(IV)	SOLMOD4:SOLSOH5	5.517E-08	5.517E-08
Th(IV)	SOLMOD4:SOLCOH	5.836E-08	5.836E-08
Th(IV)	SOLMOD4:SOLCOH2	5.844E-08	5.844E-08
Th(IV)	SOLMOD4:SOLCOH3	5.847E-08	5.847E-08
Th(IV)	SOLMOD4:SOLCOH4	5.849E-08	5.848E-08
Th(IV)	SOLMOD4:SOLCOH5	5.849E-08	5.849E-08
Np(V)	SOLMOD5:SOLSOH	4.375E-07	4.375E-07
Np(V)	SOLMOD5:SOLSOH2	3.218E-07	3.216E-07
Np(V)	SOLMOD5:SOLSOH3	2.825E-07	2.822E-07
Np(V)	SOLMOD5:SOLSOH4	2.629E-07	2.626E-07
Np(V)	SOLMOD5:SOLSOH5	2.511E-07	2.507E-07
Np(V)	SOLMOD5:SOLCOH	1.821E-06	1.821E-06
Np(V)	SOLMOD5:SOLCOH2	1.417E-06	1.416E-06
Np(V)	SOLMOD5:SOLCOH3	1.280E-06	1.278E-06
Np(V)	SOLMOD5:SOLCOH4	1.211E-06	1.209E-06
Np(V)	SOLMOD5:SOLCOH5	1.170E-06	1.168E-06
U(VI)	SOLMOD6:SOLSOH	1.000E-03	1.000E-03
U(VI)	SOLMOD6:SOLCOH	1.000E-03	1.000E-03

CONVERTED DATABASES

DATA0FM.DAT

DATA0FM.DAT 8/12/2020
atomic weights consistent with DATA0.FM4

```
# Data from DATA0.FM4 for actinides and Pitzer parameters
# Aqueous speciation written as association reactions so log k's are reversed
# from EQ36 format
# Reactions with dissolved carbonates, dissolved boron, and phosphate are re-written
# to use CO3-2, B(OH)3, and PO4-3 as the basis species to be consistent with PHREEQC
# format using relevant reactions.  This change was done to allow direct comparisons
# of log k's to values in PITZER.DAT but all are consistent with DATA0.FM4
# Additional Pitzer parameters for Br- from pitzer.dat are commented out because not in DATA0.FM4
# Perclorate Pitzer parameters included but commented out because perchlorate is suppressed by DOE for WIPP solubility modeling
# This database cannot be used for redox reactions without review and additional data
#------------------------------------------------------------------------
#------------------------------------------------------------------------
SOLUTION_MASTER_SPECIES
# Atomic weight data from 99lid via data0.ymp.R5 (DTN: SN0612T0502404.014)]
Alkalinity CO3-2      1.0          Ca0.5(CO3)0.5      50.05
B          B(OH)3                  0.0          B                  10.811
Br     Br-            0.0          Br                 79.904
C          CO3-2                   2.0          HCO3               12.011
C(4)   CO3-2                       2.0          HCO3               12.011
Ca     Ca+2                        0.0          Ca                 40.078
Cl     Cl-            0.0          Cl                 35.4527
E          e-                      0.0          0.0                0.0
H          H+                      -1.0         H                  1.00794
H(1)       H+                      -1.0         0.0
Fe         Fe+2                    0.0          Fe                 55.845
Fe(2)      Fe+2                    0.0          Fe
K          K+                      0.0          K                  39.0983
Mg     Mg+2                        0.0          Mg                 24.305
N          NO3-                    0.0    N     14.00674
N(5)       NO3-                    0.0          N
Na     Na+            0.0          Na                 22.98977
O          H2O                     0.0          O                  15.99940
O(0)       O2                      0.0          O
O(-2)      H2O                     0.0          0.0
S          SO4-2                   0.0          SO4                32.066
S(6)   SO4-2                       0.0          SO4
# Additions from EQ36 ----------------------------------
Pb                     Pb+2                     0.0          207.2              207.2
P                      PO4-3                    2.0          30.97376   30.97376
Am                     Am+3                     0.0          Am                 243.0
Np                     NpO2+                    0.0          Np                 237.0
Th                     Th+4                     0.0          Th                 232.0381
Acetate                Acetate-   1     59.05               59.05
Citrate                Citrate-3  2     189.06              189.06
Edta                   Edta-4                   2      276                     276
Oxalate                Oxalate-2  2           88                               88
Lactate                Lactate-   1           89                               89
#------------------------------------------------------------------------
# Deletions from pitzer.dat ----------------------------------
#Ba     Ba+2                    0.0          Ba                 137.327
#Li     Li+            0.0          Li                 6.941
#Mn     Mn+2                    0.0          Mn                 54.93805
#Mn(2)      Mn+2                0.0          Mn
#Sr     Sr+2                    0.0          Sr                 87.62
#------------------------------------------------------------------------
SOLUTION_SPECIES
#H+ primary master species
      H+ = H+
      log_k         0.0

#e- primary master species
      e- = e-
      log_k         0.0

#H2O primary master species
      H2O = H2O
      log_k         0.0

#Li+ primary master species
#             Li+ = Li+
```

```
#               -dw           1.03e-9
#               -Vm   -.0237   -.0690   11.5800   -2.7761 .4862 6 # supcrt

#Na+ primary master species
                Na+ = Na+
#               -dw           1.33e-9
#               -Vm  1.403  -2.285  4.419  -2.726  -5.125e-5  4.0  0.162  47.67  -3.09e-3  0.725 # supcrt modified

#K+ primary master species
                K+ = K+
#               -dw           1.96e-9
#               -Vm  3.322  -1.473  6.534  -2.712  9.06e-2  3.5  0  29.70  0  1 # supcrt modified

#Mg+2 primary master species
                Mg+2 = Mg+2
#               -dw           0.705e-9
#               -Vm  -1.410  -8.6  11.13  -2.39  1.332  5.5  1.29  -32.9  -5.86e-3  1 # supcrt modified

#Ca+2 primary master species
                Ca+2 = Ca+2
#               -dw           0.793e-9
#               -Vm  -0.3456  -7.252  6.149  -2.479  1.239  5  1.60  -57.1  -6.12e-3  1 # supcrt modified

#Sr+2 primary master species
#               Sr+2 = Sr+2
#               -dw           0.794e-9
#               -Vm  -1.57e-2  -10.15  10.18  -2.36  0.860  5.26  0.859  -27.0  -4.1e-3  1.97 # supcrt modified

#Ba+2 primary master species
#               Ba+2 = Ba+2
#               -dw           0.848e-9
#               -Vm  2.063  -10.06  1.9534  -2.36  0.4218  5  1.58  -12.03  -8.35e-3  1 # supcrt modified

#Mn+2 primary master species
#               Mn+2 = Mn+2
#               -dw           0.688e-9
#               -Vm   -.1016   -8.0295   8.9060   -2.4471  1.4006 6 # supcrt

#Fe+2 primary master species
                Fe+2 = Fe+2
#               -dw           0.719e-9
#               -Vm  -0.3255  -9.687  1.536  -2.379  0.3033  5.5  -4.21e-2  37.96  0  1 # supcrt modified

#Cl- primary master species
                Cl- = Cl-
#               -dw           2.03e-9
#               -Vm  4.465  4.801  4.325  -2.847  1.748  0  -0.331  20.16  0  1 # supcrt modified

#NO3- primary master species
                NO3- = NO3-
                log_k 0

#CO3-2 primary master species
                CO3-2 = CO3-2
#               -dw           0.955e-9
#               -Vm  5.052 0  0  -5.447  4.927  0  0.103  94.9  -1.30e-2  1 # supcrt modified

#SO4-2 primary master species
                SO4-2 = SO4-2
#               -dw           1.07e-9
#               -Vm  5.0  9.06  -8.36  -3.14  3.773  0  6.61  -27.9  -6.32e-2  0.428 # supcrt modified

#B(OH)3 primary master species
                B(OH)3 = B(OH)3
#               -dw           1.1e-9
#               -Vm 7.0643   8.8547   3.5844   -3.1451 -.2000  # supcrt

#Br- primary master species
                Br- = Br-
#               -dw           2.01e-9
```

```
#               -Vm  5.2690   6.5940   4.7450   -3.1430 1.3858 # supcrt

# From EQ36 ---------------------------------------------------------------------------------------

#Am+3 primary master species
                Am+3 =  Am+3
                log_k 0

#NpO2+ primary master species
                NpO2+ =  NpO2+
                log_k 0

#Th+4 primary master species
                Th+4 =  Th+4
                log_k 0

#Pb+2 primary master species
        Pb+2 = Pb+2
        log_k           0.0

#PO4-3 primary master species
        PO4-3 = PO4-3
        log_k           0.0

#Acetate- primary master species
                Acetate- = Acetate-
                log_k 0

#Citrate-3 primary master species
                Citrate-3 = Citrate-3
                log_k 0

#Edta-4 primary master species
                Edta-4 = Edta-4
                log_k 0

#Oxalate-2 primary master species
                Oxalate-2 = Oxalate-2
                log_k 0

#Lactate- primary master species
                Lactate- = Lactate-
                log_k 0

#-----------------------------------------------------------------------------
# Aqueous Species
#-----------------------------------------------------------------------------
H2O = OH- + H+                                          # pitzer.dat
                log_k           -13.9967                                # EQ36
#               -analytic  68.547  0  -6199.8  -24.955
#               -dw             5.27e-9
#               -Vm  1.776  0.0738  1.417  -2.782  2.347  0  0.906  0  0  1 # supcrt modified

2 H2O = O2 + 4 H+ + 4 e-                                # pitzer.dat
                -log_k       -86.0032                   # EQ36
#               -delta_h 134.79 kcal                    # pitzer.dat
#               -dw             2.35e-9                 # pitzer.dat
#               -Vm  5.7889  6.3536  3.2528  -3.0417  -0.3943 # supcrt   # pitzer.dat

CO3-2 + H+ = HCO3-                                      # pitzer.dat
                log_k           10.3392                 # EQ36.dat; pitzer.dat has 10.3391
#               delta_h -3.561  kcal                    # pitzer.dat

HCO3- + H+ = CO2 + H2O                                  # pitzer.dat
                log_k           6.3374                  # EQ36
#               delta_h       -5.738  kcal               # pitzer.dat

SO4-2 + H+ = HSO4-                                      # pitzer.dat
                log_k           1.9786                  # EQ36; pitzer.dat has 1.979
#               delta_h 4.91    kcal                    # pitzer.dat
```

```
B(OH)3 + H2O = B(OH)4- + H+                    # EQ36
        log_k          -9.239                  # EQ36, pitzer.dat has -9.239
#       delta_h 0   kcal                       # pitzer.dat

3 B(OH)4- + 2H+ = B3O3(OH)4- + 5 H2O  # EQ36
        log_k          20.1893         # EQ36
#       delta_h 0   kcal               # pitzer.dat

4 B(OH)4- + 2H+ = B4O5(OH)4-2 + 7 H2O          # EQ36
        log_k          20.8220         # EQ36
#       delta_h 0   kcal               # pitzer.dat

Ca+2 + B(OH)4- = CaB(OH)4+             # EQ36
        log_k          1.6503          # EQ36
#       delta_h 0   kcal               # pitzer.data

Mg+2 + B(OH)4- = MgB(OH)4+                     # EQ36
        log_k          1.3993          # EQ36
#       delta_h 0   kcal               # pitzer.dat

Mg+2 + H2O = MgOH+ + H+                        # pitzer.dat
        log_k          -11.8091        # EQ36 (pitzer.dat has -11.809)
#       delta_h 15.419 kcal            # pitzer.dat
                                               # log k Source: none

Pb+2 + Cl- = PbCl+                             # EQ36
    log_k      1.5                             # EQ36 (pitzer has 1.6)
#     delta_h 4.38 kcal                        # wateq4f.data
                                               # log k Source: Powell et al. (2009) Derived with SIT Model

Pb+2 + 2 Cl- = PbCl2                           # EQ36
    log_k      2.1                             # EQ36 (wateq4f.data has 1.8)
#     delta_h 1.08 kcal                        # wateq4f.dat
                                               # logk  Source: Powell et al. (2009) Derived with SIT Model

Pb+2 + 3 Cl- = PbCl3-                          # EQ36
    log_k      2.0                             # EQ36 (wateq4f.dat has 1.7)
#     delta_h 2.17 kcal                        # wateq4f.dat
                                               # log k Source: Powell et al. (2009) Derived with SIT Model

Pb+2 + H2O = PbOH+ + H+                # EQ36
    log_k     -7.46                # EQ36 (wateq4f.dat has -7.71)
#       delta_h 0    kcal                  # no data
                                           # log k Source: Powell et al. (2009) Derived with SIT Model

Pb+2 + 2 H2O = Pb(OH)2 + 2 H+                  # EQ36
    log_k     -16.94               # EQ36 (wateq4f.dat has -17.12)
#       delta_h 0    kcal                  # no data
                                           # log k Source: Powell et al. (2009)

Pb+2 + HCO3- = PbCO3 + H+                      # EQ36
    log_k     -3.89                # EQ36 (wateq4f.dat has 3.89)
#       delta_h 0    kcal                  # no data
                                           # log k Source: Powell et al. (2009) Derived with SIT Model

Pb+2 + 2 HCO3-  = Pb(CO3)2-2 + 2H+     # EQ36
    log_k     -10.55               # EQ36 (wateq4f.dat has 10.64)
#       delta_h 0    kcal                  # no data
                                           # log k Source: Powell et al. (2009) Derived with SIT Model

Pb+2 + SO4-2 = PbSO4                           # EQ36
    log_k      2.72                # EQ36 (wateq4f.dat has 2.75)
#       delta_h 0    kcal                  # no data
                                           # log k Source: Powell et al. (2009) Derived with SIT Model

Pb+2 + HCO3- + Cl- = PbCO3Cl- + H+     # EQ36
        log_k     -3.87                # EQ36
#       delta_h 0    kcal                  # no data
                                           # log k ource:Powell et al. (2009) Derived with SIT Model
```

```
Pb+2 + HCO3- + H2O = PbCO3OH- + 2H+ # EQ36
        log_k      -13.4400          # EQ36
#       delta_h 0    kcal            # no data
                                     # log k Source:Powell et al. (2009) Derived with SIT Model

Fe+2 + HCO3- = FeCO3 + H+            # EQ36
    log_k       -4.8300              # EQ36
#       delta_h 0    kcal            # no data
                                     # log k Source: Bruno et al 1992

Fe+2 + 2 HCO3- = Fe(CO3)2-2 + 2H+    # EQ36
        log_k           -13.8900             # EQ36
#       delta_h 0    kcal            # no data
                                     # log k Source: Kim et al. (2017)

Fe+2 + H2O = FeOH+ + H+              # EQ36
    log_k      -9.31          # EQ36 (wateq4f.dat has -9.5)
#     delta_h 13.2 kcal               # wateq4f.dat
                                     # log k Source: Shock et al 1997

Fe+2 + 2 H2O = Fe(OH)2 + 2 H+                # EQ36
    log_k      -20.82          # EQ36 (wateq4f.dat has -20.57)
#     delta_h 28.565 kcal              # wateq4f.dat
                                     # log k Source: Stumm & Morgan (1996)

Fe+2 + 3 H2O = Fe(OH)3- + 3 H+               # EQ36
    log_k      -31.0           # EQ36 (wateq4fg.dat also has -31.0)
#     delta_h 30.3 kcal                # wateq4f.dat
                                     # log k Source: Baes and Mesmer (1976)

Ca+2 + HCO3- = CaCO3 + H+            # EQ36
        log_k          -7.188        # EQ36
#       delta_h 3.547   kcal         # pitzer.dat

Mg+2 + HCO3- = MgCO3 + H+            # EQ36
        log_k          -7.4108       # EQ36
#       delta_h 2.535   kcal         # pitzer.dat

H+ + PO4-3 = HPO4-2                  # EQ36
    log_k     12.3426                # EQ36 (wateq4f.dat has 12.346)
#     delta_h -3.53 kcal               # wateq4f.dat

H+ + HPO4-2 = H2PO4-                 # EQ36
    log_k     7.2062         # EQ36
#     delta_h -4.52 kcal               # wateq4f.dat

2 H+ + HPO4-2 = H3PO4                # EQ36
    log_k     9.3517         # EQ36
    delta_h   -10.1 kJ       # minteq.v4.dat

Acetate- + H+ = HAcetate             # EQ36
        log_k     4.7568             # EQ36
#       delta_h     0.41       kJ    # minteq.v4.data

Acetate- + Mg+2 = MgAcetate+         # EQ36
        log_k     1.1131             # EQ36

Acetate- + Ca+2 = CaAcetate+         # EQ36
        log_k     1.1131             # EQ36

Citrate-3 + 3 H+ = H3Citrate         # EQ36
        log_k          14.27         # EQ36 Hummel et al. (2005) Derived with SIT Model

Citrate-3 + 2 H+ = H2Citrate-        # EQ36
        log_k     11.14              # EQ36 Hummel et al. (2005) Derived with SIT Model

Citrate-3 + H+ = HCitrate-2          # EQ36
        log_k      6.36              # EQ36 Hummel et al. (2005) Derived with SIT Model
```

```
Citrate-3 + H+ + Mg+2 = MgHCitrate          # EQ36
        log_k          8.96                 # EQ36 Hummel et al. (2005) Derived with SIT Model

Citrate-3 + 2 H+ + Mg+2 = MgH2Citrate+      # EQ36
        log_k          12.450               # EQ36 Hummel et al. (2005) Derived with SIT Model

Citrate-3 + Mg+2 = MgCitrate-               # EQ36
        log_k      4.81                     # EQ36 Hummel et al. (2005) Derived with SIT Model

Citrate-3 + Ca+2 = CaCitrate-               # EQ36
        log_k      4.80                     # EQ36 Hummel et al. (2005) Derived with SIT Model

Citrate-3 + H+ + Ca+2 = CaHCitrate          # EQ36
        log_k          9.28                 # EQ36 Hummel et al. (2005) Derived with SIT Model

Citrate-3 + 2 H+ + Ca+2 = CaH2Citrate+      # EQ36
        log_k      12.67                    # EQ36 Hummel et al. (2005) Derived with SIT Model

Edta-4 + 4 H+ = H4Edta                              # EQ36
        log_k      23.42                    # EQ36 Hummel et al. (2005) Derived with SIT Model

Edta-4 + 3 H+ = H3Edta-                             # EQ36
        log_k      21.19                    # EQ36 Hummel et al. (2005) Derived with SIT Model

Edta-4 + 2 H+ = H2Edta-2                    # EQ36
        log_k      18.04                    # EQ36 Hummel et al. (2005) Derived with SIT Model

Edta-4 + H+ = HEdta-3                               # EQ36
        log_k      11.24                    # EQ36 Hummel et al. (2005) Derived with SIT Model

Edta-4 + Na+ = NaEdta-3                             # EQ36
        log_k      2.80                     # EQ36 Hummel et al. (2005) Derived with SIT Model

Edta-4 + Mg+2 = MgEdta-2                    # EQ36
        log_k      10.90                    # EQ36 Hummel et al. (2005) Derived with SIT Model

Edta-4 + H+ + Mg+2 = MgHEdta-               # EQ36
        log_k          15.40                # EQ36 Hummel et al. (2005) Derived with SIT Model

Edta-4 + Ca+2 = CaEdta-2                    # EQ36
        log_k      12.69                    # EQ36 Hummel(2005)

Edta-4 + H+ + Ca+2 = CaHEdta-               # EQ36
        log_k      16.23                    # EQ36 Hummel(2005)

Oxalate-2 + 2 H+ = H2Oxalate                # EQ36
        log_k      5.6532                   # EQ36 Giambalvo

Oxalate-2 + H+ = HOxalate-                  # EQ36
        log_k      4.2596                   # EQ36 Giambalvo

Oxalate-2 + Mg+2 = MgOxalate                # EQ36
        log_k      3.7931                   # EQ36 Giambalvo

2 Oxalate-2 + Mg+2 = Mg(Oxalate)2-2         # EQ36
        log_k      5.24                     # EQ36 Jang & Kim 2016

Oxalate-2 + Ca+2 = CaOxalate                # EQ36
        log_k      3.7931                   # EQ36 Giambalvo

Lactate- + H+ = HLactate                    # EQ36
        log_k      3.8209                   # EQ36

#---------------------------------------------------------------------
# Actinides-----------------------------------------------------------

Am+3 + HCO3- = AmCO3+ + H+                          # EQ36
        log_k    -2.2388                    # EQ36

Am+3 + 2 HCO3- = Am(CO3)2- + 2 H+           # EQ36
```

```
        log_k          -7.6766              # EQ36

Am+3 + 3 HCO3- = Am(CO3)3-3 + 3 H+   # EQ36
        log_k     -15.8157              # EQ36

Am+3 + 4 HCO3- = Am(CO3)4-5 + 4H+    # EQ36
        log_k    -28.3586              # EQ36

Am+3 + H2O = AmOH+2 + H+             # EQ36
        log_k     -7.5556              # EQ36

Am+3 + 2 H2O = Am(OH)2+ + 2 H+                  # EQ36
        log_k          -15.6915              # EQ36

Am+3 + 3 H2O = Am(OH)3 + 3 H+                   # EQ36
        log_k    -25.6905              # EQ36

Am+3 + Cl- = AmCl+2                             # EQ36
        log_k    0.2393                         # EQ36

Am+3 + 2 Cl- = AmCl2+                           # EQ36
        log_k    -0.74                          # EQ36

Am+3 + SO4-2 = AmSO4+                           # EQ36
        log_k    3.2485                         # EQ36

Am+3 + 2 SO4-2 = Am(SO4)2-           # EQ36
        log_k         3.7019                    # EQ36

Am+3 + Acetate- = AmAcetate+2                   # EQ36
        log_k   2.7426                          # EQ36

Am+3 + Citrate-3 = AmCitrate         # EQ36
        log_k   8.7984                          # EQ36

Am+3 + Edta-4 = AmEdta-                         # EQ36
        log_k   18.9700                         # EQ36

Am+3 + Oxalate-2 = AmOxalate+                   # EQ36
        log_k    6.1566                         # EQ36

Am+3 + Lactate- = AmLactate+2        # EQ36
        log_k    3.7089                         # EQ36

Th+4  + 5 HCO3- = Th(CO3)5-6 + 5H+   # EQ36
        log_k   -24.5828              # EQ36

Th+4 + HCO3- + 3 H2O = Th(OH)3CO3- + 4 H+       # EQ36
        log_k   -14.0457                        # EQ36

Th+4 + 4 H2O = Th(OH)4 + 4 H+                   # EQ36
        log_k   -17.5002              # EQ36

Th+4 + 2 SO4-2 = Th(SO4)2            # EQ36
        log_k         11.5918         # EQ36

Th+4 + 3 SO4-2 = Th(SO4)3-2          # EQ36
        log_k         12.4273         # EQ36

Th+4 + Acetate- = ThAcetate+3        # EQ36
        log_k     7.3617              # EQ36

Th+4 + 2 Acetate- = Th(Acetate)2+2   # EQ36
        log_k    11.2391              # EQ36

Th+4 + Citrate-3 = ThCitrate+        # EQ36
        log_k    15.2355              # EQ36

Th+4 + Edta-4 = ThEdta                          # EQ36
        log_k    23.5570              # EQ36
```

```
Th+4 + Oxalate-2 = ThOxalate+2                  # EQ36
        log_k    11.3863                # EQ36

Th+4 + Lactate-         = ThLactate+3           # EQ36
        log_k     6.8284                # EQ36

Th+4 + 2 Lactate- = Th(Lactate)2+2      # EQ36
        log_k    11.1913                # EQ36

NpO2+ + HCO3- = NpO2CO3- + H+           # EQ36
        log_k     -5.3223               # EQ36

NpO2+ + 2 HCO3- = NpO2(CO3)2-3 + 2 H+   # EQ36
        log_k     -14.2340              # EQ36

NpO2+ + 3 HCO3- = NpO2(CO3)3-5 + 3H+    # EQ36
        log_k     -25.6859              # EQ36

NpO2+ + H2O = NpO2OH + H+               # EQ36
        log_k    -11.3084               # EQ36

NpO2+ + 2 H2O = NpO2(OH)2- + 2 H+       # EQ36
        log_k    -23.5362               # EQ36

NpO2+ + Acetate- = NpO2Acetate          # EQ36
        log_k      1.3737               # EQ36

NpO2+ + Citrate-3 = NpO2Citrate-2       # EQ36
        log_k      3.4969               # EQ36

NpO2+ + Edta-4 = NpO2Edta-3             # EQ36
        log_k      8.5352               # EQ36

NpO2+ + H+ + Edta-4 = NpO2HEdta-2       # EQ36
        log_k     15.6464               # EQ36

NpO2+ + 2 H+ + Edta-4 = NpO2H2Edta-     # EQ36
        log_k    20.8648                # EQ36

NpO2+ + Oxalate-2 = NpO2Oxalate-        # EQ36
        log_k     4.2400                # EQ36

NpO2+ + Lactate- = NpO2Lactate          # EQ36
        log_k     1.9674                # EQ36

#---------------------------------------------------------------
#---------------------------------------------------------------
#---------------------------------------------------------------

PHASES

CO2(g)
        CO2 = CO2
        log_k        -1.468
#       delta_h -4.776 kcal
#       -analytic  119.87356  2.185434e-2  -7337.8 -44.7652    669371
#       -T_c  304.2 # critical T, K
#       -P_c   72.80 # critical P, atm
#       -Omega 0.225 # acentric factor
H2O(g)
        H2O = H2O
        log_k  1.4999                           #EQ36
#       delta_h -44.03 kJ
#       -T_c  647.3 # critical T, K
#       -P_c  217.60 # critical P, atm
#       -Omega 0.344 #  acentric factor
#       -analytic   -16.5066 -2.0013E-3  2710.7  3.7646  0 2.24E-6

O2(g)
```

```
        O2 = O2
        -log_k   -2.8983
#       -analytic -7.5001 7.8981e-3 0.0 0.0 2.0027e5
#       -T_c  154.6
#       -P_c   49.80
#       -Omega 0.021

Pb2CO3Cl2(s)
        Pb2CO3Cl2 + H+ = 2 Pb+2 + 2 Cl- + HCO3-                 # EQ36 -  .dat
        log_k     0.4100                                        # EQ36 Powell et al. (2009) Derived with SIT Model

PbSO4(s)
        PbSO4 = Pb+2 + SO4-2                                    # EQ36 -  .dat
        log_k          -7.80                                    # EQ36 Powell et al. (2009) Derived with SIT Model

Cerussite
        PbCO3 + H+ = Pb+2 + HCO3-                               # EQ36 -  .dat
        log_k           -2.84                                   # EQ36 Powell et al. (2009) Derived with SIT Model
#       delta_h 4.86 kcal                                       # WATEQ4F.DAT

Litharge
        PbO + 2H+ = Pb+2 + H2O                                  # EQ36 -  .dat
        log_k       12.62                                       # EQ36 Powell et al. (2009) Derived with SIT Model
#       delta_h -16.380 kcal                                    # WATEQ4F.DAT

Ca2Edta:7H2O(s)
        Ca2Edta:7H2O = 2 Ca+2 + Edta-4 + 7 H2O                  # EQ36
        log_k      -16.8100                                     # EQ36 - Domski (2018)

MgOxalate:2H2O(s)
        MgOxalate:2H2O = Mg+2 + Oxalate-2 + 2 H2O               # EQ36
        log_k       -6.4100                                     # EQ36 - Glushinskite from AP-182

Siderite
        FeCO3 + H+ = Fe+2 + HCO3-                               # EQ36
        log_k      -0.1200                                      # EQ36 Stumm and Morgan (1996)

Chukanovite
        Fe2(OH)2CO3 + 3 H+ = 2 Fe+2 + HCO3- + 2H2O              # EQ36 -  .dat
        log_k      12.32                                        # EQ36 Kim et al (2017)

Oxychloride-Fe-3(s)
        Fe2Cl(OH)3 + 3 H+ = Cl- + 2 Fe+2 + 3 H2O                # EQ36 -  .dat
        log_k      17.08                                        # EQ36 Kim et al (2017)

Fe(OH)2-Hex
        Fe(OH)2 + 2 H+ = Fe+2 + 2 H2O                           # EQ36 -  .dat
        log_k      12.89                                        # EQ36 Kim et al (2017)

AmOHCO3(c)
        AmOHCO3 + H+ = Am+3 + CO3-2 + H2O                       # EQ36
        log_k       -8.7026                                     # EQ36: AmOHCO3(c) + 2H+ = Am+3 + HCO3- + H2O; log k = 1.6366

Am(OH)3(s)
        Am(OH)3 + 3 H+ = Am+3 + 3H2O                            # EQ36
        log_k       14.4900                                     # EQ36

NaAm(CO3)2:6H2O(c)
        NaAm(CO3)2:6H2O = Na+ + Am+3 + 2 CO3-2 + 6 H2O                  # EQ36
        log_k           -21.3915                                        # EQ36: NaAm(CO3)2:6H2O(c) + 2H+ = Na+ + Am+3
+ 2HCO3- + 6H2O; log k = -0.7131

AmPO4(c)
        AmPO4 = Am+3 + PO4-3                                    # EQ36
        log_k      -24.8021                                     # EQ36: AmPO4(c) + H+ = Am+3 + HPO4-2; log k = -12.4595

ThO2(am)
        ThO2 + 4 H+ = Th+4 + 2 H2O                              # EQ36
        log_k       10.4865                                     # EQ36
```

```
Th(SO4)2:9H2O(s)
        Th(SO4)2:9H2O = Th+4 + 2 SO4-2 + 9 H2O                  # EQ36
        log_k   -12.9982                                # EQ36

Th(SO4)2:8H2O(s)
        Th(SO4)2:8H2O = Th+4 + 2 SO4-2 + 8 H2O                  # EQ36
        log_k   -12.8955                                # EQ36

Na2Th(SO4)3:6H2O(s)                                             # Th(SO4)2:Na2SO4:6H2O in EQ36
        Na2Th(SO4)3:6H2O = Th+4 + 2 Na+ + 3 SO4-2 + 6 H2O       # EQ36
        log_k   -17.6419                                # EQ36

K2Th(SO4)3:4H2O(s)                                              # Th(SO4)2:K2SO4:4H2O(s) in EQ36
        K2Th(SO4)3:4H2O = Th+4 + 2 K+ + 3 SO4-2 + 4 H2O         # EQ36
        log_k   -18.0740                                # EQ36

K4Th(SO4)4:2H2O(s)                                              # Th(SO4)2:2K2SO4:2H2O in EQ36
        K4Th(SO4)4:2H2O = Th+4 + 4 K+ + 4 SO4-2 + 2 H2O         # EQ36
        log_k   -21.2301                                # EQ36

Th2(SO4)4:7K2SO4(s)                                             # 2[Th(SO4)2.7/2K2SO4] in EQ36
        Th2(SO4)4:7K2SO4(s) = 2 Th+4 + 14 K+ + 11 SO4-2  # EQ36
        log_k   -49.2193                                # EQ36

NpO2OH(aged)
        NpO2OH + H+ = NpO2+ + H2O                               # EQ36
        log_k   4.5164                                  # EQ36

NpO2OH(am)
        NpO2OH + H+ = NpO2+ + H2O                               # EQ36
        log_k   5.2165                                  # EQ36

Na2(NpO2)2(CO3)2:7H2O(s)                                        # 2[NaNpO2CO3:7/2H2O] in EQ36
        Na2(NpO2)2(CO3)2:7H2O = 2 NpO2+ + 2 Na+ + 2 CO3-2 + 7 H2O       # EQ36,  Na2(NpO2)2(CO3)2:7H2O + 2H+ = 2Na+ +
2NpO2+ + 2HCO3- + 7H2O
        log_k   -22.1800

Na3NpO2(CO3)2(s)
        Na3NpO2(CO3)2 = 3 Na+ + NpO2+ + 2 CO3-2                 # EQ36
        log_k   -14.1801                                # EQ36 Na3NpO2(CO3)2 + 2H+ = 3Na+ + NpO2+ + 2HCO3-, log k =
6.4983

KNpO2CO3(s)
        KNpO2CO3 = K+ + NpO2+ + CO3-2                           # EQ36
        log_k   -13.6038                                # EQ36, KNpO2CO3 + H+ = K+ + NpO2+ + HCO3-, log k = -3.2646

K3NpO2(CO3)2(s)
        K3NpO2(CO3)2 = 3 K+ + NpO2+ + 2 CO3-2                   # EQ36
        log_k   -15.9307                                # EQ36, K3NpO2(CO3)2 + 2H+ = 3K+ + NpO2+ + 2HCO3-; log k = 4.7477

H2Oxalate:2H2O(s)
        H2Oxalate:2H2O = 2 H+ + Oxalate-2 + 2 H2O               # EQ36
        log_k   -5.6615                                 # EQ36 Giambalvo

NaHOxalate:H2O(s)
        NaHOxalate:H2O = Na+ + H+ + Oxalate-2 + H2O             # EQ36
        log_k   -6.0608                                 # EQ36 Giambalvo

Na2Oxalate(s)
        Na2Oxalate = 2 Na+ + Oxalate-2                          # EQ36
        log_k   -2.4051                                 # EQ36 Giambalvo

Anhydrite
        CaSO4 = Ca+2 + SO4-2                                    # EQ36
        log_k   -4.3621                         # EQ36 (pitzer.dat has -4.362)
#       delta_h -1.71 kcal                      # WATEQ4F.DAT
#       -anal  87.836  0  -3136.79  -32.953 # 50 - 160oC, 1 - 1e3 atm, anhydrite dissolution, Blount and Dickson, 1973, Am. Mineral. 58, 323.
#       -Vm 46.1 # 136.14 / 2.95

Aphthitalite/Glaserite
```

```
        NaK3(SO4)2 =  Na+ + 3 K+ + 2 SO4-2       # EQ36
        log_k         -3.8027                    # EQ36 (pitzer.dat has -3.803)

Whewellite
        CaOxalate:H2O = Ca+2 + Oxalate-2 + H2O           # EQ36
        log_k      -8.7517                               # EQ36  Xiong (2004)

Aragonite
        CaCO3 = CO3-2 + Ca+2
        log_k         -8.2194                            # EQ36 pitzer.dat has -8.336
#       delta_h -2.589 kcal                              # pitzer.dat
#       -analytic    -171.8607   -.077993    2903.293    71.595
#       -Vm 34.04

Arcanite
        K2SO4  =  SO4-2 + 2 K+                                  # EQ36
        log_k         -1.7763                            # EQ36 (pitzer has -1.776)
#       -analytic    2.823    0.0             -1371.2
#       -Vm 65.5

Bischofite
        MgCl2:6H2O  =  Mg++ + 2 Cl- + 6 H2O              # EQ36
        log_k         4.4554                             # EQ36 (pitzer.dat has 4.455)
#       -analytic    3.524    0.0             277.6
#       Vm 127.1

Bloedite
        Na2Mg(SO4)2:4H2O  =  Mg++ + 2 Na+ + 2 SO4-2 + 4 H2O      # EQ36
        log_k         -2.3469                                   # EQ36 (pitzer.dat has -2.347)
#       -delta_H   0                                            # No data
#       -delta_H   0                # Not possible to calculate enthalpy of reaction        Bloedite
#       Vm 147

Brucite
        Mg(OH)2 + 2 H+ =  Mg++ + 2 H2O                                                          # EQ36
        log_k         17.1090                                                       # EQ36
#       Mg(OH)2  =  + 1.0000 Mg++ + 2.0000 OH-
#       log_k         -10.88
#       -delta_H   4.85    kcal/mol                                                 # pitzer.dat
#       Vm 24.6

Burkeite
        Na6CO3(SO4)2 + H+  = HCO3- + 2 SO4-2 + 6 Na+     # EQ36
        log_k         9.5671                             # EQ36

Calcite
        CaCO3 + H+ = HCO3- + Ca+2
        log_k         1.9330
#       delta_h -2.297 kcal
#       -analytic    -171.8329    -0.077993    2839.319    71.595
#       -Vm 36.9

CaCl2:4H2O(s)
        CaCl2:4H2O = Ca+2 + 2 Cl- + 4 H2O                # EQ36
        log_k         5.7171                             # EQ36

CaOxychloride_A(s)
        Ca4Cl2(OH)6:13H2O + 6 H+ = 4 Ca+2 + 2 Cl- + 19 H2O          # EQ36 -  .dat
        log_k         68.7343                                       # EQ36

CaOxychloride_B(s)
        Ca2Cl2(OH)2:H2O + 2 H+ = 2 Ca+2 + 2 Cl- + 3 H2O             # EQ36 -  .dat
        log_k          26.5313                                      # EQ46

Carnallite
        KMgCl3:6H2O  =  K+ + Mg++ + 3 Cl- + 6 H2O        # EQ36
        log_k         4.3304                             # EQ36 (pitzer has 4.330)
#       Vm 173.7

#Celestite
```

```
#       SrSO4 = Sr+2 + SO4-2                                    # pitzer.dat
#       log_k       -6.630                                      # pitzer.dat not in EQ36
#       delta_h -1.037 kcal                                     # WATEQ4F.DAT
#       -analytic  -7.14 6.11E-03  75 0 0 -1.79E-05  # Howell et al., 1992, JCED 37, 464.
#       -Vm 46.4

Epsomite
        MgSO4:7H2O  =  Mg+2 + SO4-2 + 7 H2O                     # EQ36
        log_k       -1.8811                                     # EQ36 (pitzer.dat has -1.881)
#       delta_h 2.820 kcal                                      # WATEQ4F.DAT

Gaylussite
        CaNa2(CO3)2:5H2O + 2H+ = Ca+2 + 2 HCO3- + 2 Na+ + 5 H2O         # EQ36
        log_k       11.2576                                             # EQ36

Glauberite
        Na2Ca(SO4)2  =  Ca+2 + 2 Na+ + 2 SO4-2                  # EQ36
        log_k       -5.2445                                     # EQ36 (pitzer.dat has -5.245)
#       Vm 99

Gypsum
        CaSO4:2H2O = Ca+2 + SO4-2 + 2 H2O                               # EQ36
        log_k       -4.5805                                             # EQ36 (pitzer.dat has -4.581)
#       delta_h -0.109 kcal                                             # pitzer.dat

Halite
        NaCl  =  Cl- + Na+                                                          # EQ36
        log_k       1.5704                                                          # EQ36 (pitzer.dat has 1.570)
#       delta_h 0.918 kcal                                                          # WATEQ4F.DAT
#       -analytic -713.4616   -.1201241   37302.21    262.4583    -2106915.
#       -Vm 27.1

Hexahydrite
        MgSO4:6H2O  =  Mg+2 + SO4-2 + 6 H2O                             # EQ36
        log_k       -1.6351                                             # EQ36 (pitzer.dat has -1.635)
#       -analytic    -62.666   0.0             1828.     22.187
#       Vm 132

Kainite
        KMgClSO4:3H2O  =  Cl- + K+ + Mg+2 + SO4-2 + 3 H2O               # EQ36
        log_k       -0.1926                                             # EQ36 (pitzer.dat has -0.193)

Kalicinite
        KHCO3  =  K+ + HCO3-                    # EQ36
        log_k       0.2814              # EQ36

Kieserite
        MgSO4:H2O  =  Mg+2 + SO4-2 + H2O        # EQ36
        log_k       -0.1227                     # EQ36 (pitzer.dat has -0.123)
#       Vm 53.8

Leonite
        K2Mg(SO4)2:4H2O  =  Mg+2 + 2 K+ + 2 SO4-2 + 4 H2O               # EQ36
        log_k       -3.9790                                             # EQ36 (pitzer.dat has -3.979)

Labile_Salt
        Na4Ca(SO4)3:2H2O = 4 Na+ + Ca+2 + 3 SO4-2 + 2 H2O               # EQ36
        log_k       -5.6723                                             # EQ36 (pitzer.dat has -5.672)

Magnesite
        MgCO3 + H+ =  HCO3- + Mg+2# EQ36
        log_k       2.5054              # EQ36
#       delta_h     -6.169                      # pitzer.dat
#       Vm 28.3

Mg2Cl(OH)3:4H2O
        Mg2Cl(OH)3:4H2O + 3 H+ = 2 Mg+2 + Cl- + 7 H2O   # EQ36
        log_k    26.0297                                # EQ36

Mg3Cl(OH)5:4H2O
```

```
        Mg3Cl(OH)5:4H2O + 5 H+ = 3 Mg+2 + Cl- + 9 H2O   # EQ36
        log_k     42.9600                               # EQ36 Xiong et al. (2010), see Note for Revision 3

Mercallite
        KHSO4 = K+ + H+ + SO4-2                 # EQ36
        log_k         -1.4015               # EQ36

Mirabilite
        Na2SO4:10H2O  =  SO4-2 + 2 Na+ + 10 H2O                                         # EQ36
        log_k         -1.2278                                                           # EQ36 (pitzer.dat has -1.214)
#       delta_h 18.987 kcal                                                             # WATEQ4F.DAT

Misenite
        K8H6(SO4)7  =  6 H+ + 7 SO4-2 + 8 K+    # EQ36
        log_k         -10.8061                  # EQ36 (pitzer.dat has -10.086)

Nahcolite
        NaHCO3  =  HCO3- + Na+                  # EQ36
        log_k         -0.4030               # EQ36

Natron
        Na2CO3:10H2O + H+ = HCO3- + 2 Na+ + 10 H2O      # EQ36
        log_k         9.5145                            # EQ36
#       delta_h 15.745 kcal                             # WATEQ4F.DAT

Nesquehonite
        MgCO3:3H2O + H+ = HCO3- + Mg+2 + 3 H2O                  # EQ36
        log_k         5.1722                            # EQ36
#       delta_h -5.789 kcal                             # WATEQ4F.DAT

PicromeriteSchoenite
        K2Mg(SO4)2:6H2O = 2 K+ + Mg+2 + 2 SO4-2 + 6 H2O                 # EQ36
        log_k         -4.3277

Pirssonite
        Na2Ca(CO3)2:2H2O + 2 H + = 2 Na+ + Ca+2 + 2 HCO3- + 2 H2O       # EQ36
        log_k         11.4354                           # EQ36

Polyhalite
        K2MgCa2(SO4)4:2H2O  = 2 K+ +  Mg+2 + 2 Ca+2 + 4 SO4-2 + 2 H2O   # EQ36
        log_k         -13.7441                          # EQ36 (pitzer.dat has -13.744)
#       Vm 218

Portlandite
        Ca(OH)2 + 2H+ =  Ca+2 + 2 H2O                   # EQ36
        log_k         22.8035                   # EQ36
#       delta_h -31.0 kcal                      # WATEQ4F.DAT

K2CO3:1.5H2O
        K2CO3:1.5H2O + H+ = 2 K+ + HCO3- + 1.5 H2O      # EQ36
        log_k         13.3720                           # EQ36

K8H4(CO3)6:3H2O
        K8H4(CO3)6:3H2O + 2 H+ = 8 K+ + 6 HCO3- + 3 H2O                 # EQ36
        log_k     27.6874                                       # EQ36

KNaCO3:6H2O
        KNaCO3:6H2O + H+ = K+ + Na+ + HCO3- + 6 H2O             # EQ36
        log_k     10.2233                                       # EQ36

K-Trona
        K2NaH(CO3)2:2H2O + H+ = 2 K+ + Na+ + 2 HCO3- + 2 H2O    # EQ36
        log_k     11.5757                                       # EQ36

K3H(SO4)2(s)
        K3H(SO4)2 = 3 K+ + H+ + 2 SO4-2                 # EQ36
        log_k     -3.5425                       # EQ36

Na3H(SO4)2(s)
        Na3H(SO4)2 = 3 Na+ + H+ + 2 SO4-2       # EQ36
```

```
        log_k     -0.8143                                 # EQ36

Na2CO3:7H2O(s)
        Na2CO3:7H2O + H+ = 2 Na+ + HCO3- + 7 H2O        # EQ36
        log_k     9.8791                                # EQ36

Sylvite
        KCl  = K+ + Cl-                                         # EQ36
        log_k           0.8999                          # EQ36 (pitzer.dat has 0.900)
#       -analytic     3.984     0.0             -919.55
#       Vm 37.5

Syngenite
        K2Ca(SO4)2:H2O  =  2 K+ + Ca+2 + 2 SO4-2 + H2O  # EQ36
        log_k           -7.4484                         # EQ36 (pitzer.dat has -7.448)

Tachyhydrite
        Mg2CaCl6:12H2O = 2 Mg+2 + Ca+2 + 6 Cl- + 12 H2O                 # EQ36
        log_k      17.3839                                      # EQ36 -  .dat

Thenardite
        Na2SO4 = 2 Na+ + SO4-2                  # EQ36
        log_k           -0.2875         # EQ36 -  .dat
#       delta_h -0.572 kcal             # WATEQ4F.DAT

Thermonatrite
        Na2CO3:H2O + H+ = 2 Na+ + HCO3- + H2O           # EQ36
        log_k       10.8211                             # EQ36
#       delta_h -2.802 kcal                             # WATEQ4F.DAT

Trona
        Na3H(CO3)2:2H2O =  3 Na+ + H+ + 2 CO3-2 + 2 H2O                 # EQ36
        log_k           9.2948                                       # EQ36
#       delta_h -18.0 kcal                                           # WATEQ4F.DAT
#       Vm 106

Borax
        Na2(B4O5(OH)4):8H2O = 2 Na+ + 4 B(OH)4- + 2 H+ +  1 H2O         # EQ36
        log_k           -24.4918                                     # EQ36
#       Vm 223

Boric_acid(s)
        B(OH)3 + H2O  =  B(OH)4- + H+           # EQ36
        log_k           -9.2694         # EQ36 (pitzer.dat has -0.030)

K-Pentaborate30C(s)
        KB5O8:4H2O + 8 H2O = K+ + 5 B(OH)4- + 4 H+      # EQ36
        log_k       -41.5233                            # EQ36

K-Tetraborate30C(s)
        K2B4O7:4H2O + 5 H2O = 2 K+ + 4 B(OH)4- + 2 H+   # EQ36
        log_k       -23.0495                            # EQ36

Na_Metaborate(s)
        NaBO2:4H2O = Na+ + B(OH)4- + 2 H2O              # EQ36
        log_k       0.3292                              # EQ36

Na_Pentaborate(s)
        NaB5O8:5H2O + 7 H2O = Na+ + 5 B(OH)4- + 4 H+    # EQ36
        log_k       -40.2997                            # EQ36 -  .dat

Teepleite
        Na2B(OH)4Cl = B(OH)4- + 2 Na+ + Cl-     # EQ36
        log_k           1.6012                  # EQ36

Dolomite
        CaMg(CO3)2 + 2H+ = Ca+2 + Mg+2 + 2 HCO3-        # EQ36
        log_k           3.5960                          # EQ36
#       delta_h -9.436 kcal                             # pitzer.dat
#       -Vm 64.5
```

```
Hydromagnesite5424
        Mg5(CO3)4(OH)2:4H2O + 6 H+ = 5 Mg+2 + 4 HCO3- + 6 H2O   # EQ36
        log_k          31.4900                                  # EQ36 - Robie & Hemmingway (1973)
#       delta_h -52.244 kcal                                    # WATEQ4F.DAT

Hydromagnesite4323
        Mg4(CO3)3(OH)2:3H2O + 5 H+ = 4 Mg+2 + 3 HCO3- + 5 H2O   # EQ36
        log_k      28.8104                                      # EQ36


#------------------------------------------------------------------------------
# Actinide Phases
#------------------------------------------------------------------------------

#-----------------------------------------------------------------------------------------------------------------------
#-----------------------------------------------------------------------------------------------------------------------
#-----------------------------------------------------------------------------------------------------------------------
#  Pitzer coefficients
#-----------------------------------------------------------------------------------------------------------------------
#-----------------------------------------------------------------------------------------------------------------------
PITZER
-B0
Ca+2            Edta-4          5.39            0       0       0       0       0       #
Domski(2018)
Mg+2            CaEdta-2        0               0       0       0       0       0       # Domski(2018)
Mg+2            MgEdta-2        0               0       0       0       0       0       # Domski(2018)
Na+             NaEdta-3        0.59            0       0       0       0       0       # Felmy &
Mason(2003)
Na+             Mg(Oxalate)2-2  0.07            0       0       0       0       0       # AP-182
Fe+2            Cl-             0.37324         0       0       0       0       0       # Moog et
al. (2004) 15
Na+             Fe(CO3)2-2      -0.23           0       0       0       0       0       # Kim et al
(2017)
Na+             Cl-             0.0765          0       0       0       0       0       # HMW84
Na+             SO4-2           0.01958         0       0       0       0       0       # HMW84
Na+             HSO4-           0.0454          0       0       0       0       0       # HMW84
Na+             OH-             0.0864          0       0       0       0       0       # HMW84
Na+             HCO3-           0.0277          0       0       0       0       0       # HMW84
Na+             CO3-2           0.0399          0       0       0       0       0       # HMW84
Na+             B(OH)4-         -0.0427         0       0       0       0       0       # FW86
Na+             B3O3(OH)4-      -0.056          0       0       0       0       0       # FW86
Na+             B4O5(OH)4-2     -0.11           0       0       0       0       0       # FW86
Na+             Am(CO3)2-       -0.24           0       0       0       0       0       #
FanghŠnel et al 1999 (analogue w/Cm)
Na+             Am(CO3)3-3      0.125           0       0       0       0       0       #
FanghŠnel et al 1999 (analogue w/Cm)
#Na+            ClO4-           0.0554          0       0       0       0       0       # P91
Na+             NpO2CO3-        0.1             0       0       0       0       0       # FNK95
Na+             NpO2(CO3)2-3    0.48            0       0       0       0       0       # FNK95
Na+             NpO2(CO3)3-5    1.8             0       0       0       0       0       # FNK95
Na+             H2PO4-          -0.0533         0       0       0       0       0       # P91
Na+             HPO4-2          -0.0583         0       0       0       0       0       # P91
Na+             PO4-3           0.1781          0       0       0       0       0       # P91
Na+             Th(SO4)3-2      0.12            0       0       0       0       0       # FR92
Na+             Th(CO3)5-6      1.31            0       0       0       0       0       # FR92
Na+             HOxalate-       -0.2448         0       0       0       0       0       # SAND99/Mizera
Na+             Oxalate-2       -0.2176         0       0       0       0       0       # Choppin et al
(2001)
Na+             Acetate-        0.1426          0       0       0       0       0       # SAND99/NBC96
Na+             Lactate-        -0.0563         0       0       0       0       0       # SAND99/Moore et
al. 99
Na+             H2Citrate-      -0.1296         0       0       0       0       0       # SAND99/Mizera
Na+             HCitrate-2      -0.0989         0       0       0       0       0       # SAND99/Mizera
Na+             Citrate-3       0.0887          0       0       0       0       0       # SAND99/Mizera
Na+             H3Edta-         -0.2345         0       0       0       0       0       #
Giambalvo (2002)
Na+             H2Edta-2        -0.1262         0       0       0       0       0       # Giambalvo (2002)
Na+             HEdta-3         0.5458          0       0       0       0       0       #
Giambalvo (2002)
```

Na+	Edta-4		1.10	0	0	0	0	0	# Felmy & Mason(2003)
Na+	AmEdta-		-0.2239	0	0	0	0	0	# SAND99 (Typo in original; pair should be as listed above)
Na+	NpO2Citrate-2		-0.4226	0	0	0	0	0	# SAND99 (Typo in original; pair should be as listed above)
Na+	NpO2Edta-3		0.683	0	0	0	0	0	# SAND99, PBMC98 (listed correctly in PBMC98)
Na+	NpO2Oxalate-		-0.5418	0	0	0	0	0	# SAND99 (Correctly listed in Borkowski et al. 2001)
Na+	Am(CO3)4-5		2.022	0	0	0	0	0	# FK98, FanghŠnel et al. 1995
Na+	Am(SO4)2-		-0.354	0	0	0	0	0	# FK98 (Analogue with Cm)
Na+	NpO2H2Edta-		-0.8285	0	0	0	0	0	# PBMC98
Na+	CaCitrate-	0.1742		0	0	0	0	0	# ERG_org_memo (analogy w/Mg)
Na+	CaEdta-2	0.185		0	0	0	0	0	# Domski (2018)
Na+	MgCitrate-	0.1742		0	0	0	0	0	# ERG_org_memo
Na+	NpO2HEdta-2		0.4733	0	0	0	0	0	# PBMC98
K+	Cl-		0.04835	0	0	0	0	0	# HMW84
K+	SO4-2		0.04995	0	0	0	0	0	# HMW84
K+	HSO4-		-0.0003	0	0	0	0	0	# HMW84
K+	OH-		0.1298	0	0	0	0	0	# HMW84
K+	HCO3-		0.0296	0	0	0	0	0	# HMW84
K+	CO3-2		0.1488	0	0	0	0	0	# HMW84
K+	B(OH)4-		0.035	0	0	0	0	0	# FW86
K+	B3O3(OH)4-		-0.13	0	0	0	0	0	# FW86
K+	B4O5(OH)4-2		-0.022	0	0	0	0	0	# FW86
K+	Am(CO3)2-		-0.24	0	0	0	0	0	# FK98 (analogue w/Na)
K+	Am(CO3)3-3		0.125	0	0	0	0	0	# FK98 (analogue w/Na)
K+	NpO2CO3-		0.1	0	0	0	0	0	# Novak et al. 1997 (analogue w/Na)
K+	NpO2(CO3)2-3		0.48	0	0	0	0	0	# Novak et al. 1997 (analogue w/Na)
K+	NpO2(CO3)3-5		2.34	0	0	0	0	0	# Novak et al. 1997 (calculated from K data)
K+	H2PO4-		-0.678	0	0	0	0	0	# P91
K+	HPO4-2		0.0248	0	0	0	0	0	# P91
K+	PO4-3		0.3729	0	0	0	0	0	# P91
K+	Th(SO4)3-2		0.9	0	0	0	0	0	# FR92
K+	Th(CO3)5-6		1.31	0	0	0	0	0	# FRSMHC97 (analogue w/Na)
K+	HOxalate-	-0.2448		0	0	0	0	0	# SAND99/Mizera (Analogue with Na)
K+	Oxalate-2	-0.2176		0	0	0	0	0	# SAND99/Mizera (Analogue with Na)
K+	Acetate-	0.1587		0	0	0	0	0	# SAND99/Mizera (Analogue with Na)
K+	Lactate-	-0.0563		0	0	0	0	0	# SAND99/Moore et al. 1999 (Analogue with Na)
K+	H2Citrate-	-0.1296		0	0	0	0	0	# SAND99/Mizera (Analogue with Na)
K+	HCitrate-2	-0.989		0	0	0	0	0	# SAND99/Mizera (Analogue with Na)
K+	Citrate-3	0.0887		0	0	0	0	0	# SAND99/Mizera (Analogue with Na)
K+	H3Edta-		-0.2345	0	0	0	0	0	# Giambalvo (2002)
K+	H2Edta-2	-0.1262		0	0	0	0	0	# Giambalvo (2002)
K+	HEdta-3		0.546	0	0	0	0	0	# Giambalvo (2002)
K+	Edta-4		1.10	0	0	0	0	0	# Felmy & Mason(2003)
K+	AmEdta-		-0.2239	0	0	0	0	0	# SAND99 (Analogue with Na)

K+	NpO2Citrate-2		-0.4226		0	0	0	0	0	# SAND99 (analogue w/Na; error in original)
K+	NpO2Edta-3		0.683		0	0	0	0	0	# AND99/PBMC98 (Correctly listed in latter source)
K+	NpO2Oxalate-		-0.5418		0	0	0	0	0	# SAND99/Borkowski et al. 2001; listed correctly in latter source
K+	Am(CO3)4-5		2.022		0	0	0	0	0	# FK98 (analogy with Na)
K+	Am(SO4)2-		-0.354		0	0	0	0	0	# FK98 (analogy w/Na)
K+	NpO2H2Edta-		-0.8285		0	0	0	0	0	# PBMC98 (analogy w/Na)
K+	CaCitrate-	0.1742		0	0	0	0	0	# ERG_org_memo (analogy w/Na, Mg)
K+	CaEdta-2	0.185		0	0	0	0	0	# Domski (2018)
K+	MgCitrate-	0.1742		0	0	0	0	0	# ERG_org_memo (analogy with Na)
K+	NpO2HEdta-2		0.4733		0	0	0	0	0	# PBMC98 (analogy w/Na)
Ca+2	Cl-		0.3159		0	0	0	0	0	# HMW84
Ca+2	SO4-2		0.2		0	0	0	0	0	# HMW84
Ca+2	HSO4-		0.2145		0	0	0	0	0	# HMW84
Ca+2	OH-		-0.1747		0	0	0	0	0	# HMW84
Ca+2	HCO3-		0.4		0	0	0	0	0	# HMW84
#Ca+2	ClO4-		0.4511		0	0	0	0	0	# P91
Ca+2	NpO2CO3-		0.1		0	0	0	0	0	# al Mahamid et al. 1998 (analogy w/Mg)
Ca+2	NpO2(CO3)2-3		0.48		0	0	0	0	0	# al Mahamid et al. 1998 (analogy w/Mg)
Ca+2	NpO2(CO3)3-5		2.07		0	0	0	0	0	# al Mahamid et al. 1998 (analogy w/Mg; values averaged over Na and K values)
Mg+2	Cl-		0.35235		0	0	0	0	0	# HMW84
Mg+2	SO4-2		0.221		0	0	0	0	0	# HMW84
Mg+2	HSO4-		0.4746		0	0	0	0	0	# HMW84
Mg+2	HCO3-		0.329		0	0	0	0	0	# HMW84
#Mg+2	ClO4-		0.4961		0	0	0	0	0	# P91
Mg+2	NpO2CO3-		0.1		0	0	0	0	0	# al Mahamid et al. 1998 (analogy w/Na)
Mg+2	NpO2(CO3)2-3		0.48		0	0	0	0	0	# al Mahamid et al. 1998 (analogy w/Na)
Mg+2	NpO2(CO3)3-5		2.07		0	0	0	0	0	# al Mahamid et al. 1998 (averaged Na and K values)
MgOH+	Cl-		-0.1		0	0	0	0	0	# HMW84
H+	Cl-		0.1775		0	0	0	0	0	# HMW84
H+	SO4-2		0.0298		0	0	0	0	0	# HMW84
H+	HSO4-		0.2065		0	0	0	0	0	# HMW84
#H+	ClO4-		0.1747		0	0	0	0	0	# P91
H+	Th(SO4)3-2		0.84		0	0	0	0	0	# FR92
MgB(OH)4+	Cl-		0.16		0	0	0	0	0	# FW86
CaB(OH)4+	Cl-		0.12		0	0	0	0	0	# FW86
Am+3	Cl-		0.5856		0	0	0	0	0	# FK98, Konnecke et al. 1997
Am+3	SO4-2		1.792		0	0	0	0	0	# FK98
#Am+3	ClO4-		0.8		0	0	0	0	0	# FRF90
Am+3	H2PO4-		0		0	0	0	0	0	# RFF95 (from Nd analogue)
AmCO3+	Cl-		-0.072		0	0	0	0	0	# FK98/FanghŠnel et al. 1999 (Cm analogue)
Th+4	Cl-		1.092		0	0	0	0	0	# Roy92
Th+4	SO4-2		1.56		0	0	0	0	0	# FR92
Th+4	HSO4-		1.44		0	0	0	0	0	# FR92
#Th+4	ClO4-		1.19		0	0	0	0	0	# CFN960119
AmCl+2	Cl-		0.593		0	0	0	0	0	# FK98/Konnecke et al. (Cm analogue)
NpO2+	Cl-		0.1415		0	0	0	0	0	# NFRK95
#NpO2+	ClO4-		0.257		0	0	0	0	0	# NFRK95
ThOxalate+2	Cl-		-0.343		0	0	0	0	0	# SAND99/Borkowski et al. 2001

AmAcetate+2	Cl-		0.3088		0	0	0	0	0	# ERG_org_memo
AmLactate+2	Cl-		0.8397		0	0	0	0	0	# SAND97/Moore et al 1999
AmOxalate+	Cl-		-0.9374		0	0	0	0	0	# SAND99/Borkowski et al. 2001
ThAcetate+3	Cl-		1.061		0	0	0	0	0	# SAND99
ThCitrate+	Cl-	-0.7467		0	0	0	0	0	# SAND99	
ThLactate+3	Cl-		0.6677		0	0	0	0	0	# SAND99/Moore et al. 1999
AmOH+2	Cl-		-0.055		0	0	0	0	0	# FK98/Konnecke et al. 1997 (Cm analogue)
Am(OH)2+	Cl-		-0.616		0	0	0	0	0	# FK98/Konnecke et al. 1997 (Cm analogue)
AmCl2+	Cl-		0.516		0	0	0	0	0	# FK98/Konnecke et al. 1997 (Cm analogue)
AmSO4+	Cl-		-0.091		0	0	0	0	0	# FK98 (Cm analogue)
Th(Acetate)2+2	Cl-		0.4671		0	0	0	0	0	# Moore et al. 1999
Th(Lactate)2+2	Cl-		0.5058		0	0	0	0	0	# Moore et al. 1999
CaAcetate+	Cl-		-0.0833		0	0	0	0	0	# ERG_org_memo (analogy w/Mg)
MgAcetate+	Cl-		-0.0833		0	0	0	0	0	# ERG_org_memo
#Na+	Br-	0.0973		0	0	7.692E-40	0	# pitzer.dat		
#K+	Br-	0.0569		0	0	7.39E-4	0	0	# pitzer.dat	
#H+	Br-	0.1960		0	0	-2.049E-4	0	0	# pitzer.dat	
#Mg+2	Br-	0.4327		0	0	-5.625E-5	0	0	# pitzer.dat	
#Ca+2	Br-	0.3816		0	0	-5.2275E-4	0	0	# pitzer.dat	
#Li+	Br-	0.1748			0	-1.819E-4	0	0	# pitzer.dat	
#----------										
-B1	# same references as B0									
Ca+2	Edta-4		0		0	0	0	0	0	
Mg+2	CaEdta-2	7.21		0	0	0	0	0		
Mg+2	MgEdta-2	7.27		0	0	0	0	0		
Na+	NaEdta-3	5.39		0	0	0	0	0		
Na+	Mg(Oxalate)2-2		0		0	0	0	0	0	
Fe+2	Cl-		1.13499		0	0	0	0	0	
Na+	Fe(CO3)2-2		6.26		0	0	0	0	0	
Na+	Cl-		0.2664		0	0	0	0	0	
Na+	SO4-2		1.113		0	0	0	0	0	
Na+	HSO4-		0.398		0	0	0	0	0	
Na+	OH-		0.253		0	0	0	0	0	
Na+	HCO3-		0.0411		0	0	0	0	0	
Na+	CO3-2		1.389		0	0	0	0	0	
Na+	B(OH)4-		0.089		0	0	0	0	0	
Na+	B3O3(OH)4-		-0.91		0	0	0	0	0	
Na+	B4O5(OH)4-2		-0.4		0	0	0	0	0	
Na+	Am(CO3)2-		0.224		0	0	0	0	0	
Na+	Am(CO3)3-3		4.73		0	0	0	0	0	
#Na+	ClO4-		0.2755		0	0	0	0	0	
Na+	NpO2CO3-		0.34		0	0	0	0	0	
Na+	NpO2(CO3)2-3		4.4		0	0	0	0	0	
Na+	NpO2(CO3)3-5		22.7		0	0	0	0	0	
Na+	H2PO4-		0.0396		0	0	0	0	0	
Na+	HPO4-2		1.466		0	0	0	0	0	
Na+	PO4-3		3.851		0	0	0	0	0	
Na+	Th(SO4)3-2		0		0	0	0	0	0	
Na+	Th(CO3)5-6		30		0	0	0	0	0	
Na+	HOxalate-	0.29		0	0	0	0	0		
Na+	Oxalate-2	1.74		0	0	0	0	0		
Na+	Acetate-	0.22		0	0	0	0	0		
Na+	Lactate-	0.29		0	0	0	0	0		
Na+	H2Citrate-	0.29		0	0	0	0	0		
Na+	HCitrate-2	1.74		0	0	0	0	0		
Na+	Citrate-3	5.22		0	0	0	0	0		
Na+	H3Edta-		0.29		0	0	0	0	0	
Na+	H2Edta-2	1.74		0	0	0	0	0		

Na+	HEdta-3		5.22		0	0	0	0	0
Na+	Edta-4		15.6		0	0	0	0	0
Na+	AmEdta-		0.29		0	0	0	0	0
Na+	NpO2Citrate-2		1.75		0	0	0	0	0
Na+	NpO2Edta-3		5.911		0	0	0	0	0
Na+	NpO2Oxalate-		0.29		0	0	0	0	0
Na+	Am(CO3)4-5		19.22		0	0	0	0	0
Na+	Am(SO4)2-		0.4		0	0	0	0	0
Na+	NpO2H2Edta-		0.2575		0	0	0	0	0
Na+	CaCitrate-	0.29		0	0	0	0	0	
Na+	CaEdta-2	2.405		0	0	0	0	0	
Na+	MgCitrate-	0.29		0	0	0	0	0	
Na+	NpO2HEdta-2		-1.504		0	0	0	0	0
K+	Cl-		0.2122		0	0	0	0	0
K+	SO4-2		0.7793		0	0	0	0	0
K+	HSO4-		0.1735		0	0	0	0	0
K+	OH-		0.32		0	0	0	0	0
K+	HCO3-		-0.013		0	0	0	0	0
K+	CO3-2		1.43		0	0	0	0	0
K+	B(OH)4-		0.14		0	0	0	0	0
K+	B3O3(OH)4-		0		0	0	0	0	0
K+	B4O5(OH)4-2		0		0	0	0	0	0
K+	Am(CO3)2-		0.224		0	0	0	0	0
K+	Am(CO3)3-3		4.73		0	0	0	0	0
K+	NpO2CO3-		0.34		0	0	0	0	0
K+	NpO2(CO3)2-3		4.4		0	0	0	0	0
K+	NpO2(CO3)3-5		22.7		0	0	0	0	0
K+	H2PO4-		-0.1042		0	0	0	0	0
K+	HPO4-2		1.274		0	0	0	0	0
K+	PO4-3		3.972		0	0	0	0	0
K+	Th(SO4)3-2		0		0	0	0	0	0
K+	Th(CO3)5-6		30.		0	0	0	0	0
K+	HOxalate-	0.29		0	0	0	0	0	
K+	Oxalate-2	1.74		0	0	0	0	0	
K+	Acetate-	0.3251		0	0	0	0	0	
K+	Lactate-	0.29		0	0	0	0	0	
K+	H2Citrate-	0.29		0	0	0	0	0	
K+	HCitrate-2	1.74		0	0	0	0	0	
K+	Citrate-3	5.22		0	0	0	0	0	
K+	H3Edta-		0.29		0	0	0	0	0
K+	H2Edta-2	1.74		0	0	0	0	0	
K+	HEdta-3		5.22		0	0	0	0	0
K+	Edta-4		15.6		0	0	0	0	0
K+	AmEdta-		0.29		0	0	0	0	0
K+	NpO2Citrate-2		1.75		0	0	0	0	0
K+	NpO2Edta-3		5.911		0	0	0	0	0
K+	NpO2Oxalate-		0.29		0	0	0	0	0
K+	Am(CO3)4-5		19.22		0	0	0	0	0
K+	Am(SO4)2-		0.4		0	0	0	0	0
K+	NpO2H2Edta-		0.2575		0	0	0	0	0
K+	CaCitrate-	0.29		0	0	0	0	0	
K+	CaEdta-2	2.41		0	0	0	0	0	
K+	MgCitrate-	0.29		0	0	0	0	0	
K+	NpO2HEdta-2		-1.504		0	0	0	0	0
Ca+2	Cl-		1.614		0	0	0	0	0
Ca+2	SO4-2		3.1973		0	0	0	0	0
Ca+2	HSO4-		2.53		0	0	0	0	0
Ca+2	OH-		-0.2303		0	0	0	0	0
Ca+2	HCO3-		2.977		0	0	0	0	0
#Ca+2	ClO4-		1.756		0	0	0	0	0
Ca+2	NpO2CO3-		0.34		0	0	0	0	0
Ca+2	NpO2(CO3)2-3		4.4		0	0	0	0	0
Ca+2	NpO2(CO3)3-5		22.7		0	0	0	0	0
Mg+2	Cl-		1.6815		0	0	0	0	0
Mg+2	SO4-2		3.343		0	0	0	0	0
Mg+2	HSO4-		1.729		0	0	0	0	0
Mg+2	HCO3-		0.6072		0	0	0	0	0
#Mg+2	ClO4-		2.008		0	0	0	0	0
Mg+2	NpO2CO3-		0.34		0	0	0	0	0
Mg+2	NpO2(CO3)2-3		4.4		0	0	0	0	0

Mg+2		NpO2(CO3)3-5		22.7		0	0	0	0	0	
MgOH+		Cl-		1.658		0	0	0	0	0	
H+		Cl-		0.2945		0	0	0	0	0	
H+		SO4-2		0		0	0	0	0	0	
H+		HSO4-		0.5556		0	0	0	0	0	
#H+		ClO4-		0.2931		0	0	0	0	0	
H+		Th(SO4)3-2		0		0	0	0	0	0	
MgB(OH)4+		Cl-		0		0	0	0	0	0	
CaB(OH)4+		Cl-		0		0	0	0	0	0	
Am+3		Cl-		5.6		0	0	0	0	0	
Am+3		SO4-2		15.04		0	0	0	0	0	
#Am+3		ClO4-		5.35		0	0	0	0	0	
Am+3		H2PO4-		0		0	0	0	0	0	
AmCO3+		Cl-		0.403		0	0	0	0	0	
Th+4		Cl-		13.7		0	0	0	0	0	
Th+4		SO4-2		0		0	0	0	0	0	
Th+4		HSO4-		0		0	0	0	0	0	
#Th+4		ClO4-		27.3		0	0	0	0	0	
AmCl+2		Cl-		3.15		0	0	0	0	0	
NpO2+		Cl-		0.281		0	0	0	0	0	
#NpO2+		ClO4-		0.18		0	0	0	0	0	
ThOxalate+2		Cl-		1.74		0	0	0	0	0	
AmAcetate+2		Cl-		1.74		0	0	0	0	0	
AmLactate+2		Cl-		1.74		0	0	0	0	0	
AmOxalate+		Cl-		0.29		0	0	0	0	0	
ThAcetate+3		Cl-		5.22		0	0	0	0	0	
ThCitrate+	Cl-		0.29		0	0	0	0	0		
ThLactate+3		Cl-		5.22		0	0	0	0	0	
AmOH+2		Cl-		1.6		0	0	0	0	0	
Am(OH)2+		Cl-		-0.45		0	0	0	0	0	
AmCl2+		Cl-		1.75		0	0	0	0	0	
AmSO4+		Cl-		-0.39		0	0	0	0	0	
Th(Acetate)2+2		Cl-		1.74		0	0	0	0	0	
Th(Lactate)2+2		Cl-		1.74		0	0	0	0	0	
CaAcetate+		Cl-		0.29		0	0	0	0	0	
MgAcetate+		Cl-		0.29		0	0	0	0	0	
#Na+	Br-		0.2791		0	0	10.79E-4	0	0	# pitzer.dat	
#K+		Br-		0.2212		0	0	17.40E-4	0	0	# pitzer.dat
#H+		Br-		0.3564		0	0	4.467E-4	0	0	# pitzer.dat
#Mg+2	Br-		1.753		0	0	3.8625E-3	0	0	# pitzer.dat	
#Ca+2	Br-		1.613		0	0	6.0375E-3	0	0	# pitzer.dat	
#Li+	Br-		0.2547		0	0	6.636E-4	0	0	# pitzer.dat	
#----------											
-B2		# same references as B0									
Ca+2		Edta-4		0	0	0	0	0	0		
Mg+2		CaEdta-2	0	0	0	0	0	0			
Mg+2		MgEdta-2	0	0	0	0	0	0			
Na+		NaEdta-3	0	0	0	0	0	0			
Na+		Mg(Oxalate)2-2		0	0	0	0	0	0		
Fe+2		Cl-		0	0	0	0	0	0		
Na+		Fe(CO3)2-2		0	0	0	0	0	0		
Na+		Cl-		0	0	0	0	0	0		
Na+		SO4-2		0	0	0	0	0	0		
Na+		HSO4-		0	0	0	0	0	0		
Na+		OH-		0	0	0	0	0	0		
Na+		HCO3-		0	0	0	0	0	0		
Na+		CO3-2		0	0	0	0	0	0		
Na+		B(OH)4-		0	0	0	0	0	0		
Na+		B3O3(OH)4-		0	0	0	0	0	0		
Na+		B4O5(OH)4-2		0	0	0	0	0	0		
Na+		Am(CO3)2-		0	0	0	0	0	0		
Na+		Am(CO3)3-3		0	0	0	0	0	0		
#Na+		ClO4-		0	0	0	0	0	0		
Na+		NpO2CO3-		0	0	0	0	0	0		
Na+		NpO2(CO3)2-3		0	0	0	0	0	0		
Na+		NpO2(CO3)3-5		0	0	0	0	0	0		
Na+		H2PO4-		0	0	0	0	0	0		
Na+		HPO4-2		0	0	0	0	0	0		
Na+		PO4-3		0	0	0	0	0	0		
Na+		Th(SO4)3-2		0	0	0	0	0	0		

Na+	Th(CO3)5-6		0	0	0	0	0	0
Na+	HOxalate-	0	0	0	0	0	0	
Na+	Oxalate-2	0	0	0	0	0	0	
Na+	Acetate-	0	0	0	0	0	0	
Na+	Lactate-	0	0	0	0	0	0	
Na+	H2Citrate-	0	0	0	0	0	0	
Na+	HCitrate-2	0	0	0	0	0	0	
Na+	Citrate-3	0	0	0	0	0	0	
Na+	H3Edta-		0	0	0	0	0	0
Na+	H2Edta-2	0	0	0	0	0	0	
Na+	HEdta-3		0	0	0	0	0	0
Na+	Edta-4		0	0	0	0	0	0
Na+	AmEdta-		0	0	0	0	0	0
Na+	NpO2Citrate-2		0	0	0	0	0	0
Na+	NpO2Edta-3		0	0	0	0	0	0
Na+	NpO2Oxalate-		0	0	0	0	0	0
Na+	Am(CO3)4-5		0	0	0	0	0	0
Na+	Am(SO4)2-		0	0	0	0	0	0
Na+	NpO2H2Edta-		0	0	0	0	0	0
Na+	CaCitrate-	0	0	0	0	0	0	
Na+	CaEdta-2	0	0	0	0	0	0	
Na+	MgCitrate-	0	0	0	0	0	0	
Na+	NpO2HEdta-2		0	0	0	0	0	0
K+	Cl-		0	0	0	0	0	0
K+	SO4-2		0	0	0	0	0	0
K+	HSO4-		0	0	0	0	0	0
K+	OH-		0	0	0	0	0	0
K+	HCO3-		0	0	0	0	0	0
K+	CO3-2		0	0	0	0	0	0
K+	B(OH)4-		0	0	0	0	0	0
K+	B3O3(OH)4-		0	0	0	0	0	0
K+	B4O5(OH)4-2		0	0	0	0	0	0
K+	Am(CO3)2-		0	0	0	0	0	0
K+	Am(CO3)3-3		0	0	0	0	0	0
K+	NpO2CO3-		0	0	0	0	0	0
K+	NpO2(CO3)2-3		0	0	0	0	0	0
K+	NpO2(CO3)3-5		-96.	0	0	0	0	0
K+	H2PO4-		0	0	0	0	0	0
K+	HPO4-2		0	0	0	0	0	0
K+	PO4-3		0	0	0	0	0	0
K+	Th(SO4)3-2		0	0	0	0	0	0
K+	Th(CO3)5-6		0	0	0	0	0	0
K+	HOxalate-	0	0	0	0	0	0	
K+	Oxalate-2	0	0	0	0	0	0	
K+	Acetate-	0	0	0	0	0	0	
K+	Lactate-	0	0	0	0	0	0	
K+	H2Citrate-	0	0	0	0	0	0	
K+	HCitrate-2	0	0	0	0	0	0	
K+	Citrate-3	0	0	0	0	0	0	
K+	H3Edta-		0	0	0	0	0	0
K+	H2Edta-2	0	0	0	0	0	0	
K+	HEdta-3		0	0	0	0	0	0
K+	Edta-4		0	0	0	0	0	0
K+	AmEdta-		0	0	0	0	0	0
K+	NpO2Citrate-2		0	0	0	0	0	0
K+	NpO2Edta-3		0	0	0	0	0	0
K+	NpO2Oxalate-		0	0	0	0	0	0
K+	Am(CO3)4-5		0	0	0	0	0	0
K+	Am(SO4)2-		0	0	0	0	0	0
K+	NpO2H2Edta-		0	0	0	0	0	0
K+	CaCitrate-	0	0	0	0	0	0	
K+	CaEdta-2	0	0	0	0	0	0	
K+	MgCitrate-	0	0	0	0	0	0	
K+	NpO2HEdta-2		0	0	0	0	0	0
Ca+2	Cl-		0	0	0	0	0	0
Ca+2	SO4-2		-54.24	0	0	0	0	0
Ca+2	HSO4-		0	0	0	0	0	0
Ca+2	OH-		-5.72	0	0	0	0	0
Ca+2	HCO3-		0	0	0	0	0	0
#Ca+2	ClO4-		0	0	0	0	0	0

Ca+2	NpO2CO3-		0	0	0	0	0	0
Ca+2	NpO2(CO3)2-3		0	0	0	0	0	0
Ca+2	NpO2(CO3)3-5		-48.	0	0	0	0	0
Mg+2	Cl-		0	0	0	0	0	0
Mg+2	SO4-2		-37.23	0	0	0	0	0
Mg+2	HSO4-		0	0	0	0	0	0
Mg+2	HCO3-		0	0	0	0	0	0
#Mg+2	ClO4-		0	0	0	0	0	0
Mg+2	NpO2CO3-		0	0	0	0	0	0
Mg+2	NpO2(CO3)2-3		0	0	0	0	0	0
Mg+2	NpO2(CO3)3-5		-48.	0	0	0	0	0
MgOH+	Cl-		0	0	0	0	0	0
H+	Cl-		0	0	0	0	0	0
H+	SO4-2		0	0	0	0	0	0
H+	HSO4-		0	0	0	0	0	0
#H+	ClO4-		0	0	0	0	0	0
H+	Th(SO4)3-2		0	0	0	0	0	0
MgB(OH)4+	Cl-		0	0	0	0	0	0
CaB(OH)4+	Cl-		0	0	0	0	0	0
Am+3	Cl-		0	0	0	0	0	0
Am+3	SO4-2		0	0	0	0	0	0
#Am+3	ClO4-		0	0	0	0	0	0
Am+3	H2PO4-		-92.9	0	0	0	0	0
AmCO3+	Cl-		0	0	0	0	0	0
Th+4	Cl-		-160.	0	0	0	0	0
Th+4	SO4-2		0	0	0	0	0	0
Th+4	HSO4-		0	0	0	0	0	0
#Th+4	ClO4-		0	0	0	0	0	0
AmCl+2	Cl-		0	0	0	0	0	0
NpO2+	Cl-		0	0	0	0	0	0
#NpO2+	ClO4-		0	0	0	0	0	0
ThOxalate+2	Cl-		0	0	0	0	0	0
AmAcetate+2	Cl-		0	0	0	0	0	0
AmLactate+2	Cl-		0	0	0	0	0	0
AmOxalate+	Cl-		0	0	0	0	0	0
ThAcetate+3	Cl-		0	0	0	0	0	0
ThCitrate+	Cl-	0	0	0	0	0	0	
ThLactate+3	Cl-		0	0	0	0	0	0
AmOH+2	Cl-		0	0	0	0	0	0
Am(OH)2+	Cl-		0	0	0	0	0	0
AmCl2+	Cl-		0	0	0	0	0	0
AmSO4+	Cl-		0	0	0	0	0	0
Th(Acetate)2+2	Cl-		0	0	0	0	0	0
Th(Lactate)2+2	Cl-		0	0	0	0	0	0
CaAcetate+	Cl-		0	0	0	0	0	0
MgAcetate+	Cl-		0	0	0	0	0	0
#----------								
-C0	# same references as B0							
Ca+2	Edta-4		0		0	0	0	0	0
Mg+2	CaEdta-2	0		0	0	0	0	0	
Mg+2	MgEdta-2	0		0	0	0	0	0	
Na+	NaEdta-3	0		0	0	0	0	0	
Na+	Mg(Oxalate)2-2		0		0	0	0	0	0
Fe+2	Cl-		-0.02152		0	0	0	0	0
Na+	Fe(CO3)2-2		0		0	0	0	0	0
Na+	Cl-		0.00127		0	0	0	0	0
Na+	SO4-2		0.00497		0	0	0	0	0
Na+	HSO4-		0		0	0	0	0	0
Na+	OH-		0.0044		0	0	0	0	0
Na+	HCO3-		0		0	0	0	0	0
Na+	CO3-2		0.0044		0	0	0	0	0
Na+	B(OH)4-		0.0114		0	0	0	0	0
Na+	B3O3(OH)4-		0		0	0	0	0	0
Na+	B4O5(OH)4-2		0		0	0	0	0	0
Na+	Am(CO3)2-		0.0284		0	0	0	0	0
Na+	Am(CO3)3-3		0.0007		0	0	0	0	0
#Na+	ClO4-		-0.00118	0	0	0	0	0	
Na+	NpO2CO3-		0		0	0	0	0	0
Na+	NpO2(CO3)2-3		0		0	0	0	0	0
Na+	NpO2(CO3)3-5		0		0	0	0	0	0

Na+	H2PO4-		0.00795		0	0	0	0	0
Na+	HPO4-2		0.0294		0	0	0	0	0
Na+	PO4-3		-0.05154	0	0	0	0	0	
Na+	Th(SO4)3-2		0		0	0	0	0	0
Na+	Th(CO3)5-6		0		0	0	0	0	0
Na+	HOxalate-	0.068		0	0	0	0	0	
Na+	Oxalate-2	0.122		0	0	0	0	0	
Na+	Acetate-	-0.00629	0	0	0	0	0		
Na+	Lactate-	0.047		0	0	0	0	0	
Na+	H2Citrate-	0.013		0	0	0	0	0	
Na+	HCitrate-2	0.027		0	0	0	0	0	
Na+	Citrate-3	0.047		0	0	0	0	0	
Na+	H3Edta-		0.059		0	0	0	0	0
Na+	H2Edta-2	0.054		0	0	0	0	0	
Na+	HEdta-3		-0.048		0	0	0	0	0
Na+	Edta-4		0.001		0	0	0	0	0
Na+	AmEdta-		0.002		0	0	0	0	0
Na+	NpO2Citrate-2		0.142		0	0	0	0	0
Na+	NpO2Edta-3		0		0	0	0	0	0
Na+	NpO2Oxalate-		0.095		0	0	0	0	0
Na+	Am(CO3)4-5		-0.305		0	0	0	0	0
Na+	Am(SO4)2-		0.051		0	0	0	0	0
Na+	NpO2H2Edta-		0.256		0	0	0	0	0
Na+	CaCitrate-	-0.06923	0	0	0	0	0		
Na+	CaEdta-2	0.0		0	0	0	0	0	
Na+	MgCitrate-	-0.06923	0	0	0	0	0		
Na+	NpO2HEdta-2		0		0	0	0	0	0
K+	Cl-		-0.00084	0	0	0	0	0	
K+	SO4-2		0		0	0	0	0	0
K+	HSO4-		0		0	0	0	0	0
K+	OH-		0.0041		0	0	0	0	0
K+	HCO3-		-0.008		0	0	0	0	0
K+	CO3-2		-0.0015		0	0	0	0	0
K+	B(OH)4-		0		0	0	0	0	0
K+	B3O3(OH)4-		0		0	0	0	0	0
K+	B4O5(OH)4-2		0		0	0	0	0	0
K+	Am(CO3)2-		0.0284		0	0	0	0	0
K+	Am(CO3)3-3		0.0007		0	0	0	0	0
K+	NpO2CO3-		0		0	0	0	0	0
K+	NpO2(CO3)2-3		0		0	0	0	0	0
K+	NpO2(CO3)3-5		-0.22		0	0	0	0	0
K+	H2PO4-		0		0	0	0	0	0
K+	HPO4-2		0.0164		0	0	0	0	0
K+	PO4-3		-0.0868		0	0	0	0	0
K+	Th(SO4)3-2		0		0	0	0	0	0
K+	Th(CO3)5-6		0		0	0	0	0	0
K+	HOxalate-	0.068		0	0	0	0	0	
K+	Oxalate-2	0.122		0	0	0	0	0	
K+	Acetate-	-0.0066		0	0	0	0	0	
K+	Lactate-	0.047		0	0	0	0	0	
K+	H2Citrate-	0.013		0	0	0	0	0	
K+	HCitrate-2	0.027		0	0	0	0	0	
K+	Citrate-3	0.047		0	0	0	0	0	
K+	H3Edta-		0.059		0	0	0	0	0
K+	H2Edta-2	0.054		0	0	0	0	0	
K+	HEdta-3		-0.048		0	0	0	0	0
K+	Edta-4		0.001		0	0	0	0	0
K+	AmEdta-		0.002		0	0	0	0	0
K+	NpO2Citrate-2		0.142		0	0	0	0	0
K+	NpO2Edta-3		0		0	0	0	0	0
K+	NpO2Oxalate-		0.095		0	0	0	0	0
K+	Am(CO3)4-5		-0.305		0	0	0	0	0
K+	Am(SO4)2-		0.051		0	0	0	0	0
K+	NpO2H2Edta-		0.256		0	0	0	0	0
K+	CaCitrate-	-0.06923	0	0	0	0	0		
K+	CaEdta-2	0.00		0	0	0	0	0	
K+	MgCitrate-	-0.06923	0	0	0	0	0		
K+	NpO2HEdta-2		0		0	0	0	0	0
Ca+2	Cl-		-0.00034	0	0	0	0	0	
Ca+2	SO4-2		0		0	0	0	0	0

Ca+2	HSO4-		0		0	0	0	0	0	
Ca+2	OH-		0		0	0	0	0	0	
Ca+2	HCO3-		0		0	0	0	0	0	
#Ca+2	ClO4-		-0.005		0	0	0	0	0	
Ca+2	NpO2CO3-		0		0	0	0	0	0	
Ca+2	NpO2(CO3)2-3		0		0	0	0	0	0	
Ca+2	NpO2(CO3)3-5		-0.11		0	0	0	0	0	
Mg+2	Cl-		0.00519		0	0	0	0	0	
Mg+2	SO4-2		0.025		0	0	0	0	0	
Mg+2	HSO4-		0		0	0	0	0	0	
Mg+2	HCO3-		0		0	0	0	0	0	
#Mg+2	ClO4-		0.009578	0	0	0	0	0		
Mg+2	NpO2CO3-		0		0	0	0	0	0	
Mg+2	NpO2(CO3)2-3		0		0	0	0	0	0	
Mg+2	NpO2(CO3)3-5		-0.11		0	0	0	0	0	
MgOH+	Cl-		0		0	0	0	0	0	
H+	Cl-		0.0008		0	0	0	0	0	
H+	SO4-2		0.0438		0	0	0	0	0	
H+	HSO4-		0		0	0	0	0	0	
#H+	ClO4-		0.00819		0	0	0	0	0	
H+	Th(SO4)3-2		0		0	0	0	0	0	
MgB(OH)4+	Cl-		0		0	0	0	0	0	
CaB(OH)4+	Cl-		0		0	0	0	0	0	
Am+3	Cl-		-0.0166		0	0	0	0	0	
Am+3	SO4-2		0.6		0	0	0	0	0	
#Am+3	ClO4-		-0.0048		0	0	0	0	0	
Am+3	H2PO4-		0		0	0	0	0	0	
AmCO3+	Cl-		0.0388		0	0	0	0	0	
Th+4	Cl-		-0.112		0	0	0	0	0	
Th+4	SO4-2		0		0	0	0	0	0	
Th+4	HSO4-		0		0	0	0	0	0	
#Th+4	ClO4-		-0.057		0	0	0	0	0	
AmCl+2	Cl-		-0.006		0	0	0	0	0	
NpO2+	Cl-		0		0	0	0	0	0	
#NpO2+	ClO4-		0.0081		0	0	0	0	0	
ThOxalate+2	Cl-		0.5		0	0	0	0	0	
AmAcetate+2	Cl-		-0.132		0	0	0	0	0	
AmLactate+2	Cl-		-0.332		0	0	0	0	0	
AmOxalate+	Cl-		0.248		0	0	0	0	0	
ThAcetate+3	Cl-		0.109		0	0	0	0	0	
ThCitrate+	Cl-	0.319		0	0	0	0	0		
ThLactate+3	Cl-		0.341		0	0	0	0	0	
AmOH+2	Cl-		0.05		0	0	0	0	0	
Am(OH)2+	Cl-		0.05		0	0	0	0	0	
AmCl2+	Cl-		0.01		0	0	0	0	0	
AmSO4+	Cl-		0.048		0	0	0	0	0	
Th(Acetate)2+2	Cl-		0.143		0	0	0	0	0	
Th(Lactate)2+2	Cl-		0.225		0	0	0	0	0	
CaAcetate+	Cl-		0.0987		0	0	0	0	0	
MgAcetate+	Cl-		0.0987		0	0	0	0	0	
#Na+	Br-	0.00116		0	0	-9.30E-5	0	0	# pitzer.dat	
#K+	Br-		-0.00180	0	0	0	-7.004E-5	0	0	# pitzer.dat
#H+	Br-		0.00827		0	0	-5.685E-5	0	0	# pitzer.dat
#Mg+2	Br-	0.00312		0	0	0		0	0	# pitzer.dat
#Ca+2	Br-	-0.00257	0	0	0		0	0	# pitzer.dat	
#Li+	Br-	0.0053		0	0	-2.813E-5	0	0	# pitzer.dat	

#----------

-THETA

cation-cation combinations

Na+	Fe+2	0.10945	0	0	0	0	0	# Moog et al. (2004)
Mg+2	Fe+2	0.145	0	0	0	0	0	# Moog et al. (2004)
K+	Fe+2	0.0274	0	0	0	0	0	# Moog et al. (2004)
Ca+2	Fe+2	0.0811	0	0	0	0	0	# Moog et al. (2004)
Na+	K+	-0.012	0	0	0	0	0	# HMW84
Na+	Ca+2	0.07	0	0	0	0	0	# HMW84
Na+	Mg+2	0.07	0	0	0	0	0	# HMW84

Na+	H+		0.036	0	0	0	0	0	# HMW84
Na+	Am+3		0.1	0	0	0	0	0	# FK98 (analogy with Cm)
Na+	Th+4		0.42	0	0	0	0	0	# RFSMMN
K+	Ca+2		0.032	0	0	0	0	0	# HMW84
K+	H+		0.005	0	0	0	0	0	# HMW84
K+	Am+3		0.1	0	0	0	0	0	# FK98 (analogy with Na, Cm)
K+	Th+4		0.42	0	0	0	0	0	# RFSMMN (analogy with Na)
Ca+2	Mg+2		0.007	0	0	0	0	0	# HMW84
Ca+2	H+		0.092	0	0	0	0	0	# HMW84
Ca+2	Am+3		0.2	0	0	0	0	0	# FK98 (Cm analogue)
Ca+2	Th+4		0.6	0	0	0	0	0	# RFSMMN (analogy with Mg)
Ca+2	AmCl+2		-0.014	0	0	0	0	0	# FK98 (analogy with Mg)
Ca+2	AmCl2+		-0.196	0	0	0	0	0	# FK98 (analogy with Mg)
Mg+2	H+		0.1	0	0	0	0	0	# HMW84
Mg+2	Am+3		0.2	0	0	0	0	0	# FK98 (analogue with Ca, Cm)
Mg+2	Th+4		0.6	0	0	0	0	0	# RFSMMN
Mg+2	AmCl+2		-0.014	0	0	0	0	0	# FK98 (analogy with Ca, Cm)
Mg+2	AmCl2+		-0.196	0	0	0	0	0	# FK98 (analogy with Ca, Cm)
H+	Th+4		0.6	0	0	0	0	0	# Roy92
# anion-anion combinations									
Cl-	SO4-2		0.02	0	0	0	0	0	# HMW84
Cl-	HSO4-		-0.006	0	0	0	0	0	# HMW84
Cl-	OH-		-0.05	0	0	0	0	0	# HMW84
Cl-	HCO3-		0.03	0	0	0	0	0	# HMW84
Cl-	CO3-2		-0.02	0	0	0	0	0	# HMW84
Cl-	B(OH)4-		-0.065	0	0	0	0	0	# FW86
Cl-	B3O3(OH)4-		0.12	0	0	0	0	0	# FW86
Cl-	B4O5(OH)4-2		0.074	0	0	0	0	0	# FW86
Cl-	NpO2(OH)2-		-0.24	0	0	0	0	0	# FNK95
Cl-	NpO2CO3-		-0.21	0	0	0	0	0	# FNK95
Cl-	NpO2(CO3)2-3		-0.26	0	0	0	0	0	# None
Cl-	NpO2(CO3)3-5		-0.26	0	0	0	0	0	# FNK95
Cl-	H2PO4-		0.1	0	0	0	0	0	# PS76
Cl-	Th(CO3)5-6		1.8	0	0	0	0	0	# Moore et al. 1999
Cl-	Acetate-	-0.09		0	0	0	0	0	# NBC96
SO4-2	OH-		-0.013	0	0	0	0	0	# HMW84
SO4-2	HCO3-		0.01	0	0	0	0	0	# HMW84
SO4-2	CO3-2		0.02	0	0	0	0	0	# HMW84
SO4-2	B(OH)4-		-0.012	0	0	0	0	0	# FW86
SO4-2	B3O3(OH)4-		0.1	0	0	0	0	0	# FW86
SO4-2	B4O5(OH)4-2		0.12	0	0	0	0	0	# FW86
OH-	CO3-2		0.1	0	0	0	0	0	# HMW84
#OH-	ClO4-		-0.032	0	0	0	0	0	# P91
HCO3-	CO3-2		-0.04	0	0	0	0	0	# HMW84
HCO3-	B3O3(OH)4-		-0.1	0	0	0	0	0	# FW86
HCO3-	B4O5(OH)4-2		-0.087	0	0	0	0	0	# FW86
#HCO3-	ClO4-		0.095	0	0	0	0	0	# NFRK95
#CO3-2	ClO4-		0.21	0	0	0	0	0	# NFRK95
CO3-2	NpO2(CO3)3-5		-1.9	0	0	0	0	0	# NFRK95
#ClO4-	Th(CO3)5-6		5.5	0	0	0	0	0	# FRSMHC97
#OH-	Br-	-0.065		0	0	0	0	0	# pitzer.dat
#----------									
-LAMDA									
MgOxalateNa+		0.08		0	0	0	0	0	# AP-182
MgOxalateMg+2		-0.20		0	0	0	0	0	# AP-182

```
CO2             H+              0               0       0       0       0       0       # [Harvie-
Moller-Weare convention]
CO2             Na+             0.1             0       0       0       0       0       # HMW84
CO2             K+              0.051           0       0       0       0       0       # HMW84
CO2             Ca+2            0.183           0       0       0       0       0       # HMW84
CO2             Mg+2            0.183           0       0       0       0       0       # HMW84
O2              Ca+2            0.2497          0       0       0       0       0       # YMP
DTN: SN0302T0510102.002 (data0.ypf.R1)
O2              H+              0.035284639 81.44999999 -8.09461E-11 1.21206E-13 0 0    # YMP DTN:
SN0302T0510102.002 (data0.ypf.R1)
O2              K+              1.51915E-01 1.99431E+02 7.64677E-10 -1.14341E-12 0 0    # YMP
DTN: SN0302T0510102.002 (data0.ypf.R1)
O2              Mg+2            2.29806E-01 3.05513E+02 -2.15815E-10 3.23403E-13 0 0    # YMP
DTN: SN0302T0510102.002 (data0.ypf.R1)
O2              Na+             1.60236E-01 7.28644E+01 -6.16311E-01 1.84620E-03 0 0    # YMP
DTN: SN0302T0510102.002 (data0.ypf.R1)
B(OH)3          H+              0               0       0       0       0       0       # [Harvie-
Moller-Weare convention]
B(OH)3          Na+             -0.097          0       0       0       0       0       # HMW84
B(OH)3          K+              -0.14           0       0       0       0       0       # FW86
B(OH)3          MgOH+           0               0       0       0       0       0       # [required
by zeta parameter]
B(OH)3          AmCO3+          0               0       0       0       0       0       # [required
by zeta parameter]
H3PO4           H+              0.29            0       0       0       0       0       # PS76
H3PO4           K+              -0.07           0       0       0       0       0       # PS76
Am(OH)3         H+              0               0       0       0       0       0       # [Harvie-
Moller-Weare convention]
Am(OH)3         Na+             -0.2            0       0       0       0       0       # FK98
Am(OH)3         K+              -0.2            0       0       0       0       0       # FK98
(analogy with Na)
CO2             Cl-             -0.005          0       0       0       0       0       # HMW84
CO2             SO4-2           0.097           0       0       0       0       0       # HMW84
CO2             HSO4-           -0.003          0       0       0       0       0       # HMW84
O2              Cl-             0               0       0       0       0       0       # YMP
DTN: SN0302T0510102.002 (data0.ypf.R1)
O2              Br-             -0.0347         0       0       0       0       0       # YMP
DTN: SN0302T0510102.002 (data0.ypf.R1)
O2              CO3-2           0.09648925  -277.074    2.030064E-10 -3.034302E-13      0 0 # YMP DTN:
SN0302T0510102.002 (data0.ypf.R1)
O2              HCO3-           0.0854          0       0       0       0       0       # YMP
DTN: SN0302T0510102.002 (data0.ypf.R1)
O2              NO3-            -0.0377         0       0       0       0       0       # YMP
DTN: SN0302T0510102.002 (data0.ypf.R1)
O2              OH-             5.222539E-02 1.557100E+01 -2.740323E-10 4.101025E-13 0 0        # YMP
DTN: SN0302T0510102.002 (data0.ypf.R1)
O2              SO4-2           0.087774406 -2.74085000E+02 1.32906590E-09 -1.98727658E-12      0 0 #
YMP DTN: SN0302T0510102.002 (data0.ypf.R1)
B(OH)3          Cl-             0.091           0       0       0       0       0       # FW86
B(OH)3          SO4-2           0.018           0       0       0       0       0       # FW86
B(OH)3          B3O3(OH)4-      -0.2            0       0       0       0       0       # FW86
NpO2OH          Cl-             -0.19           0       0       0       0       0       # FNK95
H3PO4           Cl-             0               0       0       0       0       0       # [Clegg-
Brimblecombe convention]
H3PO4           H2PO4-          -0.4            0       0       0       0       0       # PS76
Th(SO4)2 Cl-            0.29            0       0       0       0       0       # Roy92
Th(SO4)2 HSO4-          0.68            0       0       0       0       0       # Roy92
Am(OH)3         Cl-             -0.2            0       0       0       0       0       # FK98
NpO2Acetate     Cl-             -0.104          0       0       0       0       0       #
ERG_release_memo
AmCitrate Cl-           -0.406          0       0       0       0       0       # SAND99
NpO2Lactate     Cl-             0.015           0       0       0       0       0       #
SAND99/Moore et al. 1999
ThEdta          Cl-             0.1111          0       0       0       0       0       #
ERG_org_memo
MgOxalateCl-            0.0189          0       0       0       0       0       #
ERG_org_memo=0.0189
CaOxalate Cl-           0.0189          0       0       0       0       0       #
ERG_org_memo=0.0189
#---------------------------------------------------------------------------------------------------------
```

-PSI									
Fe+2		Na+	Cl-	-0.01605	0	0	0	0	0
	# Moog et al. (2004)								
Fe+2		K+	Cl-	-0.0252		0	0	0	0
	0	# Moog et al. (2004)							
Fe+2		Mg+2	Cl-	-0.0299		0	0	0	0
	0	# Moog et al. (2004)							
Fe+2		Ca+2	Cl-	-0.0160		0	0	0	0
	0	# Moog et al. (2004)							
Na+		K+	Cl-	-0.0018		0	0	0	0
	0	# HMW84							
Na+		K+	SO4-2	-0.01		0	0	0	0
	0	# HMW84							
Na+		K+	HCO3-	-0.003		0	0	0	0
	0	# HMW84							
Na+		K+	CO3-2	0.003		0	0	0	0
	0	# HMW84							
Na+		Ca+2	Cl-	-0.007		0	0	0	0
	0	# HMW84							
Na+		Ca+2	SO4-2	-0.055		0	0	0	0
	0	# HMW84							
Na+		Mg+2	Cl-	-0.012		0	0	0	0
	0	# HMW84							
Na+		Mg+2	SO4-2	-0.015		0	0	0	0
	0	# HMW84							
Na+		H+	Cl-	-0.004		0	0	0	0
	0	# HMW84							
Na+		H+	HSO4-	-0.0129		0	0	0	0
	0	# HMW84							
#Na+		H+	ClO4-	-0.016		0	0	0	0
	0	# NFRK95							
Na+		Th+4	Cl-	0.21		0	0	0	0
	0	# RFSMMN							
K+		Ca+2	Cl-	-0.025		0	0	0	0
	0	# HMW84							
K+		Mg+2	Cl-	-0.022		0	0	0	0
	0	# HMW84							
K+		Mg+2	SO4-2	-0.048		0	0	0	0
	0	# HMW84							
K+		H+	Cl-	-0.011		0	0	0	0
	0	# HMW84							
K+		H+	SO4-2	0.197		0	0	0	0
	0	# HMW84							
K+		H+	HSO4-	-0.0265		0	0	0	0
	0	# HMW84							
K+		Th+4	Cl-	0.21		0	0	0	0
	0	# RFSMMN (analogy with Na)							
Ca+2		Mg+2	Cl-	-0.012		0	0	0	0
	0	# HMW84							
Ca+2		Mg+2	SO4-2	0.024		0	0	0	0
	0	# None							
Ca+2		H+	Cl-	-0.015		0	0	0	0
	0	# HMW84							
Ca+2		Th+4	Cl-	0.21		0	0	0	0
	0	# RFSMMN (analogy with Mg)							
Mg+2		MgOH+	Cl-	0.028		0	0	0	0
	0	# HMW84							
Mg+2		H+	Cl-	-0.011		0	0	0	0
	0	# HMW84							
Mg+2		H+	HSO4-	-0.0178		0	0	0	0
	0	# HMW84							
Mg+2		Th+4	Cl-	0.21		0	0	0	0
	0	# RFSMMN							
H+		Th+4	Cl-	0.37		0	0	0	0
	0	# Roy92							
Cl-		SO4-2	Na+	0.0014		0	0	0	0
	0	# HMW84							
Cl-		SO4-2	Ca+2	-0.018		0	0	0	0
	0	# HMW84							

Cl-		SO4-2		Mg+2		-0.004		0	0	0	0
	0	# HMW84									
Cl-		HSO4-		Na+		-0.006		0	0	0	0
	0	# HMW84									
Cl-		HSO4-		H+		0.013		0	0	0	0
	0	# HMW84									
Cl-		OH-		Na+		-0.006		0	0	0	0
	0	# HMW84									
Cl-		OH-		K+		-0.006		0	0	0	0
	0	# HMW84									
Cl-		OH-		Ca+2		-0.025		0	0	0	0
	0	# HMW84									
Cl-		HCO3-		Na+		-0.015		0	0	0	0
	0	# HMW84									
Cl-		HCO3-		Mg+2		-0.096		0	0	0	0
	0	# HMW84									
Cl-		CO3-2		Na+		0.0085		0	0	0	0
	0	# HMW84									
Cl-		CO3-2		K+		0.004		0	0	0	0
	0	# HMW84									
Cl-		B(OH)4-		Na+		-0.0073		0	0	0	0
	0	# FW86									
Cl-		B3O3(OH)4-		Na+		-0.024		0	0	0	0
	0	# FW86									
Cl-		B4O5(OH)4-2		Na+		0.026		0	0	0	0
	0	# FW86									
Cl-		H2PO4-		K+		-0.01		0	0	0	0
	0	# PS76									
Cl-		Th(CO3)5-6		Na+		0.3		0	0	0	0
	0	# FR99									
Cl-		Th(CO3)5-6		K+		0.3		0	0	0	0
	0	# FR99 (analogy w/NNa)									
Cl-		Acetate-	Na+		0.01029		0	0	0	0	0
	# NBC96										
SO4-2		HSO4-		Na+		-0.0094		0	0	0	0
	0	# HMW84									
SO4-2		HSO4-		K+		-0.0677		0	0	0	0
	0	# HMW84									
SO4-2		HSO4-		Mg+2		-0.0425		0	0	0	0
	0	# HMW84									
SO4-2		OH-		Na+		-0.009		0	0	0	0
	0	# HMW84									
SO4-2		OH-		K+		-0.05		0	0	0	0
	0	# HMW84									
SO4-2		HCO3-		Na+		-0.005		0	0	0	0
	0	# HMW84									
SO4-2		HCO3-		Mg+2		-0.161		0	0	0	0
	0	# HMW84									
SO4-2		CO3-2		Na+		-0.005		0	0	0	0
	0	# HMW84									
SO4-2		CO3-2		K+		-0.009		0	0	0	0
	0	# HMW84									
OH-		CO3-2		Na+		-0.017		0	0	0	0
	0	# HMW84									
OH-		CO3-2		K+		-0.01		0	0	0	0
	0	# HMW84									
HCO3-		CO3-2		Na+		0.002		0	0	0	0
	0	# HMW84									
HCO3-		CO3-2		K+		0.012		0	0	0	0
	0	# HMW84									
#HCO3-		ClO4-		Na+		-0.01		0	0	0	0
	0	# NFRK95									
#CO3-2		ClO4-		Na+		-0.024		0	0	0	0
	0	# NFRK95									
#Na+	K+			Br-	-0.0022		0	0	0	0	0 # pitzer.dat
#Na+	H+			Br-	-0.012		0	0	0	0	0 # pitzer.dat
#K+		H+			Br-	-0.021		0	0	0	0
	# pitzer.dat										
#Cl-	Br-		K+		0.0000		0	0	0	0	0 # pitzer.dat
#OH-		Br-		Na+	-0.018		0	0	0	0	0 # pitzer.dat

```
#OH-	Br-	K+	-0.014	0	0	0	0	0	# pitzer.dat
#-------------------------------------------------------------------------------------------------------------------
-ZETA
O2	Ca+2	Cl-	-0.0169	0	0	0	0
	0	# YMP DTN: SN0302T0510102.002 (data0.ypf.R1)
O2	Ca+2	NO3-	0	0	0	0	0
	0	# YMP DTN: SN0302T0510102.002 (data0.ypf.R1)
O2	H+	Cl-	-0.0077	0	0	0	0
	0	# YMP DTN: SN0302T0510102.002 (data0.ypf.R1)
O2	K+	Br-	-0.00541	0	0	0	0	0
	# YMP DTN: SN0302T0510102.002 (data0.ypf.R1)
O2	K+	Cl-	-0.0211	0	0	0	0
	0	# YMP DTN: SN0302T0510102.002 (data0.ypf.R1)
O2	K+	OH-	-7.06411904E-03 -1.50750433E+01 -4.52071983E-02
4.50984598E-05	0 0	#YMP DTN: SN0302T0510102.002 (data0.ypf.R1)
O2	K+	NO3-	-0.0281	0	0	0	0
	0	# YMP DTN: SN0302T0510102.002 (data0.ypf.R1)
O2	K+	SO4-2	0	0	0	0	0
	0	# YMP DTN: SN0302T0510102.002 (data0.ypf.R1)
O2	Na+	Br-	-0.00909	0	0	0	0	0
	# YMP DTN: SN0302T0510102.002 (data0.ypf.R1)
O2	Na+	Cl-	-9.18665101E-03 -2.73899999E+00 3.25992090E-11 -
4.87958604E-14	0 0	#YMP DTN: SN0302T0510102.002 (data0.ypf.R1)
O2	Na+	CO3-2	-0.0181	0	0	0	0
	0	# YMP DTN: SN0302T0510102.002 (data0.ypf.R1)
O2	Na+	HCO3-	0	0	0	0	0
	0	# YMP DTN: SN0302T0510102.002 (data0.ypf.R1)
O2	Na+	NO3-	-0.012	0	0	0	0
	0	# YMP DTN: SN0302T0510102.002 (data0.ypf.R1)
O2	Na+	OH-	-0.0125	0	0	0	0
	0	# YMP DTN: SN0302T0510102.002 (data0.ypf.R1)
O2	Na+	SO4-2	-0.046	0	0	0	0
	0	# YMP DTN: SN0302T0510102.002 (data0.ypf.R1)
B(OH)3	Na+	SO4-2	0.046	0	0	0	0
	0	# FW86
B(OH)3	H+	Cl-	-0.0102	0	0	0	0
	0	# FW86
#-------------------------------------------------------------------------------------------------------------------
-alphas
Ca+2	Edta-4	2.0	12.0	#Domski(2018)
Mg+2	CaEdta-2	2.0	12.0	# Domski(2018)
Mg+2	MgEdta-2	2.0	12.0	# Domski(2018)
Na+	NaEdta-3	2.0	12.0	# Felmy & Mason(2003)
Na+	Mg(Oxalate)2-2	2.0	12.0	# AP-182
Fe+2	Cl-	2.0	12.0	# Moog et al. (2004) 15
Na+	Fe(CO3)2-2	2.0	12.0	# Kim et al (2017)
Na+	Cl-	2.0	12.0	# HMW84
Na+	SO4-2	2.0	12.0	# HMW84
Na+	HSO4-	2.0	12.0	# HMW84
Na+	OH-	2.0	12.0	# HMW84
Na+	HCO3-	2.0	12.0	# HMW84
Na+	CO3-2	2.0	12.0	# HMW84
Na+	B(OH)4-	2.0	12.0	# FW86
Na+	B3O3(OH)4-	2.0	12.0	# FW86
Na+	B4O5(OH)4-2	2.0	12.0	# FW86
Na+	Am(CO3)2-	2.0	12.0	# FanghŠnel et al 1999 (analogue w/Cm)
Na+	Am(CO3)3-3	2.0	12.0	# FanghŠnel et al 1999 (analogue w/Cm)
#Na+	ClO4-	2.0	12.0	# P91
Na+	NpO2CO3-	2.0	12.0	# FNK95
Na+	NpO2(CO3)2-3	2.0	12.0	# FNK95
Na+	NpO2(CO3)3-5	2.0	12.0	# FNK95
Na+	H2PO4-	2.0	12.0	# P91
Na+	HPO4-2	2.0	12.0	# P91
Na+	PO4-3	2.0	12.0	# P91
Na+	Th(SO4)3-2	2.0	12.0	# FR92
Na+	Th(CO3)5-6	2.0	12.0	# FR92
Na+	HOxalate-	2.0	12.0	# SAND99/Mizera
Na+	Oxalate-2	2.0	12.0	# Choppin et al (2001)
Na+	Acetate-	2.0	12.0	# SAND99/NBC96
Na+	Lactate-	2.0	12.0	# SAND99/Moore et al. 99
```

Na+	H2Citrate-	2.0		12.0		# SAND99/Mizera
Na+	HCitrate-2	2.0		12.0		# SAND99/Mizera
Na+	Citrate-3	2.0		12.0		# SAND99/Mizera
Na+	H3Edta-		2.0		12.0	# Giambalvo (2002)
Na+	H2Edta-2	2.0		12.0		# Giambalvo (2002)
Na+	HEdta-3		2.0		12.0	# Giambalvo (2002)
Na+	Edta-4		2.0		12.0	# Felmy & Mason(2003)
Na+	AmEdta-		2.0		12.0	# SAND99 (Typo in original; pair should be as listed above)
Na+	NpO2Citrate-2		2.0		12.0	# SAND99 (Typo in original; pair should be as listed above)
Na+	NpO2Edta-3		2.0		12.0	# SAND99, PBMC98 (listed correctly in PBMC98)
Na+	NpO2Oxalate-		2.0		12.0	# SAND99 (Correctly listed in Borkowski et al. 2001)
Na+	Am(CO3)4-5		2.0		12.0	# FK98, FanghŠnel et al. 1995
Na+	Am(SO4)2-		2.0		12.0	# FK98 (Analogue with Cm)
Na+	NpO2H2Edta-		2.0		12.0	# PBMC98
Na+	CaCitrate-	2.0		12.0		# ERG_org_memo (analogy w/Mg)
Na+	CaEdta-2	2.0		12.0		# Domski (2018)
Na+	MgCitrate-	2.0		12.0		# ERG_org_memo
Na+	NpO2HEdta-2		2.0		12.0	# PBMC98
K+	Cl-		2.0		12.0	# HMW84
K+	SO4-2		2.0		12.0	# HMW84
K+	HSO4-		2.0		12.0	# HMW84
K+	OH-		2.0		12.0	# HMW84
K+	HCO3-		2.0		12.0	# HMW84
K+	CO3-2		2.0		12.0	# HMW84
K+	B(OH)4-		2.0		12.0	# FW86
K+	B3O3(OH)4-		2.0		12.0	# FW86
K+	B4O5(OH)4-2		2.0		12.0	# FW86
K+	Am(CO3)2-		2.0		12.0	# FK98 (analogue w/Na)
K+	Am(CO3)3-3		2.0		12.0	# FK98 (analogue w/Na)
K+	NpO2CO3-		2.0		12.0	# Novak et al. 1997 (analogue w/Na)
K+	NpO2(CO3)2-3		2.0		12.0	# Novak et al. 1997 (analogue w/Na)
K+	NpO2(CO3)3-5		2.0		12.0	# Novak et al. 1997 (calculated from K data)
K+	H2PO4-		2.0		12.0	# P91
K+	HPO4-2		2.0		12.0	# P91
K+	PO4-3		2.0		12.0	# P91
K+	Th(SO4)3-2		2.0		12.0	# FR92
K+	Th(CO3)5-6		2.0		12.0	# FRSMHC97 (analogue w/Na)
K+	HOxalate-	2.0		12.0		# SAND99/Mizera (Analogue with Na)
K+	Oxalate-2	2.0		12.0		# SAND99/Mizera (Analogue with Na)
K+	Acetate-	2.0		12.0		# SAND99/Mizera (Analogue with Na)
K+	Lactate-	2.0		12.0		# SAND99/Moore et al. 1999 (Analogue with Na)
K+	H2Citrate-	2.0		12.0		# SAND99/Mizera (Analogue with Na)
K+	HCitrate-2	2.0		12.0		# SAND99/Mizera (Analogue with Na)
K+	Citrate-3	2.0		12.0		# SAND99/Mizera (Analogue with Na)
K+	H3Edta-		2.0		12.0	# Giambalvo (2002)
K+	H2Edta-2	2.0		12.0		# Giambalvo (2002)
K+	HEdta-3		2.0		12.0	# Giambalvo (2002)
K+	Edta-4		2.0		12.0	# Felmy & Mason(2003)
K+	AmEdta-		2.0		12.0	# SAND99 (Analogue with Na)
K+	NpO2Citrate-2		2.0		12.0	# SAND99 (analogue w/Na; error in original)
K+	NpO2Edta-3		2.0		12.0	# AND99/PBMC98 (Correctly listed in latter source)
K+	NpO2Oxalate-		2.0		12.0	# SAND99/Borkowski et al. 2001; listed correctly in latter source
K+	Am(CO3)4-5		2.0		12.0	# FK98 (analogy with Na)
K+	Am(SO4)2-		2.0		12.0	# FK98 (analogy w/Na)
K+	NpO2H2Edta-		2.0		12.0	# PBMC98 (analogy w/Na)
K+	CaCitrate-	2.0		12.0		# ERG_org_memo (analogy w/Na, Mg)
K+	CaEdta-2	2.0		12.0		# Domski (2018)
K+	MgCitrate-	2.0		12.0		# ERG_org_memo (analogy with Na)
K+	NpO2HEdta-2		2.0		12.0	# PBMC98 (analogy w/Na)
Ca+2	Cl-		2.0		12.0	# HMW84
Ca+2	SO4-2		1.4		12.0	# HMW84
Ca+2	HSO4-		2.0		12.0	# HMW84
Ca+2	OH-		2.0		12.0	# HMW84

Ca+2	HCO3-	2.0	12.0	# HMW84		
#Ca+2	ClO4-	2.0	12.0	# P91		
Ca+2	NpO2CO3-	2.0	12.0	# al Mahamid et al. 1998 (analogy w/Mg)		
Ca+2	NpO2(CO3)2-3	1.4	50.0	# al Mahamid et al. 1998 (analogy w/Mg)		
Ca+2	NpO2(CO3)3-5	1.4	50.0	# al Mahamid et al. 1998 (analogy w/Mg; values averaged over Na and K values)		
Mg+2	Cl-	2.0	12.0	# HMW84		
Mg+2	SO4-2	1.4	12.0	# HMW84		
Mg+2	HSO4-	2.0	12.0	# HMW84		
Mg+2	HCO3-	2.0	12.0	# HMW84		
#Mg+2	ClO4-	2.0	12.0	# P91		
Mg+2	NpO2CO3-	2.0	12.0	# al Mahamid et al. 1998 (analogy w/Na)		
Mg+2	NpO2(CO3)2-3	1.4	50.0	# al Mahamid et al. 1998 (analogy w/Na)		
Mg+2	NpO2(CO3)3-5	1.4	50.0	# al Mahamid et al. 1998 (averaged Na and K values)		
MgOH+	Cl-	2.0	12.0	# HMW84		
H+	Cl-	2.0	12.0	# HMW84		
H+	SO4-2	2.0	12.0	# HMW84		
H+	HSO4-	2.0	12.0	# HMW84		
#H+	ClO4-	2.0	12.0	# P91		
H+	Th(SO4)3-2	2.0	12.0	# FR92		
MgB(OH)4+	Cl-	2.0	12.0	# FW86		
CaB(OH)4+	Cl-	2.0	12.0	# FW86		
Am+3	Cl-	2.0	12.0	# FK98, Konnecke et al. 1997		
Am+3	SO4-2	1.4	50.0	# FK98		
#Am+3	ClO4-	2.0	12.0	# FRF90		
Am+3	H2PO4-	2.0	12.0	# RFF95 (from Nd analogue)		
AmCO3+	Cl-	2.0	12.0	# FK98/FanghŠnel et al. 1999 (Cm analogue)		
Th+4	Cl-	2.0	12.0	# Roy92		
Th+4	SO4-2	1.4	50.0	# FR92		
Th+4	HSO4-	2.0	12.0	# FR92		
#Th+4	ClO4-	2.0	12.0	# CFN960119		
AmCl+2	Cl-	2.0	12.0	# FK98/Konnecke et al. (Cm analogue)		
NpO2+	Cl-	2.0	12.0	# NFRK95		
#NpO2+	ClO4-	2.0	12.0	# NFRK95		
ThOxalate+2	Cl-	2.0	12.0	# SAND99/Borkowski et al. 2001		
AmAcetate+2	Cl-	2.0	12.0	# ERG_org_memo		
AmLactate+2	Cl-	2.0	12.0	# SAND97/Moore et al 1999		
AmOxalate+	Cl-	2.0	12.0	# SAND99/Borkowski et al. 2001		
ThAcetate+3	Cl-	2.0	12.0	# SAND99		
ThCitrate+	Cl-	2.0	12.0	# SAND99		
ThLactate+3	Cl-	2.0	12.0	# SAND99/Moore et al. 1999		
AmOH+2	Cl-	2.0	12.0	# FK98/Konnecke et al. 1997 (Cm analogue)		
Am(OH)2+	Cl-	2.0	12.0	# FK98/Konnecke et al. 1997 (Cm analogue)		
AmCl2+	Cl-	2.0	12.0	# FK98/Konnecke et al. 1997 (Cm analogue)		
AmSO4+	Cl-	2.0	12.0	# FK98 (Cm analogue)		
Th(Acetate)2+2	Cl-	2.0	12.0	# Moore et al. 1999		
Th(Lactate)2+2	Cl-	2.0	12.0	# Moore et al. 1999		
CaAcetate+	Cl-	2.0	12.0	# ERG_org_memo (analogy w/Mg)		
MgAcetate+	Cl-	2.0	12.0	# ERG_org_memo		
#Na+	Br-	0.0973	0	0	7.692E-40	0 # pitzer.dat
#K+	Br-	0.0569	0	0	7.39E-4	0 0 # pitzer.dat
#H+	Br-	0.1960	0	0	-2.049E-4	0 0 # pitzer.dat
#Mg+2	Br-	0.4327	0	0	-5.625E-5	0 0 # pitzer.dat
#Ca+2	Br-	0.3816	0	0	-5.2275E-4	0 0 # pitzer.dat
#Li+	Br-	0.1748		0	-1.819E-4	0 0 # pitzer.dat

DATA0FM_EPA.DAT

```
# DATA0FM_EPA.DAT 6/21/2021
#3/30/2022 changed earlandite solubility to value used by Domski (2019) ERMS 571052
#6/21/2021 changed log beta for CaEDTA-- to Felmy and Mason 2003 value
#2/19/2021 corrected beta(0) term for the binary Pitzer parameter for Ca2+/EDTA4- ion pair described in PPR-2019-03. Correct value is 2.49
#2/19/2021 corrected alpha(1) terms for the binary Pitzer parameters for Ca2+/EDTA4- Mg2+/MgEDTA2- and Mg2+/CaEDTA2- described in
Domski(2019)
#2/19/2021 PPR-2019-04 through -13 and EPA CC5-GEOCHEM-27d. Correct alpha(1) values are 1.4
#10/29/2020 Database has been updated to incorporate CRA-2019 completeness questions CC2-GEOCHEM-8, 10, 11, 12, 13
#10/29/2020 Updated parameters can be found by searching for the ** in the file
# atomic weights consistent with DATA0.FM4
# Data from DATA0.FM4 for actinides and Pitzer parameters
# Aqueous speciation written as association reactions so log k's are reversed
# from EQ36 format
# Reactions with dissolved carbonates, dissolved boron, and phosphate are re-written
# to use CO3-2, B(OH)3, and PO4-3 as the basis species to be consistent with PHREEQC
# format using relevant reactions.  This change was done to allow direct comparisons
# of log k's to values in PITZER.DAT but all are consistent with DATA0.FM4
# Additional Pitzer parameters for Br- from pitzer.dat are commented out because not in DATA0.FM4
# Perclorate Pitzer parameters included but commented out because perchlorate is suppressed by DOE for WIPP solubility modeling
# This database cannot be used for redox reactions without review and additional data
#-----------------------------------------------------------------------
#-----------------------------------------------------------------------
SOLUTION_MASTER_SPECIES
# Atomic weight data from 99lid via data0.ymp.R5 (DTN: SN0612T0502404.014)]
Alkalinity CO3-2      1.0          Ca0.5(CO3)0.5      50.05
B          B(OH)3                  0.0          B                  10.811
Br     Br-            0.0          Br                 79.904
C          CO3-2                   2.0          HCO3               12.011
C(4)   CO3-2                       2.0          HCO3               12.011
Ca     Ca+2                        0.0          Ca                 40.078
Cl     Cl-            0.0          Cl                 35.4527
E          e-                      0.0          0.0                0.0
H          H+                      -1.0         H                  1.00794
H(1)       H+                      -1.0         0.0
Fe         Fe+2                    0.0          Fe                 55.845
Fe(2)      Fe+2                    0.0          Fe
K          K+                      0.0          K                  39.0983
Mg     Mg+2                        0.0          Mg                 24.305
N          NO3-                    0.0    N                14.00674
N(5)       NO3-                    0.0          N
Na     Na+            0.0          Na                 22.98977
O          H2O                     0.0          O                  15.99940
O(0)       O2                      0.0          O
O(-2)      H2O                     0.0          0.0
S          SO4-2                   0.0          SO4                32.066
S(6)   SO4-2                       0.0          SO4
# Additions from EQ36 ----------------------------------
Pb                    Pb+2                    0.0          207.2              207.2
P                     PO4-3                   2.0          30.97376   30.97376
Am                    Am+3                    0.0          Am                 243.0
Np                    NpO2+                   0.0          Np                 237.0
Th                    Th+4                    0.0          Th                 232.0381
Acetate               Acetate-   1      59.05             59.05
Citrate               Citrate-3  2      189.06            189.06
Edta                  Edta-4                  2      276                276
Oxalate               Oxalate-2  2      88                88
Lactate               Lactate-   1      89                89
#-----------------------------------------------------------------------
# Deletions from pitzer.dat ----------------------------------
#Ba     Ba+2                    0.0          Ba                 137.327
#Li     Li+            0.0          Li                 6.941
#Mn     Mn+2                    0.0          Mn                 54.93805
#Mn(2)      Mn+2                0.0          Mn
#Sr     Sr+2                    0.0          Sr                 87.62
#-----------------------------------------------------------------------
SOLUTION_SPECIES
#H+ primary master species
```

```
      H+ = H+
      log_k         0.0

#e- primary master species
      e- = e-
      log_k         0.0

#H2O primary master species
      H2O = H2O
      log_k         0.0

#Li+ primary master species
#           Li+ = Li+
#           -dw           1.03e-9
#           -Vm   -.0237   -.0690   11.5800   -2.7761 .4862 6 # supcrt

#Na+ primary master species
            Na+ = Na+
#           -dw           1.33e-9
#            -Vm  1.403  -2.285  4.419  -2.726  -5.125e-5  4.0  0.162  47.67  -3.09e-3  0.725 # supcrt modified

#K+ primary master species
            K+ = K+
#           -dw           1.96e-9
#           -Vm  3.322  -1.473  6.534  -2.712  9.06e-2  3.5  0  29.70  0  1 # supcrt modified

#Mg+2 primary master species
            Mg+2 = Mg+2
#           -dw           0.705e-9
#           -Vm  -1.410  -8.6  11.13  -2.39  1.332  5.5  1.29  -32.9  -5.86e-3  1 # supcrt modified

#Ca+2 primary master species
            Ca+2 = Ca+2
#           -dw           0.793e-9
#           -Vm  -0.3456  -7.252  6.149  -2.479  1.239  5  1.60  -57.1  -6.12e-3  1 # supcrt modified

#Sr+2 primary master species
#           Sr+2 = Sr+2
#           -dw           0.794e-9
#           -Vm  -1.57e-2  -10.15  10.18  -2.36  0.860  5.26  0.859  -27.0  -4.1e-3  1.97 # supcrt modified

#Ba+2 primary master species
#           Ba+2 = Ba+2
#           -dw           0.848e-9
#           -Vm  2.063  -10.06  1.9534  -2.36  0.4218  5  1.58  -12.03  -8.35e-3  1 # supcrt modified

#Mn+2 primary master species
#           Mn+2 = Mn+2
#           -dw           0.688e-9
#           -Vm   -.1016   -8.0295   8.9060   -2.4471  1.4006 6 # supcrt

#Fe+2 primary master species
            Fe+2 = Fe+2
#           -dw           0.719e-9
#           -Vm  -0.3255  -9.687  1.536  -2.379  0.3033  5.5  -4.21e-2  37.96  0  1 # supcrt modified

#Cl- primary master species
            Cl- = Cl-
#           -dw           2.03e-9
#           -Vm  4.465  4.801  4.325  -2.847  1.748  0  -0.331  20.16  0  1 # supcrt modified

#NO3- primary master species
            NO3- = NO3-
            log_k 0

#CO3-2 primary master species
            CO3-2 = CO3-2
#           -dw           0.955e-9
#           -Vm  5.052 0  0  -5.447  4.927  0  0.103  94.9  -1.30e-2  1 # supcrt modified
```

```
#SO4-2 primary master species
        SO4-2 = SO4-2
#       -dw         1.07e-9
#       -Vm  5.0  9.06  -8.36  -3.14  3.773  0  6.61  -27.9  -6.32e-2  0.428 # supcrt modified

#B(OH)3 primary master species
        B(OH)3 = B(OH)3
#       -dw         1.1e-9
#       -Vm 7.0643   8.8547   3.5844   -3.1451 -.2000  # supcrt

#Br- primary master species
        Br- = Br-
#       -dw         2.01e-9
#       -Vm  5.2690   6.5940   4.7450   -3.1430 1.3858 # supcrt

# From EQ36 ---------------------------------------------------------------------------------------

#Am+3 primary master species
        Am+3 =  Am+3
        log_k 0

#NpO2+ primary master species
        NpO2+ =  NpO2+
        log_k 0

#Th+4 primary master species
        Th+4 =  Th+4
        log_k 0

#Pb+2 primary master species
    Pb+2 = Pb+2
    log_k       0.0

#PO4-3 primary master species
    PO4-3 = PO4-3
    log_k       0.0

#Acetate- primary master species
        Acetate- = Acetate-
        log_k 0

#Citrate-3 primary master species
        Citrate-3 = Citrate-3
        log_k 0

#Edta-4 primary master species
        Edta-4 = Edta-4
        log_k 0

#Oxalate-2 primary master species
        Oxalate-2 = Oxalate-2
        log_k 0

#Lactate- primary master species
        Lactate- = Lactate-
        log_k 0

#-----------------------------------------------------------------------------
# Aqueous Species
#-----------------------------------------------------------------------------
H2O = OH- + H+                                          # pitzer.dat
        log_k       -13.9967                                    # EQ36
#       -analytic  68.547  0  -6199.8  -24.955
#       -dw         5.27e-9
#       -Vm  1.776  0.0738  1.417  -2.782  2.347  0  0.906  0  0  1 # supcrt modified

2 H2O = O2 + 4 H+ + 4 e-                                        # pitzer.dat
        -log_k      -86.0032                                    # EQ36
#       -delta_h 134.79 kcal                                    # pitzer.dat
#       -dw         2.35e-9                                     # pitzer.dat
```

```
#               -Vm  5.7889  6.3536  3.2528  -3.0417  -0.3943 # supcrt   # pitzer.dat

CO3-2 + H+ = HCO3-                                              # pitzer.dat
        log_k           10.3392                                 # EQ36.dat; pitzer.dat has 10.3391
#       delta_h -3.561  kcal                    # pitzer.dat

HCO3- + H+ = CO2 + H2O                                          # pitzer.dat
        log_k           6.3374                  # EQ36
#       delta_h       -5.738  kcal                              # pitzer.dat

SO4-2 + H+ = HSO4-                              # pitzer.dat
        log_k           1.9786                  # EQ36; pitzer.dat has 1.979
#       delta_h 4.91    kcal                    # pitzer.dat

B(OH)3 + H2O = B(OH)4- + H+                     # EQ36
        log_k           -9.239                  # EQ36, pitzer.dat has -9.239
#       delta_h 0   kcal                        # pitzer.dat

3 B(OH)4- + 2H+ = B3O3(OH)4- + 5 H2O  # EQ36
        log_k           20.1893                 # EQ36
#       delta_h 0   kcal                # pitzer.dat

4 B(OH)4- + 2H+ = B4O5(OH)4-2 + 7 H2O           # EQ36
        log_k           20.8220         # EQ36
#       delta_h 0   kcal                # pitzer.dat

Ca+2 + B(OH)4- = CaB(OH)4+              # EQ36
        log_k           1.6503          # EQ36
#       delta_h 0   kcal                # pitzer.data

Mg+2 + B(OH)4- = MgB(OH)4+                      # EQ36
        log_k           1.3993          # EQ36
#       delta_h 0   kcal                # pitzer.dat

Mg+2 + H2O = MgOH+ + H+                         # pitzer.dat
        log_k           -11.8091        # EQ36 (pitzer.dat has -11.809)
#       delta_h 15.419 kcal             # pitzer.dat
                                                # log k Source: none

Pb+2 + Cl- = PbCl+                      # EQ36
      log_k     1.5                     # EQ36 (pitzer has 1.6)
#       delta_h 4.38 kcal               # wateq4f.data
                                                # log k Source: Powell et al. (2009) Derived with SIT Model

Pb+2 + 2 Cl- = PbCl2                    # EQ36
      log_k     2.1                     # EQ36 (wateq4f.data has 1.8)
#       delta_h 1.08 kcal               # wateq4f.dat
                                                # logk  Source: Powell et al. (2009) Derived with SIT Model

Pb+2 + 3 Cl- = PbCl3-                           # EQ36
      log_k     2.0                     # EQ36 (wateq4f.dat has 1.7)
#       delta_h 2.17 kcal               # wateq4f.dat
                                                # log k Source: Powell et al. (2009) Derived with SIT Model

Pb+2 + H2O = PbOH+ + H+                 # EQ36
      log_k     -7.46           # EQ36 (wateq4f.dat has -7.71)
#       delta_h 0    kcal               # no data
                                                # log k Source: Powell et al. (2009) Derived with SIT Model

Pb+2 + 2 H2O = Pb(OH)2 + 2 H+                   # EQ36
      log_k     -16.94          # EQ36 (wateq4f.dat has -17.12)
#       delta_h 0    kcal               # no data
                                                # log k Source: Powell et al. (2009)

Pb+2 + HCO3- = PbCO3 + H+               # EQ36
      log_k     -3.89           # EQ36 (wateq4f.dat has 3.89)
#       delta_h 0    kcal               # no data
                                                # log k Source: Powell et al. (2009) Derived with SIT Model

Pb+2 + 2 HCO3-  = Pb(CO3)2-2 + 2H+      # EQ36
```

```
      log_k      -10.55              # EQ36 (wateq4f.dat has 10.64)
#             delta_h 0    kcal                  # no data
                                                 # log k Source: Powell et al. (2009) Derived with SIT Model

Pb+2 + SO4-2 = PbSO4                             # EQ36
      log_k       2.72               # EQ36 (wateq4f.dat has 2.75)
#             delta_h 0    kcal                  # no data
                                                 # log k Source: Powell et al. (2009) Derived with SIT Model

Pb+2 + HCO3- + Cl- = PbCO3Cl- + H+       # EQ36
            log_k       -3.87                    # EQ36
#           delta_h 0    kcal                    # no data
                                                 # log k ource:Powell et al. (2009) Derived with SIT Model

Pb+2 + HCO3- + H2O = PbCO3OH- + 2H+ # EQ36
            log_k      -13.4400                  # EQ36
#           delta_h 0    kcal                    # no data
                                                 # log k Source:Powell et al. (2009) Derived with SIT Model

Fe+2 + HCO3- = FeCO3 + H+                # EQ36
      log_k       -4.8300                        # EQ36
#           delta_h 0    kcal                    # no data
                                                 # log k Source: Bruno et al 1992

Fe+2 + 2 HCO3- = Fe(CO3)2-2 + 2H+        # EQ36
            log_k            -13.8900            # EQ36
#           delta_h 0    kcal                    # no data
                                                 # log k Source: Kim et al. (2017)

Fe+2 + H2O = FeOH+ + H+                  # EQ36
      log_k      -9.31               # EQ36 (wateq4f.dat has -9.5)
#       delta_h 13.2 kcal                        # wateq4f.dat
                                                 # log k Source: Shock et al 1997

Fe+2 + 2 H2O = Fe(OH)2 + 2 H+                    # EQ36
      log_k      -20.82              # EQ36 (wateq4f.dat has -20.57)
#       delta_h 28.565 kcal                      # wateq4f.dat
                                                 # log k Source: Stumm & Morgan (1996)

Fe+2 + 3 H2O = Fe(OH)3- + 3 H+                   # EQ36
      log_k      -31.0               # EQ36 (wateq4fg.dat also has -31.0)
#       delta_h 30.3 kcal                        # wateq4f.dat
                                                 # log k Source: Baes and Mesmer (1976)

Ca+2 + HCO3- = CaCO3 + H+                # EQ36
            log_k          -7.188                # EQ36
#           delta_h 3.547   kcal                 # pitzer.dat

Mg+2 + HCO3- = MgCO3 + H+                # EQ36
            log_k          -7.4108               # EQ36
#           delta_h 2.535   kcal                 # pitzer.dat

H+ + PO4-3 = HPO4-2                              # EQ36
      log_k     12.3426                          # EQ36 (wateq4f.dat has 12.346)
#       delta_h -3.53 kcal                       # wateq4f.dat

H+ + HPO4-2 = H2PO4-                             # EQ36
      log_k     7.2062               # EQ36
#       delta_h -4.52 kcal                       # wateq4f.dat

2 H+ + HPO4-2 = H3PO4                            # EQ36
      log_k     9.3517               # EQ36
      delta_h   -10.1 kJ             # minteq.v4.dat

Acetate- + H+ = HAcetate                 # EQ36
            log_k     4.7568                     # EQ36
#           delta_h      0.41         kJ         # minteq.v4.data

Acetate- + Mg+2 = MgAcetate+             # EQ36
            log_k     1.1131                     # EQ36
```

```
Acetate- + Ca+2 = CaAcetate+                # EQ36
        log_k     1.1131                    # EQ36

Citrate-3 + 3 H+ = H3Citrate                # EQ36
        log_k          14.27                # EQ36 Hummel et al. (2005) Derived with SIT Model

Citrate-3 + 2 H+ = H2Citrate-               # EQ36
        log_k      11.14                    # EQ36 Hummel et al. (2005) Derived with SIT Model

Citrate-3 + H+ = HCitrate-2                 # EQ36
        log_k       6.36                    # EQ36 Hummel et al. (2005) Derived with SIT Model

Citrate-3 + H+ + Mg+2 = MgHCitrate          # EQ36
        log_k          8.96                 # EQ36 Hummel et al. (2005) Derived with SIT Model

Citrate-3 + 2 H+ + Mg+2 = MgH2Citrate+      # EQ36
        log_k          12.450               # EQ36 Hummel et al. (2005) Derived with SIT Model

Citrate-3 + Mg+2 = MgCitrate-               # EQ36
        log_k       4.81                    # EQ36 Hummel et al. (2005) Derived with SIT Model

Citrate-3 + Ca+2 = CaCitrate-               # EQ36
        log_k       4.80                    # EQ36 Hummel et al. (2005) Derived with SIT Model

Citrate-3 + H+ + Ca+2 = CaHCitrate          # EQ36
        log_k          9.28                 # EQ36 Hummel et al. (2005) Derived with SIT Model

Citrate-3 + 2 H+ + Ca+2 = CaH2Citrate+      # EQ36
        log_k      12.67                    # EQ36 Hummel et al. (2005) Derived with SIT Model

Edta-4 + 4 H+ = H4Edta                              # EQ36
        log_k      23.42                    # EQ36 Hummel et al. (2005) Derived with SIT Model

Edta-4 + 3 H+ = H3Edta-                             # EQ36
        log_k      21.19                    # EQ36 Hummel et al. (2005) Derived with SIT Model

Edta-4 + 2 H+ = H2Edta-2                    # EQ36
        log_k      18.04                    # EQ36 Hummel et al. (2005) Derived with SIT Model

Edta-4 + H+ = HEdta-3                               # EQ36
        log_k      11.24                    # EQ36 Hummel et al. (2005) Derived with SIT Model

Edta-4 + Na+ = NaEdta-3                             # EQ36
        log_k       2.80                    # EQ36 Hummel et al. (2005) Derived with SIT Model

Edta-4 + Mg+2 = MgEdta-2                    # EQ36
        log_k      10.90                    # EQ36 Hummel et al. (2005) Derived with SIT Model

Edta-4 + H+ + Mg+2 = MgHEdta-                       # EQ36
        log_k          15.40                # EQ36 Hummel et al. (2005) Derived with SIT Model

Edta-4 + Ca+2 = CaEdta-2                    # EQ36
        log_k      12.36                    # Felmy and Mason (2003)**
#       log_k      12.69                    # EQ36 Hummel(2005) Derived with SIT Model

Edta-4 + H+ + Ca+2 = CaHEdta-               # EQ36
        log_k      16.23                    # EQ36 Hummel(2005)

Oxalate-2 + 2 H+ = H2Oxalate                # EQ36
        log_k       5.6532                  # EQ36 Giambalvo

Oxalate-2 + H+ = HOxalate-                  # EQ36
        log_k       4.2596                  # EQ36 Giambalvo

Oxalate-2 + Mg+2 = MgOxalate                # EQ36
        log_k       3.7931                  # EQ36 Giambalvo

2 Oxalate-2 + Mg+2 = Mg(Oxalate)2-2         # EQ36
        log_k       5.24                    # EQ36 Jang & Kim 2016
```

```
Oxalate-2 + Ca+2 = CaOxalate                # EQ36
        log_k       3.7931                  # EQ36 Giambalvo

Lactate- + H+ = HLactate                    # EQ36
        log_k       3.8209                  # EQ36

#---------------------------------------------------------------------
# Actinides-----------------------------------------------------------

Am+3 + HCO3- = AmCO3+ + H+                          # EQ36
        log_k     -2.2388                   # EQ36

Am+3 + 2 HCO3- = Am(CO3)2- + 2 H+           # EQ36
        log_k          -7.6766              # EQ36

Am+3 + 3 HCO3- = Am(CO3)3-3 + 3 H+          # EQ36
        log_k     -15.8157                  # EQ36

Am+3 + 4 HCO3- = Am(CO3)4-5 + 4H+           # EQ36
        log_k    -28.3586                   # EQ36

Am+3 + H2O = AmOH+2 + H+                    # EQ36
        log_k     -7.5556                   # EQ36

Am+3 + 2 H2O = Am(OH)2+ + 2 H+                      # EQ36
        log_k         -15.6915              # EQ36

Am+3 + 3 H2O = Am(OH)3 + 3 H+                       # EQ36
        log_k    -25.6905                   # EQ36

Am+3 + Cl- = AmCl+2                                 # EQ36
        log_k    0.2393                             # EQ36

Am+3 + 2 Cl- = AmCl2+                               # EQ36
        log_k    -0.74                              # EQ36

Am+3 + SO4-2 = AmSO4+                               # EQ36
        log_k    3.2485                             # EQ36

Am+3 + 2 SO4-2 = Am(SO4)2-                  # EQ36
        log_k        3.7019                 # EQ36

Am+3 + Acetate- = AmAcetate+2                       # EQ36
        log_k   2.7426                      # EQ36

Am+3 + Citrate-3 = AmCitrate    #**updated per EPA recommendation
        log_k   8.550           #Hummel et al. (2005), 8.7984 original

Am+3 + 2 Citrate-3 = Am(Citrate)2-3    #**updated per EPA recommendation
        log_k   13.90           #Hummel et al. (2005), species not included in original

Am+3 + Edta-4 = AmEdta-         #**updated per EPA recommendation
        log_k   19.67           #Hummel et al. (2005), 18.9700 EQ36 value

Am+3 + Oxalate-2 = AmOxalate+                       # EQ36
        log_k    6.1566                             # EQ36

Am+3 + Lactate- = AmLactate+2               # EQ36
        log_k    3.7089                             # EQ36

Th+4  + 5 HCO3- = Th(CO3)5-6 + 5H+          # EQ36
        log_k   -24.5828                    # EQ36

Th+4 + HCO3- + 3 H2O = Th(OH)3CO3- + 4 H+           # EQ36
        log_k   -14.0457                            # EQ36

Th+4 + 4 H2O = Th(OH)4 + 4 H+                       # EQ36
        log_k   -17.5002                    # EQ36
```

```
Th+4 + 2 SO4-2 = Th(SO4)2                # EQ36
        log_k         11.5918            # EQ36

Th+4 + 3 SO4-2 = Th(SO4)3-2              # EQ36
        log_k         12.4273            # EQ36

Th+4 + Acetate- = ThAcetate+3            # EQ36
        log_k     7.3617                 # EQ36

Th+4 + 2 Acetate- = Th(Acetate)2+2       # EQ36
        log_k    11.2391                 # EQ36

Th+4 + Citrate-3 = ThCitrate+            # EQ36
        log_k    15.2355                 # EQ36

Th+4 + Edta-4 = ThEdta                           # EQ36
        log_k    23.5570                 # EQ36

Th+4 + Oxalate-2 = ThOxalate+2                   # EQ36
        log_k    11.3863                 # EQ36

Th+4 + Lactate-         = ThLactate+3            # EQ36
        log_k     6.8284                 # EQ36

Th+4 + 2 Lactate- = Th(Lactate)2+2       # EQ36
        log_k    11.1913                 # EQ36

NpO2+ + HCO3- = NpO2CO3- + H+                    # EQ36
        log_k     -5.3223                # EQ36

NpO2+ + 2 HCO3- = NpO2(CO3)2-3 + 2 H+            # EQ36
        log_k     -14.2340               # EQ36

NpO2+ + 3 HCO3- = NpO2(CO3)3-5 + 3H+             # EQ36
        log_k     -25.6859               # EQ36

NpO2+ + H2O = NpO2OH + H+                # EQ36
        log_k    -11.3084                # EQ36

NpO2+ + 2 H2O = NpO2(OH)2- + 2 H+        # EQ36
        log_k    -23.5362                # EQ36

NpO2+ + Acetate- = NpO2Acetate                   # EQ36
        log_k      1.3737                # EQ36

NpO2+ + Citrate-3 = NpO2Citrate-2        #**updated per EPA rec
        log_k      3.680                 #Hummel et al. (2005), 3.4969 original

NpO2+ + Edta-4 = NpO2Edta-3              #**updated per EPA recommendation
        log_k      9.230                 #Hummel et al. (2005), 8.5352 original

NpO2+ + H+ + Edta-4 = NpO2HEdta-2        #**updated per EPA recommendation
        log_k     17.06                          # Hummel et al. (2005), 15.6464 original

NpO2+ + 2 H+ + Edta-4 = NpO2H2Edta-      #**updated per EPA recommendation
        log_k    22.51                          # Hummel et al. (2005), 20.8648 original

NpO2+ + Oxalate-2 = NpO2Oxalate-         # EQ36
        log_k     4.2400                 # EQ36

NpO2+ + Lactate- = NpO2Lactate                   # EQ36
        log_k     1.9674                 # EQ36

#---------------------------------------------------------------------
#---------------------------------------------------------------------
#---------------------------------------------------------------------

PHASES

Earlandite(s)                            #**update to value selected by DOE
```

```
        Ca3Citrate2:4H2O = 3 Ca+2 + 2 Citrate-3 + 4 H2O      # EQ36
        log_k      -16.8100                                  # EQ36 - Domski (2019) from Hummel et al. 2005

CO2(g)
        CO2 = CO2
        log_k       -1.468
#       delta_h -4.776 kcal
#       -analytic  119.87356  2.185434e-2  -7337.8 -44.7652    669371
#       -T_c  304.2 # critical T, K
#       -P_c   72.80 # critical P, atm
#       -Omega 0.225 # acentric factor
H2O(g)
        H2O = H2O
        log_k  1.4999                                     #EQ36
#       delta_h -44.03 kJ
#       -T_c  647.3 # critical T, K
#       -P_c  217.60 # critical P, atm
#       -Omega 0.344 #  acentric factor
#       -analytic   -16.5066 -2.0013E-3  2710.7  3.7646  0 2.24E-6

O2(g)
        O2 = O2
        -log_k   -2.8983
#       -analytic -7.5001 7.8981e-3 0.0 0.0 2.0027e5
#       -T_c  154.6
#       -P_c   49.80
#       -Omega 0.021

Pb2CO3Cl2(s)
        Pb2CO3Cl2 + H+ = 2 Pb+2 + 2 Cl- + HCO3-                  # EQ36 -  .dat
        log_k      0.4100                                 # EQ36 Powell et al. (2009) Derived with SIT Model

PbSO4(s)
        PbSO4 = Pb+2 + SO4-2                              # EQ36 -  .dat
        log_k          -7.80                              # EQ36 Powell et al. (2009) Derived with SIT Model

Cerussite
        PbCO3 + H+ = Pb+2 + HCO3-                         # EQ36 -  .dat
        log_k           -2.84                             # EQ36 Powell et al. (2009) Derived with SIT Model
#       delta_h 4.86 kcal                                 # WATEQ4F.DAT

Litharge
        PbO + 2H+ = Pb+2 + H2O                            # EQ36 -  .dat
        log_k      12.62                                  # EQ36 Powell et al. (2009) Derived with SIT Model
#       delta_h -16.380 kcal                              # WATEQ4F.DAT

Ca2Edta:7H2O(s)
        Ca2Edta:7H2O = 2 Ca+2 + Edta-4 + 7 H2O            # EQ36
        log_k      -16.8100                               # EQ36 - Domski (2018)

MgOxalate:2H2O(s)
        MgOxalate:2H2O = Mg+2 + Oxalate-2 + 2 H2O         # EQ36
        log_k      -6.4100                                # EQ36 - Glushinskite from AP-182

Siderite
        FeCO3 + H+ = Fe+2 + HCO3-                         # EQ36
        log_k     -0.1200                                 # EQ36 Stumm and Morgan (1996)

Chukanovite
        Fe2(OH)2CO3 + 3 H+ = 2 Fe+2 + HCO3- + 2H2O        # EQ36 -  .dat
        log_k     12.32                                   # EQ36 Kim et al (2017)

Oxychloride-Fe-3(s)
        Fe2Cl(OH)3 + 3 H+ = Cl- + 2 Fe+2 + 3 H2O          # EQ36 -  .dat
        log_k     17.08                                   # EQ36 Kim et al (2017)

Fe(OH)2-Hex
        Fe(OH)2 + 2 H+ = Fe+2 + 2 H2O                     # EQ36 -  .dat
        log_k     12.89                                   # EQ36 Kim et al (2017)
```

```
AmOHCO3(c)
        AmOHCO3 + H+ = Am+3 + CO3-2 + H2O               # EQ36
        log_k       -8.7026                             # EQ36: AmOHCO3(c) + 2H+ = Am+3 + HCO3- + H2O; log k = 1.6366

Am(OH)3(s)
        Am(OH)3 + 3 H+ = Am+3 + 3H2O                        # EQ36
        log_k       14.4900                             # EQ36

NaAm(CO3)2:6H2O(c)
        NaAm(CO3)2:6H2O = Na+ + Am+3 + 2 CO3-2 + 6 H2O                  # EQ36
        log_k           -21.3915                                        # EQ36: NaAm(CO3)2:6H2O(c) + 2H+ = Na+ + Am+3
+ 2HCO3- + 6H2O; log k = -0.7131

AmPO4(c)
        AmPO4 = Am+3 + PO4-3                                # EQ36
        log_k       -24.8021                            # EQ36: AmPO4(c) + H+ = Am+3 + HPO4-2; log k = -12.4595

ThO2(am)
        ThO2 + 4 H+ = Th+4 + 2 H2O                      # EQ36
        log_k       10.4865                             # EQ36

Th(SO4)2:9H2O(s)
        Th(SO4)2:9H2O = Th+4 + 2 SO4-2 + 9 H2O              # EQ36
        log_k       -12.9982                            # EQ36

Th(SO4)2:8H2O(s)
        Th(SO4)2:8H2O = Th+4 + 2 SO4-2 + 8 H2O              # EQ36
        log_k       -12.8955                            # EQ36

Na2Th(SO4)3:6H2O(s)                                             # Th(SO4)2:Na2SO4:6H2O in EQ36
        Na2Th(SO4)3:6H2O = Th+4 + 2 Na+ + 3 SO4-2 + 6 H2O       # EQ36
        log_k       -17.6419                            # EQ36

K2Th(SO4)3:4H2O(s)                                              # Th(SO4)2:K2SO4:4H2O(s) in EQ36
        K2Th(SO4)3:4H2O = Th+4 + 2 K+ + 3 SO4-2 + 4 H2O         # EQ36
        log_k       -18.0740                            # EQ36

K4Th(SO4)4:2H2O(s)                                              # Th(SO4)2:2K2SO4:2H2O in EQ36
        K4Th(SO4)4:2H2O = Th+4 + 4 K+ + 4 SO4-2 + 2 H2O         # EQ36
        log_k       -21.2301                            # EQ36

Th2(SO4)4:7K2SO4(s)                                             # 2[Th(SO4)2.7/2K2SO4] in EQ36
        Th2(SO4)4:7K2SO4(s) = 2 Th+4 + 14 K+ + 11 SO4-2  # EQ36
        log_k       -49.2193                            # EQ36

NpO2OH(aged)
        NpO2OH + H+ = NpO2+ + H2O                       # EQ36
        log_k       4.5164                              # EQ36

NpO2OH(am)
        NpO2OH + H+ = NpO2+ + H2O                       # EQ36
        log_k       5.2165                              # EQ36

Na2(NpO2)2(CO3)2:7H2O(s)                                        # 2[NaNpO2CO3:7/2H2O] in EQ36
        Na2(NpO2)2(CO3)2:7H2O = 2 NpO2+ + 2 Na+ + 2 CO3-2 + 7 H2O       # EQ36,  Na2(NpO2)2(CO3)2:7H2O + 2H+ = 2Na+ +
2NpO2+ + 2HCO3- + 7H2O
        log_k       -22.1800

Na3NpO2(CO3)2(s)
        Na3NpO2(CO3)2 = 3 Na+ + NpO2+ + 2 CO3-2                 # EQ36
        log_k       -14.1801                            # EQ36 Na3NpO2(CO3)2 + 2H+ = 3Na+ + NpO2+ + 2HCO3-, log k =
6.4983

KNpO2CO3(s)
        KNpO2CO3 = K+ + NpO2+ + CO3-2                   # EQ36
        log_k       -13.6038                            # EQ36, KNpO2CO3 + H+ = K+ + NpO2+ + HCO3-, log k = -3.2646

K3NpO2(CO3)2(s)
        K3NpO2(CO3)2 = 3 K+ + NpO2+ + 2 CO3-2                   # EQ36
        log_k           -15.9307                            # EQ36, K3NpO2(CO3)2 + 2H+ = 3K+ + NpO2+ + 2HCO3-; log k = 4.7477
```

```
H2Oxalate:2H2O(s)
        H2Oxalate:2H2O = 2 H+ + Oxalate-2 + 2 H2O        # EQ36
        log_k           -5.6615                         # EQ36 Giambalvo

NaHOxalate:H2O(s)
        NaHOxalate:H2O = Na+ + H+ + Oxalate-2 + H2O     # EQ36
        log_k       -6.0608                             # EQ36 Giambalvo

Na2Oxalate(s)
        Na2Oxalate = 2 Na+ + Oxalate-2                  # EQ36
        log_k           -2.4051                         # EQ36 Giambalvo

Anhydrite
        CaSO4 = Ca+2 + SO4-2                            # EQ36
        log_k           -4.3621                 # EQ36 (pitzer.dat has -4.362)
#       delta_h -1.71 kcal                      # WATEQ4F.DAT
#       -anal  87.836  0  -3136.79  -32.953 # 50 - 160oC, 1 - 1e3 atm, anhydrite dissolution, Blount and Dickson, 1973, Am. Mineral. 58, 323.
#       -Vm 46.1 # 136.14 / 2.95

Aphthitalite/Glaserite
        NaK3(SO4)2 =  Na+ + 3 K+ + 2 SO4-2      # EQ36
        log_k           -3.8027                 # EQ36 (pitzer.dat has -3.803)

Whewellite
        CaOxalate:H2O = Ca+2 + Oxalate-2 + H2O          # EQ36
        log_k       -8.7517                             # EQ36  Xiong (2004)

Aragonite
        CaCO3 = CO3-2 + Ca+2
        log_k           -8.2194                         # EQ36 pitzer.dat has -8.336
#       delta_h -2.589 kcal                             # pitzer.dat
#       -analytic    -171.8607   -.077993    2903.293    71.595
#       -Vm 34.04

Arcanite
        K2SO4  =  SO4-2 + 2 K+                                  # EQ36
        log_k           -1.7763                         # EQ36 (pitzer has -1.776)
#       -analytic    2.823    0.0             -1371.2
#       -Vm 65.5

Bischofite
        MgCl2:6H2O  =  Mg++ + 2 Cl- + 6 H2O             # EQ36
        log_k           4.4554                          # EQ36 (pitzer.dat has 4.455)
#       -analytic    3.524    0.0             277.6
#       Vm 127.1

Bloedite
        Na2Mg(SO4)2:4H2O  =  Mg++ + 2 Na+ + 2 SO4-2 + 4 H2O     # EQ36
        log_k           -2.3469                                 # EQ36 (pitzer.dat has -2.347)
#       -delta_H    0                                           # No data
#       -delta_H    0               # Not possible to calculate enthalpy of reaction        Bloedite
#       Vm 147

Brucite
        Mg(OH)2 + 2 H+ =  Mg++ + 2 H2O                                                  # EQ36
        log_k           17.1090                                                 # EQ36
#       Mg(OH)2  =  + 1.0000 Mg++ + 2.0000 OH-
#       log_k           -10.88
#       -delta_H    4.85    kcal/mol                                            # pitzer.dat
#       Vm 24.6

Burkeite
        Na6CO3(SO4)2 + H+  = HCO3- + 2 SO4-2 + 6 Na+    # EQ36
        log_k           9.5671                          # EQ36

Calcite
        CaCO3 + H+ = HCO3- + Ca+2
        log_k           1.9330
#       delta_h -2.297 kcal
```

```
#       -analytic    -171.8329    -0.077993    2839.319    71.595
#       -Vm 36.9

CaCl2:4H2O(s)
        CaCl2:4H2O = Ca+2 + 2 Cl- + 4 H2O                   # EQ36
        log_k       5.7171                                  # EQ36

CaOxychloride_A(s)
        Ca4Cl2(OH)6:13H2O + 6 H+ = 4 Ca+2 + 2 Cl- + 19 H2O          # EQ36 -  .dat
        log_k       68.7343                                         # EQ36

CaOxychloride_B(s)
        Ca2Cl2(OH)2:H2O + 2 H+ = 2 Ca+2 + 2 Cl- + 3 H2O             # EQ36 -  .dat
        log_k        26.5313                                        # EQ46

Carnallite
        KMgCl3:6H2O  =  K+ + Mg++ + 3 Cl- + 6 H2O           # EQ36
        log_k       4.3304                                  # EQ36 (pitzer has 4.330)
#       Vm 173.7

#Celestite
#       SrSO4 = Sr+2 + SO4-2                                        # pitzer.dat
#       log_k       -6.630                                  # pitzer.dat not in EQ36
#       delta_h -1.037 kcal                                 # WATEQ4F.DAT
#       -analytic  -7.14 6.11E-03  75 0 0 -1.79E-05  # Howell et al., 1992, JCED 37, 464.
#       -Vm 46.4

Epsomite
        MgSO4:7H2O  =  Mg+2 + SO4-2 + 7 H2O                 # EQ36
        log_k       -1.8811                                 # EQ36 (pitzer.dat has -1.881)
#       delta_h 2.820 kcal                                  # WATEQ4F.DAT

Gaylussite
        CaNa2(CO3)2:5H2O + 2H+ = Ca+2 + 2 HCO3- + 2 Na+ + 5 H2O             # EQ36
        log_k       11.2576                                                 # EQ36

Glauberite
        Na2Ca(SO4)2  =  Ca+2 + 2 Na+ + 2 SO4-2              # EQ36
        log_k       -5.2445                                 # EQ36 (pitzer.dat has -5.245)
#       Vm 99

Gypsum
        CaSO4:2H2O = Ca+2 + SO4-2 + 2 H2O                           # EQ36
        log_k       -4.5805                                         # EQ36 (pitzer.dat has -4.581)
#       delta_h -0.109 kcal                                         # pitzer.dat

Halite
        NaCl  =  Cl- + Na+                                                      # EQ36
        log_k       1.5704                                                      # EQ36 (pitzer.dat has 1.570)
#       delta_h 0.918 kcal                                                      # WATEQ4F.DAT
#       -analytic -713.4616   -.1201241   37302.21    262.4583    -2106915.
#       -Vm 27.1

Hexahydrite
        MgSO4:6H2O  =  Mg+2 + SO4-2 + 6 H2O                         # EQ36
        log_k       -1.6351                                         # EQ36 (pitzer.dat has -1.635)
#       -analytic    -62.666   0.0            1828.     22.187
#       Vm 132

Kainite
        KMgClSO4:3H2O  =  Cl- + K+ + Mg+2 + SO4-2 + 3 H2O           # EQ36
        log_k       -0.1926                                         # EQ36 (pitzer.dat has -0.193)

Kalicinite
        KHCO3  =  K+ + HCO3-                    # EQ36
        log_k       0.2814              # EQ36

Kieserite
        MgSO4:H2O  =  Mg+2 + SO4-2 + H2O        # EQ36
        log_k       -0.1227                     # EQ36 (pitzer.dat has -0.123)
```

```
#           Vm 53.8

Leonite
            K2Mg(SO4)2:4H2O  =  Mg+2 + 2 K+ + 2 SO4-2 + 4 H2O          # EQ36
            log_k       -3.9790                                       # EQ36 (pitzer.dat has -3.979)

Labile_Salt
            Na4Ca(SO4)3:2H2O = 4 Na+ + Ca+2 + 3 SO4-2 + 2 H2O         # EQ36
            log_k       -5.6723                                       # EQ36 (pitzer.dat has -5.672)

Magnesite
            MgCO3 + H+ =  HCO3- + Mg+2# EQ36
            log_k       2.5054              # EQ36
#           delta_h     -6.169                          # pitzer.dat
#           Vm 28.3

Mg2Cl(OH)3:4H2O
            Mg2Cl(OH)3:4H2O + 3 H+ = 2 Mg+2 + Cl- + 7 H2O  # EQ36
            log_k     26.0297                              # EQ36

Mg3Cl(OH)5:4H2O
            Mg3Cl(OH)5:4H2O + 5 H+ = 3 Mg+2 + Cl- + 9 H2O  # EQ36
            log_k     42.9600                              # EQ36 Xiong et al. (2010), see Note for Revision 3

Mercallite
            KHSO4 = K+ + H+ + SO4-2             # EQ36
            log_k       -1.4015             # EQ36

Mirabilite
            Na2SO4:10H2O  =  SO4-2 + 2 Na+ + 10 H2O                                  # EQ36
            log_k       -1.2278                                                      # EQ36 (pitzer.dat has -1.214)
#           delta_h 18.987 kcal                                                      # WATEQ4F.DAT

Misenite
            K8H6(SO4)7  =  6 H+ + 7 SO4-2 + 8 K+    # EQ36
            log_k       -10.8061                    # EQ36 (pitzer.dat has -10.086)

Nahcolite
            NaHCO3  =  HCO3- + Na+              # EQ36
            log_k       -0.4030             # EQ36

Natron
            Na2CO3:10H2O + H+ = HCO3- + 2 Na+ + 10 H2O  # EQ36
            log_k       9.5145                          # EQ36
#       delta_h 15.745 kcal                             # WATEQ4F.DAT

Nesquehonite
            MgCO3:3H2O + H+ = HCO3- + Mg+2 + 3 H2O              # EQ36
            log_k       5.1722                          # EQ36
#       delta_h -5.789 kcal                             # WATEQ4F.DAT

PicromeriteSchoenite
            K2Mg(SO4)2:6H2O = 2 K+ + Mg+2 + 2 SO4-2 + 6 H2O             # EQ36
            log_k       -4.3277

Pirssonite
            Na2Ca(CO3)2:2H2O + 2 H + = 2 Na+ + Ca+2 + 2 HCO3- + 2 H2O   # EQ36
            log_k       11.4354                                         # EQ36

Polyhalite
            K2MgCa2(SO4)4:2H2O  = 2 K+ +  Mg+2 + 2 Ca+2 + 4 SO4-2 + 2 H2O  # EQ36
            log_k       -13.7441                                        # EQ36 (pitzer.dat has -13.744)
#           Vm 218

Portlandite
            Ca(OH)2 + 2H+ =  Ca+2 + 2 H2O               # EQ36
            log_k       22.8035                 # EQ36
#       delta_h -31.0 kcal                      # WATEQ4F.DAT

K2CO3:1.5H2O
```

```
        K2CO3:1.5H2O + H+ = 2 K+ + HCO3- + 1.5 H2O      # EQ36
        log_k           13.3720                         # EQ36

K8H4(CO3)6:3H2O
        K8H4(CO3)6:3H2O + 2 H+ = 8 K+ + 6 HCO3- + 3 H2O                 # EQ36
        log_k   27.6874                                 # EQ36

KNaCO3:6H2O
        KNaCO3:6H2O + H+ = K+ + Na+ + HCO3- + 6 H2O     # EQ36
        log_k   10.2233                                 # EQ36

K-Trona
        K2NaH(CO3)2:2H2O + H+ = 2 K+ + Na+ + 2 HCO3- + 2 H2O    # EQ36
        log_k   11.5757                                 # EQ36

K3H(SO4)2(s)
        K3H(SO4)2 = 3 K+ + H+ + 2 SO4-2                 # EQ36
        log_k   -3.5425                 # EQ36

Na3H(SO4)2(s)
        Na3H(SO4)2 = 3 Na+ + H+ + 2 SO4-2       # EQ36
        log_k   -0.8143                 # EQ36

Na2CO3:7H2O(s)
        Na2CO3:7H2O + H+ = 2 Na+ + HCO3- + 7 H2O        # EQ36
        log_k   9.8791                                  # EQ36

Sylvite
        KCl  = K+ + Cl-                                 # EQ36
        log_k           0.8999                          # EQ36 (pitzer.dat has 0.900)
#       -analytic   3.984   0.0             -919.55
#       Vm 37.5

Syngenite
        K2Ca(SO4)2:H2O  =  2 K+ + Ca+2 + 2 SO4-2 + H2O  # EQ36
        log_k           -7.4484                         # EQ36 (pitzer.dat has -7.448)

Tachyhydrite
        Mg2CaCl6:12H2O = 2 Mg+2 + Ca+2 + 6 Cl- + 12 H2O                 # EQ36
        log_k   17.3839                                 # EQ36 -  .dat

Thenardite
        Na2SO4 = 2 Na+ + SO4-2                  # EQ36
        log_k           -0.2875         # EQ36 -  .dat
#       delta_h -0.572 kcal             # WATEQ4F.DAT

Thermonatrite
        Na2CO3:H2O + H+ = 2 Na+ + HCO3- + H2O           # EQ36
        log_k       10.8211                     # EQ36
#       delta_h -2.802 kcal                     # WATEQ4F.DAT

Trona
        Na3H(CO3)2:2H2O =  3 Na+ + H+ + 2 CO3-2 + 2 H2O                 # EQ36
        log_k           9.2948                          # EQ36
#       delta_h -18.0 kcal                              # WATEQ4F.DAT
#       Vm 106

Borax
        Na2(B4O5(OH)4):8H2O = 2 Na+ + 4 B(OH)4- + 2 H+ +  1 H2O         # EQ36
        log_k           -24.4918                        # EQ36
#       Vm 223

Boric_acid(s)
        B(OH)3 + H2O  =  B(OH)4- + H+           # EQ36
        log_k           -9.2694         # EQ36 (pitzer.dat has -0.030)

K-Pentaborate30C(s)
        KB5O8:4H2O + 8 H2O = K+ + 5 B(OH)4- + 4 H+      # EQ36
        log_k       -41.5233                    # EQ36
```

```
K-Tetraborate30C(s)
        K2B4O7:4H2O + 5 H2O = 2 K+ + 4 B(OH)4- + 2 H+   # EQ36
        log_k     -23.0495                              # EQ36

Na_Metaborate(s)
        NaBO2:4H2O = Na+ + B(OH)4- + 2 H2O              # EQ36
        log_k     0.3292                                # EQ36

Na_Pentaborate(s)
        NaB5O8:5H2O + 7 H2O = Na+ + 5 B(OH)4- + 4 H+    # EQ36
        log_k     -40.2997                              # EQ36 -  .dat

Teepleite
        Na2B(OH)4Cl = B(OH)4- + 2 Na+ + Cl-     # EQ36
        log_k         1.6012                    # EQ36

Dolomite
        CaMg(CO3)2 + 2H+ = Ca+2 + Mg+2 + 2 HCO3-        # EQ36
        log_k         3.5960                            # EQ36
#       delta_h -9.436 kcal                             # pitzer.dat
#       -Vm 64.5

Hydromagnesite5424
        Mg5(CO3)4(OH)2:4H2O + 6 H+ = 5 Mg+2 + 4 HCO3- + 6 H2O   # EQ36
        log_k         31.4900                                   # EQ36 - Robie & Hemmingway (1973)
#     delta_h -52.244 kcal                                      # WATEQ4F.DAT

Hydromagnesite4323
        Mg4(CO3)3(OH)2:3H2O + 5 H+ = 4 Mg+2 + 3 HCO3- + 5 H2O   # EQ36
        log_k     28.8104                                       # EQ36


#-----------------------------------------------------------------------------
# Actinide Phases
#-----------------------------------------------------------------------------

#-------------------------------------------------------------------------------------------------------------------
#-------------------------------------------------------------------------------------------------------------------
#-------------------------------------------------------------------------------------------------------------------
#  Pitzer coefficients
#-------------------------------------------------------------------------------------------------------------------
#-------------------------------------------------------------------------------------------------------------------
PITZER
-B0
Ca+2            Edta-4          2.48            0       0       0       0       0       #
Domski(2018) corrected Domski(2019) ERMS 570855
Mg+2            CaEdta-2        0               0       0       0       0       0       # Domski(2018)
Mg+2            MgEdta-2        0               0       0       0       0       0       # Domski(2018)
Na+             NaEdta-3        0.59            0       0       0       0       0       # Felmy &
Mason(2003)
Na+             Mg(Oxalate)2-2  0.07            0       0       0       0       0       # AP-182
Fe+2            Cl-             0.37324         0       0       0       0       0       # Moog et
al. (2004) 15
Na+             Fe(CO3)2-2      -0.23           0       0       0       0       0       # Kim et al
(2017)
Na+             Cl-             0.0765          0       0       0       0       0       # HMW84
Na+             SO4-2           0.01958         0       0       0       0       0       # HMW84
Na+             HSO4-           0.0454          0       0       0       0       0       # HMW84
Na+             OH-             0.0864          0       0       0       0       0       # HMW84
Na+             HCO3-           0.0277          0       0       0       0       0       # HMW84
Na+             CO3-2           0.0399          0       0       0       0       0       # HMW84
Na+             B(OH)4-         -0.0427         0       0       0       0       0       # FW86
Na+             B3O3(OH)4-      -0.056          0       0       0       0       0       # FW86
Na+             B4O5(OH)4-2     -0.11           0       0       0       0       0       # FW86
Na+             Am(CO3)2-       -0.24           0       0       0       0       0       #
FanghŠnel et al 1999 (analogue w/Cm)
Na+             Am(CO3)3-3      0.125           0       0       0       0       0       #
FanghŠnel et al 1999 (analogue w/Cm)
#Na+            ClO4-           0.0554          0       0       0       0       0       # P91
Na+             NpO2CO3-        0.1             0       0       0       0       0       # FNK95
```

Na+	NpO2(CO3)2-3		0.48		0	0	0	0	0	# FNK95
Na+	NpO2(CO3)3-5		1.8		0	0	0	0	0	# FNK95
Na+	H2PO4-		-0.0533		0	0	0	0	0	# P91
Na+	HPO4-2		-0.0583		0	0	0	0	0	# P91
Na+	PO4-3		0.1781		0	0	0	0	0	# P91
Na+	Th(SO4)3-2		0.12		0	0	0	0	0	# FR92
Na+	Th(CO3)5-6		1.31		0	0	0	0	0	# FR92
Na+	HOxalate-	-0.2448		0	0	0	0	0	# SAND99/Mizera	
Na+	Oxalate-2	-0.2176		0	0	0	0	0	# Choppin et al	
(2001)										
Na+	Acetate-	0.1426		0	0	0	0	0	# SAND99/NBC96	
Na+	Lactate-	-0.0563		0	0	0	0	0	# SAND99/Moore et	
al. 99										
Na+	H2Citrate-	-0.1296		0	0	0	0	0	# SAND99/Mizera	
Na+	HCitrate-2	-0.0989		0	0	0	0	0	# SAND99/Mizera	
Na+	Citrate-3	0.0887		0	0	0	0	0	# SAND99/Mizera	
Na+	H3Edta-		-0.2345		0	0	0	0	0	#
Giambalvo (2002)										
Na+	H2Edta-2	-0.1262		0	0	0	0	0	# Giambalvo (2002)	
Na+	HEdta-3		0.5458		0	0	0	0	0	#
Giambalvo (2002)										
Na+	Edta-4		1.10		0	0	0	0	0	# Felmy &
Mason(2003)										
Na+	AmEdta-		-0.2239		0	0	0	0	0	# SAND99
(Typo in original; pair should be as listed above)										
Na+	NpO2Citrate-2		-0.4226		0	0	0	0	0	# SAND99
(Typo in original; pair should be as listed above)										
Na+	NpO2Edta-3		0.683		0	0	0	0	0	#
SAND99, PBMC98 (listed correctly in PBMC98)										
Na+	NpO2Oxalate-		-0.5418		0	0	0	0	0	# SAND99
(Correctly listed in Borkowski et al. 2001)										
Na+	Am(CO3)4-5		2.022		0	0	0	0	0	# FK98,
FanghŠnel et al. 1995										
Na+	Am(SO4)2-		-0.354		0	0	0	0	0	# FK98
(Analogue with Cm)										
Na+	NpO2H2Edta-		-0.8285		0	0	0	0	0	#
PBMC98										
Na+	CaCitrate-	0.1742		0	0	0	0	0	# ERG_org_memo	
(analogy w/Mg)										
Na+	CaEdta-2	0.185		0	0	0	0	0	# Domski (2018)	
Na+	MgCitrate-	0.1742		0	0	0	0	0	# ERG_org_memo	
Na+	NpO2HEdta-2		0.4733		0	0	0	0	0	#
PBMC98										
K+	Cl-		0.04835		0	0	0	0	0	# HMW84
K+	SO4-2		0.04995		0	0	0	0	0	# HMW84
K+	HSO4-		-0.0003		0	0	0	0	0	# HMW84
K+	OH-		0.1298		0	0	0	0	0	# HMW84
K+	HCO3-		0.0296		0	0	0	0	0	# HMW84
K+	CO3-2		0.1488		0	0	0	0	0	# HMW84
K+	B(OH)4-		0.035		0	0	0	0	0	# FW86
K+	B3O3(OH)4-		-0.13		0	0	0	0	0	# FW86
K+	B4O5(OH)4-2		-0.022		0	0	0	0	0	# FW86
K+	Am(CO3)2-		-0.24		0	0	0	0	0	# FK98
(analogue w/Na)										
K+	Am(CO3)3-3		0.125		0	0	0	0	0	# FK98
(analogue w/Na)										
K+	NpO2CO3-		0.1		0	0	0	0	0	# Novak et
al. 1997 (analogue w/Na)										
K+	NpO2(CO3)2-3		0.48		0	0	0	0	0	# Novak et
al. 1997 (analogue w/Na)										
K+	NpO2(CO3)3-5		2.34		0	0	0	0	0	# Novak et
al. 1997 (calculated from K data)										
K+	H2PO4-		-0.678		0	0	0	0	0	# P91
K+	HPO4-2		0.0248		0	0	0	0	0	# P91
K+	PO4-3		0.3729		0	0	0	0	0	# P91
K+	Th(SO4)3-2		0.9		0	0	0	0	0	# FR92
K+	Th(CO3)5-6		1.31		0	0	0	0	0	#
FRSMHC97 (analogue w/Na)										
K+	HOxalate-	-0.2448		0	0	0	0	0	# SAND99/Mizera	
(Analogue with Na)										

K+	Oxalate-2	-0.2176		0	0	0	0	0	# SAND99/Mizera (Analogue with Na)
K+	Acetate-	0.1587		0	0	0	0	0	# SAND99/Mizera (Analogue with Na)
K+	Lactate-	-0.0563		0	0	0	0	0	# SAND99/Moore et al. 1999 (Analogue with Na)
K+	H2Citrate-	-0.1296		0	0	0	0	0	# SAND99/Mizera (Analogue with Na)
K+	HCitrate-2	-0.989		0	0	0	0	0	# SAND99/Mizera (Analogue with Na)
K+	Citrate-3	0.0887		0	0	0	0	0	# SAND99/Mizera (Analogue with Na)
K+	H3Edta-		-0.2345		0	0	0	0	0 # Giambalvo (2002)
K+	H2Edta-2	-0.1262		0	0	0	0	0	# Giambalvo (2002)
K+	HEdta-3		0.546		0	0	0	0	0 # Giambalvo (2002)
K+	Edta-4		1.10		0	0	0	0	0 # Felmy & Mason(2003)
K+	AmEdta-		-0.2239		0	0	0	0	0 # SAND99 (Analogue with Na)
K+	NpO2Citrate-2		-0.4226		0	0	0	0	0 # SAND99 (analogue w/Na; error in original)
K+	NpO2Edta-3		0.683		0	0	0	0	0 # AND99/PBMC98 (Correctly listed in latter source)
K+	NpO2Oxalate-		-0.5418		0	0	0	0	0 # SAND99/Borkowski et al. 2001; listed correctly in latter source
K+	Am(CO3)4-5		2.022		0	0	0	0	0 # FK98 (analogy with Na)
K+	Am(SO4)2-		-0.354		0	0	0	0	0 # FK98 (analogy w/Na)
K+	NpO2H2Edta-		-0.8285		0	0	0	0	0 # PBMC98 (analogy w/Na)
K+	CaCitrate-	0.1742		0	0	0	0	0	# ERG_org_memo (analogy w/Na, Mg)
K+	CaEdta-2	0.185		0	0	0	0	0	# Domski (2018)
K+	MgCitrate-	0.1742		0	0	0	0	0	# ERG_org_memo (analogy with Na)
K+	NpO2HEdta-2		0.4733		0	0	0	0	0 # PBMC98 (analogy w/Na)
Ca+2	Cl-		0.3159		0	0	0	0	0 # HMW84
Ca+2	SO4-2		0.2		0	0	0	0	0 # HMW84
Ca+2	HSO4-		0.2145		0	0	0	0	0 # HMW84
Ca+2	OH-		-0.1747		0	0	0	0	0 # HMW84
Ca+2	HCO3-		0.4		0	0	0	0	0 # HMW84
#Ca+2	ClO4-		0.4511		0	0	0	0	0 # P91
Ca+2	NpO2CO3-		0.1		0	0	0	0	0 # al Mahamid et al. 1998 (analogy w/Mg)
Ca+2	NpO2(CO3)2-3		0.48		0	0	0	0	0 # al Mahamid et al. 1998 (analogy w/Mg)
Ca+2	NpO2(CO3)3-5		2.07		0	0	0	0	0 # al Mahamid et al. 1998 (analogy w/Mg; values averaged over Na and K values)
Mg+2	Cl-		0.35235		0	0	0	0	0 # HMW84
Mg+2	SO4-2		0.221		0	0	0	0	0 # HMW84
Mg+2	HSO4-		0.4746		0	0	0	0	0 # HMW84
Mg+2	HCO3-		0.329		0	0	0	0	0 # HMW84
#Mg+2	ClO4-		0.4961		0	0	0	0	0 # P91
Mg+2	NpO2CO3-		0.1		0	0	0	0	0 # al Mahamid et al. 1998 (analogy w/Na)
Mg+2	NpO2(CO3)2-3		0.48		0	0	0	0	0 # al Mahamid et al. 1998 (analogy w/Na)
Mg+2	NpO2(CO3)3-5		2.07		0	0	0	0	0 # al Mahamid et al. 1998 (averaged Na and K values)
MgOH+	Cl-		-0.1		0	0	0	0	0 # HMW84
H+	Cl-		0.1775		0	0	0	0	0 # HMW84
H+	SO4-2		0.0298		0	0	0	0	0 # HMW84
H+	HSO4-		0.2065		0	0	0	0	0 # HMW84
#H+	ClO4-		0.1747		0	0	0	0	0 # P91
H+	Th(SO4)3-2		0.84		0	0	0	0	0 # FR92
MgB(OH)4+	Cl-		0.16		0	0	0	0	0 # FW86

CaB(OH)4+	Cl-		0.12		0	0	0	0	0	# FW86
Am+3	Cl-		0.5856		0	0	0	0	0	# FK98, Konnecke et al. 1997
Am+3	SO4-2		1.792		0	0	0	0	0	# FK98
#Am+3	ClO4-		0.8		0	0	0	0	0	# FRF90
Am+3	H2PO4-		0		0	0	0	0	0	# RFF95 (from Nd analogue)
AmCO3+	Cl-		-0.072		0	0	0	0	0	# FK98/FanghŠnel et al. 1999 (Cm analogue)
Th+4	Cl-		1.092		0	0	0	0	0	# Roy92
Th+4	SO4-2		1.56		0	0	0	0	0	# FR92
Th+4	HSO4-		1.44		0	0	0	0	0	# FR92
#Th+4	ClO4-		1.19		0	0	0	0	0	# CFN960119
AmCl+2	Cl-		0.593		0	0	0	0	0	# FK98/Konnecke et al. (Cm analogue)
NpO2+	Cl-		0.1415		0	0	0	0	0	# NFRK95
#NpO2+	ClO4-		0.257		0	0	0	0	0	# NFRK95
ThOxalate+2	Cl-		-0.343		0	0	0	0	0	# SAND99/Borkowski et al. 2001
AmAcetate+2	Cl-		0.3088		0	0	0	0	0	# ERG_org_memo
AmLactate+2	Cl-		0.8397		0	0	0	0	0	# SAND97/Moore et al 1999
AmOxalate+	Cl-		-0.9374		0	0	0	0	0	# SAND99/Borkowski et al. 2001
ThAcetate+3	Cl-		1.061		0	0	0	0	0	# SAND99
ThCitrate+	Cl-	-0.7467		0	0	0	0	0	# SAND99	
ThLactate+3	Cl-		0.6677		0	0	0	0	0	# SAND99/Moore et al. 1999
AmOH+2	Cl-		-0.055		0	0	0	0	0	# FK98/Konnecke et al. 1997 (Cm analogue)
Am(OH)2+	Cl-		-0.616		0	0	0	0	0	# FK98/Konnecke et al. 1997 (Cm analogue)
AmCl2+	Cl-		0.516		0	0	0	0	0	# FK98/Konnecke et al. 1997 (Cm analogue)
AmSO4+	Cl-		-0.091		0	0	0	0	0	# FK98 (Cm analogue)
Th(Acetate)2+2	Cl-		0.4671		0	0	0	0	0	# Moore et al. 1999
Th(Lactate)2+2	Cl-		0.5058		0	0	0	0	0	# Moore et al. 1999
CaAcetate+	Cl-		-0.0833		0	0	0	0	0	# ERG_org_memo (analogy w/Mg)
MgAcetate+	Cl-		-0.0833		0	0	0	0	0	# ERG_org_memo
#Na+	Br-	0.0973		0	0	7.692E-40	0	# pitzer.dat		
#K+	Br-	0.0569		0	0	7.39E-4	0	0	# pitzer.dat	
#H+	Br-	0.1960		0	0	-2.049E-4	0	0	# pitzer.dat	
#Mg+2	Br-	0.4327		0	0	-5.625E-5	0	0	# pitzer.dat	
#Ca+2	Br-	0.3816		0	0	-5.2275E-4	0	0	# pitzer.dat	
#Li+	Br-	0.1748		0	0	-1.819E-4	0	0	# pitzer.dat	
#----------										
-B1	# same references as B0									
Ca+2	Edta-4		0		0	0	0	0	0	
Mg+2	CaEdta-2	7.21		0	0	0	0	0		
Mg+2	MgEdta-2	7.27		0	0	0	0	0		
Na+	NaEdta-3	5.39		0	0	0	0	0		
Na+	Mg(Oxalate)2-2		0		0	0	0	0	0	
Fe+2	Cl-		1.13499		0	0	0	0	0	
Na+	Fe(CO3)2-2		6.26		0	0	0	0	0	
Na+	Cl-		0.2664		0	0	0	0	0	
Na+	SO4-2		1.113		0	0	0	0	0	
Na+	HSO4-		0.398		0	0	0	0	0	
Na+	OH-		0.253		0	0	0	0	0	
Na+	HCO3-		0.0411		0	0	0	0	0	
Na+	CO3-2		1.389		0	0	0	0	0	
Na+	B(OH)4-		0.089		0	0	0	0	0	
Na+	B3O3(OH)4-		-0.91		0	0	0	0	0	
Na+	B4O5(OH)4-2		-0.4		0	0	0	0	0	

Na+	Am(CO3)2-		0.224		0	0	0	0	0
Na+	Am(CO3)3-3		4.73		0	0	0	0	0
#Na+	ClO4-		0.2755		0	0	0	0	0
Na+	NpO2CO3-		0.34		0	0	0	0	0
Na+	NpO2(CO3)2-3		4.4		0	0	0	0	0
Na+	NpO2(CO3)3-5		22.7		0	0	0	0	0
Na+	H2PO4-		0.0396		0	0	0	0	0
Na+	HPO4-2		1.466		0	0	0	0	0
Na+	PO4-3		3.851		0	0	0	0	0
Na+	Th(SO4)3-2		0		0	0	0	0	0
Na+	Th(CO3)5-6		30		0	0	0	0	0
Na+	HOxalate-	0.29		0	0	0	0	0	
Na+	Oxalate-2	1.74		0	0	0	0	0	
Na+	Acetate-	0.22		0	0	0	0	0	
Na+	Lactate-	0.29		0	0	0	0	0	
Na+	H2Citrate-	0.29		0	0	0	0	0	
Na+	HCitrate-2	1.74		0	0	0	0	0	
Na+	Citrate-3	5.22		0	0	0	0	0	
Na+	H3Edta-		0.29		0	0	0	0	0
Na+	H2Edta-2	1.74		0	0	0	0	0	
Na+	HEdta-3		5.22		0	0	0	0	0
Na+	Edta-4		15.6		0	0	0	0	0
Na+	AmEdta-		0.29		0	0	0	0	0
Na+	NpO2Citrate-2		1.75		0	0	0	0	0
Na+	NpO2Edta-3		5.911		0	0	0	0	0
Na+	NpO2Oxalate-		0.29		0	0	0	0	0
Na+	Am(CO3)4-5		19.22		0	0	0	0	0
Na+	Am(SO4)2-		0.4		0	0	0	0	0
Na+	NpO2H2Edta-		0.2575		0	0	0	0	0
Na+	CaCitrate-	0.29		0	0	0	0	0	
Na+	CaEdta-2	2.405		0	0	0	0	0	
Na+	MgCitrate-	0.29		0	0	0	0	0	
Na+	NpO2HEdta-2		-1.504		0	0	0	0	0
K+	Cl-		0.2122		0	0	0	0	0
K+	SO4-2		0.7793		0	0	0	0	0
K+	HSO4-		0.1735		0	0	0	0	0
K+	OH-		0.32		0	0	0	0	0
K+	HCO3-		-0.013		0	0	0	0	0
K+	CO3-2		1.43		0	0	0	0	0
K+	B(OH)4-		0.14		0	0	0	0	0
K+	B3O3(OH)4-		0		0	0	0	0	0
K+	B4O5(OH)4-2		0		0	0	0	0	0
K+	Am(CO3)2-		0.224		0	0	0	0	0
K+	Am(CO3)3-3		4.73		0	0	0	0	0
K+	NpO2CO3-		0.34		0	0	0	0	0
K+	NpO2(CO3)2-3		4.4		0	0	0	0	0
K+	NpO2(CO3)3-5		22.7		0	0	0	0	0
K+	H2PO4-		-0.1042		0	0	0	0	0
K+	HPO4-2		1.274		0	0	0	0	0
K+	PO4-3		3.972		0	0	0	0	0
K+	Th(SO4)3-2		0		0	0	0	0	0
K+	Th(CO3)5-6		30.		0	0	0	0	0
K+	HOxalate-	0.29		0	0	0	0	0	
K+	Oxalate-2	1.74		0	0	0	0	0	
K+	Acetate-	0.3251		0	0	0	0	0	
K+	Lactate-	0.29		0	0	0	0	0	
K+	H2Citrate-	0.29		0	0	0	0	0	
K+	HCitrate-2	1.74		0	0	0	0	0	
K+	Citrate-3	5.22		0	0	0	0	0	
K+	H3Edta-		0.29		0	0	0	0	0
K+	H2Edta-2	1.74		0	0	0	0	0	
K+	HEdta-3		5.22		0	0	0	0	0
K+	Edta-4		15.6		0	0	0	0	0
K+	AmEdta-		0.29		0	0	0	0	0
K+	NpO2Citrate-2		1.75		0	0	0	0	0
K+	NpO2Edta-3		5.911		0	0	0	0	0
K+	NpO2Oxalate-		0.29		0	0	0	0	0
K+	Am(CO3)4-5		19.22		0	0	0	0	0
K+	Am(SO4)2-		0.4		0	0	0	0	0
K+	NpO2H2Edta-		0.2575		0	0	0	0	0

K+	CaCitrate-	0.29		0	0	0	0	0		
K+	CaEdta-2	2.41		0	0	0	0	0		
K+	MgCitrate-	0.29		0	0	0	0	0		
K+	NpO2HEdta-2		-1.504		0	0	0	0	0	
Ca+2	Cl-		1.614		0	0	0	0	0	
Ca+2	SO4-2		3.1973		0	0	0	0	0	
Ca+2	HSO4-		2.53		0	0	0	0	0	
Ca+2	OH-		-0.2303		0	0	0	0	0	
Ca+2	HCO3-		2.977		0	0	0	0	0	
#Ca+2	ClO4-		1.756		0	0	0	0	0	
Ca+2	NpO2CO3-		0.34		0	0	0	0	0	
Ca+2	NpO2(CO3)2-3		4.4		0	0	0	0	0	
Ca+2	NpO2(CO3)3-5		22.7		0	0	0	0	0	
Mg+2	Cl-		1.6815		0	0	0	0	0	
Mg+2	SO4-2		3.343		0	0	0	0	0	
Mg+2	HSO4-		1.729		0	0	0	0	0	
Mg+2	HCO3-		0.6072		0	0	0	0	0	
#Mg+2	ClO4-		2.008		0	0	0	0	0	
Mg+2	NpO2CO3-		0.34		0	0	0	0	0	
Mg+2	NpO2(CO3)2-3		4.4		0	0	0	0	0	
Mg+2	NpO2(CO3)3-5		22.7		0	0	0	0	0	
MgOH+	Cl-		1.658		0	0	0	0	0	
H+	Cl-		0.2945		0	0	0	0	0	
H+	SO4-2		0		0	0	0	0	0	
H+	HSO4-		0.5556		0	0	0	0	0	
#H+	ClO4-		0.2931		0	0	0	0	0	
H+	Th(SO4)3-2		0		0	0	0	0	0	
MgB(OH)4+	Cl-		0		0	0	0	0	0	
CaB(OH)4+	Cl-		0		0	0	0	0	0	
Am+3	Cl-		5.6		0	0	0	0	0	
Am+3	SO4-2		15.04		0	0	0	0	0	
#Am+3	ClO4-		5.35		0	0	0	0	0	
Am+3	H2PO4-		0		0	0	0	0	0	
AmCO3+	Cl-		0.403		0	0	0	0	0	
Th+4	Cl-		13.7		0	0	0	0	0	
Th+4	SO4-2		0		0	0	0	0	0	
Th+4	HSO4-		0		0	0	0	0	0	
#Th+4	ClO4-		27.3		0	0	0	0	0	
AmCl+2	Cl-		3.15		0	0	0	0	0	
NpO2+	Cl-		0.281		0	0	0	0	0	
#NpO2+	ClO4-		0.18		0	0	0	0	0	
ThOxalate+2	Cl-		1.74		0	0	0	0	0	
AmAcetate+2	Cl-		1.74		0	0	0	0	0	
AmLactate+2	Cl-		1.74		0	0	0	0	0	
AmOxalate+	Cl-		0.29		0	0	0	0	0	
ThAcetate+3	Cl-		5.22		0	0	0	0	0	
ThCitrate+	Cl-	0.29		0	0	0	0	0		
ThLactate+3	Cl-		5.22		0	0	0	0	0	
AmOH+2	Cl-		1.6		0	0	0	0	0	
Am(OH)2+	Cl-		-0.45		0	0	0	0	0	
AmCl2+	Cl-		1.75		0	0	0	0	0	
AmSO4+	Cl-		-0.39		0	0	0	0	0	
Th(Acetate)2+2	Cl-		1.74		0	0	0	0	0	
Th(Lactate)2+2	Cl-		1.74		0	0	0	0	0	
CaAcetate+	Cl-		0.29		0	0	0	0	0	
MgAcetate+	Cl-		0.29		0	0	0	0	0	
#Na+	Br-	0.2791		0	0	10.79E-4	0	0	# pitzer.dat	
#K+	Br-		0.2212		0	0	17.40E-4	0	0	# pitzer.dat
#H+	Br-		0.3564		0	0	4.467E-4	0	0	# pitzer.dat
#Mg+2	Br-	1.753		0	0	3.8625E-3	0	0	# pitzer.dat	
#Ca+2	Br-	1.613		0	0	6.0375E-3	0	0	# pitzer.dat	
#Li+	Br-	0.2547		0	0	6.636E-4	0	0	# pitzer.dat	
#----------										
-B2	# same references as B0									
Ca+2	Edta-4		0	0	0	0	0	0		
Mg+2	CaEdta-2	0	0	0	0	0	0			
Mg+2	MgEdta-2	0	0	0	0	0	0			
Na+	NaEdta-3	0	0	0	0	0	0			
Na+	Mg(Oxalate)2-2		0	0	0	0	0	0		
Fe+2	Cl-		0	0	0	0	0	0		

Na+	Fe(CO3)2-2		0	0	0	0	0	0
Na+	Cl-		0	0	0	0	0	0
Na+	SO4-2		0	0	0	0	0	0
Na+	HSO4-		0	0	0	0	0	0
Na+	OH-		0	0	0	0	0	0
Na+	HCO3-		0	0	0	0	0	0
Na+	CO3-2		0	0	0	0	0	0
Na+	B(OH)4-		0	0	0	0	0	0
Na+	B3O3(OH)4-		0	0	0	0	0	0
Na+	B4O5(OH)4-2		0	0	0	0	0	0
Na+	Am(CO3)2-		0	0	0	0	0	0
Na+	Am(CO3)3-3		0	0	0	0	0	0
#Na+	ClO4-		0	0	0	0	0	0
Na+	NpO2CO3-		0	0	0	0	0	0
Na+	NpO2(CO3)2-3		0	0	0	0	0	0
Na+	NpO2(CO3)3-5		0	0	0	0	0	0
Na+	H2PO4-		0	0	0	0	0	0
Na+	HPO4-2		0	0	0	0	0	0
Na+	PO4-3		0	0	0	0	0	0
Na+	Th(SO4)3-2		0	0	0	0	0	0
Na+	Th(CO3)5-6		0	0	0	0	0	0
Na+	HOxalate-	0	0	0	0	0	0	
Na+	Oxalate-2	0	0	0	0	0	0	
Na+	Acetate-	0	0	0	0	0	0	
Na+	Lactate-	0	0	0	0	0	0	
Na+	H2Citrate-	0	0	0	0	0	0	
Na+	HCitrate-2	0	0	0	0	0	0	
Na+	Citrate-3	0	0	0	0	0	0	
Na+	H3Edta-		0	0	0	0	0	0
Na+	H2Edta-2	0	0	0	0	0	0	
Na+	HEdta-3		0	0	0	0	0	0
Na+	Edta-4		0	0	0	0	0	0
Na+	AmEdta-		0	0	0	0	0	0
Na+	NpO2Citrate-2		0	0	0	0	0	0
Na+	NpO2Edta-3		0	0	0	0	0	0
Na+	NpO2Oxalate-		0	0	0	0	0	0
Na+	Am(CO3)4-5		0	0	0	0	0	0
Na+	Am(SO4)2-		0	0	0	0	0	0
Na+	NpO2H2Edta-		0	0	0	0	0	0
Na+	CaCitrate-	0	0	0	0	0	0	
Na+	CaEdta-2	0	0	0	0	0	0	
Na+	MgCitrate-	0	0	0	0	0	0	
Na+	NpO2HEdta-2		0	0	0	0	0	0
K+	Cl-		0	0	0	0	0	0
K+	SO4-2		0	0	0	0	0	0
K+	HSO4-		0	0	0	0	0	0
K+	OH-		0	0	0	0	0	0
K+	HCO3-		0	0	0	0	0	0
K+	CO3-2		0	0	0	0	0	0
K+	B(OH)4-		0	0	0	0	0	0
K+	B3O3(OH)4-		0	0	0	0	0	0
K+	B4O5(OH)4-2		0	0	0	0	0	0
K+	Am(CO3)2-		0	0	0	0	0	0
K+	Am(CO3)3-3		0	0	0	0	0	0
K+	NpO2CO3-		0	0	0	0	0	0
K+	NpO2(CO3)2-3		0	0	0	0	0	0
K+	NpO2(CO3)3-5		-96.	0	0	0	0	0
K+	H2PO4-		0	0	0	0	0	0
K+	HPO4-2		0	0	0	0	0	0
K+	PO4-3		0	0	0	0	0	0
K+	Th(SO4)3-2		0	0	0	0	0	0
K+	Th(CO3)5-6		0	0	0	0	0	0
K+	HOxalate-	0	0	0	0	0	0	
K+	Oxalate-2	0	0	0	0	0	0	
K+	Acetate-	0	0	0	0	0	0	
K+	Lactate-	0	0	0	0	0	0	
K+	H2Citrate-	0	0	0	0	0	0	
K+	HCitrate-2	0	0	0	0	0	0	
K+	Citrate-3	0	0	0	0	0	0	
K+	H3Edta-		0	0	0	0	0	0

K+	H2Edta-2	0	0	0	0	0	0	
K+	HEdta-3		0	0	0	0	0	0
K+	Edta-4		0	0	0	0	0	0
K+	AmEdta-		0	0	0	0	0	0
K+	NpO2Citrate-2		0	0	0	0	0	0
K+	NpO2Edta-3		0	0	0	0	0	0
K+	NpO2Oxalate-		0	0	0	0	0	0
K+	Am(CO3)4-5		0	0	0	0	0	0
K+	Am(SO4)2-		0	0	0	0	0	0
K+	NpO2H2Edta-		0	0	0	0	0	0
K+	CaCitrate-	0	0	0	0	0	0	
K+	CaEdta-2	0	0	0	0	0	0	
K+	MgCitrate-	0	0	0	0	0	0	
K+	NpO2HEdta-2		0	0	0	0	0	0
Ca+2	Cl-		0	0	0	0	0	0
Ca+2	SO4-2		-54.24	0	0	0	0	0
Ca+2	HSO4-		0	0	0	0	0	0
Ca+2	OH-		-5.72	0	0	0	0	0
Ca+2	HCO3-		0	0	0	0	0	0
#Ca+2	ClO4-		0	0	0	0	0	0
Ca+2	NpO2CO3-		0	0	0	0	0	0
Ca+2	NpO2(CO3)2-3		0	0	0	0	0	0
Ca+2	NpO2(CO3)3-5		-48.	0	0	0	0	0
Mg+2	Cl-		0	0	0	0	0	0
Mg+2	SO4-2		-37.23	0	0	0	0	0
Mg+2	HSO4-		0	0	0	0	0	0
Mg+2	HCO3-		0	0	0	0	0	0
#Mg+2	ClO4-		0	0	0	0	0	0
Mg+2	NpO2CO3-		0	0	0	0	0	0
Mg+2	NpO2(CO3)2-3		0	0	0	0	0	0
Mg+2	NpO2(CO3)3-5		-48.	0	0	0	0	0
MgOH+	Cl-		0	0	0	0	0	0
H+	Cl-		0	0	0	0	0	0
H+	SO4-2		0	0	0	0	0	0
H+	HSO4-		0	0	0	0	0	0
#H+	ClO4-		0	0	0	0	0	0
H+	Th(SO4)3-2		0	0	0	0	0	0
MgB(OH)4+	Cl-		0	0	0	0	0	0
CaB(OH)4+	Cl-		0	0	0	0	0	0
Am+3	Cl-		0	0	0	0	0	0
Am+3	SO4-2		0	0	0	0	0	0
#Am+3	ClO4-		0	0	0	0	0	0
Am+3	H2PO4-		-92.9	0	0	0	0	0
AmCO3+	Cl-		0	0	0	0	0	0
Th+4	Cl-		-160.	0	0	0	0	0
Th+4	SO4-2		0	0	0	0	0	0
Th+4	HSO4-		0	0	0	0	0	0
#Th+4	ClO4-		0	0	0	0	0	0
AmCl+2	Cl-		0	0	0	0	0	0
NpO2+	Cl-		0	0	0	0	0	0
#NpO2+	ClO4-		0	0	0	0	0	0
ThOxalate+2	Cl-		0	0	0	0	0	0
AmAcetate+2	Cl-		0	0	0	0	0	0
AmLactate+2	Cl-		0	0	0	0	0	0
AmOxalate+	Cl-		0	0	0	0	0	0
ThAcetate+3	Cl-		0	0	0	0	0	0
ThCitrate+	Cl-	0	0	0	0	0	0	
ThLactate+3	Cl-		0	0	0	0	0	0
AmOH+2	Cl-		0	0	0	0	0	0
Am(OH)2+	Cl-		0	0	0	0	0	0
AmCl2+	Cl-		0	0	0	0	0	0
AmSO4+	Cl-		0	0	0	0	0	0
Th(Acetate)2+2	Cl-		0	0	0	0	0	0
Th(Lactate)2+2	Cl-		0	0	0	0	0	0
CaAcetate+	Cl-		0	0	0	0	0	0
MgAcetate+	Cl-		0	0	0	0	0	0
#----------								
-C0	# same references as B0							
Ca+2	Edta-4		0		0	0	0	0	0
Mg+2	CaEdta-2	0		0	0	0	0	0	

Mg+2	MgEdta-2	0		0	0	0	0	0	
Na+	NaEdta-3	0		0	0	0	0	0	
Na+	Mg(Oxalate)2-2		0		0	0	0	0	0
Fe+2	Cl-		-0.02152		0	0	0	0	0
Na+	Fe(CO3)2-2		0		0	0	0	0	0
Na+	Cl-		0.00127		0	0	0	0	0
Na+	SO4-2		0.00497		0	0	0	0	0
Na+	HSO4-		0		0	0	0	0	0
Na+	OH-		0.0044		0	0	0	0	0
Na+	HCO3-		0		0	0	0	0	0
Na+	CO3-2		0.0044		0	0	0	0	0
Na+	B(OH)4-		0.0114		0	0	0	0	0
Na+	B3O3(OH)4-		0		0	0	0	0	0
Na+	B4O5(OH)4-2		0		0	0	0	0	0
Na+	Am(CO3)2-		0.0284		0	0	0	0	0
Na+	Am(CO3)3-3		0.0007		0	0	0	0	0
#Na+	ClO4-		-0.00118	0	0	0	0	0	
Na+	NpO2CO3-		0		0	0	0	0	0
Na+	NpO2(CO3)2-3		0		0	0	0	0	0
Na+	NpO2(CO3)3-5		0		0	0	0	0	0
Na+	H2PO4-		0.00795		0	0	0	0	0
Na+	HPO4-2		0.0294		0	0	0	0	0
Na+	PO4-3		-0.05154	0	0	0	0	0	
Na+	Th(SO4)3-2		0		0	0	0	0	0
Na+	Th(CO3)5-6		0		0	0	0	0	0
Na+	HOxalate-	0.068		0	0	0	0	0	
Na+	Oxalate-2	0.122		0	0	0	0	0	
Na+	Acetate-	-0.00629	0	0	0	0	0		
Na+	Lactate-	0.047		0	0	0	0	0	
Na+	H2Citrate-	0.013		0	0	0	0	0	
Na+	HCitrate-2	0.027		0	0	0	0	0	
Na+	Citrate-3	0.047		0	0	0	0	0	
Na+	H3Edta-		0.059		0	0	0	0	0
Na+	H2Edta-2	0.054		0	0	0	0	0	
Na+	HEdta-3		-0.048		0	0	0	0	0
Na+	Edta-4		0.001		0	0	0	0	0
Na+	AmEdta-		0.002		0	0	0	0	0
Na+	NpO2Citrate-2		0.142		0	0	0	0	0
Na+	NpO2Edta-3		0		0	0	0	0	0
Na+	NpO2Oxalate-		0.095		0	0	0	0	0
Na+	Am(CO3)4-5		-0.305		0	0	0	0	0
Na+	Am(SO4)2-		0.051		0	0	0	0	0
Na+	NpO2H2Edta-		0.256		0	0	0	0	0
Na+	CaCitrate-	-0.06923	0	0	0	0	0		
Na+	CaEdta-2	0.0		0	0	0	0	0	
Na+	MgCitrate-	-0.06923	0	0	0	0	0		
Na+	NpO2HEdta-2		0		0	0	0	0	0
K+	Cl-		-0.00084	0	0	0	0	0	
K+	SO4-2		0		0	0	0	0	0
K+	HSO4-		0		0	0	0	0	0
K+	OH-		0.0041		0	0	0	0	0
K+	HCO3-		-0.008		0	0	0	0	0
K+	CO3-2		-0.0015		0	0	0	0	0
K+	B(OH)4-		0		0	0	0	0	0
K+	B3O3(OH)4-		0		0	0	0	0	0
K+	B4O5(OH)4-2		0		0	0	0	0	0
K+	Am(CO3)2-		0.0284		0	0	0	0	0
K+	Am(CO3)3-3		0.0007		0	0	0	0	0
K+	NpO2CO3-		0		0	0	0	0	0
K+	NpO2(CO3)2-3		0		0	0	0	0	0
K+	NpO2(CO3)3-5		-0.22		0	0	0	0	0
K+	H2PO4-		0		0	0	0	0	0
K+	HPO4-2		0.0164		0	0	0	0	0
K+	PO4-3		-0.0868		0	0	0	0	0
K+	Th(SO4)3-2		0		0	0	0	0	0
K+	Th(CO3)5-6		0		0	0	0	0	0
K+	HOxalate-	0.068		0	0	0	0	0	
K+	Oxalate-2	0.122		0	0	0	0	0	
K+	Acetate-	-0.0066		0	0	0	0	0	
K+	Lactate-	0.047		0	0	0	0	0	

K+	H2Citrate-	0.013		0	0	0	0	0
K+	HCitrate-2	0.027		0	0	0	0	0
K+	Citrate-3	0.047		0	0	0	0	0
K+	H3Edta-		0.059		0	0	0	0
K+	H2Edta-2	0.054		0	0	0	0	0
K+	HEdta-3		-0.048		0	0	0	0
K+	Edta-4		0.001		0	0	0	0
K+	AmEdta-		0.002		0	0	0	0
K+	NpO2Citrate-2		0.142		0	0	0	0
K+	NpO2Edta-3		0		0	0	0	0
K+	NpO2Oxalate-		0.095		0	0	0	0
K+	Am(CO3)4-5		-0.305		0	0	0	0
K+	Am(SO4)2-		0.051		0	0	0	0
K+	NpO2H2Edta-		0.256		0	0	0	0
K+	CaCitrate-	-0.06923	0	0	0	0	0	
K+	CaEdta-2	0.00		0	0	0	0	0
K+	MgCitrate-	-0.06923	0	0	0	0	0	
K+	NpO2HEdta-2		0		0	0	0	0
Ca+2	Cl-		-0.00034	0	0	0	0	0
Ca+2	SO4-2		0		0	0	0	0
Ca+2	HSO4-		0		0	0	0	0
Ca+2	OH-		0		0	0	0	0
Ca+2	HCO3-		0		0	0	0	0
#Ca+2	ClO4-		-0.005		0	0	0	0
Ca+2	NpO2CO3-		0		0	0	0	0
Ca+2	NpO2(CO3)2-3		0		0	0	0	0
Ca+2	NpO2(CO3)3-5		-0.11		0	0	0	0
Mg+2	Cl-		0.00519		0	0	0	0
Mg+2	SO4-2		0.025		0	0	0	0
Mg+2	HSO4-		0		0	0	0	0
Mg+2	HCO3-		0		0	0	0	0
#Mg+2	ClO4-		0.009578	0	0	0	0	0
Mg+2	NpO2CO3-		0		0	0	0	0
Mg+2	NpO2(CO3)2-3		0		0	0	0	0
Mg+2	NpO2(CO3)3-5		-0.11		0	0	0	0
MgOH+	Cl-		0		0	0	0	0
H+	Cl-		0.0008		0	0	0	0
H+	SO4-2		0.0438		0	0	0	0
H+	HSO4-		0		0	0	0	0
#H+	ClO4-		0.00819		0	0	0	0
H+	Th(SO4)3-2		0		0	0	0	0
MgB(OH)4+	Cl-		0		0	0	0	0
CaB(OH)4+	Cl-		0		0	0	0	0
Am+3	Cl-		-0.0166		0	0	0	0
Am+3	SO4-2		0.6		0	0	0	0
#Am+3	ClO4-		-0.0048		0	0	0	0
Am+3	H2PO4-		0		0	0	0	0
AmCO3+	Cl-		0.0388		0	0	0	0
Th+4	Cl-		-0.112		0	0	0	0
Th+4	SO4-2		0		0	0	0	0
Th+4	HSO4-		0		0	0	0	0
#Th+4	ClO4-		-0.057		0	0	0	0
AmCl+2	Cl-		-0.006		0	0	0	0
NpO2+	Cl-		0		0	0	0	0
#NpO2+	ClO4-		0.0081		0	0	0	0
ThOxalate+2	Cl-		0.5		0	0	0	0
AmAcetate+2	Cl-		-0.132		0	0	0	0
AmLactate+2	Cl-		-0.332		0	0	0	0
AmOxalate+	Cl-		0.248		0	0	0	0
ThAcetate+3	Cl-		0.109		0	0	0	0
ThCitrate+	Cl-	0.319		0	0	0	0	0
ThLactate+3	Cl-		0.341		0	0	0	0
AmOH+2	Cl-		0.05		0	0	0	0
Am(OH)2+	Cl-		0.05		0	0	0	0
AmCl2+	Cl-		0.01		0	0	0	0
AmSO4+	Cl-		0.048		0	0	0	0
Th(Acetate)2+2	Cl-		0.143		0	0	0	0
Th(Lactate)2+2	Cl-		0.225		0	0	0	0
CaAcetate+	Cl-		0.0987		0	0	0	0
MgAcetate+	Cl-		0.0987		0	0	0	0

```
#Na+        Br-                0.00116                0          0          -9.30E-5   0          0          # pitzer.dat
#K+                 Br-                -0.00180               0          0          -7.004E-5  0          0          # pitzer.dat
#H+                 Br-                0.00827                0          0          -5.685E-5  0          0          # pitzer.dat
#Mg+2       Br-                0.00312                0          0          0                     0          0          # pitzer.dat
#Ca+2       Br-                -0.00257   0           0          0                     0          0          # pitzer.dat
#Li+        Br-                0.0053                 0          0          -2.813E-5  0          0          # pitzer.dat
#-----------------------------------------------------------------------------------------------------------
-THETA
# cation-cation combinations
Na+                Fe+2                0.10945                0          0          0          0          0          # Moog et
al. (2004)
Mg+2               Fe+2                0.145                  0          0          0          0          0          # Moog et
al. (2004)
K+                 Fe+2                0.0274                 0          0          0          0          0          # Moog et
al. (2004)
Ca+2               Fe+2                0.0811                 0          0          0          0          0          # Moog et
al. (2004)
Na+                K+                  -0.012                 0          0          0          0          0          # HMW84
Na+                Ca+2                0.07                   0          0          0          0          0          # HMW84
Na+                Mg+2                0.07                   0          0          0          0          0          # HMW84
Na+                H+                  0.036                  0          0          0          0          0          # HMW84
Na+                Am+3                0.1                    0          0          0          0          0          # FK98
(analogy with Cm)
Na+                Th+4                0.42                   0          0          0          0          0          #
RFSMMN
K+                 Ca+2                0.032                  0          0          0          0          0          # HMW84
K+                 H+                  0.005                  0          0          0          0          0          # HMW84
K+                 Am+3                0.1                    0          0          0          0          0          # FK98
(analogy with Na, Cm)
K+                 Th+4                0.42                   0          0          0          0          0          #
RFSMMN (analogy with Na)
Ca+2               Mg+2                0.007                  0          0          0          0          0          # HMW84
Ca+2               H+                  0.092                  0          0          0          0          0          # HMW84
Ca+2               Am+3                0.2                    0          0          0          0          0          # FK98
(Cm analogue)
Ca+2               Th+4                0.6                    0          0          0          0          0          #
RFSMMN (analogy with Mg)
Ca+2               AmCl+2              -0.014                 0          0          0          0          0          # FK98
(analogy with Mg)
Ca+2               AmCl2+              -0.196                 0          0          0          0          0          # FK98
(analogy with Mg)
Mg+2               H+                  0.1                    0          0          0          0          0          # HMW84
Mg+2               Am+3                0.2                    0          0          0          0          0          # FK98
(analogue with Ca, Cm)
Mg+2               Th+4                0.6                    0          0          0          0          0          #
RFSMMN
Mg+2               AmCl+2              -0.014                 0          0          0          0          0          # FK98
(analogy with Ca, Cm)
Mg+2               AmCl2+              -0.196                 0          0          0          0          0          # FK98
(analogy with Ca, Cm)
H+                 Th+4                0.6                    0          0          0          0          0          # Roy92
# anion-anion combinations
Cl-                SO4-2               0.02                   0          0          0          0          0          # HMW84
Cl-                HSO4-               -0.006                 0          0          0          0          0          # HMW84
Cl-                OH-                 -0.05                  0          0          0          0          0          # HMW84
Cl-                HCO3-               0.03                   0          0          0          0          0          # HMW84
Cl-                CO3-2               -0.02                  0          0          0          0          0          # HMW84
Cl-                B(OH)4-             -0.065                 0          0          0          0          0          # FW86
Cl-                B3O3(OH)4-          0.12                   0          0          0          0          0          # FW86
Cl-                B4O5(OH)4-2         0.074                  0          0          0          0          0          # FW86
Cl-                NpO2(OH)2-          -0.24                  0          0          0          0          0          # FNK95
Cl-                NpO2CO3-            -0.21                  0          0          0          0          0          # FNK95
Cl-                NpO2(CO3)2-3        -0.26                  0          0          0          0          0          # None
Cl-                NpO2(CO3)3-5        -0.26                  0          0          0          0          0          # FNK95
Cl-                H2PO4-              0.1                    0          0          0          0          0          # PS76
Cl-                Th(CO3)5-6          1.8                    0          0          0          0          0          # Moore et
al. 1999
Cl-                Acetate-            -0.09                  0          0          0          0          0          # NBC96
SO4-2              OH-                 -0.013                 0          0          0          0          0          # HMW84
SO4-2              HCO3-               0.01                   0          0          0          0          0          # HMW84
```

```
SO4-2           CO3-2           0.02            0       0       0       0       0       # HMW84
SO4-2           B(OH)4-         -0.012          0       0       0       0       0       # FW86
SO4-2           B3O3(OH)4-      0.1             0       0       0       0       0       # FW86
SO4-2           B4O5(OH)4-2     0.12            0       0       0       0       0       # FW86
OH-             CO3-2           0.1             0       0       0       0       0       # HMW84
#OH-            ClO4-           -0.032          0       0       0       0       0       # P91
HCO3-           CO3-2           -0.04           0       0       0       0       0       # HMW84
HCO3-           B3O3(OH)4-      -0.1            0       0       0       0       0       # FW86
HCO3-           B4O5(OH)4-2     -0.087          0       0       0       0       0       # FW86
#HCO3-          ClO4-           0.095           0       0       0       0       0       # NFRK95
#CO3-2          ClO4-           0.21            0       0       0       0       0       # NFRK95
CO3-2           NpO2(CO3)3-5    -1.9            0       0       0       0       0       # NFRK95
#ClO4-          Th(CO3)5-6      5.5             0       0       0       0       0       #
FRSMHC97
#OH-            Br-             -0.065          0       0       0       0       0       # pitzer.dat
#-----------------------------------------------------------------------------------------------
-LAMDA
MgOxalateNa+                    0.08            0       0       0       0       0       # AP-182
MgOxalateMg+2                   -0.20           0       0       0       0       0       # AP-182
CO2             H+              0               0       0       0       0       0       # [Harvie-
Moller-Weare convention]
CO2             Na+             0.1             0       0       0       0       0       # HMW84
CO2             K+              0.051           0       0       0       0       0       # HMW84
CO2             Ca+2            0.183           0       0       0       0       0       # HMW84
CO2             Mg+2            0.183           0       0       0       0       0       # HMW84
O2              Ca+2            0.2497          0       0       0       0       0       # YMP
DTN: SN0302T0510102.002 (data0.ypf.R1)
O2              H+              0.035284639     81.44999999     -8.09461E-11    1.21206E-13 0  0    # YMP DTN:
SN0302T0510102.002 (data0.ypf.R1)
O2              K+              1.51915E-01     1.99431E+02     7.64677E-10     -1.14341E-12    0  0    # YMP
DTN: SN0302T0510102.002 (data0.ypf.R1)
O2              Mg+2            2.29806E-01     3.05513E+02     -2.15815E-10    3.23403E-13     0  0    # YMP
DTN: SN0302T0510102.002 (data0.ypf.R1)
O2              Na+             1.60236E-01     7.28644E+01     -6.16311E-01    1.84620E-03     0  0    # YMP
DTN: SN0302T0510102.002 (data0.ypf.R1)
B(OH)3          H+              0               0       0       0       0       0       # [Harvie-
Moller-Weare convention]
B(OH)3          Na+             -0.097          0       0       0       0       0       # HMW84
B(OH)3          K+              -0.14           0       0       0       0       0       # FW86
B(OH)3          MgOH+           0               0       0       0       0       0       # [required
by zeta parameter]
B(OH)3          AmCO3+          0               0       0       0       0       0       # [required
by zeta parameter]
H3PO4           H+              0.29            0       0       0       0       0       # PS76
H3PO4           K+              -0.07           0       0       0       0       0       # PS76
Am(OH)3         H+              0               0       0       0       0       0       # [Harvie-
Moller-Weare convention]
Am(OH)3         Na+             -0.2            0       0       0       0       0       # FK98
Am(OH)3         K+              -0.2            0       0       0       0       0       # FK98
(analogy with Na)
CO2             Cl-             -0.005          0       0       0       0       0       # HMW84
CO2             SO4-2           0.097           0       0       0       0       0       # HMW84
CO2             HSO4-           -0.003          0       0       0       0       0       # HMW84
O2              Cl-             0               0       0       0       0       0       # YMP
DTN: SN0302T0510102.002 (data0.ypf.R1)
O2              Br-             -0.0347         0       0       0       0       0       # YMP
DTN: SN0302T0510102.002 (data0.ypf.R1)
O2              CO3-2           0.09648925      -277.074        2.030064E-10    -3.034302E-13   0  0 # YMP DTN:
SN0302T0510102.002 (data0.ypf.R1)
O2              HCO3-           0.0854          0       0       0       0       0       # YMP
DTN: SN0302T0510102.002 (data0.ypf.R1)
O2              NO3-            -0.0377         0       0       0       0       0       # YMP
DTN: SN0302T0510102.002 (data0.ypf.R1)
O2              OH-             5.222539E-02    1.557100E+01    -2.740323E-10   4.101025E-13 0  0    # YMP
DTN: SN0302T0510102.002 (data0.ypf.R1)
O2              SO4-2           0.087774406     -2.74085000E+02 1.32906590E-09  -1.98727658E-12 0  0    #
YMP DTN: SN0302T0510102.002 (data0.ypf.R1)
B(OH)3          Cl-             0.091           0       0       0       0       0       # FW86
B(OH)3          SO4-2           0.018           0       0       0       0       0       # FW86
B(OH)3          B3O3(OH)4-      -0.2            0       0       0       0       0       # FW86
```

```
NpO2OH          Cl-                     -0.19           0       0       0       0       0       # FNK95
H3PO4           Cl-                     0               0       0       0       0       0       # [Clegg-
Brimblecombe convention]
H3PO4           H2PO4-                  -0.4            0       0       0       0       0       # PS76
Th(SO4)2 Cl-                    0.29            0       0       0       0       0       # Roy92
Th(SO4)2 HSO4-                  0.68            0       0       0       0       0       # Roy92
Am(OH)3         Cl-                     -0.2            0       0       0       0       0       # FK98
NpO2Acetate     Cl-                     -0.104          0       0       0       0       0       #
ERG_release_memo
AmCitrate Cl-                   -0.406          0       0       0       0       0       # SAND99
NpO2Lactate     Cl-                     0.015           0       0       0       0       0       #
SAND99/Moore et al. 1999
ThEdta          Cl-                     0.1111          0       0       0       0       0       #
ERG_org_memo
MgOxalateCl-                    0.0189          0       0       0       0       0       #
ERG_org_memo=0.0189
CaOxalate Cl-                   0.0189          0       0       0       0       0       #
ERG_org_memo=0.0189
#---------------------------------------------------------------------------------------------------------
-PSI
Fe+2            Na+             Cl-             -0.01605 0      0       0       0       0
        # Moog et al. (2004)
Fe+2            K+              Cl-             -0.0252         0       0       0       0
        0       # Moog et al. (2004)
Fe+2            Mg+2            Cl-             -0.0299         0       0       0       0
        0       # Moog et al. (2004)
Fe+2            Ca+2            Cl-             -0.0160         0       0       0       0
        0       # Moog et al. (2004)
Na+             K+              Cl-             -0.0018         0       0       0       0
        0       # HMW84
Na+             K+              SO4-2           -0.01           0       0       0       0
        0       # HMW84
Na+             K+              HCO3-           -0.003          0       0       0       0
        0       # HMW84
Na+             K+              CO3-2           0.003           0       0       0       0
        0       # HMW84
Na+             Ca+2            Cl-             -0.007          0       0       0       0
        0       # HMW84
Na+             Ca+2            SO4-2           -0.055          0       0       0       0
        0       # HMW84
Na+             Mg+2            Cl-             -0.012          0       0       0       0
        0       # HMW84
Na+             Mg+2            SO4-2           -0.015          0       0       0       0
        0       # HMW84
Na+             H+              Cl-             -0.004          0       0       0       0
        0       # HMW84
Na+             H+              HSO4-           -0.0129         0       0       0       0
        0       # HMW84
#Na+            H+              ClO4-           -0.016          0       0       0       0
        0       # NFRK95
Na+             Th+4            Cl-             0.21            0       0       0       0
        0       # RFSMMN
K+              Ca+2            Cl-             -0.025          0       0       0       0
        0       # HMW84
K+              Mg+2            Cl-             -0.022          0       0       0       0
        0       # HMW84
K+              Mg+2            SO4-2           -0.048          0       0       0       0
        0       # HMW84
K+              H+              Cl-             -0.011          0       0       0       0
        0       # HMW84
K+              H+              SO4-2           0.197           0       0       0       0
        0       # HMW84
K+              H+              HSO4-           -0.0265         0       0       0       0
        0       # HMW84
K+              Th+4            Cl-             0.21            0       0       0       0
        0       # RFSMMN (analogy with Na)
Ca+2            Mg+2            Cl-             -0.012          0       0       0       0
        0       # HMW84
Ca+2            Mg+2            SO4-2           0.024           0       0       0       0
        0       # None
```

Ca+2		H+	Cl-		-0.015	0	0	0	0
	0	# HMW84							
Ca+2		Th+4	Cl-		0.21	0	0	0	0
	0	# RFSMMN (analogy with Mg)							
Mg+2		MgOH+	Cl-		0.028	0	0	0	0
	0	# HMW84							
Mg+2		H+	Cl-		-0.011	0	0	0	0
	0	# HMW84							
Mg+2		H+	HSO4-		-0.0178	0	0	0	0
	0	# HMW84							
Mg+2		Th+4	Cl-		0.21	0	0	0	0
	0	# RFSMMN							
H+		Th+4	Cl-		0.37	0	0	0	0
	0	# Roy92							
Cl-		SO4-2	Na+		0.0014	0	0	0	0
	0	# HMW84							
Cl-		SO4-2	Ca+2		-0.018	0	0	0	0
	0	# HMW84							
Cl-		SO4-2	Mg+2		-0.004	0	0	0	0
	0	# HMW84							
Cl-		HSO4-	Na+		-0.006	0	0	0	0
	0	# HMW84							
Cl-		HSO4-	H+		0.013	0	0	0	0
	0	# HMW84							
Cl-		OH-	Na+		-0.006	0	0	0	0
	0	# HMW84							
Cl-		OH-	K+		-0.006	0	0	0	0
	0	# HMW84							
Cl-		OH-	Ca+2		-0.025	0	0	0	0
	0	# HMW84							
Cl-		HCO3-	Na+		-0.015	0	0	0	0
	0	# HMW84							
Cl-		HCO3-	Mg+2		-0.096	0	0	0	0
	0	# HMW84							
Cl-		CO3-2	Na+		0.0085	0	0	0	0
	0	# HMW84							
Cl-		CO3-2	K+		0.004	0	0	0	0
	0	# HMW84							
Cl-		B(OH)4-	Na+		-0.0073	0	0	0	0
	0	# FW86							
Cl-		B3O3(OH)4-	Na+		-0.024	0	0	0	0
	0	# FW86							
Cl-		B4O5(OH)4-2	Na+		0.026	0	0	0	0
	0	# FW86							
Cl-		H2PO4-	K+		-0.01	0	0	0	0
	0	# PS76							
Cl-		Th(CO3)5-6	Na+		0.3	0	0	0	0
	0	# FR99							
Cl-		Th(CO3)5-6	K+		0.3	0	0	0	0
	0	# FR99 (analogy w/NNa)							
Cl-		Acetate-	Na+		0.01029	0	0	0	0
	# NBC96								
SO4-2		HSO4-	Na+		-0.0094	0	0	0	0
	0	# HMW84							
SO4-2		HSO4-	K+		-0.0677	0	0	0	0
	0	# HMW84							
SO4-2		HSO4-	Mg+2		-0.0425	0	0	0	0
	0	# HMW84							
SO4-2		OH-	Na+		-0.009	0	0	0	0
	0	# HMW84							
SO4-2		OH-	K+		-0.05	0	0	0	0
	0	# HMW84							
SO4-2		HCO3-	Na+		-0.005	0	0	0	0
	0	# HMW84							
SO4-2		HCO3-	Mg+2		-0.161	0	0	0	0
	0	# HMW84							
SO4-2		CO3-2	Na+		-0.005	0	0	0	0
	0	# HMW84							
SO4-2		CO3-2	K+		-0.009	0	0	0	0
	0	# HMW84							

```
OH-             CO3-2           Na+             -0.017          0       0       0       0
        0       # HMW84
OH-             CO3-2           K+              -0.01           0       0       0       0
        0       # HMW84
HCO3-           CO3-2           Na+             0.002           0       0       0       0
        0       # HMW84
HCO3-           CO3-2           K+              0.012           0       0       0       0
        0       # HMW84
#HCO3-          ClO4-           Na+             -0.01           0       0       0       0
        0       # NFRK95
#CO3-2          ClO4-           Na+             -0.024          0       0       0       0
        0       # NFRK95
#Na+    K+              Br-     -0.0022         0       0       0       0       0       # pitzer.dat
#Na+    H+              Br-     -0.012          0       0       0       0       0       # pitzer.dat
#K+             H+              Br-     -0.021          0       0       0       0       0
        # pitzer.dat
#Cl-    Br-             K+      0.0000          0       0       0       0       0       # pitzer.dat
#OH-    Br-             Na+     -0.018          0       0       0       0       0       # pitzer.dat
#OH-    Br-             K+      -0.014          0       0       0       0       0       # pitzer.dat
#------------------------------------------------------------------------------------------------------------------------
-ZETA
O2              Ca+2            Cl-             -0.0169         0       0       0       0
        0       # YMP DTN: SN0302T0510102.002 (data0.ypf.R1)
O2              Ca+2            NO3-            0               0       0       0       0
        0       # YMP DTN: SN0302T0510102.002 (data0.ypf.R1)
O2              H+              Cl-             -0.0077         0       0       0       0
        0       # YMP DTN: SN0302T0510102.002 (data0.ypf.R1)
O2              K+              Br-             -0.00541        0       0       0       0       0
        # YMP DTN: SN0302T0510102.002 (data0.ypf.R1)
O2              K+              Cl-             -0.0211         0       0       0       0
        0       # YMP DTN: SN0302T0510102.002 (data0.ypf.R1)
O2              K+              OH-             -7.06411904E-03 -1.50750433E+01 -4.52071983E-02
4.50984598E-05  0  0    #YMP DTN: SN0302T0510102.002 (data0.ypf.R1)
O2              K+              NO3-            -0.0281         0       0       0       0
        0       # YMP DTN: SN0302T0510102.002 (data0.ypf.R1)
O2              K+              SO4-2           0               0       0       0       0
        0       # YMP DTN: SN0302T0510102.002 (data0.ypf.R1)
O2              Na+             Br-             -0.00909        0       0       0       0       0
        # YMP DTN: SN0302T0510102.002 (data0.ypf.R1)
O2              Na+             Cl-             -9.18665101E-03 -2.73899999E+00 3.25992090E-11 -
4.87958604E-14  0  0  #YMP DTN: SN0302T0510102.002 (data0.ypf.R1)
O2              Na+             CO3-2           -0.0181         0       0       0       0
        0       # YMP DTN: SN0302T0510102.002 (data0.ypf.R1)
O2              Na+             HCO3-           0               0       0       0       0
        0       # YMP DTN: SN0302T0510102.002 (data0.ypf.R1)
O2              Na+             NO3-            -0.012          0       0       0       0
        0       # YMP DTN: SN0302T0510102.002 (data0.ypf.R1)
O2              Na+             OH-             -0.0125         0       0       0       0
        0       # YMP DTN: SN0302T0510102.002 (data0.ypf.R1)
O2              Na+             SO4-2           -0.046          0       0       0       0
        0       # YMP DTN: SN0302T0510102.002 (data0.ypf.R1)
B(OH)3          Na+             SO4-2           0.046           0       0       0       0
        0       # FW86
B(OH)3          H+              Cl-             -0.0102         0       0       0       0
        0       # FW86
#------------------------------------------------------------------------------------------------------------------------
-alphas
Ca+2            Edta-4          1.4             12.0            #Domski(2018) Domski(2019) PPR-2019-
04 to -13
Mg+2            CaEdta-2        1.4             12.0            # Domski(2018) Domski(2019) PPR-2019-04 to -13
and CC5-GEOCHEM-27d
Mg+2            MgEdta-2        1.4             12.0            # Domski(2018) Domski(2019) PPR-2019-04 to -13
Na+             NaEdta-3        2.0             12.0            # Felmy & Mason(2003)
Na+             Mg(Oxalate)2-2  2.0             12.0            # AP-182
Fe+2            Cl-             2.0             12.0            # Moog et al. (2004) 15
Na+             Fe(CO3)2-2      2.0             12.0            # Kim et al (2017)
Na+             Cl-             2.0             12.0            # HMW84
Na+             SO4-2           2.0             12.0            # HMW84
Na+             HSO4-           2.0             12.0            # HMW84
Na+             OH-             2.0             12.0            # HMW84
```

Na+	HCO3-		2.0		12.0	# HMW84
Na+	CO3-2		2.0		12.0	# HMW84
Na+	B(OH)4-		2.0		12.0	# FW86
Na+	B3O3(OH)4-		2.0		12.0	# FW86
Na+	B4O5(OH)4-2		2.0		12.0	# FW86
Na+	Am(CO3)2-		2.0		12.0	# FanghŠnel et al 1999 (analogue w/Cm)
Na+	Am(CO3)3-3		2.0		12.0	# FanghŠnel et al 1999 (analogue w/Cm)
#Na+	ClO4-		2.0		12.0	# P91
Na+	NpO2CO3-		2.0		12.0	# FNK95
Na+	NpO2(CO3)2-3		2.0		12.0	# FNK95
Na+	NpO2(CO3)3-5		2.0		12.0	# FNK95
Na+	H2PO4-		2.0		12.0	# P91
Na+	HPO4-2		2.0		12.0	# P91
Na+	PO4-3		2.0		12.0	# P91
Na+	Th(SO4)3-2		2.0		12.0	# FR92
Na+	Th(CO3)5-6		2.0		12.0	# FR92
Na+	HOxalate-	2.0		12.0		# SAND99/Mizera
Na+	Oxalate-2	2.0		12.0		# Choppin et al (2001)
Na+	Acetate-	2.0		12.0		# SAND99/NBC96
Na+	Lactate-	2.0		12.0		# SAND99/Moore et al. 99
Na+	H2Citrate-	2.0		12.0		# SAND99/Mizera
Na+	HCitrate-2	2.0		12.0		# SAND99/Mizera
Na+	Citrate-3	2.0		12.0		# SAND99/Mizera
Na+	H3Edta-		2.0		12.0	# Giambalvo (2002)
Na+	H2Edta-2	2.0		12.0		# Giambalvo (2002)
Na+	HEdta-3		2.0		12.0	# Giambalvo (2002)
Na+	Edta-4		2.0		12.0	# Felmy & Mason(2003)
Na+	AmEdta-		2.0		12.0	# SAND99 (Typo in original; pair should be as listed above)
Na+	NpO2Citrate-2		2.0		12.0	# SAND99 (Typo in original; pair should be as listed above)
Na+	NpO2Edta-3		2.0		12.0	# SAND99, PBMC98 (listed correctly in PBMC98)
Na+	NpO2Oxalate-		2.0		12.0	# SAND99 (Correctly listed in Borkowski et al. 2001)
Na+	Am(CO3)4-5		2.0		12.0	# FK98, FanghŠnel et al. 1995
Na+	Am(SO4)2-		2.0		12.0	# FK98 (Analogue with Cm)
Na+	NpO2H2Edta-		2.0		12.0	# PBMC98
Na+	CaCitrate-	2.0		12.0		# ERG_org_memo (analogy w/Mg)
Na+	CaEdta-2	2.0		12.0		# Domski (2018)
Na+	MgCitrate-	2.0		12.0		# ERG_org_memo
Na+	NpO2HEdta-2		2.0		12.0	# PBMC98
K+	Cl-		2.0		12.0	# HMW84
K+	SO4-2		2.0		12.0	# HMW84
K+	HSO4-		2.0		12.0	# HMW84
K+	OH-		2.0		12.0	# HMW84
K+	HCO3-		2.0		12.0	# HMW84
K+	CO3-2		2.0		12.0	# HMW84
K+	B(OH)4-		2.0		12.0	# FW86
K+	B3O3(OH)4-		2.0		12.0	# FW86
K+	B4O5(OH)4-2		2.0		12.0	# FW86
K+	Am(CO3)2-		2.0		12.0	# FK98 (analogue w/Na)
K+	Am(CO3)3-3		2.0		12.0	# FK98 (analogue w/Na)
K+	NpO2CO3-		2.0		12.0	# Novak et al. 1997 (analogue w/Na)
K+	NpO2(CO3)2-3		2.0		12.0	# Novak et al. 1997 (analogue w/Na)
K+	NpO2(CO3)3-5		2.0		12.0	# Novak et al. 1997 (calculated from K data)
K+	H2PO4-		2.0		12.0	# P91
K+	HPO4-2		2.0		12.0	# P91
K+	PO4-3		2.0		12.0	# P91
K+	Th(SO4)3-2		2.0		12.0	# FR92
K+	Th(CO3)5-6		2.0		12.0	# FRSMHC97 (analogue w/Na)
K+	HOxalate-	2.0		12.0		# SAND99/Mizera (Analogue with Na)
K+	Oxalate-2	2.0		12.0		# SAND99/Mizera (Analogue with Na)
K+	Acetate-	2.0		12.0		# SAND99/Mizera (Analogue with Na)
K+	Lactate-	2.0		12.0		# SAND99/Moore et al. 1999 (Analogue with Na)
K+	H2Citrate-	2.0		12.0		# SAND99/Mizera (Analogue with Na)
K+	HCitrate-2	2.0		12.0		# SAND99/Mizera (Analogue with Na)
K+	Citrate-3	2.0		12.0		# SAND99/Mizera (Analogue with Na)
K+	H3Edta-		2.0		12.0	# Giambalvo (2002)
K+	H2Edta-2	2.0		12.0		# Giambalvo (2002)

K+	HEdta-3		2.0		12.0	# Giambalvo (2002)
K+	Edta-4		2.0		12.0	# Felmy & Mason(2003)
K+	AmEdta-		2.0		12.0	# SAND99 (Analogue with Na)
K+	NpO2Citrate-2		2.0		12.0	# SAND99 (analogue w/Na; error in original)
K+	NpO2Edta-3		2.0		12.0	# AND99/PBMC98 (Correctly listed in latter source)
K+	NpO2Oxalate-		2.0		12.0	# SAND99/Borkowski et al. 2001; listed correctly in latter source
K+	Am(CO3)4-5		2.0		12.0	# FK98 (analogy with Na)
K+	Am(SO4)2-		2.0		12.0	# FK98 (analogy w/Na)
K+	NpO2H2Edta-		2.0		12.0	# PBMC98 (analogy w/Na)
K+	CaCitrate-	2.0		12.0		# ERG_org_memo (analogy w/Na, Mg)
K+	CaEdta-2	2.0		12.0		# Domski (2018)
K+	MgCitrate-	2.0		12.0		# ERG_org_memo (analogy with Na)
K+	NpO2HEdta-2		2.0		12.0	# PBMC98 (analogy w/Na)
Ca+2	Cl-		2.0		12.0	# HMW84
Ca+2	SO4-2		1.4		12.0	# HMW84
Ca+2	HSO4-		2.0		12.0	# HMW84
Ca+2	OH-		2.0		12.0	# HMW84
Ca+2	HCO3-		2.0		12.0	# HMW84
#Ca+2	ClO4-		2.0		12.0	# P91
Ca+2	NpO2CO3-		2.0		12.0	# al Mahamid et al. 1998 (analogy w/Mg)
Ca+2	NpO2(CO3)2-3		1.4		50.0	# al Mahamid et al. 1998 (analogy w/Mg)
Ca+2	NpO2(CO3)3-5		1.4		50.0	# al Mahamid et al. 1998 (analogy w/Mg; values averaged over Na and K values)
Mg+2	Cl-		2.0		12.0	# HMW84
Mg+2	SO4-2		1.4		12.0	# HMW84
Mg+2	HSO4-		2.0		12.0	# HMW84
Mg+2	HCO3-		2.0		12.0	# HMW84
#Mg+2	ClO4-		2.0		12.0	# P91
Mg+2	NpO2CO3-		2.0		12.0	# al Mahamid et al. 1998 (analogy w/Na)
Mg+2	NpO2(CO3)2-3		1.4		50.0	# al Mahamid et al. 1998 (analogy w/Na)
Mg+2	NpO2(CO3)3-5		1.4		50.0	# al Mahamid et al. 1998 (averaged Na and K values)
MgOH+	Cl-		2.0		12.0	# HMW84
H+	Cl-		2.0		12.0	# HMW84
H+	SO4-2		2.0		12.0	# HMW84
H+	HSO4-		2.0		12.0	# HMW84
#H+	ClO4-		2.0		12.0	# P91
H+	Th(SO4)3-2		2.0		12.0	# FR92
MgB(OH)4+	Cl-		2.0		12.0	# FW86
CaB(OH)4+	Cl-		2.0		12.0	# FW86
Am+3	Cl-		2.0		12.0	# FK98, Konnecke et al. 1997
Am+3	SO4-2		1.4		50.0	# FK98
#Am+3	ClO4-		2.0		12.0	# FRF90
Am+3	H2PO4-		2.0		12.0	# RFF95 (from Nd analogue)
AmCO3+	Cl-		2.0		12.0	# FK98/FanghŠnel et al. 1999 (Cm analogue)
Th+4	Cl-		2.0		12.0	# Roy92
Th+4	SO4-2		1.4		50.0	# FR92
Th+4	HSO4-		2.0		12.0	# FR92
#Th+4	ClO4-		2.0		12.0	# CFN960119
AmCl+2	Cl-		2.0		12.0	# FK98/Konnecke et al. (Cm analogue)
NpO2+	Cl-		2.0		12.0	# NFRK95
#NpO2+	ClO4-		2.0		12.0	# NFRK95
ThOxalate+2	Cl-		2.0		12.0	# SAND99/Borkowski et al. 2001
AmAcetate+2	Cl-		2.0		12.0	# ERG_org_memo
AmLactate+2	Cl-		2.0		12.0	# SAND97/Moore et al 1999
AmOxalate+	Cl-		2.0		12.0	# SAND99/Borkowski et al. 2001
ThAcetate+3	Cl-		2.0		12.0	# SAND99
ThCitrate+	Cl-	2.0		12.0		# SAND99
ThLactate+3	Cl-		2.0		12.0	# SAND99/Moore et al. 1999
AmOH+2	Cl-		2.0		12.0	# FK98/Konnecke et al. 1997 (Cm analogue)
Am(OH)2+	Cl-		2.0		12.0	# FK98/Konnecke et al. 1997 (Cm analogue)
AmCl2+	Cl-		2.0		12.0	# FK98/Konnecke et al. 1997 (Cm analogue)
AmSO4+	Cl-		2.0		12.0	# FK98 (Cm analogue)

Th(Acetate)2+2		Cl-			2.0		12.0		# Moore et al. 1999	
Th(Lactate)2+2		Cl-			2.0		12.0		# Moore et al. 1999	
CaAcetate+		Cl-			2.0		12.0		# ERG_org_memo (analogy w/Mg)	
MgAcetate+		Cl-			2.0		12.0		# ERG_org_memo	
#Na+	Br-		0.0973		0	0	7.692E-40	0	# pitzer.dat	
#K+		Br-		0.0569		0	0	7.39E-4	0	0	# pitzer.dat
#H+		Br-		0.1960		0	0	-2.049E-4	0	0	# pitzer.dat
#Mg+2	Br-		0.4327		0	0	-5.625E-5	0	0	# pitzer.dat
#Ca+2	Br-		0.3816		0	0	-5.2275E-4	0	0	# pitzer.dat
#Li+	Br-		0.1748			0	-1.819E-4	0	0	# pitzer.dat

INPUT FILES

GWB_DOE

```
DATABASE C:/PHREEQC/DATABASES/DATA0FM.dat
TITLE Actinide solubility calculations using minimum to 5x GWB brine volume, Salado minerals and MgO backfill 3/30/2022
simulate equilibrium calculations for CRA19 DPA calcite not suppressed
SOLUTION_SPECIES
H2O + 0.01e- = H2O-0.01
    log_k -9
END
SOLUTION 1 GWB 1x brine CRA-2019 Domski and Sisk-Scott ERMS 571178 and Conc_density_calcs_CRA-2019_PA.xlsx
        units       moles/l
        pH          6.0
        pe          7.0
        temp        25.
        density     1.2366
        Na          3.53
        K           0.467
        Mg          1.02
        Ca          0.014
        Cl          5.86
        C(4)        0.016
        S(6)        0.177
        B           0.158
        Br          0.0266
        Acetate     0.0283
        Citrate     0.0023
        EDTA        7.92e-05
        Oxalate     0.0113
        Fe          1.0E-08
        Pb          1.0E-08
        Am          1.0E-8    #equilibrium with Am(OH)3(s)
        Np          1.0E-8    #equilibrium with KNpO2CO3
        Th          1.0E-8    #equilibrium with ThO2(am)
EQUILIBRIUM_PHASES #Domski and Sisk-Scott ERMS 571178 Table 4 and output file gwb_1x.6o - equilibrate with all minerals
        Hydromagnesite5424 0.0      7.34
        Brucite                     0.0     36.7
        Anhydrite          0.0      166.0
        Halite                      0.0     3490.
        Litharge           0.0      4.35
        Fe(OH)2-Hex                 0.0     46.1
        Calcite                     0.0     0.0
        Glauberite         0.0      0.0
        Whewellite                  0.0     0.0
        Cerussite          0.0      0.0
        Borax                       0.0     0.0
        Mg3Cl(OH)5:4H2O             0.0     0.0
        Oxychloride-Fe-3(s) 0.0     0.0
        Am(OH)3(s)                  0.0     1.0
        KNpO2CO3(s)                 0.0     1.0
        ThO2(am)           0.0      1.0
SELECTED_OUTPUT
 -file        GWB_DOE_sel.out
 -high_precision true
 -pH true
 -temperature
 -ionic_strength
 -water
 -percent_error
 -totals Na K Mg Ca Cl S(6) C(4) B Br Fe Pb Oxalate Acetate EDTA Citrate Th Am Np
 -molalities H+
 -equilibrium_phases Hydromagnesite5424 Brucite Anhydrite Halite Litharge Fe(OH)2-Hex Calcite
   Glauberite Whewellite Cerussite Borax Mg3Cl(OH)5:4H2O Oxychloride-Fe-3(s) Am(OH)3(s) KNpO2CO3(s) ThO2(am)
 -saturation_indices Hydromagnesite5424 Brucite Anhydrite Halite Litharge Fe(OH)2-Hex Calcite
   Glauberite Whewellite Cerussite Borax Mg3Cl(OH)5:4H2O Oxychloride-Fe-3(s) CO2(g) Am(OH)3(s) KNpO2CO3(s) ThO2(am)
SAVE SOLUTION 1
END
```

```
SOLUTION 2 GWB 2x brine CRA-2019 Domski and Sisk-Scott ERMS 571178 and Conc_density_calcs_CRA-2019_PA.xlsx
        units   moles/l
        pH              6.0
        pe              7.0
        temp            25.
        density         1.2356
        Na              3.53
        K               0.467
        Mg              1.02
        Ca              0.014
        Cl              5.86
        C(4)            0.016
        S(6)            0.177
        B               0.158
        Br              0.0266
        Acetate         0.0142
        Citrate         0.00115
        EDTA            3.96e-05
        Oxalate         0.00565
        Fe              1.0E-08
        Pb              1.0E-08
        Am              1.0E-8  #equilibrium with Am(OH)3(s)
        Np              1.0E-8  #equilibrium with KNpO2CO3
        Th              1.0E-8  #equilibrium with ThO2(am)
EQUILIBRIUM_PHASES #Domski and Sisk-Scott ERMS 571178 Table 4 and output file gwb_1x.6o - equilibrate with all minerals
        Hydromagnesite5424      0.0     7.34
        Brucite                 0.0     36.7
        Anhydrite       0.0     166.0
        Halite                  0.0     3490.
        Litharge        0.0     4.35
        Fe(OH)2-Hex             0.0     46.1
        Calcite                 0.0     0.0
        Glauberite      0.0     0.0
        Whewellite              0.0     0.0
        Cerussite       0.0     0.0
        Borax                   0.0     0.0
        Mg3Cl(OH)5:4H2O         0.0     0.0
        Oxychloride-Fe-3(s)     0.0     0.0
        Am(OH)3(s)              0.0     1.0
        KNpO2CO3(s)             0.0     1.0
        ThO2(am)        0.0     1.0
SAVE SOLUTION 2
END
SOLUTION 3 GWB 3x brine CRA-2019 Domski and Sisk-Scott ERMS 571178 and Conc_density_calcs_CRA-2019_PA.xlsx
        units   moles/l
        pH              6.0
        pe              7.0
        temp            25.
        density         1.23526
        Na              3.53
        K               0.467
        Mg              1.02
        Ca              0.014
        Cl              5.86
        C(4)            0.016
        S(6)            0.177
        B               0.158
        Br              0.0266
        Acetate         0.00945
        Citrate         0.000768
        EDTA            2.64e-05
        Oxalate         0.00377
        Fe              1.0E-08
        Pb              1.0E-08
        Am              1.0E-8  #equilibrium with Am(OH)3(s)
        Np              1.0E-8  #equilibrium with KNpO2CO3
        Th              1.0E-8  #equilibrium with ThO2(am)
EQUILIBRIUM_PHASES #Domski and Sisk-Scott ERMS 571178 Table 4 and output file gwb_1x.6o - equilibrate with all minerals
        Hydromagnesite5424      0.0     7.34
        Brucite                 0.0     36.7
```

```
        Anhydrite               0.0     166.0
        Halite                          0.0     3490.
        Litharge                0.0     4.35
        Fe(OH)2-Hex                     0.0     46.1
        Calcite                         0.0     0.0
        Glauberite              0.0     0.0
        Whewellite                      0.0     0.0
        Cerussite               0.0     0.0
        Borax                           0.0     0.0
        Mg3Cl(OH)5:4H2O                 0.0     0.0
        Oxychloride-Fe-3(s)     0.0     0.0
        Am(OH)3(s)                      0.0     1.0
        KNpO2CO3(s)                     0.0     1.0
        ThO2(am)                0.0     1.0
SAVE SOLUTION 3
END
SOLUTION 4 GWB 4x brine CRA-2019 Domski and Sisk-Scott ERMS 571178 and Conc_density_calcs_CRA-2019_PA.xlsx
        units   moles/l
        pH              6.0
        pe              7.0
        temp            25.
        density         1.2351
        Na              3.53
        K               0.467
        Mg              1.02
        Ca              0.014
        Cl              5.86
        C(4)            0.016
        S(6)            0.177
        B               0.158
        Br              0.0266
        Acetate         0.00709
        Citrate         0.000576
        EDTA            1.98e-05
        Oxalate         0.00282
        Fe              1.0E-08
        Pb              1.0E-08
        Am              1.0E-8  #equilibrium with Am(OH)3(s)
        Np              1.0E-8  #equilibrium with KNpO2CO3
        Th              1.0E-8  #equilibrium with ThO2(am)
EQUILIBRIUM_PHASES #Domski and Sisk-Scott ERMS 571178 Table 4 and output file gwb_1x.6o - equilibrate with all minerals
        Hydromagnesite5424      0.0     7.34
        Brucite                         0.0     36.7
        Anhydrite               0.0     166.0
        Halite                          0.0     3490.
        Litharge                0.0     4.35
        Fe(OH)2-Hex                     0.0     46.1
        Calcite                         0.0     0.0
        Glauberite              0.0     0.0
        Whewellite                      0.0     0.0
        Cerussite               0.0     0.0
        Borax                           0.0     0.0
        Mg3Cl(OH)5:4H2O                 0.0     0.0
        Oxychloride-Fe-3(s)     0.0     0.0
        Am(OH)3(s)                      0.0     1.0
        KNpO2CO3(s)                     0.0     1.0
        ThO2(am)                0.0     1.0
SAVE SOLUTION 4
END
SOLUTION 5 GWB 5x brine CRA-2019 Domski and Sisk-Scott ERMS 571178 and Conc_density_calcs_CRA-2019_PA.xlsx
        units   moles/l
        pH              6.0
        pe              7.0
        temp            25.
        density         1.235
        Na              3.53
        K               0.467
        Mg              1.02
        Ca              0.014
        Cl              5.86
```

```
        C(4)                    0.016
        S(6)                    0.177
        B                       0.158
        Br                      0.0266
        Acetate                 0.00567
        Citrate                 0.000461
        EDTA                    1.58e-05
        Oxalate                 0.00226
        Fe                      1.0E-08
        Pb                      1.0E-08
        Am                      1.0E-8      #equilibrium with Am(OH)3(s)
        Np                      1.0E-8      #equilibrium with KNpO2CO3
        Th                      1.0E-8      #equilibrium with ThO2(am)
EQUILIBRIUM_PHASES #Domski and Sisk-Scott ERMS 571178 Table 4 and output file gwb_1x.6o - equilibrate with all minerals
        Hydromagnesite5424      0.0         7.34
        Brucite                             0.0         36.7
        Anhydrite               0.0         166.0
        Halite                              0.0         3490.
        Litharge                0.0         4.35
        Fe(OH)2-Hex                         0.0         46.1
        Calcite                             0.0         0.0
        Glauberite              0.0         0.0
        Whewellite                          0.0         0.0
        Cerussite               0.0         0.0
        Borax                               0.0         0.0
        Mg3Cl(OH)5:4H2O                     0.0         0.0
        Oxychloride-Fe-3(s)     0.0         0.0
        Am(OH)3(s)                          0.0         1.0
        KNpO2CO3(s)                         0.0         1.0
        ThO2(am)                0.0         1.0
SAVE SOLUTION 5
END
```

ERDA6_DOE

```
DATABASE C:/PHREEQC/DATABASES/DATA0FM.dat
TITLE Actinide solubility calculations using minimum to 5x GWB brine volume, Salado minerals and MgO backfill 3/31/2022
simulate equilibrium calculations for CRA19 DPA calcite not suppressed
KNOBS
-diagonal_scale
-step_size 10
-pe_step_size 5
-iterations 200
SOLUTION_SPECIES
H2O + 0.01e- = H2O-0.01
      log_k -9
END
SOLUTION 1 ERDA-6 brine 1x brine CRA-2019 Domski and Sisk-Scott ERMS 571178 and Conc_density_calcs_CRA-2019_PA.xlsx
              units       moles/l
              pH                  6.0
              pe                  7.0
              temp                25.
              density             1.20138
              B                   0.063
              Na                  4.871
              Mg                  0.019
              K                   0.097
              Ca                  0.012
              Cl                  4.80
              S(6)                0.170
              Br                  0.011
              C(4)                0.016
              Acetate             0.0283
              Citrate             0.0023
              EDTA                7.92e-05
              Oxalate             0.0113
              Am                  1.0E-8      #equilibrium with Am(OH)3(s)
              Np                  1.0E-8      #equilibrium with KNpO2CO3
              Th                  1.0E-8      #equilibrium with ThO2(am)
EQUILIBRIUM_PHASES #Domski and Sisk-Scott ERMS 571178 Table 4 - equilibrate with all minerals except calcite
              Hydromagnesite5424  0.0         7.19
              Brucite                         0.0         35.9
              Anhydrite           0.0         163.0
              Halite                          0.0         3410.
              Litharge            0.0         4.26
              Fe(OH)2-Hex                     0.0         45.1
              Calcite                         0.02        0.0
              Glauberite          0.0         0.0
              Whewellite                      0.0         0.0
              Cerussite           0.0         0.0
              Borax                           0.0         0.0
              Mg3Cl(OH)5:4H2O                 0.0         0.0
              Oxychloride-Fe-3(s) 0.0         0.0
              Am(OH)3(s)                      0.0         1.0
              KNpO2CO3(s)                     0.0         1.0
              ThO2(am)            0.0         1.0
              CO2(g)
SELECTED_OUTPUT
 -file        ERDA6_DOE_sel.out
 -high_precision false
 -pH true
 -temperature
 -ionic_strength
 -water
 -percent_error
 -totals Na K Mg Ca Cl S(6) C(4) B Br Fe Pb Oxalate Acetate EDTA Citrate Th Am Np
 -molalities H+
SAVE SOLUTION 1
END
SOLUTION 2 ERDA-6 2x brine CRA-2019 Domski and Sisk-Scott ERMS 571178 and Conc_density_calcs_CRA-2019_PA.xlsx
              units       moles/l
              pH                  6.0
```

```
        pe                      7.0
        temp                    25.
        density                 1.20038
        B                       0.063
        Na                      4.87
        Mg                      0.019
        K                       0.097
        Ca                      0.012
        Cl                      4.80
        S(6)                    0.170
        Br                      0.011
        C(4)                    0.016
        Acetate                 0.0142
        Citrate                 0.00115
        EDTA                    3.96e-05
        Oxalate                 0.00565
        Am                      1.0E-8      #equilibrium with Am(OH)3(s)
        Np                      1.0E-8      #equilibrium with KNpO2CO3
        Th                      1.0E-8      #equilibrium with ThO2(am)
EQUILIBRIUM_PHASES #Domski and Sisk-Scott ERMS 571178 Table 4 - equilibrate with all minerals except calcite
        Hydromagnesite5424      0.0         7.19
        Brucite                             0.0         35.9
        Anhydrite               0.0         163.0
        Halite                              0.0         3410.
        Litharge                0.0         4.26
        Fe(OH)2-Hex                         0.0         45.1
        Calcite                             0.02        0.0
        Glauberite              0.0         0.0
        Whewellite                          0.0         0.0
        Cerussite               0.0         0.0
        Borax                               0.0         0.0
        Mg3Cl(OH)5:4H2O                     0.0         0.0
        Oxychloride-Fe-3(s)     0.0         0.0
        Am(OH)3(s)                          0.0         1.0
        KNpO2CO3(s)                         0.0         1.0
        ThO2(am)                0.0         1.0
        CO2(g)
SAVE SOLUTION 2
END
SOLUTION 3 ERDA-6 3x brine CRA-2019 Domski and Sisk-Scott ERMS 571178 and Conc_density_calcs_CRA-2019_PA.xlsx
        units       moles/l
        pH                      6.0
        pe                      7.0
        temp                    25.
        density                 1.20004
        B                       0.063
        Na                      4.87
        Mg                      0.019
        K                       0.097
        Ca                      0.012
        Cl                      4.80
        S(6)                    0.170
        Br                      0.011
        C(4)                    0.016
        Acetate                 0.00945
        Citrate                 0.000768
        EDTA                    2.64e-05
        Oxalate                 0.00377
        Am                      1.0E-8      #equilibrium with Am(OH)3(s)
        Np                      1.0E-8      #equilibrium with KNpO2CO3
        Th                      1.0E-8      #equilibrium with ThO2(am)
EQUILIBRIUM_PHASES #Domski and Sisk-Scott ERMS 571178 Table 4 equilibrate with all minerals except calcite
        Hydromagnesite5424      0.0         7.19
        Brucite                             0.0         35.9
        Anhydrite               0.0         163.0
        Halite                              0.0         3410.
        Litharge                0.0         4.26
        Fe(OH)2-Hex                         0.0         45.1
        Calcite                             0.02        0.0
        Glauberite              0.0         0.0
```

```
        Whewellite                      0.0     0.0
        Cerussite       0.0             0.0
        Borax                           0.0     0.0
        Mg3Cl(OH)5:4H2O                 0.0     0.0
        Oxychloride-Fe-3(s) 0.0         0.0
        Am(OH)3(s)                      0.0     1.0
        KNpO2CO3(s)                     0.0     1.0
        ThO2(am)        0.0             1.0
        CO2(g)
SAVE SOLUTION 3
END
SOLUTION 4 ERDA-6 4x brine CRA-2019 Domski and Sisk-Scott ERMS 571178 and Conc_density_calcs_CRA-2019_PA.xlsx
        units   moles/l
        pH              6.0
        pe              7.0
        temp            25.
        density         1.19988
        B               0.063
        Na              4.87
        Mg              0.019
        K               0.097
        Ca              0.012
        Cl              4.80
        S(6)            0.170
        Br              0.011
        C(4)            0.016
        Acetate         0.00709
        Citrate         0.000576
        EDTA            1.98e-05
        Oxalate         0.00282
        Am              1.0E-8  #equilibrium with Am(OH)3(s)
        Np              1.0E-8  #equilibrium with KNpO2CO3
        Th              1.0E-8  #equilibrium with ThO2(am)
EQUILIBRIUM_PHASES #Domski and Sisk-Scott ERMS 571178 Table 4 - equilibrate with all minerals except calcite
        Hydromagnesite5424 0.0          7.19
        Brucite                         0.0     35.9
        Anhydrite       0.0             163.0
        Halite                          0.0     3410.
        Litharge        0.0             4.26
        Fe(OH)2-Hex                     0.0     45.1
        Calcite                         0.02    0.0
        Glauberite      0.0             0.0
        Whewellite                      0.0     0.0
        Cerussite       0.0             0.0
        Borax                           0.0     0.0
        Mg3Cl(OH)5:4H2O                 0.0     0.0
        Oxychloride-Fe-3(s) 0.0         0.0
        Am(OH)3(s)                      0.0     1.0
        KNpO2CO3(s)                     0.0     1.0
        ThO2(am)        0.0             1.0
        CO2(g)
SAVE SOLUTION 4
END
SOLUTION 5 ERDA-6 5x brine CRA-2019 Domski and Sisk-Scott ERMS 571178 and Conc_density_calcs_CRA-2019_PA.xlsx
        units   moles/l
        pH              6.0
        pe              7.0
        temp            25.
        density         1.19978
        B               0.063
        Na              4.87
        Mg              0.019
        K               0.097
        Ca              0.012
        Cl              4.80
        S(6)            0.170
        Br              0.011
        C(4)            0.016
        Acetate         0.00567
        Citrate         0.000461
```

```
        EDTA                    1.58e-05
        Oxalate                 0.00226
        Am                      1.0E-8      #equilibrium with Am(OH)3(s)
        Np                      1.0E-8      #equilibrium with KNpO2CO3
        Th                      1.0E-8      #equilibrium with ThO2(am)
EQUILIBRIUM_PHASES #Domski and Sisk-Scott ERMS 571178 Table 4 - equilibrate with all minerals
        Hydromagnesite5424 0.0      7.19
        Brucite                     0.0     35.9
        Anhydrite           0.0     163.0
        Halite                      0.0     3410.
        Litharge            0.0     4.26
        Fe(OH)2-Hex                 0.0     45.1
        Calcite                     0.02    0.0
        Glauberite          0.0     0.0
        Whewellite                  0.0     0.0
        Cerussite           0.0     0.0
        Borax                       0.0     0.0
        Mg3Cl(OH)5:4H2O             0.0     0.0
        Oxychloride-Fe-3(s) 0.0     0.0
        Am(OH)3(s)                  0.0     1.0
        KNpO2CO3(s)                 0.0     1.0
        ThO2(am)            0.0     1.0
        CO2(g)
SAVE SOLUTION 5
END
```

GWB_EPADB

```
DATABASE C:/PHREEQC/DATABASES/DATA0FM_EPA.dat
TITLE Actinide solubility calculations using GWB brine, Salado minerals and MgO backfill 3/30/2022
simulate equilibrium calculations for CRA19 DPA changes include EPA database and calcite SI 0.03 to aid convergence
SOLUTION_SPECIES
H2O + 0.01e- = H2O-0.01
    log_k -9
Edta-4 + Mg+2 = MgEdta-2                # EQ36
        log_k   9.20                    # original Hummel et al. (2005) value is 10.9
#modify MgEDTA-2 log beta to improve fit to Choppin et al. (2001) apparent log betas (as corrected by Hummel et al. 2005)
Th+4 + Edta-4 = ThEdta                  # EQ36
        log_k   24.6                    # original Hummel et al. (2005) value is 23.557
#modify ThEDTA log beta to improve fit to Choppin et al. (2001) apparent log betas (as corrected by Hummel et al. 2005)
END
SOLUTION 1 GWB 1x brine CRA-2019 Domski and Sisk-Scott ERMS 571178 and Conc_density_calcs_CRA-2019_PA.xlsx
        units       moles/l
        pH              6.0
        pe              7.0
        temp            25.
        density         1.2366
        Na              3.53
        K               0.467
        Mg              1.02
        Ca              0.014
        Cl              5.86
        C(4)            0.016
        S(6)            0.177
        B               0.158
        Br              0.0266
        Acetate         0.0283
        Citrate         0.0023
        EDTA            7.92e-05
        Oxalate         0.0113
        Fe              1.0E-08
        Pb              1.0E-08
        Am              1.0E-8      #equilibrium with Am(OH)3(s)
        Np              1.0E-8      #equilibrium with KNpO2CO3
        Th              1.0E-8      #equilibrium with ThO2(am)
EQUILIBRIUM_PHASES #Domski and Sisk-Scott ERMS 571178 Table 4 and output file gwb_1x.6o - equilibrate with all minerals
        Hydromagnesite5424  0.0     7.34
        Brucite                     0.0     36.7
        Anhydrite           0.0     166.0
        Halite                      0.0     3490.
        Litharge            0.0     4.35
        Fe(OH)2-Hex                 0.0     46.1
        Calcite                     0.03    0.0
        Glauberite          0.0     0.0
        Whewellite                  0.0     0.0
        Cerussite           0.0     0.0
        Borax                       0.0     0.0
        Mg3Cl(OH)5:4H2O             0.0     0.0
        Oxychloride-Fe-3(s) 0.0     0.0
        Am(OH)3(s)                  0.0     1.0
        KNpO2CO3(s)                 0.0     1.0
        ThO2(am)            0.0     1.0
SELECTED_OUTPUT
 -file      GWB_EPADB_sel.out
 -high_precision true
 -pH true
 -temperature
 -ionic_strength
 -water
 -percent_error
 -totals Na K Mg Ca Cl S(6) C(4) B Br Fe Pb Th Am Np Oxalate Acetate EDTA Citrate
 -molalities H+
 -equilibrium_phases Hydromagnesite5424 Brucite Anhydrite Halite Litharge Fe(OH)2-Hex Calcite
   Glauberite Whewellite Cerussite Borax Mg3Cl(OH)5:4H2O Oxychloride-Fe-3(s) Am(OH)3(s) KNpO2CO3(s) ThO2(am)
 -saturation_indices Hydromagnesite5424 Brucite Anhydrite Halite Litharge Fe(OH)2-Hex Calcite
```

```
   Glauberite Whewellite Cerussite Borax Mg3Cl(OH)5:4H2O Oxychloride-Fe-3(s) CO2(g) Am(OH)3(s) KNpO2CO3(s) ThO2(am)
SAVE SOLUTION 1
END
SOLUTION 2 GWB 2x brine CRA-2019 Domski and Sisk-Scott ERMS 571178 and Conc_density_calcs_CRA-2019_PA.xlsx
        units       moles/l
        pH                  6.0
        pe                  7.0
        temp                25.
        density             1.2356
        Na                  3.53
        K                   0.467
        Mg                  1.02
        Ca                  0.014
        Cl                  5.86
        C(4)                0.016
        S(6)                0.177
        B                   0.158
        Br                  0.0266
        Acetate             0.0142
        Citrate             0.00115
        EDTA                3.96e-05
        Oxalate             0.00565
        Fe                  1.0E-08
        Pb                  1.0E-08
        Am                  1.0E-8    #equilibrium with Am(OH)3(s)
        Np                  1.0E-8    #equilibrium with KNpO2CO3
        Th                  1.0E-8    #equilibrium with ThO2(am)
EQUILIBRIUM_PHASES #Domski and Sisk-Scott ERMS 571178 Table 4 and output file gwb_1x.6o - equilibrate with all minerals
        Hydromagnesite5424  0.0       7.34
        Brucite                       0.0       36.7
        Anhydrite           0.0       166.0
        Halite                        0.0       3490.
        Litharge            0.0       4.35
        Fe(OH)2-Hex                   0.0       46.1
        Calcite                       0.03      0.0
        Glauberite          0.0       0.0
        Whewellite                    0.0       0.0
        Cerussite           0.0       0.0
        Borax                         0.0       0.0
        Mg3Cl(OH)5:4H2O               0.0       0.0
        Oxychloride-Fe-3(s) 0.0       0.0
        Am(OH)3(s)                    0.0       1.0
        KNpO2CO3(s)                   0.0       1.0
        ThO2(am)            0.0       1.0
SAVE SOLUTION 2
END
SOLUTION 3 GWB 3x brine CRA-2019 Domski and Sisk-Scott ERMS 571178 and Conc_density_calcs_CRA-2019_PA.xlsx
        units       moles/l
        pH                  6.0
        pe                  7.0
        temp                25.
        density             1.23526
        Na                  3.53
        K                   0.467
        Mg                  1.02
        Ca                  0.014
        Cl                  5.86
        C(4)                0.016
        S(6)                0.177
        B                   0.158
        Br                  0.0266
        Acetate             0.00945
        Citrate             0.000768
        EDTA                2.64e-05
        Oxalate             0.00377
        Fe                  1.0E-08
        Pb                  1.0E-08
        Am                  1.0E-8    #equilibrium with Am(OH)3(s)
        Np                  1.0E-8    #equilibrium with KNpO2CO3
        Th                  1.0E-8    #equilibrium with ThO2(am)
```

```
EQUILIBRIUM_PHASES #Domski and Sisk-Scott ERMS 571178 Table 4 and output file gwb_1x.6o - equilibrate with all minerals
        Hydromagnesite5424 0.0     7.34
        Brucite                    0.0     36.7
        Anhydrite          0.0     166.0
        Halite                     0.0     3490.
        Litharge           0.0     4.35
        Fe(OH)2-Hex                0.0     46.1
        Calcite                    0.03    0.0
        Glauberite         0.0     0.0
        Whewellite                 0.0     0.0
        Cerussite          0.0     0.0
        Borax                      0.0     0.0
        Mg3Cl(OH)5:4H2O            0.0     0.0
        Oxychloride-Fe-3(s) 0.0    0.0
        Am(OH)3(s)                 0.0     1.0
        KNpO2CO3(s)                0.0     1.0
        ThO2(am)           0.0     1.0
SAVE SOLUTION 3
END
SOLUTION 4 GWB 4x brine CRA-2019 Domski and Sisk-Scott ERMS 571178 and Conc_density_calcs_CRA-2019_PA.xlsx
        units      moles/l
        pH                 6.0
        pe                 7.0
        temp               25.
        density            1.2351
        Na                 3.53
        K                  0.467
        Mg                 1.02
        Ca                 0.014
        Cl                 5.86
        C(4)               0.016
        S(6)               0.177
        B                  0.158
        Br                 0.0266
        Acetate            0.00709
        Citrate            0.000576
        EDTA               1.98e-05
        Oxalate            0.00282
        Fe                 1.0E-08
        Pb                 1.0E-08
        Am                 1.0E-8  #equilibrium with Am(OH)3(s)
        Np                 1.0E-8  #equilibrium with KNpO2CO3
        Th                 1.0E-8  #equilibrium with ThO2(am)
EQUILIBRIUM_PHASES #Domski and Sisk-Scott ERMS 571178 Table 4 and output file gwb_1x.6o - equilibrate with all minerals
        Hydromagnesite5424 0.0     7.34
        Brucite                    0.0     36.7
        Anhydrite          0.0     166.0
        Halite                     0.0     3490.
        Litharge           0.0     4.35
        Fe(OH)2-Hex                0.0     46.1
        Calcite                    0.03    0.0
        Glauberite         0.0     0.0
        Whewellite                 0.0     0.0
        Cerussite          0.0     0.0
        Borax                      0.0     0.0
        Mg3Cl(OH)5:4H2O            0.0     0.0
        Oxychloride-Fe-3(s) 0.0    0.0
        Am(OH)3(s)                 0.0     1.0
        KNpO2CO3(s)                0.0     1.0
        ThO2(am)           0.0     1.0
SAVE SOLUTION 4
END
SOLUTION 5 GWB 5x brine CRA-2019 Domski and Sisk-Scott ERMS 571178 and Conc_density_calcs_CRA-2019_PA.xlsx
        units      moles/l
        pH                 6.0
        pe                 7.0
        temp               25.
        density            1.235
        Na                 3.53
        K                  0.467
```

```
        Mg                  1.02
        Ca                  0.014
        Cl                  5.86
        C(4)                0.016
        S(6)                0.177
        B                   0.158
        Br                  0.0266
        Acetate             0.00567
        Citrate             0.000461
        EDTA                1.58e-05
        Oxalate             0.00226
        Fe                  1.0E-08
        Pb                  1.0E-08
        Am                  1.0E-8    #equilibrium with Am(OH)3(s)
        Np                  1.0E-8    #equilibrium with KNpO2CO3
        Th                  1.0E-8    #equilibrium with ThO2(am)
EQUILIBRIUM_PHASES #Domski and Sisk-Scott ERMS 571178 Table 4 and output file gwb_1x.6o - equilibrate with all minerals
        Hydromagnesite5424 0.0      7.34
        Brucite                     0.0       36.7
        Anhydrite          0.0      166.0
        Halite                      0.0       3490.
        Litharge           0.0      4.35
        Fe(OH)2-Hex                 0.0       46.1
        Calcite                     0.03      0.0
        Glauberite         0.0      0.0
        Whewellite                  0.0       0.0
        Cerussite          0.0      0.0
        Borax                       0.0       0.0
        Mg3Cl(OH)5:4H2O             0.0       0.0
        Oxychloride-Fe-3(s) 0.0     0.0
        Am(OH)3(s)                  0.0       1.0
        KNpO2CO3(s)                 0.0       1.0
        ThO2(am)           0.0      1.0
SAVE SOLUTION 5
END
```

ERDA6_EPADB

```
DATABASE C:/PHREEQC/DATABASES/DATA0FM_EPA.dat
TITLE Actinide solubility calculations using minimum to 5x ERDA-6 brine volume, Salado minerals and MgO backfill 3/31/2022
simulate equilibrium calculations for CRA19 DPA all DOE assumptions and EPA database, calcite SI = 0.03 to aid convergence
KNOBS
-diagonal_scale
-step_size 10
-pe_step_size 5
-iterations 200
SOLUTION_SPECIES
H2O + 0.01e- = H2O-0.01
    log_k -9
Edta-4 + Mg+2 = MgEdta-2                # EQ36
        log_k    9.20                   # original Hummel et al. (2005) value is 10.9
#modify MgEDTA-2 log beta to improve fit to Choppin et al. (2001) apparent log betas (as corrected by Hummel et al. 2005)
Th+4 + Edta-4 = ThEdta                  # EQ36
        log_k    24.6                   # original Hummel et al. (2005) value is 23.557
#modify ThEDTA log beta to improve fit to Choppin et al. (2001) apparent log betas (as corrected by Hummel et al. 2005)
END
SOLUTION 1 ERDA-6 brine 1x brine CRA-2019 Domski and Sisk-Scott ERMS 571178 and Conc_density_calcs_CRA-2019_PA.xlsx
        units       moles/l
        pH                  6.0
        pe                  7.0
        temp                25.
        density             1.20138
        B                   0.063
        Na                  4.871
        Mg                  0.019
        K                   0.097
        Ca                  0.012
        Cl                  4.80
        S(6)                0.170
        Br                  0.011
```

```
        C(4)                0.016
        Acetate             0.0283
        Citrate             0.0023
        EDTA                7.92e-05
        Oxalate             0.0113
        Am                  1.0E-8      #equilibrium with Am(OH)3(s)
        Np                  1.0E-8      #equilibrium with KNpO2CO3
        Th                  1.0E-8      #equilibrium with ThO2(am)
EQUILIBRIUM_PHASES #Domski and Sisk-Scott ERMS 571178 Table 4 - equilibrate with all minerals except calcite
        Hydromagnesite5424  0.0         7.19
        Brucite                         0.0         35.9
        Anhydrite           0.0         163.0
        Halite                          0.0         3410.
        Litharge            0.0         4.26
        Fe(OH)2-Hex                     0.0         45.1
        Calcite                         0.03        0.0
        Glauberite          0.0         0.0
        Whewellite                      0.0         0.0
        Cerussite           0.0         0.0
        Borax                           0.0         0.0
        Mg3Cl(OH)5:4H2O                 0.0         0.0
        Oxychloride-Fe-3(s) 0.0         0.0
        Am(OH)3(s)                      0.0         1.0
        KNpO2CO3(s)                     0.0         1.0
        ThO2(am)            0.0         1.0
SELECTED_OUTPUT
 -file      ERDA6_EPADB_sel.out
 -high_precision false
 -pH true
 -temperature
 -ionic_strength
 -water
 -percent_error
 -totals Na K Mg Ca Cl S(6) C(4) B Br Fe Pb Th Am Np Oxalate Acetate EDTA Citrate
 -molalities H+
SAVE SOLUTION 1
END
SOLUTION 2 ERDA-6 2x brine CRA-2019 Domski and Sisk-Scott ERMS 571178 and Conc_density_calcs_CRA-2019_PA.xlsx
        units       moles/l
        pH                  6.0
        pe                  7.0
        temp                25.
        density             1.20038
        B                   0.063
        Na                  4.87
        Mg                  0.019
        K                   0.097
        Ca                  0.012
        Cl                  4.80
        S(6)                0.170
        Br                  0.011
        C(4)                0.016
        Acetate             0.0142
        Citrate             0.00115
        EDTA                3.96e-05
        Oxalate             0.00565
        Am                  1.0E-8      #equilibrium with Am(OH)3(s)
        Np                  1.0E-8      #equilibrium with KNpO2CO3
        Th                  1.0E-8      #equilibrium with ThO2(am)
EQUILIBRIUM_PHASES #Domski and Sisk-Scott ERMS 571178 Table 4 - equilibrate with all minerals except calcite
        Hydromagnesite5424  0.0         7.19
        Brucite                         0.0         35.9
        Anhydrite           0.0         163.0
        Halite                          0.0         3410.
        Litharge            0.0         4.26
        Fe(OH)2-Hex                     0.0         45.1
        Calcite                         0.03        0.0
        Glauberite          0.0         0.0
        Whewellite                      0.0         0.0
        Cerussite           0.0         0.0
```

```
        Borax                           0.0     0.0
        Mg3Cl(OH)5:4H2O                 0.0     0.0
        Oxychloride-Fe-3(s)  0.0        0.0
        Am(OH)3(s)                      0.0     1.0
        KNpO2CO3(s)                     0.0     1.0
        ThO2(am)             0.0        1.0
SAVE SOLUTION 2
END
SOLUTION 3 ERDA-6 3x brine CRA-2019 Domski and Sisk-Scott ERMS 571178 and Conc_density_calcs_CRA-2019_PA.xlsx
        units       moles/l
        pH                  6.0
        pe                  7.0
        temp                25.
        density             1.20004
        B                   0.063
        Na                  4.87
        Mg                  0.019
        K                   0.097
        Ca                  0.012
        Cl                  4.80
        S(6)                0.170
        Br                  0.011
        C(4)                0.016
        Acetate             0.00945
        Citrate             0.000768
        EDTA                2.64e-05
        Oxalate             0.00377
        Am                  1.0E-8  #equilibrium with Am(OH)3(s)
        Np                  1.0E-8  #equilibrium with KNpO2CO3
        Th                  1.0E-8  #equilibrium with ThO2(am)
EQUILIBRIUM_PHASES #Domski and Sisk-Scott ERMS 571178 Table 4 equilibrate with all minerals except calcite
        Hydromagnesite5424  0.0     7.19
        Brucite                     0.0     35.9
        Anhydrite           0.0     163.0
        Halite                      0.0     3410.
        Litharge            0.0     4.26
        Fe(OH)2-Hex                 0.0     45.1
        Calcite                     0.03    0.0
        Glauberite          0.0     0.0
        Whewellite                  0.0     0.0
        Cerussite           0.0     0.0
        Borax                       0.0     0.0
        Mg3Cl(OH)5:4H2O             0.0     0.0
        Oxychloride-Fe-3(s) 0.0     0.0
        Am(OH)3(s)                  0.0     1.0
        KNpO2CO3(s)                 0.0     1.0
        ThO2(am)            0.0     1.0
SAVE SOLUTION 3
END
SOLUTION 4 ERDA-6 4x brine CRA-2019 Domski and Sisk-Scott ERMS 571178 and Conc_density_calcs_CRA-2019_PA.xlsx
        units       moles/l
        pH                  6.0
        pe                  7.0
        temp                25.
        density             1.19988
        B                   0.063
        Na                  4.87
        Mg                  0.019
        K                   0.097
        Ca                  0.012
        Cl                  4.80
        S(6)                0.170
        Br                  0.011
        C(4)                0.016
        Acetate             0.00709
        Citrate             0.000576
        EDTA                1.98e-05
        Oxalate             0.00282
        Am                  1.0E-8  #equilibrium with Am(OH)3(s)
        Np                  1.0E-8  #equilibrium with KNpO2CO3
```

```
        Th                      1.0E-8      #equilibrium with ThO2(am)
EQUILIBRIUM_PHASES #Domski and Sisk-Scott ERMS 571178 Table 4 - equilibrate with all minerals except calcite
        Hydromagnesite5424 0.0      7.19
        Brucite                     0.0     35.9
        Anhydrite          0.0      163.0
        Halite                      0.0     3410.
        Litharge           0.0      4.26
        Fe(OH)2-Hex                 0.0     45.1
        Calcite                     0.03    0.0
        Glauberite         0.0      0.0
        Whewellite                  0.0     0.0
        Cerussite          0.0      0.0
        Borax                       0.0     0.0
        Mg3Cl(OH)5:4H2O             0.0     0.0
        Oxychloride-Fe-3(s) 0.0     0.0
        Am(OH)3(s)                  0.0     1.0
        KNpO2CO3(s)                 0.0     1.0
        ThO2(am)           0.0      1.0
SAVE SOLUTION 4
END
SOLUTION 5 ERDA-6 5x brine CRA-2019 Domski and Sisk-Scott ERMS 571178 and Conc_density_calcs_CRA-2019_PA.xlsx
        units       moles/l
        pH                      6.0
        pe                      7.0
        temp                    25.
        density                 1.19978
        B                       0.063
        Na                      4.87
        Mg                      0.019
        K                       0.097
        Ca                      0.012
        Cl                      4.80
        S(6)                    0.170
        Br                      0.011
        C(4)                    0.016
        Acetate                 0.00567
        Citrate                 0.000461
        EDTA                    1.58e-05
        Oxalate                 0.00226
        Am                      1.0E-8      #equilibrium with Am(OH)3(s)
        Np                      1.0E-8      #equilibrium with KNpO2CO3
        Th                      1.0E-8      #equilibrium with ThO2(am)
EQUILIBRIUM_PHASES #Domski and Sisk-Scott ERMS 571178 Table 4 - equilibrate with all minerals
        Hydromagnesite5424 0.0      7.19
        Brucite                     0.0     35.9
        Anhydrite          0.0      163.0
        Halite                      0.0     3410.
        Litharge           0.0      4.26
        Fe(OH)2-Hex                 0.0     45.1
        Calcite                     0.03    0.0
        Glauberite         0.0      0.0
        Whewellite                  0.0     0.0
        Cerussite          0.0      0.0
        Borax                       0.0     0.0
        Mg3Cl(OH)5:4H2O             0.0     0.0
        Oxychloride-Fe-3(s) 0.0     0.0
        Am(OH)3(s)                  0.0     1.0
        KNpO2CO3(s)                 0.0     1.0
        ThO2(am)           0.0      1.0
SAVE SOLUTION 5
END
```

GWB_EPA

```
DATABASE C:/PHREEQC/DATABASES/DATA0FM_EPA.dat
TITLE Actinide solubility calculations using minimum to 5x GWB brine volume, Salado minerals and MgO backfill 3/30/2022
revised actinide solubility calculations for CRA19 DPA using EPA assumptions and database
SOLUTION_SPECIES
H2O + 0.01e- = H2O-0.01
     log_k -9
Edta-4 + Mg+2 = MgEdta-2                    # EQ36
          log_k     9.20                    # original Hummel et al. (2005) value is 10.9
#modify MgEDTA-2 log beta to improve fit to Choppin et al. (2001) apparent log betas (as corrected by Hummel et al. 2005)
Th+4 + Edta-4 = ThEdta                      # EQ36
          log_k     24.6                    # original Hummel et al. (2005) value is 23.557
#modify ThEDTA log beta to improve fit to Choppin et al. (2001) apparent log betas (as corrected by Hummel et al. 2005)
END
SOLUTION 1 GWB 1x brine CRA-2019 Domski and Sisk-Scott ERMS 571178 and Conc_desity_calcs_CRA-2019_PA.xlsx
          units       moles/l
          pH                  6.0
          pe                  7.0
          temp                25.
          density             1.2366
          Na                  3.53
          K                   0.467
          Mg                  1.02
          Ca                  0.014
          Cl                  5.86
          C(4)                0.016
          S(6)                0.177
          B                   0.158
          Br                  0.0266
          Acetate             0.0283
          Citrate             0.0023
          EDTA                7.92e-05
          Oxalate             0.0113
          Am                  1.0E-8    #equilibrium with Am(OH)3(s)
          Np                  1.0E-8    #equilibrium with KNpO2CO3
          Th                  1.0E-8    #equilibrium with ThO2(am)
EQUILIBRIUM_PHASES #Domski and Sisk-Scott ERMS 571178 Table 4 and output file gwb_1x.6o - equilibrate with all minerals
          Hydromagnesite5424 0.0        7.34
          Brucite                       0.0         36.7
          Anhydrite          0.0        166.0
          Halite                        0.0         3490.
          Aragonite          0.0        0.0
          Glauberite         0.0        0.0
          Whewellite                    0.0         0.0
          Borax                         0.0         0.0
          Mg3Cl(OH)5:4H2O               0.0         0.0
          Am(OH)3(s)                    0.0         1.0
          KNpO2CO3(s)                   0.0         1.0
          ThO2(am)           0.0        1.0
SELECTED_OUTPUT
 -file        GWB_EPA_sel.out
 -high_precision true
 -pH true
 -temperature
 -ionic_strength
 -water
 -percent_error
 -totals Na K Mg Ca Cl S(6) C(4) B Br Th Am Np Oxalate Acetate EDTA Citrate
 -molalities H+
 -equilibrium_phases Hydromagnesite5424 Brucite Anhydrite Halite Aragonite
    Glauberite Whewellite Borax Mg3Cl(OH)5:4H2O Am(OH)3(s) KNpO2CO3(s) ThO2(am)
 -saturation_indices Hydromagnesite5424 Brucite Anhydrite Halite Aragonite Calcite
    Glauberite Whewellite Borax Mg3Cl(OH)5:4H2O CO2(g) Am(OH)3(s) KNpO2CO3(s) ThO2(am)
SAVE SOLUTION 1
END
SOLUTION 2 GWB 2x brine CRA-2019 Domski and Sisk-Scott ERMS 571178 and Conc_desity_calcs_CRA-2019_PA.xlsx
          units       moles/l
          pH                  6.0
```

```
        pe                  7.0
        temp                25.
        density             1.2356
        Na                  3.53
        K                   0.467
        Mg                  1.02
        Ca                  0.014
        Cl                  5.86
        C(4)                0.016
        S(6)                0.177
        B                   0.158
        Br                  0.0266
        Acetate             0.0142
        Citrate             0.00115
        EDTA                3.96e-05
        Oxalate             0.00565
        Am                  1.0E-8      #equilibrium with Am(OH)3(s)
        Np                  1.0E-8      #equilibrium with KNpO2CO3
        Th                  1.0E-8      #equilibrium with ThO2(am)
EQUILIBRIUM_PHASES #Domski and Sisk-Scott ERMS 571178 Table 4 and output file gwb_1x.6o - equilibrate with all minerals
        Hydromagnesite5424  0.0         7.34
        Brucite                         0.0         36.7
        Anhydrite           0.0         166.0
        Halite                          0.0         3490.
        Aragonite           0.0         0.0
        Glauberite          0.0         0.0
        Whewellite                      0.0         0.0
        Borax                           0.0         0.0
        Mg3Cl(OH)5:4H2O                 0.0         0.0
        Am(OH)3(s)                      0.0         1.0
        KNpO2CO3(s)                     0.0         1.0
        ThO2(am)            0.0         1.0
SAVE SOLUTION 2
END
SOLUTION 3 GWB 3x brine CRA-2019 Domski and Sisk-Scott ERMS 571178 and Conc_desity_calcs_CRA-2019_PA.xlsx
        units       moles/l
        pH                  6.0
        pe                  7.0
        temp                25.
        density             1.23526
        Na                  3.53
        K                   0.467
        Mg                  1.02
        Ca                  0.014
        Cl                  5.86
        C(4)                0.016
        S(6)                0.177
        B                   0.158
        Br                  0.0266
        Acetate             0.00945
        Citrate             0.000768
        EDTA                2.64e-05
        Oxalate             0.00377
        Am                  1.0E-8      #equilibrium with Am(OH)3(s)
        Np                  1.0E-8      #equilibrium with KNpO2CO3
        Th                  1.0E-8      #equilibrium with ThO2(am)
EQUILIBRIUM_PHASES #Domski and Sisk-Scott ERMS 571178 Table 4 and output file gwb_1x.6o - equilibrate with all minerals
        Hydromagnesite5424  0.0         7.34
        Brucite                         0.0         36.7
        Anhydrite           0.0         166.0
        Halite                          0.0         3490.
        Aragonite           0.0         0.0
        Glauberite          0.0         0.0
        Whewellite                      0.0         0.0
        Borax                           0.0         0.0
        Mg3Cl(OH)5:4H2O                 0.0         0.0
        Am(OH)3(s)                      0.0         1.0
        KNpO2CO3(s)                     0.0         1.0
        ThO2(am)            0.0         1.0
SAVE SOLUTION 3
```

```
END
SOLUTION 4 GWB 4x brine CRA-2019 Domski and Sisk-Scott ERMS 571178 and Conc_desity_calcs_CRA-2019_PA.xlsx
        units       moles/l
        pH                  6.0
        pe                  7.0
        temp                25.
        density             1.23510
        Na                  3.53
        K                   0.467
        Mg                  1.02
        Ca                  0.014
        Cl                  5.86
        C(4)                0.016
        S(6)                0.177
        B                   0.158
        Br                  0.0266
        Acetate             0.00709
        Citrate             0.000576
        EDTA                1.98e-05
        Oxalate             0.00282
        Am                  1.0E-8      #equilibrium with Am(OH)3(s)
        Np                  1.0E-8      #equilibrium with KNpO2CO3
        Th                  1.0E-8      #equilibrium with ThO2(am)
EQUILIBRIUM_PHASES #Domski and Sisk-Scott ERMS 571178 Table 4 and output file gwb_1x.6o - equilibrate with all minerals
        Hydromagnesite5424  0.0         7.34
        Brucite                         0.0         36.7
        Anhydrite           0.0         166.0
        Halite                          0.0         3490.
        Aragonite           0.0         0.0
        Glauberite          0.0         0.0
        Whewellite                      0.0         0.0
        Borax                           0.0         0.0
        Mg3Cl(OH)5:4H2O                 0.0         0.0
        Am(OH)3(s)                      0.0         1.0
        KNpO2CO3(s)                     0.0         1.0
        ThO2(am)            0.0         1.0
SAVE SOLUTION 4
END
SOLUTION 5 GWB 5x brine CRA-2019 Domski and Sisk-Scott ERMS 571178 and Conc_desity_calcs_CRA-2019_PA.xlsx
        units       moles/l
        pH                  6.0
        pe                  7.0
        temp                25.
        density             1.235
        Na                  3.53
        K                   0.467
        Mg                  1.02
        Ca                  0.014
        Cl                  5.86
        C(4)                0.016
        S(6)                0.177
        B                   0.158
        Br                  0.0266
        Acetate             0.00567
        Citrate             0.000461
        EDTA                1.58e-05
        Oxalate             0.00226
        Am                  1.0E-8      #equilibrium with Am(OH)3(s)
        Np                  1.0E-8      #equilibrium with KNpO2CO3
        Th                  1.0E-8      #equilibrium with ThO2(am)
EQUILIBRIUM_PHASES #Domski and Sisk-Scott ERMS 571178 Table 4 and output file gwb_1x.6o - equilibrate with all minerals
        Hydromagnesite5424  0.0         7.34
        Brucite                         0.0         36.7
        Anhydrite           0.0         166.0
        Halite                          0.0         3490.
        Aragonite           0.0         0.0
        Glauberite          0.0         0.0
        Whewellite                      0.0         0.0
        Borax                           0.0         0.0
        Mg3Cl(OH)5:4H2O                 0.0         0.0
```

```
        Am(OH)3(s)              0.0     1.0
        KNpO2CO3(s)             0.0     1.0
        ThO2(am)        0.0     1.0
SAVE SOLUTION 5
END
```

ERDA6_EPA

```
DATABASE C:/PHREEQC/DATABASES/DATA0FM_EPA.dat
TITLE Actinide solubility calculations using ERDA-6 brine, Salado minerals and MgO backfill 3/31/2022
simulate equilibrium calculations for CRA19 DPA using EPA assumptions and database
SOLUTION_SPECIES
H2O + 0.01e- = H2O-0.01
    log_k -9
Edta-4 + Mg+2 = MgEdta-2                # EQ36
        log_k   9.20                    # original Hummel et al. (2005) value is 10.9
#modify MgEDTA-2 log beta to improve fit to Choppin et al. (2001) apparent log betas (as corrected by Hummel et al. 2005)
Th+4 + Edta-4 = ThEdta                  # EQ36
        log_k   24.6                    # original Hummel et al. (2005) value is 23.557
#modify ThEDTA log beta to improve fit to Choppin et al. (2001) apparent log betas (as corrected by Hummel et al. 2005)
END
SOLUTION 1 ERDA-6 brine 1x brine CRA-2019 Domski and Sisk-Scott ERMS 571178 and Conc_density_calcs_CRA-2019_PA.xlsx
        units       moles/l
        pH                  6.0
        pe                  7.0
        temp                25.
        density             1.20138
        B                   0.063
        Na                  4.871
        Mg                  0.019
        K                   0.097
        Ca                  0.012
        Cl                  4.80
        S(6)                0.170
        Br                  0.011
        C(4)                0.016
        Acetate             0.0283
        Citrate             0.0023
        EDTA                7.92e-05
        Oxalate             0.0113
        Am                  1.0E-8  #equilibrium with Am(OH)3(s)
        Np                  1.0E-8  #equilibrium with KNpO2CO3
        Th                  1.0E-8  #equilibrium with ThO2(am)
EQUILIBRIUM_PHASES #Domski and Sisk-Scott ERMS 571178 Table 4 - equilibrate with all minerals except calcite
        Hydromagnesite5424  0.0     7.19
        Brucite                     0.0     35.9
        Anhydrite           0.0     163.0
        Halite                      0.0     3410.
        Aragonite           0.0     0.0
        Glauberite          0.0     0.0
        Whewellite                  0.0     0.0
        Borax                       0.0     0.0
        Mg3Cl(OH)5:4H2O             0.0     0.0
        Am(OH)3(s)                  0.0     1.0
        KNpO2CO3(s)                 0.0     1.0
        ThO2(am)            0.0     1.0
SELECTED_OUTPUT
 -file      ERDA6_EPA_sel.out
 -high_precision true
 -pH true
 -temperature
 -ionic_strength
 -water
 -percent_error
 -totals Na K Mg Ca Cl S(6) C(4) B Br Th Am Np Oxalate Acetate EDTA Citrate
 -molalities H+
 -equilibrium_phases Hydromagnesite5424 Brucite Anhydrite Halite Aragonite
   Glauberite Whewellite Borax Mg3Cl(OH)5:4H2O Am(OH)3(s) KNpO2CO3(s) ThO2(am)
 -saturation_indices Hydromagnesite5424 Brucite Anhydrite Halite Aragonite Calcite
   Glauberite Whewellite Borax Mg3Cl(OH)5:4H2O CO2(g) Am(OH)3(s) KNpO2CO3(s) ThO2(am)
SAVE SOLUTION 1
END
SOLUTION 2 ERDA-6 2x brine CRA-2019 Domski and Sisk-Scott ERMS 571178 and Conc_density_calcs_CRA-2019_PA.xlsx
        units       moles/l
        pH                  6.0
```

```
        pe                      7.0
        temp                    25.
        density                 1.20038
        B                       0.063
        Na                      4.87
        Mg                      0.019
        K                       0.097
        Ca                      0.012
        Cl                      4.80
        S(6)                    0.170
        Br                      0.011
        C(4)                    0.016
        Acetate                 0.0142
        Citrate                 0.00115
        EDTA                    3.96e-05
        Oxalate                 0.00565
        Am                      1.0E-8      #equilibrium with Am(OH)3(s)
        Np                      1.0E-8      #equilibrium with KNpO2CO3
        Th                      1.0E-8      #equilibrium with ThO2(am)
EQUILIBRIUM_PHASES #Domski and Sisk-Scott ERMS 571178 Table 4 - equilibrate with all minerals except calcite
        Hydromagnesite5424      0.0         7.19
        Brucite                             0.0         35.9
        Anhydrite               0.0         163.0
        Halite                              0.0         3410.
        Aragonite               0.0         0.0
        Glauberite              0.0         0.0
        Whewellite                          0.0         0.0
        Borax                               0.0         0.0
        Mg3Cl(OH)5:4H2O                     0.0         0.0
        Am(OH)3(s)                          0.0         1.0
        KNpO2CO3(s)                         0.0         1.0
        ThO2(am)                0.0         1.0
SAVE SOLUTION 2
END
SOLUTION 3 ERDA-6 3x brine CRA-2019 Domski and Sisk-Scott ERMS 571178 and Conc_density_calcs_CRA-2019_PA.xlsx
        units       moles/l
        pH                      6.0
        pe                      7.0
        temp                    25.
        density                 1.20004
        B                       0.063
        Na                      4.87
        Mg                      0.019
        K                       0.097
        Ca                      0.012
        Cl                      4.80
        S(6)                    0.170
        Br                      0.011
        C(4)                    0.016
        Acetate                 0.00945
        Citrate                 0.000768
        EDTA                    2.64e-05
        Oxalate                 0.00377
        Am                      1.0E-8      #equilibrium with Am(OH)3(s)
        Np                      1.0E-8      #equilibrium with KNpO2CO3
        Th                      1.0E-8      #equilibrium with ThO2(am)
EQUILIBRIUM_PHASES #Domski and Sisk-Scott ERMS 571178 Table 4 equilibrate with all minerals except calcite
        Hydromagnesite5424      0.0         7.19
        Brucite                             0.0         35.9
        Anhydrite               0.0         163.0
        Halite                              0.0         3410.
        Aragonite               0.0         0.0
        Glauberite              0.0         0.0
        Whewellite                          0.0         0.0
        Borax                               0.0         0.0
        Mg3Cl(OH)5:4H2O                     0.0         0.0
        Am(OH)3(s)                          0.0         1.0
        KNpO2CO3(s)                         0.0         1.0
        ThO2(am)                0.0         1.0
SAVE SOLUTION 3
```

```
END
SOLUTION 4 ERDA-6 4x brine CRA-2019 Domski and Sisk-Scott ERMS 571178 and Conc_density_calcs_CRA-2019_PA.xlsx
        units       moles/l
        pH                  6.0
        pe                  7.0
        temp                25.
        density             1.19988
        B                   0.063
        Na                  4.87
        Mg                  0.019
        K                   0.097
        Ca                  0.012
        Cl                  4.80
        S(6)                0.170
        Br                  0.011
        C(4)                0.016
        Acetate             0.00709
        Citrate             0.000576
        EDTA                1.98e-05
        Oxalate             0.00282
        Am                  1.0E-8      #equilibrium with Am(OH)3(s)
        Np                  1.0E-8      #equilibrium with KNpO2CO3
        Th                  1.0E-8      #equilibrium with ThO2(am)
EQUILIBRIUM_PHASES #Domski and Sisk-Scott ERMS 571178 Table 4 - equilibrate with all minerals except calcite
        Hydromagnesite5424  0.0         7.19
        Brucite                         0.0         35.9
        Anhydrite           0.0         163.0
        Halite                          0.0         3410.
        Aragonite           0.0         0.0
        Glauberite          0.0         0.0
        Whewellite                      0.0         0.0
        Borax                           0.0         0.0
        Mg3Cl(OH)5:4H2O                 0.0         0.0
        Am(OH)3(s)                      0.0         1.0
        KNpO2CO3(s)                     0.0         1.0
        ThO2(am)            0.0         1.0
SAVE SOLUTION 4
END
SOLUTION 5 ERDA-6 5x brine CRA-2019 Domski and Sisk-Scott ERMS 571178 and Conc_density_calcs_CRA-2019_PA.xlsx
        units       moles/l
        pH                  6.0
        pe                  7.0
        temp                25.
        density             1.19978
        B                   0.063
        Na                  4.87
        Mg                  0.019
        K                   0.097
        Ca                  0.012
        Cl                  4.80
        S(6)                0.170
        Br                  0.011
        C(4)                0.016
        Acetate             0.00567
        Citrate             0.000461
        EDTA                1.58e-05
        Oxalate             0.00226
        Am                  1.0E-8      #equilibrium with Am(OH)3(s)
        Np                  1.0E-8      #equilibrium with KNpO2CO3
        Th                  1.0E-8      #equilibrium with ThO2(am)
EQUILIBRIUM_PHASES #Domski and Sisk-Scott ERMS 571178 Table 4 - equilibrate with all minerals
        Hydromagnesite5424  0.0         7.19
        Brucite                         0.0         35.9
        Anhydrite           0.0         163.0
        Halite                          0.0         3410.
        Aragonite           0.0         0.0
        Glauberite          0.0         0.0
        Whewellite                      0.0         0.0
        Borax                           0.0         0.0
        Mg3Cl(OH)5:4H2O                 0.0         0.0
```

```
        Am(OH)3(s)              0.0     1.0
        KNpO2CO3(s)             0.0     1.0
        ThO2(am)        0.0     1.0
SAVE SOLUTION 5
END
```